THE UNIVERSITY *of* EDINBURGH

Controls on ice dynamics of the Greenland Ice Sheet

Joshua J. Williams

Submitted for the degree of Doctor of Philosophy

The University of Edinburgh

2021

Abstract

In recent decades, the Greenland Ice Sheet has lost mass at an accelerating rate, such that it is now the largest individual cryospheric contributor to global sea level rise. This mass loss occurs as a combination of an increase in the melting of ice at the ice sheet surface as well as increased submarine melting and iceberg calving at marine-terminating outlet glaciers, with these processes driven by increasing atmospheric and oceanic temperatures. Understanding the dynamic processes by which ice is discharged into the oceans or moved from higher to lower elevations where air temperatures are warmer is crucial, as the acceleration of ice flow in either case would lead to enhanced ice loss from the ice sheet. This thesis produces considerable new observations and investigates the processes controlling the ice dynamics of the Greenland Ice Sheet within three distinct regions of the ice sheet: the southwest land-terminating margin, the interior accumulation zone, and Sermilik Fjord in southeast Greenland which is characterised by the presence of fast-flowing marine-terminating outlet glaciers.

This thesis first investigates the dynamic response of the south-western land terminating sector of the Greenland Ice Sheet to multi-annual variability in surface meltwater forcing. Within this land-terminating region, the drainage of surface meltwater to the bed and its impact upon the subglacial hydrological system exerts a critical control on ice motion. This link between subglacial hydrology and ice dynamics is termed 'hydro-dynamic coupling' and is of fundamental importance to land-terminating regions of the ice sheet as it controls the transfer of ice from cooler, high elevation regions to warmer, low elevation regions where surface melting, and thus mass loss, is greater. Previous work has shown that over multi-decadal timescales, a persistent increase in the production of surface meltwater has driven a long-term slowdown. However, following a period of sustained high melt peaking with the record melt year experienced in 2012, the regional climate has cooled. This thesis aims to investigate the net impact of this reversal in climate forcing on ice dynamics through its impact upon hydro-dynamic coupling.

To address this, feature tracking is applied to the entire Landsat archive covering the southwest Greenland land-terminating sector in order to quantify changes in annual ice velocity across a 10,600 km^2 sector of the Greenland Ice Sheet during the period 1992-2019, and in particular during the recent cooler 2013-2019 period. Between the early-2000s and 2012, a slowdown in ice motion is observed, consistent with previous results. However, from 2013 to 2019, an acceleration in ice motion occurred, coincident with atmospheric cooling and a 15 % reduction in mean surface melt production relative to the period 2003-2012. This acceleration is strongest nearer the ice margin and is strongly related to ice thickness. This thesis hypothesises that under thinner ice, increases in basal water pressure offset a greater proportion of the ice overburden pressure, leading to a greater acceleration when compared to thicker ice further inland. These findings indicate that hydro-dynamic coupling provides the major control on 'short-term' variations in ice motion within the ablation zone of Greenland's land-terminating margins over multi-annual timescales. Furthermore, these findings confirm that these regions of the ice sheet are resilient to the dynamic impacts associated with increases in surface meltwater production.

The thesis next explores multi-decadal changes in ice velocity within the interior accumulation zone of the Greenland Ice Sheet, an area across which our understanding of recent dynamic change and the processes driving any change is extremely limited. Changes in the ice dynamics of the ice sheet interior are important as the greater ice thickness means that any increase in ice motion will result in a much larger increase in mass flux when compared to marginal regions, and this long-term response of inland regions of the ice sheet to dynamic perturbations originating at the terminus is hypothesised to represent a major component of Greenland's sea level rise contribution. Here, recent satellite-derived annual ice velocity measurements are combined with GPS measurements from the mid-1990s at sites spanning the 2000 m (a.s.l.) elevation contour to quantify the multi-decadal ice velocity change within the ice sheet interior. The results

show a complex pattern of long-term velocity change, with inland acceleration almost ubiquitous along the west coast, reaching 28.1 ± 7.8 m yr^{-1} inland of Jakobshavn Isbrae, contrasting with very limited evidence of acceleration inland of tidewater glaciers on the east coast, despite similar acceleration and retreat observed at the glacier termini. It is hypothesised that this may be related to the underlying subglacial topography whereby glaciers with extensive subglacial troughs, extending considerable distances inland, are generally characterised by inland acceleration. In contrast, sites where inland acceleration is not observed are almost all upstream of a sharp rise in bed topography, consistent with recent research suggesting that such steep bedrock slopes act as to limit the propagation of any perturbation originating at the terminus. These results indicate that acceleration and thinning perturbations at tidewater glacier termini can propagate for distances >100 km inland, accelerating mass loss by increasing the draw-down of greater volumes of thicker ice from the interior toward the lower elevation margins. However, in regions where inland acceleration is not observed, the local bed topography likely limits the extent to which change at the terminus can propagate inland, such that they will be more resilient to future changes in outlet glacier dynamics.

The final results chapter turns to Sermilik Fjord in southeast Greenland, in which a range of remotely-sensed data is combined to investigate and compare the dynamic response of a group of tidewater glaciers to a common climate forcing. The glaciers studied include Helheim Glacier, one of the largest and fastest-flowing outlet glaciers draining the Greenland Ice Sheet, and any dynamic change at Helheim Glacier would thus represent a significant change in the flux of mass from the ice sheet to the ocean. Moreover, by comparing the response of neighbouring glaciers to a common climate forcing, the importance of local geometrical factors such as bed and fjord geometry upon ice dynamics, and thus the transfer of mass to the ocean, can be better understood.

Since 2014, the near-terminus region at Helheim has accelerated by 2.5-3 km

yr^{-1} and retreated by >4 km, with retreat in both 2017 and 2019 extending further inland than during its recent pronounced maximum retreat position in 2005. Mass balance data shows that it has continually lost mass such that the near-terminus region is now 20-100 m thinner than it was in 2005, consistent with a long-term increase in observed air temperatures and modelled submarine melt rates. The front 5 km of the glacier is now within 25-50 m of flotation, indicating that the glacier is in a much more unstable configuration currently than during its previous maximum retreat in 2005. This concern regarding instability is supported by applying the same analyses to the neighbouring Fenris Glacier and Midgard Glacier, which have been subject to essentially equivalent climate forcing and have also undergone consistent mass loss since at least the early-2000s. Both of these glaciers thinned to flotation, after which they underwent dramatic retreat and acceleration, although the timing of this dynamic change differed between glaciers, likely reflecting the different morphological settings and characteristics of the individual glaciers. These results therefore suggest that differences in local fjord morphology and glacier geometry have affected the timing of the response of the glaciers studied to increased air and ocean temperatures, although the fundamental mechanism, the thinning of the near-terminus region towards flotation, remains the same. As a consequence, this thesis argues that Helheim Glacier is poised for a dramatic retreat under continued atmospheric and oceanic warming, which would be unprecedented in at least the last ∼120 years.

This thesis thus presents several advances in our understanding of the processes controlling dynamic change across the Greenland Ice Sheet, with observations spanning land- and marine-terminating margins as well as the interior accumulation zone. The thesis concludes by discussing the implications of these advances in the context of informing future projects of dynamic mass loss from both land- and marine-terminating margins of the ice sheet under future climate change.

Lay summary

In the past 25 years, increasing air and ocean temperatures have caused increased mass loss from the Greenland Ice Sheet, both through melting at the surface of the ice sheet and icebergs breaking off from large 'tidewater' glaciers that drain into the ocean. However, the processes by which the ice sheet responds to changes in climate are complex, and many uncertainties remain. It is therefore crucial to better understand how the dynamics of the ice sheet change in response to climate warming in order to improve projections of sea level rise during the 21st Century and beyond.

When ice melts at the surface of the ice sheet, it forms surface meltwater which can gather in lakes and rivers before draining to the base of the ice sheet. This impacts upon the speed at which the ice flows, a process termed 'hydro-dynamic coupling', whereby the presence of meltwater acts to lubricate the base of the ice sheet, reducing friction and allowing the ice to slide forward more quickly. Initial research suggested that as the climate warms and Greenland experiences increased surface melting, the ice would flow more quickly as a result of this lubrication, increasing mass loss as more ice is drawn down to lower elevations where air temperatures are warmer. However, more recent research has shown that this meltwater at the base of the ice sheet can form subglacial channels which allow the water to drain more quickly, reducing the lubricating effect and thus ice flow. This thesis presents observations of ice flow across a 10,600 km^2 land-terminating region of the ice sheet for the period 1992-2019 and shows that a 30 % rise in surface melting is coincident with a median ice deceleration of 15 % during the period 2003-2012. This supports previous work which hypothesised that a long-term increase in melting at the surface would result in the formation of larger and more widespread channels at the base of the ice sheet, allowing meltwater to drain more quickly, thus increasing friction and reducing the ice flow velocity. Since the year of record melt experienced in 2012, the regional climate cooled and surface melting fell by 15 %, with the ice flow accelerating by 8 % as a result.

This is likely because as less water accesses the base of the ice sheet, it takes longer for channels to form, and any channels that do form are smaller and less spatially extensive. As a result, meltwater that is present at the ice sheet base can lubricate the ice sheet for a longer period of time before draining away, allowing the ice to flow faster. These results thus build on previous research by expanding our understanding of multi-decadal hydro-dynamic coupling to include periods of reduced surface melting; more specifically, they support suggestions that hydro-dynamic coupling is the key control on short-term variations in ice dynamics across the southwest Greenland land-terminating sector, and that this sector of the ice sheet is resilient to the dynamic impacts of increased melting at the ice sheet surface.

The thesis next investigates dynamic change within the ice sheet interior inland from marine-terminating glaciers, a region where our understanding of dynamic change is very limited. However, the retreat of fast-flowing tidewater glaciers at the ice sheet margin causes thinning and acceleration to spread into the interior, and this is thought to be responsible for a majority of the dynamic component of Greenland's sea level rise contribution on a centennial timescale. By combining GPS measurements of ice velocity from the 1990s with satellite-derived velocity measurements covering 2014-2018 at sites around the 2000 m (a.s.l.) elevation contour, this thesis presents the first direct observations of multi-decadal ice velocity change within the ice sheet interior of marine-terminating catchments. The pattern of interior velocity change is complex, with evidence of ice flow acceleration in western Greenland, yet very limited ice flow acceleration in eastern Greenland, despite similar acceleration and retreat of tidewater glaciers at the margins of both regions. This is inferred to be largely due to the differences in the underlying topography, whereby the presence of steep subglacial bedrock slopes across east Greenland limits the ability for the terminus thinning and acceleration to spread inland. In contrast, tidewater glaciers in west Greenland are often underlain by deep troughs that extend considerable distances inland, allowing terminus thinning and acceleration to spread far into the ice sheet interior.

These results indicate that dynamic change near the ice sheet margin can drive faster flow >100 km into the ice sheet interior, increasing the drawn down of thicker ice to lower elevations, and thus enhancing ice mass loss. However, the limited ice flow acceleration observed in east Greenland indicates that this region may be more resilient to future outlet glacier change.

A significant proportion of the Greenland Ice Sheet's contribution to global sea level rise results from mass loss at its marine-terminating glaciers. Helheim Glacier, located in southeast Greenland, is one of the largest and fastest-flowing glaciers draining the Greenland Ice Sheet. During the early-2000s, Helheim Glacier underwent dramatic retreat and acceleration, but subsequently re-advanced during cooler conditions in 2006. However, persistently high ocean and atmospheric temperatures have ensured that Helheim Glacier has in fact been continuously losing mass since 2003, despite this re-advance. This thesis uses a range of remotely-sensed data to show that since 2014, Helheim Glacier has accelerated and retreated to a greater extent than that observed during 2003-2005. More importantly, as the glacier has been losing mass over the past two decades, it is currently much thinner than during its peak retreat in 2005. As the glacier continues to lose mass, it will pass a certain threshold beyond which the ice will float and rapidly disintegrate. This process has already been observed at the glaciers neighbouring Helheim Glacier, which have been subjected to the same climate forcing and thus provide a clear analogue for the future response of Helheim Glacier under continued warming. The results therefore suggest that with continued warming of the ocean and atmosphere, Helheim Glacier is likely to undergo an imminent and dramatic retreat.

This thesis therefore presents several important advances in our understanding of how the Greenland Ice Sheet will respond to future climate warming. These advances stem from observations in both land-terminating and marine-terminating margins of the ice sheet, as well as from the ice sheet interior. The thesis concludes by discussing the implications of these findings in the wider context of

Greenland Ice Sheet stability and suggesting directions for future research.

Declaration

I declare that this thesis has been composed solely by myself, and that it contains only my work except where otherwise specified, or where the work is explicitly indicated below to have formed part of a jointly-authored publication. This work has not been submitted for any other degree or professional qualification.

The candidate confirms that appropriate credit has been given within the thesis where reference has been made to the work of others.

Chapter 4

Citation: Williams, J.J., Gourmelen, N. and Nienow, P. (2020) Dynamic response of the Greenland Ice Sheet to recent cooling, *Scientific Reports*, **10**, 1647. DOI: https://doi.org/10.1038/s41598-020-58355-2
Author contributions: JJW performed all of the data processing and analyses. All authors contributed to the design of the study and the writing of the paper.

Chapter 5

Citation: Williams, J.J., Gourmelen, N. and Nienow, P. (2021) Complex multi-decadal ice dynamical change inland of marine-terminating glaciers on the Greenland Ice Sheet, *Journal of Glaciology*, Cambridge University Press, pp. 1-14 DOI: 10.1017/jog.2021.31.
Author contributions: JJW performed all of the data processing and analyses. All authors contributed to the design of the study and the writing of the paper.

Chapter 6

Citation: Williams, J.J., Gourmelen, N., Nienow, P., Bunce, C. and Slater D. (Manuscript in review) Helheim Glacier poised for dramatic retreat

Author contributions: JJW, NG and PN contributed to the design of the study. JJW performed the data processing and analyses. CB assisted with data processing and figure creation. DS estimated submarine melt rates and subglacial discharge. NG produced surface elevation change estimates. All authors contributed to the writing of the paper.

Joshua J. Williams

May 2021

Acknowledgements

First and foremost, I would like to thank my supervisors Noel Gourmelen and Pete Nienow for their support, guidance, and enthusiasm throughout the past four and a half years, even if the extended conversations regarding day-to-day minutiae preceding each meeting have contributed to a slightly delayed submission. In particular, Noel has provided excellent technical support throughout, and I greatly appreciate his patience when dealing with my frankly dire programming endeavours during the early years of my PhD. Pete has offered invaluable assistance with planning and guiding my research, as well as providing extensive critiques of both my published papers and PhD thesis, which are greatly improved as a result. Both have done all of this with great humour, and I could not have asked for a better pair of supervisors. I would also like to thank the wider glaciology community at the University of Edinburgh for providing a supportive and lively research environment, in particular Charlie for remote sensing and GIS support and Donald for providing data and useful comments for my third results chapter. In addition, I would like to thank my examiners, Dr Dan Goldberg and Dr Hamish Pritchard, for providing useful critique that has certainly improved the thesis.

This research would not have been possible without the generous funding of the NERC E3 Doctoral Training Partnership, who provided me with a fully-funded scholarship alongside the necessary funding to pay for computing costs and travel to various scientific conferences. I would like to thank Stephanie Robin who has been of consistent support and has done an excellent job of managing the DTP.

There are also a number of individuals who deserve particular acknowledgement. Thanks to Michael Biggart for the evenings of BTEC European football, back-to-back dating shows and misery drinking, and for contributions to the coveted backheel assist during Sunday morning 6-a-side. Thanks also to Louis, Andy

and Aythya for making up the more erudite component of the Drummond Street book club and for introducing me to the world of literature. Thanks to Boris for always being happy to help with programming, even if harbouring a great hatred of MATLAB, and for gracing the Bruntsfield Palace with the inexhaustible joys of Mariokart 8. Thanks to Frazer Christie for excellent behaviour and attendance at conferences, for contribution to Milan Fashion Week 2019 and co-authorship within the Open Access Journal of Oceanography and Fisheries (which sadly didn't fit into this thesis), and for appreciation of US soft-rock doyens Hall & Oates. Thanks to Kyle for excellent culinary performance and the many trips to the Turkish baths. Thanks to Victoria and Jenna for the many trips to the Highlands and for always being there. Thanks to Hannah, Alex, Max, and Ewan for the many pub quiz victories. Thanks to Sam for contribution to craft beer consumption. Thanks to Stijn for helping get the code set up on the supercomputer, and to Jordan, Olivier, and Berend for many memorable adventures in Edinburgh and the Netherlands. Thanks to the Exeter lads for downloading and refreshing my papers numerous times in order to get my metrics up, and for pretending to read said papers. Thanks also to my fellow PhD students past and present for sharing the highs and lows of a PhD, in particular Thom, Emiel, Charlie, Laura, Rosie, Polly and Richard. Thanks to Lou for putting up with my nonsense, supporting me through the latter stages of the PhD, and for introducing me to the 1995 BBC adaptation of Jane Austen's Pride and Prejudice starring Colin Firth.

Finally, I would like to thank my parents, Louise and Ian Williams, and wider family for their continued support, encouragement, and belief in me throughout my postgraduate studies.

Contents

List of Figures

List of Tables

Chapter 1

Introduction

The Greenland Ice Sheet contains approximately 2.9 million km^3 of ice, equivalent to ~7.4 m of sea level rise (Morlighem et al., 2017). Whilst the traditional consensus was that the Greenland Ice Sheet is relatively insensitive to changes in climate, with dynamic change occurring over millennia (e.g. Houghton et al., 2001; Huybrechts et al., 1991; Huybrechts and De Wolde, 1999; Oerlemans, 1991; van de Wal and Oerlemans, 1994), it is now understood to constitute one of the most sensitive components of the Earth System to climate change, capable of undergoing significant dynamic change over short (e.g., decadal, annual, seasonal, and diurnal) timescales (i.e., Bevan et al., 2012; Howat et al., 2005; Howat et al., 2008a; Joughin et al., 2004; King, 2018; King et al., 2020; Luckman et al., 2006; Moon and Joughin, 2008; Rignot and Kanagaratnam, 2006a). As such, understanding the dynamics of the Greenland Ice Sheet and the processes that drive ice-motion is crucial in order to accurately project future changes in sea level rise (Meredith et al., 2019; Oppenheimer et al., 2019).

The response of the Greenland Ice Sheet to climate change can be understood through its mass balance. Greenland gains mass through snowfall within the interior accumulation region, and the flow of ice transfers mass from this inland region to the lower elevation ablation region near the coast, where mass is lost through a combination of melting and runoff at the surface and the calving of icebergs at the front of marine-terminating (tidewater) outlet glaciers (Figure 1.1).

Over a full melt-year, if accumulation equals ablation, the ice sheet is in balance, whereas should ablation outpace accumulation, the ice sheet has a negative mass balance (Benn and Evans, 2010).

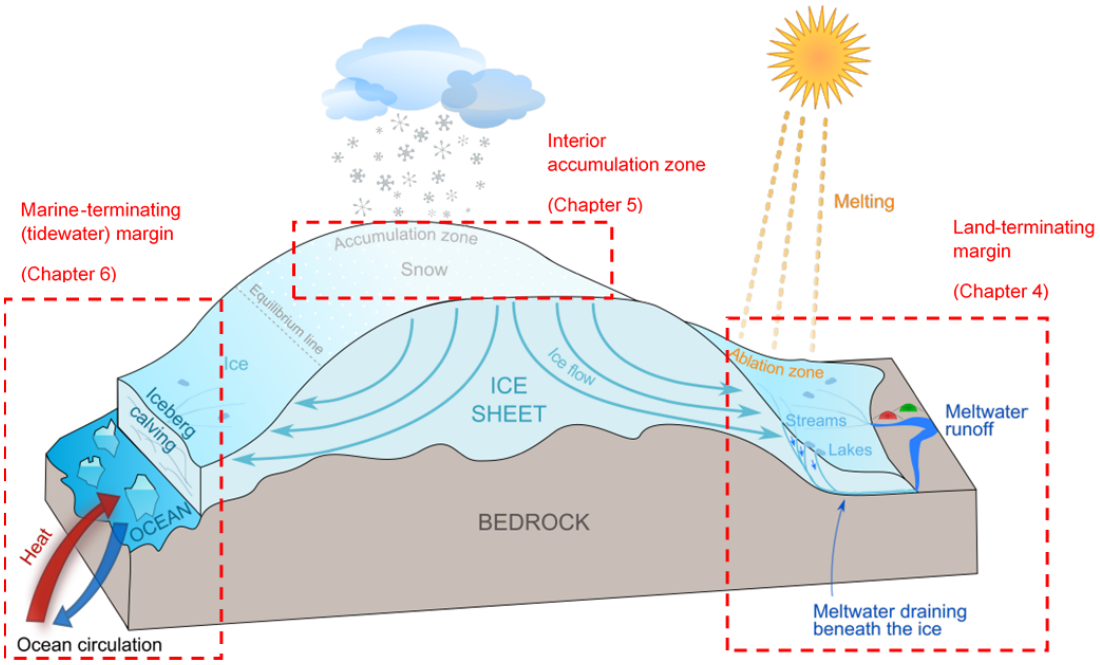

Figure 1.1: *Components of the Greenland Ice Sheet mass budget. Adapted from Tedstone, 2015*

Prior to the 20th Century, current best estimates suggest the Greenland Ice Sheet was close to balance (Box and Colgan, 2013; Hanna et al., 2013; Khan et al., 2015), followed by a period of modest mass loss of -75.1 ± 29.4 Gt yr^{-1} between 1900 and 1983 (Kjeldsen et al., 2015). Whilst some estimates indicated continued mass loss through the 1990s (Krabill, 2004; Rignot et al., 2008; Shepherd et al., 2012), recent studies indicate that the ice sheet was instead close to a state of balance during this period (Figure 1.2, Box and Colgan, 2013; Shepherd et al., 2019; Zwally et al., 2011) before a substantial increase in mass loss began in the late-1990s and early 2000s (Figure 1.2, Mouginot et al., 2019; Pritchard et al., 2009; Rignot and Kanagaratnam, 2006a; Shepherd et al., 2012, 2019; van den Broeke et al., 2009; van den Broeke et al., 2016; Vaughan et al., 2013; Velicogna and Wahr, 2006).

Rates of mass loss have remained consistently above 200 Gt yr^{-1} since 2002

(Mouginot et al., 2019; Rignot and Kanagaratnam, 2006a; Shepherd et al., 2012, 2019; Velicogna and Wahr, 2006), peaking at 345 ± 66 Gt yr^{-1} in 2011 and totalling 3902 ± 342 Gt during the period 1992-2018, equivalent to a sea level contribution of 10.8 ± 0.9 mm (Figure 1.2, Shepherd et al., 2019). The partitioning of ice loss between negative surface mass balance (SMB, increased melting and/or decreased accumulation) and increased dynamic loss has varied over the observational period, and while approximately equal during the 2000s (van den Broeke et al., 2009), the SMB component contributed to 84 % of the mass loss between 2009 and 2012 (Enderlin et al., 2014). The most recent IMBIE estimate (produced by combining and comparing 26 individual satellite-derived estimates of changes to ice sheet volume, flow, and gravitational potential) indicates an approximately even split over the period 1992-2018 (Figure 1.2, Shepherd et al., 2019), although estimates within the wider literature remain varied (Khan et al., 2015; Mouginot et al., 2019).

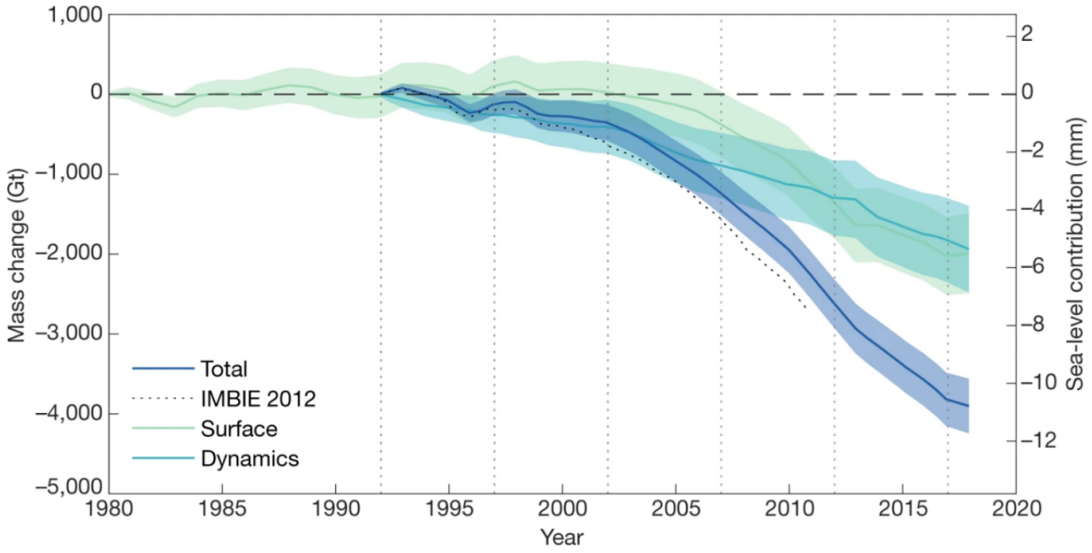

Figure 1.2: *Cumulative anomalies in the total mass, SMB, and ice dynamics of the Greenland Ice Sheet. Total mass change (blue) and mass change through dynamic thinning (light blue) cover the period 1992-2018, and SMB change (green) covers the period 1980-2018. The change in SMB is determined from three regional climate models relative to their mean over the period 1980-1990. The change associated with ice dynamics is determined as the difference between the change in total and surface mass. The estimated 1 standard deviation uncertainties of the cumulative changes are shown by the shaded envelopes. The dotted line shows the results from the previous IMBIE assessment (Shepherd et al., 2012), and the vertical dashed lines mark consecutive 5-year epochs. Reproduced from Shepherd et al., 2019.*

Annual air temperatures across the Greenland Ice Sheet have been increasing since the mid-20th Century (Trusel, 2018, Figure 1.3) and mean summer air temperatures became positive during the mid-1990s (Mernild et al., 2011). Furthermore, Arctic surface air temperatures have increased by more than double the global average since the start of the 21st Century (Meredith et al., 2019; Overland et al., 2019). Coastal weather stations around the Greenland Ice Sheet show evidence of significant atmospheric warming between 1991 and 2019, with average temperature increases of 1.7°C, 4.4°C and 2.7°C in summer, winter, and spring respectively during this period (Hanna et al., 2020). This warming has been particularly pronounced in the west and northwest, where winter temperatures have warmed by ∼6-6.5°C during this period (Hanna et al., 2020), and this has extended to the highest elevations within the Greenland interior, with Summit Station (3216 m a.s.l.) warming by 2.7 ± 0.3°C between 1982 and 2011 (McGrath et al., 2013). Air temperatures peaked in the extreme melt year of 2012, during which a maximum of 98.6 % of the ice sheet surface experienced melt, including the usually cold 'dry snow zone' at high altitudes across the ice sheet interior (Nghiem et al., 2012). Increases in air temperature drive an increase in ice sheet surface melt and thus a reduction in surface mass balance (Fettweis et al., 2017; Noël et al., 2017; van den Broeke et al., 2016); across the period 1991-2015, Greenland's surface mass balance fell by an average of 10.2 Gt yr^{-1} (van den Broeke et al., 2016).

Since 2012, Greenland has experienced a period of relative stability in mass balance (Bevis, 2019) and air temperatures over Greenland have cooled, particularly since 2013/14 (Hanna et al., 2020). This cooling is coincident with a return to a predominantly positive NAO phase, acting both to reduce incoming solar radiation and enhance snowfall (Tedesco et al., 2017). However, since 2019, GRACE data indicates a return to high surface melt rates (Sasgen et al., 2020), and a recent analysis of remote sensing and model data indicates that the summer of 2019 saw extreme melt across the Greenland Ice Sheet, second only to 2012 in runoff magnitude during the period 1948-2019 (Tedesco and Fettweis, 2020).

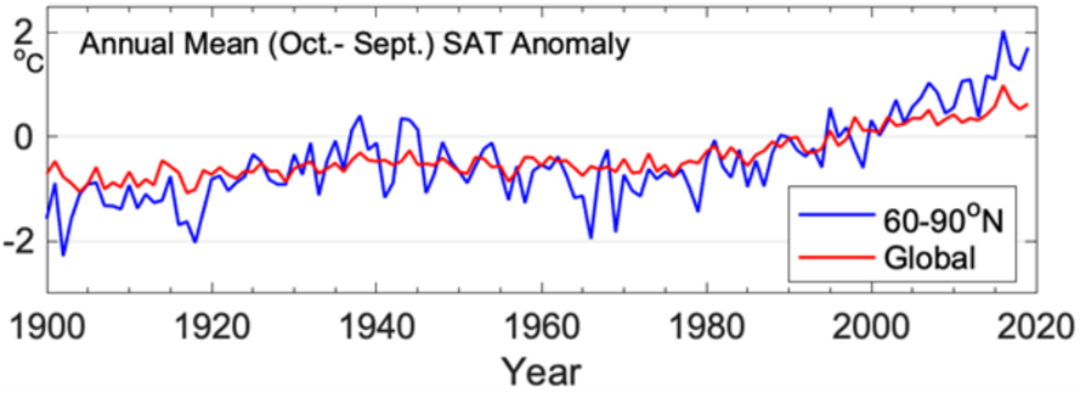

Figure 1.3: *Arctic (land stations north of 60°N; blue line) and global (red line) mean annual land surface air temperature (SAT) anomalies for the period 1900-2019 relative to the 1981-2010 mean value. Reproduced from Overland et al., 2019.*

Atmospheric warming exerts a critical control on the dynamics of Greenland's land-terminating sectors, where the production of surface meltwater influences the development of the drainage network beneath the ice, which in turn modulates ice flow through the resultant impacts on basal water pressure (Andrews et al., 2014; Bartholomew et al., 2011a; Bartholomew et al., 2010, 2011b, 2012; Davison et al., 2019; Nienow et al., 2017; Stevens et al., 2016; Tedstone et al., 2015). Whilst it was originally proposed that melt and ice flow would scale positively within these regions (Parizek and Alley, 2004; Zwally et al., 2002), more recent work shows an inverse relationship (Stevens et al., 2016; Tedstone et al., 2015), indicating that Greenland's land-terminating sectors may be dynamically resilient to climate warming, although the increases in surface melt production contribute to enhanced mass loss regardless.

Greenland's tidewater glaciers, which drain ice from extensive inland basins, have been subject to large increases in dynamic mass loss over the past 20 years (King, 2018; King et al., 2020; Rignot and Kanagaratnam, 2006a; van den Broeke et al., 2009). The four largest (Jakobshavn Isbrae, Petermann Glacier, Kangerlugssuaq, and Helheim Glacier) collectively drain approximately 22 % of the total ice sheet area (Nick et al., 2013), and accounted for ∼50 % of ice loss due to increased solid

ice discharge between 2000 and 2012 (Enderlin et al., 2014). Acceleration of ice flow results in a thinning of the ice, termed 'dynamic thinning'. Dynamic thinning has been observed at all latitudes across the Greenland Ice Sheet, penetrating up to 120 km into the interior (Pritchard et al., 2009), with the strongest dynamic thinning signals located along the southeast and northwest coasts (Csatho et al., 2014; Pritchard et al., 2009; Velicogna et al., 2014). The propagation of dynamic thinning into the interior is thought to be of particular importance, as modelling work suggests that approximately 75 % of dynamic mass loss from the Greenland Ice Sheet results from the longer-term diffusive response of the ice sheet to initial perturbations at tidewater glacier termini (Price et al., 2011).

Changes in atmospheric temperature can influence tidewater glacier dynamics through enhancing crevassing and iceberg calving, the drainage of meltwater to the bed and associated impacts upon subglacial hydrology, the export of freshwater at the terminus acting to drive a fjord circulation which in turns enhances warm water transport to the glacier front, and SMB-driven changes in ice geometry. Greenland's marine-terminating margins are also influenced by ocean properties (i.e., temperature, salinity, velocity) where the ice meets the ocean, with these ocean properties in turn modulated by regional ocean circulation (Catania et al., 2020). Greenland is located at the confluence of the export pathway of cold, fresh Polar Water (PW) from the Arctic Ocean and the anticlockwise recirculation of warm, saline, subtropical Atlantic Water (AW) within the subpolar gyre (Figure 1.4, Catania et al., 2020; Straneo and Heimbach, 2013). PW is transported south along the east coast of Greenland within the East Greenland Coastal Current (EGCC), and AW flows through the Irminger Current (IC), an extension of the North Atlantic Current (NAC) that flows southwest of Iceland and meets the EGCC south of the Denmark Strait (Figure 1.4). The merged East Greenland – Irminger Current subsequently travels along the southeast coast, around the southern tip of Greenland at Cape Farewell, and finally flows northward towards Baffin Bay as the West Greenland Current (WGC).

On Greenland's continental shelves, colder PW is generally found in the surface layer (upper ∼100-200 m), partially buffering the coast from warm AW by blocking surface pathways (Sutherland and Pickart, 2008). However, AW is denser than PW due to its salinity, despite being warmer (Joughin et al., 2012), and so is typically found underlying PW at ∼100 to ∼1000 m depth, where it can access Greenland's deep glacial fjords (Sutherland and Pickart, 2008). Indeed, surveys have shown that fjords contain a thick layer of warm (0 – 4°C), saline, subsurface AW beneath a layer of PW (Christoffersen et al., 2011; Holland et al., 2008; Johnson et al., 2011; Rignot et al., 2010; Straneo et al., 2010), and it is the influence of this warm AW layer than can have a large impact on submarine terminus melt should it come into contact with glacier ice (Joughin et al., 2012).

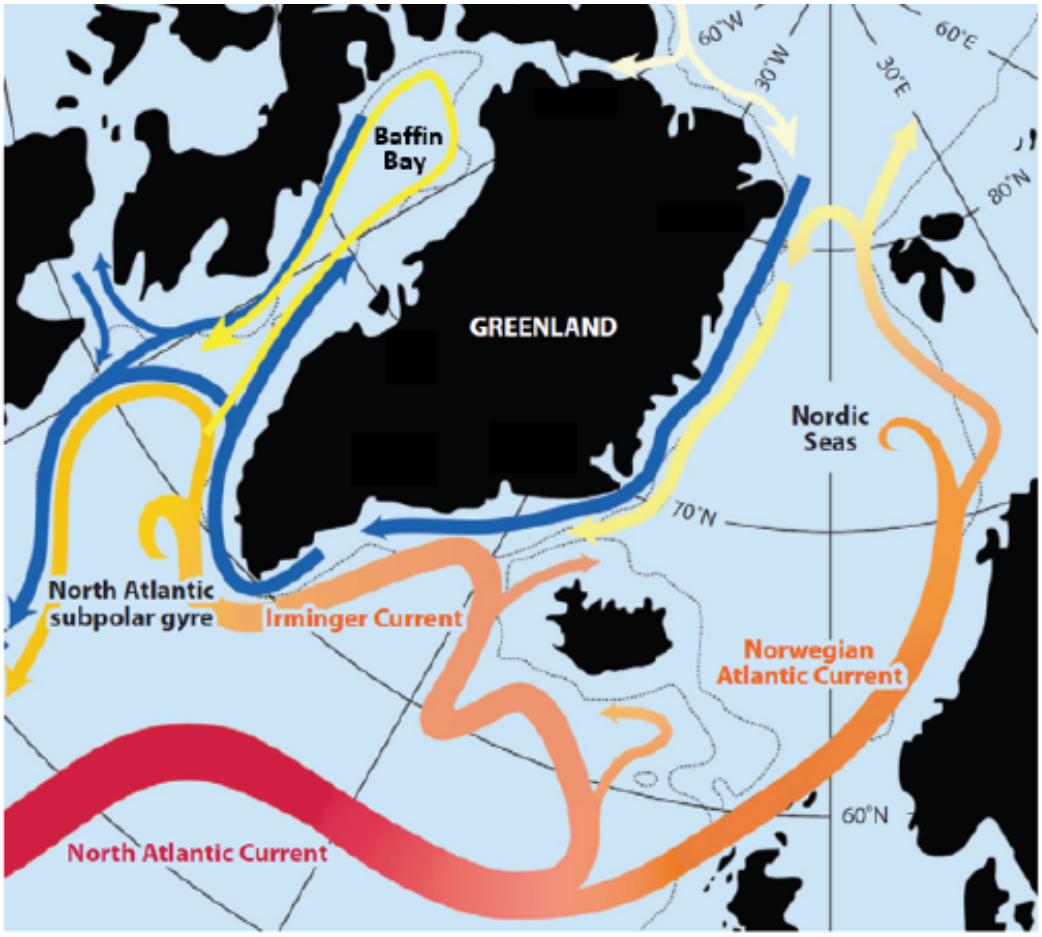

Figure 1.4: *Ocean circulation around Greenland, with the major ocean currents annotated. The colours of the currents describe their temperature, with the red to yellow colours representing warm, saline Atlantic Water and the blue representing cold, fresh Polar Water. Modified from Straneo and Cenedese, 2015*

The recent retreat, acceleration, and thinning of Greenland's marine-terminating outlet glaciers has been coincident with a warming of the upper 500-1000 m of the subpolar North Atlantic, extending to Baffin Bay, which began in the mid-1990s and has continued through the 2010s (Bersch et al., 2007; Holland et al., 2008; Holliday et al., 2008; Myers et al., 2007; Straneo and Heimbach, 2013). This warming is unprecedented in the historical record outside of a similar warm period during the 1930s (F Straneo, 2013; Polyakov et al., 2005). Since the 1990s, ocean temperature and salinity have increased rapidly within the subpolar gyre (Holliday et al., 2008), with some of the highest salinity and temperatures ever recorded within the IC measured after 1995, and an overall warming trend of $+0.03$°C yr^{-1} between 1984 and 2005 (Myers et al., 2007). Off the coast of west Greenland, sea surface temperature (SST) anomalies show a significant increasing trend of $+0.096$°C yr^{-1} within the upper 0-300 m during the period 1983-2004 (Stein, 2006), and the mean 150-600 m depth averaged temperature within Disko Bay rose from 1.7°C in 1995 to 3.3°C in 1998, remaining around this level thereafter (Holland et al., 2008). Modelled subsurface ocean temperatures show an increase of 1.5°C offshore of southeast and southwest Greenland between 1994 and 2005, followed by a subsequent cooling, an increase of 2-2.5°C offshore of northwest Greenland between 1997 and 2005, and an increase of <0.5°C after 2005 in the far north (Rignot et al., 2012).

Model projections indicate that under continued warming, a marked increase in both surface runoff (Gregory et al., 2020; Hofer et al., 2020) and dynamic mass loss (Choi et al., 2021) from the Greenland Ice Sheet will occur over the 21st Century. Despite this, a range of uncertainties remain with respect to Greenland's response to both atmospheric and oceanic forcing, and so capturing the dynamic response of the ice sheet to climatic forcing within models remains difficult (Pattyn et al., 2018), as evidenced by the large spread in projections of ice sheet volume change and sea level contribution by 2100 (Fürst et al., 2015; Goelzer et al., 2020; Meredith et al., 2019; Vizcaino et al., 2015). Consequently, an improved understanding of the processes controlling the dynamics of the GrIS

is needed if the response of the ice sheet to predicted climate change is to be more accurately determined; and this thesis has the ambition to improve this process understanding.

1.1 Outline of Thesis

This thesis aims to improve our understanding of the mechanisms controlling the discharge of ice from both land and marine-terminating sectors of the Greenland Ice Sheet on multi-annual to multi-decadal timescales. It primarily uses remotely sensed observations to investigate the response of ice motion to changes in atmospheric and oceanic forcing, with the inclusion of field-based GPS data in order to measure change within inland regions of the ice sheet. The thesis specifically seeks to provide an improved process-based understanding of the response of the Greenland Ice Sheet to global climate change, such that the response of the ice sheet to future warming can be better projected, and is organised into three research themes:

1. **The dynamic response of the southwest Greenland land-terminating sector to recent climate cooling.** Air temperatures across the southwest Greenland Ice Sheet have warmed during the 1990s and 2010s (Box et al., 2009; Hanna et al., 2012, 2020), peaking in 2012 (Nghiem et al., 2012) and driving increased production of surface meltwater. This meltwater can drain to the bed, where it exerts a key control on ice dynamics within the southwest Greenland land-terminating sector through its influence on the development of the subglacial hydrological system. On multi-decadal timescales, previous work has shown that a persistent increase in surface meltwater production drives a long-term slowdown in ice velocity (Stevens et al., 2016; Tedstone et al., 2015). This has been attributed to an increase in both the size and spatial extent of efficient subglacial channels in response to enhanced meltwater inputs, with the result of increased drainage of waters from the inefficient, distributed component of the subglacial hy-

drological system, acting to reduce regional basal water pressures and so ice motion (Tedstone et al., 2015). However, since the record melt of 2012, air temperatures have cooled (Hanna et al., 2020) and the mass balance of the Greenland Ice Sheet has been relatively stable (Bevis, 2019). By undertaking feature tracking of the entire Landsat archive covering the southwest Greenland land-terminating sector, this theme quantifies changes in annual ice velocity across a 10,600 km^2 sector of the Greenland Ice Sheet during the period 1992-2019 in order to assess the long-term response of ice motion to surface melt forcing, and in particular, to the reduced surface melt forcing from 2013 to 2019. The response of the southwest land-terminating margin to a reduced surface melt forcing has previously only been studied on a seasonal timescale (Joughin et al., 2008b; Sole et al., 2013; van de Wal et al., 2015), and so the ultimate aim of this theme is to provide a better understanding of the mechanisms driving ice motion on a multi-annual timescale.

2. **Quantifying multi-decadal ice dynamical change inland of marine-terminating glaciers on the Greenland Ice Sheet.** Since the late-1990s through early-2000s, the Greenland Ice Sheet has undergone increased dynamic mass loss as a result of the near-terminus retreat, acceleration and thinning of marine-terminating glaciers (King, 2018; King et al., 2020; Rignot and Kanagaratnam, 2006a; Shepherd et al., 2012, 2019). However, our understanding of changes in the dynamics of inland regions is far more limited, yet it has been projected that the majority of Greenland's future contribution to sea level rise will be as a result of the ability for perturbations originating at tidewater glacier termini to propagate upglacier and drive increased ice flow and thinning within the ice sheet interior (Price et al., 2011). Subsequent theoretical work has indicated that there may be geometrical constraints (i.e., bed topography, ice thickness, ice surface slope) on the ability for thinning and acceleration to propagate inland (Felikson et al., 2017, 2020). However, there is very little direct observational evidence

to constrain these modelling and theoretical studies, with observations of velocity change within inland regions limited to sparse GPS measurements of seasonal velocity variability inland of a few individual glaciers (Ahlstrøm et al., 2013; Sole et al., 2011) alongside a single multi-annual study observing velocity change up to 80-100 km inland of the grounding line at Zacharie Isstrom in northeast Greenland (Mouginot et al., 2015). Moreover, whilst it is possible to obtain ice-sheet-wide measurements of dynamic thinning by differentiating modelled SMB from surface elevation change measurements (McMillan et al., 2016; Pritchard et al., 2009; Zwally et al., 2011), the required accuracy to map the expected dynamic thinning in the interior is well below the combined uncertainty of the altimetry and SMB models. In this theme, recent satellite-derived annual ice velocities from the period 2014-2018 (Gardner et al., 2018, 2019) are combined with estimates of annual ice velocity during the period 1993-1997 from a ring of 161 GPS sites around the 2000 m (a.s.l.) surface elevation contour (Thomas et al., 2000; Thomas et al., 1998; Thomas, 2001). By combining these data sources, the multi-decadal response of inland regions of the Greenland Ice Sheet to the dramatic changes observed at tidewater glacier termini is quantified, providing the first robust observational evidence of inland ice dynamics on an ice-sheet-wide scale and covering multiple decades.

3. **Investigating recent dynamic change at marine-terminating glaciers within Sermilik Fjord, southeast Greenland.** Located at the head of Sermilik Fjord, southeast Greenland, Helheim Glacier is one of the largest discharging and fastest-flowing glaciers on the Greenland Ice Sheet, draining approximately 7 % of the total ice sheet area (Rignot and Kanagaratnam, 2006a). During the period 2002-2005, Helheim Glacier underwent dramatic retreat, acceleration, and dynamic thinning (Howat et al., 2005; Howat et al., 2008b; Luckman et al., 2006; Stearns and Hamilton, 2007), after which it stabilised and re-advanced (Bevan et al., 2012; Howat et al., 2011; Kehrl et al., 2017; Miles et al., 2016), although it has since remained in negative mass

balance (Mouginot et al., 2019). Recent estimates show a large increase in solid ice discharge from Helheim Glacier during the period 2014-2019, such that it is now at least the second largest contributor to Greenland's solid ice discharge (Mankoff et al., 2020; Mouginot et al., 2019). Through combining satellite-derived measurements of ice velocity, terminus position and surface elevation, this theme investigates the recent dynamic changes at Helheim Glacier. More specifically, it does so in the context of its prior maximum retreat, acceleration and thinning during 2005, and utilises air temperature data from a proximal weather station alongside modelled submarine melt rates to assess the impact of recent atmospheric and oceanic forcing upon the observed change. In addition, this theme also investigates dynamic change at the neighbouring Fenris Glacier and Midgard Glacier, which also drain into Sermilik Fjord, over the same time period. This enables insights into whether glaciers within the same fjord system, and thus likely subject to very similar atmospheric and oceanic forcing, show similar or differing responses to external climatic forcing, and whether the responses of Fenris Glacier and Midgard Glacier can be used as analogues for the future response of Helheim Glacier.

1.2 Thesis Structure and Format

Following this introduction, Chapter 2 provides a detailed review of ice dynamical change in both land and marine-terminating sectors of the Greenland Ice Sheet, including the fundamental processes controlling ice motion, the coupling of subglacial hydrology and ice dynamics, ice-ocean interactions, and the mechanisms by which thinning and acceleration induced by a perturbation at the terminus may propagate inland. Chapter 3 describes the methodologies used to analyse the remotely sensed data that is used in this thesis, with more specific details found later in the individual results chapters. Chapters 4-6 present the main results, following the three themes as introduced above. Finally, Chapter 7 provides a synthesis and summary of the key findings and places them in the wider

context of ongoing research being undertaken investigating the future stability of the Greenland Ice Sheet.

Chapters 4, 5 and 6 have been written as standalone papers in order to rapidly report their key findings to the wider research community through peer-reviewed journals. Chapters 4 and 5 have been published (Williams et al., 2020, 2021), while Chapter 6 has been submitted for publication.

Chapter 2

Background

The Greenland Ice Sheet loses mass through the melting of the ice sheet surface, and both submarine melting and the calving of icebergs at its marine-terminating outlet glaciers, and these processes respond to changes in atmospheric and oceanic properties (i.e., Cowton et al., 2018; Holland et al., 2008; Joughin et al., 2008a; Murray et al., 2010, 2015; Seale et al., 2011; Straneo and Heimbach, 2013). The interaction between ice sheet dynamics and climatic forcing differs between land-terminating and marine-terminating sectors of the ice sheet, with the former solely driven by atmospheric forcing through surface melting and glacier hydrology, and the latter also affected by ice-ocean interactions.

This background chapter first addresses the fundamental mechanisms of ice flow, before providing a broad introduction to glacier hydrology. Our understanding of glacier hydrology results from many decades of research into alpine glaciers, and it was only from the start of the 21st Century that the link between hydrology and dynamics of the Greenland Ice Sheet began to receive attention, with many of the concepts derived from alpine glaciers being applicable. As such, an overview of the research conducted at alpine glaciers is given to provide the foundation of glacier hydrology and hydro-dynamic coupling, after which observations within the southwest Greenland land-terminating sector are reviewed. The dynamic change observed, and its heterogeneity, across Greenland's tidewater glaciers is then discussed along with the key oceanic, atmospheric, and morpho-

logical controls. The chapter concludes by discussing the mechanisms through which perturbations at tidewater glacier termini can propagate into the ice sheet interior, which has been proposed as a crucial control on future sea-level rise (Felikson et al., 2017, 2020; Price et al., 2011).

2.1 Mechanisms of Ice Flow

Glacier ice moves slowly downslope under gravity, flowing from the high-elevation accumulation area to the low-elevation ablation area where ice is lost through melting at the surface, as well as through submarine melting and the calving of icebergs at marine-terminating margins.

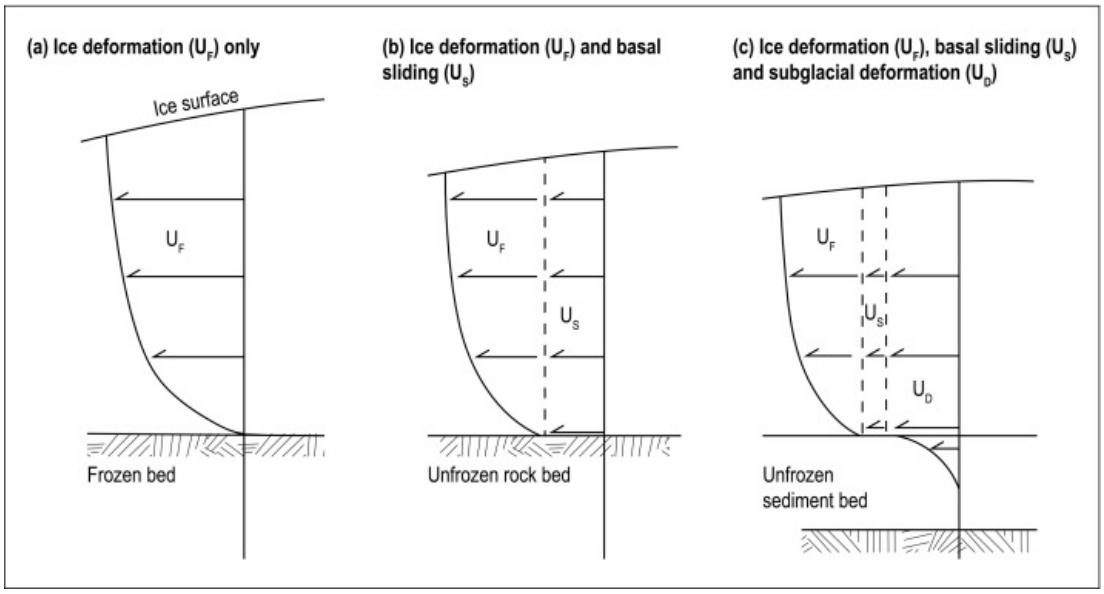

Figure 2.1: *Schematic diagrams showing the vertical distribution of velocity for three different types of glacier motion;* ***(a)*** *internal deformation (UF) only,* ***(b)*** *internal deformation (UF) and basal sliding (US), and* ***(c)*** *internal deformation (UF), basal sliding (US) and soft-bed deformation (UD). The horizontal arrows refer to the velocity of ice motion at their respective depths. Reproduced from Chandler and Evans, 2021 following Boulton, 1996.*

As a result, the response of the Greenland Ice Sheet to climate change, and thus Greenland's contribution to future sea level rise, is strongly dependent upon the mechanisms and rates of glacier flow (Figure 2.1), which occurs through

a combination of internal deformation within or between ice crystals (Section 2.1.1), basal sliding as a result of the presence of water at the ice-bed interface (Section 2.1.2), and the deformation of the underlying bed should the glacier be underlain by soft, deformable sediments (Section 2.1.3).

Gravity pulls a glacier downward, with a gravitational driving stress (τ_d) acting on the full ice column and affecting both internal deformation and basal sliding. τ_d is principally due to the weight of the overlying ice and the slope of the ice surface, and takes the form:

$$\tau_d = P_i g H \ tan \ \alpha \tag{2.1}$$

Where P_i is the ice density (typically 917 kg m^{-3}), g is the gravitational acceleration (9.8 m s^{-2}), H is the ice thickness, and α represents the surface slope (Benn and Evans, 2010). From this, it can be seen that both a thickening of glacier ice, and an increase in surface slope (for example through a disproportionate increase in downstream ablation relative to upstream accumulation), will result in an increased driving stress, and so faster ice motion.

This driving stress must be counteracted by resistive stresses, else the glacier ice would accelerate without limit and quickly melt away. As such, glacier flow can be described as a force-balance equation, in which the gravitational driving stress is balanced by a combination of resistive stresses (Benn and Evans, 2010; Jiskoot, 2011). On most glaciers, where the ice is grounded at the bed, resistance is primarily as a result of friction at the bed, commonly termed basal drag, but can also include lateral drag from valley/trough walls and shear margins, and dynamical resistance to ice flow via pulling and pushing due to longitudinal stress gradients within the ice (Benn and Evans, 2010; Jiskoot, 2011). Where ice is not grounded, for example ice shelves and the floating ice tongues of some marine-terminating glaciers, bed resistance is zero and so the driving stress is balanced by the latter two resistive stresses.

Rates of ice flow therefore depend upon the driving and resistive stresses that act on a glacier but are also controlled by the way in which glacier ice can deform (through internal deformation, or 'creep'), and whether a glacier can slide over its bed (Jiskoot, 2011). These flow mechanisms are considered in more detail in the following sections.

2.1.1 Internal Deformation

Internal deformation is composed of deformation resulting from movement within or between individual ice crystals (Benn and Evans, 2010), and where large stresses are applied rapidly, brittle failure and fracturing (Jiskoot, 2011), and is the dominant flow mechanism where the ice is frozen to the bed. The rate of internal deformation can be approximated by Glen's Flow Law (Glen, 1955) which takes the form:

$$\varepsilon = A\tau^n \tag{2.2}$$

Where τ is the applied stress, A is the ice 'softness' parameter, which increases exponentially with temperature (Cuffey and Paterson, 2010), and n is a constant that depends upon the applied stress (Jiskoot, 2011) and the creep mechanism operating (Hooke, 2005). Whilst n can be in the range of $1.5 < n < 4.2$, a mean of n=3 is commonly used for temperate glaciers (Cuffey and Paterson, 2010), such that strain rates increase non-linearly with applied stress (Benn and Evans, 2010). The relation between applied stress and glacier flow is approximately proportional to the fourth power of ice thickness and the third power of ice surface slope (Jiskoot, 2011). Given the resistance of basal drag acting at the bed, and lateral drag at the margins, glaciers moving predominantly via internal deformation are generally characterised by a maximum ice flow at the surface, which decreases as a fourth-order polynomial with depth to almost zero at the ice-bed interface (Jiskoot, 2011, Figure 2.1a). The transverse velocity profile has a parabolic shape, with a maximum in the centre and decreasing velocity towards the lateral margins (Figure 2.2).

Factors other than ice temperature and applied stress can influence the creep rate of glacier ice. Ice crystals deform along cleavage planes, controlled by the molecular structure, approximately 100-1000 times more easily than in any other direction (Hooke, 2005), and so in polycrystalline ice, deformation rates also depend upon the aggregate orientation of ice crystals, commonly termed the 'ice crystal fabric' (Benn and Evans, 2010). In addition, the presence of impurities or water within the ice can influence deformational flow, the latter important within basal ice which may have a water content an order of magnitude greater than that of ice nearer the surface (Hubbard et al., 2003), and so may deform more easily.

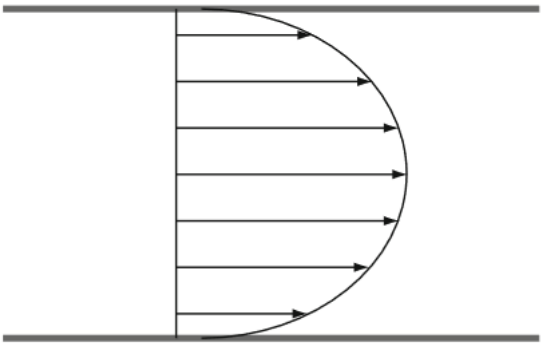

Figure 2.2: *Diagram showing an approximate parabolic transverse ice velocity profile. The length of the arrow represents the velocity at that location across the glacier. Reproduced from Jiskoot, 2011.*

Whilst deformation rates increase non-linearly with applied stress, changes to ice thickness, surface slope, temperature and water/impurity content are relatively slow, and so changes in ice velocity as a result of internal deformation occur rather slowly.

2.1.2 Basal Sliding

In glaciers that are not frozen to their bed (such that the ice-bed interface is at the pressure melting point), basal motion will occur whereby the ice slides over its bed, which can account for a significant proportion of ice flow and allow much faster flow speeds (Benn and Evans, 2010; Cuffey and Paterson, 2010; Hooke,

2005; Jiskoot, 2011; Kamb et al., 1985). Our understanding of basal slip has its origins in Weertman's theory of sliding (Weertman, 1957, 1964), which addresses how ice at the pressure melting point is able to flow past bumps in the bed topography through the processes of regelation and enhanced creep.

Regelation (Weertman, 1957, 1964) describes the mechanism whereby local high pressure immediately upstream of a bedrock obstacle reduces the pressure melting point, thus driving local melting of the ice (Cuffey and Paterson, 2010). This meltwater then flows to the downstream side of the obstacle where pressures are lower and the water subsequently refreezes, releasing latent heat which is conducted through the obstacle (due to the temperature gradient) and assists in the upstream melting (Benn and Evans, 2010). Regelation is most effective with small obstacles, given the increasing inefficiency of heat conduction as obstacle size increases (Benn and Evans, 2010).

Enhanced creep occurs as a result of the non-linear variance in strain rate with applied stress (Equation 2.2), whereby excess stress concentrations on the upstream side of a bedrock obstacle drive locally high strain rates, allowing the ice to deform around and over the obstacle (Weertman, 1957). A larger obstacle would result in a larger upstream region of enhanced stress, and so enhanced creep is more effective for large obstacles than small ones (Cuffey and Paterson, 2010).

Weertman's theory of sliding, however, is subject to the assumption of a temperate ice mass separated from a rough, undeformable and impermeable bedrock by a thin film of water, and is unlikely to be entirely realistic as it does not account for the formation of water-filled cavities on the downstream side of bedrock bumps (Cuffey and Paterson, 2010) where the pressure exerted by the weight of the overlying ice (ice overburden pressure, P_i) is lowest.

Subsequent models of sliding emphasised the importance of water-filled cavities

(Lliboutry, 1968, 1979; Lliboutry, 1987), which affect sliding behaviour in several ways. The formation of cavities (cavitation) can submerge small bumps on the bed, especially when formed in the lee of large bedrock obstacles, and thus reduce the bed roughness (Fowler, 1987; Schoof, 2005). Pressurised water within cavities exerts a net downglacier force on the ice at the downstream side of the cavity (Hooke, 2005), increasing the downglacier driving force. Thirdly, and perhaps most importantly, as water cannot support a shear stress, the basal shear stress above water-filled cavities is locally zero, such that the area of ice-bed coupling is reduced and stresses concentrate on the remaining areas of contact (Lliboutry, 1968, 1979), reducing basal drag and increasing the efficiency of regelation and ice deformation, both of which increase the sliding rate.

The minimum overburden pressure at which water can force its way between the ice and the underlying bed is termed the separation pressure (P_s), and thus where water pressure (P_w) is equal to the separation pressure ($P_w = P_s$), cavities begin to form. If P_w increases, for example where more water is supplied to the subglacial drainage system than can be drained away, cavities increase in size as $P_w > P_s$, submerging more of the bed and further increasing sliding speed (Cuffey and Paterson, 2010). Faster sliding is therefore related to low effective pressures (N, the difference between P_i and P_w), and can become unstable where P_w passes a critical threshold (P_c), which may lead to non-linear acceleration (Iken, 1981).

To maintain large cavities and fast sliding, the volume of water at the bed must be sufficient to fill the cavity space and with P_w high enough to prevent cavity closure by ice creep (Cuffey and Paterson, 2010). However, the growth of cavities both increases the capacity of the subglacial drainage system and forces a transition from a distributed, linked-cavity based subglacial drainage system to an efficient, conduit based subglacial drainage system, which reduces P_w and thus sliding (Jiskoot, 2011; Kamb, 1987; Lliboutry, 1968). As such, basal sliding through cavitation can be considered to have two 'modes' of sliding (Jiskoot, 2011); a 'fast mode' whereby water at the bed drains through linked cavities,

characterised by a direct relationship between subglacial P_w and ice motion, and a 'slow mode' whereby water at the bed drains efficiently through large conduits, characterised by an inverse relationship between subglacial P_w and ice motion. A change between these two forms of subglacial drainage can drive sudden changes in sliding velocity (Kamb, 1987; Lliboutry, 1968), and is considered in more detail in section 2.2.

2.1.3 Soft-Bed Deformation

Early theoretical analyses of basal sliding assumed a rigid and impermeable bed (Cuffey and Paterson, 2010), however glacier ice can also be underlain by poorly-consolidated or unlithified sediments, termed glacial till, which can deform as a result of stresses imposed by the overlying ice (Benn and Evans, 2010; Hooke, 2005; Jiskoot, 2011). Observations at Whillans Ice Stream in Antarctica (Alley et al., 1986; Blankenship et al., 1986) indicated that the presence of a deformable glacial till at the ice-bed interface may contribute significantly to the motion of glacier ice, in addition to the sliding of ice along the top of the till.

As with basal sliding, the deformation of subglacial till is strongly controlled by water pressure at the bed (Cuffey and Paterson, 2010), as unconsolidated sediments readily deform under applied shear stress when a large fraction of their pore space, the space between individual granules, is filled with pressurised water (Jiskoot, 2011). Water enters the intergranular pore space through Darcian flow, as a result of elevation differences and pressure gradients which combine to define the hydraulic potential, with water flowing from regions of high hydraulic potential (high elevation, high pressure) to low hydraulic potential (low elevation, low pressure) (Cuffey and Paterson, 2010). If the rate of water input into the till is greater than the evacuation of water from the till, the pore water pressure, the water pressure within the intergranular pore space, increases. This weakens the till, allowing the sediment to deform more readily and thus increasing ice motion. Where large clasts of sediment at the ice-bed interface are partially embedded in ice and partially in till, they can be pushed forward by the motion of the ice and

'plough' through the till, enhancing soft-bed deformation (Brown et al., 1987; Iverson et al., 1999; Iverson, 1999).

However, the contribution of soft-bed deformation to ice motion may be substantially less than originally postulated (Iverson et al., 1995; Piotrowski et al., 2001, 2004). An increased P_w at the ice-bed interface is indicative of a reduced effective pressure, and so the overlying ice will be approaching flotation, thus transmitting less shear stress to the subglacial sediment (Clarke, 2005). As such, a negative feedback exists between subglacial P_w and soft-bed deformation rates, thus favouring sliding via ice-bed decoupling. This is supported by observations of surface uplift during speed-up events (Iverson et al., 1995). Alternatively, it has been argued that where the water layer thickens at the bed, shear stresses will be focused on fewer sediment particles, increasing their likelihood to plough through the bed and thus increase soft-bed deformation (Iverson, 2011; Thomason and Iverson, 2008). It is clear that much of the impact of subglacial water on soft-bed deformation remains unknown, and it is beyond the scope of this literature review to attempt to bring the seemingly disparate modes into a common framework. Regardless, the presence of 'sticky spots' (Alley, 1993) at the glacier bed, for example bedrock protrusions, bare-rock set within till, regions of efficient drainage or regions where water freezes to the bed (Cuffey and Paterson, 2010), further limit the rate of soft-bed deformation. Such 'sticky spots' are thought to be the norm as opposed to the exception for ice-sheet beds, and so it is plausible that soft-bed deformation is not as widespread and pervasive as first conceived (Piotrowski et al., 2001, 2004).

2.2 The Glacier Hydrological System

The hydrological system of a glacier or ice sheet is composed of three distinct subsystems; supraglacial hydrology, which concerns the production and transfer of meltwater on and across the ice surface, englacial hydrology, which concerns the transfer of surface meltwater through the glacier ice, and subglacial hydrol-

ogy, with concerns the drainage of water at the ice-bed interface. Each of these subsystems is composed of a variety of features, as illustrated in Figure 2.3.

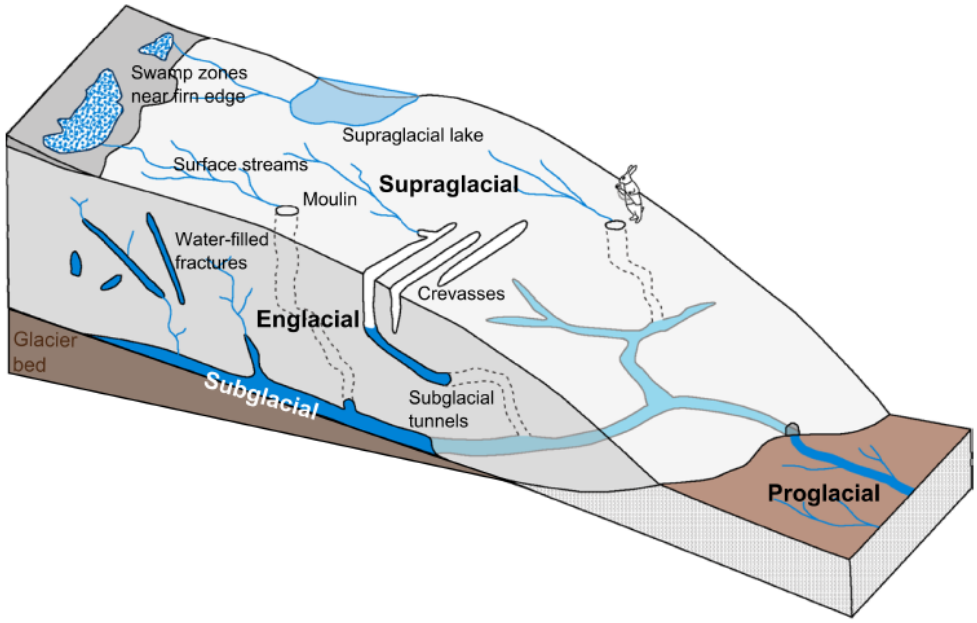

Figure 2.3: *Elements of the subglacial hydrological system of a land-terminating sector, reproduced from Tedstone, 2015 following Cuffey and Paterson, 2010.*

2.2.1 The routing of meltwater on the ice sheet surface to the bed

Water enters the glacio-hydrological system through rainfall or melting at the ice-sheet surface, with the latter being the dominant source and typically commencing sometime during spring and ceasing in autumn, a period termed the 'melt season'. The majority of this water is routed to the ice sheet bed, where it exerts a fundamental control on ice dynamics (Chu, 2014; Davison et al., 2019; Fountain and Walder, 1998; Hubbard and Nienow, 1997; Iken and Bindschadler, 1986; Nienow et al., 2017).

Should melting occur where snow or firn is present, the meltwater must percolate through the snowpack/firn, during which it can locally re-freeze (Pfeffer et al., 1991) or be stored within the porous firn (Harper et al., 2012). Storage within firn across Greenland is hypothesised to act as a buffer against the sea level

rise contribution of the Greenland Ice Sheet, with an estimated storage sink size of 322 ± 44 to 1289^{+388}_{-252} Gt that would take on the order of decades to fill (Harper et al., 2012). However, more recent work in west Greenland indicates that this meltwater storage within firn has been limited as a result of a series of warm summers during the period 2009-2015 (Machguth et al., 2016). At elevations >1900 m, the firn has densified, reducing the ability for meltwater to percolate into the pore space, and at lower elevations more abundant melt has filled the pore space such that the firn has lost most of its capacity to store water, both acting to increase meltwater runoff over the ice sheet surface (Machguth et al., 2016).

In southeast Greenland, considerable water storage has been observed within an existing firn aquifer located approximately 5-50 m below the surface (Forster et al., 2014; Koenig et al., 2014; Miège et al., 2016). This aquifer covers an estimated area of 21,900 (Miège et al., 2016) to 70,000 km^2 (Forster et al., 2014) and may store up to 140 ± 20 Gt of water (Forster et al., 2014; Koenig et al., 2014), equating to ∼0.4 mm of sea level rise. Modelling studies indicate that the firn aquifer can drain to the bed via crevasses (Poinar et al., 2017, 2019), and suggest that the aquifer and crevasses should be considered as a common system which may drive a delayed routing of large volumes of meltwater to the bed, possibly outside of the melt season (Poinar et al., 2017, 2019).

Where meltwater does not re-freeze or become stored within firn, it reaches the impermeable ice sheet surface and subsequently flows downslope through sheet flow or via an arborescent network of incised supraglacial channels (Benn and Evans, 2010), the latter of which are formed through thermal erosion during meltwater flow (Mantelli et al., 2015; Smith et al., 2015) and convey water at speeds of a few m s^{-1} (Cuffey and Paterson, 2010). Near the margin, supraglacial streams may flow to the edge of the ice sheet, discharging water directly into the proglacial environment, while further inland they predominantly drain englacially into the ice sheet through moulins or crevasses (Figure 2.3; Catania and Neumann, 2010; Davison et al., 2019; Koziol et al., 2017; Nienow et al., 2017; Smith et al., 2015).

These surface-to-bed connections are initially formed where crevasses intersect the supraglacial drainage system. As a result of meltwater ponding within them, crevasses can subsequently extend to the bed via 'hydrofracture' to form a moulin (van der Veen, 2007), a near-vertical conduit extending through the glacier ice (Cuffey and Paterson, 2010). As water is denser than ice, the outward pressure exerted by the water on the walls and base of a crevasse can overcome the ice overburden pressure acting to close the fracture (Scambos et al., 2000; Van Der Veen, 1998; van der Veen, 2007; Weertman, 1972), allowing the crevasse to reach the bed. A considerable proportion of moulins in Greenland, however, form away from crevasse fields (Hoffman et al., 2018), and in these cases observational and model evidence points to fracturing being driven by the rapid drainage of supraglacial lakes (Das et al., 2008; Hoffman et al., 2018).

Once a surface-to-bed connection is made, the flow of water through the moulin will keep the moulin open through frictional heat dissipation (Cuffey and Paterson, 2010), provided that the rate of melting exceeds the rate of ice creep closure (Fountain and Walder, 1998). At higher surface elevations, the combination of reduced surface meltwater availability and greater creep closure rates as a result of thicker ice means that moulin density decreases (Koziol et al., 2017; Poinar et al., 2015), with an estimated upper limit of ∼1600 m in western Greenland (Poinar et al., 2015). As a result, meltwaters produced at higher elevations are often transported considerable distances from their source before they enter the englacial hydrological system (Nienow et al., 2017; Poinar et al., 2015). Given that larger volumes of water are required to form and maintain moulins at higher elevations, lake hydrofracture is thought to be dominant process driving moulin formation further inland (Koziol et al., 2017).

2.2.2 Subglacial Drainage System Structure

Surface meltwater that drains via moulins subsequently travels through englacial pathways (pathways within the ice) to the glacier bed. Where the bed is temper-

ate (maintained at the pressure melting point), liquid water can persist, facilitating the development of a subglacial drainage system and the flow of ice through basal motion, as introduced in Section 2.1.2. Within the subglacial drainage system, water flows in the direction of the steepest hydraulic potential gradient (Shreve, 1972), primarily controlled by the ice surface and bedrock topographies (Fountain and Walder, 1998; Shreve, 1972), but varying spatially and temporally as a result of heterogeneous subglacial drainage system structure (Andrews et al., 2014; Hubbard et al., 1995; Nienow et al., 2017). The subglacial drainage system is thought to be composed of various components, summarised and grouped by their hydraulic efficiency in Figure 2.4, which control the ability for water to drain across the bed (Fountain and Walder, 1998; Hubbard and Nienow, 1997).

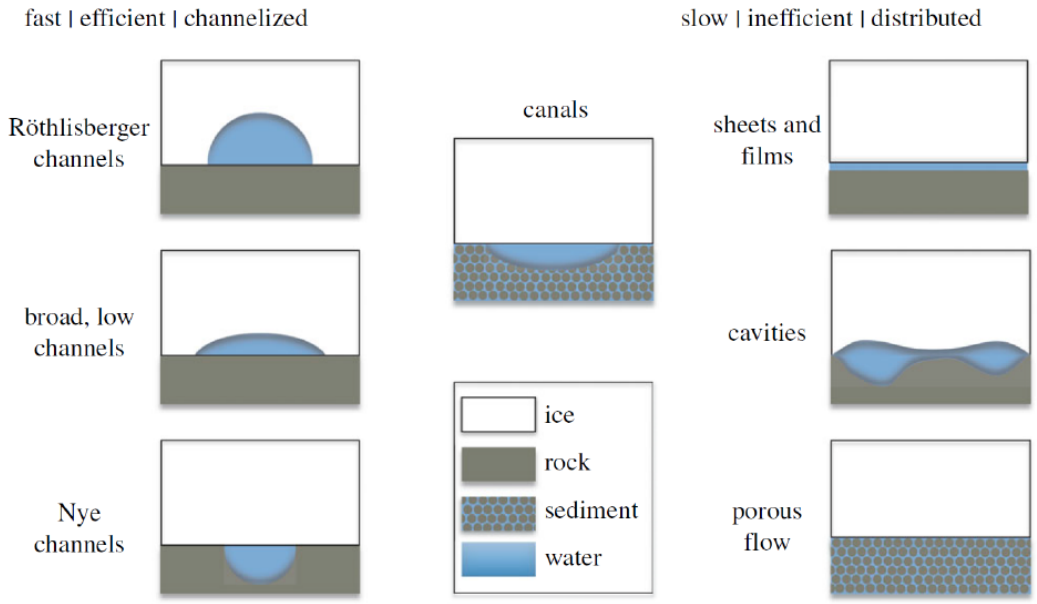

Figure 2.4: *Idealised 'elements' of the subglacial drainage system, grouped into those associated with 'fast', 'efficient' or 'channelised' drainage, versus those associated with 'slow', 'inefficient' or 'distributed' drainage. Canals may be classified as within either group. Reproduced from Flowers, 2015.*

A distributed subglacial drainage system is characterised by slow, inefficient transport of basal water and a positive scaling between subglacial discharge and subglacial water pressure (Cuffey and Paterson, 2010; Fountain and Walder, 1998; Hubbard and Nienow, 1997). A variety of water flow mechanisms within a distributed drainage system have been proposed, the simplest of which is through a

thin meltwater film across the areas of the bed characterised by regelation (Weertman, 1972). However, such a film requires a flat, debris-free, impermeable bed, whereas the glacier bed is often rough and topographically variable (Fountain and Walder, 1998). Moreover, were such a film to reach of thickness of $\sim>4$ mm, it would become unstable and collapse into a system of channels (Walder, 1982). As such, it is unlikely that a meltwater film accounts for anything more than a small proportion of the total subglacial meltwater flux (Fountain and Walder, 1998; Hubbard and Nienow, 1997). Instead, it is thought that the majority of drainage within a distributed drainage system occurs through a network of linked cavities (Fountain and Walder, 1998; Hallet, 1990; Hubbard and Nienow, 1997; Sharp et al., 1989; Walder and Hallet, 1979), although water transport within a distributed subglacial drainage system may also occur via Darcian flow through the underlying glacial till (Boulton and Hindmarsh, 1987), or through a network of shallow canals (Walder and Fowler, 1994).

As introduced in Section 2.1.2, meltwater can collect within cavities on the downstream side of bedrock bumps, where ice-overburden pressure is less than the basal water pressure (Lliboutry, 1968). These cavities may be linked via small channels, or orifices, forming a complex 'linked-cavity' network (Fountain and Walder, 1998; Hubbard and Nienow, 1997; Walder and Hallet, 1979), as illustrated by Figures 2.5 and 2.6B. Cavities can expand where increased basal water pressure is sufficiently high to overcome the greater ice overburden pressure exerted on the new, larger cavity (Iken, 1981), and so larger cavities are characterised by greater subglacial water pressures. This acts to prevent the meltwater from concentrating within few larger cavities, thus stabilising the anabranching linked-cavity network (Kamb, 1987). As meltwater can be produced through geothermal or frictional melting across large areas of a glacier bed (Benn and Evans, 2010; Petrunin et al., 2013), even where a channelised drainage system exists, a more widespread distributed system is likely to be present within the areas between or outside of the channels, acting to transfer meltwater from these regions into the channelised system (Hubbard et al., 1995; Hubbard and Nienow, 1997).

Whereas in a distributed drainage system the ice overburden pressure is balanced by the subglacial water pressure, if water is able to flow more rapidly such that frictional melting of the surrounding ice is greater than the creep closure rate, a drainage system composed of a network of efficient Röthlisberger channels (or 'R-channels') can form (Fountain and Walder, 1998; Röthlisberger, 1972), as illustrated by Figure 2.6A. These channels are incised upward into the ice, have a large cross-sectional area and are able to efficiently drain water, as evidenced by dye tracer studies that indicate flow rates from tens of cm s^{-1} to $\sim$1 m s^{-1} (Iken and Bindschadler, 1986; Seaberg et al., 1988; Stenborg, 1969).

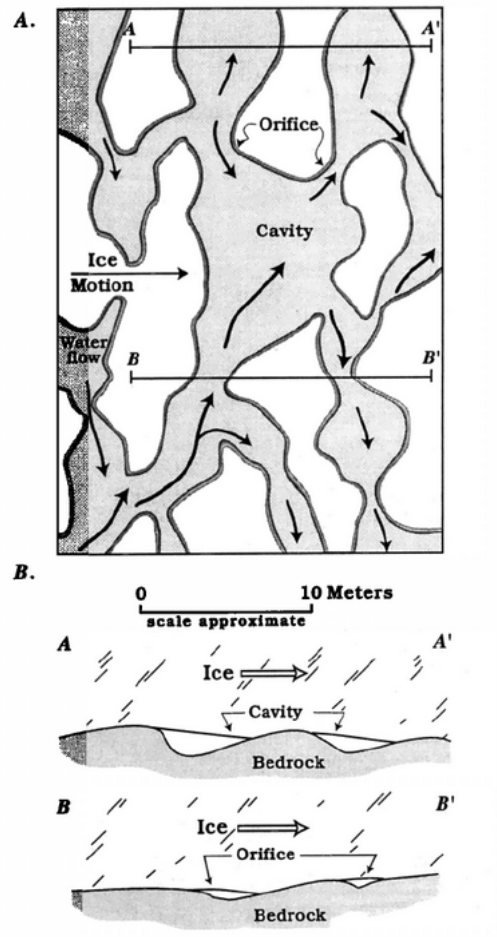

Figure 2.5: *Idealised subglacial linked-cavity network in* ***(A)*** *plan view and* ***(B)*** *cross section, after Kamb, 1987. Unshaded areas represent regions of ice-rock contact, and shaded regions represent ice-rock separation (cavities). Flow directions within cavities are indicated by arrows. Reproduced from Fountain and Walder, 1998.*

Where the subglacial water pressure is greater than ice overburden pressure,

R-channels increase in size, whereas should water pressure fall below ice overburden pressure, channel diameter contracts at a rate proportional to the third power of the difference between ice overburden pressure and water pressure (Nye, 1953). As such, the capacity of the drainage system can adjust to variability in the strength of the water supply (Cuffey and Paterson, 2010). As wall melting increases as water flux increases, the pressure gradient scales inversely with steady state water flux (Fountain and Walder, 1998; Hubbard and Nienow, 1997), in contrast to that of a distributed drainage system. As such, this allows larger, lower pressure channels to capture water from smaller, higher pressure channels, facilitating the formation of an arborescent (branching) network of channels in which a large number of higher-pressure tributaries feed into fewer, lower-pressure main channels (2.6a, Fountain and Walder, 1998; Hubbard and Nienow, 1997; Röthlisberger, 1972; Shreve, 1972). A channelised subglacial drainage system transports water more effectively than a distributed drainage system, and so is characterised by a lower steady state water pressure (Walder, 1986), and covers a relatively small proportion of the glacier bed (Hubbard and Nienow, 1997).

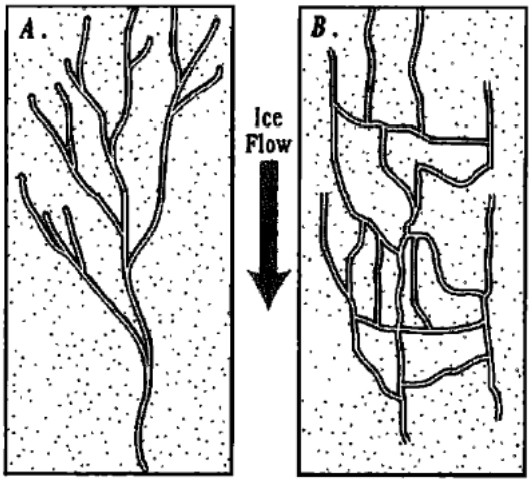

Figure 2.6: *Idealised plan view of* ***(A)*** *an arborescent, efficient subglacial drainage system composed of channels and* ***(B)*** *a non-arborescent, inefficient subglacial drainage system. Reproduced from Fountain and Walder, 1998.*

2.2.3 Subglacial Drainage System Evolution

The structure of the subglacial drainage system is a major control on spatial and temporal patterns of subglacial P_w, and thus rates of basal motion (Bingham et al., 2003; Fountain and Walder, 1998; Mair, 2002; Rippin et al., 2005). Whilst water can be produced at the bed through frictional melting and/or the influence of the geothermal heat flux (Benn and Evans, 2010; Petrunin et al., 2013), in reality, for regions outside of Antarctica and central Greenland, the flux of surface meltwater to the bed dominates the water budget of the subglacial drainage system and thus determines the subglacial drainage structure, although the latter is limited to daylight hours within the summer months (Fountain and Walder, 1998; Hubbard and Nienow, 1997; Nienow et al., 2017; Röthlisberger, 1972). As such, the subglacial drainage system evolves over diurnal and seasonal timescales in response to meltwater inputs (Andrews et al., 2014; Bartholomew et al., 2011a; Bartholomew et al., 2010; Fountain and Walder, 1998; Hubbard et al., 1995; Hubbard and Nienow, 1997), as surmised in Figure 2.7.

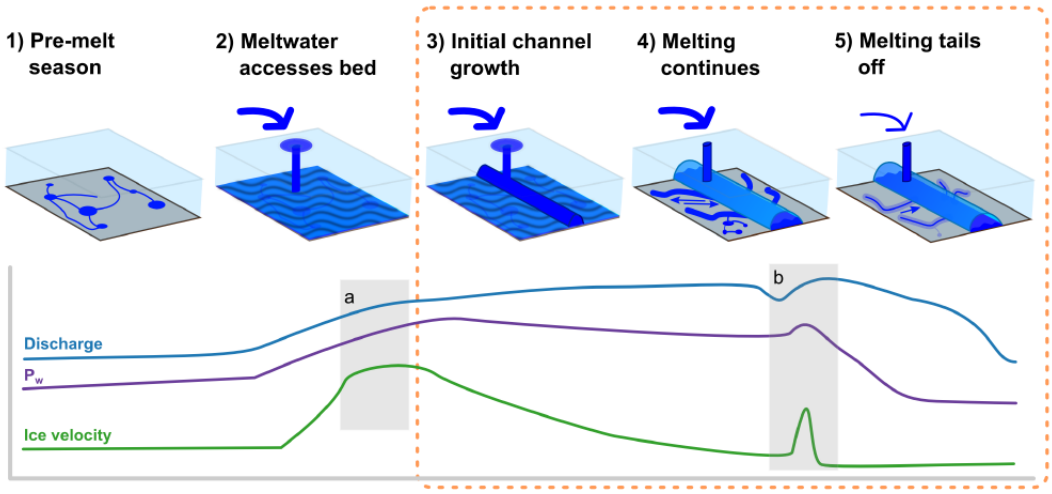

Figure 2.7: *Illustration of coupled seasonal hydrology-dynamics, after Iken and Bindschadler, 1986; Bingham et al., 2003; Bartholomew et al., 2010. Steps 3-5, outlined in orange, can occur additionally each time there is a step increase in the rate of surface meltwater supply to the ice-bed interface. Arrows in steps 4 and 5 show the direction of diurnal P_w gradients. Boxes (a) and (b) refer to 'spring events' and transient increases in the rate of meltwater supply. Reproduced from Tedstone, 2015.*

During winter (Figure 2.7 step 1), the water supply to the bed is provided by basal melt, supplemented by any stored meltwater, and is insufficient to form or

maintain a channelised subglacial drainage system (Hubbard and Nienow, 1997). In these circumstances, a distributed drainage system underlays the glacier ice, as evidenced by high borehole water pressures and dye tracing indicating slow water flow velocities (Nienow et al., 1998). Moreover, as a linked-cavity system is maintained primarily by basal sliding, it should survive the absence of a strong meltwater forcing over winter (Fountain and Walder, 1998).

Surface melting commences at the onset of the melt season, causing meltwater to reach the glacier bed. This increased meltwater input exceeds the capacity of the distributed subglacial drainage system, forcing a transient acceleration of ice motion for a period of hours to days, commonly termed a 'spring event' (Figure 2.7 step 2, box a; Hooke et al., 1989; Iken et al., 1983; Iken and Bindschadler, 1986; Mair et al., 2001; Mair et al., 2003). As the distributed drainage system is unable to remove all of the meltwater arriving at the bed, P_w increases, partly counteracting P_i and thus reducing the amount of contact between the ice and the bed (Cuffey and Paterson, 2010), a process termed 'hydraulic jacking'. This reduces the friction at the bed, and thus increases the rate of basal sliding, and is evidenced by observations of surface uplift coincident with the onset of the melt season (Iken et al., 1983), indicating ice-bed separation. During this period of the melt season, ice velocity scales positively with subglacial discharge.

With the delivery of further surface meltwater to the subglacial drainage system, subglacial P_w increases until it passes a critical threshold (P_c) at which point the linked cavity system will collapse and form an efficient channelised system (Figure 2.7 step 3, Kamb, 1987). Consequently, subglacial P_w decreases and hydraulic jacking becomes less widespread, causing a reduction in ice velocity. Over the remainder of the melt season, the channelised drainage system increases in spatial extent (Bingham et al., 2003; Nienow et al., 1998) and efficiency (Hock and Hooke, 1993), migrating upglacier at a rate determined by the retreat of the summer snowline and expansion of the ablation area (Bingham et al., 2003; Nienow et al., 1998). As the presence of a snowpack increases the local albedo,

thus reducing meltwater production, and acts to store water at the surface, thus delaying and smoothing its delivery to the glacier bed, its removal results in a much greater magnitude of meltwater delivery (Gordon et al., 1998), allowing subglacial P_w to rapidly increase and drive channelisation. Moreover, as channels convey water at low P_w (Kamb, 1987; Walder, 1986), once a channel is formed it produces a locally steep hydraulic gradient between the high P_w distributed drainage system and the low P_w channel, increasing the water flow within the distributed drainage system, hence increasing melt through frictional heat, and driving further channelisation (Nienow et al., 1998). The expansion of an efficient drainage system drives a gradual decline in ice velocity due to the inverse relationship between meltwater input and P_w once a channelised drainage system is formed (Figure 2.7 step 4), although there is some variability as a result of diurnal meltwater fluxes and the influence of additional meltwater pulses or rainfall inputs.

As the input of surface meltwater varies diurnally, with melt only occurring during the daylight hours, pressure gradients between the channelised drainage system and surrounding distributed drainage system fluctuate. During the daytime, rising meltwater inputs force water out of channels and into the surrounding bed, whereas during the night, water is forced out of the surrounding bed back into the channelised drainage system, driving a diurnal variability in water pressure and thus ice motion (Hubbard et al., 1995; Nienow et al., 2005). In addition, whilst an efficient drainage system results in a reduced subglacial P_w and ice velocities, any short-term delivery of meltwater that exceeds the capacity of the subglacial drainage system, for example large rainfall events (Gordon et al., 1998; Vieli et al., 2004) or an extreme melt or drainage event (Bingham et al., 2006; Boon et al., 2003; Stone and Clarke, 1996; Vieli et al., 2004), will drive a short-term spike in subglacial P_w, leading to a transient ice velocity acceleration (Figure 2.7, box b, Copland et al., 2003; Iken and Bindschadler, 1986).

At the end of the melt season, the inputs of surface meltwater to the bed cease

with the cessation of surface melting, and so the large R-channels can no longer maintain their size through wall melting and so gradually close via ice deformation (Figure 2.7 step 5). This results in a return to an inefficient, distributed drainage system that persists over the course of the following winter (Figure 2.7 step 1), accompanied by an increase in basal friction and thus a reduction in ice velocity. Over the course of the winter, the subglacial drainage system gradually re-pressurises through basal melting and cavity closure, and so ice velocities slowly increase. Some meltwater remains trapped in subglacial cavities, causing some degree of ice-bed separation during the winter (Iken and Truffer, 1997). Greater surface melting in the preceding summer drives more extensive and longer lasting channelisation, resulting in increased drainage of the distributed drainage system and so reducing the amount of water that is stored over the following winter (Burgess et al., 2013; Sole et al., 2013), reducing the degree of ice-bed separation. As such, winter velocities are inversely related to surface melting in the preceding summer.

Meltwater at the ice-bed interface can also be produced through basal melting as a result of basal friction and the effect of geothermal heat (Karlsson et al., 2021). However, the production rate of basal melt is essentially constant throughout the year, and as a result is not thought to be important in terms of the seasonal evolution of the subglacial hydrological system.

2.2.4 Hydrology and Dynamics of the Greenland Ice Sheet

Whilst the importance of hydro-dynamic coupling to the dynamics of alpine glaciers has long been recognised and subject to comprehensive research, prior to the early-2000s little consideration was given to the hydrology of the Greenland Ice Sheet (Nienow et al., 2017). The large ice thicknesses (compared to alpine glaciers) and cold, impermeable, ice surface were generally considered to prevent the drainage of surface meltwaters to the glacier bed (Nienow et al., 2017), although drainage of meltwaters through crevasses was observed up to ∼10 km inland of the ice margin at Jakobshavn Isbrae in west Greenland (Echelmeyer et al., 1991; Echelmeyer and Harrison, 1990). However, this drainage of meltwater

was not thought to impact basal motion on a seasonal timescale (Echelmeyer and Harrison, 1990).

One of the first indications that surface meltwaters could drain to the bed and influence Greenland's ice dynamics came from satellite radar interferometry data at Ryder Glacier, north Greenland (Joughin et al., 1996). Supraglacial lakes were inferred to have drained at the end of the 1995 melt season, pressurising the subglacial drainage system and driving an increase in the sliding velocity by approximately 3 times (Joughin et al., 1996). Subsequent research since the early-2000s has hypothesised and subsequently shown that surface meltwaters can drain through over 1 km thick ice via hydrofracture (Das et al., 2008; Doyle et al., 2013; Hoffman et al., 2011; van der Veen, 2007), and confirmed the critical role of hydro-dynamic coupling within the Greenland Ice Sheet system (Chu, 2014; Davison et al., 2019; Flowers, 2015; Nienow et al., 2017).

The following subsection reviews in more detail the research into hydro-dynamic coupling at Greenland's land-terminating margins. The impact of subglacial hydrology at marine-terminating margins is introduced in Section 2.3.5.

Hydrology and Dynamics at Land-Terminating Margins

The majority of research into hydro-dynamic coupling has been focused on Greenland's land-terminating margins, notably the Leverett Glacier catchment in south west Greenland (Davison et al., 2019, Figure 2.8). Land-terminating margins are isolated from the impact of oceanic processes, and so provide an ideal study site for investigating the response of the Greenland Ice Sheet to surface melt forcing (Fitzpatrick et al., 2013; Lindbäck et al., 2014).

Initial research at Swiss Camp, ~35 km from the ice-sheet margin in west Greenland (Figure 2.8), during the summers of 1996-1999 observed ice velocity acceleration of ~5-25 % above the midwinter average during periods of summer melt, followed by deceleration after the melting ceased (Zwally et al., 2002). This indi-

cated that basal sliding was enhanced via the rapid transfer of surface meltwaters to the ice-bed interface and the resultant increase in subglacial water pressure. Moreover, interannual variability in the magnitude of surface melting positively correlated with variability in the magnitude of ice flow acceleration, suggesting a mechanism by which the Greenland Ice Sheet could respond rapidly, and on a large-scale, to climate warming (Zwally et al., 2002). Subsequent numerical simulations using a flowline model showed that should there indeed exist a positive relationship between magnitudes of surface melting and flow acceleration, such a meltwater-driven acceleration of ice motion has the potential to increase Greenland's contribution to sea level rise by 0.15 – 0.4 m by 2500 (Parizek and Alley, 2004). In these model simulations, melt-driven acceleration near the ice margin draws down ice from the ice sheet interior to lower elevations where ablation rates are greater, reducing the mean ice sheet surface elevation and causing the ablation zone to expand (Parizek and Alley, 2004).

Satellite observations indicated widespread seasonal acceleration of ice flow across west Greenland during the summer of 2006, with strong summer acceleration across the land-terminating margin (+50 – 100 %) and more limited acceleration (<+15 %) at tidewater outlets (Joughin et al., 2008b). At Russell Glacier (Figure 2.8), peak daily velocities were reached within 1-2 hours of peak daily surface melting, with surface uplift of ∼1-4 cm indicating ephemeral cavity growth, and a positive link between surface melting and ice flow acceleration (Shepherd et al., 2009). Subsequent work covering 10 glacier catchments in west Greenland observed that late-summer acceleration was positively correlated with modelled runoff, extended up to ∼100 km inland, and that the spatial variation in the magnitude of acceleration was linked to the locations of supraglacial sinks, such as lakes and moulins (Palmer et al., 2011).

However, a 17-year record across 8 GPS sites (making up the 'K-transect', Figure 2.8) indicates that whilst ice velocity indeed increased with increases in surface melt over periods of days, the multi-annual record shows that between 1991 and 2007, annual ice velocity decreased slightly (van de Wal et al., 2008) and shows no

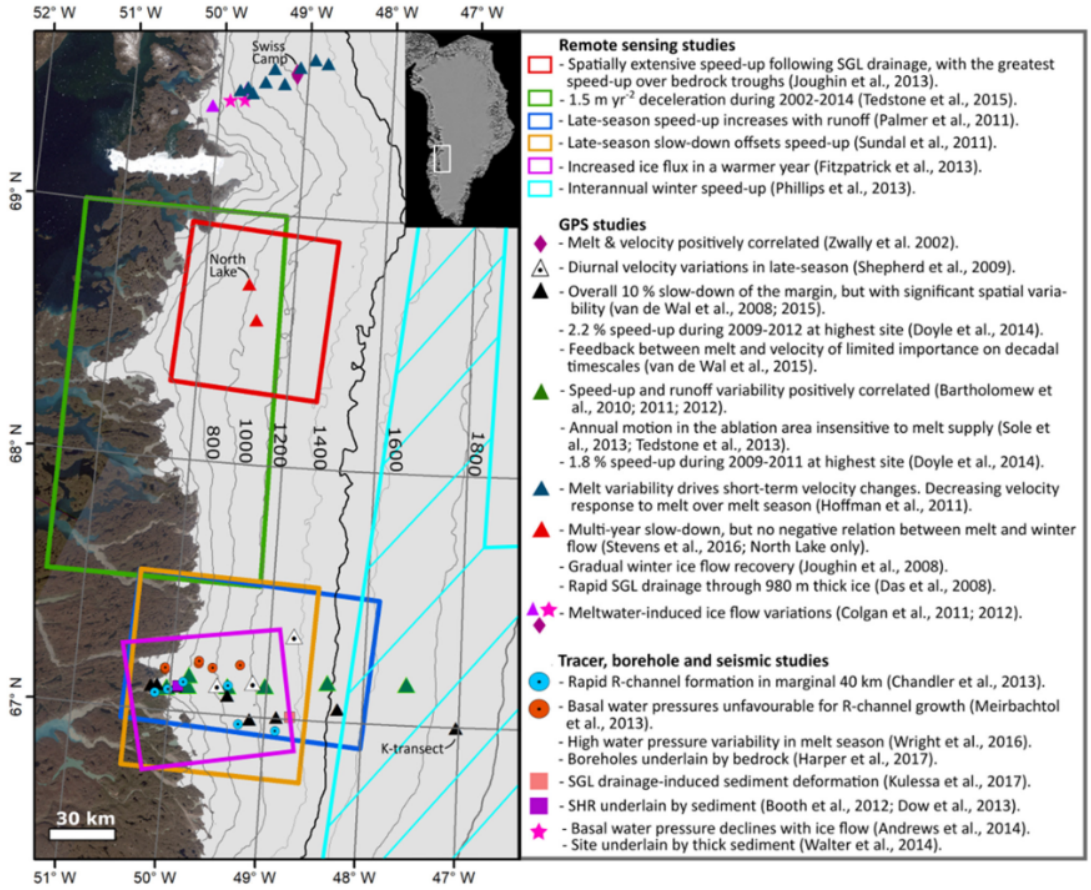

Figure 2.8: *Overview of key observations at the south west Greenland land-terminating sector. Coloured boxes delimit the approximate study area of remote sensing studies, with the study area of Phillips et al., 2013 extending off figure. Also shown are: Swiss Camp (lilac diamond, Zwally et al., 2002); FOXX and GULL GPS and borehole sites (pink stars, Andrews et al., 2014); K-transect sites (black triangles); Leverett GPS sites (dark green triangles); Russell GPS sites (white dotted triangles, Shepherd et al., 2009); Lake F (pale pink square); moulins used for gas tracer injection (blue dotted circles, Chandler et al., 2013); boreholes presented in Wright et al., 2016 (orange dotted circles). Contours are from the GIMP DEM (Howat et al., 2014) and are displayed at 200 m intervals. The bold contour (1500 m) represents the approximate elevation of the equilibrium line during 1991-2011 (Van De Wal et al., 2012). "SGL" stands for supraglacial lake. These data are overlaid on a true colour composite Landsat 7 image mosaic. Inset is a MEaSUREs MODIS mosaic (Haran et al., 2015), with white rectangle showing the approximate location of the south west land-terminating sector within the Greenland Ice Sheet. Reproduced from Davison et al., 2019.*

correlation with annual ablation rate. These results suggest that the previously proposed positive surface melt/ice velocity feedback is a seasonal process, with a limited impact over multi-annual timescales (van de Wal et al., 2008), suggesting that the subglacial drainage system may adjust over the melt season to accommodate the increased meltwater input. Analysis of 35-day mean velocities calculated

from satellite SAR data across the southwest Greenland land-terminating sector indicate that whilst peak rates of ice flow acceleration are positively correlated with increasing surface melt, deceleration occurs once a critical surface runoff threshold is passed (Sundal et al., 2011). This inverse surface melt/ice velocity relationship mirrors that of alpine glaciers whereby velocities increase in the early melt season, driving the formation of an efficient subglacial drainage system that transmits water at lower pressure, thus increasing basal friction and reducing sliding velocity through the late melt season (Sundal et al., 2011; Truffer et al., 2005).

In contrast, other studies have argued that the timing and rate of meltwater input, rather than the volume itself, are more critical for driving ice acceleration (Bartholomaus et al., 2008; Bartholomew et al., 2011a; Bartholomew et al., 2010, 2012; Schoof, 2010). GPS observations of ice velocity at 24-hour temporal resolution show that the early melt season ice acceleration is a function of numerous short-lived (1 day to 1 week) speed-up events (Bartholomew et al., 2011a; Bartholomew et al., 2010, 2012), analogous to 'spring events' observed on alpine glaciers during which meltwater first accesses the inefficient, distributed subglacial drainage system (Hooke et al., 1989; Iken et al., 1983; Iken and Bindschadler, 1986; Mair et al., 2001; Mair et al., 2003). These meltwater inputs drive an initial transient acceleration, and force a morphological transition to an efficient, channelised system when and where the input of meltwater is of sufficient magnitude (Chandler et al., 2013; Kamb, 1987; Schoof, 2010), and this channelised system migrates inland over the course of the melt season in response to the later melt onset at higher elevations (Bartholomew et al., 2011a; Bartholomew et al., 2010, 2011b, 2012; Chandler et al., 2013). Once an efficient subglacial drainage system is formed, ice flow decelerates through the remainder of the melt season, and any further short-term acceleration can only be driven by a larger meltwater pulse (Bartholomew et al., 2012; Cowton et al., 2013), for example via the drainage of a supraglacial lake (Das et al., 2008; Hoffman et al., 2011), intense rainstorms (Doyle et al., 2015) or simply by further increases in surface melt supply in the early melt season (Cowton et al., 2013).

Following the cessation of melt at the end of the melt season, ice flow decelerates to an annual minimum (Joughin et al., 2008b; Sole et al., 2013; Zwally et al., 2002), prior to a gradual re-pressurisation of the subglacial drainage system over winter through basal sliding and geothermal heat (Fitzpatrick et al., 2013). As observed in Alaska (Burgess et al., 2013), greater melt in the preceding summer is observed to precondition the following winter for reduced ice flow as a result of the drainage of high P_w regions of the distributed drainage system by larger and more extensive subglacial channels (Andrews et al., 2014; Sole et al., 2013). An observed slowdown in ice velocity for a land-terminating margin in West Greenland in 2012 was attributed to this slower winter flow following enhanced melt inputs in the preceding summer (Tedstone et al., 2013). Whilst this process may be enhanced, or dampened, depending on the volume of water stored subglacially over the winter (Chu et al., 2016), the net effect is to counter-act the summer speed-up in ice velocity, such that annual ice motion is relatively insensitive to variations in surface melt forcing (Sole et al., 2013; Tedstone et al., 2013).

More recently, research has focused on whether increasing surface melt rates would increase ice flow velocities on a multi-annual timescale. Whilst early work posited a multi-annual positive feedback between increasing surface melt rates and acceleration of ice motion (Parizek and Alley, 2004; Zwally et al., 2002), it has since been shown that a multi-annual increase in surface melt production has driven a long-term ice velocity slowdown within southwest Greenland (Figure 2.9, Hoffman et al., 2016; Stevens et al., 2016; Tedstone et al., 2015; van de Wal et al., 2008, 2015).

GPS velocities along the K-transect show an average slowdown of 10 % between 1991 and 2007 (van de Wal et al., 2008, 2015), and at North Lake, GPS velocities show a slowdown of -0.9 $\pm$ 1.1 m yr^{-2} between 2006 and 2014 (Stevens et al., 2016). Over a much larger, 8000 km^2 region of southwest Greenland extending inland to a surface elevation of 1100 m (a.s.l.), Tedstone et al., 2015 observed a 12 % slowdown in mean annual ice velocity between 1985-1994 and 2007-2014,

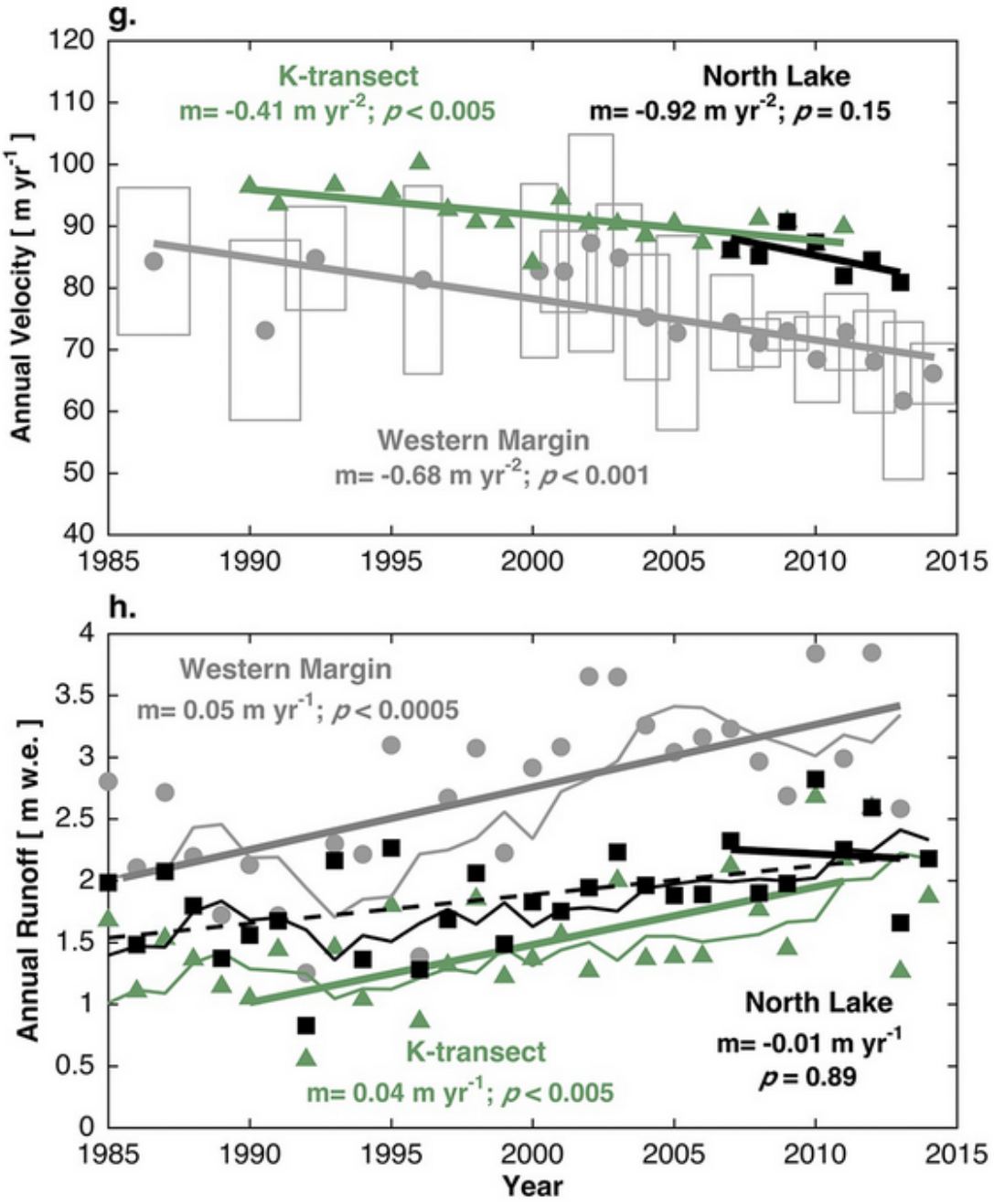

Figure 2.9: *Trends through* ***(A)*** *annual ice velocity measurements and* ***(B)*** *annual runoff estimates at North Lake (black, Stevens et al., 2016), K-transect (green, van de Wal et al., 2015), and the western margin (grey, Tedstone et al., 2015) for the period 1985-2014. The widths of the grey boxes surrounding the western margin ice velocity estimates in subplot A refer to the total timespan of the pairs of Landsat images acquired during each period, and the height of the boxes represents* $\pm 1\sigma$ *(Tedstone et al., 2015). Reproduced from Stevens et al., 2016.*

coincident with a 50 % increase in surface melt rates. This slowdown began in approximately 2002 and continued at an average rate of -1.5 m yr^{-2} between

2002 and 2014 (Tedstone et al., 2015). Only 17-33 % of this slowdown could be attributed to a change in deformation rate due to changes in ice thickness and surface slope (Tedstone et al., 2015), implying that the majority of the velocity signal was controlled by processes acting at the bed. As such, the observed multi-annual deceleration has been attributed to the seasonal formation of larger and more spatially and temporally extensive efficient subglacial channels under enhanced surface melting, which would in turn enhance the drainage of high-pressure waters from the more extensive distributed component of the subglacial drainage system (Andrews et al., 2014; Hoffman et al., 2016; Tedstone et al., 2015), thus reducing regional basal P_w and hence ice velocity. These hydraulically isolated regions of the bed are thought to take several years to recharge (Hoffman et al., 2016), driving a widespread and extended period of depressurisation and increased basal traction following their drainage.

The inland extent to which an efficient subglacial drainage system can form, and the behaviour of inland regions of the land-terminating ice sheet in response to surface meltwater production, are poorly understood (Davison et al., 2019; Nienow et al., 2017). Observations from boreholes, dye tracing and ice velocity data indicate efficient channels extending between 40-80 km inland (Bartholomew et al., 2011a; Bartholomew et al., 2010, 2011b, 2012; Chandler et al., 2013; Das et al., 2008; Doyle et al., 2013; Fitzpatrick et al., 2013), and efficient channels have been modelled to extend up to 50 km inland, under 900 m thick ice (de Fleurian et al., 2016; Koziol and Arnold, 2018). Further inland, R-channel formation is inhibited by thicker ice (and hence greater ice overburden pressures) and shallower surface slopes, leading to creep closure speeds of hours to days where channels are not completely pressurised to overburden (Dow et al., 2014; Doyle et al., 2014). Moreover, surface strain rates suggest an upper limit of ∼1600 m (a.s.l.) for crevasse and moulin formation (Poinar et al., 2015), at least within the relatively slow-flowing region inland of the southwest land-terminating sector. Consequently, there is likely very little delivery of surface meltwaters to the bed within these interior regions, possibly limited to high elevation supraglacial lake

drainage (Dow et al., 2014), such that any period of basal pressurisation would be extremely limited in duration. As such, it has been suggested that processes observed at alpine glaciers and the land-terminating margin may not hold for interior regions (Dow et al., 2014; Doyle et al., 2014).

GPS velocity measurements at a site 140 km from the margin, 50 km within the accumulation area, at an elevation of 1840 m (a.s.l.) show both a seasonal velocity cycle of up to 8.1 % above the wintertime average, and a 2.2 % increase in annual velocity between the cooler 2009 (51.78 ± 0.01 m yr^{-1}) and the warmer 2012 (51.92 ± 0.01 m yr^{-1}) (Figure 2.10, Doyle et al., 2014), in contrast to the deceleration observed at lower elevations across the same time period (Tedstone et al., 2013). These observations suggest that in this inland region, there is sufficient transfer of surface meltwater to the bed to induce a seasonal acceleration, but an insufficient quantity to develop efficient subglacial channels, with the result that surface melt and ice velocity scale positively (Doyle et al., 2014). These observations, however, are extremely limited in both spatial and temporal extent, and it therefore remains unclear how significant they are to wider ice sheet dynamics.

2.3 Tidewater Glacier Dynamics and Controls

The Greenland Ice Sheet is drained by fast-flowing (> 100 m yr^{-1}) tidewater (marine-terminating) glaciers (Figure 2.11, Catania et al., 2020), largely concentrated along the north-western and south-eastern coasts. Whilst changes in ice sheet dynamics were originally thought to occur over millennial timescales, making only a small net contribution to global sea level rise (Houghton et al., 2001), subsequent research has shown that Greenland's tidewater glaciers can undergo rapid and high-magnitude responses to climatic perturbations (Howat et al., 2005; Howat et al., 2007, 2008b; Joughin et al., 2014; Joughin et al., 2004, 2008a; King, 2018; King et al., 2020; Moon and Joughin, 2008; Moon et al., 2015; Moon et al., 2020; Mouginot et al., 2015; Rignot and Kanagaratnam, 2006a; Thomas et al.,

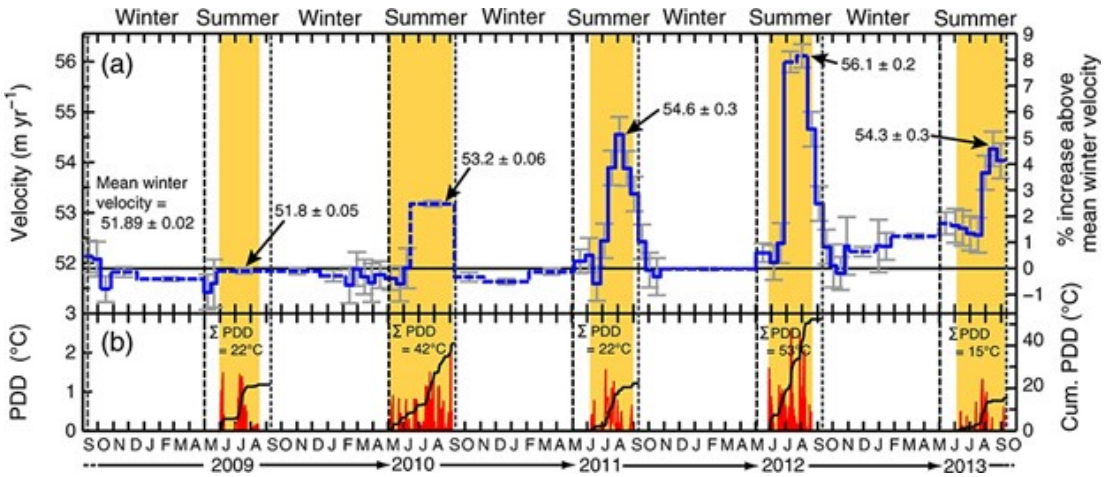

Figure 2.10: ***(a)*** *Velocity (blue line) at GPS site S10 (1840 m a.s.l., 67.00°N 47.02°W) between September 2008 and October 2013. Where the blue line is dashed, it indicates averaging periods of over 15 days, which may reduce the apparent amplitude of velocity variations (i.e., summer 2009 and summer 2010). The horizontal grey line represents the mean winter velocity (51.89 m yr^{-1}) averaged across all five winters.* ***(b)*** *Positive degree days (PDD) at S10 in red, with cumulative PDD in black. The orange shading highlights the melt seasons, and the vertical dashed black lines delineate the summer (1st May to 10th September), winter (10th September to 1st May), and annual (1st May to 1st May) averaging periods used in this study. Reproduced from Doyle et al., 2014.*

2003). Tidewater glacier behaviour is extremely complex, and their dynamics are controlled by a variety of processes, operating across multiple spatial and temporal scales, through their interaction with the atmosphere, ocean, and local morphology (Catania et al., 2020).

2.3.1 The Tidewater Glacier Cycle

Whilst tidewater glacier dynamics have been observed to show considerable seasonal fluctuations (Meier and Post, 1987), their long-term behaviour during periods of quasi-stable climate forcing is characterised by phases of slow (∼10 to 50 m yr^{-1}), centennial advance and rapid (100 to >1000 m yr^{-1}), decadal retreat, which have been conceptually modelled as the 'tidewater glacier cycle' (Figure 2.12, Amundson, 2016; McNabb and Hock, 2014; Meier and Post, 1987; Post, 1975; Post et al., 2011).

From a stable, advanced configuration (Figure 2.12a), an initial climatic perturbation can drive a dynamic transition to the rapid retreat phase (Figure 2.12b) as

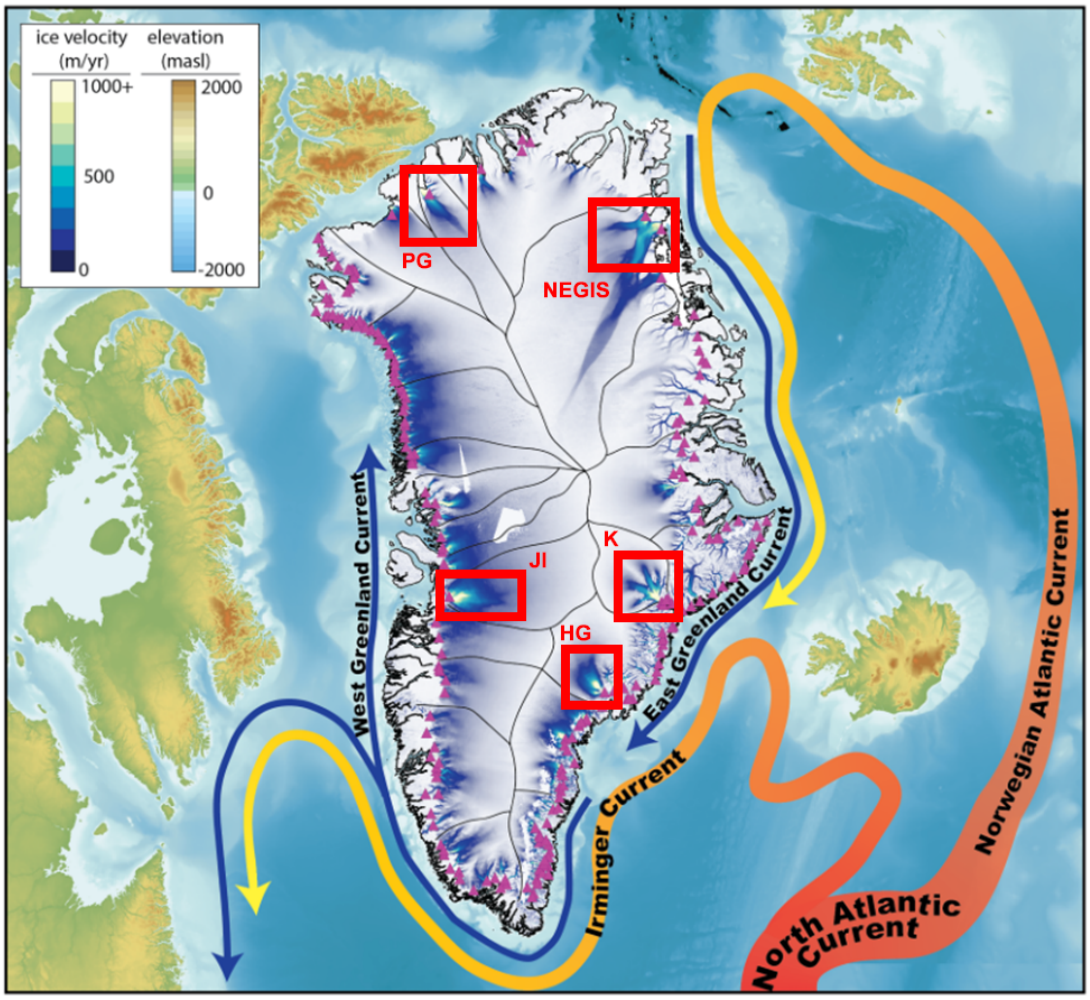

Figure 2.11: *The locations of tidewater glaciers with flow rates above 50 m yr^{-1} (purple triangles) draining from the Greenland Ice Sheet, and surrounding ocean currents. The size of ocean current arrows indicates water mass, and the colour indicates heat transport. Surface ice flow speeds are from Joughin et al., 2010. Locations of major tidewater glaciers shown within red boxes; Jakobshavn Isbrae (JI), Petermann Glacier (PG), the Northeast Greenland Ice Stream (NEGIS), terminating in 79 North Glacier and Zacharie Isstrøm, Kangerdlugssuaq (K), and Helheim Glacier (HG). Modified from Catania et al., 2020.*

the terminus recedes from a stabilising bedrock high in deeper waters behind it, or through a narrow lateral constriction into a widening fjord (Post, 1975; Post et al., 2011). This results in a loss of basal and/or lateral resistance, resulting in increases in velocity, dynamic thinning, and calving rates (Amundson, 2016; Meier and Post, 1987; Pfeffer, 2007; Post et al., 2011).

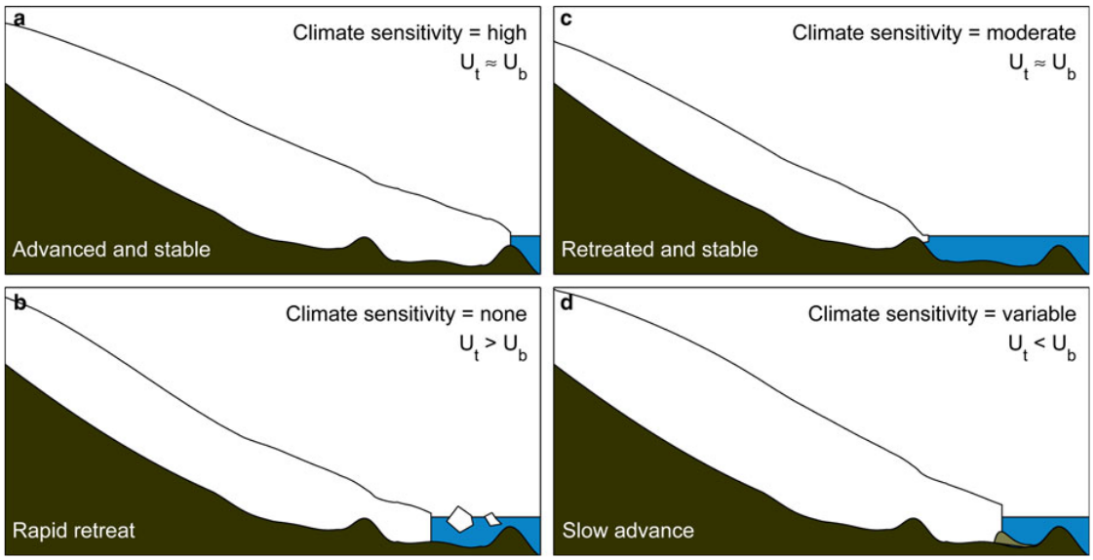

Figure 2.12: *Schematic of the tidewater glacier cycle.* ***(a)*** *Advanced, stable configuration with high sensitivity to climate.* ***(b)*** *Rapid terminus retreat initiated by a climatic perturbation and driven by glacier dynamics. Once initiated, sensitivity to climate may be limited.* ***(c)*** *Retreated, stable configuration with moderate climate sensitivity.* ***(d)*** *Slow advance enabled by increased resistance from a terminal moraine. A calving retreat can be triggered prior to the terminus advancing to the end of the fjord through a rise in ELA or climatic perturbation. U_t is the terminus velocity and U_b is the balance velocity (net surface and basal mass balance divided by the cross-sectional area of the terminus). Reproduced from Amundson, 2016.*

Retreat down a reverse bed-slope thus drives a positive feedback whereby retreat rate increases as the front retreats into deeper waters (Meier and Post, 1987; Post, 1975), and once retreat is initiated, it is argued to proceed independently of the size of any climatic perturbation (Amundson, 2016; Post et al., 2011). However, observations across 36 Alaskan tidewater glaciers indicates that the retreat phase may occur in steps, with 1 to 2-year bursts of retreat interspersed with periods of stability (McNabb and Hock, 2014), possibly driven by variations in bedrock geometry and/or sea surface temperatures. Glacier stability can only be regained through a retreat into shallower waters and/or into a narrower fjord width, or a retreat out of the water entirely (Figure 2.12c, Amundson, 2016; Post et al., 2011). This reduces buoyancy forces at the terminus and so reduces the rate of calving, in turn reducing ice velocity and so the drawdown of ice.

Re-advance (Figure 2.12d) can be initiated by climate cooling (Amundson, 2016)

and/or through changes in glacier geometry. For example, an accumulation area ratio (AAR), the ratio of the accumulation area to the total glacier area (Post et al., 2011), greater than ∼0.8 generally favours advance (Post et al., 2011), and so re-advance is also facilitated by a lowering of the ELA (Amundson, 2016). Advance into deeper waters, however, is inhibited due to negative feedbacks of increased velocity, calving, and so loss of near-terminus flow resistance (Amundson, 2016; Meier and Post, 1987; Post et al., 2011). Consequently, tidewater glacier re-advance is thought to require the development of a terminal moraine, which acts to reduce buoyancy forces at the terminus, keep the glacier grounded, insulate the ice front from warm, erosive seawater and thus reduce submarine melt rates and calving (Amundson, 2016; Fischer and Powell, 1998; Meier and Post, 1987; Nick et al., 2007; Post and Motyka, 1995; Post et al., 2011). This moraine is slowly moved forward via proximal erosion and distal deposition (Meier and Post, 1987), and thus the rate of advance is thought to be determined by the rate of sediment erosion and the availability of erosive material. As such, the advance phase proceeds very slowly, and can persist for centuries to millennia (McNabb and Hock, 2014; Meier and Post, 1987; Post et al., 2011).

Eventually, an extended glacier geometry is achieved, rendering the glacier increasingly susceptible to climatic forcing as the AAR decreases (Figure 2.12a, Post et al., 2011), and so the cycle begins anew. It should be noted that a sufficient climatic perturbation may trigger retreat prior to a complete re-advance (Amundson, 2016).

2.3.2 Ice sheet-wide Trends in Tidewater Glacier Behaviour

Aerial imagery since the early-20th Century has shown that tidewater glaciers in Greenland retreated throughout the late-1920s/early-1930s (Bjørk et al., 2012; Kjeldsen et al., 2015) in line with increases in air temperatures during this period (Box et al., 2009), with subsequent re-advance as air temperatures cooled in the following decades. Advances in satellite remote sensing revealed that widespread thinning, retreat and acceleration of Greenland's tidewater glaciers began in the

late-1990s/early-2000s (Holland et al., 2008; Howat et al., 2005; Howat et al., 2007, 2008b; Joughin et al., 2004, 2008a; King et al., 2020; Luckman et al., 2006; Mankoff et al., 2020; Moon and Joughin, 2008; Rignot and Kanagaratnam, 2006a; Thomas et al., 2003), leading to an increase in solid ice discharge such that dynamic change now accounts for 48-66 % of mass loss from the ice sheet (Mouginot et al., 2019; Shepherd et al., 2019). A study surveying 199 tidewater glaciers observed that 188 of 199 retreated between 2000 and 2010 (Murray et al., 2015), and a more recent study of 276 tidewater glaciers observed retreat during the period 2000-2015 across 99 % and 96 % of studied glaciers along the northwest and southeast coasts respectively (Figure 2.13, Bunce et al., 2018).

Along the east coast, tidewater glaciers underwent a two- to threefold increase in terminus retreat rate during the period 2000-2005 compared to 1980-2000 (Jiskoot et al., 2012), with mass loss increasing from 48 km^3 yr^{-1} in 2000 to 67 km^3 yr^{-1} in 2005 (Rignot and Kanagaratnam, 2006a), although retreat slowed with a return to cooler air temperatures during 2006/07 (Moon and Joughin, 2008). Outlet glaciers in west Greenland began retreating during the mid to late-1990s through to the early-2000s (Catania et al., 2018; Howat et al., 2010; Mcfadden et al., 2011). Out of 59 glaciers studied, Mcfadden et al., 2011 observed retreats of > 1 km at 20 glaciers between 2000 and 2009, with the largest being the 12.8 km retreat of Jakobshavn Isbrae. In contrast to the east coast, tidewater glacier retreat in the west, particularly the northwest, has remained sustained through the 2000s and 2010s (Bunce et al., 2018; King et al., 2020), although Jakobshavn Isbrae began to decelerate and re-advance in 2016 (Khazendar et al., 2019). Retreat has been more limited in north Greenland with rates of 10s-100s m yr^{-1} (Hill et al., 2017), though it remains pervasive, with 17 of 21 glaciers studied by Hill et al., 2017 observed to have retreated between 2000 and 2015. The largest change has been observed at Petermann Glacier, which saw a 27 km retreat and 270 km^2 loss of its floating ice tongue beginning in 2010 (Falkner et al., 2011; Hill et al., 2018; Nick, 2012).

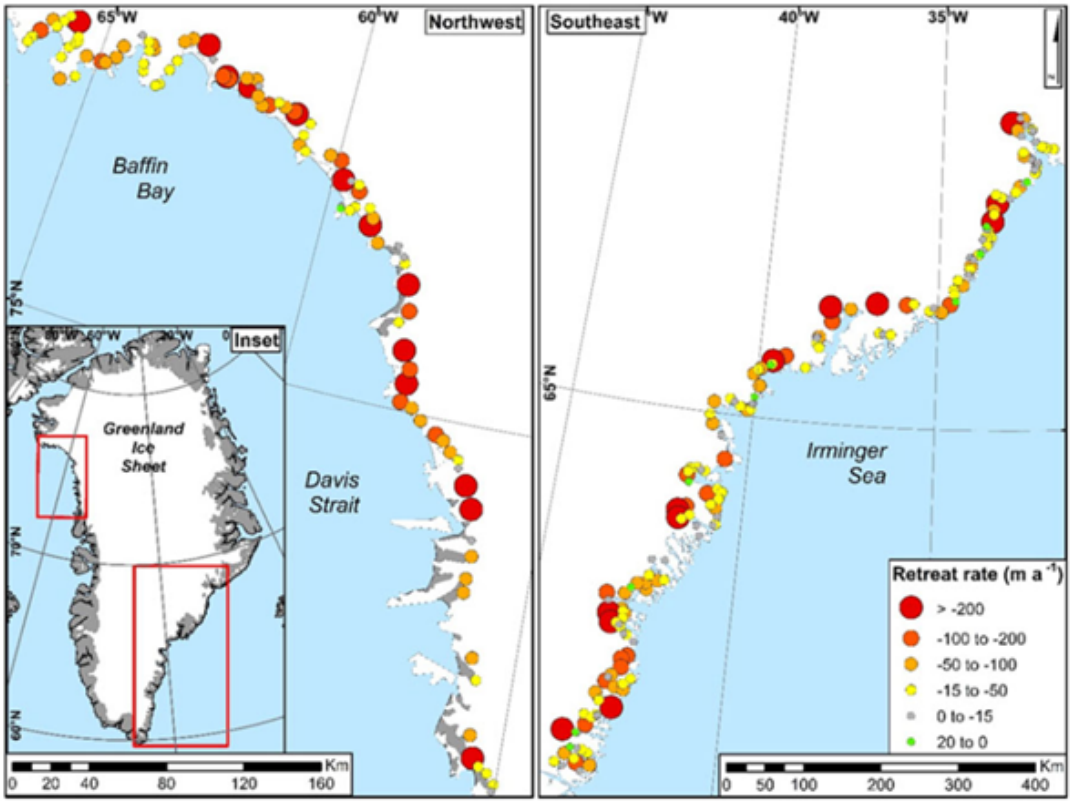

Figure 2.13: *Mean annual retreat rates of outlet glaciers in northwest and southeast Greenland. The size and colour of circles represent the mean annual retreat rate for each glacier for the period 2000-2015. Reproduced from Bunce et al., 2018.*

2.3.3 Heterogeneity in Tidewater Glacier Behaviour

Whilst the synchronous onset of retreat, thinning and acceleration of tidewater glaciers is indicative of some common climatic forcing (Howat et al., 2008b; Luckman et al., 2006; Moon and Joughin, 2008; Seale et al., 2011), significant variability in mass loss is observed at spatial scales ranging from across a region of the ice sheet to an individual fjord system (Figure 2.11, Bunce et al., 2018; Catania et al., 2018; Motyka et al., 2017; Seale et al., 2011). In east Greenland, significant retreat was observed during the period 2001-2005 south of 69°N, whereas north of this latitude tidewater glaciers were characterised by minimal or no change during the same period (Figure 2.14, Seale et al., 2011). This regional difference was attributed to the transport of warm subtropical waters via the Irminger Current, and thus into the south-eastern fjords (Seale et al., 2011), with the presence of warm Atlantic waters within these fjords confirmed by sub-

sequent hydrographic measurements (Christoffersen et al., 2012; Straneo et al., 2010, 2012).

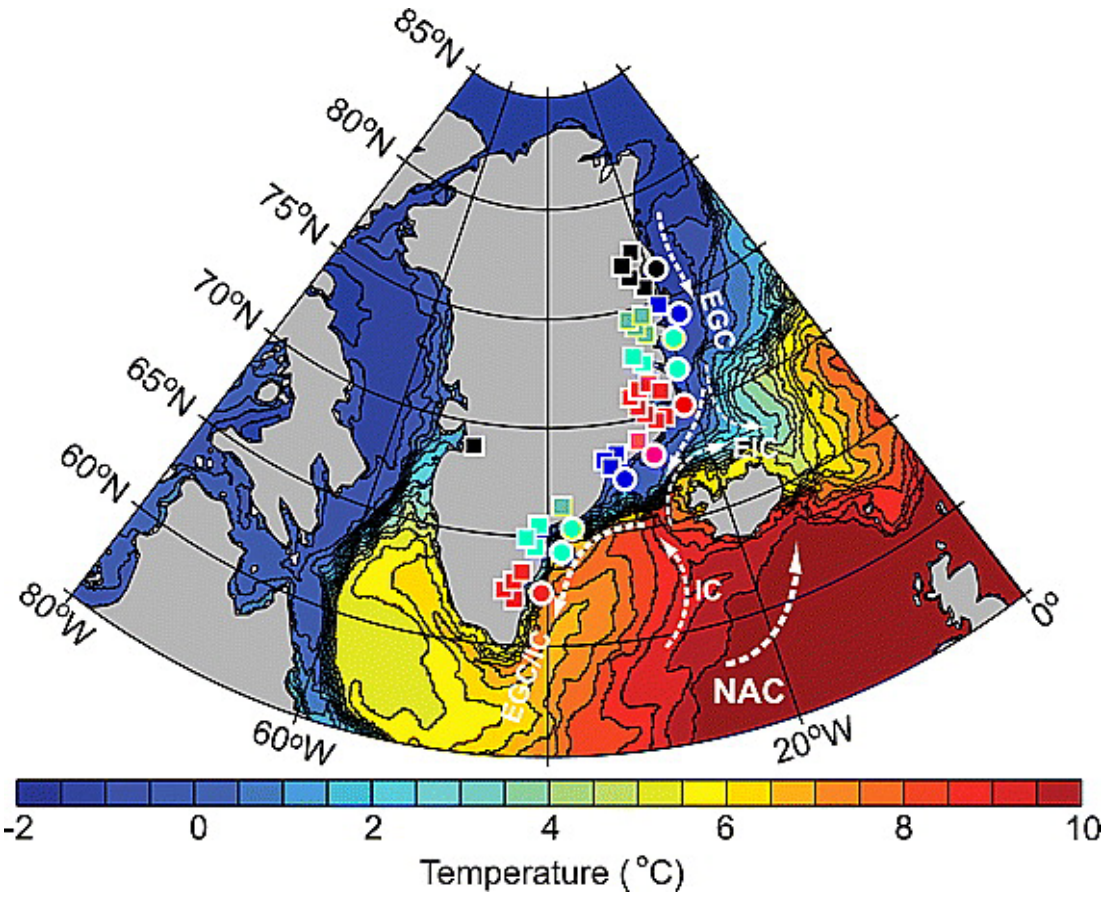

Figure 2.14: *Map of Greenland and adjacent seas showing mean annual sea surface temperatures (°C) in 2004 from ocean model reanalysis. Coloured squares show locations of surveyed glaciers and coloured dots show locations where subsurface temperatures were examined in ocean reanalysis. White dashed arrows illustrate the main ocean currents, which are the North Atlantic Current (NAC), Irminger Current (IC), East Greenland Current (EGC), and Icelandic Current (IC). Reproduced from Seale et al., 2011.*

In addition, each tidewater glacier is set within a unique fjord system, with particular ice, fjord, and bedrock geometries (Carr et al., 2013; Catania et al., 2018). Across 13 tidewater glaciers in west Greenland, multi-annual retreat began quasi-synchronously, with retreat onset at 9 of the 13 glaciers studied beginning in 1998 (Catania et al., 2018). However, considerable variability was observed in the magnitude, duration, and rate of retreat, with no clear subregional pattern (Catania et al., 2018). Asynchronous behaviour has also been observed within individual fjord systems. Kangiata Nunaata Sermia and Narsap Sermia terminate

within the Godthåbsfjord system, located in southwest Greenland, and the former has retreated 22 km from its Little Ice Age (LIA) maximum (1761 AD), with 0.8 km of this retreat occurring since 1985, after which it has stabilised in shallow water (Motyka et al., 2017). In contrast, Narsap Sermia only began retreating from its LIA moraine between 2004 and 2006, after which it re-stabilised, before undergoing a rapid 3.3 km retreat during the period 2010-2014 (Motyka et al., 2017). As such, it can be difficult to pinpoint the exact mechanisms that control and regulate tidewater glacier dynamics.

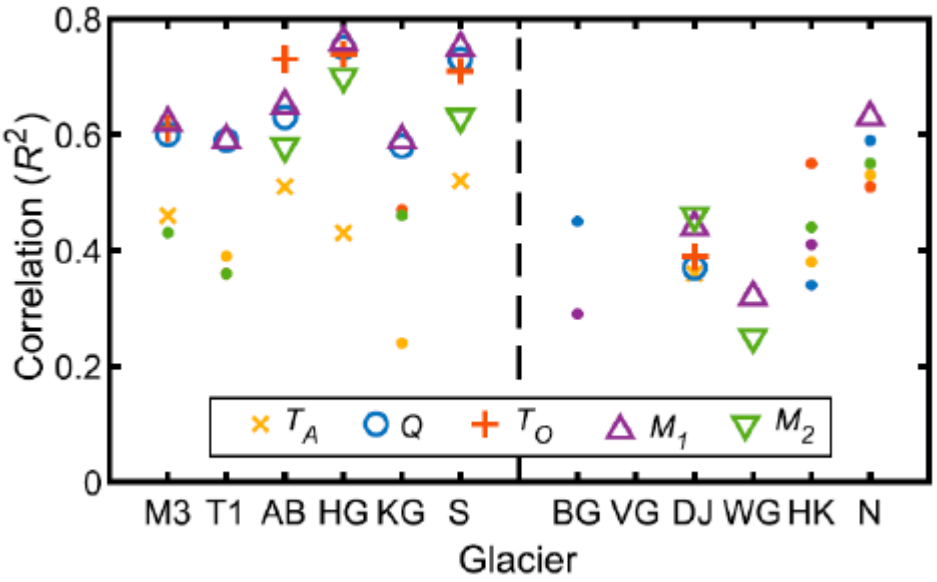

Figure 2.15: *R^2 values for the relationship of terminus position (P) with air temperature (T_A), runoff (Q), ocean temperature (T_O), and the combined effects of oceanic and atmospheric forcing (M1 and M2) at each glacier and for the averaged regional southern (S) and northern (N) trends, split north and south of 69°N. The dashed line separates the southern (left) and northern (right) glacier subsets. Reproduced from Cowton et al., 2018.*

However, despite these complexities, recent work shows that regional tidewater glacier retreat in east Greenland can be explained by the simple variables of air temperature, meltwater runoff and ocean temperature (Cowton et al., 2018). Across 10 glaciers in east Greenland, 54 % of the regional terminus position change during the period 1993-2012 can be attributed to the combined influence of meltwater runoff (and thus air temperature) and ocean temperature, rising to up to 76 % at individual glaciers (Figure 2.15, Cowton et al., 2018). As such, it

may be possible for the future response of tidewater glaciers to climate warming to be predicted by simple forcing parameters.

2.3.4 Oceanic Controls on Tidewater Glaciers

Iceberg Calving

Where glaciers terminate in water, calving, or the mechanical loss of ice from the glacier front (Benn et al., 2007b), is a fundamentally important component of the mass budget, contributing substantially to ice losses from the Greenland Ice Sheet. It is proposed to be a two-step process involving the fracture of ice, followed by the transport of detached icebergs away from the ice front (Bassis and Jacobs, 2013), although the precise mechanisms of calving vary in space and time (Benn et al., 2007a; Catania et al., 2020). Four basic mechanisms of calving have been postulated as follows:

1. **The stretching of ice in response to large-scale velocity gradients**
   Tensile stresses associated with along and across-flow gradients in ice velocity are usually sufficiently large enough to drive the formation of crevasses (Benn et al., 2007b), for example through longitudinal stretching, as the velocity of ice commonly increases towards glacier termini. Such crevasses can propagate downwards, particularly when filled with water (through hydrofracture, Section 2.2.1), and calving is suggested to occur where the crevasse depth equals the ice height above sea level (Benn et al., 2007a).

2. **Force imbalance at ice fronts**
   Large stress gradients typically occur at floating glacier termini as a result of an imbalance between forces acting outward from and inward to the frontal ice cliff (Benn and Evans, 2010; Benn et al., 2007b; Reeh, 1968). Above sea level, the outward-directed cryostatic pressure is essentially unopposed, whilst below the waterline it is always greater than the opposing pressure exerted by the water column (hydrostatic pressure), except at the

base (Benn and Evans, 2010; Benn et al., 2007b). This force imbalance creates a zone of high stress at the surface, facilitating crevasse formation and thus calving (Benn et al., 2007b; Reeh, 1968).

3. **Undercutting of the terminus by subaqueous melting**

   Where melt rates at or below the waterline are greater than subaerial melt rates, the calving front will be progressively undercut, increasing the force imbalance and promoting calving through a torquing of the overhanging ice (Bartholomaus et al., 2012; Benn and Evans, 2010; Benn et al., 2007b; Fried et al., 2015; Luckman et al., 2015; O'Leary and Christoffersen, 2013). In Greenland, this is an important calving mechanism for thinner, well-grounded outlet glaciers (Catania et al., 2020; Fried et al., 2015), especially those characterised by the presence of subglacial meltwater plumes (Chauché et al., 2014; Fried et al., 2018). In the case of the latter, this mechanism produces local terminus embayments associated with the discharge of subglacial water at the grounding line. Where subaqueous undercutting is the dominant calving mechanism, the long-term calving rate is equal to the rate of terminus undercutting by subaqueous melting, and so depends on water properties such as temperature, density, and circulation (Benn et al., 2007b; Luckman et al., 2015).

4. **Buoyant forces at a glacier terminus**

   Buoyant flexure can trigger crevasse propagation and calving via two main methods. Where subaerial calving losses exceed subaqueous calving losses, a projecting subaqueous 'ice foot' can develop (Benn and Evans, 2010; Benn et al., 2007b; Mercenier et al., 2020) which is unstable and can fail catastrophically. Alternatively, where the terminus region of a tidewater glacier thins towards the ice thickness at which it will float, buoyancy forces increase, with calving occurring once buoyancy forces are sufficiently high (Benn and Evans, 2010; Benn et al., 2007b; James et al., 2014; Van Der Veen, 1998). In this case, buoyant flexure at the grounding line likely drives

the formation of basal crevasses (James et al., 2014; Van Der Veen, 1998), which can propagate upwards to connect to existing surface crevasses and drive large volume, full-thickness, laterally-extensive tabular calving events (Amundson et al., 2010; Bassis and Jacobs, 2013; Fried et al., 2018; James et al., 2014; Warren et al., 2001). This calving mechanism tends to occur where a tidewater glacier occupies a deeply incised fjord (Catania et al., 2020), for example Helheim Glacier in southeast Greenland, which was observed to undergo significant buoyancy-driven calving, dominated by large events (>1 km^3), during the summers of 2010 and 2011 (James et al., 2014). As buoyant flexure typically requires the export of full-thickness, tabular icebergs, the calving rate is sensitive to the presence of a proglacial ice melange (Amundson et al., 2010) which provides a stabilising backstress on the glacier front.

The 'Calving Problem'

It remains unclear as to whether ice losses by calving are the cause or the result of ice flow acceleration (Benn et al., 2007a). Calving may be the 'master' of glacier dynamics, whereby mass loss through the calving of icebergs at the glacier terminus results in dynamic changes up-glacier, such as flow acceleration (Howat et al., 2005; Joughin et al., 2004; Meier and Post, 1987). Alternatively, calving may be the 'slave' to glacier dynamics, whereby dynamical and/or geometrical changes to the glacier result in the retreat of the calving front, thereby increasing the rate of ice delivery to the front, and thus increasing calving fluxes (Fischer and Powell, 1998; Van Der Veen, 1996; van der Veen, 2002). In reality, it is likely that there is no simple unidirectional causal relationship between ice dynamic processes and calving processes (Benn et al., 2007a), with both comprising parts of the complex ice-atmosphere-ocean system. This complexity means that there is currently no all-embracing calving law that has been validated at tidewater glaciers (Benn et al., 2017a), which limits our ability to project the response of the Greenland Ice Sheet to climate change within coupled ice-ocean models.

Submarine Melting

Submarine melting is the direct mechanism by which oceanic heat melts glacier ice and thus influences tidewater glacier dynamics through triggering calving, retreat, and ice flow acceleration, as evidenced by both direct observations and model studies (Carroll et al., 2016; Fried et al., 2015; Holland et al., 2008; Jenkins, 2011; Luckman et al., 2015; Motyka et al., 2003; O'Leary and Christoffersen, 2013; Rignot et al., 2016; Slater et al., 2015, 2017, 2018; Slater et al., 2019b; Straneo and Heimbach, 2013; Truffer and Motyka, 2016). This process also impacts floating ice, whereby submarine melting beneath the ice causes high thinning rates, initiating rift formation which can in turn result in the disintegration of a floating ice shelf or tongue (Truffer and Motyka, 2016). This process has been proposed to have driven the disintegration of the floating ice tongue at Jakobshavn Isbrae in west Greenland, in turn leading to major acceleration and retreat of the glacier (Holland et al., 2008).

Submarine melt is thought to be a function of near-terminus ocean conditions, for example ocean temperature, salinity, and circulation (Jenkins, 2011; Joughin et al., 2012), as well as the presence and magnitude of meltwater plumes (Jenkins, 2011; Mankoff et al., 2016; Slater et al., 2015; Sutherland et al., 2019). The latter occur during summer, whereby surface meltwater drains from the ice surface to the subglacial drainage system and is subsequently ejected at the base of the glacier terminus into the fjord, where it rises due to buoyancy to form localised, vigorous turbulent meltwater plumes that in turn entrain warmer ocean waters, driving rapid submarine melt (Figure 2.16; Jenkins, 2011; Mankoff et al., 2016; Slater et al., 2015; Sutherland et al., 2019).

Two distinct methods of submarine melting have thus been proposed; subglacial discharge driven melting through plume upwelling and ambient 'background' melting of the terminus away from these plumes (Catania et al., 2020). Initially, plume-driven melting was considered the major source of submarine melting, with ambient melting typically assumed to be negligible (Carroll et al., 2016; Cowton et al., 2015). However, more recent observations indicate that

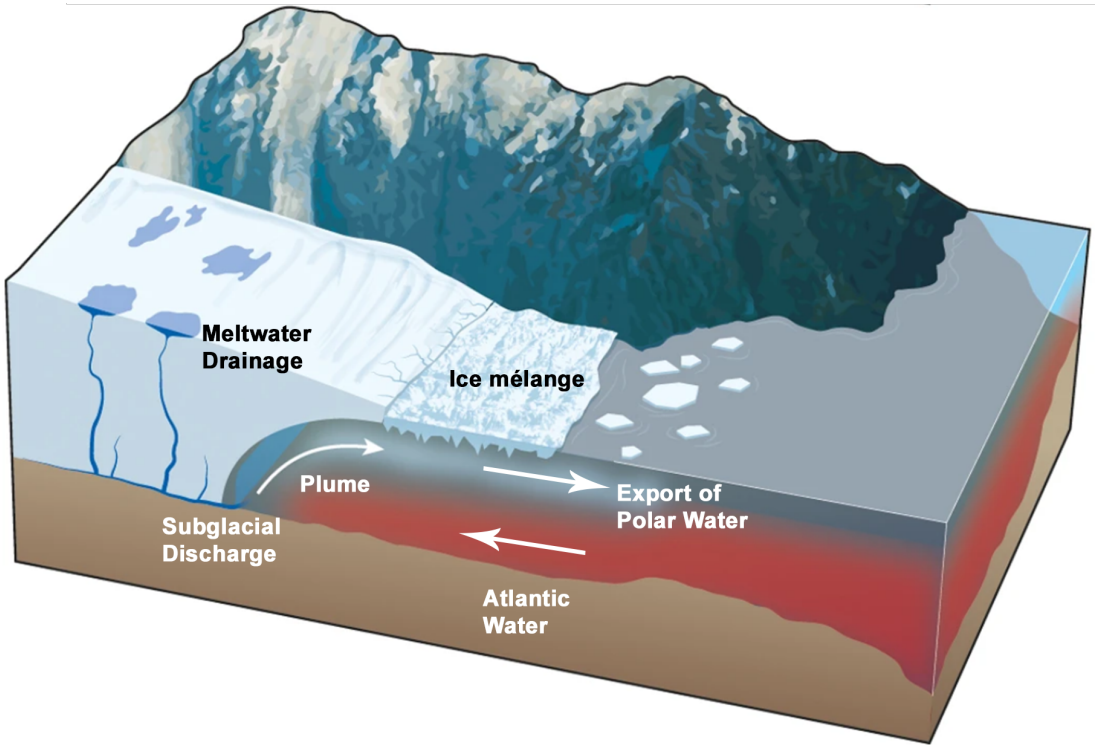

Figure 2.16: *Simple diagram illustrating the circulation within a glacial fjord showing the drainage of meltwater to the glacier bed and the subglacial discharge of freshwater at the terminus forming a buoyant plume, which in turn drives an overturning circulation within the fjord that exports cold Polar Water near the surface and draws in warm Atlantic Water at depth. Modified from Straneo and Heimbach, 2013.*

ambient melting may play an important role in net submarine melting (Slater et al., 2018; Sutherland et al., 2019), as meltwater plumes may drive a horizontal recirculation which enhances ocean velocity across large sections of the terminus, thus enhancing ambient melting (Slater et al., 2018).

Measurements and estimates of submarine melt rates have been made via direct hydrographic observations (Inall et al., 2014; Motyka et al., 2003; Rignot et al., 2010), ocean models (Jenkins, 2011; Sciascia et al., 2013; Slater et al., 2015) and remote sensing observations (Enderlin and Howat, 2013; Rignot and Jacobs, 2002), and range from centimetres to over 10 metres per day, although these values differ between glaciers and remain uncertain.

Fjord Circulation

Glacial meltwater released at the ice front rises buoyantly and flows down-fjord, establishing a fjord circulation cell in which an opposing flow draws warm ocean water at depth from the fjord mouth or coastal shelf into the fjord, and toward the glacier front (Figure 2.16, Carroll et al., 2015; Cowton et al., 2016; Jenkins, 2011; Motyka et al., 2003; Rignot et al., 2010; Sciascia et al., 2013; Straneo et al., 2011). This in turn enhances submarine melting by increasing the availability of oceanic heat at the terminus (Cowton et al., 2016; Straneo and Heimbach, 2013); numerical modelling of Kangerlugssuaq Fjord in east Greenland suggests that between the periods 1993-2001 and 2002-2011, circulation of water within the fjord resulted in an approximately 50 % increase in the ocean heat available for melting at the Kangerlugssuaq Glacier ice front (Cowton et al., 2016). The presence of buoyancy driven fjord circulation is evidenced by direct observations of warm Atlantic waters within tidewater glacier fjords (Straneo et al., 2010), the emergence of sediment-laden meltwater plumes down-fjord following the onset of surface melting in summer (Bunce et al., 2021; Tedstone and Arnold, 2012), and is also supported by theoretical modelling (Cowton et al., 2015). Warm ocean water can also be exchanged with the fjord through a shelf-driven intermediary circulation (Cowton et al., 2016; Jackson et al., 2014, 2018), which is the major mechanism of fjord exchange in winter in the absence of meltwater discharge. Fjord circulation can also be affected by the addition of freshwater via the melting of icebergs (Davison et al., 2020a) as well as wind forcing (Fraser and Inall, 2018; Jackson et al., 2014, 2018).

Proglacial Mélange Presence

Many tidewater glaciers flowing from the Greenland Ice Sheet are characterised by a proglacial ice mélange, a dense mix of sea ice and icebergs (Howat et al., 2010; Moon et al., 2015). This mélange may be transient, forming in winter and disintegrating in summer, or perennial, but with seasonal variability in its strength and structure. The presence (or absence) of a proglacial ice mélange is suggested to be a control on glacier dynamics through exerting a resistive buttressing stress on the

terminus (Reeh et al., 2001; Sohn et al., 1998), and/or preventing iceberg calving (Amundson et al., 2010; Cassotto et al., 2015). Observations at Jakobshavn Isbrae (Amundson et al., 2010; Cassotto et al., 2015) and other west Greenland tidewater glaciers (Moon et al., 2015) show a clear correspondence between seasonal mélange conditions and terminus change. In winter, cooler temperatures promote sea ice growth, which strengthens the mélange through binding icebergs together, ultimately preventing calving of full-thickness icebergs and facilitating glacier advance (Amundson et al., 2010; Cassotto et al., 2015; Moon et al., 2015). Weakening or loss of the mélange in summer promotes calving and so drives terminus retreat.

Mélange presence has also been attributed to multi-year dynamic change (Bevan et al., 2019; Howat et al., 2010). Anomalously low mélange formation in early-2003 is suggested to have triggered a multi-year retreat at Ingia Isbrae, Umiamako Isbrae and Sermeq Silardleq in west Greenland (Howat et al., 2010). The loss of mélange resulted in an extended period during which the glaciers calved, which may have led to terminus retreat beyond a stable pinning point, thus inducing a long-term instability (Howat et al., 2010). At Kangerlugssuaq Glacier in east Greenland, weakened mélange during the winters of 2016/17 and 2017/18, suggested to have been caused as a result of the penetration of anomalously warm surface waters into the fjord in 2016, enabled year-round calving for 2 consecutive years, resulting in the glacier retreating to its furthest point inland in 80 years (Figure 2.17, Bevan et al., 2019). In winter 2019, the mélange re-formed, and the glacier re-advanced by 3.5 km (Figure 2.17, Bevan et al., 2019).

2.3.5 Atmospheric Controls on Tidewater Glaciers

Warming air temperatures drive an increase in summer surface melting, which can impact tidewater glacier dynamics through several processes. First, surface melting drives surface lowering, in turn steepening the ice surface and so increasing ice flow rates through internal deformation (Catania et al., 2020; Cuffey and Paterson, 2010; Felikson et al., 2017). This can in turn create a positive feedback

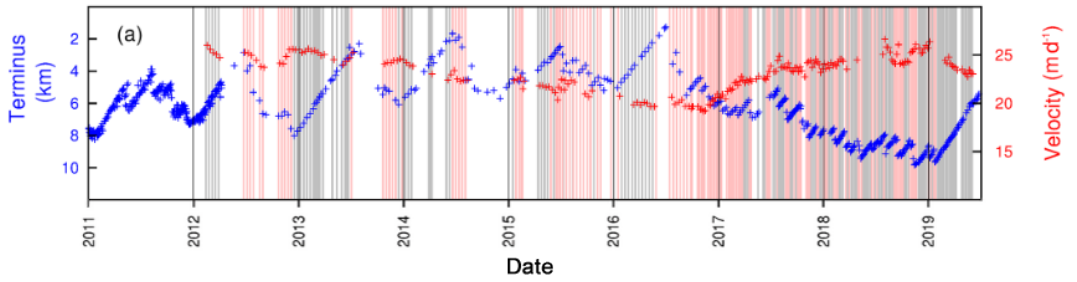

Figure 2.17: *Time series of terminus position (blue) and ice velocity (red) at Kangerlussuaq between 2011 and 2019. The vertical bars indicate the presence (grey) or absence (pink) of a rigid proglacial ice mélange. Reproduced from Bevan et al., 2019.*

that enhances ice flow into warmer, lower-elevation regions and further increases surface melt, and thus surface slope. In addition, should surface meltwater enter crevasses, the pressure of the water can offset the overburden pressure exerted by the weight of the ice, allowing the hydrofracture of crevasses deeper into the ice and thus enhancing calving (Benn and Evans, 2010; Benn et al., 2007b; Cook et al., 2014; Nick et al., 2010; Van Der Veen, 1998).

Greenland's marine terminating outlet glaciers can also be impacted by the generation of surface meltwater through its impact upon their subglacial hydrology. However, whilst it is expected that the broad glacio-hydrological processes observed at alpine glaciers and Greenland's land-terminating margin are likely to be similar at tidewater glaciers, our understanding of subglacial hydrology at tidewater glaciers is far more uncertain (Nienow et al., 2017). In contrast to alpine glaciers and Greenland's land-terminating margins, tidewater glacier margins are sensitive to a number of mechanisms affecting their dynamics, such as ice/ocean interactions (Holland et al., 2008; Rignot et al., 2012; Wood et al., 2018), iceberg calving (Benn et al., 2007b), and the presence of a proglacial mélange (Amundson et al., 2010; Moon et al., 2015), making it more difficult to attribute change in ice motion to hydrological forcing. Moreover, traditional field methods of hydrological investigation are extremely difficult to undertake at fast-flowing tidewater glaciers (Nienow et al., 2017).

However, both remote sensing and field-based studies have provided some insight into hydro-dynamic behaviour at tidewater glacier outlets. GPS velocity measurements between 36 and 72 km from the margin at Kangiata Nunaata Sermia in south west Greenland suggest that seasonal ice velocity variations are controlled by surface meltwater induced changes to the subglacial hydrological system, with an efficient subglacial drainage system extending at least 48 km inland (Sole et al., 2011). The magnitudes of these velocity variations are less than those at the land-terminating margin (Sole et al., 2011), consistent with larger scale remote sensing observations of west Greenland that show a seasonal acceleration of tidewater glaciers of < 15 %, compared to $50 - 100$ % at the land-terminating margin (Joughin et al., 2008b). Similarly, satellite-derived velocity measurements of the near-terminus at 5 stable tidewater glaciers in west Greenland show a mid-summer deceleration, indicative of subglacial drainage evolution (Howat et al., 2010). Further south, recent remote sensing observations at Kangiata Nunaata Sermia, Narsap Sermia and Akullersuup Sermia show seasonal speed-up at these glaciers coincident with surface melt onset, and subsequent slow-down following inferred subglacial channelisation (Davison et al., 2020b).

At Helheim Glacier in east Greenland, seasonal dynamic thinning has been attributed to the penetration of meltwater to the ice-bed interface, with no corresponding signal in ice front position (Bevan et al., 2015). Over multi-annual timescales, however, numerical modelling of Helheim Glacier suggests that multi-year dynamic changes are unlikely to be driven by basal lubrication as a result of the propagation of surface meltwater to the bed, which alone drives a modest 150 m of modelled frontal retreat as opposed to the $\sim$7 km of retreat observed in the mid-2000s (Nick et al., 2009). On an ice-sheet-wide, multi-annual scale, a study of 55 Greenlandic tidewater glaciers suggests that the dynamics of some are characterised by evolving subglacial drainage systems whereas other are not (Moon et al., 2014), and this may be related to the availability of surface meltwater and/or the presence of perennial firn aquifers. Outside of Greenland, observations at Perito Moreno Glacier, a lake-terminating glacier in Patagonia, show a

strong positive correlation between ice velocity and air temperature (Sugiyama et al., 2011), suggesting persistent inefficient subglacial drainage with little seasonal drainage evolution. In contrast, long-term changes in ice flow of Kronebreen, Svalbard, appear to be controlled by the presence and location of an efficient subglacial drainage system (How et al., 2017). Despite a range of studies, it therefore remains unclear the extent to which changes in subglacial hydrology characterise tidewater glacier systems, and to which they impact tidewater glacier dynamics on both seasonal and multi-annual timescales.

Subglacial hydrology may also impact upon tidewater glacier dynamics through an interaction with proglacial fjords, as introduced in Section 2.3.4. The discharge of subglacial water at the grounding lines of tidewater glaciers can influence both fjord circulation, whereby warm ocean water is drawn towards the glacier at depth (Carroll et al., 2015; Cowton et al., 2016; Sciascia et al., 2013; Straneo et al., 2011), and submarine melting of the ice front (Bunce et al., 2021; Motyka et al., 2003; Slater et al., 2015). In the case of the latter, model simulations indicate that the presence of a distributed subglacial drainage can increase the rate of submarine melting by up to a factor of 5 compared to a channelised drainage system, as a distributed drainage system results in water motion and the presence of warmer water across a larger proportion of the calving front (Slater et al., 2015). Consequently, whilst it remains unclear as to the direct impact of subglacial hydrology on basal sliding at tidewater glaciers, it is evident that it can influence patterns and magnitudes of ocean-driven melting, which in turn impacts tidewater glacier dynamics. Indeed, recent model results project an increase in subglacial discharge from tidewater glacier termini on the order of hundreds to thousands of $m^3\ s^{-1}$ by 2100 (a relative increase of approximately 2 to 8 times present values) (Slater et al., 2020). Moreover, associated modelled retreat via submarine melting (a function of both subglacial discharge and oceanic thermal forcing) across 191 tidewater glaciers projects a median retreat of 4.2 km by 2100 under the high emission RCP8.5 scenario (Slater et al., 2019b).

2.3.6 Morphological Controls on Tidewater Glacier Dynamics

Alongside oceanic and atmospheric forcing, tidewater glacier dynamics are fundamentally controlled by glacier geometry and the morphology of the glacier bed and lateral boundaries (Bunce et al., 2018; Carr et al., 2013; Catania et al., 2018, 2020). Observations show that increases in retreat rate can be associated with retreat into a widening fjord, retreat from a lateral pinning point, and/or retreat down a retrograde bed-slope (Bunce et al., 2018; Catania et al., 2018; Warren and Glasser, 1992).

Changes in fjord width at the terminus may accompany terminus retreat. If all else is equal, a glacier with a wider terminus, or with increasing terminus width as it retreats, will be more sensitive to climatic perturbations (Enderlin et al., 2013). This is as a result of reduced flow resistance from the lateral margins (Raymond, 1996), and conservation of mass requiring a reduction in ice thickness to maintain the same ice flux, thus promoting calving at the terminus (Bunce et al., 2018; Jamieson et al., 2012). Modelled glacier response to ocean warming on decadal to millennial timescales suggests retreat into a widening fjord may exert a stronger control on retreat than the presence or absence of a terminal moraine (Åkesson et al., 2018).

The presence of a terminus moraine facilitates glacier stability by providing flow resistance, limiting warm water access to the glacier front, and reducing buoyancy-driven calving (Enderlin et al., 2018; Post et al., 2011). Consequently, outlet glaciers resting on retrograde bed-slopes on the back side of terminal moraines are generally considered to be more susceptible to retreat in response to an external forcing (Bunce et al., 2018; Carr et al., 2013; Catania et al., 2018, 2020; Meier and Post, 1987). As introduced in Section 2.3.1, once retreat is initiated, retreat may continue down a reverse bed-slope until the glacier front reaches a prograde bed-slope further up-fjord (Catania et al., 2018; Meier and Post, 1987;

Weertman, 1974). This retreat results from a positive feedback, whereby retreat down a reverse bed-slope increases the area of the ice front in contact with warm ocean waters, thus increasing submarine melting and calving, and driving further retreat (Gudmundsson et al., 2012; Meier and Post, 1987; Post, 1975). This process was observed during the early to mid-2000s retreat of tidewater glaciers in southeast Greenland (Howat et al., 2008b; Joughin et al., 2008a), which was preceded by the formation of a flat or reverse-sloped surface topography near the terminus, indicating that the subsequent retreat was influenced by the presence of a reverse bed slope (Howat et al., 2008b).

Recent work based on the dynamics of 15 tidewater glaciers in west Greenland shows that the rate of glacier retreat accelerates through overdeepenings in the underlying bed topography (Catania et al., 2018), and the morphology of these overdeepenings can be used as a predictive measure for retreat extent (Figure 2.18). Moreover, whilst the near-synchronous onset of retreat (1998 $\pm$ 3 years) is indicative of a wider climate forcing, there is some evidence that the subtle differences in the time of retreat onset may also be influenced by bed topography, as those glaciers that began retreating earliest were resting on reverse bed-slopes (Catania et al., 2018). In addition, even narrow overdeepenings were observed to be important in modulating glacier retreat, likely due to the focusing of subglacial discharge driving localised melt of the terminus, thereby enhancing local retreat (Catania et al., 2018).

However, uncertainties in our knowledge of Greenland's basal topography remain, especially in under-sampled regions (Morlighem et al., 2017), limiting our ability to project the future behaviour of tidewater glaciers (Catania et al., 2020). Furthermore, the influence of overdeepened bed topography on outlet glacier dynamics remains subject to debate, with modelling studies suggesting that stable grounding line positions can be achieved on a reverse bed-slope (Jamieson et al., 2012; Nick et al., 2010). This is supported by the recent transient stabilisation and re-advance of Jakobshavn Isbrae (Khazendar et al., 2019) on a reverse-sloping bed (An et al., 2017).

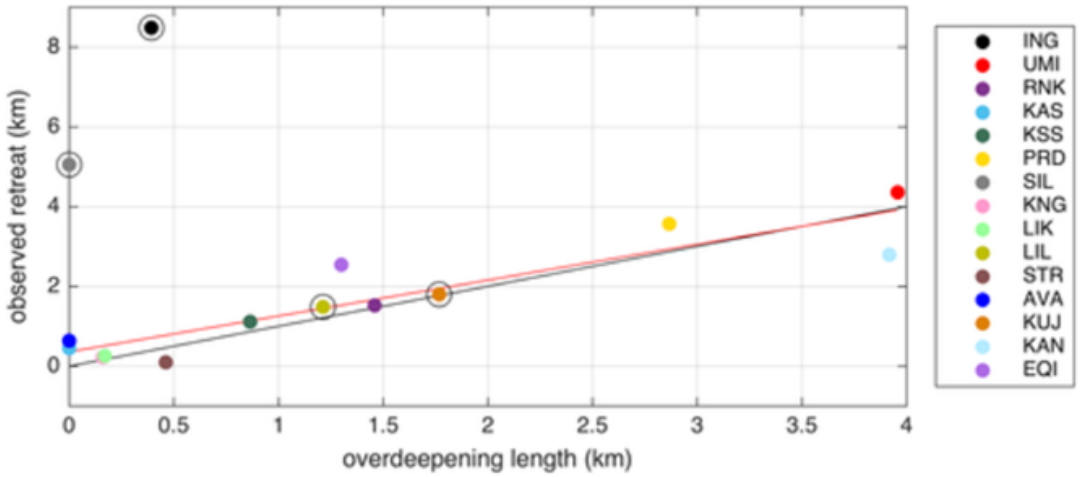

Figure 2.18: *Overdeepening length upstream of the terminus at the time of progressive retreat onset against total retreat observed since progressive retreat onset. Points outlined with black circles have poorly constrained bed topography at retreat onset locations. The black line gives the 1:1 relationship, and red line shows a linear regression (R^2 = 0.8) using only glaciers with well constrained bed topography. Reproduced from Catania et al., 2018.*

2.3.7 Inland Propagation of Terminus Change

Retreat and acceleration of tidewater glaciers draining the Greenland Ice Sheet has resulted in dynamic thinning, which is initiated at tidewater glacier termini and subsequently diffuses inland (Felikson et al., 2017, 2020; Nye, 1960; Payne et al., 2004; Price et al., 2011; van der Veen, 2001). As this diffusion of dynamic thinning is not instantaneous, the Greenland Ice Sheet continues responding to a given dynamic perturbation long after that original perturbation ceases (Price et al., 2011); for example, the loss of back-stress following disintegration of a floating ice tongue or an increase in strain rate as the terminus retreats into deeper water. The associated long-term mass loss represents Greenland's 'committed' sea level rise contribution, which would still occur in the absence of any further climatic forcing and associated changes in ice dynamics and SMB (Price et al., 2011). In relation to these delayed responses, modelling work estimates that the retreat, acceleration, and dynamic thinning of Greenland's outlet glaciers during the period 2000-2009 will result in a minimum committed sea level rise contribution of 6 $\pm$ 2 mm by 2100, irrespective of any future climatic forcing and associated dynamic change (Price et al., 2011).

Recent work (Felikson et al., 2017, 2020) suggests that there may be geometrical constraints on the ability for thinning perturbations to propagate inland. These studies calculate the Péclet number (Pe), a nondimensional number that describes the ratio of the rate at which a kinematic wave diffuses upstream or advects downstream, and which is a function of ice thickness and surface slope (and thus basal topography). These studies contend that where ice is thick and with a low surface gradient, Pe is low, thus enhancing the up-glacier translation of a given thinning perturbation. Conversely, where ice is thin and steep, Pe is high, and it is harder for thinning perturbations originating at the terminus to diffuse up-glacier due to the impact of the down-glacier advection of ice, which may overprint any thinning perturbation (Felikson et al., 2017). Based upon observations of cumulative volume loss from DEM differencing across 16 glaciers in west Greenland, it was estimated that 94 % of the up-glacier dynamic mass loss resulting from terminus perturbations would occur between the terminus and the location at which Pe = 3 (Felikson et al., 2017), thus offering a possible empirical threshold by which to measure the ability of changes at the margin to propagate inland. The greater the distance between the terminus and the location at which Pe = 3, the greater the distance a perturbation will propagate upglacier, and thus the greater the contribution to future sea-level rise. One constraint on up-glacier thinning limits was inferred to be the heads of subglacial troughs, which can be found tens to hundreds of kilometres inland from tidewater glacier termini (Morlighem et al., 2014), where steep bed slopes restrict diffusive thinning from propagating further inland. Consequently, the variability in glacier geometry is proposed as an explanation for the observed heterogenous response of Greenland's tidewater glaciers to oceanic and atmospheric warming (Felikson et al., 2017).

This analysis was extended by Felikson et al., 2020, who applied it to 141 tidewater glaciers across the Greenland Ice Sheet. They sampled between 6 and 24 flowlines per glacier, and calculated the thinning limit by taking the single furthest inland thinning limit, before subtracting one standard deviation of the distances

to all predicted flowline thinning limits for that particular glacier, thereby taking into account the across flow uncertainty (Felikson et al., 2020). At each tidewater glacier studied, total thinning was measured by differencing a 1978-1987 DEM (Korsgaard et al., 2016) from the ArcticDEM, which represents the ∼2015 ice sheet surface elevation (Porter et al., 2018a). Of the 141 total glaciers studied, 72 exhibited dynamic thinning that was limited to within the spatial extent of the DEM difference. From these 72 tidewater glaciers, the authors argue that the Pe = 3 threshold represents the location where 89 % of dynamic change has occurred (with an interquartile range of 74-100 %). This limit is associated with 'knickpoints' in basal topography, defined as regions where bed elevation raises by >= 300 m over a distance of <= 100 km (Felikson et al., 2020).

The authors identify two end-member geometries; those characterised by shallow bed topography and permitting diffusion far inland, and those characterised by the presence of steep, mountainous bed topography with knickpoints that set clear and strong limits to the inland diffusion of thinning (Felikson et al., 2020). Following this, they identify two distinct groups of glaciers with a high potential for dynamic mass loss for two separate reasons (Figure 2.19). The first group are those with a high ice flux (>5 km^3 yr^{-1}) but with knickpoints (and thus thinning limits) close to the margin (<150 km), for example Helheim Glacier and Kangerlugssuaq in southeast Greenland. They hypothesise that high-flux glaciers have more erosive power and so create knickpoints that set thinning limits closer to the ice margin (Felikson et al., 2020). The second group are those glaciers with a relatively low ice flux but where thinning limits extend far inland (> 200 km); these glaciers do not receive as much attention as the high-flux glaciers but have the potential for a large dynamic mass loss contribution. For example, northwest Greenland is characterised by shallow bed topography, resulting in 9 of the 12 glaciers between Upernavik Isstrøm Central and Cornell Gletscher having predicted thinning limits >250 km from the margin (Felikson et al., 2020). Moreover, as the rate of diffusion slows as thinning spreads inland (van der Veen, 2001), these glaciers will continue to thin over longer timescales, consistent with

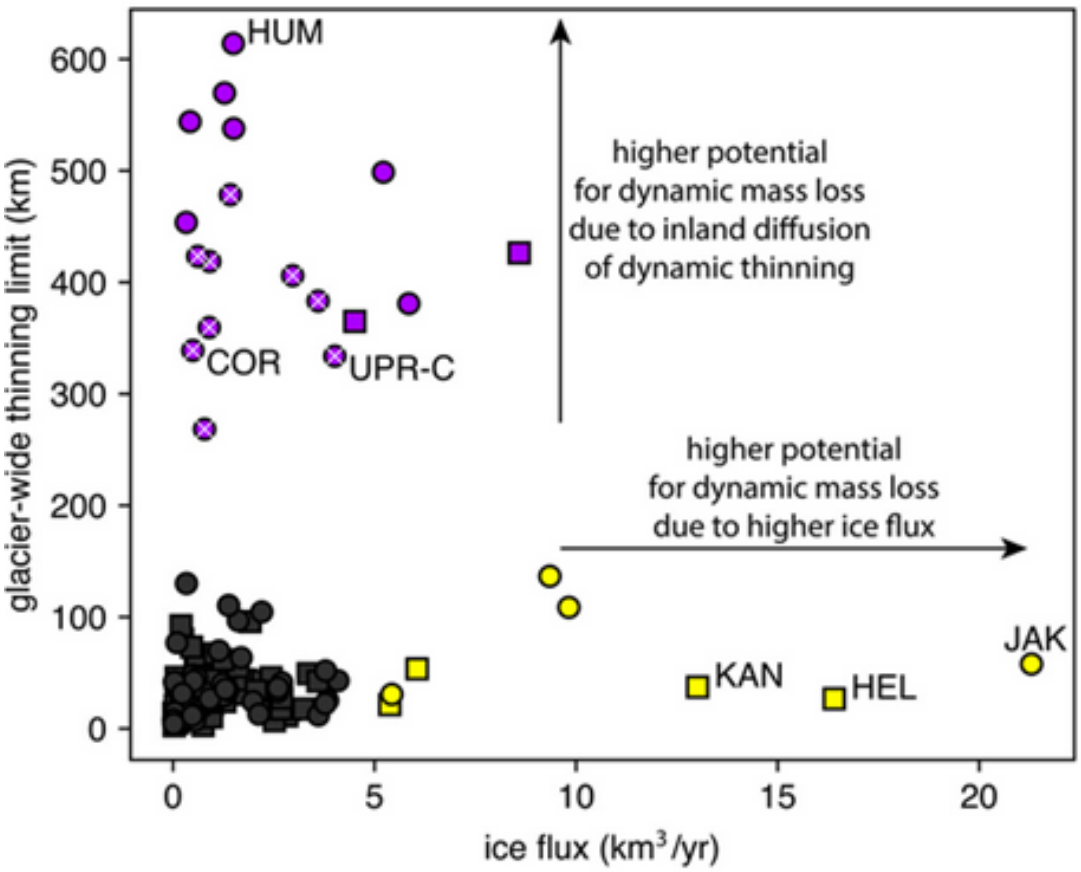

Figure 2.19: *Distances from ice sheet margin to thinning limits plotted against ice fluxes for 141 glaciers in regions of gentle (circles) and mountainous (squares) bed topography. Purple markers indicate a group of glaciers with thinning limits > 200 km from the ice margin, and yellow markers indicate a group of glaciers with an ice flux of >5 km^3 yr^{-1}. White x's inside purple markers indicate nine glaciers in NW, discussed in text. Black markers indicate the remaining glaciers studied with thinning limits < 200 km from the ice margin and an ice flux < 5 km^3 yr^{-1}. Reproduced from Felikson et al., 2020.*

recent observations that northwest Greenland is the only region which is experiencing an ongoing and sustained increase in ice discharge since the mid-2000s (King et al., 2020).

2.4 Summary of motivation for thesis

Understanding how the Greenland Ice Sheet responds dynamically to oceanic and atmospheric warming is crucial if we are to project accurately Greenland's future contribution to global sea level. The body of literature which addresses Green-

land's ice dynamics has grown rapidly over the past two decades; however, many uncertainties remain which inhibit our ability to predict with confidence rates of ice sheet mass loss under future climate change. At Greenland's land-terminating margins, previous research has shown that over multi-decadal timescales, a persistent increase in the production of surface meltwater has driven a long-term reduction in ice motion. However, since 2012, the southwest Greenland land-terminating margin has experienced a cooler regional climate, and it remains unclear how this impacts hydro-dynamic coupling and thus ice motion on a multi-annual timescale. At higher elevations within the interior accumulation zone, our understanding of ice dynamic change is extremely limited at an ice sheet scale, both in land- and marine-terminating basins, with direct observations limited to sparse GPS measurements. Changes in the ice dynamics of the ice sheet interior are of great significance as given the greater thickness of the ice, any increase in ice velocity will result in a much larger mass flux compared to an equivalent change in ice motion near the margin. At marine-terminating margins, it remains unclear how important long-term oceanic and atmospheric forcing is in driving tidewater glacier change when compared to the local fjord morphology and ice geometry. Moreover, improving our understanding of how the ice dynamics of Greenland's tidewater glaciers respond to a changing climate is complicated by the fact that these glaciers may respond non-linearly to climate forcing, and by the multitude of temporally and spatially overlapping processes at play that are challenging to observe. During the remainder of this thesis, certain aspects of these many uncertainties are addressed, with the overall aim of providing an improved process-based understanding of the behaviour of the Greenland Ice Sheet, thereby enabling improved projections of the ice sheet's response to future global warming.

Chapter 3

Data and Methods

The research presented in this thesis utilises a range of remotely sensed data and derived data products, as well as in-situ GPS data and measured and modelled oceanic and atmospheric indices. The results chapters 4-6 which follow this chapter each have their own Methods section, detailing the most relevant information for that particular chapter. This chapter aims to provide a broader overview and context of the data and methods used in the thesis, as well as more detailed descriptions of the methods in the case that they are not described in full within the respective results chapters.

3.1 Remote Sensing in Glaciology

The growing availability of airborne and spaceborne sensors has greatly improved our ability to assess glaciological conditions and study changes in the Cryosphere (Bishop et al., 2014). For over four decades, satellite sensors have observed the Greenland Ice Sheet (Cooper and Smith, 2019; Pope et al., 2014; Pritchard et al., 2011), facilitating the measurement of a variety of glaciological characteristics and their change through time, such as ice surface elevation, ice velocity, glacier front position and the albedo of the ice surface, as well as the mapping of surface melt extent and glaciological facies, amongst other uses (Cooper and Smith, 2019). Satellite remote sensing is particularly useful within the field of glaciology due to the often inaccessible and inhospitable study locations, resulting in logistically

difficult, financially expensive, and spatially limited field campaigns. Satellite imagery permits year-round, real-time, and long-term studies as well as ice-sheet-wide coverage, with an increasing amount of remotely-sensed data and derived data products being freely available to the researcher (Pope et al., 2014).

3.2 Data Sources

3.2.1 Landsat

At nearly 50 years of continuous, unbroken data collection, the Landsat series of satellites represents the longest temporal record of civilian spaceborne Earth observations (Wulder et al., 2019), with later missions designed to complement and continue the prior record (Pope et al., 2014). As a result, the main characteristics have remained the same between satellites (i.e., 16-day temporal resolution, multispectral imagery collected across multiple bands). Landsat-1 through Landsat-3 collected data using the Multispectral Scanner (MSS) sensor across four bands with 6-bit radiometric resolution and a spatial resolution of 60 m (Mather, 2004; Wulder et al., 2019). As the six detectors on the MSS deteriorated at different rates, MSS imagery can show a phenomenon known as six-line banding (Mather, 2004). The quality of Landsat imagery was improved with the addition of the Thematic Mapper (TM) to Landsat-4 and Landsat-5, which collected data across 7 spectral bands at 8-bit radiometric resolution and up to 30 m spatial resolution (Wulder et al., 2019). The spatial resolution of Landsat was further increased to 15 m with the addition of the panchromatic band to the Enhanced Thematic Mapper (ETM+) of Landsat-7, which launched in April 1999. However, the scan line corrector (SLC) on the ETM+ failed during May 2003 (Mather, 2004), and so horizontal striping affects scenes imaged after this event, resulting in $\sim$20 % of pixels not being scanned in each image (Ahn and Howat, 2011; Chen et al., 2011). As a result, Landsat-5 imagery continued to be downlinked to ground-receiving stations until January 2013. Landsat-8 launched in February 2013, with the Operational Land Imager (OLI) providing a considerable upgrade over the previous sensors in radiometric resolution (12-bit) and internal geometric accuracy, as well

as through the addition of several new spectral bands (Fahnestock et al., 2016; Roy et al., 2014; Wulder et al., 2019). Currently, approximately 1200 images are added to the USGS Landsat archive every day (∼475 Landsat-7, ∼740 Landsat-8, Wulder et al., 2019).

In 2008, the Landsat data policy changed, and the Landsat archive became free and open (Woodcock et al., 2008). This provided an unprecedented volume of observations in time and space captured during a period of rapid climatic change, facilitating accelerated scientific developments (Wulder et al., 2019; Zhu et al., 2019). Indeed, Landsat data has been used to investigate changes in tidewater glacier extent (Bunce et al., 2018; Murray et al., 2015), ice motion (Joughin et al., 2018; Mouginot et al., 2015; Mouginot et al., 2017; Rosenau et al., 2015; Tedstone et al., 2015), and supraglacial lake extent (Miles et al., 2017; Williamson et al., 2018), amongst other applications, across the Greenland Ice Sheet. Access to Landsat data remains freely available through both the USGS (`https://earthexplorer.usgs.gov/`) and ESA (`https://eocat.esa.int`) archives.

Landsat data is the predominant remotely sensed data source used in this thesis. In Chapter 4, feature tracking is applied to pairs of Landsat-5, Landsat-7, and Landsat-8 imagery to measure ice velocity within the southwest Greenland land-terminating sector. In Chapter 5, ice velocities produced from Landsat imagery as part of the ITS-LIVE dataset (Gardner et al., 2018, 2019) are used in combination with in-situ GPS velocity measurements to investigate changes in ice motion within the ice sheet interior. In addition, in Chapter 6, Landsat-8 data is used to map terminus positions of marine-terminating glaciers within Sermilik Fjord between 2014 and present, and MEaSUREs monthly velocity data derived from Landsat imagery (Howat, 2020) are extracted from the near-terminus regions of the same glaciers to assess changes in ice motion over the same time period.

3.2.2 Sentinel-2

Sentinel-2 is a constellation of two satellites (Sentinel-2A, Sentinel 2-B, launched June 2015 and March 2017 respectively) as part of the European Copernicus Programme, providing systematic global acquisitions of high resolution multi-spectral imagery with a high revisit frequency (Drusch et al., 2012), with free and open access to data. The visible and near-infrared bands have a 10 m spatial resolution, and the revisit period over Greenland is 5-days (Drusch et al., 2012), representing improvements over Landsat-8 (15 m panchromatic band, 16-day revisit). Sentinel-2 imagery can be combined with Landsat 8 imagery to provide a more frequent revisit time of ∼3 days (i.e., Williamson et al., 2018). As with Landsat data, Sentinel-2 imagery is freely accessible from both the USGS (`https://earthexplorer.usgs.gov/`) and ESA (`https://eocat.esa.int`) archives and has been used for terminus mapping (Fahrner et al., 2021) and other applications (Moyer et al., 2019; Williamson et al., 2018) across the Greenland Ice Sheet, although its use in producing velocity fields has thus far been more limited (Kääb et al., 2016; Nagy et al., 2019). In this thesis, Sentinel-2 data in is used in conjunction with Landsat-8 data to map terminus positions at marine-terminating glaciers within Sermilik Fjord at high temporal resolution (Chapter 6).

3.2.3 CryoSat-2

Launched in April 2010, CryoSat-2 is a radar altimeter specific for ice applications, with an orbit reaching latitudes of 88° and thus maximising coverage over the polar regions. Since its launch in 2010, CryoSat-2 data has been widely used to measure surface elevation and elevation change on an ice-sheet-scale for the Greenland Ice Sheet (Helm et al., 2014; McMillan et al., 2016; Nilsson et al., 2016; Sandberg Sørensen et al., 2018). The inter-track spacing is half that of ICESat and an order of magnitude smaller than Envisat or ERS-1/2, offering a high observation density. As opposed to traditional altimeters which measure surface elevation at the point of closest approach (the point at the surface closest to the satellite), the interferometric mode of CryoSat-2 can be used to map 5 km wide

swaths of surface elevation at 500 m resolution for each satellite pass, providing up to two orders of magnitude more surface elevation measurements than traditional altimeters (Foresta et al., 2016, 2018; Gourmelen et al., 2018). CryoSat-2 data is used in Chapter 6 to measure the change in surface elevation between late-2010 and early-2020 at marine-terminating glaciers within Sermilik Fjord, and is freely available from ESA (https://science-pds.cryosat.esa.int/, https://eocat.esa.int).

3.2.4 Airborne Topographic Mapper

The Airborne Topographic Mapper (ATM) is a lidar altimeter that can map surface topography from an aircraft flying at 400-800 m altitude with an accuracy of 10-20 cm. The data is limited in spatial extent to the flight lines flown by the aircraft, yet as flights have been flown across the entire ice sheet, ATM data have been used in a wide range of studies investigating surface elevation change across different regions and outlets of the Greenland Ice Sheet (Howat et al., 2007; Kehrl et al., 2017; Lewis et al., 2017; Millan et al., 2018; Morlighem et al., 2013). ATM surface elevation measurements from the mid-2000s are used in Chapter 6 to contextualise recent dynamic change at marine-terminating glaciers within Sermilik Fjord. The Pre-IceBridge ATM data used within Chapter 6 are freely available from the NSIDC (https://nsidc.org/data/BLATM2/versions/1).

3.2.5 MODIS

The Moderate Resolution Imaging Spectoradiometer (MODIS) is an imaging sensor on board the Terra and Aqua satellites. MODIS data is of low spatial resolution (250 – 1000 m) but very high temporal resolution, surveying the entire Earth surface every 1-2 days (Pope et al., 2014). As such, it has been used for mapping terminus positions and glacier area change across wide areas at high temporal resolutions (Box and Decker, 2011; Howat et al., 2010; Schild and Hamilton, 2013; Seale et al., 2011), as well as for other applications such as investigating changes in ice surface temperature (Hall et al., 2013; Shuman et al., 2014) and map-

ping snow grain size (Lyapustin et al., 2009). MODIS imagery and derived-data products can be freely accessed from the USGS (https://earthexplorer.usgs.gov/), NASA (https://ladsweb.modaps.eosdis.nasa.gov/), and the NSIDC (https://nsidc.org/data/modis/index.html). Here, MODIS data is used to provide background imagery for geospatial figures (Chapter 4).

3.2.6 Modèle Atmosphérique Régionale (MAR)

The Modèle Atmosphérique Régionale (MAR) is a regional atmospheric model that combines atmospheric modelling (Gallee and Schayes, 1994) with the Soil Ice Snow Vegetation Atmosphere Transfer Scheme (De Ridder and Gallée, 1998) to simulate realistic surface mass balance (SMB), air-snow interactions, and atmospheric circulation over the ice sheets. MAR has been extensively used and evaluated to simulate surface energy balance and SMB processes across the Greenland Ice Sheet (Delhasse et al., 2018, 2020; Fettweis et al., 2011; Fettweis, 2007; Fettweis et al., 2013; Fettweis et al., 2017; Tedesco and Fettweis, 2020). In this thesis, model SMB data is obtained from MAR v3.10 forced by NCEP-NCARv1 re-analysis at an annual temporal resolution. The raw data has a spatial resolution of 20 km, but this is interpolated to a finer resolution of 1 km, and this higher resolution product is used here. The MAR model code can be accessed via https://mar.cnrs.fr/, and the MAR data used in this thesis was provided by Dr Xavier Fettweis (pers. comm.).

3.3 Estimation of Ice Flow Velocities using Feature Tracking

Feature tracking defines tracking the displacement of surface features, for example crevasses, boulders, or patterns of debris/ice, across pairs of images (in this case optical satellite scenes) covering the same geographic area but separated in time. As the time interval between the images is known, these displacement estimates can be converted to velocity estimates. A reference template, Ωr, is chosen

within the first (reference) image centred around a pixel (x,y). A template of the same size is then extracted from the second (search) image, but translated by (u,v) pixels within a specified search window, Ωs, as illustrated in Figure 3.1 (Debella-Gilo and Kääb, 2011). This is then compared to Ωr using a function of similarity. The operation is repeated for different values of (u,v), and the position of maximum similarity is a measure of displacement, which is then converted to velocity (Dehecq et al., 2015).

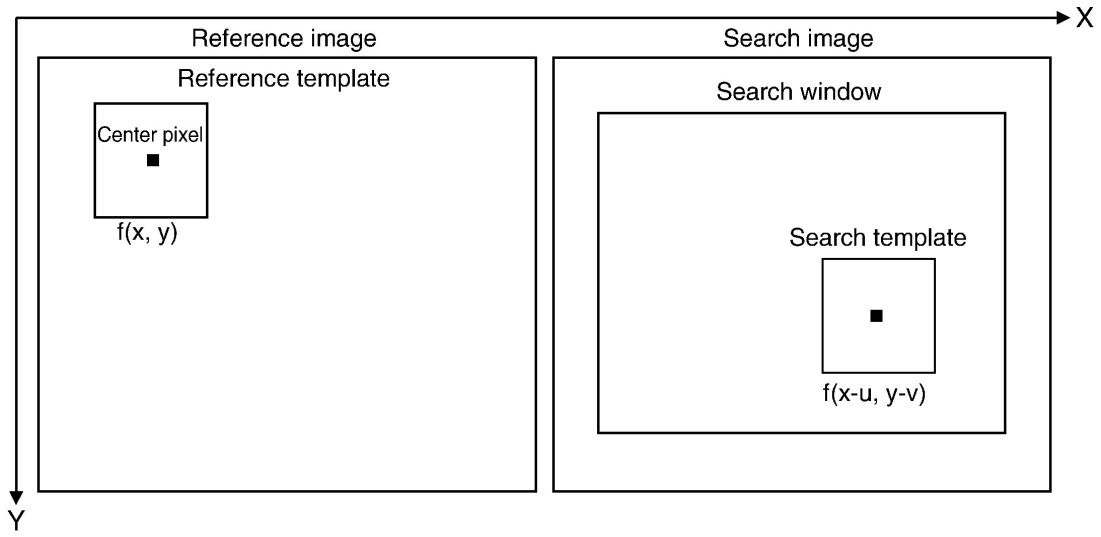

Figure 3.1: *Schematic representation of the feature tracking procedure, showing an image pair with the reference template, central pixel, search template and the search window. Reproduced from Debella-Gilo and Kääb, 2011.*

This has been applied to the ice sheets since the early-1990s (Scambos et al., 1992), and improvements in both satellite sensors and computing power have substantially increased the scope of the technique. For instance, the higher radiometric resolution and internal geometric accuracy of Landsat-8 OLI allows for the tracking of subtle snowdrift patterns, extending the velocity mapping capability beyond crevassed areas (Fahnestock et al., 2016; Jeong and Howat, 2015). In this thesis, I utilise and develop a previously developed processing chain (Dehecq et al., 2015) to extract velocities from Landsat imagery covering the south west Greenland land-terminating sector. As a detailed description of the processing chain is contained within Dehecq et al., 2015, a more concise description is provided here. The feature tracking process requires a number of steps to be com-

pleted before a robust velocity estimate can be extracted. These are summarised in Figure 3.2 and addressed in the following subsections.

3.3.1 Image Acquisition

For the purpose of utilising the entire Landsat archive to calculate ice velocities over large areas, manual selection of image pairs is implausible. As such, the selection of image pairs is purely based upon the date and time of their acquisition, and their location. Here, I have updated the feature-tracking processing chain to automatically find every WRS2 path/row that intersects a shapefile outlining a given area of interest (AOI), in this case the southwest Greenland land-terminating sector (66.41 to 69.52 N, 51.78 to -45.45 W, see Chapter 4 Methods, Figure 4.5), and subsequently semi-automatically download every Landsat 5, Landsat 7, and Landsat 8 scene for each of the path/row coordinates. After determining all of the WRS2 path/row combinations that cover the AOI, a list of every scene for each sensor (Landsat 5/7/8) within these path/row combinations is created via the USGS EarthExplorer interface (`earthexplorer.usgs.gov/`). For Landsat 5 and Landsat 7, each scene on these lists is then downloaded by interfacing with the EarthExplorer JSON API using Python. Landsat 8 imagery is stored on Amazon Web Services (AWS) which allows the added benefit of downloading individual bands, further speeding up the image acquisition process (i.e., Mouginot et al., 2017). Consequently, Landsat 8 imagery is downloaded directly from the AWS API using Python. Both of these image acquisition methods offer download speeds of $>$10 Mb s^{-1}, and order of magnitude greater than what can usually be achieved via the Bulk Download Application provided by the USGS ($\sim$1 Mb s^{-1}), and moreover they can be run overnight using a Linux screen.

Additional Landsat 5 and Landsat 7 imagery is stored within ESA data repositories. This cannot be accessed via an API, and so the most efficient way to access the data is via the FireFox DownThemAll extension, which allows parallel downloading of up to 4 scenes at once. To maximise spatial coverage of the AOI and resultant velocity mosaics, all available scenes are downloaded from both USGS

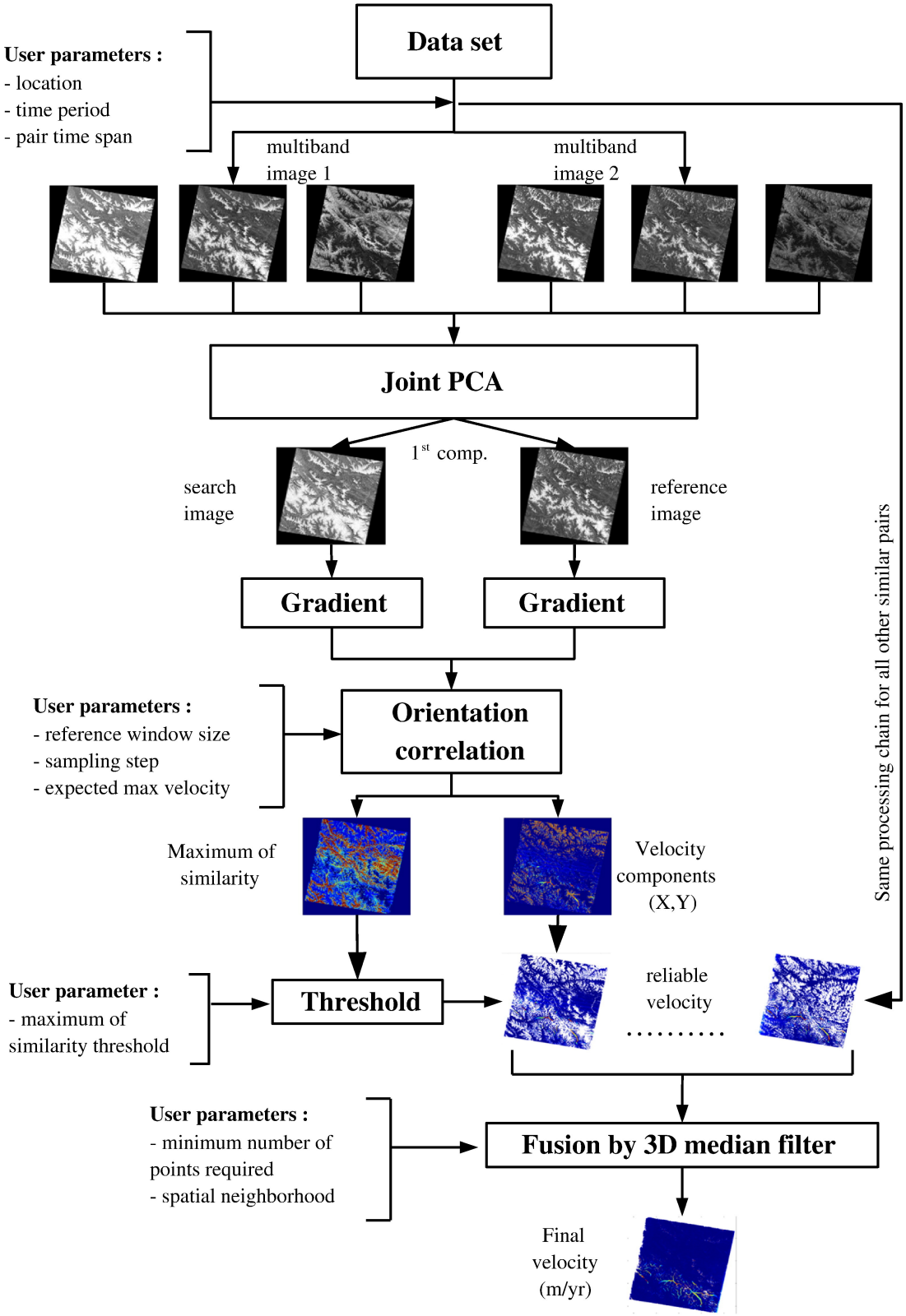

Figure 3.2: *Processing strategy to derive glacier velocities from a complete multispectral satellite archive. Reproduced from Dehecq et al., 2015.*

and ESA repositories, and any duplicates are subsequently removed.

Imagery from the earlier Landsat 1-3 missions is characterised by much larger errors in georeferencing and orthorectification and is very limited in availability. As such, these older data are excluded from the analysis.

3.3.2 Temporal Baseline

Once the imagery is acquired, pairs of images must be identified based on the desired temporal baseline separation. This must be appropriate for the flow velocity of the region under investigation, with larger baselines required for slower-flowing ice (Dehecq et al., 2015). A temporal baseline of approximately one year (368±16 days) is chosen to minimise the influence of seasonal ice flow variability as the objective of the analysis carried out during this thesis was to retrieve interannual ice velocity trends. This results in a total of 2665 pairs of Landsat images across 14 path/rows (See Chapter 4 Methods, Figures 4.6, 4.7), an increase of >5 and >3 times respectively that used in previous work focused on this region of the ice sheet (Tedstone et al., 2015). As using images 16 days either side of the 368-day baseline may still introduce bias whereby, for example, a 384-day period could disproportionately sample faster flow in summer (Joughin et al., 2018) (or vice versa), an assessment of the impact of varying baseline durations on annual ice velocity is conducted within Chapter 4.

3.3.3 Parameter Choice

Prior to running the processing chain, several key parameter values need to be determined. The first of these is the appropriate spectral band or bands. Radiation is reflected and emitted from the surface over a range of wavelengths, and the clarity of surface features can differ depending upon the wavelength at which they are observed. The precise wavelength ranges of each spectral band designation are broadly equivalent for Landsat 5 through Landsat 8. The optimal spectral band combination for this region of the ice sheet was determined through

thorough testing in previous work to be bands 2 and 3 for Landsat 5 and 7, and bands 3 and 4 for Landsat 8, covering the wavelengths ∼0.52-0.69 μm (Tedstone et al., 2015). Whilst the panchromatic band 8 offers greater spatial resolution for Landsat 7 and 8 imagery, combining bands of different spatial resolution can introduce a bias whereby the coarser resolution Landsat 5 imagery may not be able to resolve features, such that the feature tracking algorithm may instead lock onto stable features, whereas features can be resolved, and thus tracked, within the higher resolution Landsat 7 and 8 imagery (Dehecq et al., 2019). As such, should the resultant velocities produced from 15 m resolution Landsat 7/8 imagery be compared to those produced from the 30 m resolution Landsat 5 imagery, an apparent speed-up from ∼0 m yr^{-1} to a value significantly greater can be introduced (Dehecq et al., 2019). Consequently, the aforementioned bands are used as both the wavelengths that they cover and their spatial resolution are consistent across sensors.

The most critical parameter is argued to be the reference template size (Dehecq et al., 2015). This defines the area centred around the sampling pixel (x,y) in the reference image, which is then treated as the reference pattern to be matched within the search window of the search image (Figure 3.1). If the reference template size is too small, it can be problematic due to ambiguities arising from repetitive surface textures (i.e., crevasses), resulting in spurious matches (Debella-Gilo et al., 2012; Jeong et al., 2017). Increasing the reference template size increases its uniqueness but results in an exponential increase in computing time and can cause increased geometric distortion of features within the template (Debella-Gilo et al., 2012; Dehecq et al., 2015). As such, the aim is to identify a reference template size that contains higher signal variability in relation to noise variability with minimum geometric distortion, that is also appropriate for the ice velocity of the study region and the time separation of the image pair (Ahn and Howat, 2011; Debella-Gilo et al., 2012). Extensive testing in prior work found a reference template size of 44 pixels (1320 m) to be optimal for the northern ∼60 % of the study region (Tedstone et al., 2015), however this was insufficient

to generate velocity fields with good spatial coverage in the Leverett Glacier region further south. As such, here a reference window of 80 pixels (2400 m) was necessary to produce velocity fields with a spatial coverage extending ∼120 km further south than those produced in Tedstone et al., 2015.

The search window defines the region within the search image across which the reference template is translated to search for matching offsets (Figure 3.1). This should be set to slightly larger than the expected maximum displacement based upon prior velocity estimates for the region of interest, as this will reduce both computing time as well as the potential for mismatches (Dehecq et al., 2015; Messerli and Grinsted, 2015). As such, the search window size is chosen to be slightly larger than prior velocity estimates for southwest Greenland (Joughin et al., 2010).

The spacing, or step-size, defines the spatial resolution of the final velocity field by setting the grid spacing at which offsets are calculated. A higher spacing value decreases computing time at the expense of spatial resolution. Spacing is set to 8 pixels, giving a spatial resolution of 240 m for the velocity fields.

The choice of feature tracking algorithm can also affect results. Normalised Cross-Correlation (NCC) is commonly used when studying glacier velocities (Heid and Kääb, 2012; Messerli and Grinsted, 2015). The normalisation accounts for variations in brightness and contrast within a sequence of imagery, for example as a result of differing illumination angles (Debella-Gilo and Kääb, 2011), however as this algorithm operates in the spatial domain, it is time-consuming compared to algorithms operating in the frequency domain (Heid and Kääb, 2012). Moreover, NCC is easily dominated by large differences in digital numbers, which often characterises glacial areas where white snow, darker ice and black rocks are often present (Heid and Kääb, 2012). Whilst this is not problematic if these differences are present in both the reference and search images, it is common that snow patches may disappear between images, and rocks can move independently

of glacier motion through rolling or sliding at the ice surface (Heid and Kääb, 2012).

An alternative feature tracking algorithm is Orientation Correlation (OC). This is a fast, illumination invariant feature tracking method (Fitch et al., 2002) that is not affected by uniform areas, which are common in glacial regions (Heid and Kääb, 2012). Moreover, OC also performs better than NCC for Landsat 7 SLC-off imagery and is argued to outperform similar Fourier methods (Heid and Kääb, 2012).

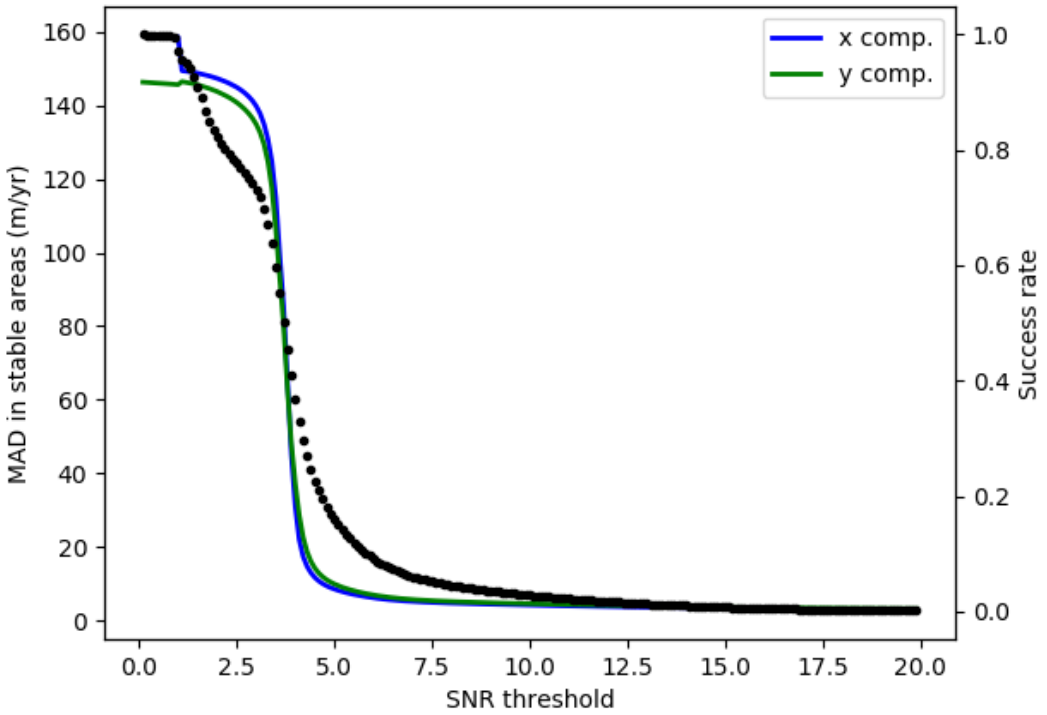

Figure 3.3: *Median absolute deviation (MAD) of the x and y velocity components in stable (off-ice) areas (blue and green lines), and the success rate (black dots), for different SNR thresholds.*

As a manual inspection of results is not feasible, outliers and/or mismatches can be removed from the velocity outputs by filtering with a signal-to-noise ratio (SNR) threshold (Dehecq et al., 2015), whereby pixels with an SNR of less than the threshold value are removed prior to the fusion of velocity fields. The choice

of SNR threshold is a compromise between retaining the maximum number of velocity estimates whilst removing most of the mismatches and enhancing the certainty in the retained velocity estimates (Dehecq et al., 2015). The SNR threshold can be determined by looking at where the median absolute deviation (MAD) of velocities within stable, off-ice regions becomes asymptotic above a certain SNR threshold, in this case SNR≈6 (Figure 3.3). As the success rate (the percentage of velocity estimates within a defined area which have an SNR value greater than the SNR threshold) continues to decrease as more of the velocity field is removed for higher SNR threshold values, an SNR threshold of 6 is used.

3.3.4 Pre-Processing

To improve the performance of the feature tracking algorithm, the imagery is subject to pre-processing and image enhancement. As multiple bands of data are used, a principal component analysis (PCA) is used to reduce the redundancy in the multispectral data, enhancing the signal from the two bands into a single, uncorrelated value (Dehecq et al., 2015; Mather, 2004).

The optimum combination of spectral bands was identified by Tedstone et al., 2015; Tedstone, 2015 through running a PCA on a range of band combinations, and for each combination calculating the velocity fields and subsequently computing the success rate, defined as the percentage of velocity estimates within a given area with a signal-to-noise ratio greater than a user-defined threshold, in both on- and off-ice regions. The optimal band combination is thus defined as that which gives the highest success rate, which was found to be those covering the wavelengths of ∼0.52-0.69 μm, specifically bands 2 and 3 for Landsat 5 and 7, and bands 3 and 4 for Landsat 8 (Tedstone et al., 2015; Tedstone, 2015). The first principal component is used as it contains the largest percentage of total scene variance (Dehecq et al., 2015).

Sobel kernels are then used to compute the intensity gradients in x and y, emphasising the detailed, high-frequency components such as crevasses, and dampening

the low-frequency components such as the effects of large-scale basal topography (Dehecq et al., 2015; Mather, 2004). Features are then tracked via orientation correlation.

3.3.5 Feature Tracking

To track the displacement of surface features, the processing chain illustrated in Figure 3.2 was updated to use the Image Georectification and Feature Tracking Toolbox (ImGRAFT, Messerli and Grinsted, 2015). In feature tracking, sub-pixel precision is achieved by running the cross-correlation at coarse steps, with the resultant offset field then interpolated to a higher resolution. The interpolation scheme within the previous feature tracking toolbox (from GAMMA Remote Sensing, https://www.gamma-rs.ch/) generated aliasing towards pixel integers, whereas that within ImGRAFT did not. As such, following the pre-processing steps described in the preceding section, feature tracking is undertaken using the OC algorithm within ImGRAFT.

3.3.6 Post-Processing and Fusion

Coregistration of the processed velocity fields is required as artificial offsets as a result of georeferencing errors in the original imagery can contribute to erroneous velocities (Dehecq et al., 2015; Rosenau et al., 2015). This is particularly problematic for image pairs with a short time separation, where such artificial offsets can account for a significant fraction of the measured surface displacement between images, particularly in slow-flowing regions (Fahnestock et al., 2016). In the original processing chain, Global Land Survey (GLS) images are used reference images for coregistration of the Landsat images (Dehecq et al., 2015). However, as GLS images are not available for every path/row covering the study region, a median coregistration is applied to the output velocity fields in order to remove errors associated with georeferencing, whereby we calculate the median velocity over stable ground (where velocity should equal zero) and remove this from the calculated ice velocity at each pixel (Tedstone et al., 2015).

The coregistered velocity fields are then fused via a spatio-temporal median over annual or multi-year periods in order to exploit the redundancy offered by many overlapping image pairs to produce robust velocity outputs (Dehecq et al., 2015). Low-quality velocity estimates are removed through filtering by a threshold signal-to-noise ratio value (snr threshold = 6). For Landsat 7 and 8 data, velocities are grouped into 1- and 2-year periods, whereas for Landsat 5 data, the results into 4-year periods (as fewer pairs are available and given the difficulty in producing velocity outputs with good coverage over the southern sector of the study region). The final velocity field for each time period is composed of the median value of all velocity fields within the time period at each pixel. The median value is used as this is not sensitive to large outliers, and so can filter out the impact of any erroneous values that remained above the signal-to-noise ratio threshold. The output velocity merges are re-projected to Polar Stereographic given that the path/row combinations span several UTM zones.

This processing chain was used to produce the velocity data used within Chapter 4. Different velocity products were used within Chapters 5 and 6, however the fundamental processing concepts remain the same between them. More details regarding uncertainties, seasonality, velocity time series creation and inter-mission bias are given within Chapter 4.

3.4 Calculating multi-decadal ice velocity change within the accumulation area of the Greenland Ice Sheet

The estimation of ice velocity using feature tracking has traditionally been limited to faster flowing regions near the ice sheet margins, and so almost all of our current observations of long-term change are concentrated in this region of the ice sheet. In contrast, reported observations of ice dynamical change at distances $>\sim$50 km

from the margin have very low spatial and temporal resolution, such that our understanding of changes in the dynamics of inland regions of the ice sheet is far more limited compared to that of marginal regions. Recent advances in satellite imaging, in particular an increase in radiometric resolution, have extended the spatial extent across which ice velocities can be mapped into the ice sheet interior (Fahnestock et al., 2016; Jeong and Howat, 2015). Whilst this is not possible using older satellite imagery, it is possible to measure multi-decadal velocity change within the accumulation area through combining recent satellite-image-derived ice velocities with in-situ GPS measurements from the NASA-led PARCA project (Thomas et al., 2000; Thomas et al., 1998; Thomas, 2001).

3.4.1 The PARCA Project

The Program for Arctic Regional Climate Assessment (PARCA), which began in 1993, represents an international scientific effort to study the Greenland Ice Sheet and better understand its contributions to global sea level rise. As part of this project, a network of 161 GPS stations was set up during 1993 to circumnavigate the 2000 m elevation contour of the Greenland Ice Sheet (except for the southwest where the stakes were placed at higher elevations to avoid nunataks, mountains, and crevasses), with the aim of measuring the mass balance of the central ice sheet (Thomas et al., 2000; Thomas et al., 1998; Thomas, 2001). The GPS stations were spaced by approximately 30 km, and at each station an annual ice velocity was calculated using GPS observations recorded over a one-year return period sometime between 1993-1997, with a precision of < 0.5 m yr^{-1} and better than 0.2 m yr^{-1} in most cases (Thomas et al., 1998). In addition, measurements of surface elevation and ice thickness were collected at each station, the latter using ice penetrating radar.

The locations of the PARCA GPS sites are displayed in Figure 3.4. It should be noted that whilst the GPS sites are located at approximately the same surface elevation, there are considerable differences in the distance from their respective glacier termini, with a notable increase in distance inland in the north and

north-east.

3.4.2 NASA MEaSUREs ITS-LIVE velocities

The NASA MEaSUREs ITS-LIVE ice velocity product provides global measurements of glacier and ice sheet surface velocities at high temporal resolution and a spatial resolution of 240 m, with annual mean surface velocities produced for the years 1985-2018 from Landsat 4-8 imagery (Gardner et al., 2019). Velocity data is available for the Greenland Ice Sheet, Antarctica, Canadian High Arctic, Alaska and western North America, Iceland, Patagonia, High Mountain Asia, and Svalbard and the Russian Arctic. These velocities were processed using the JPL autonomous Repeat Image Feature Tracking (autoRIFT) processing chain (Gardner et al., 2018, 2019). Whilst the autoRIFT processing chain differs in some respects to that described in section 3.3, the fundamental principles remain the same, and so only a brief description is provided here.

Image pairs were processed for all images within the same WRS2 path-row with a time separation of <546 days and a cloud cover of <60 %. In addition, to increase the data density prior to the launch of Landsat 8 in 2013, image pairs were processed from adjacent or near-adjacent orbit swaths with a time separation of 10-96 days. Features were tracked using NCC, with the search window based upon the expected displacement for a given region. Annual velocity maps were created by taking the error-weighted average of all the image-pair velocity fields which have a centre date that falls within that calendar year. A full description of autoRIFT is provided within Gardner et al., 2018, and full documentation of the ITS-LIVE dataset are available through the following: https://its-live.jpl.nasa.gov/#documentation.

A full description of the post-processing steps applied to the ITS-LIVE and PARCA annual velocity data by which velocity change was determined is given within the methods section of Chapter 5 and so is not repeated here.

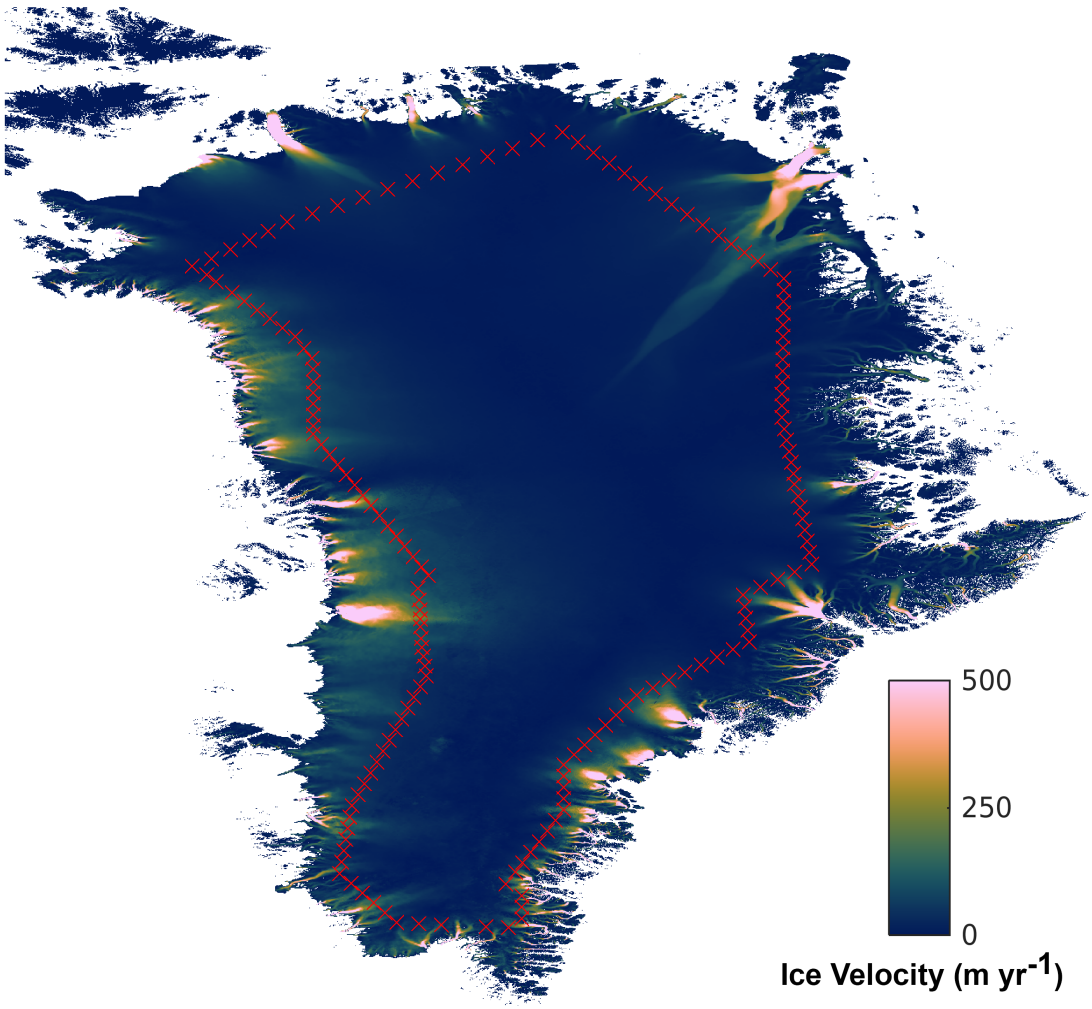

Figure 3.4: *Locations of the 161 PARCA GPS sites (red crosses) within the accumulation area of the Greenland Ice Sheet. The base image is the 2016 velocity field from the NASA MEaSUREs ITS-LIVE v0 product (Gardner et al., 2018, 2019).*

3.4.3 Estimating the Impact of Seasonality

GPS data from 1850 m (a.s.l.) in south west Greenland, during the period 2009-2012, reveal a strong seasonal velocity cycle, with summer velocities up to 8.1 % above the winter mean (Doyle et al., 2014). Whilst this sector is land-terminating as opposed to marine-terminating and thus potentially undergoing different dynamic processes, seasonal velocity variability has been observed near the margins of tidewater glaciers in Greenland (Lemos et al., 2018) and up to at least ∼70 km inland at Kangiata Nunaata Sermia in southwest Greenland (Sole et al., 2011), although it is not clear how much further inland such variability extends. Given that ice velocity is extracted at pixels with pair lengths both longer and shorter

than 365 days, it is necessary to calculate the potential impact of such seasonality on the satellite-image-derived velocities, as any disproportionate sampling of summer vs winter days may result in artificially high or low velocities.

Following previous work (i.e., Hanna et al., 2008, 2012, 2013, 2014, 2020; Hofer et al., 2017; Leeson et al., 2018; Noël et al., 2015), summer is defined as the months June, July, and August (hereafter JJA), a period spanning 91 days and making up ∼25 % of the year, with 'winter' spanning 274 days and making up ∼75 % of the year. For each GPS site, at each pixel in the 3*3 grid around the site, the centre-date and effective pair length are used to calculate the number of days in the sampling period that fall within JJA, and this is divided by the effective pair length to give a percentage of the sampling period that represents summer. A reference velocity is calculated at each pixel by taking the average velocity across the 3*3-pixel window for the period 2014-2018, and then subtracting this from the velocity at that pixel for each year (2014-2018) in turn, giving an 'adjusted velocity'. As a result, for the pixels within the 3*3 window centred on each GPS site, and for each year in the period 2014-2018, the percentage summer coverage against the adjusted velocity can be plotted to assess the impact of any seasonality. To compare across all GPS sites, the adjusted velocities are normalised through the following at each pixel as shown in equation 3.1:

$$Adjusted\,Velocity\,(\%) = \frac{Velocity_{(i,j)}\ (m\ yr^{-1}) - Reference\ Velocity_{(i,j)}\ (m\ yr^{-1})}{Reference\ Velocity_{(i,j)}\ (m\ yr^{-1})} \cdot 100 \tag{3.1}$$

When integrating the data across all GPS sites, for four of the five years (2014, 2015, 2016, 2018) there is a negative correlation between adjusted velocity and the percentage of summer coverage (Figure 3.5). Considering a larger spatial scale, for an 11*11-pixel window centred around each GPS site, the same analysis shows a similar pattern, that is, no correlation (2014, 2015) or a negative correlation (2016, 2018) for four of the five years in the study period (Figure 3.6). These trends are influenced by outliers, notably when using a small window size (3*3-pixels,

Figure 3.5), which appear to be concentrated at individual GPS sites. There is no consistent pattern with these outliers; with a window size of 3*3-pixels, in four of the five years (2014, 2015, 2016, 2018) a strong negative adjusted ice velocity with a summer coverage of 100 % is observed (Figure 3.5), whereas in 2017 the apparent positive trend may be driven by strong positive adjusted velocity at a single site with a summer coverage of ∼90 %. When more pixels are included with a larger window size (Figure 3.6), the trends are reduced, which supports the conclusion that there is no broad seasonal pattern at the PARCA GPS sites during the period 2014-2018.

This analysis is repeated, but instead of dividing by the reference velocity at each individual pixel within the 3*3-pixel window around the GPS site, it is divided by the mean reference velocity across the entire 3*3-pixel window as shown in equation 3.2:

$$Adjusted\,Velocity\,(\%) = \frac{Velocity_{(i,j)}\ (m\ yr^{-1}) - Reference\ Velocity_{mean}\ (m\ yr^{-1})}{Reference\ Velocity_{mean}\ (m\ yr^{-1})} \cdot 100 \tag{3.2}$$

Similarly, for four of the five years (2014, 2015, 2016, 2018) there exists a negative correlation between adjusted velocity and the percentage of summer coverage (Figure 3.7). With a larger 11*11-pixel window, there is either a very small negative correlation (2015, 2016, 2018) or no trend (2014, 2017) (Figure 3.8). As such, whilst there is variance between GPS sites, there is no coherent pattern showing clear evidence of seasonality in the velocity data at these elevations and so the ITS-LIVE data is not filtered by pair length.

3.4.4 Surface Mass Balance Data

In order to compare the measurements of velocity change within the accumulation zone to changes in SMB, modelled surface melt production and SMB from MAR v3.10 (Fettweis et al., 2017) are extracted from the same 3*3-pixel window around each GPS site, and mean values of each are calculated for the periods

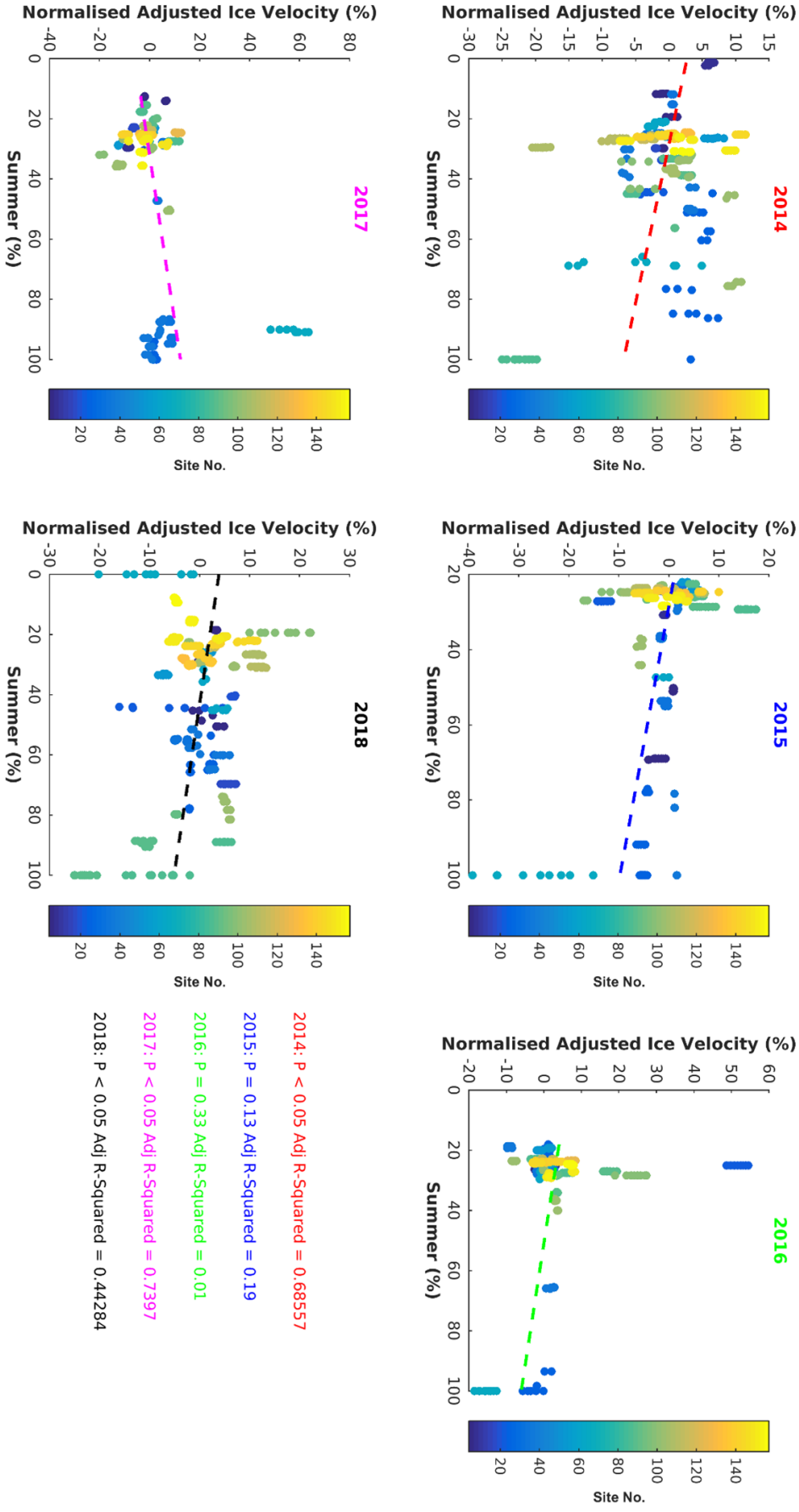

Figure 3.5: *Normalised adjusted ice velocity (%) against summer coverage (%), calculated using equation 3.1, for all pixels in a 3*3-pixel (0.72*0.72 km) window centred around each of the 45 GPS sites included in the analysis for* **(A)** *2014,* **(B)** *2015,* **(C)** *2016,* **(D)** *2017,* **(E)** *2018. The scatter points are coloured by their GPS site number. A linear model is fit to each year of data, with the p-value and adjusted R^2 displayed in the lower right. The calculation of the adjusted ice velocity and summer coverage are described in Section 3.4.3.*

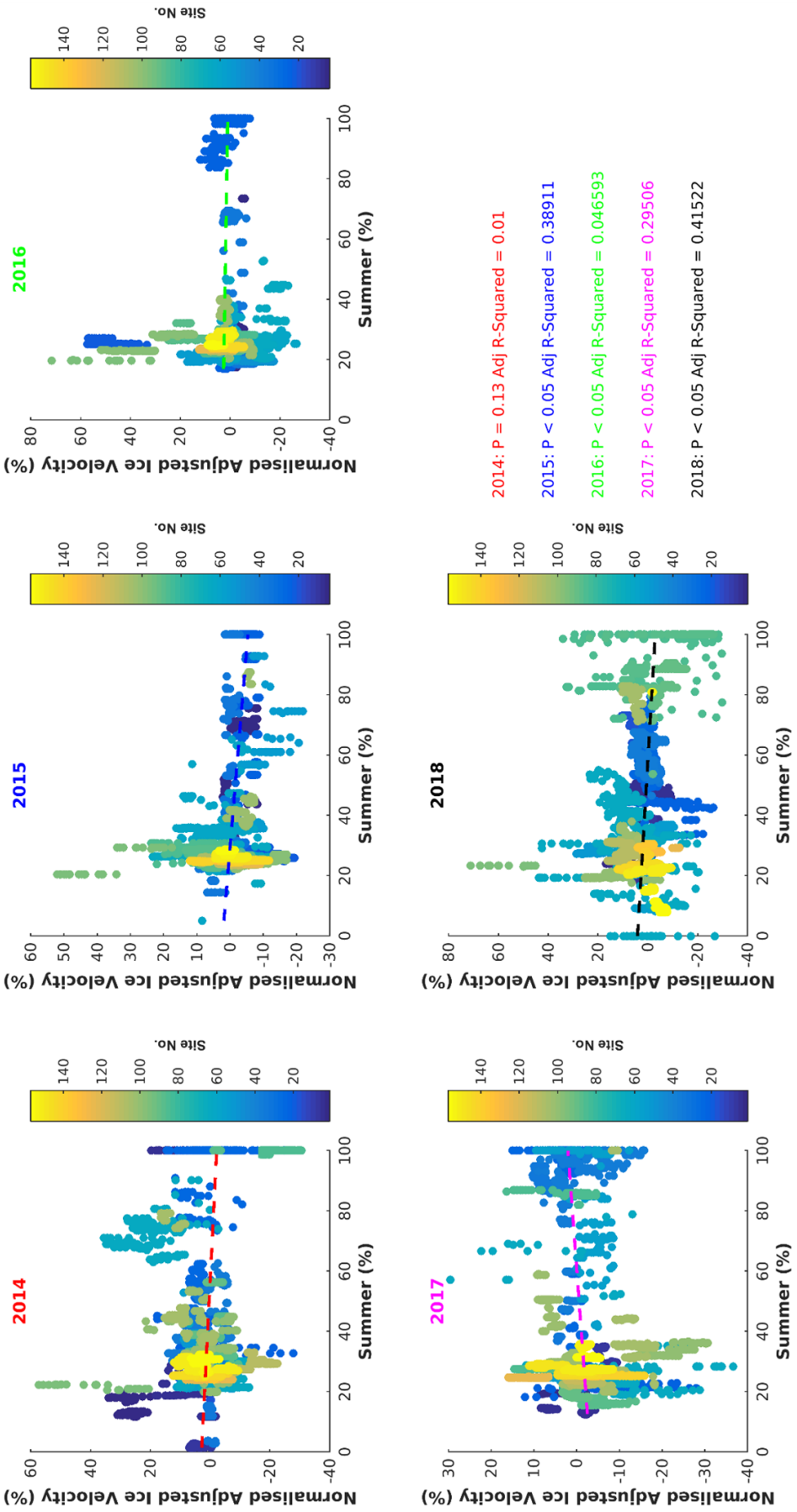

Figure 3.6: *Normalised adjusted ice velocity (%) against summer coverage (%), calculated using equation 3.1, for all pixels in a 11*11-pixel (2.64*2.64 km) window centred around each of the 45 GPS sites included in the analysis for* ***(A)*** *2014,* ***(B)*** *2015,* ***(C)*** *2016,* ***(D)*** *2017,* ***(E)*** *2018. The scatter points are coloured by their GPS site number. A linear model is fit to each year of data, with the p-value and adjusted R^2 displayed in the lower right. The calculation of the adjusted ice velocity and summer coverage are described in Section 3.4.3.*

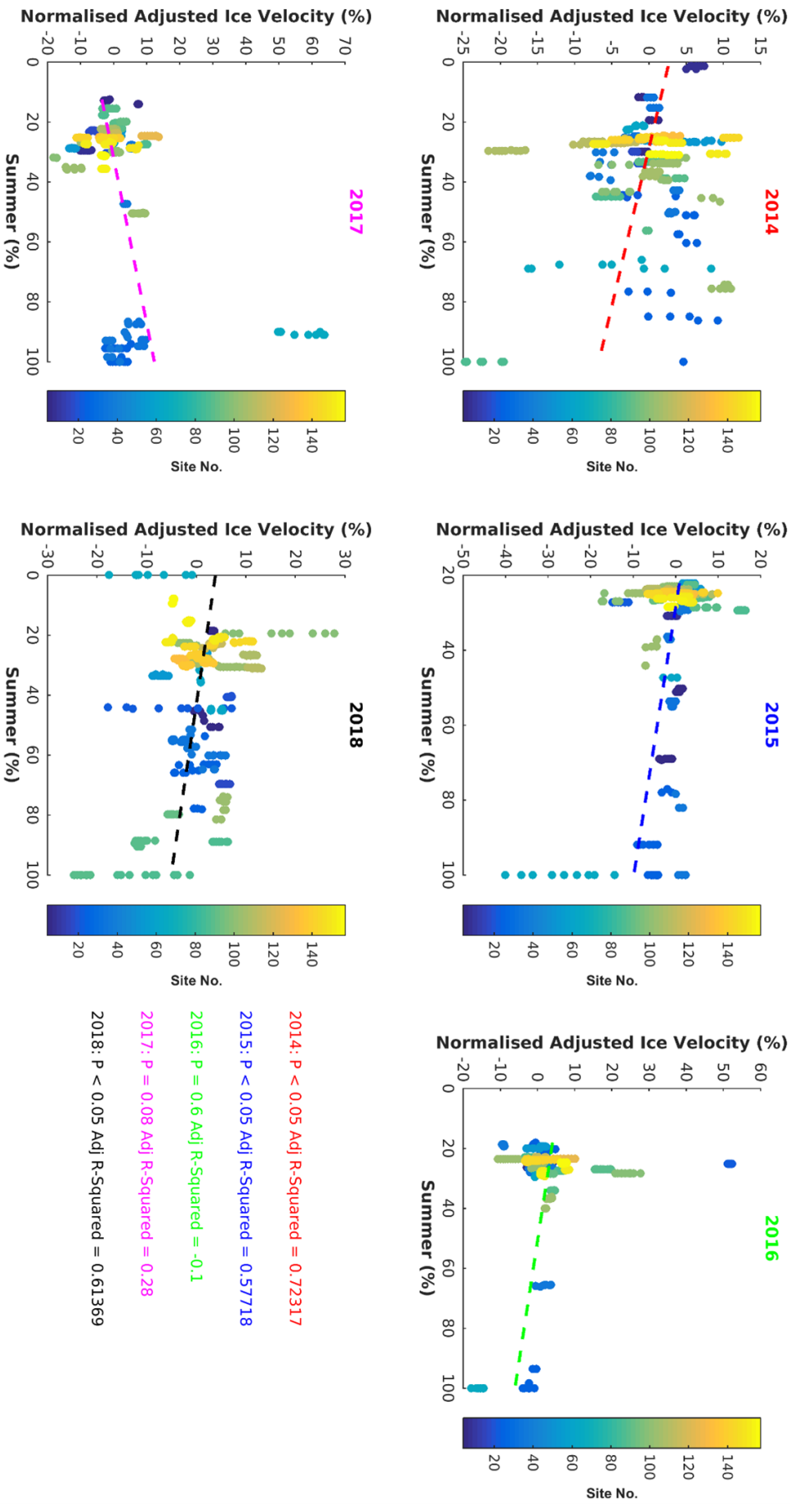

Figure 3.7: *Normalised adjusted ice velocity (%) against summer coverage (%), calculated using equation 3.2, for all pixels in a 3*3-pixel (0.72*0.72 km) window centred around each of the 45 GPS sites included in the analysis for* ***(A)*** *2014,* ***(B)*** *2015,* ***(C)*** *2016,* ***(D)*** *2017,* ***(E)*** *2018. The scatter points are coloured by their GPS site number. A linear model is fit to each year of data, with the p-value and adjusted R^2 displayed in the lower right. The calculation of the adjusted ice velocity and summer coverage are described in Section 3.4.3.*

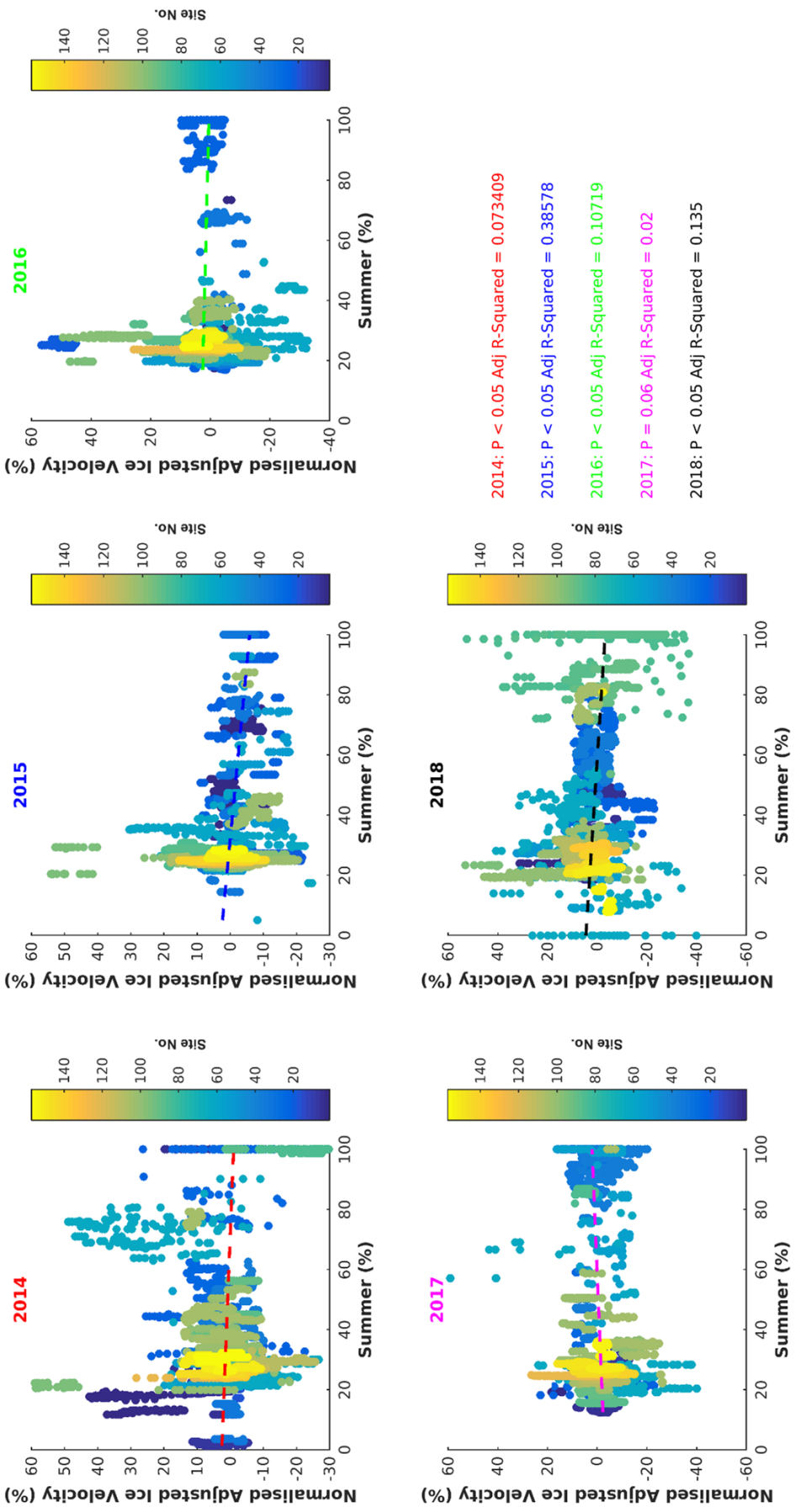

Figure 3.8: *Normalised adjusted ice velocity (%) against summer coverage (%), calculated using equation 3.2, for all pixels in a 11*11-pixel (2.64*2.64 km) window centred around each of the 45 GPS sites included in the analysis for* ***(A)*** *2014,* ***(B)*** *2015,* ***(C)*** *2016,* ***(D)*** *2017,* ***(E)*** *2018. The scatter points are coloured by their GPS site number. A linear model is fit to each year of data, with the p-value and adjusted R^2 displayed in the lower right. The calculation of the adjusted ice velocity and summer coverage are described in Section 3.4.3.*

1990-1999 and 2014-2018. These are then differenced to calculate the change in modelled melt production and SMB between the GPS and satellite velocity measurement periods.

3.4.5 Impact of changing geometry on ice velocity

To investigate whether the observations of inland velocity change presented in Chapter 5 can be supported by supported by changes in surface slope and ice thickness through their impacts upon local driving stress, the expected change in velocity as a result of changes in ice thickness and surface slope at PARCA GPS site 36, inland of Jakobshavn Isbrae, is estimated using equation 3.3:

$$\delta u_s = u_s(3\frac{\delta S}{S} + 4\frac{\delta H}{H}) \tag{3.3}$$

where u_s represents the initial ice surface velocity, S and H represent the initial surface slope and ice thickness, respectively, and δS and δH represent the change in surface slope and ice thickness, respectively.

The use of equation 3.3 assumes that velocity change is as a result of changes in internal deformation (through changes in ice thickness and surface slope) alone, with no contribution from changes in basal sliding or subglacial till deformation. This is a justifiable assumption as modelling work indicates that the propagation of terminus perturbations inland is unlikely to be caused by changes in basal lubrication (Nick et al., 2009). Instead, this work argues that acceleration leads to thinning of nearby upstream ice, steepening the glacier surface and so increasing the driving stress, with the result of further increasing acceleration and causing thinning and acceleration to propagate upstream (Nick et al., 2009). Consequently, estimating the change in ice velocity as a result of changes in ice thickness and surface slope through equation 3.3 will capture the expected velocity change associated with the inland propagation of ice flow acceleration initiated at the terminus.

3.5 Investigating dynamic change at tidewater glaciers within Sermilik Fjord, southeast Greenland

A range of remotely-sensed data and derived data products are used to investigate dynamic change at Helheim Glacier, Fenris Glacier and Midgard Glacier, which drain into Sermilik Fjord. Introductions to Landsat and Sentinel imagery are given in Sections 3.2.1 and 3.2.2 respectively, and to CryoSat-2 and ATM altimetry in Sections 3.2.3 and 3.2.4 respectively, and so are not repeated here.

3.5.1 Monthly Ice Velocity

To determine near-terminus ice velocity at a monthly resolution, the MEaSUREs Selected Glacier Site Velocity from Optical Images V3 (Howat, 2020) product is used for the period 2014 through 2019. This velocity product has a spatial resolution of 100 m and is produced from Landsat 4-8 and ASTER imagery, with the panchromatic band 8 used for Landsat-7/8, bands 2-4 for Landsat-4/5, and bands 1-3 for ASTER imagery. The most recent (V3) version of this data product uses the Surface Extraction from TIN based Search-space Minimization (SESTM) algorithm to produce ice velocities from Landsat-8 imagery, as this algorithm allows for more efficient processing of Landsat-8 OLI imagery within a high-performance computing environment (Noh and Howat, 2017). The Multi-Image Multi-Chip (MIMC) algorithm (Ahn and Howat, 2011) is used to process the data from Landsat 4-7 and ASTER, as this algorithm was specifically designed for imagery with lower bit resolution, as well as for SLC-off Landsat-7 imagery.

Site	Minimum Velocity (m yr^{-1})	AOI Coverage Threshold (%)
Helheim Glacier	3000	50
Fenris Glacier	800	20
Midgard North Glacier	1000	50

Table 3.1: Input parameters for velocity time series creation at Helheim Glacier, Fenris Glacier, and Midgard North Glacier.

At each glacier, an area of interest (AOI) is defined in the near-terminus

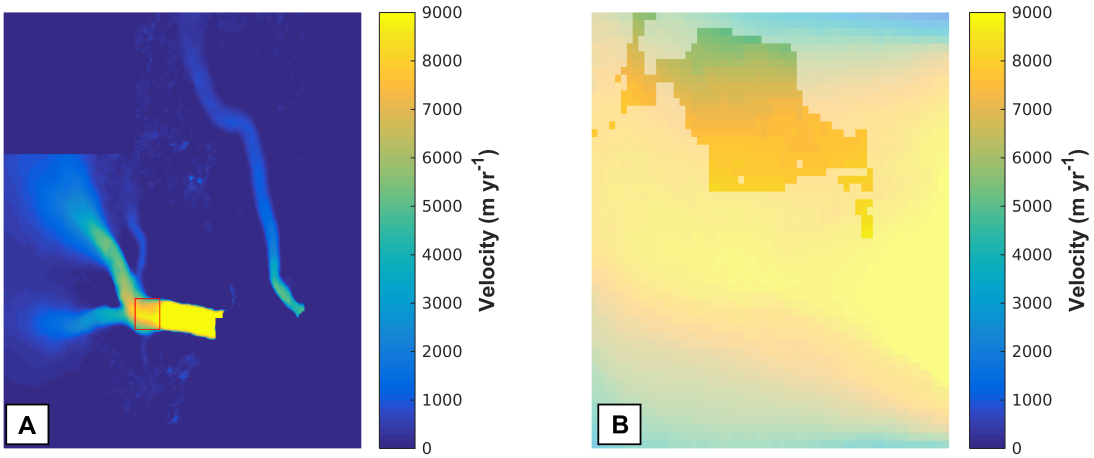

Figure 3.9: *Maps displaying the location of pixels extracted for the velocity time series of Helheim Glacier.* ***(A)*** *AOI (red rectangle) used for velocity extraction.* ***(B)*** *Pixels common to all years, displayed over a semi-transparent velocity field. The velocity data displayed is from MEaSUREs Selected Glacier Site Velocity Maps from Optical Images V3 (Howat, 2020).*

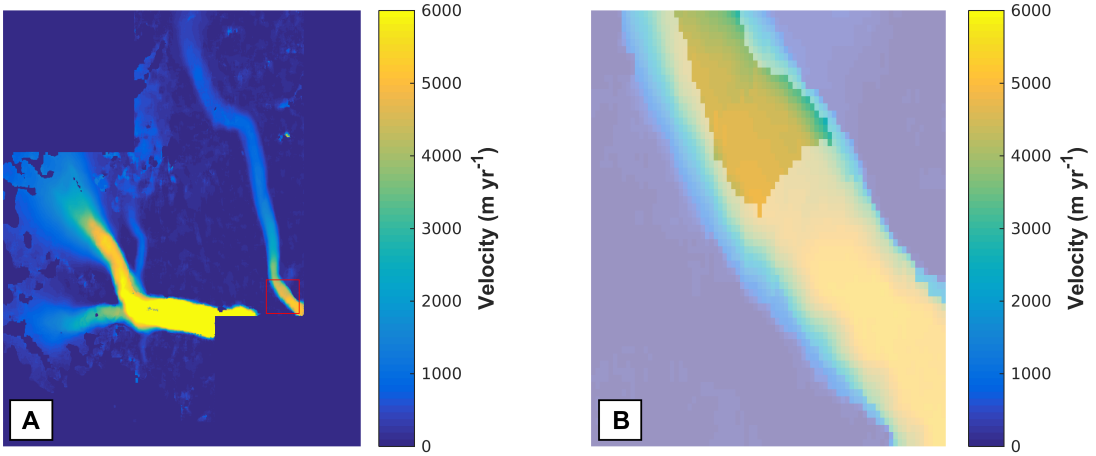

Figure 3.10: *Maps displaying the location of pixels extracted for the velocity time series of Fenris Glacier.* ***(A)*** *AOI (red rectangle) used for velocity extraction.* ***(B)*** *Pixels common to all years, displayed over a semi-transparent velocity field. The velocity data displayed is from MEaSUREs Selected Glacier Site Velocity Maps from Optical Images V3 (Howat, 2020).*

region. Within these AOI, for each month of data, pixels flowing slower than a threshold minimum velocity are removed and the month is then included in the time series should the remaining pixels cover a threshold percentage area of the AOI (parameters for each site are given in Table 3.1). The pixels common to all remaining months of data are then calculated to avoid any spatial bias, and velocity is then taken as the median velocity over the common pixels for each

month in turn. These pixels are shown for each glacier in Figures 3.9, 3.10, and 3.11. As the velocity data coverage near the front of Midgard South is poor, it is not possible to plot a velocity time series for this site.

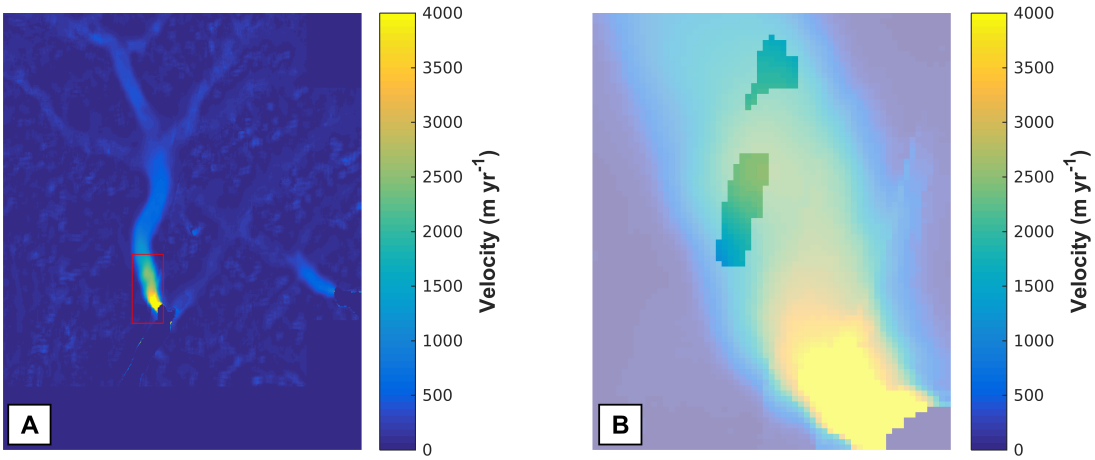

Figure 3.11: *Maps displaying the location of pixels extracted for the velocity time series of Midgard North Glacier.* ***(A)*** *AOI (red rectangle) used for velocity extraction.* ***(B)*** *Pixels common to all years, displayed over a semi-transparent velocity field. The velocity data displayed is from MEaSUREs Selected Glacier Site Velocity Maps from Optical Images V3 (Howat, 2020).*

3.5.2 Mapping Glacier Terminus Position

Terminus positions were mapped using the Google Earth Digitisation Tool (GEEDiT) (Lea, 2018) from all available Level 1T Landsat 8 Operational Land Imager (15 m resolution) and Sentinel-2 (10 m resolution) satellite imagery from 2014 through 2020. Annual terminus positions were derived from Landsat 7, Landsat 8, and Sentinel-2 imagery for the period 2000-2020 whereby images were mapped as close to August 31st as possible. The presence of proglacial ice mélange prohibited mapping for certain scenes, particularly in winter at Midgard North and South. Where multiple scenes were available for the same date, the terminus position was mapped from the Sentinel-2 scene, if available, due to the higher spatial resolution, else the terminus position was mapped from the first available image.

Changes in terminus position were assessed using the curvilinear box method

(Figure 3.12) along a glacier centreline using MaQiT (Lea, 2018), with box widths of 5 km, 1.5 km, 1 km, and 1 km used for Helheim Glacier, Fenris Glacier, Midgard North Glacier and Midgard South Glacier, respectively. This is an extension of the commonly used box method (Moon and Joughin, 2008), with the advantage that the defined box does not have to be rectilinear such that the box can follow directionally non-linear glacier flow (Lea et al., 2014; Lea, 2018). Margin change is measured by defining a box of fixed-width spanning the centreline that intersects with the margin, and subsequently dividing the area of the box by its width (Figure 3.12). This provides a more representative width-averaged measure of margin change compared to simply measuring change along an individual flowline.

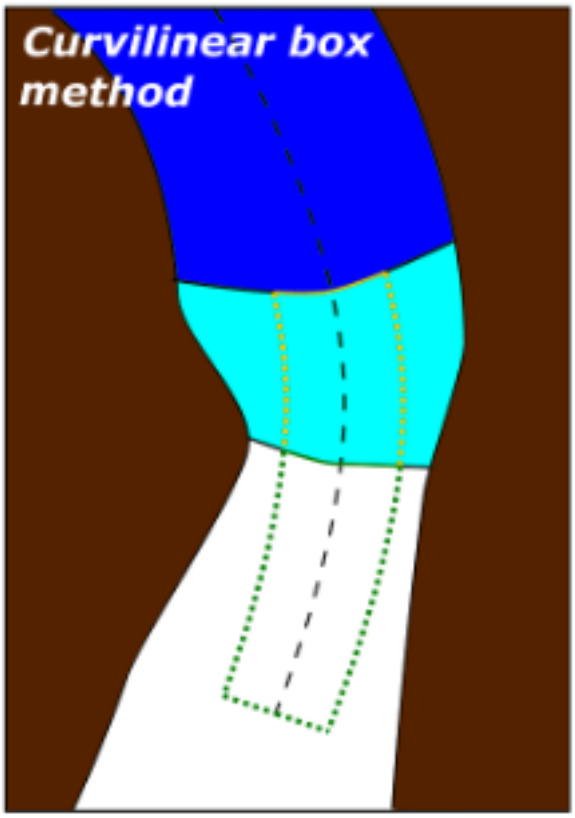

Figure 3.12: *An illustration of the curvilinear box method for margin change quantification, showing the retreat of a marine-terminating glacier with ice (white), the former glacier extent (light blue), and open water (dark blue). Adapted from Lea, 2018.*

To account for uncertainty resulting from the geolocational accuracy of the imagery, a section of coastline with Helheim Fjord was digitised for 30 scenes

for both Landsat-8 and Sentinel-2 imagery, where there should be no discernible change (Brough et al., 2019; Bunce et al., 2018). From this, root mean squared errors of ±4.8 m and ±3.1 m were estimated for Landsat-8 and Sentinel-2 imagery respectively, both of which are less than the respective pixel sizes (15 m and 10 m respectively).

3.5.3 Surface Elevation Change

Digital Elevation Models (DEMs) from the Oceans Melting Greenland L3 Glacier and Land Ice Surface Topography Interferometer airborne radar (GLISTIN-A) product (OMG, 2020) are used to assess surface elevation change for the period 2016-2019. The initial L2 data represents surface elevation measurements collected at a spatial resolution of 3 m, with a precision of <50 cm, using Ka-band (8.4 mm) radar, which limits the penetration into snow and firn and increases the interferometric accuracy. This data was then averaged into 50 m resolution bins to produce the L3 DEMs. Each data point is given an elevation quality flag which describes the data quality based upon the height above mean sea level, the standard deviation of the L2 points within the averaging bin, and the number of L2 points within the averaging bin. Low quality estimates are removed by filtering out data points where the quality flag > 0. GLISTIN-A swaths 15 and 16 are used for both Helheim and Fenris Glaciers, swath 17 is used for Midgard Glacier.

The uncertainty associated with the ATM measurements is on the order of centimetres to decimetres (Brunt et al., 2017; Krabill et al., 2002), and a comparison between ATM and GLISTIN-A elevation measurements at 16000 coincident points covering the main trunk of Jakobshavn Isbrae and surrounding slower flowing ice finds a mean difference of 0.18 m between the two datasets (standard deviation = 2.15 m), demonstrating the high accuracy of the GLISTIN-A data (Khazendar et al., 2019).

To evaluate decadal change in surface elevation at each glacier, the 2016-2019

OMG elevation data are sampled along a Pre-IceBridge Airborne Topographic Mapper (ATM) flightline over the near-terminus region (Thomas and Studinger, 2010). The sampled OMG elevation data are then compared to the ATM L2 Icessn elevation data collected along the same flightline, with these flights flown on 19/05/2005 at Helheim Glacier, 11/05/2007 at Fenris Glacier and Midgard South Glacier, and 31/07/2008 at Midgard North Glacier. Both GLISTIN-A and ATM L2 Icessn elevation measurements are referenced to mean sea level by subtracting the GOCO05c geoid (Fecher et al., 2017).

3.5.4 Regional Surface Elevation Change from CryoSat-2 Radar Altimetry

For each of the three glaciers studied, regional surface elevation change estimates are generated using CryoSat-2 radar altimetry for the period 2010-2020. As introduced in section 3.2.3, swath altimetry with CryoSat-2 provides up to two orders of magnitude more surface elevation measurements than traditional POCA altimeters (Foresta et al., 2016, 2018; Gourmelen et al., 2018). Moreover, as swath processing does not rely on retracking, it can measure surface elevation even with atypical waveforms without a clearly defined leading edge, for example in regions characterised by complex terrain (Jakob et al., 2021). As a result, CryoSat-2 is currently the only radar altimeter that is able to measure surface elevation change at high resolution for glaciers (Jakob et al., 2021).

There are, however, uncertainties that can affect surface elevation measurements from CryoSat-2. For example, the formation of refrozen ice layers associated with exceptional surface melting events causes a vertical rise in the reflective surface within the snowpack, introducing a positive elevation bias (Nilsson et al., 2015). During August-September 2012 (following the exceptional July 2012 melt event), this bias resulted in an apparent elevation increase of 56±26 cm in the area of the North Greenland Eemian Ice Drilling Project, located within the accumulation zone in northwest Greenland (Nilsson et al., 2015). In addition, CryoSat-2

elevation measurements can be biased on a seasonal timescale due to the impacts of winter accumulation (Gray et al., 2019). Within the southeast Greenland periphery, winter snowfall can reach 2-3 m over the course of the season. This accumulation, and associated firn compaction, results in the strongly-reflecting melt layer from the previous summer sinking downwards, resulting in an apparent decrease in elevation on the order of 2 m (Gray et al., 2019). This is also impacted by the presence of the overlying dry snow, which acts to slow the radar waves, contributing to the apparent decrease in the measured surface height (Gray et al., 2019).

Despite such uncertainties, over most regions, surface elevation change measurements from CryoSat-2 over annual and multi-annual timescales are consistent with in-situ, airborne and meteorological observations (Gourmelen et al., 2018; Gray et al., 2015; Gray et al., 2019; Jakob et al., 2021; McMillan et al., 2014a). Moreover, the elevation changes measured in Chapter 6 are on the order of 10-20 metres over a multi-annual time period, and thus it is unlikely that the uncertainty sources presented in the preceding paragraph are significant enough to affect the interpretation of the results.

3.5.5 Ocean and Atmospheric Forcing

3.5.6 Additional Data

In addition to the data and methods described in the preceding subsections, the following were also undertaken, however as they are described in detail within Chapter 6, such detail is not repeated here:

- Bed topography and ice thickness data were extracted from BedMachineV3 (Morlighem et al., 2017) and from these a flotation elevation was calculated.
- Submarine melting and subglacial discharge are derived as in Slater et al., 2019b.
- Air temperature was measured at the Tasiilaq meteorological station located

near the mouth of Sermilik Fjord (65.615°N, 37.637°W, Cappelen et al., 2020).

Chapter 4

Dynamic response of the Greenland ice sheet to recent cooling

The subglacial hydrological system exerts an important control on ice motion through its evolution in response to surface meltwater inputs. Within the southwest land-terminating region of the ice sheet, early work suggested that ice motion would scale positively with surface melting (Zwally et al., 2002). However, it has been shown more recently that a long-term increase in surface melting drives a slowdown in ice motion over multi-annual timescales (Stevens et al., 2016; Tedstone et al., 2015). Since the extreme melt experienced in 2012, the southwest land-terminating sector has cooled and surface meltwater production has decreased (Hanna et al., 2020), and it remains unclear whether the resultant evolution of the subglacial hydrological system has impacted regional ice motion. This chapter applies feature tracking to the entire Landsat archive across this sector of the ice sheet, an area of approximately 10,600 km^2, between 1985 and 2019 in order to assess the long-term response of ice motion to surface melt forcing and, in particular, to the reduced surface melt forcing from 2013 to 2019. The results are limited to the ablation zone, which motivates the work presented in Chapter 5 whereby multi-decadal changes in ice dynamics are investigated across the accumulation zone of the Greenland Ice Sheet.

This chapter was published in *Scientific Reports* in February 2020.

Authors: Joshua J. Williams[1], Noel Gourmelen[1] and Peter Nienow[1]

1. School of Geosciences, University of Edinburgh, Edinburgh, EH8 9XP, UK

Citation: Williams, J.J.[1], Gourmelen, N.[1] and Nienow, P.[1] (2020) Dynamic response of the Greenland Ice Sheet to recent cooling, *Scientific Reports*, **10**, 1647. DOI: https://doi.org/10.1038/s41598-020-58355-2

Author contributions: JJW performed all of the data processing and analyses. All authors contributed to the design of the study and the writing of the paper.

Acknowledgements: J.J.W. and P.N. were funded by a UK Natural Environment Research Council (NERC) doctoral training partnership grant (NE/L002558/1). N.G was funded by ESA grants Dragon10302 and Dragon32437. The Landsat imagery was provided by the United States Geological Survey and the European Space Agency third party missions program. Dr. Xavier Fettweis provided the MAR v3.10 SMB data.

4.1 Abstract

The subglacial hydrological system critically controls ice motion at the margins of the Greenland Ice Sheet. However, over multi-annual timescales, the net impact of hydro-dynamic coupling on ice motion remains poorly understood. Here, we present annual ice velocities from 1992-2019 across a $\sim 10,600$ km^2 land-terminating area of southwest Greenland. From the early-2000s through to $\sim$ 2012, we observe a slowdown in ice motion in response to increased surface melt, consistent with previous research. From 2013 to 2019 however, we observe an acceleration in ice motion coincident with atmospheric cooling and a ~ 15 % reduction in mean surface melt production relative to 2003-2012. We find that ice velocity speed-up is greater in marginal areas, and is strongly correlated with ice thickness. We hypothesise that under thinner ice, increases in basal water pressure offset a larger proportion of the ice overburden pressure, leading to reduced effective pressure and thus greater acceleration when compared to thicker ice further inland. Our findings indicate that hydro-dynamic coupling provides the major control on changes in ice motion across the ablation zone of land terminating margins of the Greenland Ice Sheet over multi-annual timescales.

4.2 Introduction

The Greenland Ice Sheet (GrIS) has lost mass at an accelerating rate over the past two decades, with persistent mass loss observed since 1998 (Hanna et al., 2013; Mouginot et al., 2019; Rignot et al., 2011; Shepherd et al., 2012; van den Broeke et al., 2016). Approximately 52 % of this mass loss can be attributed to surface melt (Shepherd et al., 2019), which increased in the late 2000s and early 2010s to levels unprecedented since at least 1900 (Fettweis et al., 2017). Increases in surface melt have been driven by increasing air temperatures over Greenland since the mid-1980s (Cappelen et al., 2017; Fettweis et al., 2017) and variability in cloud cover, both of which are forced by larger scale circulation patterns (Fettweis et al., 2013; Hanna et al., 2016; Hofer et al., 2019; Nghiem et al., 2012; Serreze and Barry, 2011). Increased cloud-cover warms the ice sheet interior through the

trapping of longwave radiation (Cullather et al., 2018; Van Tricht et al., 2016), whereas a reduction in summer cloud cover since 1995 has driven enhanced melt in the ablation zone through increasing the shortwave flux (Hofer et al., 2017, 2019). Moreover, the seasonal migration of the snowline causes the exposure of dark bare-ice, decreasing the albedo of the ice surface and reducing meltwater re-freezing, further driving surface melt and runoff (Ryan et al., 2019). Alongside changes in surface mass balance, roughly 48 % of mass loss is due to increases in ice discharge through Greenland's marine terminating outlet glaciers (Shepherd et al., 2019). However, the dynamic response of the ice sheet to variability in surface mass balance and ocean conditions remains a large source of uncertainty in projecting future sea level rise (IPCC, 2013).

Land-terminating margins are isolated from processes acting at the ice/ocean boundary, and thus provide ideal study sites for investigating how the ice-sheet responds to atmospheric, and thus surface melt forcing (Fitzpatrick et al., 2013; Lindbäck et al., 2014). This is particularly prescient as the largely land-terminating margin in South West Greenland exhibits a strong and sustained negative mass balance (Andersen et al., 2015; van den Broeke et al., 2009), and is projected to make a greater contribution to sea level rise with continued atmospheric warming and associated increases in surface runoff (Tedesco and Fettweis, 2012).

Each summer, surface meltwaters drain from the ice-sheet surface to the bed via moulins and crevasses (Andrews et al., 2014; Chandler et al., 2013; Das et al., 2008; van der Veen, 2007) where their impact on friction at the ice-bed interface is fundamentally important in controlling ice velocity (Fountain and Walder, 1998; Iken and Bindschadler, 1986). Whilst initial research postulated that as these seasonal meltwaters drain to the base of the ice sheet, they would pressurise the basal hydrological system, reduce friction at the bed and so enhance glacier sliding (Zwally et al., 2002), other studies have argued that variability in meltwater input, rather than the volume itself, is more critical for driving ice acceleration (Bartholomaus et al., 2008; Schoof, 2010).

Both short-term and sustained increases in surface meltwater delivery to the glacier bed drive an increase in basal water pressure above the ice overburden pressure, reducing friction at the bed and so forcing a transient acceleration (Bartholomew et al., 2010, 2011b; Schoof, 2010). These inputs force a morphological switch from an inefficient, distributed subglacial drainage system to an efficient, channelised system when and where subglacial discharge is sufficiently turbulent to open subglacial channels (Bingham et al., 2005; Chandler et al., 2013; Kamb, 1987; Schoof, 2010). This introduces a negative feedback whereby as the drainage system capacity increases in response to enhanced meltwater input, basal water pressures decrease as subglacial channels allow the efficient evacuation of subglacial water (Chandler et al., 2013; Tedstone et al., 2013), forcing a deceleration of the ice later in the melt season (Andrews et al., 2014; Nienow et al., 2017; Schoof, 2010).

More recently, research has focused on whether this hydro-dynamical coupling of ice flow at land-terminating margins results in a long-term trend in ice-motion in response to long-term increases in surface melt (Hoffman et al., 2016; Tedstone et al., 2015). Multi-annual ice velocity slowdowns in southwest Greenland since the early-mid 2000s have been reported by numerous studies based on both GPS data (Stevens et al., 2016; van de Wal et al., 2008, 2015) and large-scale satellite-derived observations (Joughin et al., 2018; Tedstone et al., 2015). Ice velocities from GPS stations along a transect in Southwest Greenland, extending $\sim$150 km inland from the margin between surface elevations of 340 m and 1850 m above sea level (a.s.l), show a 10 % average slowdown from 1991-2007 (van de Wal et al., 2008, 2015), coincident with increasing surface melt, and GPS data at North Lake show a slowdown of -0.9 $\pm$ 1.1 m yr^{-2} from 2006-2014 (Stevens et al., 2016). Over a much larger 8000 km^2 region of Southwest Greenland, Tedstone et al., 2015 showed that ice velocity had decreased by 12 % in 2007-14 compared to 1985-94, despite a 50 % increase in surface meltwater production, with ice velocity decreasing by 1.5 m yr^{-2} between 2002 and 2014. This long-term

slowdown is attributed to the expansion of subglacial channels, both up-glacier and in their dimensions, as a result of the long-term increase in surface melt, enhancing the drainage of waters from the more extensive distributed component of the subglacial drainage system, thus reducing regional basal water pressures and so ice velocities (Nienow et al., 2017; Tedstone et al., 2015). The distributed component of the subglacial drainage system encompasses varying degrees of connectivity, and it is hypothesised that the reduction of basal water pressures in the weakly-connected areas of the drainage system specifically (Andrews et al., 2014; Hoffman et al., 2016) are critical to the observed slow-down as their recharge is slow (on the order of years (Hoffman et al., 2016)), resulting in widespread and extended depressurisation and so increased basal traction.

Since the record surface melt in 2012 (Hanna et al., 2013), a period of relative stability in mass balance (Bevis, 2019) has been observed across Greenland, with 2017 having the lowest maximum surface melt extent since 1996 (Tedesco et al., 2017). This stability is coincident with positive Arctic and North Atlantic Oscillations, promoting cyclonic conditions thereby reducing incoming solar radiation and enhancing precipitation (Tedesco et al., 2017). Given that the proposed hydro-dynamic mechanism for a long-term velocity slowdown requires a continual increase in surface melt (Hoffman et al., 2016; Tedstone et al., 2015), it would be expected that ice motion would respond to a sustained change in surface run-off and begin to stabilise or accelerate as surface melt decreases and the distributed subglacial hydrological system re-pressurises. Under reduced surface melt forcing, we would expect the up-glacier extent of efficient subglacial channels to decrease, allowing regions of the distributed drainage system that were, in previous years, drained by efficient channels to re-pressurise through the gradual recharge of meltwater via basal melting. Numerous GPS data show that this process occurs on a seasonal timescale, whereby following the deceleration of ice motion to a minimum in the late melt season, measured ice velocities show a gradual increase over the following winter (Joughin et al., 2008b; Sole et al., 2013; van de Wal et al., 2015); this process has not however been observed to-date on a multi-annual

timescale. This study therefore extends the West Greenland ice velocity time series, both spatially and temporally, in order to investigate how ice motion has responded to recent reductions in surface melt forcing, with the ultimate aim of improving our understanding of the mechanisms driving ice sheet motion.

Here we present observations of ice velocity from 1992-2019 across a predominantly land-terminating area of $\sim 10,600$ km^2 in SW Greenland, extending ~ 300 km along the margin and ~ 50 km inland to an elevation of 1300 m. Our study region is considerably larger than that of Tedstone et al., 2015, extending a further ~ 120 km to the south. We apply feature tracking to 2665 pairs of Landsat scenes, separated by 352-384 days, over 14 path/row combinations. Subsequently, we derive robust ice velocity and uncertainty estimates for periods of 1, 2 and 4 years to construct a time series from 1992 to 2019, and assess the spatial distribution of velocity change between 1992-2003 and 2003-2012, and 2010-2012 and 2017-2019. Finally, we assess the implications of our results for future land-terminating ice-sheet motion in a warming climate in light of the dynamic response of the study region to the recent variability in meltwater forcing.

4.3 Results

4.3.1 Spatial Pattern of Velocity Change

Ice velocity displays a clear slowdown across the study site (Figure 4.1A) between the periods 1992-2003 and 2003-2012, with 93.1 % (9895 km^2) of the region exhibiting reduced velocity in the latter period, and a mean regional slowdown of ~ 15.3 % (Figure 4.2A).

The slowdown is greatest at lower ice thicknesses and decreases in magnitude inland as surface elevation and ice thickness increase (Figure 4.2C), although deceleration characterises all ice thicknesses assessed and extends further inland than in previous work (Tedstone et al., 2015). We would expect this to be the case as at higher elevations further inland, lower surface melt rates, thicker ice

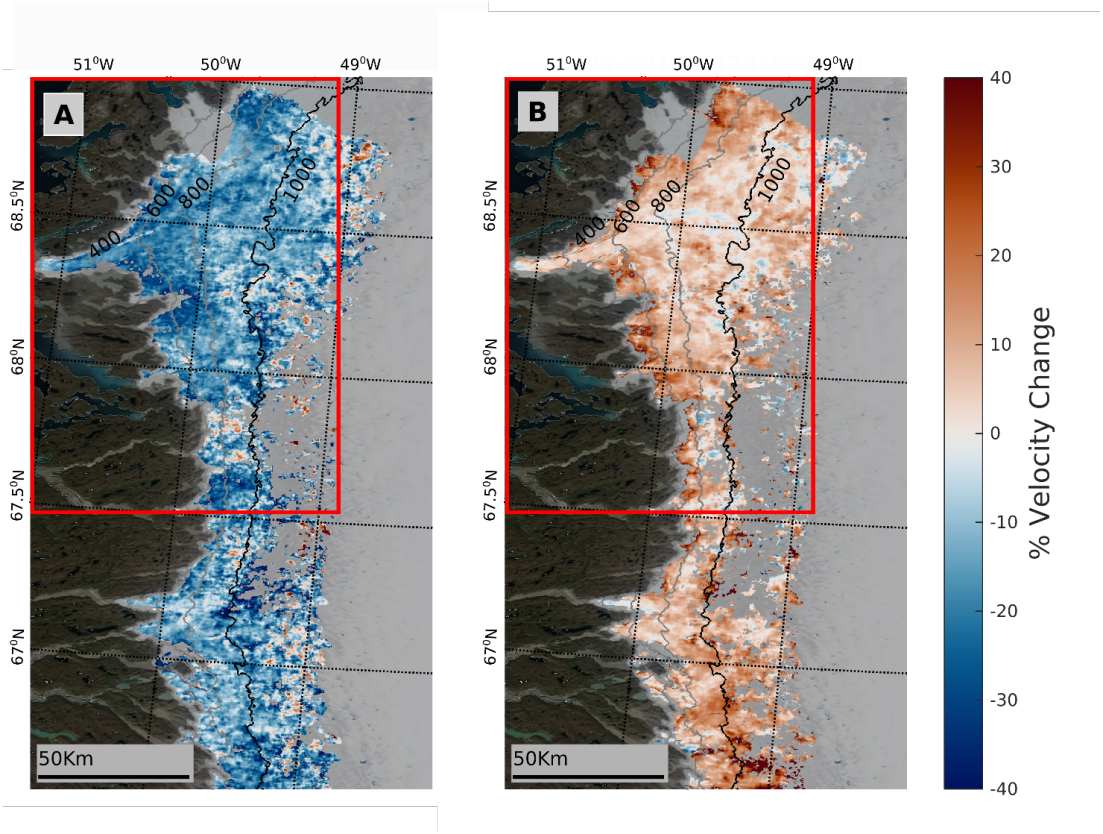

Figure 4.1: *Spatial change in ice velocity (%) between the* ***(A)*** *2003-2012 and 1992-2003 and* ***(B)*** *2017-2019 and 2010-2012 reference periods. Data above 1300 m (a.s.l.) are filtered out in order to remove spurious points that characterise higher elevations. The red rectangle denotes the region studied in Tedstone et al., 2015. Ice surface elevation contours (grey lines) are from Howat et al., 2014, with the 1000 m contour bold to make clear the area across which the velocity time series was calculated (Figure 4.3). The two tidewater glaciers to the north of the study region are masked out as they are undergoing different dynamic processes to the rest of the region. The base image is a MODIS (Terra) corrected reflectance image from EOSDIS NASA Worldview (https://worldview.earthdata.nasa.gov/).*

and shallower surface slopes slow channel growth, allowing subglacial water pressures to remain higher in smaller subglacial channels (Chandler et al., 2013; Dow et al., 2014; Meierbachtol et al., 2013b).

Subsequently, we observe a mean region-wide acceleration of ~7.9 % between the periods 2010-2012 and 2017-2019 (Figure 4.1B), with 89.6 % (8218 km^2) of this second change map exhibiting increased velocity during the latter period (Figure 4.2B). This acceleration in ice motion is proportionally largest at lower ice thicknesses and decreases as ice thickness increases but is observed across all

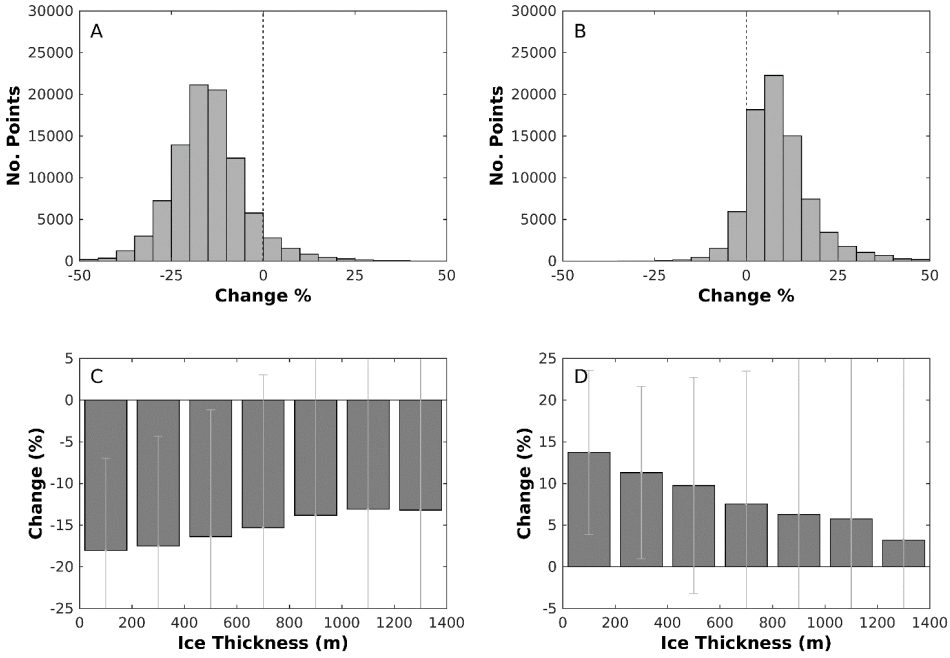

Figure 4.2: *Histogram of ice velocity change across the study region and percentage change across ice thicknesses for the two changemaps displayed in Figure 4.1. Plots A and C relate to Figure 4.1A (2003/2012 – 1992/2003), and plots B and D relate to Figure 4.1B (2017/2019 – 2010/2012).* ***(A)*** *Percentage change in ice velocities across the region displayed in Figure 4.1A in 5 % bins.* ***(B)*** *Percentage change in ice velocities across the region displayed in Figure 4.1B in 5 % bins.* ***(C)*** *Median percentage change in each 200 m ice thickness band between 0 m and 1400 m for the changemap displayed in Figure 4.1A.* ***(D)*** *Median percentage change in each 200 m ice thickness band between 0 m and 1400 m for the changemap displayed in Figure 4.1B. The error bars display the interquartile range. Ice surface elevation data is from Howat et al., 2014, and ice thickness data are from Morlighem et al., 2017.*

ice thicknesses studied (Figure 4.2D).

4.3.2 Ice Velocity and Surface Melt/Runoff Time Series

To investigate changes in ice motion (Figure 4.3A), we follow recent work by assessing anomalies in annual velocity (see Section 4.4.2) whereby only pixels common to all the velocity fields presented in the time series are used in the computation of the median velocity anomalies (Dehecq et al., 2019). Most of the common points fall between 600 m and 1000 m elevation (a.s.l.) due to the hypsometry of our study region (Figure 4.4), although we observe >50 % coverage in each 100 m elevation band between 100 m and 900 m. In total, we compute

velocity anomalies across 71703 common measurements (4130 km^2), an order of magnitude greater than previous work (Tedstone et al., 2015, their Figure 2C).

Over the time period from 1992 to 2019, the ice velocity anomaly time series reveals a mean slowdown of -0.72 $\pm$ 0.08 m yr^{-2} (R^2 = 0.70, p $<$ 0.01). The quality of the fit is further improved via break point analysis (see Section 4.4.2) which recognises three statistically distinct periods based on the pattern of velocity changes (R^2 = 0.85 (Fig. 4.3A)). Between 1992 and 2003, we observe a period exhibiting no significant trend (-0.03 $\pm$ 0.23 m yr^{-2}, p = 0.69). A substantial slowdown of -1.64 $\pm$ 0.37 m yr^{-2} (p $<$ 0.01), starting around 2003 (but which could range from 2002-2004 due to a gap in our data), occurs until 2012, after which the most recent period of ice motion exhibits a significant increasing trend (0.58 $\pm$ 0.37 m yr^{-2}, p $<$ 0.05).

We use the regional climate model MAR v3.10 (Fettweis et al., 2013; Fettweis et al., 2017) to calculate the mean surface melt production anomaly during the three distinct periods identified in our ice velocity anomaly time series; 1992-2003, 2003-2012, and 2012-2019 (Figure 4.3B). Mean surface melt production anomalies across our study region rose by $\sim$30 % from -0.18 m yr^{-1} to 0.45 m yr^{-1} (w.e.) ($\sim$2.15 m yr^{-1} to $\sim$2.77 m yr^{-1} (w.e.)) between 1992-2003 and 2003-2012.

Following this period of sustained higher surface melt production, a $\sim$ 15 % decrease to 0.06 m yr^{-1} ($\sim$2.39 m yr^{-1}) is observed for 2012-2019, when compared to the 2003-2012 mean. The period of ice velocity decrease therefore coincides with a period of enhanced ice surface melt, while rates of constant and accelerating ice velocity occur during periods of lower surface melt.

Previous work has argued that there is a significant relationship between antecedent surface melt production and ice velocity (Tedstone et al., 2015). More recent work however suggests that this may be a statistical construct (Stevens et al., 2016), whereby as more antecedent melt years are included in the average

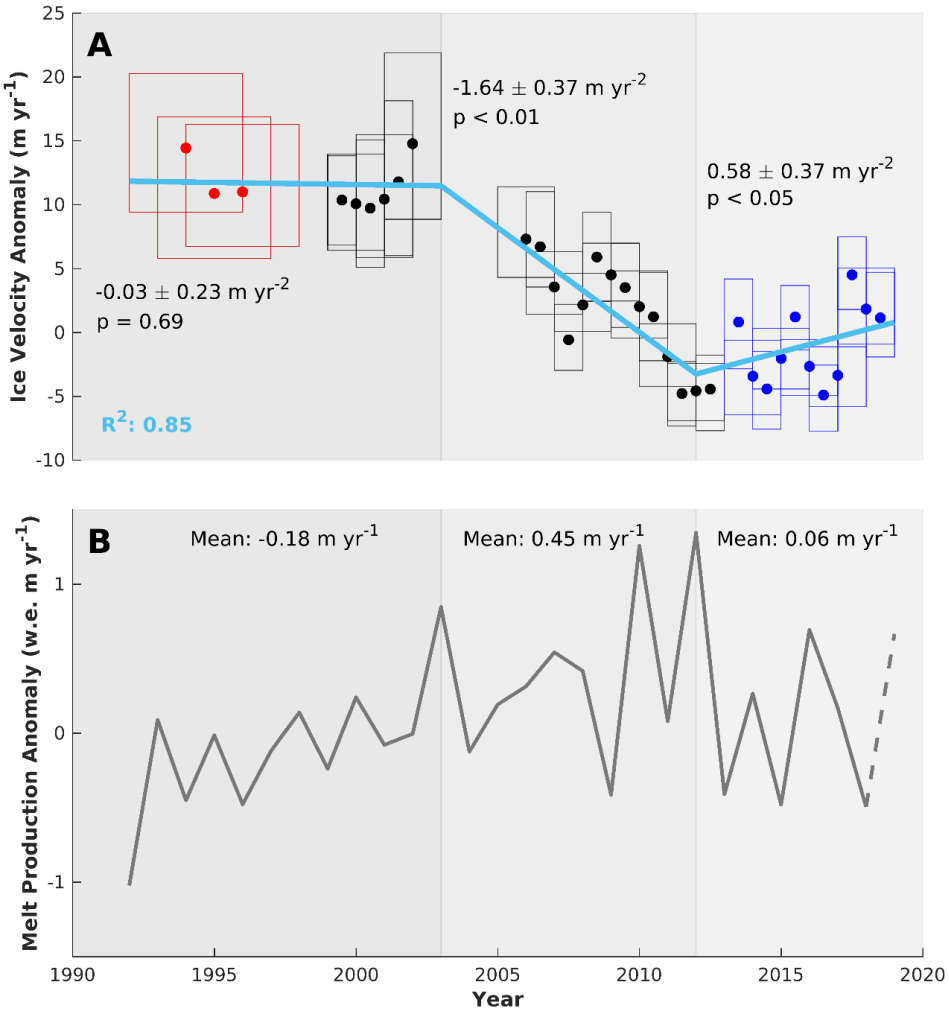

Figure 4.3: ***(A)*** *Median ice velocity anomalies (m yr^{-1}) during each period calculated by sampling the common pixels between all velocity fields in the times series. Red boxes indicate Landsat 5 data, black boxes indicate Landsat 7 data, and blue boxes indicate Landsat 8 data. The width of each box corresponds to the total time period of the pairs in Landsat scenes fused for each period. The height of each box corresponds to the interquartile range and the light blue line displays the trends in ice velocity computed by a segmented linear regression (see Section 4.4.2).* ***(B)*** *Annual modelled surface melt production anomaly (grey) (Fettweis et al., 2017) in water equivalent (w.e.) m yr^{-1} (see Section 4.4.6). A dotted line is used to display the data for 2019 as this is currently incomplete. The background shades are used to differentiate the three distinct periods of dynamic behaviour.*

value, R^2 tends further towards 1 (Figure 4.15) as the data becomes increasingly smoothed and the individual points become less independent. With only one period of sustained slowdown, we are unable to test whether ice velocity slowdown is in response to a gradual increase in surface melt or to the passing of some surface melt threshold. Moreover, the response times of ice velocity to increases and de-

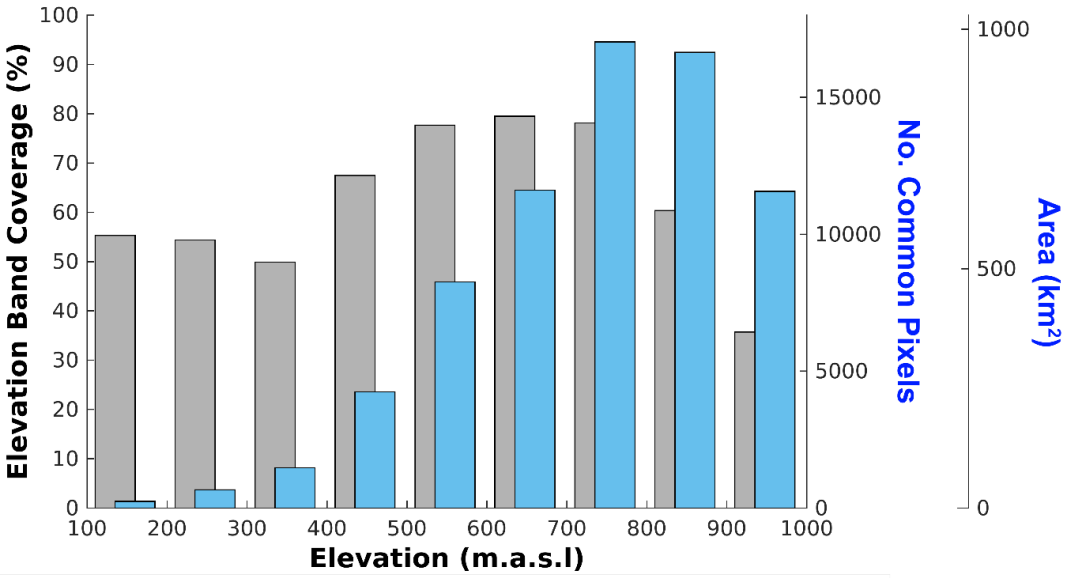

Figure 4.4: *Percentage coverage of each 100 m elevation band by common sampling pixels (grey, left axis) and the altitudinal distribution in the common sampling pixels used in the computation of median ice velocities (blue, right axes).*

creases in surface melt forcing appear to differ – surface melt displays a long-term increasing trend from the early-mid 1990s before ice velocities begin to decrease in $\sim$ 2003, whereas ice velocities stabilise and begin accelerating almost instantly in response to the large reduction in surface melt forcing from 2013 onwards. To investigate the impact of year-to-year variability in surface melt production on year-to-year velocity, we calculate a linear regression through detrended velocity and melt production anomaly time series (Figure 4.16), which gives an R^2 of 0.08 ($p = 0.11$), indicating that there is no significant relationship between annual ice velocity and annual runoff, consistent with earlier work (Sole et al., 2013; Stevens et al., 2016; van de Wal et al., 2015).

4.3.3 Discussion

Changes in ice thickness and surface gradient can contribute to changes in ice motion through their associated impacts on driving stress. Thinning at the margins of the Greenland Ice Sheet has been observed since the early 1990s (Shepherd et al., 2012), and from 1992-1998, the southwest Greenland land-terminating sector thinned by $\sim 0.02 - 0.4$ m yr^{-1} (Sandberg Sørensen et al., 2018; Sole et al.,

2008). A period of stability characterised the late 1990s and early to mid-2000s (Sandberg Sørensen et al., 2018), followed by rapid thinning ($\sim 1 - 1.5$ m yr^{-1}). Whilst some datasets assume a constant thinning of a similar magnitude through to 2014 (Helm et al., 2014), recent work points to a maximum thinning rate in 2012, after which thinning has continued at a more moderate rate (McMillan et al., 2016), albeit with differences in thinning trends between drainage basins (Nilsson et al., 2016; Sandberg Sørensen et al., 2018). Prior modelling work in our study region (Tedstone et al., 2015) indicates that changes in driving stress due to thinning could only explain 17-33 % of the slowdown signal beyond 10 km from the ice-margin, and none of the signal beyond 50 km. This modelling work applied 20 m of thinning over 30 years, equating to a thinning rate of -0.66 m yr^{-1}. Outside of the period 2007-2011, there is no evidence for thinning rates greater than this during our study period (Helm et al., 2014; Pritchard et al., 2009; Sandberg Sørensen et al., 2018; Sole et al., 2008), and we thus do not believe that thinning rates could be responsible for more slowdown than already reported in Tedstone et al., 2015. Moreover, continued thinning from 2012 would be expected to continue to reduce ice motion, which contrasts with the acceleration in ice velocity observed during this period. As such, these findings imply that most of the ice velocity signal is controlled by processes operating at the ice-bed interface.

The subglacial hydrological system exerts a critical control on ice motion at land-terminating margins of the Greenland Ice Sheet (Chu, 2014; Nienow et al., 2017). Our results provide support for a previously postulated mechanism (Tedstone et al., 2015), whereby under a sustained multi-annual increase in surface meltwater production, the subglacial drainage system is characterised by both a gradual increase in the extent of channelisation, as well as the time during which these channels remain open and are thus able to evacuate water from the surrounding distributed drainage system (Hubbard et al., 1995). These conditions promote the drainage of waters from weakly-connected (Hoffman et al., 2016) regions of the distributed drainage system, thereby reducing basal water pressure and associated basal lubrication and hence ice velocity over longer (decadal) timescales

as effective pressures increase. Whilst it is hypothesised that increasing runoff to the bed will increase sediment pore water pressure, resulting in reduced sediment shear strength, increased sediment deformation and thus enhanced ice flow (Kulessa et al., 2017), such behaviour contrasts with the observations reported here and elsewhere (Joughin et al., 2018; Tedstone et al., 2015; van de Wal et al., 2008, 2015). Consequently, our results suggest either that extensive layers of subglacial till are not ubiquitous across our study region or if they are present, the tills have not deformed pervasively in response to the sustained period of enhanced meltwater input.

Surface melt production in our study region peaks in 2012, decreasing thereafter (although surface mass balance remains negative), consistent with trends observed across the ice-sheet (Tedesco et al., 2017). Concurrent with decreasing meltwater runoff, we observe an acceleration in ice velocity. During the period of sustained high melt, the drainage of basal waters from a larger area of the distributed drainage system causes a gradual depressurisation of the background water pressure with an associated increase in effective pressure. Reduced surface meltwater production would result in seasonally less extensive and smaller subglacial channels and consequently these channels will undergo faster creep closure (Schoof, 2010). This results in a reduced time-period over which the main subglacial channels can evacuate water from the surrounding weakly connected, hydraulically distributed regions. As water pressure is no longer being systematically reduced, the background water pressure can increase through a gradual re-pressurisation of the subglacial hydrological system, as meltwater can recharge from basal melting without being evacuated by efficient subglacial channels.

Effective pressure (N) is calculated as $N = P_i - P_w$, where P_i refers to the ice overburden pressure and P_w to the basal water pressure (Meier and Post, 1987; Schoof, 2010). Repressurising the subglacial hydrological system causes basal water pressure (P_w) to increase, thus reducing effective pressure and causing ice to accelerate. As effective pressure is a function of ice thickness, for the same

increase in basal water pressure we would anticipate acceleration to be greater where ice is thinner. Although we expect channel closure to occur earlier and faster under thicker ice (due to higher ice overburden pressure) (Chandler et al., 2013; Dow et al., 2014; Meierbachtol et al., 2013b), modelling studies suggest that once channel pressure falls to 90 % of overburden pressure, there is less than 2 days difference in closure time for channels with a cross-sectional area of 10 m^2 compared to <1 m^2 (Dow et al., 2014). Moreover, it has been suggested that maximum channel closure rates are similar at both marginal and interior sites (Meierbachtol et al., 2013b). Consequently, we argue that any variation in repressurisation due to channel closure rates will only have a small impact upon effective pressures when compared to variability in ice thickness (which ranges from 0 – 1400 m across our study area). As a result, we hypothesise that the observed acceleration is greater for marginal regions of thinner ice due to the impact of basal meltwater recharge on water pressure in these areas offsetting a larger proportion of the ice overburden pressure (Figure 4.2D).

The inland limit and spatial extent of efficient channel formation is subject to considerable debate (Davison et al., 2019; Nienow et al., 2017). Borehole and tracer studies and ice velocity records have been used to infer channels extending 40-80 km inland (Bartholomew et al., 2011a; Bartholomew et al., 2011b, 2012; Chandler et al., 2013; Das et al., 2008; Doyle et al., 2013; Fitzpatrick et al., 2013), with high flow velocities of traced waters and the rapid transmission of pulses of meltwater from the ice sheet surface to the margin indicating efficient drainage (Nienow et al., 2017; Smith et al., 2017). These observations are supported by modelling studies, whereby efficient channels have been modelled up to 50 km inland, under 900 m thick ice (de Fleurian et al., 2016; Koziol and Arnold, 2018). The spatial extent of channelisation is influenced by the distribution of surface-to-bed connections, with high moulin density conducive to widespread and rapid channel development (Banwell et al., 2016). Further inland, ice thickness increases, surface slopes become shallower and runoff production decreases, leading to enhanced creep closure due to higher effective pressures and reduc-

tions in hydropotential gradients and wall-melting (Davison et al., 2019; Hooke et al., 1990; Nye, 1953; Schoof, 2010). Under these conditions, modelling studies suggest that at a certain elevation and ice-thickness, efficient subglacial channels will not develop (Dow et al., 2014; Meierbachtol et al., 2013b) in which case melt and ice-velocity are expected to scale positively (Doyle et al., 2014). Velocity measurements 140 km from the margin (Doyle et al., 2014), within the accumulation area of the Leverett catchment, indicate a 2.2 % increase in annual velocity between 2009 and 2012. In our study, we are unable to determine whether a positive change in ice velocity has occurred at elevations above 1300 m (a.s.l.) due to increasing noise in our dataset further inland. However, GPS observations reveal reduced velocities to at least 80 km inland (at ∼1500 m a.s.l) in the years of record surface melt in 2010 (Sole et al., 2013) and 2012 (Tedstone et al., 2013) when compared to 2009.

Whilst multi-annual ice velocity slowdowns in southwest Greenland since the early-mid 2000s are observed here and in a number of other studies (Joughin et al., 2018; Stevens et al., 2016; Tedstone et al., 2015; van de Wal et al., 2008, 2015), differences between studies exist regarding the magnitude of slowdown, and the proposed mechanism(s) driving this dynamic change. For example, whilst GPS data show a slowdown of -0.9 ± 1.1 m yr^{-2} at North Lake from 2006-2014 (Stevens et al., 2016), satellite radar data from 2000/01 to 2016/17 reveal no significant trend (-0.2 m yr^{-2}, p=0.62, Joughin et al., 2018). At a regional scale, this radar data suggests a weaker slowdown trend than that reported either here, or by Tedstone et al., 2015 (-1.5 m yr^{-2} from 2002-2014, -12 % between 1985-1994 and 2007-2014), across the same study area, with little in the way of significant changes between 2001/01 and 2016/17 across much of the southwest margin (Joughin et al., 2018). Methodological differences between the studies may affect the conclusions drawn as this study and that of Tedstone et al., 2015 applied feature tracking to image pairs either side of an annual baseline (352-400 days in Tedstone et al., 2015, 352-384 days here), whereas Joughin et al., 2018 composed mosaics of winter velocities, comprised of data sampled between September and

May. This raises the possibility that the previously observed slowdown (Tedstone et al., 2015) may be related to some local process, rather than regional-scale surface melt forcing (Joughin et al., 2018), for example water piracy as a result of dynamic thinning on Jakobshavn Isbrae has been suggested as a driver of slowdown in the north of the West Greenland land-terminating sector (Joughin et al., 2018). However, by extending the study area ∼120 km to the south, and by increasing the number of common pixels used in our time series by an order of magnitude compared to that of Tedstone et al., 2015, we extend confidence in the observed slowdown of ice motion from the early-mid 2000s. Moreover, by calculating an ice velocity anomaly (Dehecq et al., 2019), we remove the influence of any biases between sensors from the observed trends, further increasing confidence that this sector of the ice sheet underwent significant deceleration during this period.

A variety of models exist to simulate the subglacial drainage system and its impact on ice dynamics in response to increasing meltwater fluxes in a warming climate (De Fleurian et al., 2018). However, whilst current models can reproduce observed dynamics of Greenland's land-terminating margins over days/weeks (Dow et al., 2014; Schoof, 2010), on a seasonal timescale (Hewitt, 2013; Hoffman et al., 2016; Koziol and Arnold, 2018), and across several years (de Fleurian et al., 2016; Poinar et al., 2019), there is a need to consider the longer, decadal and multi-decadal response of ice motion to surface meltwater forcing in order to better reproduce observed dynamics and project future change. On a decadal scale, recent modelling predicts increased ice-motion and thus ice flux into the ablation zone under enhanced summer melt within 44 km of the ice-margin (Gagliardini and Werder, 2018, their Figure 5C). These predictions contrast with the results presented both here and from other GPS and satellite-derived observations (Joughin et al., 2018; Stevens et al., 2016; Tedstone et al., 2013, 2015; van de Wal et al., 2008, 2015). Further work is therefore required to investigate what aspects of the model set-up or framework cause the modelled ice-motion to accelerate on a multi-annual timescale in response to increasing surface runoff, in contrast to

numerous observations reported in this and other studies. Whilst we do observe reduced slowdown as ice thickness increases, our results and those of others show that ice motion within the ablation area has slowed as a result of increased surface runoff, and we do not observe any appreciable or spatially extensive increases in ice velocity as a result of an extended period of high surface melt. We therefore argue that in order to better represent ice dynamical processes and project future changes in coupled hydro-dynamic models, the models must better utilise the available data from field and satellite observations both in model set-up and for assessing model performance, and there is a need for changes in the numeric representation of processes, including ice-hydrology coupling.

Our findings demonstrate that ice at surface elevations below 1300 m (a.s.l.) in the South West land-terminating region of the GrIS underwent deceleration during the mid to late-2000s and early-2010s with subsequent acceleration following sustained reductions in surface melt production, with this acceleration proportionally greater in areas of thinner ice. We hypothesise that this recent acceleration is driven by increases in basal water pressure offsetting a larger proportion of ice overburden pressure, and thus causing a greater reduction in effective pressure under thinner ice. This behaviour has not been observed previously on a multi-annual timescale. Whilst we have demonstrated that changes affecting the subglacial hydrological system are the most likely driver of ice velocity change in our study region, we are unable to conclusively state whether antecedent melt production is the predominant factor controlling ice motion, or whether some threshold in the amount of melt is required in order to drive a change in velocity. However, it is clear from our results that the period of ice deceleration occurred during a period of sustained high melt production, and ice motion accelerated subsequently as melt production decreased to consistently lower values from 2013 onwards. Moreover, we observed no indication of an ongoing slowdown once surface melt production exhibited a sustained decrease. Thus, the behaviour observed supports a process-based understanding of the links between hydrology and ice dynamics in this land-terminating sector of the Greenland ice sheet. The

results displayed in this study show that the observed trends in ice velocity are not statistical artefacts or the result of biases between sensors (Dehecq et al., 2019). Further, we see no evidence of speed-up at the elevations studied under a warming climate, irrespective of the bed conditions. Future work is required to improve observations of change at higher elevations, and at other land-terminating sectors of the ice sheet, in order to assess the extent to which these processes operate on an ice sheet scale.

Furthermore, while the results presented here relate specifically to land-terminating margins, it has been argued that the dynamics of tidewater glaciers are a product of both oceanic and atmospheric forcing (Cowton et al., 2018; Slater et al., 2019a), with the latter potentially driving a positive feedback as a result of its influence upon fjord water circulation and thus submarine melt (Cowton et al., 2018; Slater et al., 2017, 2018). This positive feedback contrasts with our findings at land-terminating margins, indicating that at an ice-sheet scale, the relationship between hydrology and ice dynamics is complex and spatially variable. Since the extent to which surface melt processes impact on tidewater glacier dynamics remains uncertain, analysis of existing large-scale, multi-decadal datasets (Mouginot et al., 2019) at marine-terminating margins should be undertaken with respect to surface melt change, in order to better project the future response of the Greenland ice sheet to changing atmospheric and oceanic conditions.

4.4 Methods

Repeat image feature-tracking of pairs of multispectral satellite images is often used to derive glacier surface velocity (Dehecq et al., 2015; Fahnestock et al., 2016; Heid and Kääb, 2012; Jeong et al., 2017). Here, we apply these techniques to calculate ice motion from Landsat imagery. The major strength of Landsat data is the continuous archive of imagery across multiple missions, from 1972 to present, available at a synoptic scale (Pope et al., 2014; Wulder et al., 2016). This imagery is freely available through the US Geological Sur-

vey (via https://earthexplorer.usgs.gov/) and the European Space Agency (via https://eo-sso-idp.eo.esa.int/). Given the poor availability of imagery and larger errors in georeferencing and orthorectification from Landsat 1-3, we limit our analysis to imagery from Landsat 5-8, covering the time period 1985 to present.

We calculate every Landsat path/row that intersects our study region (66.41 to 69.52 N, -51.78 to -45.45 W, Figure 4.5) and apply feature-tracking to all possible pairs of length 368±16 days for each path/row combination from 1985 to 2019 (Figure 4.6 and 4.7). This amounts to a total of 2665 pairs across 14 path/rows, an increase of >5 times the number of pairs and nearly 3 times the number of path/rows used by Tedstone et al., 2015. The temporal baseline of ∼1 year is used to minimise the impact of any seasonal variability in interannual ice velocity.

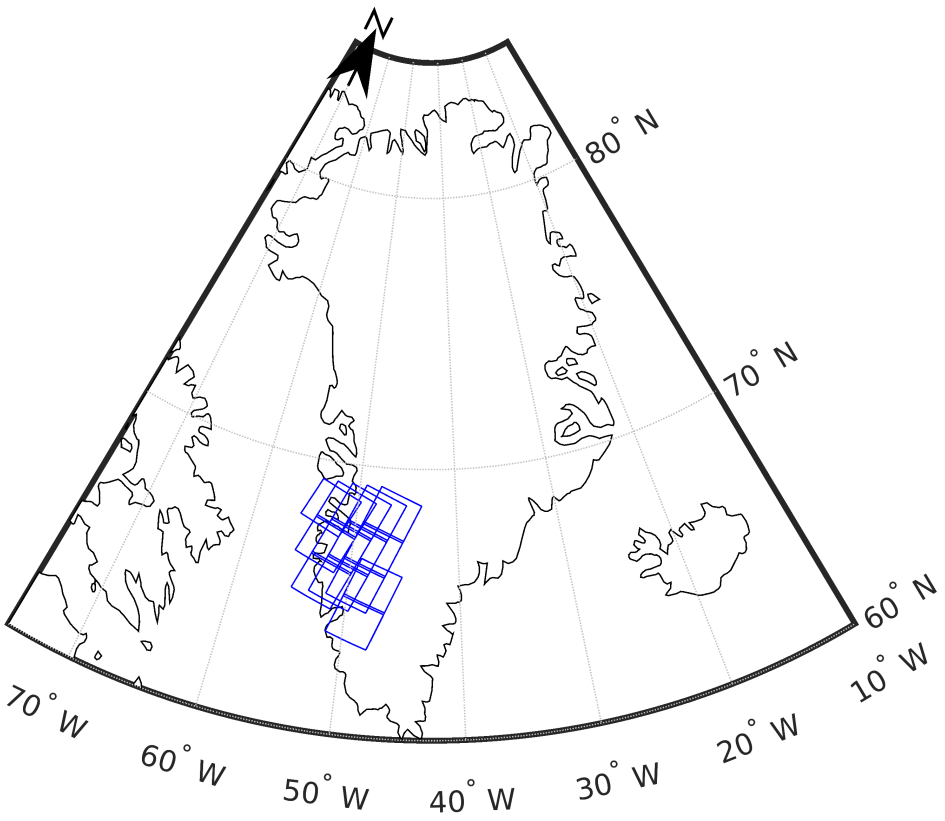

Figure 4.5: *Map displaying the coverage of the WRS2 path/row combinations used in this study. Each path/row is displayed as a blue square.*

Using images 16 days either side of the 368-day baseline may introduce bias whereby, for example, a 384-day period could disproportionately sample faster flow in summer (Joughin et al., 2018) (or vice versa). To test the impact of a varying temporal baseline, we quantify the proportion of summer coverage along our velocity time series, displayed in Figure 4.8, and follow Tedstone et al., 2015 in using mean summer and winter GPS velocities (127.6 m yr^{-1} and 81.6 m yr^{-1} respectively) from Leverett Glacier sites (Sole et al., 2013; Tedstone et al., 2013) to convert this into the potential impact upon annual velocity.

By applying a linear regression to the resultant time series, we observe no significant trend (-0.05 $\pm$ 0.03 m yr^{-2}, p = 0.16). We also apply a linear regression to the periods calculated by the segmented linear regression of our velocity anomaly time series, and find no significant trend introduced for any subsection of the time series (0.15 $\pm$ 0.11 m yr^{-2}, p = 0.21, 0.25 $\pm$ 0.13 m yr^{-2}, p = 0.08, 0.25 $\pm$ 0.19 m yr^{-2}, p = 0.22, for segments 1 through 3 respectively). Consequently, we argue that the trends in annual ice velocity are not artefacts of a varying temporal baseline.

Joughin et al., 2018 used winter velocities (1st Sept - 31st May) to assess interannual change, arguing that this should minimise any seasonal variation. However, GPS data from multiple studies indicate that ice flow varies considerably through winter (Colgan et al., 2012; Joughin et al., 2008b; Sole et al., 2013; van de Wal et al., 2015) and so introduces problems when attempting to determine net winter velocity from a subset of winter, as the particular period sampled will impact upon the final velocity. This is especially important given the slower-flowing nature of land-terminating margins. Consequently, we argue that calculating velocities with a temporal baseline of $\sim$1 year best captures changes in interannual ice velocity. Moreover, our temporal baseline of 352-384 days is shorter than that of Tedstone et al., 2015 (352-400 days), which should reduce any impact of disproportionate sampling.

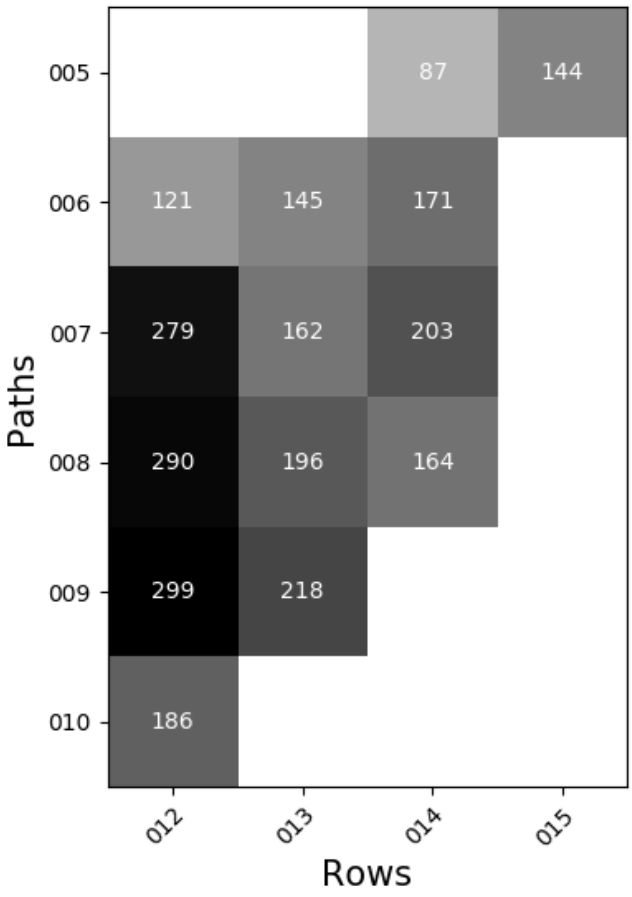

Figure 4.6: *Heatmap displaying the number of image pairs for each WRS2 path/row combination. Darker shading denotes more image pairs, with the exact number noted in white for each path/row.*

2786

2787 The feature-tracking processing chain is explained in detail in Dehecq et al., 2015.
2788 Here, we use oriented correlation, matching the feature of gradient orientation for
2789 each pixel (Fitch et al., 2002), as this is found to give improved spatial coverage
2790 of the output velocity fields compared to normalised cross-correlation. Following
2791 Tedstone et al., 2015, we use a combination of spectral bands at wavelengths
2792 ∼0.52-0.69 μm (bands 2+3 for Landsat 5 and 7, 3+4 for Landsat 8), and we
2793 enhance the images by applying a principal component analysis to these bands.
2794 Subsequently, a high-pass gaussian filter is used to enhance surface features such
2795 as crevasses and reduce the impact of temporally stable features relating to the
2796 basal topography (Dehecq et al., 2015; Tedstone et al., 2015).

2797

Whilst we use the same grid spacing of 8 pixels (240m) as Tedstone et al.,

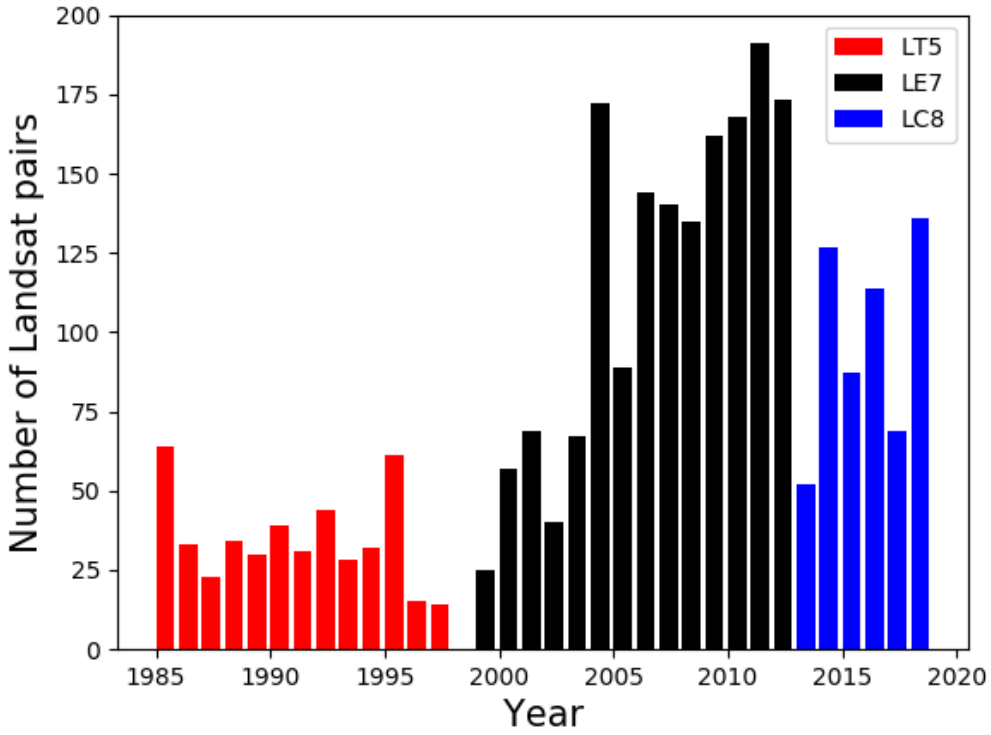

Figure 4.7: *Bar chart displaying the number of Landsat image pairs for each year. Image pairs from Landsat 5, 7 and 8 scenes are displayed in red, black and blue bars respectively.*

2015, we use a larger reference window size of 80 pixels (2400m). We found that this was necessary to generate velocity fields with good spatial coverage across the margin in the Leverett Glacier region, to the south of the region studied by Tedstone et al., 2015. We follow Dehecq et al., 2015 by performing feature tracking for selected cloud-free pairs with different reference window sizes, and subsequently choosing the size at which errors over stable ground are minimised and become asymptotic as the reference window size is increased further. The search window is automatically set based on the maximum expected displacement over the pair duration from prior velocity observations (Joughin et al., 2010).

As reference images (i.e. Global Land Survey) are not available for every path/row, we apply a median coregistration to the output velocity fields in order

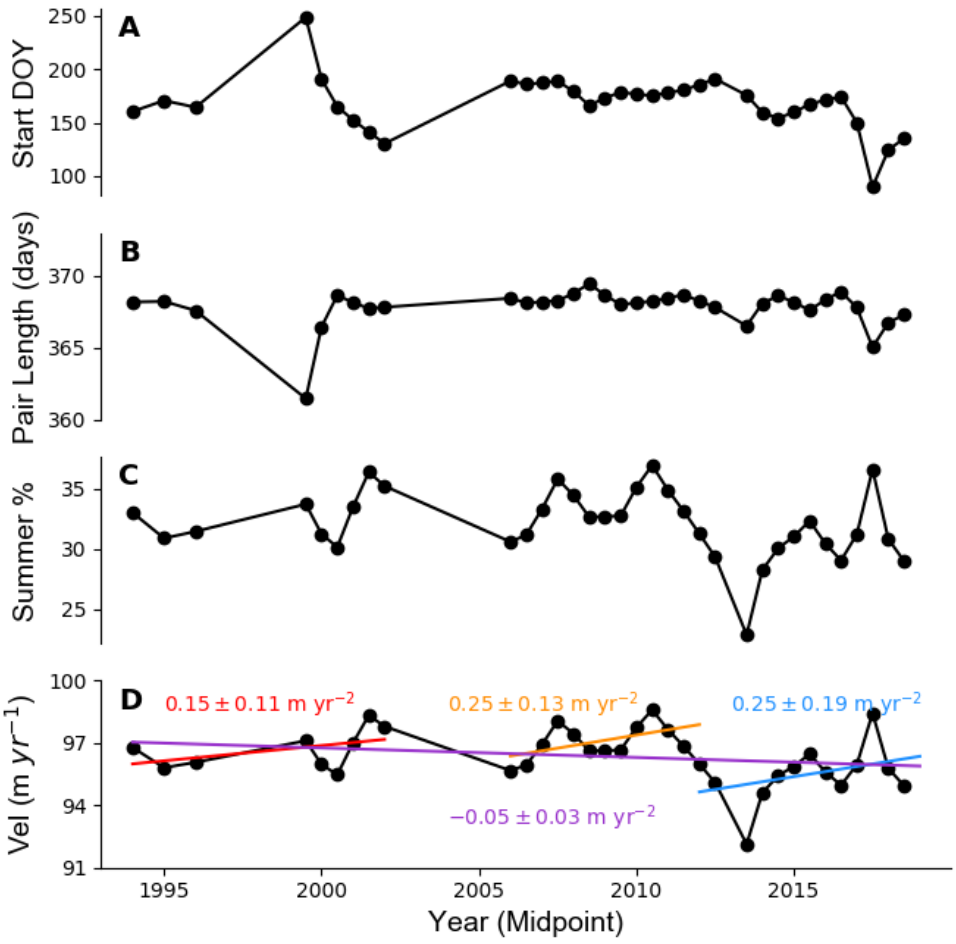

Figure 4.8: *Temporal baseline analysis of the Landsat image pairs used in each period of the time series in Figure 4.3 (with the year displayed as the midpoint of the time period).* ***(A)*** *The average start day-of-year (DOY) of all image pairs in each period,* ***(B)*** *the average baseline duration of all pairs,* ***(C)*** *the percentage of the baseline duration that falls within summer, defined as May 1st – August 31st,* ***(D)*** *the annual velocity expected in the ablation zone of the Leverett Glacier catchment (see Methods), based upon the percentage of summer and winter coverage, and the average baseline duration for each period. Linear regressions for the entire time series (purple), as well as for each segment (red, orange, blue), are displayed.*

to remove errors associated with georeferencing, whereby we calculate the median velocity over stable ground (where velocity should equal zero) and remove this from the calculated ice velocity at each pixel (following Tedstone et al., 2015). Coregistration is particularly important for slower-flowing regions as artificial offsets may contribute to a significant proportion of any change signal.

The coregistered velocity fields are then fused via a spatio-temporal median over annual or multi-year periods in order to exploit the redundancy offered by many overlapping image pairs to produce robust velocity outputs. We remove low-quality velocity estimates through filtering by a threshold signal-to-noise ratio value (snr threshold = 6). Following previous work (Dehecq et al., 2015; Tedstone et al., 2015), we identify this threshold value by calculating the value beyond which the median absolute deviation of velocities over stable ground becomes asymptotic (Figure 3.3). For Landsat 7 and 8 data, we group velocities into 1- and 2-year periods, whereas for Landsat 5 data, we group the results into 4-year periods (as fewer pairs are available and given the difficulty in producing velocity outputs with good coverage over the southern sector of our study region). The final velocity field for each time period is composed of the median value of all velocity fields within the time period at each pixel. We use the median value as this is not sensitive to large outliers, and so can filter out the impact of any erroneous values that remained above the signal-to-noise ratio threshold. The output velocity merges are re-projected to Polar Stereographic given that the path/row combinations span several UTM zones.

To calculate the uncertainty at each pixel for the fused velocity fields, we compute a 1σ confidence interval for each component of the velocity field based on the median absolute deviation of the velocity over stable ground and the number of velocity estimates used in the calculation of the median (Dehecq et al., 2015). This follows the form:

$$\sigma = \frac{k}{2} \cdot \frac{MAD}{N^{\alpha}} \tag{4.1}$$

Where MAD is the median absolute deviation over stable ground, N is the number of velocity fields used in the computation of the median velocity, σ is the 1σ confidence interval, and k and α are parameters determined for each time period from the stable ground velocity which is known to equal zero. This relationship is extrapolated on-ice using the appropriate values of MAD and N at each pixel in order to give the uncertainty of the ice velocity estimates for each time period.

Following Tedstone et al., 2015, we discard pixels with $\sigma > 60$ m yr^{-1} from the subsequent analyses. In addition, we mask out the tidewater glaciers to the very north of the study region in order to remove any influence of ice experiencing different dynamic processes from our land-terminating results.

To compute a multi-annual ice velocity time series, we first remove all points above the 60 m yr^{-1} uncertainty threshold from each merged output. Given that the velocity fields become increasingly noisy at higher surface elevations, we use the Greenland Ice Mapping Project DEM (Howat et al., 2014) to limit our analysis to pixels below 1000 m above sea-level. As there are differences in spatial coverage between time periods, there exists a compromise to be made between spatial and temporal coverage, with the aim to assess change across many common pixels whilst retaining a high temporal resolution. We retain only the velocity fields with an area coverage above 9250 km^2. If we apply a minimum coverage threshold of 9000 km^2, we lose ~35 % of our common points (1429 km^2). Increasing the minimum coverage threshold to 9500 km^2 results in the loss of data from the time series, which increases as the threshold increases further. As such, we take 9250 km^2 as the coverage threshold which offers the best compromise between spatial and temporal coverage. The median velocity is subsequently calculated across the 71703 pixels common to all the remaining merged velocity fields (Figure 4.9) in order to avoid spatial bias influencing the change signal. By multiplying this by the area of an individual pixel (240*240 m), we calculate a common areal coverage of 4130 km^2. This represents an order of magnitude increase in the number of common pixels, and thus common area, between velocity merges when compared to Tedstone et al., 2015. The associated uncertainty is estimated across the same pixels in the form:

$$\sqrt{\sum_{i=1}^{N} \frac{\sigma_i^2}{N}} \tag{4.2}$$

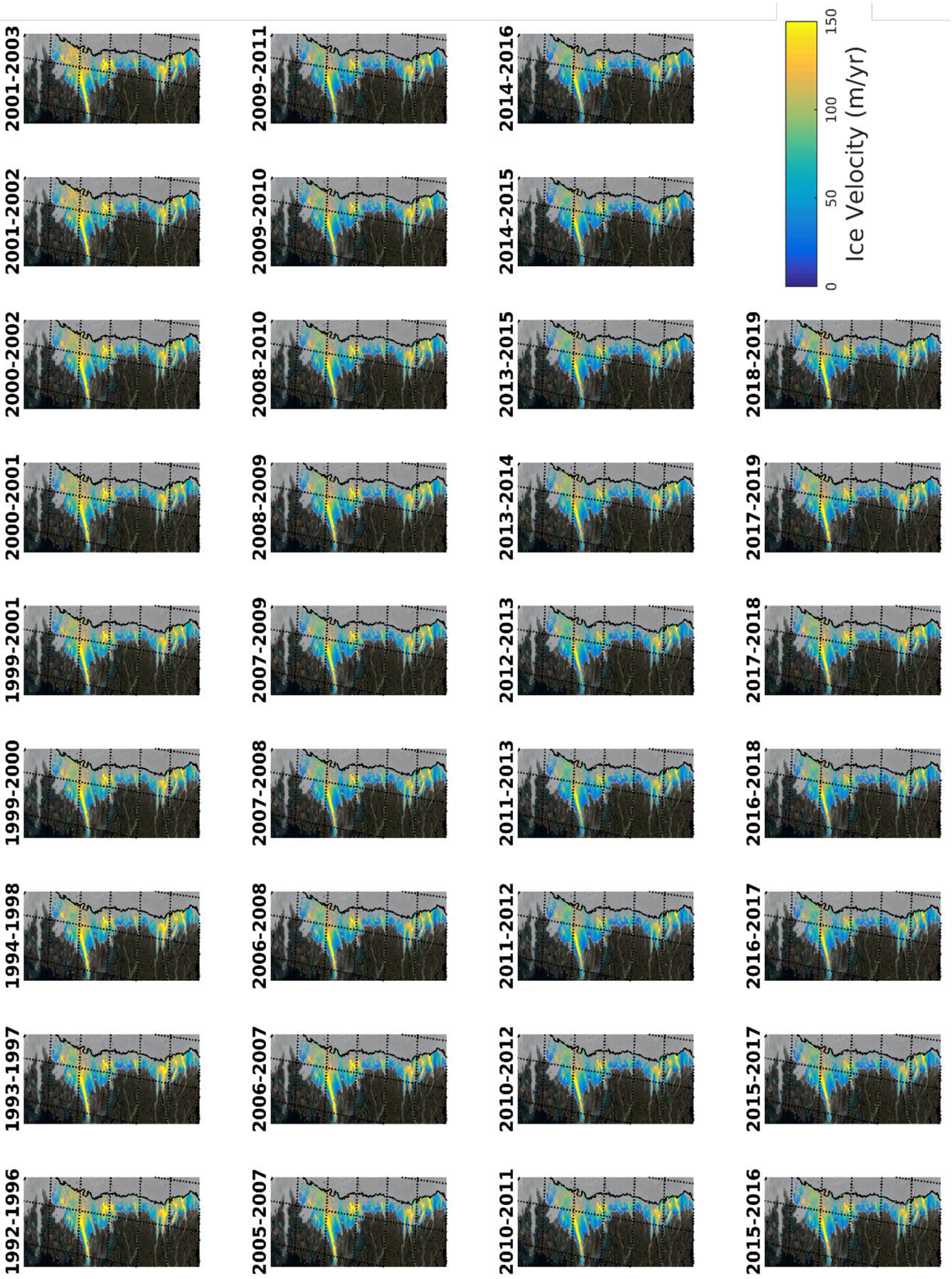

Figure 4.9: *Ice velocities (m yr^{-1}) during each time period. Only the pixels common to all periods are displayed. The black contour displays 1000 m surface elevation, and the velocity fields are displayed over a MODIS (Terra) corrected reflectance image from EOSDIS NASA Worldview (https://worldview.earthdata.nasa.gov/).*

4.4.1 Anomaly-based Time Series

Time series of ice velocity are commonly displayed in terms of difference in velocity magnitude (Heid and Kääb, 2012; Lemos et al., 2018; Moon et al., 2015; Tedstone et al., 2015). Recent work (Dehecq et al., 2019) indicates that velocity magnitude has a biased mean, with this bias increasing with the standard deviation of the velocity components (and so with noise). Consequently, this causes an artificial negative velocity trend, particularly so in slow-flowing sectors and where velocities are not significantly larger than noise, when calculating a multi-mission time series.

To mitigate this effect, we follow the velocity anomaly approach of Dehecq et al., 2019. First, we calculate a mean of all velocity pairs covering the period 1992-2017 described as V_0. The velocity anomaly is defined as the value of the difference vector $V_t - V_0$ projected on the mean velocity vector:

$$dv = \frac{(V_t - V_0) \cdot V_0}{\|V_0\|} = \frac{(V_{x,t} - V_{x,0}) \cdot V_{x,0} + (V_{y,t} - V_{y,0}) \cdot V_{y,0}}{\|V_0\|} \tag{4.3}$$

The result of this approach is to centre the noise distribution symmetrically around zero (Figure 4.10) such that there is no bias in the mean value, removing any artificial slowdown trends due to variability in noise magnitude between sensors (Dehecq et al., 2019). The resultant velocity anomaly fields are displayed in Figure 4.11.

4.4.2 Calculating a Long-Term Ice Velocity Trend

To assess the long-term trends in our time series, we first compute a simple linear regression through the data, which gives a velocity change of -0.72 $\pm$ 0.08 m yr^{-2} from 1992 to 2019 ($R^2 = 0.70$, $p < 0.01$). Whilst a long-term slowdown is clear from the time series, it also shows a period of sustained high velocity, followed by a period of slowdown, and then an apparent stabilisation. Consequently, we test whether the data can be divided into three statistically different segments (Figures 4.12, 4.13 and 4.14).

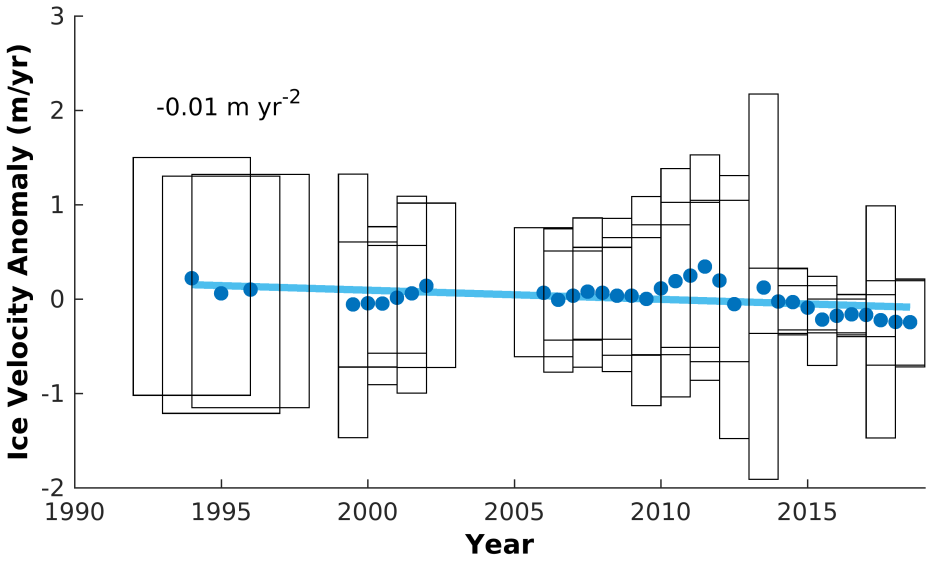

Figure 4.10: *Off-ice velocity anomaly (m yr^{-1}) time series. The width of each box refers to the time period covered by that data point, and the height of the box displays the interquartile range. The light blue line shows a linear regression fit to the data.*

We use the non-parametric Mann-Whitney Wilcoxon Test to determine whether the medians of independent populations are similar. We split the times series into two segments, 1992-2012 and 2002-2019, and test all possible pairs of breakpoints at 0.2-year intervals along each. We also compute the root mean squared error (RMSE) for each pair. This describes how close the observed data points are to the modelled fit, with lower RMSE indicating a better fit to the data. For the first period, we find that for breakpoints between 1996 and 2011, the null hypothesis of equal medians can be rejected (Figure 4.12C). This means that pre- and post-1996, populations are significantly different with 95 % confidence. From Figure 4.12B, we observe that for pre- and post-2000 populations, the null hypothesis can be rejected with 99 % certainty ($p = 0.01$). The minimum RMSE (Figure 4.12A) is during 2003, however there is a region of low RMSE from 2002-2005 which arises from a gap in our dataset. From this, we take a breakpoint of 2003 given that this year has the lowest RMSE (and so the best fit to the velocity anomaly time series) and separates two populations with statistically different medians at the 99 % confidence interval.

For the second period (Figure 4.13), the null hypothesis of equal medians can

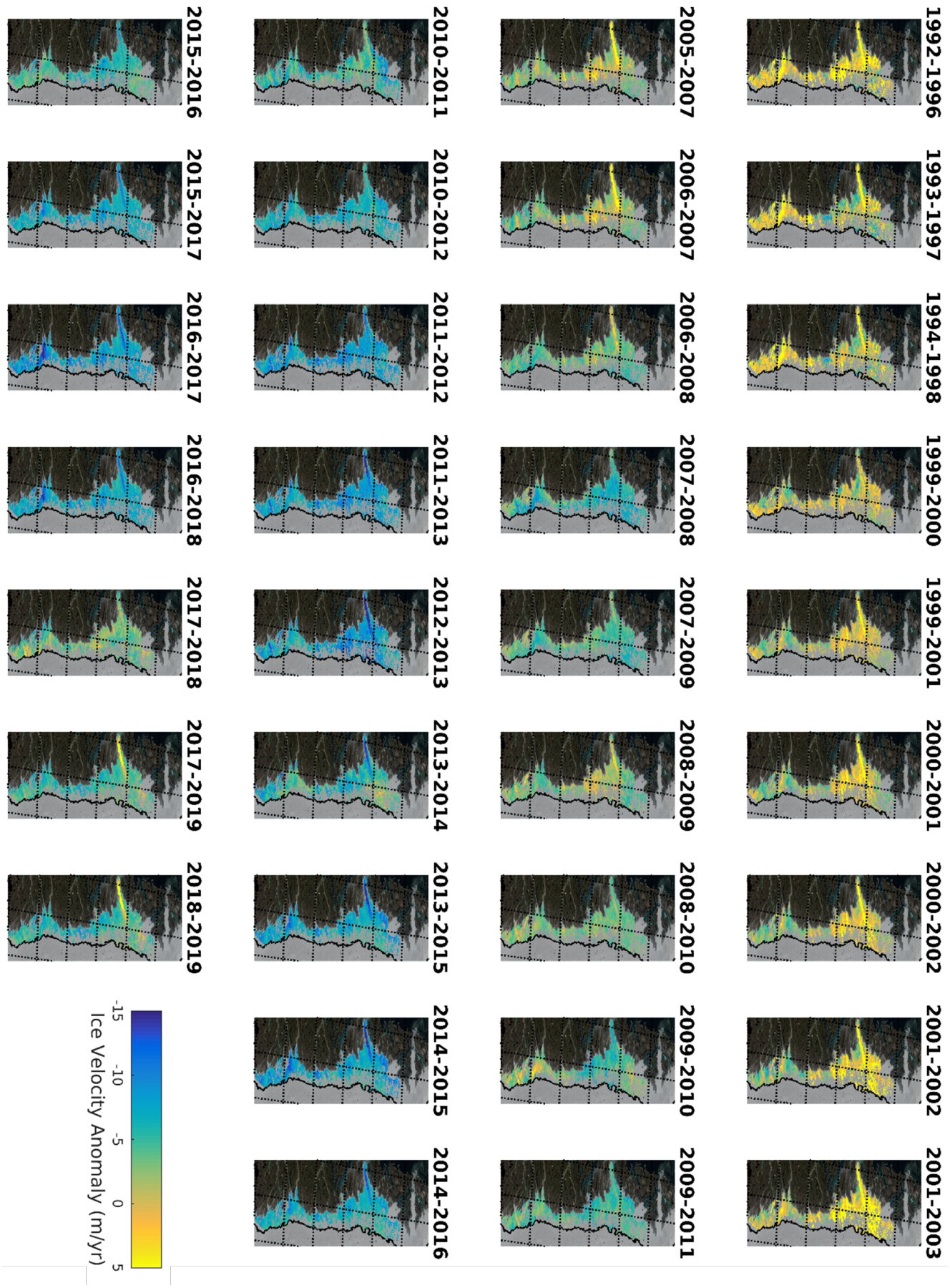

Figure 4.11: *Ice velocity anomalies (m yr^{-1}) during each time period. Only the pixels common to all periods are displayed. The black contour displays 1000 m surface elevation, and the velocity fields are displayed over a MODIS (Terra) corrected reflectance image from EOSDIS NASA Worldview (https://worldview.earthdata.nasa.gov/).*

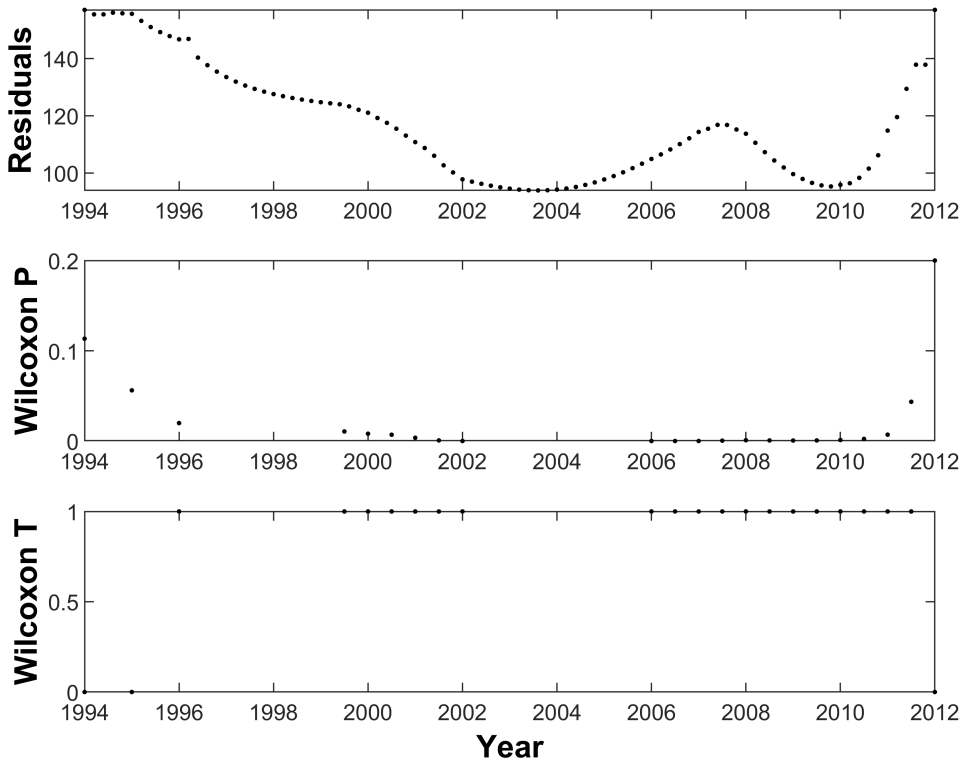

Figure 4.12: *Statistical significance of two periods of ice motion between 1994 and 2012.* ***(A)*** *Residuals displayed as the RMSE of a two-trend model fitted to the ice velocity anomaly data at each tested breakpoint.* ***(B)*** *Probability that the observed result occurred by chance if the null hypothesis that medians are equal is true.* ***(C)*** *Hypothesis test of the Wilcoxon rank sum test for equal medians, testing that the probability of two populations are similar at the 95 % confidence interval. 0 denotes that the hypothesis of equal medians cannot be rejected, 1 denotes that the hypothesis of equal medians can be rejected.*

be rejected for breakpoints between 2006 and 2012. A minimum in RMSE is observed in 2012, and so we take this as the second breakpoint in our time series, which also separates two populations with statistically different medians (p=0.01). As a result, we select the pair of breakpoints with the lowest RMSE, that are statistically significant with 99 % certainty, which gives breaks at 2003 and 2012, and an improved R^2 of 0.85.

The RMSE of each pair of breakpoints tested with the Mann-Whitney Wilcoxon test are displayed in Figure 4.14. Whilst the breakpoints with the lowest RMSE are 2003 and 2012, there is a large area of low RMSE for pairs of breakpoints

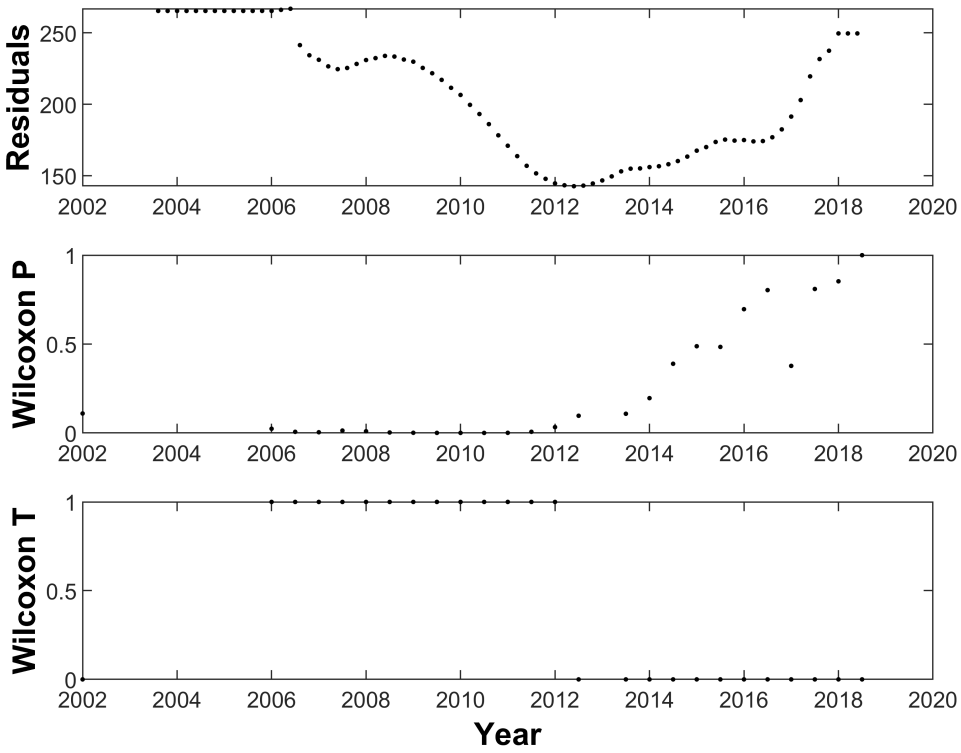

Figure 4.13: *Statistical significance of two periods of ice motion between 2002 and 2019.* ***(A)*** *Residuals displayed as the RMSE of a two-trend model fitted to the ice velocity anomaly data at each tested breakpoint.* ***(B)*** *Probability that the observed result occurred by chance if the null hypothesis that medians are equal is true.* ***(C)*** *Hypothesis test of the Wilcoxon rank sum test for equal medians, testing that the probability of two populations are similar at the 95 % confidence interval. 0 denotes that the hypothesis of equal medians cannot be rejected, 1 denotes that the hypothesis of equal medians can be rejected.*

between ∼2002-2005 and ∼2010-2014, although the null hypothesis cannot be rejected for a breakpoint between 2013-2014. Consequently, whilst we cannot conclusively state any exact dates for the pair of breakpoints in the time series, we conclude that our ice velocity time series can be divided into three statistically different segments, with the breakpoints during the periods 2002-2005 and 2010-2012.

4.4.3 Impacts of Calculating a Multi-Mission Trend

It is important to consider that the second break in our time series (Figure 4.3) corresponds closely with the change in sensor between Landsat 7 and Landsat 8.

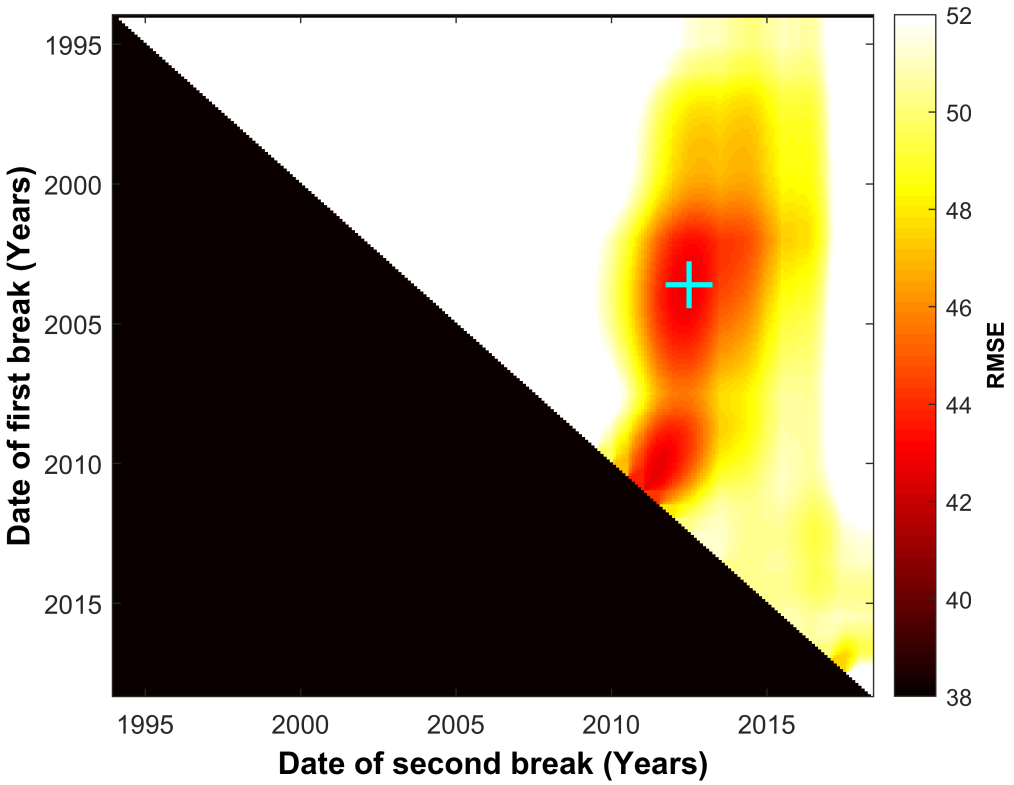

Figure 4.14: *Hypothesis test of the Wilcoxon rank-sum test for statistically different medians between three periods of ice velocity anomalies. The coloured half shows the root mean square errors (RMSE) of a three-segment linear model fitted to all possible combinations of two break dates at intervals of 0.2 years. The centre of the cyan cross denotes the location of the pair of breakpoints with the lowest combined RMSE. The black area is shaded for simplicity as it mirrors the coloured sector.*

Whilst numerous studies have calculated velocity trends using multiple sensors, recent research (Dehecq et al., 2019; Joughin et al., 2018) indicates that biases exist between missions and sensors. This is especially important to consider where breakpoints in a time series coincide with changes in sensor or mission, as it cannot initially be ruled out that a change in trend is simply the result of biases between sensors/missions. Over time, the Landsat missions have improved in radiometric quality, decreasing both noise and the number of potential mismatches (Dehecq et al., 2019). In addition, Landsat 8 has a 12-bit radiometric quantisation, as opposed to 8-bit for Landsat 5 and 7. Whilst this enables the tracking of subtle surface features and the extension of offset-tracking to regions beyond crevassed areas (Fahnestock et al., 2016), ice features that were not previously

visible can now be tracked, leading to an apparent speed-up (Dehecq et al., 2019). Sensor resolution has also improved from 30*30 m to 15*15 m with the introduction of the panchromatic band (band 8) in Landsat 7 and 8. This can lead to biases in high strain regions (Joughin et al., 2018), where higher resolution can lead to increased tracking of sharp features, and on narrow glaciers where coarser resolution imagery is more likely to lock onto stable ground.

In the Himalayas, it has been possible to correct for this as sufficient Landsat 5 imagery exists alongside Landsat 7 imagery, and Landsat 7 imagery is available post-2013 such that pairs of Landsat 5 and Landsat 7, as well as Landsat 7 and Landsat 8, scenes can be compared over essentially the same time period (Dehecq et al., 2019) in order to calculate the offset between missions. This work indicates that velocities obtained from Landsat 8 scenes are higher than those from Landsat 7 scenes, which are in turn greater than those from Landsat 5 scenes (Dehecq et al., 2019). These biases are largely < 5 m yr^{-1}, however can reach as high as 10–15 m yr^{-1} for some glaciers (Dehecq et al., 2019, their Figures S12 and S13). Whilst insufficient imagery is available to calculate a similar correction for Greenland (or Antarctica), were we to apply a correction to account for biases between sensors, this would be added to velocities calculated from Landsat 5 and 7 and so would not change our conclusions. We would instead observe a slight decreasing trend from the early 1990s through the early 2000s, followed by a steeper slowdown from ∼2003 to 2012, after which velocities would return to a more stable trend.

As biases between missions are mostly located on narrow glaciers and at high elevations, we would expect these biases to be considerably reduced in our study region. In order to remove any biases resulting from changes in sensor resolution, we limit our analysis to the same 30*30 m spatial resolution and spectral band combination (∼0.52-0.69 μm) for all three sensors. Moreover, the ice velocity anomaly approach acts to limit the influence of reductions in sensor noise over time. Consequently, we are confident that our dataset is robust against any biases

introduced by using multiple sensors.

4.4.4 Statistical Links between Ice Velocity and Surface Melt Production

Previous work argues for a statistical link between antecedent melt production and ice motion, whereby including the four prior years of melt production is suggested to explain 44-50 % of the observed ice motion (Tedstone et al., 2015). However, subsequent work has argued that the fact that an improved correlation is observed when multiple years of runoff are included is "an expected outcome of analysing two variables with long-term temporal trends, even if the mechanism generating these trends is unrelated to the annual variability" (Stevens et al., 2016, p. 11301). By repeating the analysis presented in Tedstone et al., 2015, we show that R^2 tends towards 1 as more antecedent melt years are included (Figure 4.15). As such, it is not trivial to statistically link trends in ice motion and surface melt production.

To investigate the link between year-to-year variations in melt production and ice velocity, we detrend both time series and apply a linear regression to the resultant detrended time series. The segmented linear regression presented in Figure 4.3 was used to detrend the ice velocity anomaly time series. Following this, we detrended the melt production anomaly by calculating separate linear regressions for the same three time periods.

Our detrended regression gives an R^2 of 0.08 ($p = 0.11$), suggesting the year-to-year variation in melt production has no significant impact on year-to-year variations in ice velocity (Figure 4.16).

It is plausible that there are alternative metrics that would better correlate with year-to-year variations in ice velocity, for example the frequency and magnitude of pulses of meltwater supply to the subglacial drainage system. Once an

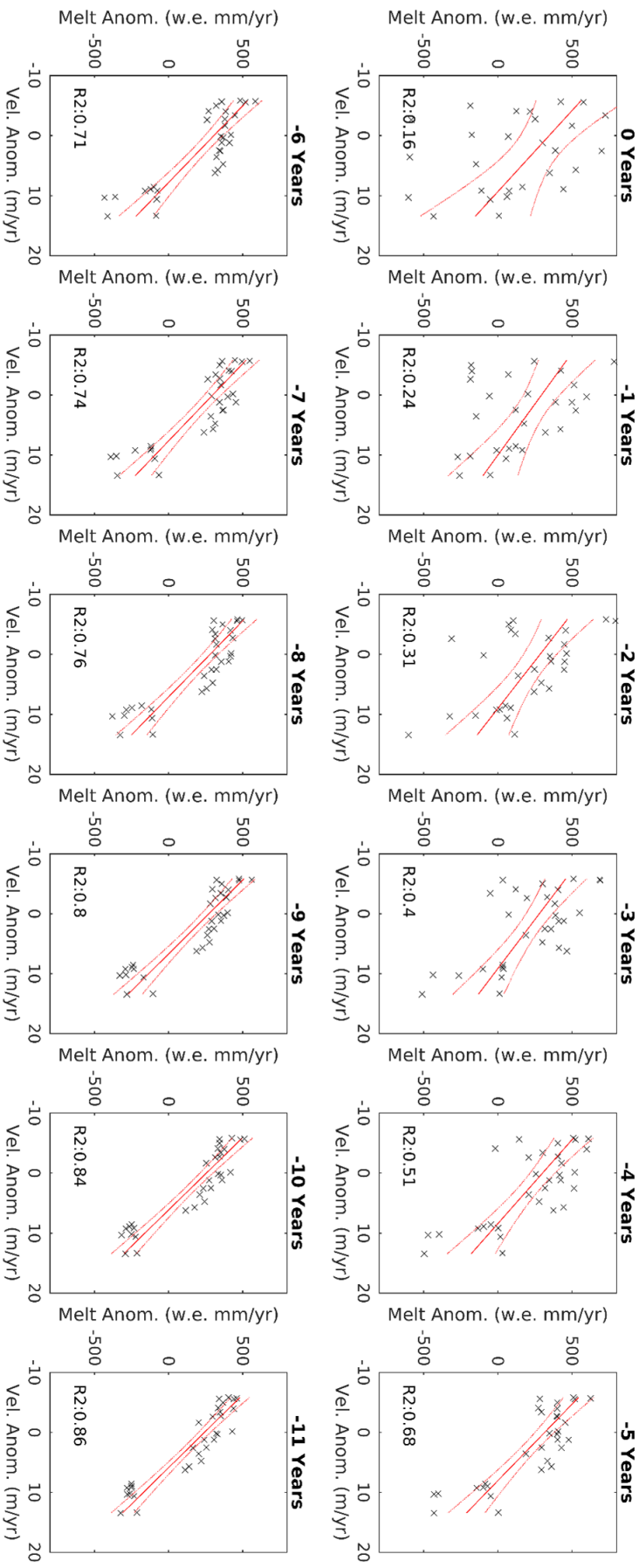

Figure 4.15: *Linear regressions between ice velocity anomalies ($m\ yr^{-1}$) and antecedent surface melt production anomalies (w.e. $mm\ yr^{-1}$). The title of each plot refers to the number of years of melt data prior to each velocity point that were included. The R2 value of each regression is displayed within each subplot.*

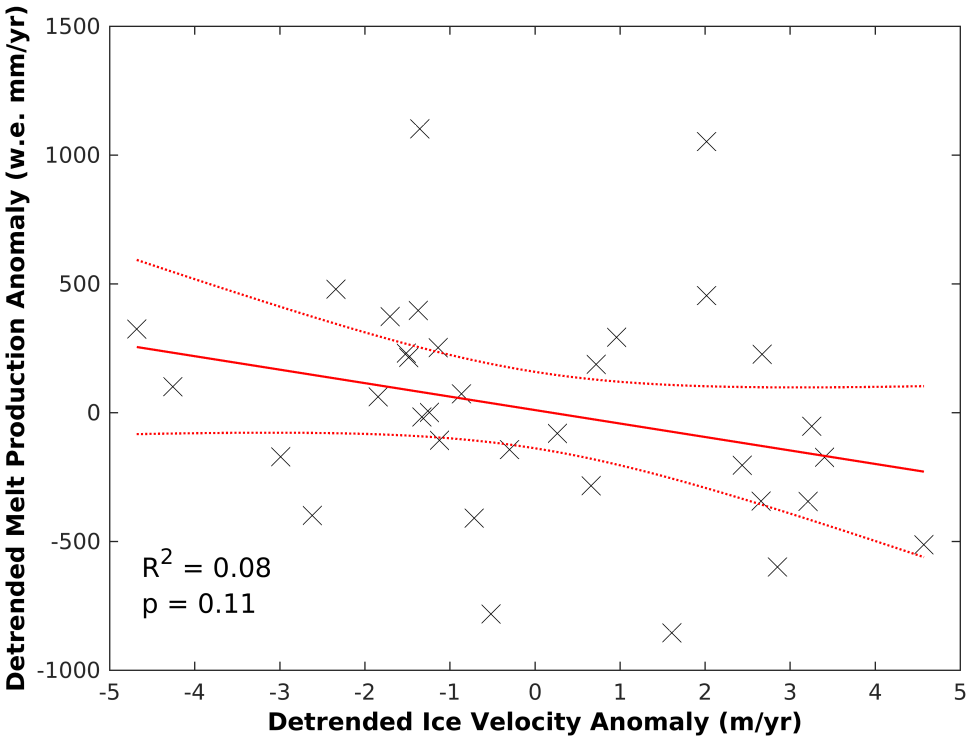

Figure 4.16: *Linear regression between detrended ice velocity anomalies (m yr^{-1}) and detrended melt production anomalies (mm yr^{-1}). The regression is displayed by the solid red line, with confidence bounds displayed by the dotted red lines.*

efficient subglacial drainage system is formed, ice flow decelerates through the remainder of the melt season, and any further short-term acceleration can only be driven by a larger meltwater pulse (Bartholomew et al., 2012; Cowton et al., 2013). This can occur via the drainage of a supraglacial lake (Das et al., 2008; Hoffman et al., 2011), an intense rainstorm (Doyle et al., 2015), or an extreme melt event (Tedstone et al., 2013). However, the impact of such events occurs only over a period of hours (Das et al., 2008) to days (Cowton et al., 2013; Doyle et al., 2015; Tedstone et al., 2013), and moreover, there is no evidence to suggest that melt seasons on Greenland are changing in terms of their overall behaviour.

4.4.5 Spatial Trends in Ice Velocity

To investigate spatial trends in velocity change across our study region, we construct a change map displaying the percentage ice velocity change between the following periods; 1992-2003 and 2003-2012, 2010-2012 and 2017-2019. Median

ice velocity for each period was calculated through fusing all of the constituent velocity fields via a spatio-temporal median, as described previously. We calculate uncertainty of the percentage change through a linear combination of the uncertainties of each period in the form:

$$\sqrt{{c_1}^2 + {c_2}^2} \tag{4.4}$$

Where c_1 is the first period (i.e. 1992-2003) and c_2 is the second period (i.e. 2003-2012). We remove pixels with uncertainty greater than 60 m yr^{-1}. We also filter by Velocity Vector Coherence (VVC, Dehecq et al., 2015), which describes the alignment of the velocity vectors. This follows the form:

$$VVC(i,j) = \frac{\left\| \sum_{t \in T} \vec{V}(i,j,t) \right\|}{\sum_{t \in T} \left\| \vec{V}(i,j,t) \right\|} \tag{4.5}$$

Where T is the set of N velocity estimates V(i,j,t) merged to obtain the median velocity $\vec{V}$(i,j) at pixel(i,j). We filter out all pixels with VVC < 0.45. In addition, we erode the edge of our ice mask by 3 pixels in order to limit the influence of noise at the ice margin. We then calculated the median percentage change in ice velocity across the remaining pixels for the full study region.

4.4.6 Surface Mass Balance

We obtain surface mass balance (SMB) data from the MAR v3.10 regional climate model (Fettweis et al., 2017), forced by NCEP-NCARv1 from 1992 to 2019. We limit our analyses of SMB below an ice surface elevation upper limit of 1600 m (a.s.l.). Little lake drainage occurs above this elevation (Howat et al., 2013; Johansson et al., 2013; Selmes et al., 2013) and it has been argued that this is an approximate maximum elevation where crevasses, and thus moulins, are likely to form (Poinar et al., 2015). Whilst surface meltwater can runoff from elevations above this, surficial drainage is less likely to occur in high elevation regions due to the shallower surface slope (Selmes et al., 2013). Consequently, below this threshold elevation, we can be confident that surface meltwater drains to the

ice-bed interface, and so influences ice motion. Regardless, melt at all elevations has increased from the 1958-1987 average in the period 1988-2013 (Poinar et al., 2015), with the difference between the means of the period being positive at $p < 0.05$ from 400-2600m (a.s.l.).

Chapter 5

Complex multi-decadal ice dynamical change inland of marine-terminating glaciers on the Greenland Ice Sheet

Almost all of our current observations of dynamic change within Greenland are concentrated at or near the margins of the ice sheet as exemplified by the results presented in Chapter 4. As a result, our comparative lack of observations within the ice sheet interior represents a major uncertainty with respect to Greenland's likely contribution to future sea-level rise. This is particularly important as modelling projections indicate that the majority of Greenland's dynamic sea level rise contribution will result from perturbations originating at tidewater glacier termini propagating up-glacier and driving increased ice flow and thinning within the ice sheet interior (Price et al., 2011). Recent advances in satellite imaging have enabled the extension of feature tracking into the ice sheet interior (Fahnestock et al., 2016). As a result, through combining recent satellite-derived annual ice velocities (Gardner et al., 2018, 2019) with GPS measurements from the mid-1990s near the 2000 m surface elevation contour (Thomas et al., 2000; Thomas et al., 1998; Thomas, 2001), this chapter presents the first direct observational evidence of multi-decadal ice dynamical change within the accumulation zone of

the Greenland Ice Sheet, on an ice-sheet-wide scale. The results exhibit a complex pattern of ice dynamical change, and this pattern is hypothesised to be linked to variability in basal topography and ice geometry, important controls on ice dynamics which are investigated further in Chapter 6.

This chapter was published in *Journal of Glaciology* in March 2021.

Authors: Joshua J. Williams[1], Noel Gourmelen[1] and Peter Nienow[1]

1. School of Geosciences, University of Edinburgh, Edinburgh, EH8 9XP, UK

Citation: Williams, J.J.[1], Gourmelen, N.[1] and Nienow, P.[1] (2021) Complex multi-decadal ice dynamical change inland of marine-terminating glaciers on the Greenland Ice Sheet, *Journal of Glaciology*, Cambridge University Press, pp. 1-14. DOI: 10.1017/jog.2021.31.

Author contributions: JJW performed all of the data processing and analyses. All authors contributed to the design of the study and the writing of the paper.

Acknowledgements: JJW was funded by a UK Natural Environment Research Council (NERC) doctoral training partnership grant (NE/L002558/1). Dr. Xavier Fettweis provided the MAR v3.10 SMB data and Dr Denis Felikson provided helpful discussion with regards to the propagation of terminus perturbations inland.

5.1 Abstract

Greenland's future contribution to sea-level rise is strongly dependent on the extent to which dynamic perturbations, originating at the margin, can drive increased ice flow within the ice sheet interior. However, reported observations of ice dynamical change at distances >∼50 km from the margin have very low spatial and temporal resolution. Consequently, the likely response of the ice sheet's interior to future oceanic and atmospheric warming is poorly constrained. Through combining GPS and satellite-image-derived ice velocity measurements, we measure multi-decadal (1993-1997 to 2014-2018) velocity change at 45 inland sites, encompassing all regions of the ice sheet. We observe an almost ubiquitous acceleration inland of tidewater glaciers in west Greenland, consistent with acceleration and retreat at glacier termini, suggesting that terminus perturbations have propagated considerable distances (>100 km) inland. In contrast, outside of Kangerlugssuaq, we observe no acceleration inland of tidewater glaciers in east Greenland despite terminus retreat and near-terminus acceleration, and suggest propagation may be limited by the influence of basal topography and ice geometry. This pattern of inland dynamical change indicates that Greenland's future contribution to sea-level will be spatially complex and will depend on the capacity for dynamic changes at individual outlet glacier termini to propagate inland.

5.2 Introduction

The Greenland Ice Sheet (GrIS) has lost mass to the ocean at an increasing rate over recent decades (Enderlin et al., 2014; King, 2018; Mouginot et al., 2019; Rignot et al., 2011; Rignot et al., 2008; Shepherd et al., 2012, 2019, and now has the largest contribution to global sea level rise of any individual ice body (Bamber et al., 2018; Vaughan et al., 2013). Estimates indicate that ∼48 to 66 % of this mass loss can be attributed to glacier dynamics, with this dynamic loss driven by the acceleration and retreat of marine-terminating glaciers and increasing by 14 % between 1985-1999 and 2007-2018 (King et al., 2020), and the remaining ∼34 to 52 % due to surface mass balance (Mouginot et al., 2019; Shepherd et al.,

2019). Following a step-increase in ice discharge in the early-2000s, the Greenland Ice Sheet is suggested to have entered a state of persistent mass loss (King et al., 2020), and recent model intercomparison work projects a future sea level rise contribution of 32 ± 17 to 90 ± 50 mm by 2100 (Goelzer et al., 2020). Almost all of our current observations of long-term change are concentrated at the margins of the ice sheet, which have been characterised by thinning (McMillan et al., 2016; Pritchard et al., 2009; Sandberg Sørensen et al., 2018) and both substantial velocity accelerations (Joughin et al., 2010, 2018; Moon et al., 2012; Rignot and Kanagaratnam, 2006b) and near-ubiquitous retreat of marine-terminating outlet glaciers (Bunce et al., 2018; Murray et al., 2015), especially in the north west and southeast.

In contrast, our understanding of changes in the dynamics of inland regions of the ice sheet is far more limited, and yet any such changes would be important for several reasons. At land-terminating margins, whilst the impacts of variable hydrological forcing on ice flow have been well-studied nearer the ice margin (Bartholomew et al., 2010; Sole et al., 2013; Tedstone et al., 2015; van de Wal et al., 2008, 2015), it remains unclear whether meltwater can access the bed, and efficient subglacial channels form, further into the ice sheet interior where the ice is thicker and rates of surface melting are lower (Nienow et al., 2017). This is particularly important given that as the ELA rises in response to projected increases in surface melt (Hanna et al., 2008), the area of the ice sheet surface undergoing melt will increase exponentially due to the hypsometry of the ice sheet surface (Bartholomew et al., 2011a; Machguth et al., 2016). Furthermore, some studies have postulated that ice motion will scale positively with surface melting at high elevations (Doyle et al., 2014; Gagliardini and Werder, 2018), and others that the presence of liquid water within the englacial hydrological system may increase ice deformation rates over time scales of years to decades (Phillips et al., 2010, 2013). More generally, considering conservation of mass, the thickness of ice in the interior is considerably greater than that at the margin, and so any increase in ice motion has the potential to result in a much larger increase in

mass flux when compared to marginal regions (Doyle et al., 2014), particularly for marine-terminating margins which are characterised by faster flow velocities and can discharge any increase in mass flux directly into the ocean. As a consequence, future sea level change projections are strongly dependent on how quickly mass can be transported from the ice sheet interior to the margin (Felikson et al., 2017, 2020; Price et al., 2008; Price et al., 2011), as well as the time required for the ice sheet to reach a new steady-state following a perturbation. For example, modelling work indicates that ∼75 % of the projected sea-level rise from Greenland, which would result from the response of the ice sheet to forcing over the past few decades, is yet to come (Price et al., 2011). Furthermore, additional estimates suggest thinning may continue for hundreds (Wang et al., 2012) to thousands (Price et al., 2008) of years until a new steady state is reached.

Several mechanisms have been proposed to drive change in the ice dynamics within regions inland of Greenland's tidewater glacier termini. Changes to the surface slope and thickness of the ice, as a result of ice dynamical and/or surface mass balance (SMB) change, impact upon the driving stress, in turn affecting rates of ice flow through internal deformation of the ice (Cuffey and Paterson, 2010). Such a change in driving stress, and thus internal deformation, can be driven through the up-glacier propagation of changes at the terminus of tidewater glaciers (Felikson et al., 2017, 2020; Howat et al., 2008a; Nick et al., 2009; Price et al., 2008; Price et al., 2011); for example, the loss of back-stress as a result of the loss of a floating ice tongue, or an increase in strain rate as the terminus retreats into deeper water (Price et al., 2011). This perturbs the force-balance, and the resultant acceleration leads to thinning of nearby upstream ice, steepening the local glacier surface thereby increasing the driving stress, resulting in further acceleration causing thinning and acceleration to propagate upstream (Nick et al., 2009). The propagation of this thinning can be modelled as a diffusive kinematic wave (Felikson et al., 2017, 2020; Nick et al., 2009; Nye, 1960, 1963; Price et al., 2011). This process can initiate a dramatic change in inland velocities, as observed during large 'surging' events at some Arctic ice caps (McMillan et al.,

2014b; Willis et al., 2018; Zheng et al., 2019).

Recent work (Felikson et al., 2017, 2020) suggests there may be geometrical constraints on the ability for thinning (and thus velocity) perturbations to propagate inland. These studies calculate the Péclet number (Pe), which describes the ratio of the rate at which a kinematic wave diffuses upstream or advects downstream. A threshold value of Pe = 3 is argued to represent the location at which 89 % of dynamic change has occurred (Felikson et al., 2020), thus offering a possible empirical threshold by which to measure the ability of changes at the margin to propagate inland. Through applying this to 141 tidewater glaciers across the Greenland Ice Sheet, Felikson et al., 2020 suggest that two end-member geometries describe those glaciers with the greatest potential for dynamic mass loss; those with a relatively low mass flux but with basal topography permitting thinning to diffuse far inland (i.e., northwest Greenland), and those with high mass flux but with thinning limits close to the margin (i.e., southeast Greenland).

In spite of the wealth of studies, there is little observational data to constrain these theoretical and model results, especially at higher elevations further inland. Direct observations of velocity change inland of fast-flowing marine-terminating outlet glaciers are limited to sparse GPS measurements of seasonal flow variations at a few individual glaciers (Ahlstrøm et al., 2013; Sole et al., 2011), and a single long-term (multi-decadal) study observing changes in ice motion extending ∼80-100 km from the grounding line at Zacharie Isstrom in northeast Greenland (Mouginot et al., 2015). Recent measurements of mass change from ICESat and ICESat-2 show thinning extending inland to elevations of 2000-2500 m (a.s.l.) in western and southern Greenland, particularly inland of Jakobshavn Isbrae and tidewater glaciers in the north west, and to 1500 m (a.s.l.) in northeast Greenland (Smith et al., 2020), although thinning is the result of both dynamic change and changes in SMB. To disentangle the relative contribution of dynamic and SMB, thereby isolating the dynamic signal of mass loss, surface elevation change can be corrected with SMB fields derived from regional climate models (Felikson et

al., 2017; McMillan et al., 2016; Pritchard et al., 2009; Zwally et al., 2011). The majority of pronounced dynamic thinning is found in a relatively narrow set of regions; Jakobshavn Isbrae, Upernavik Isstrom and Steenstrup Glacier on the west coast, Kangerlugssuaq in the southeast, and Zacharie Isstrom in the northeast (McMillan et al., 2016). Whilst dynamic thinning has been observed to penetrate inland of fast-flowing outlet glaciers (McMillan et al., 2016; Pritchard et al., 2009; Zwally et al., 2011), the amplitude of thinning from a small perturbation in ice velocity is expected to be well below the combined uncertainty of altimetry and SMB models and so the inland limit of dynamic thinning comes with large uncertainty. Consequently, there is a need for additional robust measurements of dynamics, and thus potentially dynamic change, within the accumulation zone of the GrIS in order to quantify how the interior of the GrIS has responded to climate warming and associated ice marginal dynamic perturbations.

During the period 1993-1997, a line of 161 stakes located ∼30 km apart, was installed in a 'girdle' around the entire GrIS at approximately the 2000 m elevation contour as part of the NASA-led PARCA project, in order to estimate the mass balance of the ice sheet interior (Thomas et al., 2000; Thomas et al., 1998; Thomas, 2001). At each stake, annual ice velocity was calculated using GPS observations recorded over a one-year return period sometime between 1993-1997. This period was characterised by stable mass balance (Sandberg Sørensen et al., 2018) and preceded both the recent rapid acceleration in ice motion observed at many of Greenland's marine-terminating outlet glaciers (Bevan et al., 2012; Hill et al., 2018; Holland et al., 2008; Joughin et al., 2004; Luckman et al., 2006; Murray et al., 2010; Thomas et al., 2003), and the slowdown in the south-west land-terminating sector (Stevens et al., 2016; Tedstone et al., 2015; van de Wal et al., 2015; Williams et al., 2020), which both began in the late-1990s to early-2000s. Whilst inland velocity measurements have previously been limited to GPS data, the launch of Landsat-8 in 2013, amongst other advances in satellite imaging, has led to the extension of large-scale feature tracking into the ice sheet interior (Fahnestock et al., 2016; Gardner et al., 2018, 2019). Since 2013, some

marine-terminating glaciers have continued to accelerate whilst others have stabilised or slowed down (Joughin et al., 2018, 2020; Khazendar et al., 2019; Lemos et al., 2018; Mankoff et al., 2020). Few, however, have remained stable since the 1990s or returned to speeds comparable to those prior to the initial acceleration (Bevan et al., 2012; Joughin et al., 2018).

Here, we compare recent satellite-image-derived velocities in the ice sheet interior to those collected at the PARCA GPS stakes along the 2000 m elevation contour in the mid-1990s to quantify how the interior of the GrIS has responded to the period of dramatic change observed at marine-terminating margins of the GrIS during the 2000s and 2010s. We measure multi-decadal ice velocity change at 45 sites inland of tidewater margins, encompassing all regions of the ice sheet. Subsequently, we assess the observed pattern of change with respect to the patterns of velocity change at the margins, ice geometrical constraints and modelled surface mass balance from MAR v3.10 (Fettweis et al., 2017).

5.3 Data and Methods

5.3.1 PARCA ice velocities around the 2000 m traverse

The PARCA data consists of GPS receivers at 161 stakes, located approximately 30 km apart and spanning the entire 2000 m elevation contour of the Greenland Ice Sheet, except for the southwest where the stakes were placed at higher elevations to avoid nunataks, mountains and crevasses (Thomas et al., 2000; Thomas et al., 1998). At each GPS station, an annual ice velocity (m yr^{-1}) was recorded within the period 1993-1997, as well as surface elevation (m a.s.l.) and ice thickness (m), the latter of which was measured by ice penetrating radar. The precision of annual velocity measurements from these GPS sites is < 0.5 m yr^{-1}, and better than 0.2 m yr^{-1} in most cases (Thomas et al., 1998). We apply a conservative uncertainty of $\pm$ 0.5 m yr^{-1} at all sites.

It should be noted that whilst the GPS sites are located at approximately the

same surface elevation, there are considerable differences in the distance from their respective glacier termini (Figure 5.9), with a notable increase in distance inland in the north and north-east.

5.3.2 NASA MEaSUREs ITS-LIVE ice velocities

Recent advances in satellite imaging have enabled the routine mapping of ice velocities (Dehecq et al., 2015; Fahnestock et al., 2016), with enhanced coverage in the interiors of the ice sheets (Gardner et al., 2018). Here, we use the NASA MEaSUREs ITS-LIVE annual velocity mosaics (v0) of the Greenland ice sheet, generated from Landsat imagery through the auto-RIFT feature tracking processing chain (Gardner et al., 2018), covering the period 1985-2018 and gridded to 240 m (Gardner et al., 2019). Full documentation for this dataset are available through the following; https://its-live.jpl.nasa.gov/#documentation. We use this dataset as the ice velocity measurements extend to the 2000 m elevation contour and both effective pair length (dt) and centre date are provided at each pixel such that we can assess the impact of any seasonality introduced in our analyses. Moreover, a recent assessment of satellite-image-derived ice velocities within the Greenland interior shows that when compared to GPS velocities from 2015-2019, located ∼150 km from the ice divide in the Northeast Greenland Ice Stream (NEGIS; 75°38 N, 35°60 W), ITS-LIVE velocities from 2013-2018 are characterised by the lowest bias (0.31 m) of all velocity products assessed (Hvidberg et al., 2020). For the calculation of multi-decadal ice velocity change, we use the data spanning 2014-2018, produced from Landsat-8 imagery. Whilst Landsat-8 imagery was used to compute the 2013 velocity field, it was used in conjunction with Landsat-7 imagery, and so the uncertainties are much higher than for 2014-2018 given the lower radiometric resolution of Landsat-7 compared to Landsat-8. Given the slow ice speeds within the interior, any such uncertainty can make up a considerable part of the observed change, hence we do not include data earlier than 2014 in our analyses.

5.3.3 ITS-LIVE velocity extraction at PARCA GPS sites

Prior to velocity extraction, we exclude pixels with a velocity below 10 m yr^{-1}, reasoning that the associated uncertainties constitute an unacceptably high percentage at very low velocities. Following this thresholding, we extract ice velocity (m yr^{-1}), ice velocity uncertainty (m yr^{-1}), effective pair length (days) and effective centre date from a 3*3-pixel (720*720 m) window around each of the 161 PARCA GPS sites, taking the median value of each from the extracted window. We repeat this for each year in the period 2014-2018, and then calculate the median velocity and uncertainty across the 2014-2018 period (calculated from whichever years we have data at a given GPS site) to account for any year-to-year variability in ice velocity.

Seasonal variability in ice velocities have been observed near the margins of tidewater glaciers in Greenland (Lemos et al., 2018), as well as up to at least ∼70 km inland at Kangiata Nunaata Sermia in southwest Greenland (Sole et al., 2011) and at an elevation of 1850 m (a.s.l.), 140 km inland in the southwest land-terminating sector (Doyle et al., 2014). We calculate the potential impact of such seasonality on the satellite-image-derived velocity data at the PARCA GPS sites, as described in the Chapter 3, and observe no coherent pattern showing any clear evidence of seasonality in the velocity data at these elevations.

5.3.4 Calculating velocity change

For each GPS site, we use the 2014-2018 median ITS-LIVE velocity to calculate a decadal velocity change through the following:

$$Velocity\ Change\ (m\ yr^{-1}) = ITSLIVE\ Velocity_{2014-2018}\ -\ GPS\ Velocity \tag{5.1}$$

$$Velocity\ Change\ (\%) = \frac{ITSLIVE\ Velocity_{2014-2018}\ -\ GPS\ Velocity}{GPS\ Velocity} \cdot 100 \tag{5.2}$$

It should be noted that for inland regions where the ice is flowing much more slowly than at the margins, any uncertainties in the ice velocity measurements may equal a considerable proportion of any measured velocity change. Following this, we first remove any sites where the measured velocity change (m yr^{-1}) is less than or equal to the 2014-2018 median velocity uncertainty (m yr^{-1}) extracted from the ITS-LIVE data added to the 0.5 m uncertainty of the GPS measurements (Thomas et al., 1998). To assess temporal variability, at each GPS site we calculate the standard deviation of the annual velocity for the period 2014-2018. We remove any GPS sites where our measured velocity change (2014-2018 median) is less than or equal to the standard deviation at that site. The locations of these sites are shown in Figure 5.10. Following this filtering, we measure decadal velocity change at 45 GPS sites.

At these 45 sites, ITS-LIVE velocity uncertainties range from 0.1 to 11.5 m yr^{-1}, with a mean uncertainty of 1.8 m yr^{-1}, for the years 2014-2018 (Figure 5.11). At the majority of the GPS sites included in our analyses, both median ice velocity uncertainty (m yr^{-1}) and the ice velocity standard deviation (m yr^{-1}) across the 2014-2018 ITS-LIVE data is very low, often less than 1-2 m yr^{-1} (Figure 5.11). In addition, almost all of the GPS sites have ITS-LIVE data in all 5 years (2014-2018, Figure 5.11D), such that the median velocity and velocity uncertainty are representative of the entire period, thereby limiting any temporal bias.

We observe absolute magnitudes of change ranging from -9.4 $\pm$ 3.3 to +28.1 $\pm$ 8.3 m yr^{-1} (Figure 5.1A), and also report these as percentage changes (Figure 5.1B). Where there are multiple GPS sites inland of a glacier, we report the range of velocity change values observed across these sites, and we also report the combined ITS-LIVE and GPS uncertainties.

5.3.5 Velocity time series creation

To compare acceleration in the interior with changes in ice motion at the margins, we create time series of ice velocity at the ice sheet margin using the full ITS-

LIVE dataset from 1985 to 2018 (Gardner et al., 2018, 2019). For each glacier studied, we define an area of interest (AOI) near the terminus. Within this AOI, we then remove pixels that are flowing slower than a specified minimum velocity, as well as pixels with an uncertainty greater than a specified threshold value, for each year of ITS-LIVE data. These velocity and uncertainty thresholds differ between sites, with full input parameters given in Table 5.2. We then calculate the pixels common to all years of ITS-LIVE data within the AOI, such that there is no spatial bias influencing the time series. These pixels are shown for each site in Figures 5.12 through 5.28.

At fast-flowing outlet glaciers, the pair lengths used to compute velocity are often smaller than those further inland where greater temporal separation is necessary to measure displacement given the slower flow speeds. Seasonal velocity variability has been observed at several of Greenland's tidewater glaciers from both GPS measurements (Sole et al., 2011) and satellite remote sensing (Lemos et al., 2018), and may impact upon the extracted velocities and thus time series. As such, we calculate the percentage of summer (JJA) coverage at each common pixel for each year using the centre-date and effective pair length, as described in Section 3.4.3. We then calculate the median summer coverage across all common pixels for each year of data, and colour-code the scatter points in Figures 5.3, 5.4 and 5.5 by these values.

5.3.6 Surface mass balance

Changes in ice motion can be driven by changes in surface mass balance (SMB), for example through meltwater input to the bed (Tedstone et al., 2015), cryo-hydrologic warming (Phillips et al., 2010, 2013), or simply the impact on local driving stress through ice thinning and surface slope change (Tedstone et al., 2015). We obtain SMB data from the MAR v3.10 regional climate model (Fettweis et al., 2017), forced by NCEP-NCARv1 from 1992 to 2019. Modelled melt production and SMB are extracted from a 3 by 3-pixel window around each GPS station, for the years 1990-1999 and 2014-2018. Mean values are calculated for

each of these time periods, which are then differenced to calculate the change in modelled melt production and SMB between the GPS and satellite velocity measurement periods.

5.4 Results

5.4.1 Multi-Decadal velocity change around the 2000 m traverse

We observe a near-ubiquitous acceleration inland of marine-terminating glaciers on the west coast (Figure 5.1). Across four GPS sites ~117 km inland of the terminus of Jakobshavn Isbrae, the largest and fastest flowing outlet glacier of the GrIS (Holland et al., 2008; Joughin et al., 2004, 2020; Khazendar et al., 2019), we observe an acceleration ranging from 7.6 ± 4.2 to 28.1 ± 7.8 m yr^{-1}.

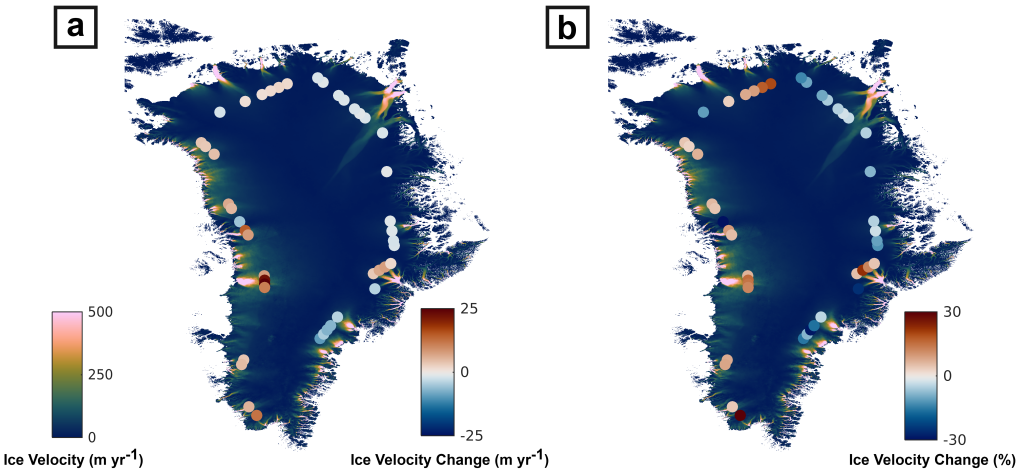

Figure 5.1: *Ice velocity change (**a:** m yr^{-1}, **b:** %) at 45 GPS sites inland of tidewater margins between the periods 1993-1997 and 2014-2018. The base image is the 2016 velocity field from the NASA MEaSUREs ITS-LIVE v0 product (Gardner et al., 2018, 2019).*

Similarly, we observe accelerations up-glacier from Narsap Sermia (3.6 ± 0.8 to 4.6 ± 1.6 m yr^{-1}) in the southwest, and inland of Rinks Isbrae (7.8 ± 2.7 to 14.6 ± 7.5 m yr^{-1}), Upernavik Isstrom (4.9 ± 1.9 to 6.3 ± 2.2 m yr^{-1}) and Kong Oscar Glacier (3.3 ± 1.0 to 3.7 ± 2.4 m yr^{-1}) respectively in central to north

west Greenland. The only glacier where we observe inland deceleration on the west coast is Umiamako Isbrae (-5.5 ± 2.8 m yr^{-1}).

North Greenland is characterised by very small changes in inland flow (-1.8 ± 0.7 to +2.1 ± 0.8 m yr^{-1}), with minor accelerations of 1.1 ± 0.4 m yr^{-1} and 1.0 ± 0.3 to 2.1 ± 0.3 m yr^{-1} inland of Petermann Glacier and Ryder Glacier, respectively. In contrast, the NEGIS (which drains into 79 North Glacier and Zacharie Isstrom) has seen a slowdown by -1.3 ± 0.7 to -1.8 ± 0.6 m yr^{-1}. To the north of the NEGIS, Academy Glacier also shows inland deceleration (-1.3 ± 0.2 to -1.8 ± 0.2 m yr^{-1}).

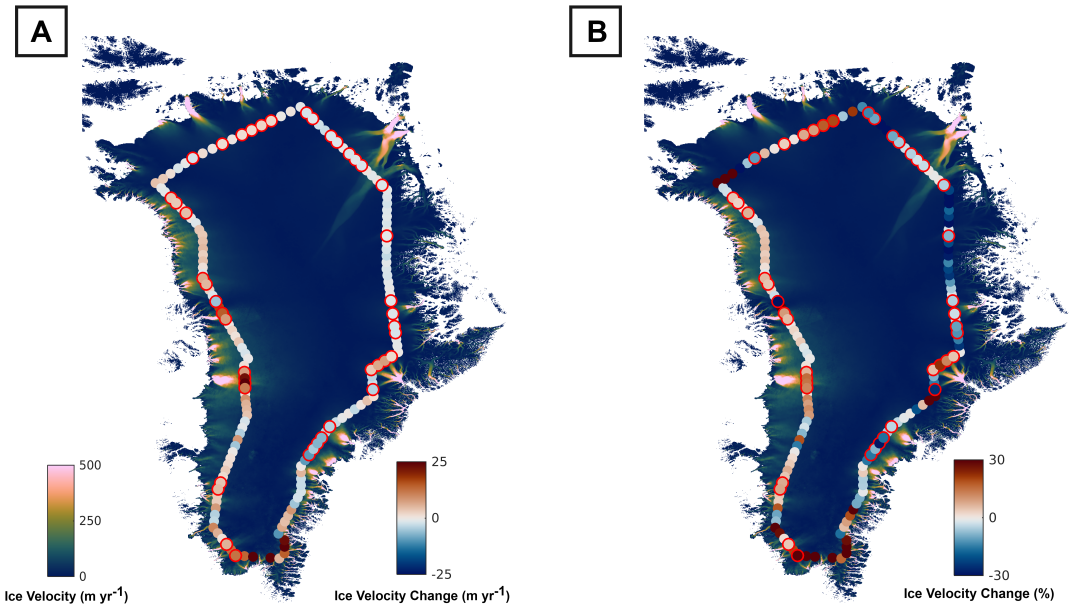

Figure 5.2: *Ice velocity change (**a:** m yr^{-1}, **b:** %) at all PARCA GPS sites inland of tidewater margins between the periods 1993-1997 and 2014-2018. The sites with a red outline are those 45 that remain after filtering and are displayed in Figure 5.1 and used in the rest of the analyses. The base image is the 2016 velocity field from the NASA MEaSUREs ITS-LIVE v0 product (Gardner et al., 2018, 2019).*

In contrast to west Greenland, interior acceleration has been largely absent from the east coast. In central-east Greenland, the inland region draining into Daugaard-Jensen Glacier has decelerated by -1.3 ± 0.4 to -1.5 ± 0.3 m yr^{-1}. Further south, Kangerlugssuaq has a more complex pattern, with a 1.7 ± 0.8 to 7.5 ± 2.2 m yr^{-1} interior acceleration inland of two of its flow branches, and a -4.0 ± 1.9 m yr^{-1} deceleration inland of the most southerly branch. In the south-east,

we observe decelerations inland of Helheim Glacier (-4.1 ± 1.2 to -6.8 ± 1.3 m yr^{-1}) and Ikertivaq (-4.9 ± 2.0 to -9.4 ± 2.8 m yr^{-1}).

Assessing velocity change at all PARCA sites, regardless of any uncertainties that would otherwise cause to be filtered out in our analyses, does not qualitatively change the overall results (Figure 5.2). There is a predominant acceleration observed along the west coast and no change or a slowdown observed along the east coast outside of Kangerlugssuaq. The PARCA sites within the southwest Greenland land-terminating margin differ to the rest of the west coast in that some evidence of slowdown is observed, however this may be due to the dynamics of land-terminating regions being different to those observed inland of tidewater glaciers.

We next assess multi-decadal (1985-2018) time series of near-terminus ITS-LIVE ice velocity (Gardner et al., 2018, 2019) downstream of our inland velocity change measurements to investigate whether the observed inland velocity change may be driven by the up-glacier propagation of acceleration at the terminus.

5.4.2 Near-terminus velocity change

Numerous studies have measured multi-annual ice velocity change near the terminus of Greenland's tidewater glaciers (e.g. Bevan et al., 2012; Howat et al., 2007, 2008b; Joughin et al., 2008a, 2010, 2018; Moon et al., 2012; Mouginot et al., 2015; Murray et al., 2010; Rignot and Kanagaratnam, 2006a). Through assessing ITS-LIVE ice velocity change (Gardner et al., 2018, 2019) from 1985 to 2018 at tidewater glacier margins (Figure 5.3) alongside these studies, we observe that those sites where ice velocities were greater between 2014-2018 than during the 1990s have also undergone large and/or rapid perturbations downstream. Conversely, five of the six sites without inland acceleration also exhibit acceleration downstream (Figure 5.4).

Where multiple GPS sites are present upstream of an individual glacier terminus, inland change is largely consistent across these GPS sites (Figure 5.1). At

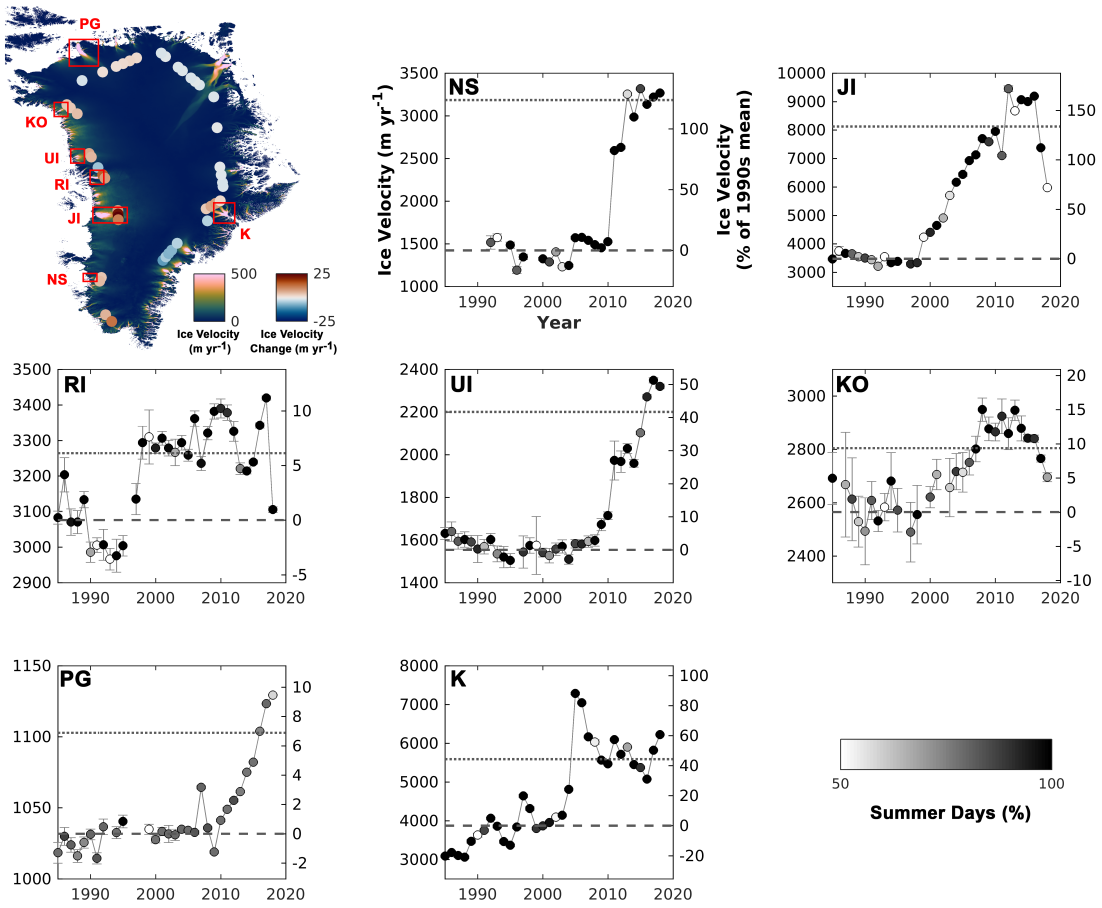

Figure 5.3: *Time series of ITS-LIVE ice velocity (m yr^{-1}) from 1985 to 2018 measured near the terminus (see Figures 5.12-5.18 for exact locations) for glaciers inland of which multi-decadal acceleration is observed;* ***(NS)*** *Narsap Sermia,* ***(JI)*** *Jakobshavn Isbrae,* ***(RI)*** *Rinks Isbrae,* ***(UI)*** *Upernavik Isstrom (Central),* ***(KO)*** *Kong Oscar Glacier,* ***(PG)*** *Petermann Glacier,* ***(K)*** *Kangerlugssuaq. Scatter points are colour-coded in greyscale by the percentage of summer (JJA) days over which ice velocities were measured in that particular year (see Sections 3.4.3 and 5.3.5). At each site, only points common to every annual velocity field included in the time series were used for velocity extraction (see Figures 5.12-5.18). The dashed line displays the average velocity between 1990-1999, and the dotted line displays the average velocity between 2014-2018. Input parameters are given in Table 5.2.*

Kangerlugssuaq however, the response is more complex. While the glacier terminus underwent a substantial acceleration between 2000 and 2006 (Bevan et al., 2012; Howat et al., 2007, 2008b; Khan et al., 2014; Rignot and Kanagaratnam, 2006a), flow diverges into four distinct branches inland (Figure 5.5), with acceleration inland of the central flow branches (2 and 3) and deceleration inland of the most southerly branch (1) between 1993-1997 and 2014-2018.

For the flow branches (2 and 3) where we observe inland acceleration (of 3.2

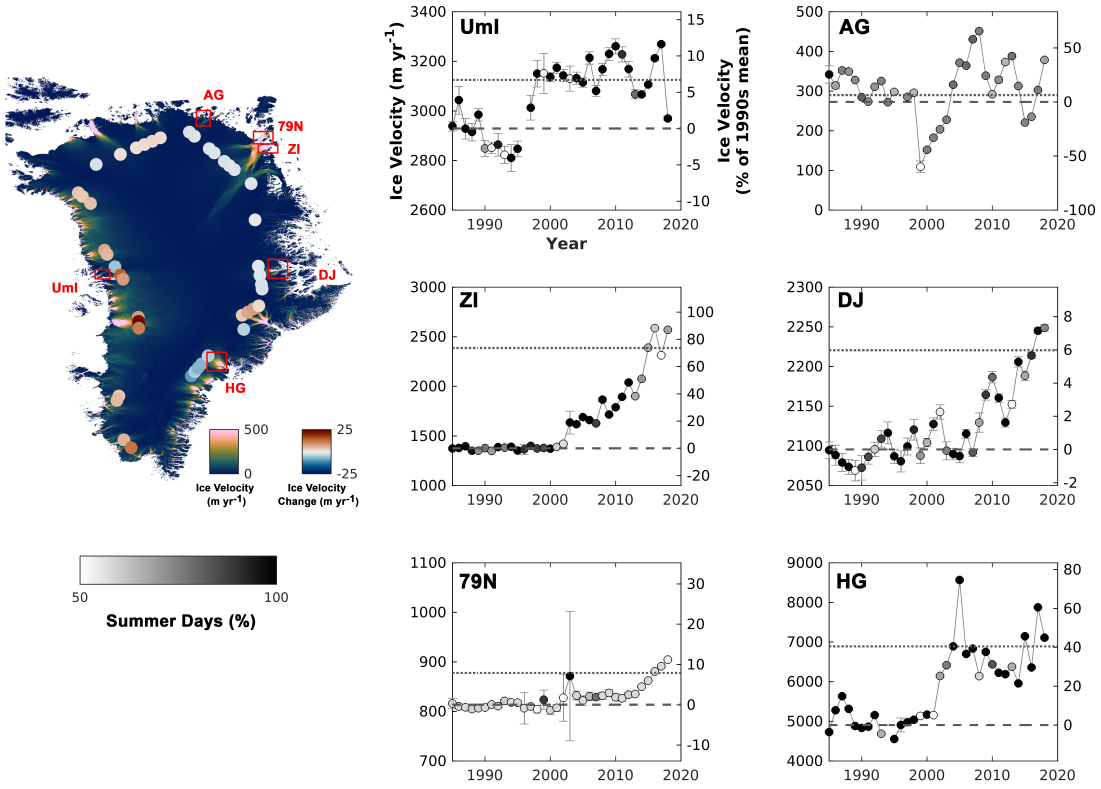

Figure 5.4: *Time series of ITS-LIVE ice velocity (m yr^{-1}) from 1985 to 2018 measured near the terminus (see Figures 5.19-5.24 for exact locations)) for glaciers inland of which no multi-decadal acceleration is observed;* ***(UmI)*** *Umiamako Isbrae,* ***(AG)*** *Academy Glacier,* ***(79N)*** *79 North Glacier,* ***(ZI)*** *Zacharie Isstrom,* ***(DJ)*** *Daugaard-Jensen Glacier,* ***(HG)*** *Helheim Glacier. Scatter points are colour-coded in greyscale by the percentage of summer days over which ice velocities were measured for that particular year (see Sections 3.4.3 and 5.3.5). At each site, only points common to every annual velocity field included in the time series were used for velocity extraction (see Figures 5.19-5.24). The dashed line displays the average velocity between 1990-1999, and the dotted line displays the average velocity between 2014-2018. Input parameters are given in Table 5.2.*

± 1.0 to 6.5 ± 1.4 m yr^{-1} and 1.7 ± 0.8 to 7.5 ± 2.2 m yr^{-1} respectively, Figure 5.1), we observe downstream speed-ups of approximately 100 m yr^{-1} (∼25%) and 75 m yr^{-1} (∼20%) between ∼2000 and ∼2008 (Figure 5.5). A similar ∼100 m yr^{-1} acceleration is observed at the most easterly branch (4), although the GPS sites inland of this flow branch are filtered out of our analysis. For the most southerly flow branch (1), inland of which we observe a deceleration (-4.0 ± 1.9 m yr^{-1}, Figure 5.1), we observe minimal downstream change (Figure 5.5), indicating that differences in downstream flow dynamics may explain the different inland responses of upstream tributaries at Kangerlugssuaq.

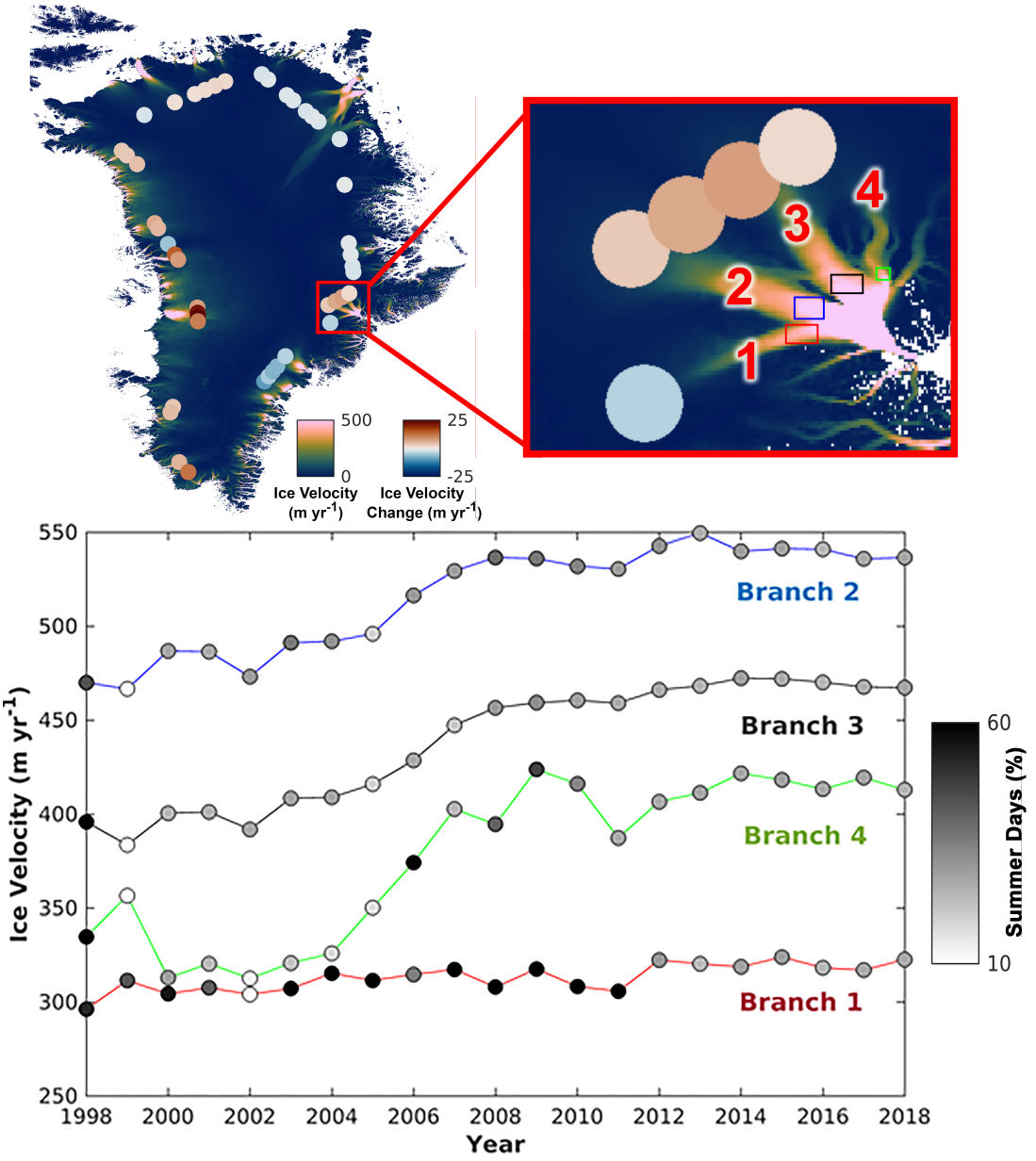

Figure 5.5: *Time series of ITS-LIVE ice velocity (m yr^{-1}) from 1998 to 2018 measured at the four flow branches of Kangerlugssuaq, with velocity extraction from pixels within the rectangle on each branch. Scatter points are colour-coded by the percentage of summer days over which ice velocities were measured for that particular year (see Sections 3.4.3 and 5.3.5). At each site, only the points common to every velocity field included in the time series were used for velocity extraction (see Figures 5.25-5.28). Input parameters are given in Table 5.2.*

5.4.3 Influence of ice geometry

Whilst glaciers that show interior acceleration are characterised by downstream acceleration, several glaciers that have also experienced downstream speed-up exhibit no inland acceleration. Consequently, dynamical change at the mar-

gin alone is not necessarily indicative of interior acceleration. To assess whether downstream ice geometry can explain the inland heterogeneity in velocity change between 1993-1997 and 2014-2018, we compare the observed velocity change to basal topography and the extent of subglacial troughs (Figure 5.6, Table 5.1). It is clear that for six out of the eight of glaciers where we observe inland acceleration, the overdeepened subglacial trough extends further or at least a comparable distance inland to the PARCA GPS stations (Table 5.1). This is most evident at Jakobshavn Isbrae, where we observe inland acceleration at 4 GPS sites, all of which lie within an extensive region underlain by deep basal topography (Figure 5.6). Conversely, for four of the seven glaciers where we observe inland deceleration, the GPS stations are largely located far beyond the maximum extent of any subglacial trough, indicating that subglacial topography (and thus ice geometry) may play an important role limiting the propagation distance of perturbations at the terminus for certain glaciers. This pattern, however, is not ubiquitous; for example, we do not observe inland acceleration at 79 North Glacier or Zacharie Isstrom despite extensive subglacial troughs while conversely, we observe acceleration inland of Kangerlugssuaq despite the GPS sites being located ∼50 km further inland than the head of the respective subglacial trough.

5.4.4 Influence of surface mass balance

Within the accumulation zone in southwest Greenland, increases in surface melt have been hypothesised to drive acceleration through hydro-dynamic coupling (Doyle et al., 2014) and/or cryo-hydrologic warming (Phillips et al., 2010, 2013). Data from MAR v3.10 (Fettweis et al., 2017) suggest ice-sheet-wide increases in modelled surface melt production within the interior (Figure 5.7A, 5.7B) between the periods 1990-1999 and 2014-2018. The largest increases (42 - 270 mm yr^{-1}) are observed in the west and southeast, whereas increases in the north and north east are very small (0 - 45 mm yr^{-1}). All of the PARCA GPS sites are characterised by positive SMBs during both the 1990-1999 and 2014-2018 periods (Figure 5.7C, 5.7D), which ranges from ∼90-200 mm yr^{-1} in the north to more positive values of ∼200-1900 mm yr^{-1} and ∼300-650 mm yr^{-1} along the east and

west coasts, respectively.

5.5 Discussion

5.5.1 Mechanisms driving inland change

Our results reveal a complex pattern of inland velocity change over the ∼20-year period between 1993-1997 and 2014-2018, for which there exist several possible driving mechanisms.

Whilst we do observe increases in modelled surface melt production at all of the GPS sites, and decreases in modelled SMB at most (Figure 5.7), we see no evidence that any of the sites have undergone a transition from the accumulation to the ablation zone during the study period. Although cryo-hydrologic warming may also occur in the wet snow zone of the lower accumulation zone (Phillips et al., 2013), all 45 sites remain well within the accumulation zone as evidenced by positive modelled SMBs during 2014-2018 (all >∼10 cm w.e., with a mean of 43 cm w.e., Figure 5.7D). This is consistent with in-situ stake observations which show no evidence of negative SMB above ∼1700 m (a.s.l.) across 17 sites in Greenland (Machguth et al., 2016), and a persistent positive SMB at site S10 (1850 m a.s.l.) of the K-transect in southwest Greenland (Van De Wal et al., 2012), despite increases in surface melt at this site (Doyle et al., 2014). Furthermore, analysis of surface strain rates indicates that moulins and crevasses are unlikely to form above 1600 m (a.s.l.), and so meltwater access to the englacial drainage system is likely limited at these elevations (Poinar et al., 2015) and will instead flow along surface streams into moulins further downstream.

Glacier Name *Location*	Distance of PARCA GPS Site from Terminus (km) Min	 Max	Subglacial Trough Length (km)* *(Morlighem and others, 2014)*	Trough Length - Average Distance Inland (km)	Inland Velocity Change (m yr^{-1}) Min	 Max
Central and South West						
Narsap Sermia	92	92	77	-15	3.6	4.6
Jakobshavn Isbrae	117	118	170	52.5	7.6	28.1
North West						
Rinks Isbrae	90	94	88	-4	7.8	14.6
Umiamako Isbrae	115	115	39	-76	-5.5	-5.5
Upernavik Isstrom (C)	97	97	90	-7	4.9	6.3
Kong Oscar Glacier	85	86	101	15.5	3.3	3.7
North						
Petermann Glacier	200	200	400	200	1.1	1.1
Ryder Glacier	180	216	191	-7	1	2.1
Academy Glacier	153	165	102	-57	-1.8	-1.3
North East						
79 North Glacier	210	219	404	189.5	-1.6	-1.5
Zacharie Isstrom	190	240	377	162	-1.8	-1.3
Central and South East						
Daugaard-Jensen Glacier	108	137	70**	-52.5	-1.5	-1.3
Kangerlugssuaq	131	141	87	-49	-4	7.5
Helheim Glacier	118	120	68	-51	-6.8	-4.1
Ikertivaq	96	130	0	-113	-9.4	-4.9

Table 5.1: *Comparison of PARCA GPS distance inland and measured velocity change (m yr^{-1}) between 1993-1997 and 2014-2018 with the extent of subglacial troughs (Morlighem et al., 2014, their Table S1) at 15 tidewater glaciers on the Greenland Ice Sheet. As neighbouring GPS sites may have differing distances from the margin, we compare the average distance of these sites inland of a particular glacier to the subglacial trough length at that glacier. *Subglacial trough lengths were calculated by Morlighem et al., 2014 using the longest flowline that connects the ice front to the interior of the ice sheet, and do not necessarily follow the glacier centreline. **Daugaard-Jensen Glacier is stated to have a trough length of 70 km in the main manuscript, with a maximum trough length of 124 km given in the SI.*

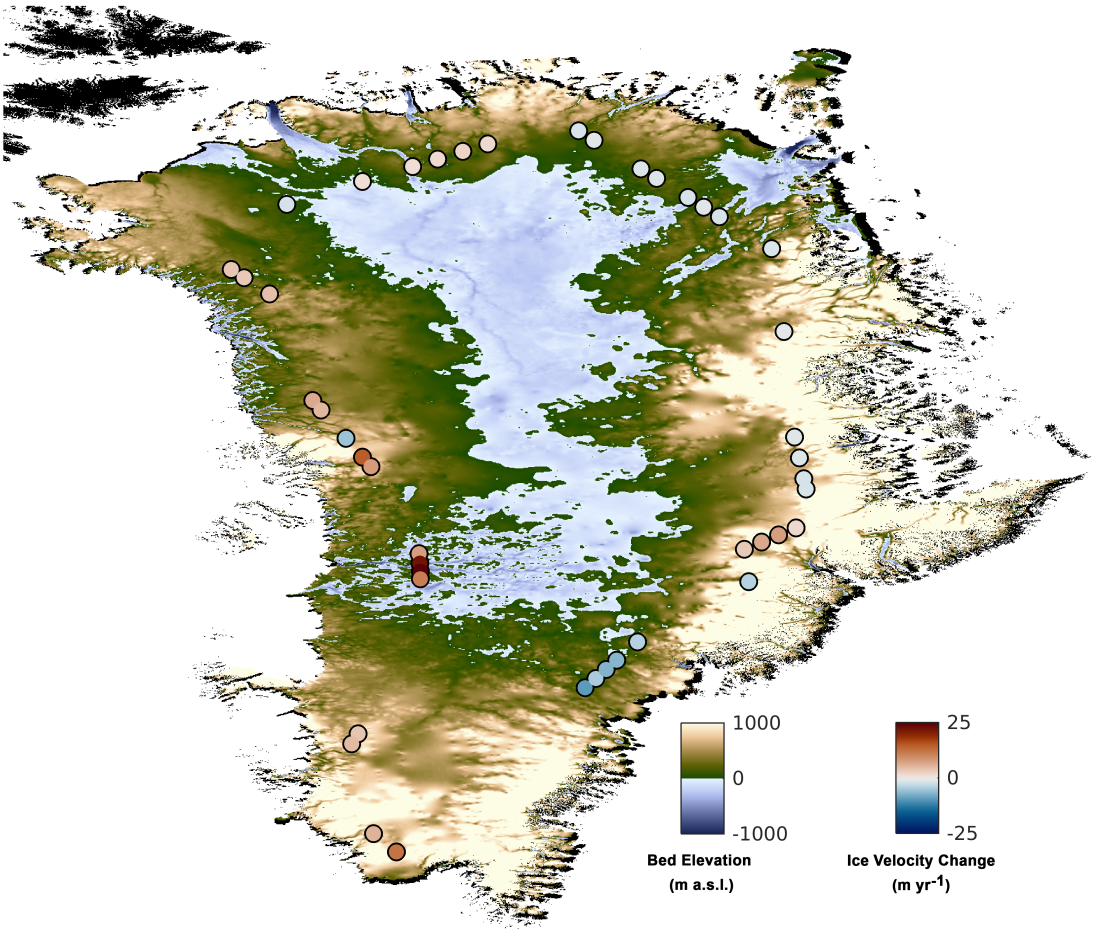

Figure 5.6: *Ice velocity change (m yr^{-1}) at 45 GPS sites inland of tidewater margins between the periods 1993-1997 and 2014-2018, compared to basal topography from BedMachineV3 (Morlighem et al., 2017).*

Ice flow may also be affected by the presence of firn aquifers, which are thought to be extensive in southeast Greenland (Brangers et al., 2020; Miège et al., 2016) and which may store significant quantities of meltwater for several decades (Forster et al., 2014; Harper et al., 2012; Miller et al., 2018). Water stored in firn may increase ice motion through latent heat transfer (Phillips et al., 2010, 2013; Poinar et al., 2017) and/or through drainage to the bed (Miège et al., 2016; Poinar et al., 2017, 2019). In the case of the latter, the presence of a firn aquifer may buffer the supply of meltwater to the bed, and thus possibly mask any long-term trend between ice velocity and meltwater production. However, drainage from firn aquifers is thought to most likely occur where there exists a downstream crevasse field through which it can drain to the bed (Miège et al.,

2016), and so may have a limited impact upon ice flow at the inland locations assessed in this study.

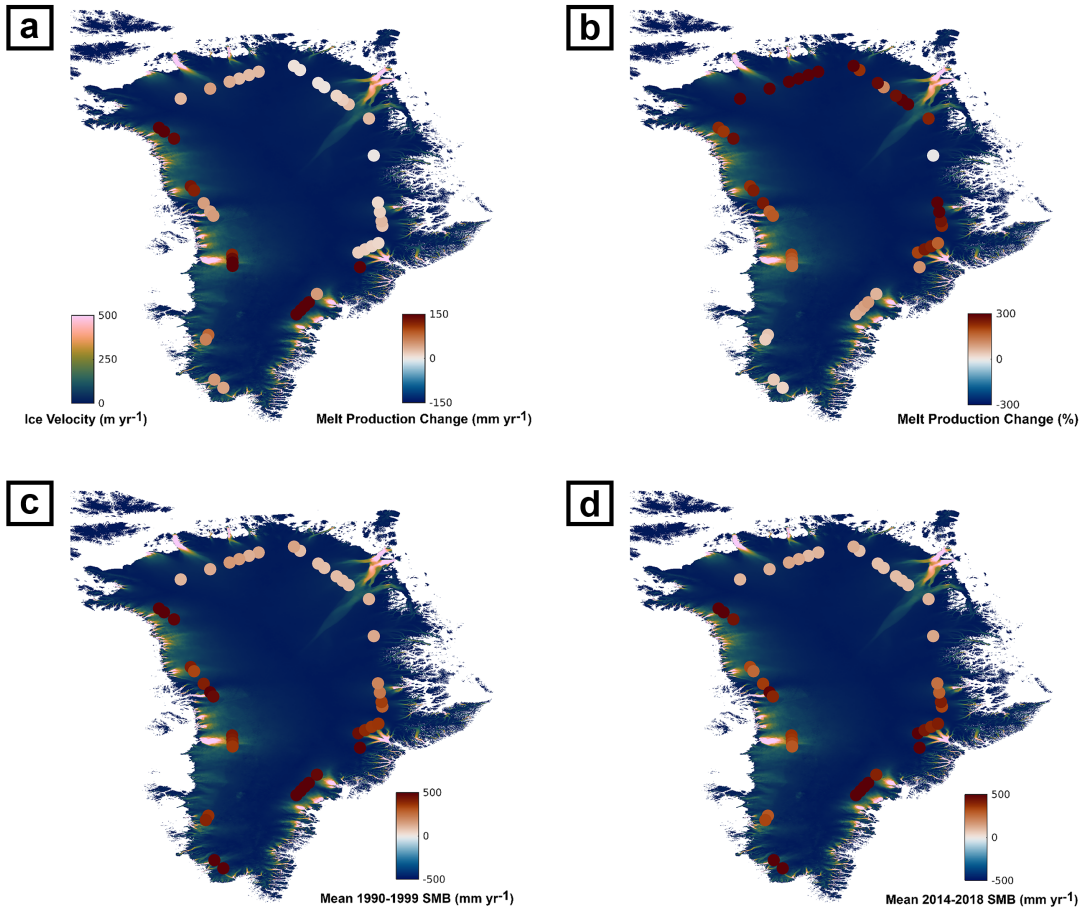

Figure 5.7: ***(a)*** *Modelled surface melt production change (mm* yr^{-1}*),* ***(b)*** *modelled surface melt production change (%),* ***(c)*** *mean modelled 1990-1999 SMB (mm* yr^{-1}*) and* ***(d)*** *mean modelled 2014-2018 SMB (mm* yr^{-1}*) at 45 GPS sites inland of tidewater margins. Modelled melt production change is calculated between the 1990-1999 and 2014-2018 means. The base image is the 2016 velocity field from the NASA MEaSUREs ITS-LIVE v0 product (Gardner et al., 2018, 2019). Modelled surface melt production and SMB data are from MAR v3.10 (Fettweis et al., 2017).*

Changes in surface slope and/or ice thickness through both ice dynamical and SMB-related processes cause changes in driving stress and can thus contribute to changes in ice motion through changes to the internal deformation rate. To assess whether the velocity changes observed may be explained by changes in local driving stress, we estimate the expected change in velocity as a result of changes in ice thickness and surface slope at PARCA GPS site 36, inland of Jakobshavn Isbrae, where we observe the largest velocity increase. Applying this calcula-

tion elsewhere is difficult as the observed velocity changes are small (Figure 5.1), the uncertainties associated with the surface elevation change are proportionally large, and the potential errors associated with the following 20-year approximate surface elevation change reconstruction, and thus the 1990s slope estimate, are too great, thus reducing confidence in our ability to make any meaningful comparison.

We extract ice thickness and surface slope, the latter calculated using surface elevation and under the assumption that ice flows in the direction of the steepest slope, at this location from BedMachineV3 (Morlighem et al., 2017), and consider this as representative for the period 2014-2018. We then use the CCI surface elevation change (SEC) v2.0 product (Sandberg Sørensen et al., 2018; Simonsen and Sørensen, 2017) to calculate the cumulative SEC at each pixel within the 3*3-pixel window surrounding site 36, across the periods 1993-1997, 1998-2002, 2003-2007, 2007-2011, and 2012-2016. By adding this SEC to the ice thickness from BedMachineV3, we get a rough estimate of the initial ice thickness in 1993. Similarly, by adding the cumulative SEC to the BedMachineV3 surface elevation within the same 3*3-pixel window, we calculate an approximate initial surface slope for 1993. We subsequently calculate the change in ice thickness and surface slope.

The first-order change in surface velocity (δu_s) as a result of changes in ice thickness and surface slope can be characterised by the following (Tedstone et al., 2015):

$$\delta u_s = u_s(3\frac{\delta S}{S} + 4\frac{\delta H}{H}) \tag{5.3}$$

Where u_s represents the initial ice surface velocity (194.5 m yr^{-1}), S and H represent the initial surface slope (0.018 m/m) and ice thickness (1740.2 m) respectively, and δS and δH represent the change in surface slope (0.001 m/m) and ice thickness (-7.2 m) respectively. The resultant approximation for a change in deformational velocity is 35.02 m yr^{-1}, which is within the uncertainty range of the observed velocity change (28.1 $\pm$ 7.8 m yr^{-1}) and thus compares well.

We also assess the role that SMB-driven thickness changes play in driving velocity change (Mernild et al., 2013). There has been extensive SMB-driven thinning around Greenland (Mouginot et al., 2019; van den Broeke et al., 2009), for example, at site 36, modelled melt production increases by 150 mm yr^{-1} between the 1990-1999 and 2014-2018 means (Figure 5.7A). However, we observe no obvious spatial correlation between changes in ice velocity (Figure 5.1) and modelled surface melt production. Whilst we do observe large increases in surface melting ($>$ 100 mm yr^{-1}) at some GPS sites where we observe acceleration (i.e., inland of Jakobshavn Isbrae, Upernavik Isstrom, and Kong Oscar Glacier in the central to northwest), the GPS sites on the east coast show an almost pervasive deceleration despite increases in modelled melt production. This is most notable at the south-eastern GPS sites, where increases in modelled melt production are of a similar or greater magnitude (47 – 270 mm yr^{-1}) to those in the central and northwest (42 – 162 mm yr^{-1}).

To assess the impact of this SMB forcing alone, we follow Tedstone et al., 2015 by taking a 100 km transect, extending 50 km either side of site 36, and calculating the slope change from the linear change in ice thickness over this distance. Modelled melt production increased by 184.5 mm yr^{-1} and 41.3 mm yr^{-1} between the 1990-1999 and 2014-2018 means at the downstream and upstream ends of the transect respectively, a difference of 143.2 mm yr^{-1}, and the concurrent change in accumulation rate is negligible. Assuming a linear increase in melt production over 20 years, this gives a total thinning of 1.5m and a steepening of 0.000015 m/m.

Applying the above equation (5.3), we estimate the associated change in deformational velocity as -0.18 m yr^{-1}, indicating that at site 36, SMB changes alone are unable to explain the observed velocity acceleration, and may counteract some of the observed velocity increase. The modelling therefore suggests that in this inland region of the ice sheet, changes in surface slope are insuffi-

cient to overcome the reduction in driving stress caused by thinning. At all other sites where we observe acceleration, modelled melt production increase is either similar (northwest Greenland) or less than that observed inland of Jakobshavn Isbrae (Figure 5.7A). As such, assuming a relatively consistent ice sheet hypsometry, this suggests that change in SMB may often act to oppose acceleration and is unlikely to drive an inland velocity change of more than several tens of cm yr^{-1}.

Changes to surface mass balance (SMB) have also been hypothesised to influence ice motion through cryo-hydrologic warming in regions transitioning from the accumulation to the ablation region (Phillips et al., 2010, 2013). Despite increases in modelled melt production, we observe that all of the PARCA GPS sites have strongly positive modelled SMB in both the 1990-1999 and 2014-2018 periods (Figure 5.7C, 5.7D), and so we observe no evidence of a transition between accumulation and ablation zones at any site, with all 45 GPS sites remaining well within the accumulation zone.

As a result, we argue that our observations of inland acceleration are most likely driven by the upstream propagation of changes initiated at the terminus (Felikson et al., 2017; Howat et al., 2005; Howat et al., 2007; Joughin et al., 2008a; Nick et al., 2009; Price et al., 2008; Price et al., 2011). This mechanism is discussed in more detail in the subsequent sections.

5.5.2 Observed velocity changes and regional differences

We observe almost ubiquitous acceleration across the GPS sites inland of tidewater glaciers in west Greenland with a slowdown at Umiamako Isbrae being the only exception. The largest acceleration is observed ~117 km inland from the terminus of Jakobshavn Isbrae (7.6 ± 4.2 to 28.1 ± 7.8 m yr^{-1}), which is unsurprising given the high magnitude of acceleration and thinning observed near the terminus between the late-1990s and early-2010s (Holland et al., 2008; Joughin et al., 2014; Joughin et al., 2004, 2008a, 2018; Luckman, 2005; Moon et al., 2012), primarily as a result of reduced back-stress through the loss of its floating ice

tongue (Holland et al., 2008; Joughin et al., 2004; Motyka et al., 2011; Thomas, 2004). Moreover, modelling of dynamic thinning suggests that faster ice flow facilitates a larger magnitude propagation inland, with modelled thinning rates at 2000 m elevation of nearly -0.4 m yr^{-1} within a drainage system with a mean flow velocity of ~120 m yr^{-1} as opposed to an ice-sheet-wide average of approximately -0.1 m yr^{-1} with a mean velocity of ~60 m yr^{-1} (Wang et al., 2012), and Jakobshavn Isbrae is the fastest flowing outlet glacier on the Greenland Ice Sheet (i.e. Joughin et al., 2004, 2018).

We also observe inland acceleration at other tidewater glaciers in west Greenland that have undergone terminus retreat and associated near-terminus acceleration, such that their 2014-2018 ice velocities were greater than during the 1990s (Figure 5.3). For example, the northern and central branches of Upernavik Isstrom underwent rapid calving, retreat and acceleration beginning during the mid-late 2000s (Khan et al., 2013; Larsen et al., 2016), and Narsap Sermia accelerated and retreated by approximately 3.3 km between 2010 and 2014, primarily as a result of increased submarine melting (Motyka et al., 2017). Similarly, Kong Oscar Glacier and Rinks Isbrae retreated by several kilometres during the mid-2000s (Bevan et al., 2012) and the mid-late 1990s (Catania et al., 2018) respectively, in conjunction with acceleration (Figure 5.3). Inland of these west coast glaciers, we observe acceleration ranging from 3.3 ± 1.0 to 3.7 ± 2.4 m yr^{-1} inland of Kong Oscar Glacier up to 14.6 ± 7.5 m yr^{-1} inland of Rinks Isbrae. However, we observe a clear contrast between the dynamics of west and east Greenland. Whilst outlet glaciers on the west coast almost all demonstrate inland acceleration, there is little evidence of propagation of downstream change inland of tidewater glacier termini on the east coast. We observe no evidence of inland acceleration at Helheim Glacier, Zacharie Isstrom and 79 North Glacier, all of which have undergone significant frontal retreat and acceleration at some point between our measurement periods of 1993-1997 and 2014-2018 (Bevan et al., 2012; Howat et al., 2005; Howat et al., 2007, 2008b; Mouginot et al., 2015; Murray et al., 2010; Rignot and Kanagaratnam, 2006a; our Figure 5.4).

The duration of a specific terminus perturbation does not appear to control the likelihood of that perturbation propagating inland. We observe inland acceleration at sites with long-term perturbations (Jakobshavn Isbrae, Upernavik Isstrom, Kong Oscar Glacier) as well as at sites with relatively short-term accelerations (i.e. Kangerlugssuaq, Narsap Sermia), although all sites where we observe acceleration were flowing faster in their terminus regions during 2014-2018 than 1990-1999. Moreover, we observe no inland acceleration at Zacharie Isstrom despite continual acceleration since the early-2000s, or at Helheim Glacier which underwent a rapid speed-up of short duration from ∼2002-2005 (Figure 5.4). It may be that perturbations at the terminus have yet to propagate to the PARCA GPS sites inland of some tidewater glaciers, particularly in the north and north east (Figure 5.9) where the GPS sites are ∼165-240 km inland from the terminus as opposed to ∼85-141 km on the east and west coasts. Thinning has been observed to propagate along ice streams in West Antarctica at rates of 6-15 km yr^{-1} (Konrad et al., 2017) while acceleration near the terminus of Kangerlugssuaq propagated 10 km up-glacier between 2005 and 2006 (Howat et al., 2007). Whilst recent work observes propagation rates in the lowest 20 km of Jakobshavn Isbrae an order of magnitude faster than the local mean flow speed (Riel et al., 2021), rates of propagation have not been observed further inland, or elsewhere in Greenland, and we are unable to determine propagation rates given the gap in our time series. Surface velocities derived from Landsat missions prior to Landsat-8 are characterised by both a reduced spatial coverage in inland regions, due to insufficient radiometric resolution to measure subtle features on the ice sheet surface (Fahnestock et al., 2016), and increased uncertainties, which are particularly problematic given the slow surface velocities as one moves inland. Regardless, it is plausible that perturbations have not yet had the time to propagate sufficiently far inland to be observed at the PARCA GPS sites in north east Greenland, especially given that the rate of propagation will slow as it moves further inland (van der Veen, 2001). This is supported by separate velocity measurements, which show no evidence of acceleration beyond ∼80-100 km and ∼50 km inland of Zacharie Isstrom and

79 North Glacier respectively (Mouginot et al., 2015; their Figure 2). Further south at Daugaard-Jensen and Helheim Glaciers however, the PARCA GPS sites are a comparable distance inland to those on the west coast, as well as those at Kangerlugssuaq, which have undergone acceleration in response to terminus perturbations, indicating that there may be an alternative control on the speed and/or limit of propagation (i.e., Felikson et al., 2017, 2020).

5.5.3 Influence of basal topography and ice geometry

Basal topography is a crucial factor controlling ice flow. Beneath the Greenland ice sheet, widespread ice-filled valleys have been observed to extend significantly deeper below sea-level and farther inland than previously thought (Morlighem et al., 2014), thereby channelling ice flow over distances from tens to hundreds of kilometres. Since deep troughs and the associated thicker ice lead to both higher driving stresses and warmer ice, they will encourage faster ice flow and potentially greater propagation distances (Wang et al., 2012). We observe almost ubiquitous interior acceleration in the central and northwest regions, across areas that are characterised by low surface slopes and bed topography that remains below sea level for tens to hundreds of kilometres inland (Morlighem et al., 2017).

For example, Jakobshavn Isbrae flows through a subglacial valley extending ∼170 km inland (Morlighem et al., 2014), whereas the PARCA GPS sites are located ∼117 km from the terminus (Table 5.1). Under these conditions, not only do we observe the large acceleration at the terminus, but this acceleration is likely to be channelled to, and beyond, the site at which we measure inland velocity change in this study. Similar patterns are observed at other west coast glaciers, where PARCA GPS sites are closer to the margin than the extent of the associated subglacial valleys, or, if further inland than the head of the valley, are at least within the theoretical stress-coupling length (4-10x the ice-thickness (Kamb and Echelmeyer, 1986)) of the maximum subglacial valley extent. In contrast, the one glacier on the west coast where we do not observe inland acceleration is Umiamako Isbrae, despite near-terminus flow velocities ∼200 m yr^{-1} greater in the 2000s and

2010s compared to the early- to mid-1990s (Figure 5.4). Here, an overdeepened subglacial valley extends just ∼39 km from the terminus (Morlighem et al., 2014), whereas the PARCA GPS site is located ∼115 km inland.

In the north, we observe no inland acceleration at Academy Glacier, where the head of the submarine valley is ∼57 km closer to the terminus than the PARCA GPS sites. Similarly, outside of two flow branches of Kangerlugssuaq, we observe no evidence of interior propagation on the east coast, where despite the existence of deep subglacial valleys (Morlighem et al., 2017), basal topography rises quickly to plateaus above sea level (Morlighem et al., 2014), suggesting that these rapid rises in basal topography may limit the inland propagation of any thinning perturbation. This is the case at Helheim Glacier and Daugaard-Jensen Glacier, which are both grounded below sea-level for ∼70 km, whereupon rises in basal topography over a short-distance have been theorised to prevent rapid glacier retreat or ice sheet drawdown (Morlighem et al., 2014). Given that the PARCA GPS sites inland of Helheim Glacier and Daugaard-Jensen Glacier are approximately 118-120 km and 108-137 km from the terminus respectively, it is plausible that any perturbation at the terminus is limited by the rapid rise in basal topography at the end of the subglacial trough, such that no inland response is observed in our study.

This hypothesis, and our observations, are largely consistent with recent work that argues that steep rises (termed 'knickpoints') in bedrock topography act to limit the extent of inland thinning, such that the gentle basal topography of the northwest facilitates the propagation of thinning far into the ice sheet interior, and the mountainous basal topography of the central east and southeast limits propagation to near the margin (Felikson et al., 2020). We observe inland acceleration at Rinks Isbrae, Upernavik Isstrom and Kong Oscar Glacier in the northwest, consistent with proposed thinning limits of >400 km, >300 km and ∼500 km, respectively (Felikson et al., 2020). Likewise, our observation of no inland speed-up at Umiamako Isbrae is consistent with a thinning limit of 43.8 km,

considerably downstream of the PARCA GPS site. Our results are also in agreement on the east coast, where Daugaard-Jensen Glacier and Helheim Glacier are characterised by thinning limits of 53.5 km and 26.7 km (Felikson et al., 2020), again located >50 km downstream of the PARCA GPS sites and in line with lack of inland acceleration observed in this study. Whilst both 79 North and Zacharie Isstrom show no inland acceleration despite extensive subglacial valleys extending beyond the PARCA GPS sites, as noted previously, it is plausible that since these sites are several hundred kilometres from the margin, the propagation speed is such that any downstream perturbation has not yet reached them. Alternatively, knickpoints in bed topography may limit any dynamic propagation to approximately 100-120 kilometres inland of the termini of these glaciers, considerably downstream from the PARCA GPS sites in this region (Felikson et al., 2020).

Our observations of inland acceleration at Jakobshavn Isbrae, Narsap Sermia and Kangerlugssuaq, however, are in contrast to the thinning limits suggested by Felikson et al., 2020 at these glaciers (57.9 km, 37.3 km, and 35.3 km respectively). As Felikson et al., 2020 argue that the Pe = 3 threshold accounts for 89 % (with an interquartile range of 76-100 %) of the total dynamic loss, our observations of acceleration inland of these glaciers may represent the remaining ∼11 % of dynamic change that has propagated beyond the empirical thinning limit. Alternatively, at Jakosbhavn Isbrae, there may be some uncertainty associated with the choice of flowline within the Pe analysis, with earlier work indicating a thinning limit of 240 km (Felikson et al., 2017) compared to the more recent 57.9 km estimate (Felikson et al., 2020).

Whilst we observe acceleration inland of the suggested thinning limits at Jakobshavn Isbrae and Narsap Sermia, these accelerations remain consistent with the extent of underlying subglacial troughs (Table 5.1). In contrast, at Kangerlugssuaq our observed acceleration is both ∼100 km inland of the thinning limit proposed by Felikson et al., 2020, and ∼49 km inland of the maximum subglacial trough extent. Consequently, whilst basal topography and ice geometry appear to

offer a compelling explanation for much of the observed inland velocity change, it is clear that the processes controlling tidewater glacier dynamics are complex. As such, multiple controls will likely impact the ability for a terminus perturbation to propagate inland, thus affecting how different inland regions of the Greenland Ice Sheet have responded and will continue to respond to climate warming.

5.5.4 Comparison with other studies

Recent measurements of mass change between 2003 and 2019 from ICESat and ICESat-2 show a clear pattern of coastal thinning around the entire periphery of the Greenland Ice Sheet, which decreases inland and changes to thickening at 2000-2500 m (a.s.l.) in southern and western Greenland, and at 1500 m (a.s.l.) in the north east (Smith et al., 2020). Thinning extends furthest inland at Jakobshavn Isbrae and in the northwest, consistent with our observations of multi-decadal accelerations in these inland regions. Similarly, mass change is far more limited in extent in the central east and northeast regions where we do not observe inland acceleration, although in the southeast, thinning appears to extend to approximately the locations of the GPS sites at which we observe no acceleration. As the dynamic component of mass change is not isolated in these ICESat and ICESat-2 data, the south-eastern thinning may be influenced by a decrease in SMB, which has contributed to 36 $\pm$ 12 % of mass loss in this region between 1972 and 2018 (Mouginot et al., 2019).

Measurements of surface elevation change can be used to isolate the dynamic component of a thinning signal through the differencing of measured elevation change and modelled SMB (i.e., McMillan et al., 2016) or comparing the rate of change between adjacent fast- and slow-flowing areas within the same climatic setting (Pritchard et al., 2009). This methodology has revealed extensive dynamic thinning, penetrating deep into the ice sheet interior. At Jakobshavn Isbrae, thinning has been observed ~120 km inland (Pritchard et al., 2009), extending upwards of 2000 m surface elevation as early as 2001 (Thomas et al., 2003). Similar pervasive thinning has been observed inland of other fast-flowing tide-

water glaciers, notably Helheim Glacier, Kangerlugssuaq, Upernavik Isstrom and Zacharie Isstrom (McMillan et al., 2016; Pritchard et al., 2009). On a regional scale, the northwest and southeast margins are characterised by the strongest dynamic thinning (Csatho et al., 2014; Pritchard et al., 2009; Zwally et al., 2011) although the furthest propagation of thinning inland is observed in the west and northwest, with thinning in the southeast less extensive (Csatho et al., 2014; Zwally et al., 2011). Moreover, in the southeast, the inland extent of dynamic thinning has been observed to rapidly decrease between the period 2003-2005 and 2009 (Csatho et al., 2014), and outside of Kangerlugssuaq, significant signals of dynamic thinning are not clear (McMillan et al., 2016).

These observations are reinforced by modelling work, which indicates that dynamic thinning may penetrate deep into the ice sheet in as little as ten years of an initial perturbation, with modelled thinning rates of up to 40 cm yr^{-1} extending to 2000 m elevation in central west and northwest Greenland (Wang et al., 2012). For the fast-flowing outlet glaciers of Jakobshavn Isbrae, Helheim Glacier and Kangerlugssuaq, modelling of dynamic thinning along the centre-profile between 2003 and 2005 suggests thinning during this period would reach ∼80-100 km inland of the terminus at Jakobshavn Isbrae and ∼30-40 km inland at both Helheim Glacier and Kangerlugssuaq (Price et al., 2011).

Our work largely supports these studies. We observe a strong interior acceleration inland of Jakobshavn Isbrae, a region characterised by extremely strong dynamic thinning (Csatho et al., 2014; McMillan et al., 2016; Pritchard et al., 2009; Zwally et al., 2011), with speed-ups of smaller magnitude inland of other west coast tidewater glaciers. We observe interior acceleration upstream of two of the main flow branches of Kangerlugssuaq on the east coast, and do not measure any long-term interior acceleration inland of Helheim Glacier or Zacharie Isstrom, despite indications of some penetration of dynamic thinning inland at these glaciers (McMillan et al., 2016; Pritchard et al., 2009). Our observations in northeast Greenland are supported by other satellite-image-derived velocities,

which indicate little if any interior acceleration inland of Zacharie Isstrom and 79 North Glacier beyond approximately ∼80-100 km and ∼50 km from the terminus respectively (Mouginot et al., 2015).

5.6 Conclusions

In this study, we present the first multi-decadal analysis of ice-sheet-wide changes in ice velocity within the accumulation zone of the Greenland Ice Sheet. Along the west coast, we observe evidence of inland acceleration, most likely in response to perturbations originating at tidewater glacier termini. In contrast, away from Kangerlugssuaq, we observe no inland acceleration on the east coast, despite acceleration and thinning at the terminus of many of these marine-terminating glaciers. The complexity within the observed pattern of inland change likely reflects a range of controls, including the speed at which a perturbation can propagate inland, and the influence of ice geometry and basal topography in facilitating or limiting the extent to which a perturbation can propagate up-glacier.

These findings are of great importance with regards to Greenland's future contribution to global sea-level rise, as they indicate that ice acceleration at many tidewater glaciers has the potential to propagate considerable distances into the ice-sheet interior, accelerating the draw-down of greater volumes of thicker ice toward the margins, thus accelerating mass loss. Moreover, our results indicate that this mass loss as a result of the draw-down of ice from the interior should be further exacerbated by future acceleration and thinning perturbations at tidewater margins. However, our results also support recent work that indicates that local ice geometry and bed topography are crucial in facilitating or limiting the ability for a perturbation at the terminus to propagate inland (Felikson et al., 2017, 2020; Morlighem et al., 2014, 2017), and suggest that as a result of steep down-glacier bed topography, inland regions in east Greenland may be more resilient to the impacts of future outlet glacier acceleration than those in the west. This is consistent with recent work that suggests that the presence of steep subglacial

knickpoints limits the extent to which thinning can diffuse inland, particularly in the southeast, whereas the gentle bed topography of the northwest facilitates the propagation of thinning hundreds of kilometres inland (Felikson et al., 2020). Consequently, we expect that Greenland's future contribution to global sea-level rise will be spatially complex and will depend on the ability for dynamic changes at the termini of individual outlet glaciers to propagate inland.

5.7 Supplementary Information

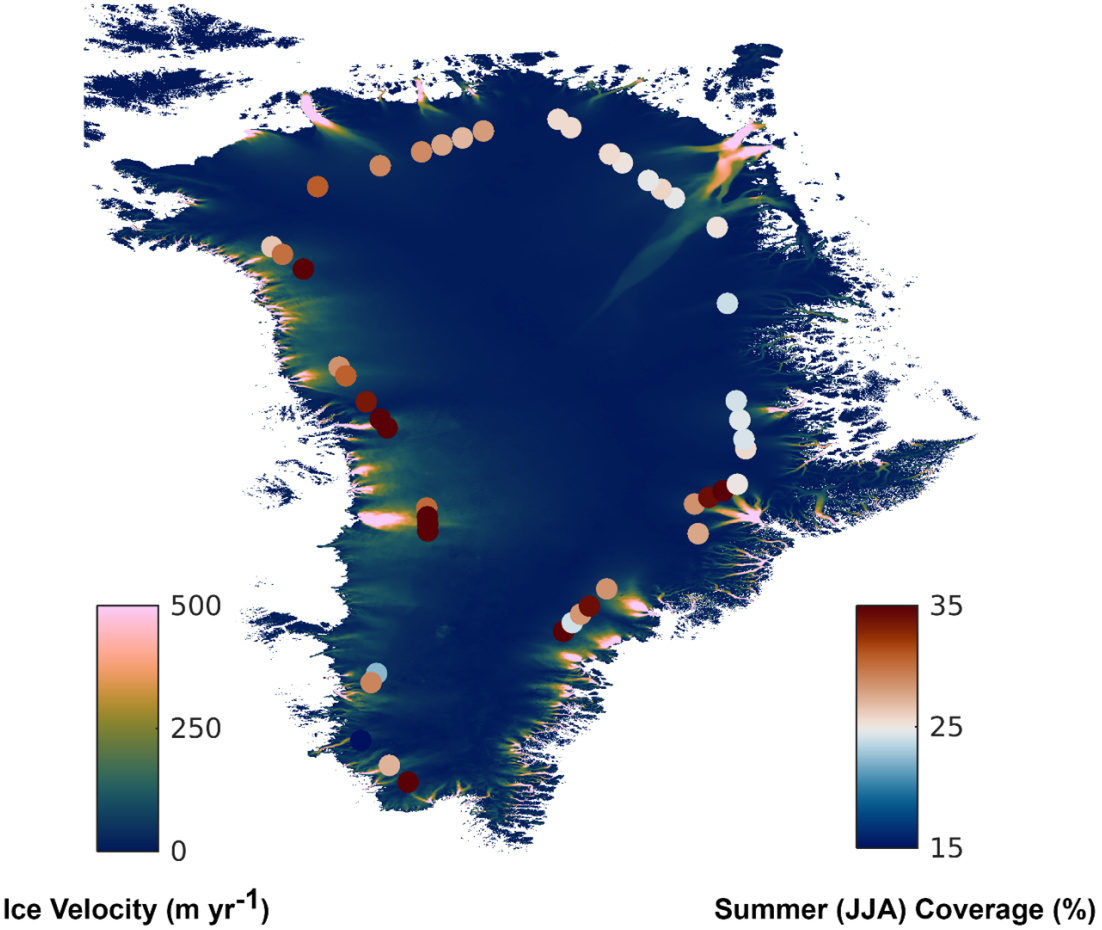

Figure 5.8: *Median 2014-2018 summer coverage (%) within a 3*3-pixel window centred on 45 GPS sites used in our analysis, with summer taken as JJA. The base image is the 2016 velocity field from the NASA ITS-LIVE v0 product (Gardner et al., 2018, 2019).*

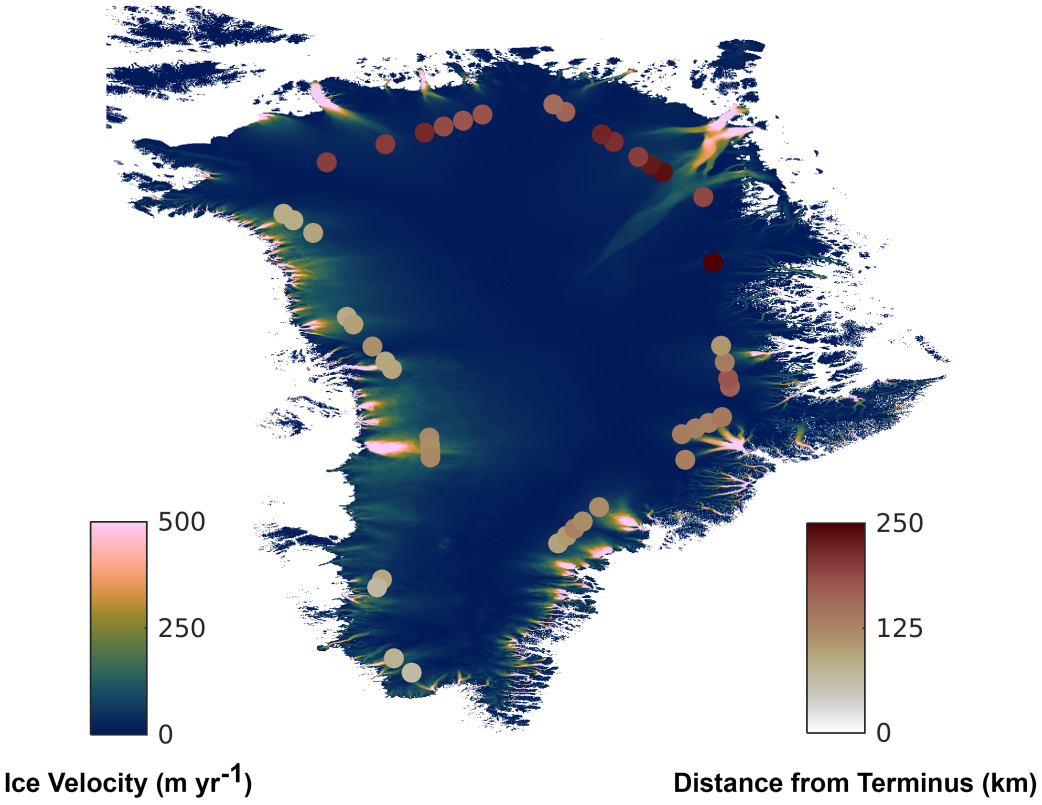

Figure 5.9: *Distance from terminus of the 45 GPS sites inland of tidewater margins used in our analyses. The base image is the 2016 velocity field from the NASA ITS-LIVE v0 product (Gardner et al., 2018, 2019).*

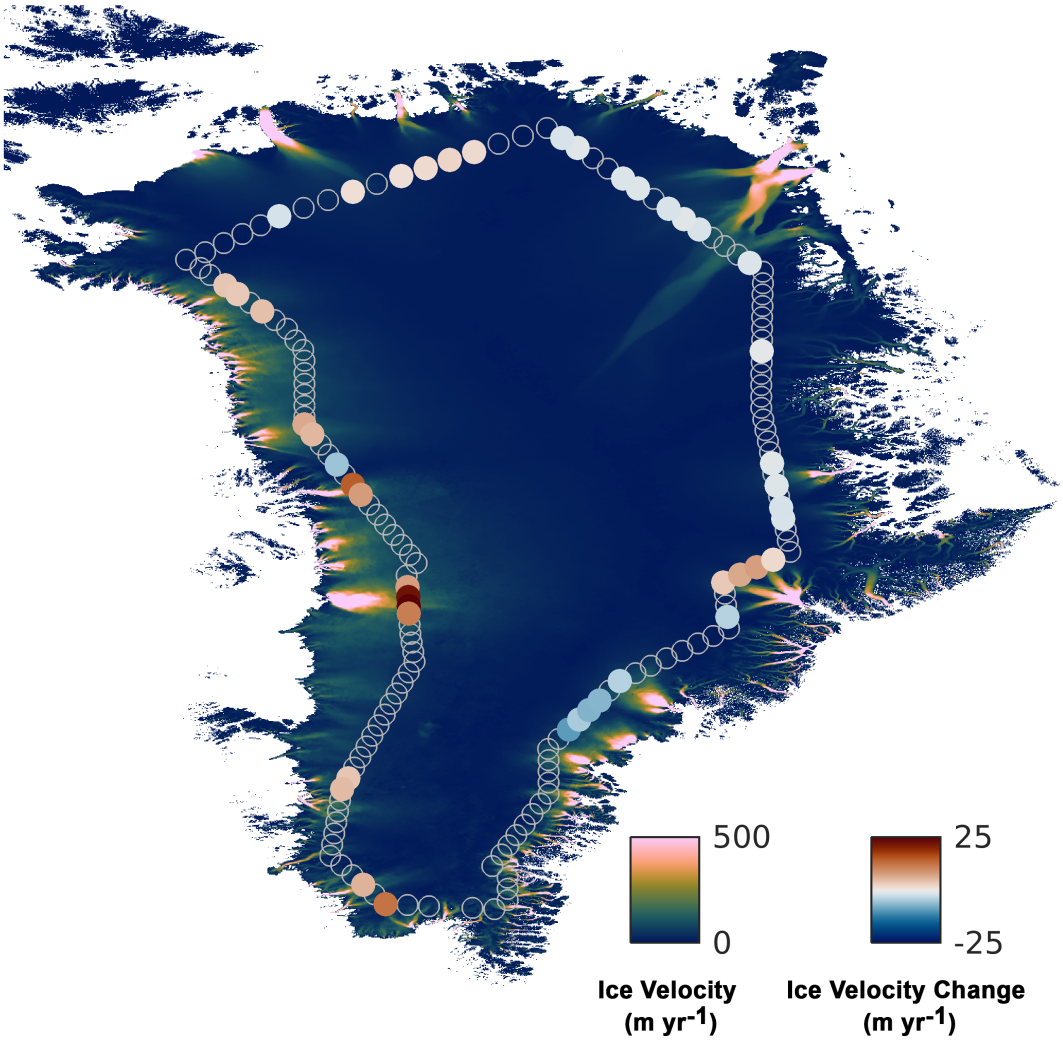

Figure 5.10: *Ice velocity change (m yr^{-1}) at 45 GPS sites inland of tidewater margins between the periods 1993-1997 and 2014-2018. GPS sites that were filtered out of our analysis are shown as empty circles. The base image is the 2016 velocity field from the NASA MEaSUREs ITS-LIVE v0 product (Gardner et al., 2018, 2019).*

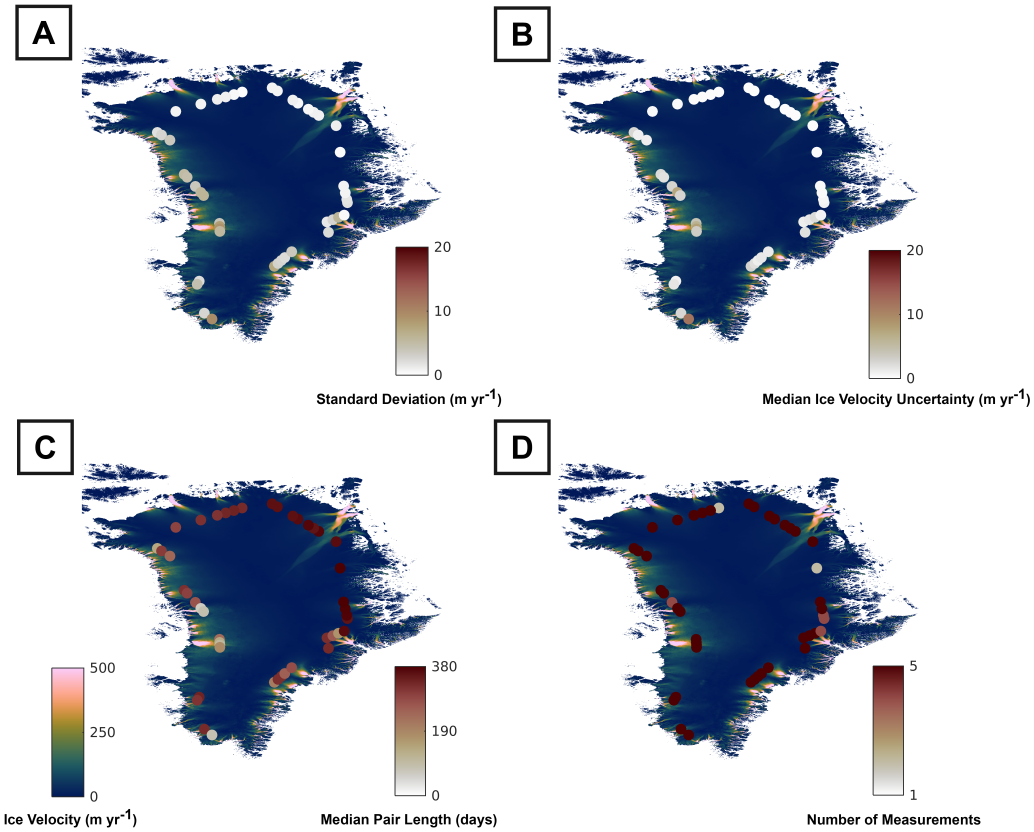

Figure 5.11: ***(A)*** *Standard deviation of 2014-2018 ITS-LIVE ice velocity measurements (m yr^{-1}),* ***(B)*** *median ITS-LIVE ice velocity uncertainty (m yr^{-1}),* ***(C)*** *median ITS-LIVE pair length, and* ***(D)*** *the number of ITS-LIVE measurement years at the 45 GPS sites included in our analyses. The base image is the 2016 velocity field from the NASA ITS-LIVE v0 product (Gardner et al., 2018, 2019).*

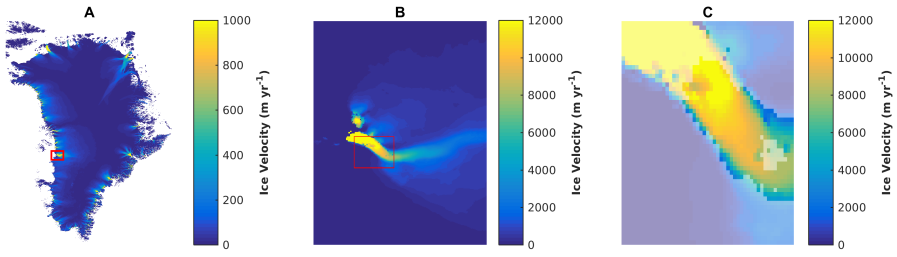

Figure 5.12: *Maps displaying the location of pixels extracted for the velocity time series of Jakobshavn Isbrae.* ***(A)*** *Location of Jakobshavn Isbrae in Greenland.* ***(B)*** *AOI (red rectangle) used for velocity extraction.* ***(C)*** *Pixels common to all years, displayed over a semi-transparent velocity field. In all cases, the velocity data in this figure is the 2016 velocity field from the NASA ITS-LIVE v0 product (Gardner et al., 2018, 2019).*

Glacier Name	Centre Latitude (degrees N)	Centre Longitude (degrees E)	Window Size (pixels x)	Window Size (pixels y)	Minimum Velocity (m yr-1)	Error Threshold (m yr-1)
Figure 2						
Jakobshavn Isbrae	69.12	-49.55	51	51	1500	400
Narsap Sermia	64.66	-49.88	51	51	1000	400
Kangerlugssuaq	68.64	-33	61	61	1000	400
Upernavik Isstrom	72.95	-54.07	81	41	800	400
Kong Oscar Glacier	76.04	-59.55	81	41	2000	400
Petermann Glacier	80.48	-59.6	81	41	500	40
Rinks Isbrae	71.77	-51.44	121	61	2000	400
Figure 3						
Helheim Glacier	66.38	-38.25	61	61	3000	400
Daugaard-Jensen Glacier	71.8	-28.93	161	161	1000	60
79 North Glacier	79.46	-22.05	151	301	200	400
Zacharie Isstrom	78.3	-21	101	101	1000	300
Academy Glacier	81.63	-32.3	31	31	100	60
Umiamako Isbrae	71.76	-51.61	51	51	500	400
Figure 4						
Kangerlugssuaq Branch 1	68.8	-34.01	61	61	50	200
Kangerlugssuaq Branch 2	68.94	-33.85	61	61	200	100
Kangerlugssuaq Branch 3	69.05	-33.35	61	61	300	100
Kangerlugssuaq Branch 4	69.05	-32.92	21	21	200	200

Table 5.2: *Input parameters for ITS-LIVE velocity time series extraction at glaciers in Figures 5.3 through 5.5.*

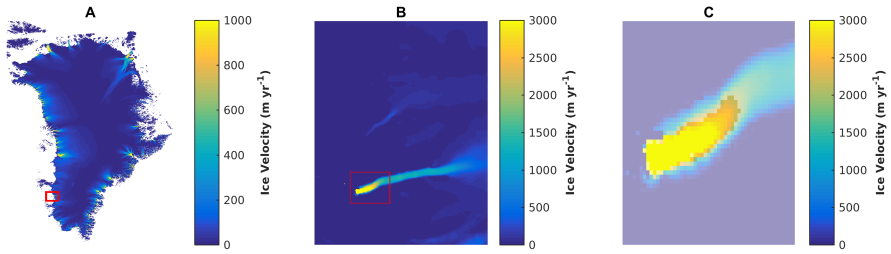

Figure 5.13: *Maps displaying the location of pixels extracted for the velocity time series of Narsap Sermia.* ***(A)*** *Location of Narsap Sermia in Greenland.* ***(B)*** *AOI (red rectangle) used for velocity extraction.* ***(C)*** *Pixels common to all years, displayed over a semi-transparent velocity field. In all cases, the velocity data in this figure is the 2016 velocity field from the NASA ITS-LIVE v0 product (Gardner et al., 2018, 2019).*

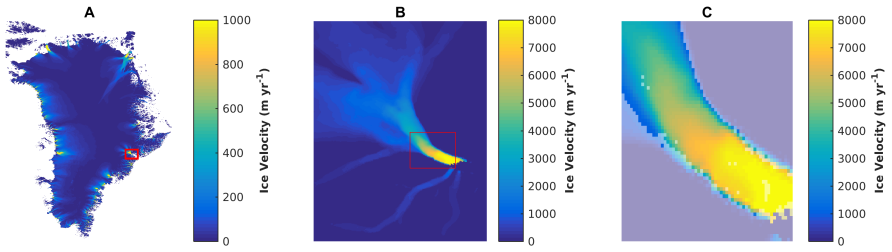

Figure 5.14: *Maps displaying the location of pixels extracted for the velocity time series of Kangerlugssuaq.* ***(A)*** *Location of Kangerlugssuaq in Greenland.* ***(B)*** *AOI (red rectangle) used for velocity extraction.* ***(C)*** *Pixels common to all years, displayed over a semi-transparent velocity field. In all cases, the velocity data in this figure is the 2016 velocity field from the NASA ITS-LIVE v0 product (Gardner et al., 2018, 2019).*

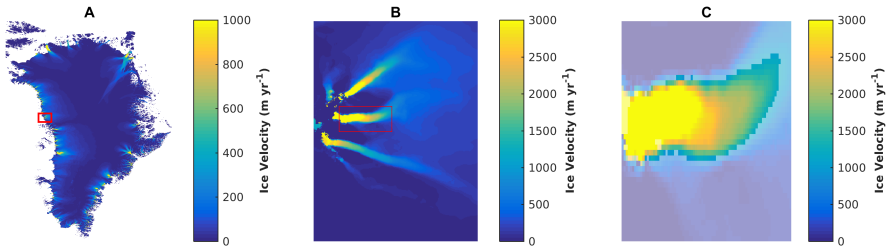

Figure 5.15: *Maps displaying the location of pixels extracted for the velocity time series of Upernavik Isstrom.* ***(A)*** *Location of Upernavik Isstrom in Greenland.* ***(B)*** *AOI (red rectangle) used for velocity extraction.* ***(C)*** *Pixels common to all years, displayed over a semi-transparent velocity field. In all cases, the velocity data in this figure is the 2016 velocity field from the NASA ITS-LIVE v0 product (Gardner et al., 2018, 2019).*

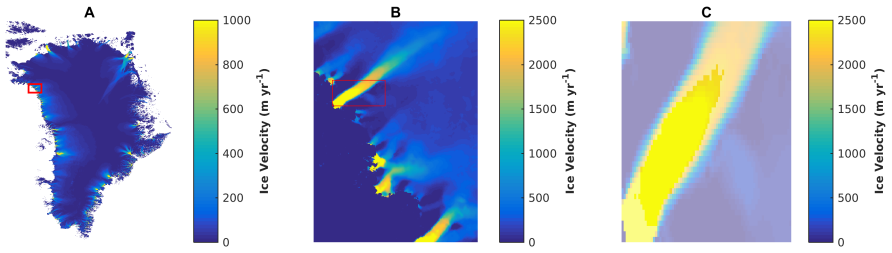

Figure 5.16: *Maps displaying the location of pixels extracted for the velocity time series of Kong Oscar Glacier.* ***(A)*** *Location of Kong Oscar Glacier in Greenland.* ***(B)*** *AOI (red rectangle) used for velocity extraction.* ***(C)*** *Pixels common to all years, displayed over a semi-transparent velocity field. In all cases, the velocity data in this figure is the 2016 velocity field from the NASA ITS-LIVE v0 product (Gardner et al., 2018, 2019).*

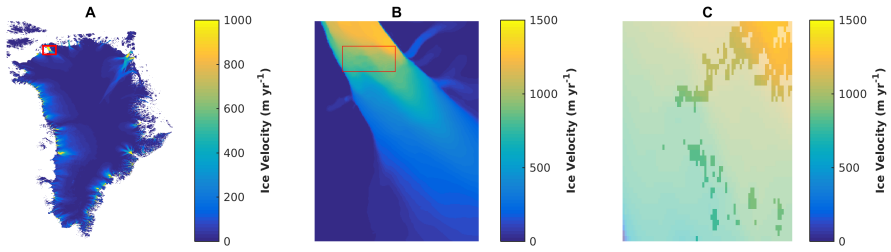

Figure 5.17: *Maps displaying the location of pixels extracted for the velocity time series of Petermann Glacier.* ***(A)*** *Location of Petermann Glacier in Greenland.* ***(B)*** *AOI (red rectangle) used for velocity extraction.* ***(C)*** *Pixels common to all years, displayed over a semi-transparent velocity field. In all cases, the velocity data in this figure is the 2016 velocity field from the NASA ITS-LIVE v0 product (Gardner et al., 2018, 2019).*

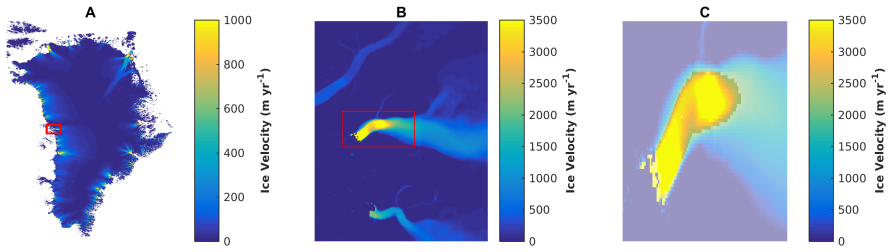

Figure 5.18: *Maps displaying the location of pixels extracted for the velocity time series of Rinks Isbrae.* ***(A)*** *Location of Rinks Isbrae in Greenland.* ***(B)*** *AOI (red rectangle) used for velocity extraction.* ***(C)*** *Pixels common to all years, displayed over a semi-transparent velocity field. In all cases, the velocity data in this figure is the 2016 velocity field from the NASA ITS-LIVE v0 product (Gardner et al., 2018, 2019).*

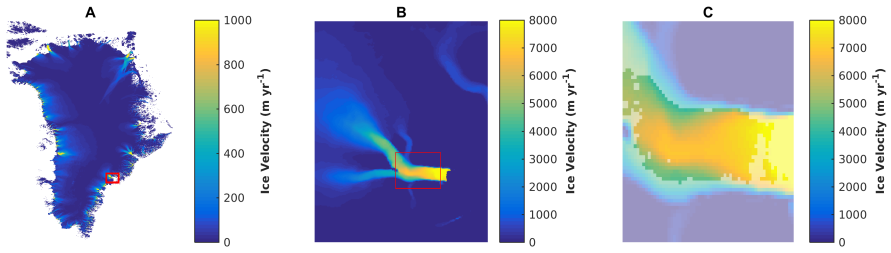

Figure 5.19: *Maps displaying the location of pixels extracted for the velocity time series of Helheim Glacier.* ***(A)*** *Location of Helheim Glacier in Greenland.* ***(B)*** *AOI (red rectangle) used for velocity extraction.* ***(C)*** *Pixels common to all years, displayed over a semi-transparent velocity field. In all cases, the velocity data in this figure is the 2016 velocity field from the NASA ITS-LIVE v0 product (Gardner et al., 2018, 2019).*

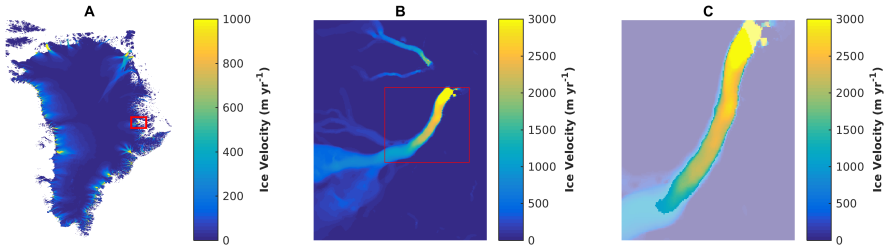

Figure 5.20: *Maps displaying the location of pixels extracted for the velocity time series of Daugaard-Jensen Glacier.* ***(A)*** *Location of Daugaard-Jensen Glacier in Greenland.* ***(B)*** *AOI (red rectangle) used for velocity extraction.* ***(C)*** *Pixels common to all years, displayed over a semi-transparent velocity field. In all cases, the velocity data in this figure is the 2016 velocity field from the NASA ITS-LIVE v0 product (Gardner et al., 2018, 2019).*

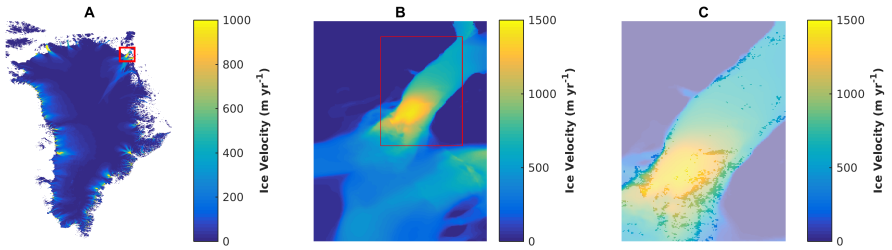

Figure 5.21: *Maps displaying the location of pixels extracted for the velocity time series of 79 North Glacier.* ***(A)*** *Location of 79 North Glacier in Greenland.* ***(B)*** *AOI (red rectangle) used for velocity extraction.* ***(C)*** *Pixels common to all years, displayed over a semi-transparent velocity field. In all cases, the velocity data in this figure is the 2016 velocity field from the NASA ITS-LIVE v0 product (Gardner et al., 2018, 2019).*

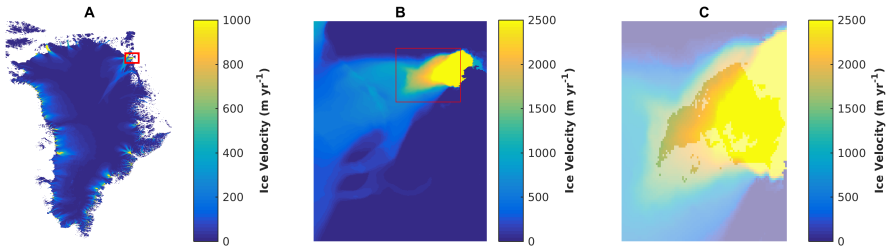

Figure 5.22: *Maps displaying the location of pixels extracted for the velocity time series of Zacharie Isstrom.* ***(A)*** *Location of Zacharie Isstrom in Greenland.* ***(B)*** *AOI (red rectangle) used for velocity extraction.* ***(C)*** *Pixels common to all years, displayed over a semi-transparent velocity field. In all cases, the velocity data in this figure is the 2016 velocity field from the NASA ITS-LIVE v0 product (Gardner et al., 2018, 2019).*

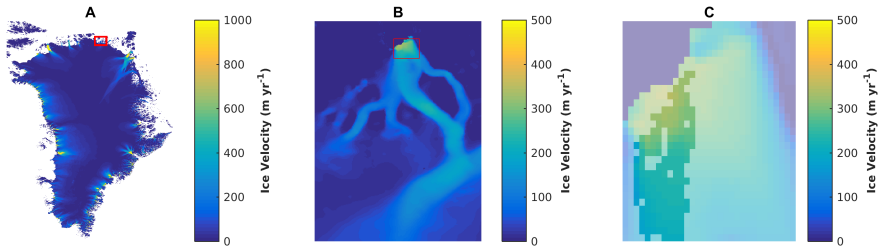

Figure 5.23: *Maps displaying the location of pixels extracted for the velocity time series of Academy Glacier.* ***(A)*** *Location of Academy Glacier in Greenland.* ***(B)*** *AOI (red rectangle) used for velocity extraction.* ***(C)*** *Pixels common to all years, displayed over a semi-transparent velocity field. In all cases, the velocity data in this figure is the 2016 velocity field from the NASA ITS-LIVE v0 product (Gardner et al., 2018, 2019).*

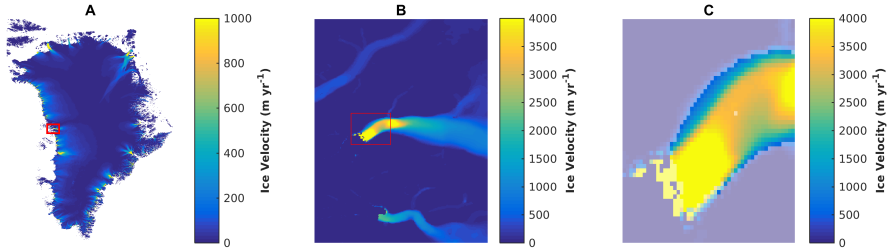

Figure 5.24: *Maps displaying the location of pixels extracted for the velocity time series of Umiamako Isbrae.* ***(A)*** *Location of Umiamako Isbrae in Greenland.* ***(B)*** *AOI (red rectangle) used for velocity extraction.* ***(C)*** *Pixels common to all years, displayed over a semi-transparent velocity field. In all cases, the velocity data in this figure is the 2016 velocity field from the NASA ITS-LIVE v0 product (Gardner et al., 2018, 2019).*

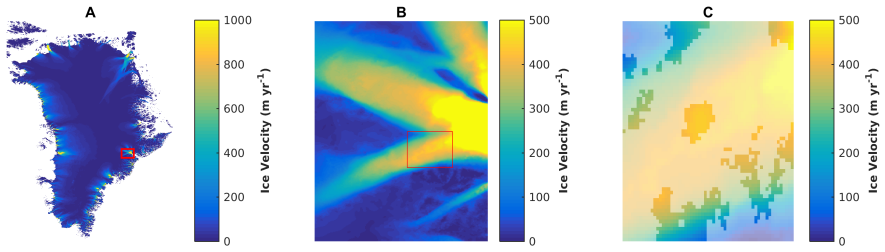

Figure 5.25: *Maps displaying the location of pixels extracted for the velocity time series of Kangerlugssuaq Branch 1.* ***(A)*** *Location of Kangerlugssuaq Branch 1 in Greenland.* ***(B)*** *AOI (red rectangle) used for velocity extraction.* ***(C)*** *Pixels common to all years, displayed over a semi-transparent velocity field. In all cases, the velocity data in this figure is the 2016 velocity field from the NASA ITS-LIVE v0 product (Gardner et al., 2018, 2019).*

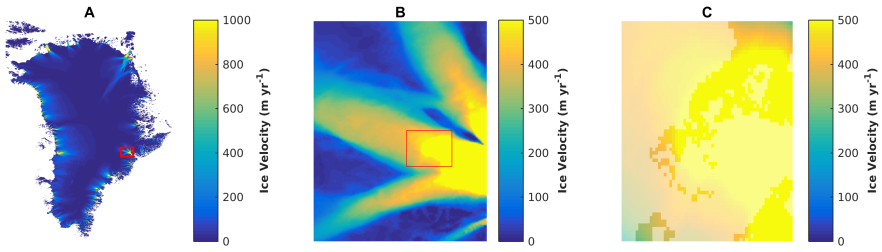

Figure 5.26: *Maps displaying the location of pixels extracted for the velocity time series of Kangerlugssuaq Branch 2.* ***(A)*** *Location of Kangerlugssuaq Branch 2 in Greenland.* ***(B)*** *AOI (red rectangle) used for velocity extraction.* ***(C)*** *Pixels common to all years, displayed over a semi-transparent velocity field. In all cases, the velocity data in this figure is the 2016 velocity field from the NASA ITS-LIVE v0 product (Gardner et al., 2018, 2019).*

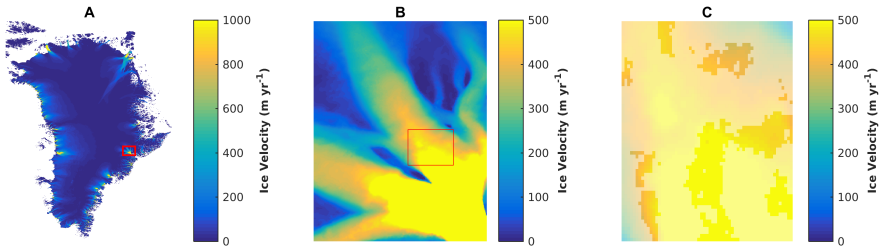

Figure 5.27: *Maps displaying the location of pixels extracted for the velocity time series of Kangerlugssuaq Branch 3.* ***(A)*** *Location of Kangerlugssuaq Branch 3 in Greenland.* ***(B)*** *AOI (red rectangle) used for velocity extraction.* ***(C)*** *Pixels common to all years, displayed over a semi-transparent velocity field. In all cases, the velocity data in this figure is the 2016 velocity field from the NASA ITS-LIVE v0 product (Gardner et al., 2018, 2019).*

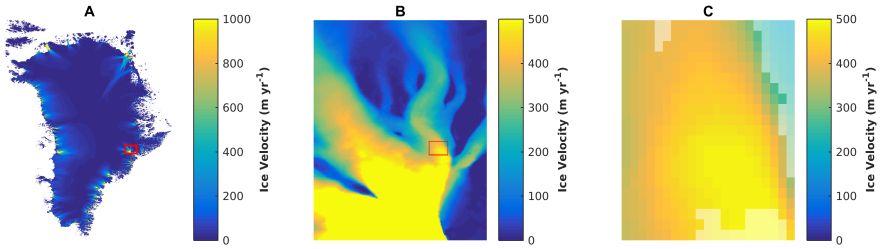

Figure 5.28: *Maps displaying the location of pixels extracted for the velocity time series of Kangerlugssuaq Branch 4.* ***(A)*** *Location of Kangerlugssuaq Branch 4 in Greenland.* ***(B)*** *AOI (red rectangle) used for velocity extraction.* ***(C)*** *Pixels common to all years, displayed over a semi-transparent velocity field. In all cases, the velocity data in this figure is the 2016 velocity field from the NASA ITS-LIVE v0 product (Gardner et al., 2018, 2019).*

Chapter 6

Helheim Glacier poised for dramatic retreat

A significant proportion of the Greenland Ice Sheet's contribution to global sea level rise is as a result of mass loss from its marine-terminating glaciers. Helheim Glacier, located at the head of Sermilik Fjord in southeast Greenland, is one of the largest and fastest-flowing glaciers draining the Greenland Ice Sheet, and last underwent a period of dramatic retreat during the early-2000s (Howat et al., 2005; Howat et al., 2007; Luckman et al., 2006; Stearns and Hamilton, 2007), after which it stabilised and re-advanced (Bevan et al., 2012; Howat et al., 2011; Kehrl et al., 2017; Miles et al., 2016). Recent estimates indicate that since 2014, Helheim Glacier has seen a large increase in its solid ice discharge (Mankoff et al., 2020), indicating that it may have entered a state of thinning, retreat, and acceleration similar to that which occurred during the early-2000s. This chapter utilises an array of remotely-sensed data and data sources to investigate recent dynamic changes at Helheim Glacier, as well as at the neighbouring Fenris Glacier and Midgard Glacier, and places this change in context with that observed in the early-2000s. In addition, proximal air temperature data and modelled submarine melt rates are used to infer the impact of atmospheric and oceanic forcing upon the observed dynamic change. The results reinforce the role of climatic forcing in driving changes in Greenland's ice dynamics, as shown in Chapter 4, as well as the importance of basal topography and ice geometry in modulating

the response of the Greenland Ice Sheet to climatic forcing, as shown in Chapter 5.

This chapter has been submitted for publication.

Authors: Joshua J. Williams[1], Noel Gourmelen[1], Peter Nienow[1], Charlie Bunce[1] and Donald Slater[1,2]

1. School of Geosciences, University of Edinburgh, Edinburgh, EH8 9XP, UK
2. School of Geography and Sustainable Development, University of St Andrews, St Andrews, KY16 9AL, UK

Citation: Williams, J.J.[1], Gourmelen, N.[1], Nienow, P.[1], Bunce, C.[1] and Slater, D.[1,2] (Manuscript in review) Helheim Glacier poised for dramatic retreat.

Author contributions: JJW, NG and PN contributed to the design of the study. JJW performed the data processing and analyses. NG derived surface elevation change estimates from altimetry data. CB assisted with data processing and figure creation. DS estimated submarine melt rates and subglacial discharge. All authors contributed to the writing of the paper.

Acknowledgements: JJW and CB were funded by a UK Natural Environment Research Council (NERC) doctoral training partnership grant (NE/L002558/1). DS acknowledges NERC Independent Research Fellowship NE/T011920/1. NG is supported by the European Space Agency's CryoTEMPO grant 4000128095/19/I-DT. We also thank M. Morlighem for providing open access to BedMachine.

6.1 Abstract

Helheim Glacier is a large tidewater glacier draining the Greenland Ice Sheet that underwent significant retreat and acceleration in the early-2000s, accounting for an appreciable proportion of the ice sheet's mass loss during that period. Using a range of remotely sensed datasets, we show that despite a subsequent re-advance, the glacier has continued to lose mass and thin, and has recently retreated further than its maximum retreat in 2005. Critically, the near-terminus is ∼20-100 m thinner than during 2005, and the front 5 km is within 25-50 m of flotation, with retrograde bed slopes extending several kilometres inland of the terminus. The neighbouring Fenris and Midgard Glaciers have both undergone recent large-scale and rapid retreat once their near-terminus regions began to float, suggesting that under projected climate warming and associated glacier thinning, Helheim Glacier is poised to pass a threshold whereby the near-terminus region will retreat rapidly.

6.2 Introduction

The Greenland Ice Sheet is a major contributor to global sea level rise (Bamber et al., 2018; van den Broeke et al., 2016). Approximately 50 % of Greenland's mass loss is due to increasing ice loss from its marine-terminating outlet glaciers (Shepherd et al., 2019), particularly in the southeast where solid ice discharge increased from an average of 136 ± 6 Gt yr^{-1} during 1972-1980 to an average of 160 ± 2 Gt yr^{-1} during 2010-2018 (Mouginot et al., 2019), totalling ∼25 % of the ice-sheet-wide mass loss due to solid ice discharge since 1990, the largest regional contribution. Located at the head of Sermilik Fjord, Helheim Glacier (66.4°N, 38°W) is one of the largest and fastest-flowing glaciers in Greenland, contributing 6-7 % of the total ice discharge from the Greenland Ice Sheet (Mankoff et al., 2020).

After several decades of stability (Bevan et al., 2012; Bjørk et al., 2012; Miles et al., 2016), Helheim Glacier underwent dramatic retreat, near-front accelera-

tion and dynamic thinning between 2003 and 2005 (Howat et al., 2005; Howat et al., 2008b; Luckman et al., 2006; Stearns and Hamilton, 2007), thought to be driven by increased oceanic and/or atmospheric temperatures (Andresen et al., 2012; Cowton et al., 2018; Joughin et al., 2008a; Straneo et al., 2011), followed by stabilisation and re-advance from 2006 (Bevan et al., 2012; Howat et al., 2011; Kehrl et al., 2017; Miles et al., 2016). Recent estimates, however, show a large increase in Helheim's solid ice discharge from ∼2014 through 2019, such that it is now at least the second-largest discharging Greenlandic glacier (Mankoff et al., 2020) and one of the sectors of the Greenland Ice Sheet losing mass the fastest (Mouginot et al., 2019). It remains unclear, however, how the dynamics of Helheim Glacier have changed during this recent period of enhanced ice discharge, as well as what this recent change means for the future evolution of the glacier.

Here, we combine satellite-derived measurements of ice velocity, terminus position and surface elevation alongside estimates of bed topography and mass balance to examine recent dynamical change at Helheim Glacier. The same analyses are undertaken for the neighbouring Fenris and Midgard Glaciers in order to both contextualise the observed change at Helheim Glacier and provide analogues for its future evolution.

6.3 Data and Methods

To determine near-terminus ice velocity, we use the MEaSUREs Selected Glacier Site Velocity from Optical Images V3 (Howat, 2020) for the period 2014 through 2019 and extract velocities from an AOI ('Area of Interest') near the terminus of each glacier. As the velocity data coverage near the front of Midgard South is poor, we are unable to plot a velocity time series for this site.

Terminus positions were manually digitised from all available Landsat 8 and Sentinel-2 satellite imagery from 2014 through 2020 using the Google Earth Digitisation Tool (GEEDiT) (Lea, 2018). Annual terminus positions were mapped

for the period 2000-2020 using Landsat 7, Landsat 8, and Sentinel-2 imagery, using images as close to August 31st as possible. We estimate a RMSE of ±4.8 m and ±3.1 m for Landsat-8 and Sentinel-2 imagery respectively, both of which are less than the respective pixel sizes (see Chapter 3 for more detail). Changes in terminus position were assessed using the curvilinear box method along a glacier centreline using MaQiT (Lea, 2018).

To assess surface elevation change, we use 50 m resolution DEMs for the period 2016-2019 from the Oceans Melting Greenland (OMG) L3 GLISTIN-A product (OMG, 2020). To evaluate decadal change in surface elevation at each glacier, we sample the 2016-2019 OMG elevation data along a Pre-IceBridge Airborne Topographic Mapper (ATM) flightline over the near-terminus region (Thomas and Studinger, 2010). The sampled OMG elevation data are then compared to the ATM L2 Icessn elevation data collected along the same flightline, with these flights flown on 19/05/2005 at Helheim Glacier, 11/05/2007 at Fenris Glacier and Midgard South Glacier, and 31/07/2008 at Midgard North Glacier.

We also generate regional surface elevation change between 2010 and 2020 using CryoSat-2 radar altimetry. CryoSat-2 time-dependent surface elevations are processed following the method described in Gourmelen et al., 2018. Monthly time-series of height change for each of the three glaciers are then generated following the approach described in Malczyk et al., 2020. The pixels across which these elevation measurements were collected are displayed in Section 6.7. For each glacier, we also include mass balance data from Mouginot et al., 2019 (their Dataset S2).

For each of the profiles along which we extracted surface elevation data, we extract bed topography and ice thickness from BedMachineV3 (Morlighem et al., 2017). We then calculate the flotation elevation (h_f) at each point along the profile as follows:

$$h_f = H * (1 - \frac{\rho_{ice}}{\rho_{ocean}}) \tag{6.1}$$

Where H is the ice thickness, ρ_{ice} is the density of ice (917 kg m^{-3}) and ρ_{ocean} is the density of seawater (1025 kg m^{-3}).

Submarine melt rates are estimated as in Slater et al., 2019b using the parameterisation $0.142Q^{0.31}TF^{1.18}$, in which Q is subglacial discharge and TF is ocean thermal forcing. Subglacial discharge is estimated by summing surface runoff volumes from RACMO2.3p2 (Noël et al., 2018) over the hydrological catchment for the glacier in question. Ocean thermal forcing is estimated by extrapolating ocean properties on the continental shelf (from EN4; Good et al., 2013) into the fjord. Melt rates are calculated monthly and then averaged over each year. We also use surface air temperatures measured at the Tasiilaq meteorological station near the mouth of Sermilik Fjord (Cappelen et al., 2020).

It remains difficult to produce formal uncertainties for modelled submarine melt rates. They are certainly greater than 0, and they can't be larger than the ice velocity because otherwise there would be no icebergs, however there are so few direct observations at vertical front tidewater glaciers such that the theory that predicts submarine melt rates (Jenkins, 2011) has not really been tested. Observations are largely limited to Antarctic ice shelves (Jenkins et al., 2010) where the theory appears to perform relatively well, however these ice shelves are very different environments to those in Greenland as they have a horizontal (as opposed to a vertical) interface with the ocean, and ocean waters are warmer and move much faster in Greenland. For most tidewater glaciers in Greenland (and elsewhere), the lack of an ice shelf prevents access to the ocean cavity from above, and ship access is inhibited by icebergs, sea ice and ice melange (Sutherland et al., 2019). Our only observations outside of Antarctica are from LeConte Glacier in Alaska (Sutherland et al., 2019), where submarine melt rates were observed to be two orders of magnitude greater than those predicted by theory, providing support for the high submarine melt rates suggested by several recent studies

(Fried et al., 2015; Slater et al., 2018; Wagner et al., 2019).

Despite this, the prevailing consensus is that theoretically, submarine melt rates should scale sub-linearly with subglacial runoff and approximately linearly with ocean temperature, and this is supported by direct observations (Luckman et al., 2015; Motyka et al., 2013). Therefore, we have more confidence in modelling the relative change in submarine melt rates over time. As a result, the modelled submarine melt rates present in this chapter are discussed with reference to their relative change over time as opposed to their precise values.

6.4 Results

6.4.1 Helheim Glacier

Helheim Glacier has been characterised by a persistently negative mass balance ranging between -5.0 and -13.2 Gt yr^{-1} since 2003/04 (Figure 6.1c, Mouginot et al., 2019) and a long-term negative trend in glacier-wide surface elevation initiated in the mid-2000s (Shepherd et al., 2019) and averaging >10 m of thinning between late-2010 and early-2020 (Figure 6.1c). Within 5 km of the terminus, we observe surface thinning of >50 m between 2016 and 2019, and a strong reduction in surface slope reaching to near-horizontal by 2018 and 2019 (Figure 6.1d). The 2019 surface in the near-terminus region is 20-100 m thinner than during 2005 and is only 25-50 m above flotation. Whilst the bed topography in the centre of the glacier is largely flat with a 100 m elevation gain between 2 and 4 km inland, the northern and southern sectors are underlain by reverse bed slopes, extending 1-2 km and 3-4 km inland of the 2019 terminus respectively (Figure 6.1a, 6.1e).

During the period 2014-2020, we observe a near-terminus acceleration of 2.5-3 km yr^{-1} and concomitant terminus retreat of 4 km from summer 2014 to summer 2019, with retreat beyond the 2005 extent in 2017 and 2019 (Figure 6.1f). The observed pattern of retreat and acceleration shows some seasonality, with large re-advances (2-3 km) during the winters of 2015/16 and 2017/18, limited

re-advance (∼1 km) during the winters of 2016/17, 2018/19 and 2019/20, and no re-advance during the winter of 2014/15.

6.4.2 Fenris Glacier

Fenris Glacier has had a negative mass balance since 2003/04, ranging from -0.6 to -2.0 Gt yr^{-1} (Figure 6.2c, Mouginot et al., 2019), and an average surface thinning of 15 m across the glacier trunk between late-2010 and mid-2020 (Figure 6.2c). The near-terminus region thinned by >50 m between 2007 and 2016, with the front 1 km of the glacier floating in early-2016 and early-2017 (Figure 6.2d). Thinning continued through 2018 such that by early-2019, the front ∼2.5 km of the glacier was floating. This is supported by the presence of large tabular icebergs within the proglacial fjord that have not overturned (see Figure 6.10). Fenris Glacier is underlain by a steep retrograde bed slope extending at least 6 km inland of the 2007 terminus (Figure 6.2a, 6.2e), and the surface elevation data (Figure 6.2d) indicates that by 2019, the grounding line had retreated down this slope to a region of flat bed topography.

Fenris Glacier was characterised by relatively stable ice velocity during the period 2014-2017 before an initial acceleration of approximately 1 km yr^{-1} near the front from early-2017 through 2018, coincident with the absence of a 2016/17 winter re-advance of the terminus (Figure 6.2f). This preceded a rapid acceleration to 4.5 km yr^{-1} and terminus retreat of 3 km beginning in early-2019.

6.4.3 Midgard Glacier

Midgard Glacier has been characterised by a permanently negative mass balance between 2000 and 2018 (Figure 6.3c), with a minimum of -5.1 Gt yr^{-1} in 2012. The surface of Midgard Glacier has thinned by an average of >10 m across the wider glacier area during the period 2010-2020 (Figure 6.3c).

Midgard North Glacier thinned by 100 to 300 m and retreated by >6 km between 2008 and 2016, and the glacier has been grounded on a steep prograde

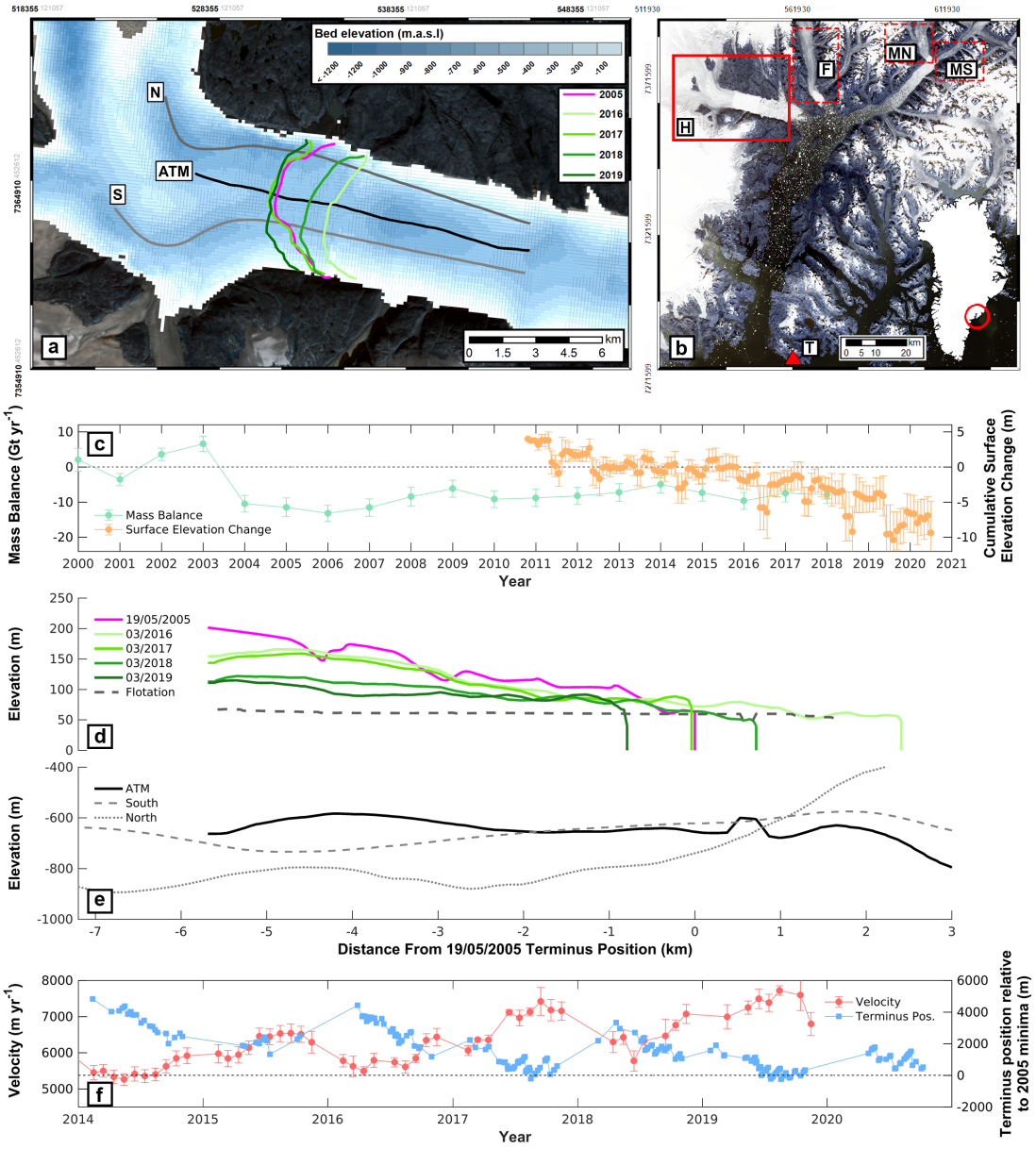

Figure 6.1: ***(a)*** *Helheim Glacier bed topography overlain with summer minimum terminus positions for the indicated years. The ATM profile follows a Pre-IceBridge flightline, and the northern (N) and southern (S) profiles were drawn manually to illustrate the bed topography in these regions of the glacier.* ***(b)*** *Map of Sermilik Fjord with red rectangles showing the locations of Helheim Glacier (H), Fenris Glacier (F), Midgard North Glacier (MN) and Midgard South Glacier (MS). The location of the Tasiilaq meteorological station (T) is displayed with the red triangle.* ***(c)*** *Glacier total mass balance (green, Gt* yr^{-1}*) and cumulative surface elevation change (orange, m) from CryoSat-2 altimetry with associated uncertainty, averaged across the wider glacier area (Figure 6.7).* ***(d)*** *Surface elevation along the ATM profile. The dashed line represents the surface elevation at which the ice will float.* ***(e)*** *Bed topography along the profiles displayed in (a).* ***(f)*** *Near-terminus ice velocity (red) with associated uncertainty and terminus position (blue), plotted relative to the 2005 minima.*

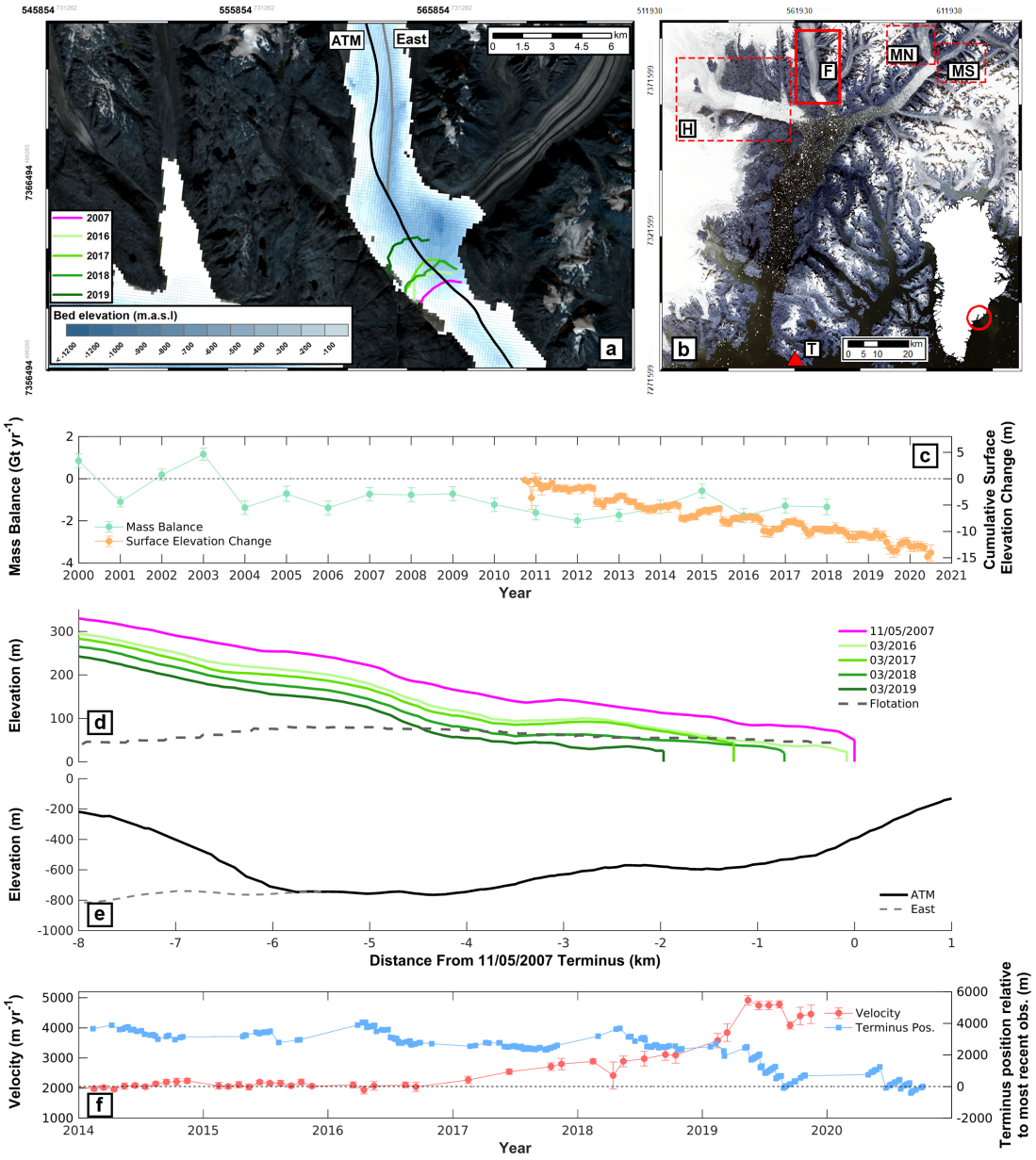

Figure 6.2: *Equivalent to Figure 6.1 for Fenris Glacier. The ATM elevation data and associated summer minimum terminus position are from 2007, and an eastern (East) profile was drawn manually to illustrate the bed topography in this region of the glacier. Terminus positions in* ***(f)*** *are plotted relative to the most recent observation.*

slope since at least 2016 (Figure 6.3e). We observe a subsequent thinning of 20 m between 2016 and 2017, after which the surface elevation has remained stable (Figure 6.3d). During the period 2014-2020, Midgard North Glacier has been characterised by terminus stability, with seasonal advance of ∼1 km in winter and retreat back to its stable position in summer (Figure 6.3f). The near-terminus ice velocity underwent a gradual slow-down during this period, with some inter-

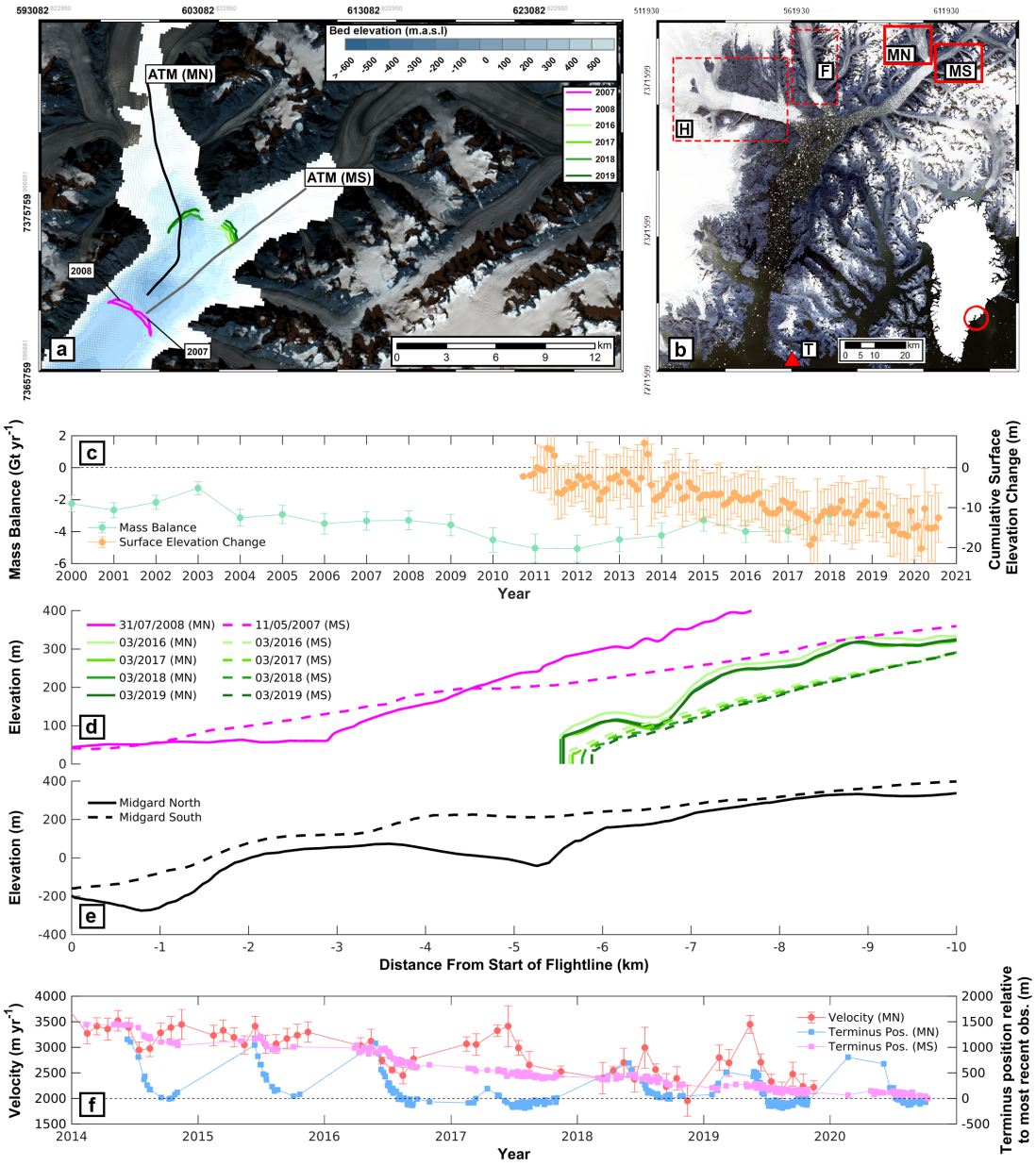

Figure 6.3: *Equivalent to Figure 6.1 for Midgard North Glacier and Midgard South Glacier. The ATM elevation data and associated summer minimum terminus position are from 2007 for Midgard South, and 2008 for Midgard North. Terminus positions in* ***(f)*** *are plotted relative to the most recent observation.*

annual variability.

In contrast to the other glaciers studied, Midgard South Glacier underwent gradual thinning of its surface alongside a consistent terminus retreat from 2014 through 2020. The terminus retreat totalled ∼1.5 km and exhibited only limited evidence of seasonality (Figure 6.3d, 6.3f), indicating that the glacier may

have become essentially land-terminating.

6.4.4 Ocean and Atmospheric Forcing

Submarine melt rates and subglacial runoff (Figure 6.4a, 6.4b) exhibit considerable inter-annual variability with a multi-decadal increase at all three glaciers. At Helheim Glacier, the annual mean modelled submarine melt rate has increased by >10 % between the periods 1980-1989 and 2010-2019. Between 2010 and 2019, modelled submarine melt rates have been at least as great as, if not greater than, those of the mid-2000s during which period the glacier underwent substantial retreat, acceleration, and thinning. We also observe consistent increases in modelled submarine melt rates at Fenris and Midgard glaciers, with an increase of >20 % between the 1980-1989 and 2010-2019 means at Fenris Glacier. All three glaciers have seen a gradual increase in annual mean modelled subglacial runoff, from 40-80 m^3 s^{-1} during the 1980s to 70-120 m^3 s^{-1} between 2010 and 2019.

Air temperatures in Tasiilaq have increased over the past 40 years, from a mean of -1.8°C during 1980-1989 to a mean of 0.3°C during 2010-2019 (Figure 6.4c).

6.5 Discussion

The three glaciers studied have continuously lost mass between 2003 and 2018, with 2003 characterised by a large, quasi-synchronous increase in mass loss at all three sites (Figure 6.1c, 6.2c, 6.3c, Mouginot et al., 2019), suggesting a sensitivity to a regional environmental forcing, driven by warming of the atmosphere and/or ocean (Howat et al., 2008b; Luckman et al., 2006; Moon and Joughin, 2008; Seale et al., 2011). Warming of the ocean increases submarine melt, and subsequently calving, at glacier termini (Straneo and Heimbach, 2013), and increased surface melt due to increased air temperatures may accelerate calving through hydrofracture (Nick et al., 2013) and/or increased basal water pressure and thus sliding (Sugiyama et al., 2011). An additional hypothesis suggests retreat may be driven by increased calving following the loss of buttressing ice mélange (Amundson et

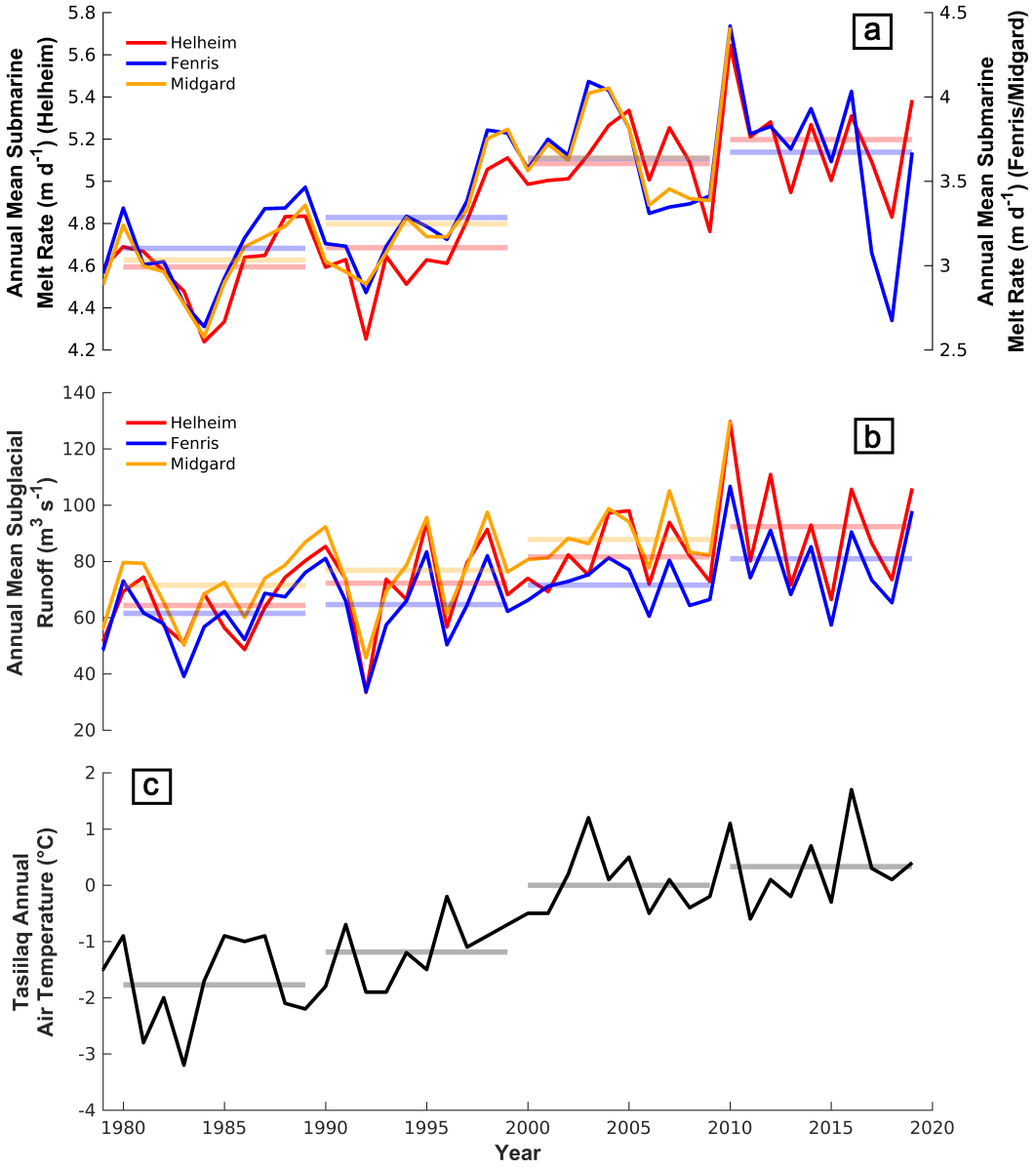

Figure 6.4: ***(a)*** *Annual mean submarine melt rate (m d^{-1}) and* ***(b)*** *annual mean subglacial runoff (m^3 s^{-1}) at the termini of Helheim, Fenris and Midgard Glaciers for the period 1979-2019. Data for Midgard Glacier stops in 2010 when the glacier split into two distinct branches.* ***(c)*** *Annual mean air temperature at Tasiilaq (°C) for the period 1979-2019 (Cappelen et al., 2020). The horizontal lines in all plots represent 10-year means.*

al., 2010; Bevan et al., 2019).

Whilst it has proven difficult to disentangle the relative importance of particular oceanic and atmospheric processes in driving terminus retreat (i.e., Bevan

et al., 2012; Moon et al., 2015; Murray et al., 2015), significant relationships have been found between oceanic and atmospheric warming and southeast Greenland tidewater glacier retreat over multiple decades (Cowton et al., 2018). We observe a step increase in mean modelled submarine melt rates at all three sites, and a step increase in mean annual air temperature at Tasiilaq, between the periods 1990-1999 and 2000-2010 (Figure 6.4). Mean observed air temperatures and mean modelled submarine melt rates remained elevated during 2010-2019 (Figure 6.4), driving the persistently negative mass balance observed at all three glaciers during this period (Mouginot et al., 2019).

Helheim Glacier last underwent a period of sustained retreat between 2003 and 2005, during which the front retreated by >7 km, and the near-terminus region accelerated by 5 km yr^{-1} (Howat et al., 2005; Howat et al., 2008b) and dynamically thinned by 100 m (Stearns and Hamilton, 2007). Whilst Helheim Glacier slowed and underwent some re-advance between 2006 and 2014 (Bevan et al., 2012; Howat et al., 2011; Kehrl et al., 2017; Miles et al., 2016), during the past 6 years we observe an acceleration (2.5-3 km yr^{-1}) and retreat (3-4 km) similar in magnitude to those of the early-2000s. This is supported by recent measurements of an approximately 10 Gt yr^{-1} increase in solid ice discharge from Helheim Glacier between 2014 and 2019 (Mankoff et al., 2020). The total retreat we measure is less than that in 2003-2005; however, this is because the glacier did not re-advance to its pre-2003 extent between 2006 and 2014, and we observe retreat further inland than its 2005 minimum extent during the summers of 2017 and 2019 (Figure 6.1f). Moreover, the near-terminus region is 20-100 m thinner than during 2005 and much closer to flotation, indicating that the glacier is currently in a more unstable configuration than during its peak retreat in 2005.

The broad trends in behaviour at Helheim Glacier are also observed at the neighbouring Fenris and Midgard Glaciers, suggesting a largely coherent response to the same long-term climate forcing. Fenris Glacier saw little dynamic change during the 2000s, with a decadal area change of -0.3 km^2 a^{-1} (Box and Decker, 2011)

and maximum retreat of -1.6 km (Walsh et al., 2012) during 2000-2010. Between 2000 and 2018, the glacier gradually retreated by 2 km (Figures 6.5, 6.6), before the ice front thinned to flotation in early-2018, leading to a rapid retreat of 3-4 km (Figure 6.2e) that is unprecedented in at least the last 20 years. Midgard Glacier underwent a major retreat during the mid-2000s (Box and Decker, 2011; Walsh et al., 2012, Figures 6.5) which is likely a result of thinning to flotation, supported by the very low surface elevations ($<$ 50 m a.s.l.) extending down-fjord during 2007 and 2008 (Figure 6.3d). Whilst the precise timing and magnitude of retreat differs between the glaciers studied, the fundamental mechanism, thinning to flotation as a result of a persistent negative mass balance, is the same. As such, the changes observed at Fenris and Midgard Glaciers provide an analogue for the expected future change at Helheim Glacier under continued mass loss, further supporting our suggestion that it is poised for a dramatic retreat.

The precise timing of acceleration and retreat in response to the long-term climate forcing differs between the glaciers studied, likely reflecting the different morphological settings and characteristics of the three glaciers, as has been observed elsewhere in Greenland (Catania et al., 2018). For example, glaciers overlaying deeper bed topography and/or with wider trunks are likely to be closer to flotation such that less thinning is required to initiate a rapid, unstable retreat following a given perturbation (Enderlin et al., 2013). At Fenris Glacier, where the glacier trunk is narrow in comparison to Helheim and Midgard Glaciers, it may be that only the eastern region of the glacier trunk is floating due to the much deeper underlying bed topography compared to the western region of the trunk (Figure 6.2a). This influence of glacier geometry also contributes to the likely instability of Helheim Glacier, as it is characterised by a wide glacier trunk ($\sim$6 km), where the northern and southern sections of the glacier are underlain by retrograde bed slopes (Figure 6.1a, 6.1e). With continued mass loss, thinning, and retreat down these reverse slopes, the near-terminus region of Helheim Glacier will move rapidly towards flotation and thus rapid retreat beyond what has previously been observed.

During the 1930s, warmer air temperatures (Box et al., 2009) were coincident with retreat at Helheim Glacier (Bjørk et al., 2012; Khan et al., 2014; Khan et al., 2020) with the terminus reaching approximately the same glacier extent as 2011/12 (Khan et al., 2014). However, following this retreat during the 1930s, Helheim Glacier gained mass and re-advanced such that during the period 1900-1983, it was in near-balance (Khan et al., 2014; Khan et al., 2020; Kjeldsen et al., 2015) and recent data shows that between 1972 and 2003, it was characterised by an almost consistently positive mass balance (Mouginot et al., 2019). Consequently, between 1875 and 2012, Helheim Glacier lost only 31 ± 21 Gt of mass (Khan et al., 2020), orders of magnitude less than the mass loss from Jakosbhavn Isbrae (1518 ± 189 Gt) and Kangerlussuaq (1381 ± 178 Gt).

Helheim Glacier last saw large-scale retreat and acceleration during the early-2000s (Howat et al., 2005; Howat et al., 2008b), after which it slowed and re-advanced (Bevan et al., 2012; Howat et al., 2011; Kehrl et al., 2017; Miles et al., 2016). However, in contrast to the post-1930s re-advance, mass balance has remained negative at Helheim Glacier since 2003 (Mouginot et al., 2019), such that the glacier has continued to thin and lose mass despite re-advancing and decelerating. Therefore, we argue that despite the fact that the glacier has re-advanced following its last two periods of major retreat, it is currently in a far more precarious position than during either of these past retreats as a result of sustained thinning towards flotation over the past two decades. Moreover, not only is the near-terminus region much closer to flotation, but dynamic thinning (Csatho et al., 2014; McMillan et al., 2016; Pritchard et al., 2009) and a prolonged negative surface mass balance (Khan et al., 2014; Khan et al., 2020; Mouginot et al., 2019; Sandberg Sørensen et al., 2018) mean that the ice inland is also much thinner, as supported by the altimetry data presented here (Figure 6.1c). The current surface topography thus points to a different future dynamic trajectory when compared with the 2005 retreat.

The geometry of the fjord may exert a stabilising influence on the future evolution of Helheim Glacier. Within the central region of ice flow there is a bedrock high (Figure 6.1a) that may act as a pinning point should the glacier retreat this far inland. Similarly, strong lateral flow convergence from Helheim Glacier's three branches of ice flow may stabilise the terminus, even in regions with a reverse-sloping bed (Frank et al., 2021; Gudmundsson et al., 2012). However, both the bedrock high and the convergence of Helheim Glacier's flow branches are located >6 km inland of the 2019 terminus, and thus the glacier would already have retreated significantly should it reach this point. Moreover, the bedrock high is more of a 'nunatak-like' feature with deep bed topography either side than an across-fjord sill, and thus ocean water may be able to attack the terminus from either side of this point, limiting any stabilising impact.

Re-advance has been observed at other major tidewater glaciers draining the Greenland Ice Sheet following previous large-scale retreat. For example, Jakobshavn Isbrae has re-advanced since 2016/17 following an extended period of retreat (Joughin et al., 2020; Khazendar et al., 2019), and Kangerlussuaq re-advanced from 2019 following a transient retreat (Bevan et al., 2019), with both of these re-advances occurring up retrograde bed slopes. These events have both been linked to localised cooling of ocean waters and the associated presence of a rigid winter ice melange, facilitating greater winter advance (Bevan et al., 2019; Joughin et al., 2020). However, whilst Helheim Glacier may undergo some re-advance should the local climate cool, analogous to that which occurred in 2006 (Bevan et al., 2012; Howat et al., 2011; Kehrl et al., 2017; Miles et al., 2016), unless local air and ocean temperatures cool to levels sufficient to facilitate mass gain for an extended period, this will only be a transient re-advance as the glacier will continue to thin and lose mass. Both air and ocean temperatures are projected to continue to rise, driving greater rates of surface (Hofer et al., 2020) and submarine melting (Slater et al., 2020). Under continued climate warming, we argue that a critical threshold will be reached at Helheim Glacier through thinning to flotation, which would drive a dramatic retreat analogous to those

observed at the neighbouring Fenris and Midgard glaciers. Such a retreat event is inferred to have occurred during the Holocene, beginning between 10.5 – 9.6 ka BP, after which Helheim Glacier remained retreated for most of the Holocene, despite cold events at 9.3 and 8.2 ka and during the early-Neoglacial, until a re-advance beginning at 0.3 ka BP (Bjørk et al., 2018). This supports our suggestion that should Helheim Glacier continue to thin to flotation, a much larger retreat is possible than has been observed since the end of the Little Ice Age, suggesting that Helheim Glacier is approaching a tipping point into a new dynamic state.

6.6 Conclusion

We have shown that Helheim Glacier has recently retreated and accelerated to an extent similar to that observed during its well-studied dynamic change in the early-2000s. Critically, however, the near-terminus region is ∼20-100 m thinner than during its previous maximum retreat in 2005, such that the terminus within ∼5 km of the ice front is within ∼25-50 m of flotation. This thinning and retreat has been driven by a persistent negative mass balance since 2003 as a result of anomalously warm atmospheric and oceanic temperatures which have shown a sustained increase since 1980. Although temporary re-advance is possible, with further oceanic and atmospheric warming we expect that Helheim Glacier will continue to thin and lose mass, eventually passing a threshold whereby the near-terminus region floats and rapidly accelerates and retreats. Such a retreat would be the most extensive within the observational record, exceeding that which occurred in the 1930s and the early-2000s. Moreover, Holocene records (Bjørk et al., 2018) indicate that after a similar retreat occurred beginning between 10.5 – 9.6 ka, Helheim Glacier remained retreated until 0.3 ka, despite cold events at 9.3 and 8.2 ka and during the early-Neoglacial, suggesting that re-advance would be difficult. As such, we argue Helheim Glacier is poised for a rapid retreat that may represent a tipping point into a new dynamic state.

6.7 Supplementary Information

6.7.1 Midgard Glacier Flow Branches

In 2010, Midgard Glacier split into separate flow branches (see Figure 6.5) and these are treated separately in our analysis (named Midgard North Glacier and Midgard South Glacier), apart from where the data does not distinguish between them, which is the case for the CryoSat-2 surface elevation change data and the Mouginot et al., 2019 mass balance data.

6.7.2 Midgard Glacier Bed Topography

At both Midgard North and Midgard South, the bed topography elevation estimates are greater than the surface elevation measurements, and so we do not calculate a flotation elevation for these sites. Despite the uncertainty in the exact values, we include the bed topography data in our results at these glaciers as the shape of the bed is important in itself, and this data represents the current best estimate.

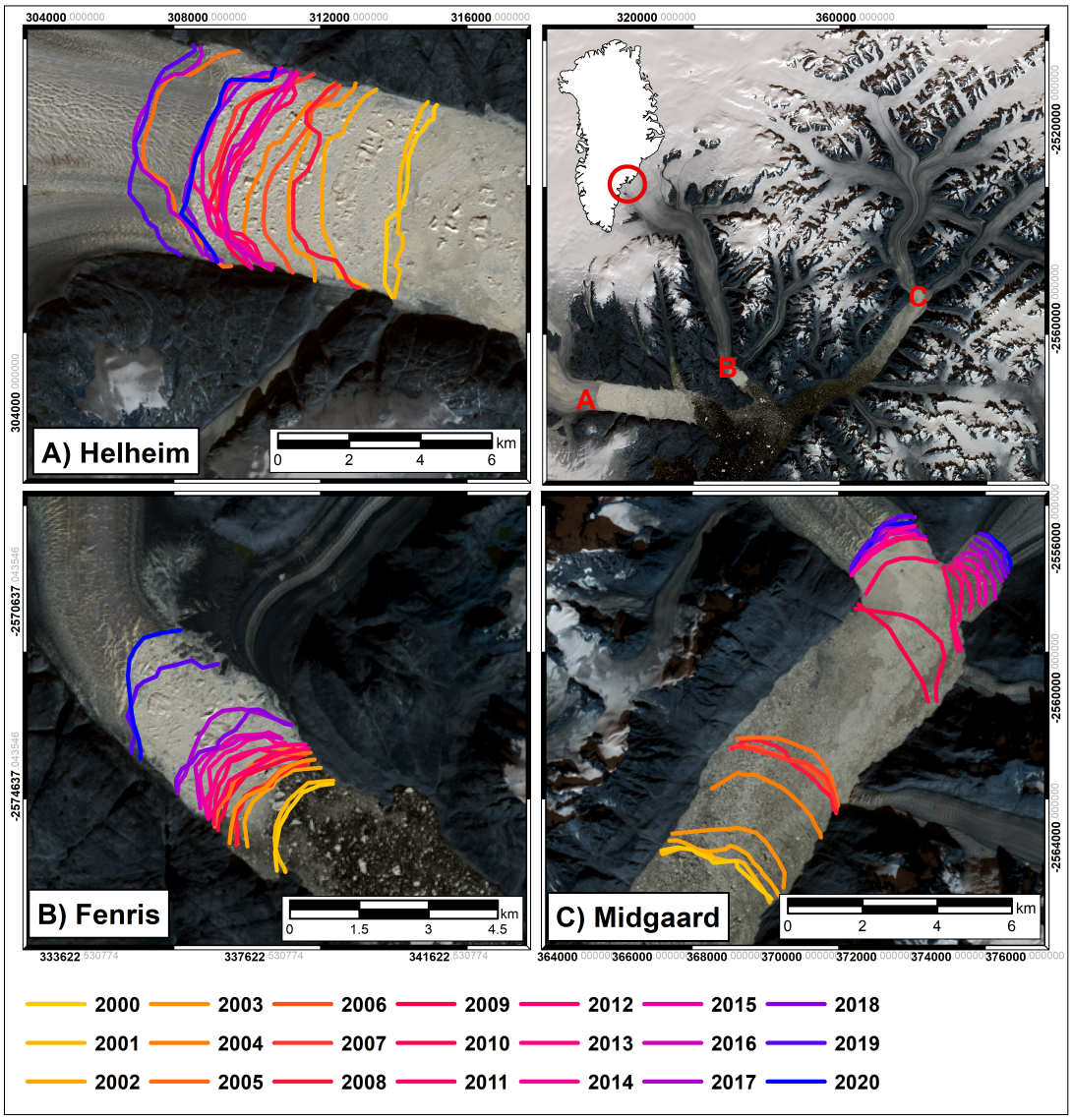

Figure 6.5: *Terminus positions from 2000-2020 at* ***(A)*** *Helheim Glacier,* ***(B)*** *Fenris Glacier, and* ***(C)*** *Midgard Glacier.*

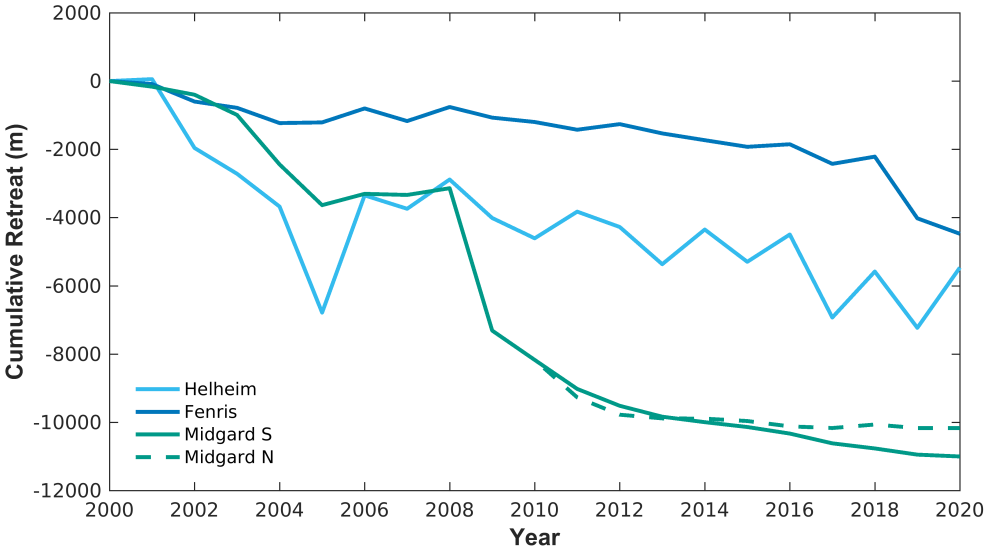

Figure 6.6: *Cumulative retreat (m) of the terminus at Helheim Glacier, Fenris Glacier, Midgard North Glacier and Midgard South Glacier from 2000-2020.*

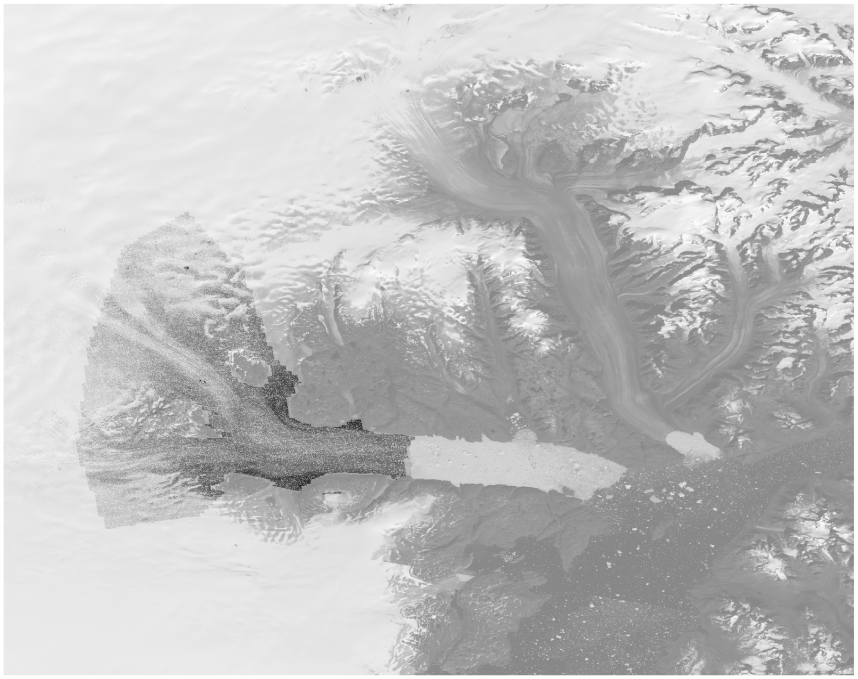

Figure 6.7: *Map displaying the pixels at which CryoSat-2 elevation data was extracted to produce the surface elevation time series for Helheim Glacier, displayed in Figure 6.1c. The base image is a Landsat 7 ETM+ band 8 mosaic from the MEaSUREs GIMP 2000 Image Mosaic V1 (Howat, 2017).*

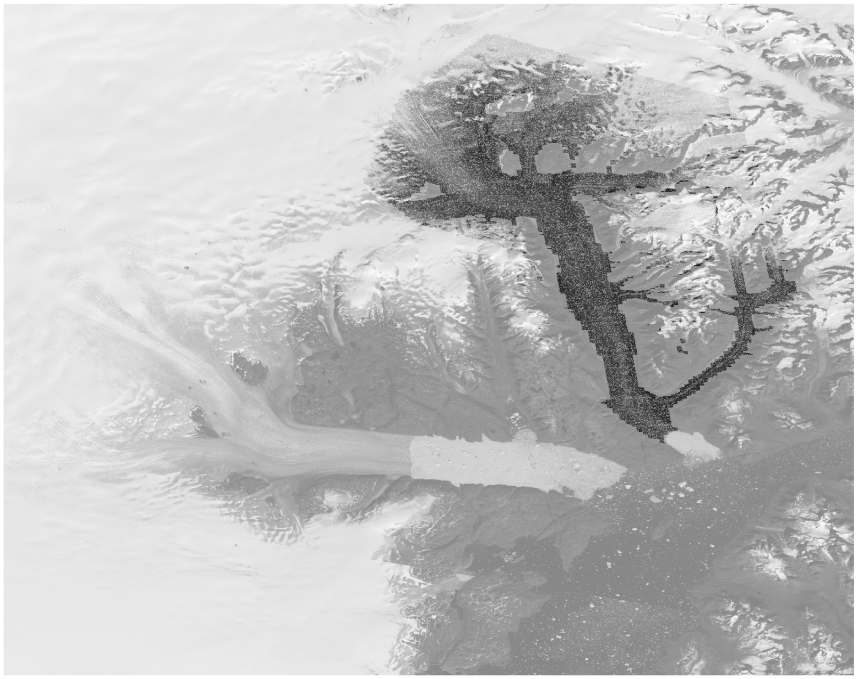

Figure 6.8: *Map displaying the pixels at which CryoSat-2 elevation data was extracted to produce the surface elevation time series for Fenris Glacier, displayed in Figure 6.2c. The base image is a Landsat 7 ETM+ band 8 mosaic from the MEaSUREs GIMP 2000 Image Mosaic V1 (Howat, 2017).*

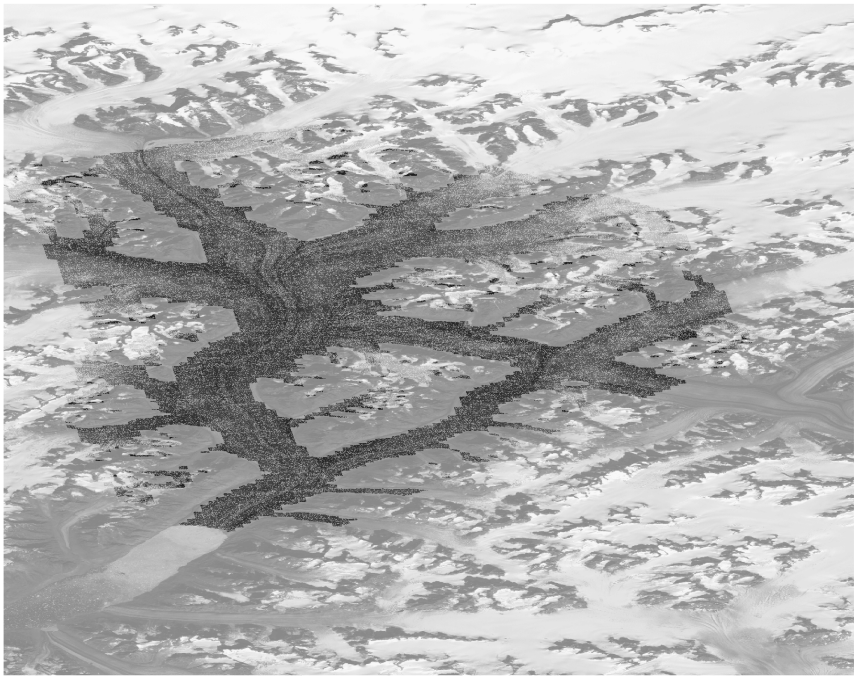

Figure 6.9: *Map displaying the pixels at which CryoSat-2 elevation data was extracted to produce the surface elevation time series for Midgard Glacier, displayed in Figure 6.3c. The base image is a Landsat 7 ETM+ band 8 mosaic from the MEaSUREs GIMP 2000 Image Mosaic V1 (Howat, 2017).*

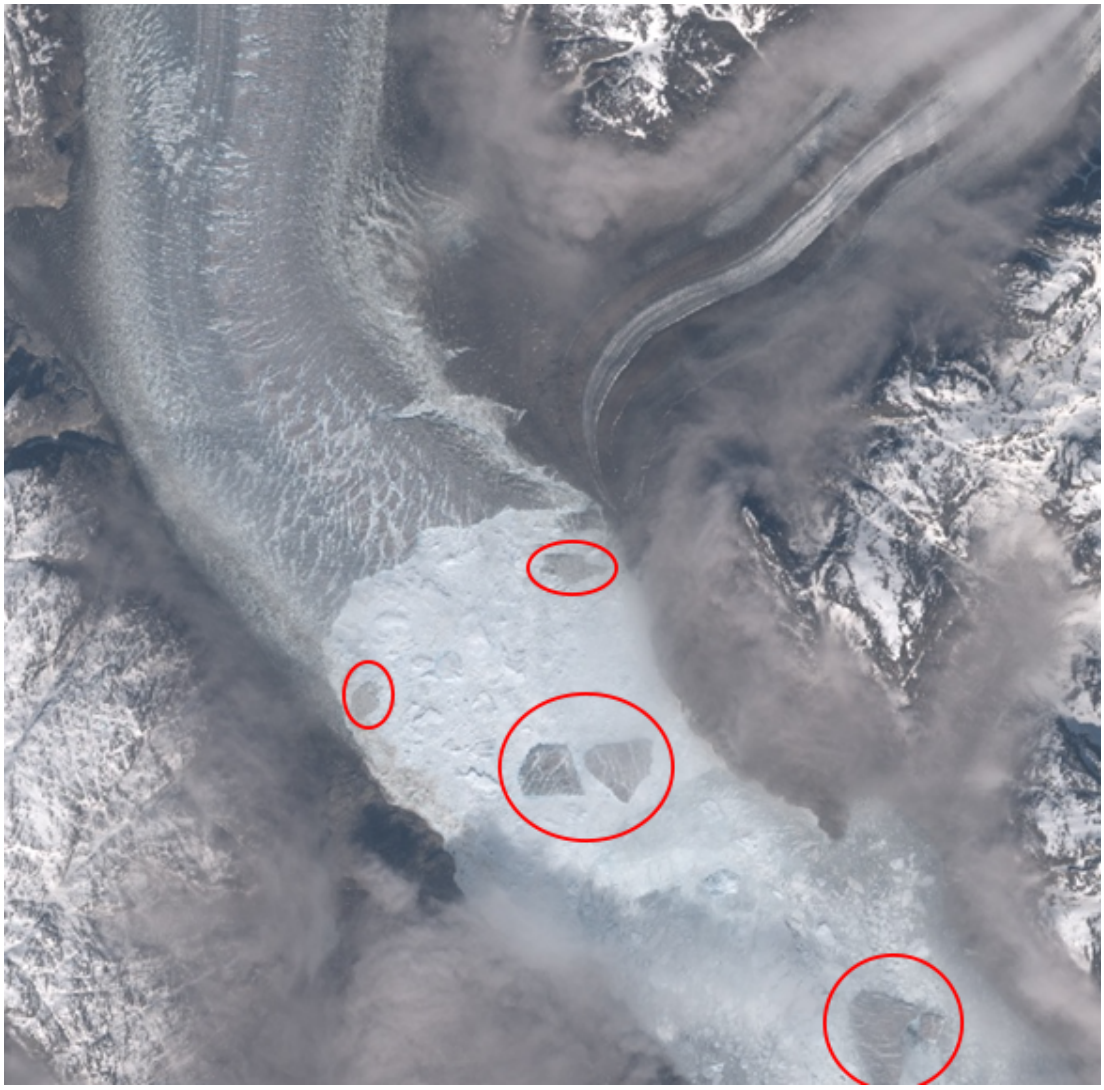

Figure 6.10: *Examples of large tabular icebergs (highlighted by red circles) that have not overturned within the proglacial fjord of Fenris Glacier, and thus provide evidence that the near-terminus region is floating. The background image is a Landsat 8 (band 8) scene from 24/05/2019.*

Chapter 7

Discussion and Conclusions

The overall aim of this thesis has been to improve our understanding of the dynamics of the Greenland Ice Sheet in order to facilitate improved projections of how the ice sheet will respond to future climate warming. This work has been motivated by the response of the Greenland Ice Sheet to recent climate change in the form of increased atmospheric and oceanic temperatures, as illustrated by widespread thinning, acceleration, and retreat of marine terminating glaciers across all regions of the ice sheet margin since the late-1990s/early-2000s (Bevan et al., 2012; Bunce et al., 2018; Hill et al., 2018; Joughin et al., 2008a; McMillan et al., 2016; Murray et al., 2015; Pritchard et al., 2009; Rignot and Kanagaratnam, 2006a). Furthermore, the potential dynamic response of land-terminating sectors of the ice sheet to atmospheric warming and associated surface melt-ice-dynamics coupling is of ongoing concern (Davison et al., 2019; Nienow et al., 2017). Despite a rapid growth in the research interest in mass loss from the Greenland Ice Sheet and its associated impacts, we still lack the ability to predict with confidence rates of mass loss under future climate change, with uncertainty stemming from the non-linear response of the ice sheet to climate forcing, and the multitude of processes at play that occur on overlapping timescales and are often challenging to observe (Catania et al., 2020; Davison et al., 2019; Nienow et al., 2017). Consequently, a better understanding of the mechanisms driving recent and contemporary dynamical change and the discharge of ice from the Greenland Ice Sheet is crucial for improving the representation of ice dynamics

and their response to climate forcing within the ice sheet models used to predict the behaviour of the Greenland Ice Sheet under future climate change.

The first section of this concluding chapter provides a summary of the main findings of this thesis as previously reported in Chapters 4-6. This is followed by a discussion that considers the implications of these findings with reference to the wider literature, after which the chapter ends with suggestions for priorities regarding the future direction of research into Greenland's dynamics followed by concluding remarks.

7.1 Summary of Findings

Chapter 4 builds upon the recent research into understanding the net impact of hydro-dynamic coupling on ice motion across the land-terminating margins of the Greenland Ice Sheet. On a multi-decadal timescale, prior studies have provided evidence for a mechanism whereby a long-term sustained increase in surface melt-water production causes a long-term slowdown in annual ice velocity as a result of an increase in the size and extent of efficient subglacial channels which enhance the drainage of basal meltwaters from the inefficient drainage system, thereby reducing 'background' basal water pressure across extensive areas (Stevens et al., 2016; Tedstone et al., 2015). However, since the exceptional melt of 2012, re-gional air temperatures have cooled (Tedesco et al., 2017) and as a consequence, we would thus expect the geometric and spatial extent of subglacial channels to decrease, thereby enabling the distributed drainage system to re-pressurise via the recharge of meltwater through basal melting, with the overall impact of in-creasing annual ice velocity. This 're-pressurisation' effect has been observed on a seasonal timescale from GPS data (Joughin et al., 2008b; Sole et al., 2013; van de Wal et al., 2015); however, these observations are spatially limited, and the process has yet to be observed on a multi-annual timescale. In order to address this and determine whether the recent cooling has indeed impacted ice dynamics across Greenland's land-terminating glacier margins, feature tracking was applied

to the entire Landsat archive between 1985 and 2019 across a 10,600 km^2 region of southwest Greenland, extending 300 km along the margin and 50 km inland, reaching an elevation of 1300 m (a.s.l.).

Between the periods 1992-2003 and 2003-2012, modelled surface melt production increased by approximately 30 %, while ∼93 % of the study area experienced a reduction in ice velocity, with a mean regional slowdown of ∼15 %. By assessing the time series of velocity change across the pixels common to each velocity field (totalling an area of 4130 km^2), ice velocity decreased by 1.64 ± 0.37 m yr^{-2} between 2003 and 2012, results which are consistent with prior work (Stevens et al., 2016; Tedstone et al., 2015). Following this period of enhanced atmospheric temperatures, regional cooling drove a 15 % reduction in modelled surface melt production between the periods 2010-2012 and 2017-2019. This cooling is coincident with a mean region-wide re-acceleration of 8 % across the study area, with 90 % of the study area re-accelerating. The velocity time series shows a mean acceleration of 0.58 ± 037 m yr^{-2} between 2012 and 2019 across the 4130 km^2 area common to all included velocity fields.

These results support the hypothesis that under a reduced melt forcing, the subglacial drainage system will gradually re-pressurise, and ice flow will thus accelerate. However, whilst it may be expected that channels would close earlier and faster under thicker ice (Chandler et al., 2013; Dow et al., 2014; Meierbachtol et al., 2013a), thereby enhancing the re-acceleration further inland compared to nearer the margin, the results in Chapter 4 show that this re-acceleration is proportionally largest in areas of lower ice thickness. This is consistent with modelling studies that suggest there is very little difference in closure time between channels with cross-sectional area of 10 m^2 compared to <1 m^2 (Dow et al., 2014), and that maximum rates of channel closure are similar at marginal and inland sites (Meierbachtol et al., 2013a). We thus hypothesise that marginal regions show a proportionally greater re-acceleration because the recharge of basal meltwaters in these regions offsets a larger proportion of the ice overburden pressure.

Our findings indicate that hydro-dynamic coupling provides the major control on ice motion within the ablation zone of Greenland's land-terminating margins over multi-annual timescales and reaffirms that these regions of the ice sheet are resilient to the dynamic impacts of increases in surface meltwater production. It remains unclear how higher elevation regions of the ice-sheet, with thicker ice, will respond to future variations in surface meltwater forcing, as well as the extent to which surface melt processes are and will continue to impact upon tidewater glacier dynamics.

The uncertainty regarding dynamic change across the higher elevation ice sheet interior is addressed in Chapter 5. This is particularly important as Greenland's future contribution to sea level rise is strongly dependent on the extent to which dynamic perturbations, originating at the margin, can drive increased ice flow within the interior (Felikson et al., 2017, 2020; King et al., 2020; Price et al., 2011). Measurements of ice velocity within the interior were originally limited to spatially and temporally sparse GPS data (Ahlstrøm et al., 2013; Sole et al., 2011). However, recent advances in satellite imaging have enabled the mapping of ice velocities through feature tracking at considerable distances into the ice sheet interior (Fahnestock et al., 2016). By combining recent satellite-derived annual ice velocities from the period 2014-2018 (Gardner et al., 2019) with estimates of annual ice velocity during the period 1993-1997 observed by a ring of GPS sites around the 2000 m (a.s.l.) surface elevation contour (Thomas et al., 2000; Thomas et al., 1998; Thomas, 2001), multi-decadal changes in ice velocity are quantified at 45 GPS sites inland of tidewater glaciers and encompassing all regions of the ice sheet.

The results of this study show an almost ubiquitous acceleration inland of tidewater glaciers in west Greenland, consistent with retreat and acceleration at glacier termini. Interior acceleration reaches 28.1 $\pm$ 7.8 m yr^{-1} at a site approximately 117 km inland of Jakobshavn Isbrae. An estimation of the change in surface velocity as a result of total changes in ice thickness and surface slope at the same

site gives a comparable velocity change of 35.02 m yr^{-1}, whereas the estimated change in surface velocity as a result of SMB-driven ice thickness and surface slope change is -0.18 m yr^{-1}. This therefore supports the indication that dynamic perturbations at the terminus have propagated distances of over 100 km inland in west Greenland, and that the observed inland velocity change cannot have been driven by changes in SMB. In contrast, and with the exception of Kangerlugssuaq no acceleration is observed inland of tidewater glaciers in east Greenland despite near-ubiquitous terminus retreat and near-terminus acceleration. This suggests that propagation may be limited by the influence of basal topography and ice geometry, as has been suggested by recent work (Felikson et al., 2017, 2020). Indeed, we find that inland acceleration is observed in regions characterised by shallow surface slopes and deep basal topography that remains below sea level for tens to hundreds of kilometres into the ice sheet (Morlighem et al., 2014, 2017). By contrast, sites where no acceleration is observed are almost all upstream of a sharp rise or 'step' in basal topography, thought to limit the propagation of a thinning perturbation (Felikson et al., 2017, 2020; Morlighem et al., 2014). These findings are of significance with regards to Greenland's future contribution to global sea level rise, as they indicate that ice acceleration at the termini of many tidewater glaciers has the potential to propagate into the ice-sheet interior, accelerating the draw-down of greater volumes of thicker ice toward the margins, thus accelerating mass loss. However, these results also support recent work that indicates that local bed topography and ice geometry are crucial in facilitating or limiting the ability for a perturbation at the terminus to propagate inland (Felikson et al., 2017, 2020; Morlighem et al., 2014, 2017). This indicates that as a result of steep and pronounced down-glacier bed topographic steps, inland regions in east Greenland may be more resilient to the impacts of future outlet glacier acceleration than those in the west.

The final results chapter investigates recent dynamical change at the marine-terminating Helheim Glacier, and the neighbouring Fenris Glacier and Midgard Glacier, in southeast Greenland. Helheim Glacier drains approximately 7 % of

the ice sheet area (Rignot and Kanagaratnam, 2006a), and underwent significant thinning, acceleration, and retreat between 2002 and 2005 (Howat et al., 2005; Howat et al., 2008a; Luckman et al., 2006; Stearns and Hamilton, 2007), after which it re-advanced and decelerated (Bevan et al., 2012; Howat et al., 2011; Kehrl et al., 2017). Recent research indicates that Helheim Glacier has undergone a substantial increase in solid ice discharge since 2014, such that it now has at least the second largest discharge of any Greenlandic glacier (Mankoff et al., 2020). In this chapter, a range of satellite-derived data are combined with estimates of bed topography in order to examine this recent dynamic change, and the same analyses are applied to the neighbouring Fenris Glacier and Midgard Glacier to contextualise the observed change at Helheim Glacier and investigate how tidewater glaciers located within the same fjord system may differ in their response to a common climatic forcing.

Recent mass balance data (Mouginot et al., 2019) show that despite re-advancing from 2006, Helheim Glacier has continued to lose mass and thin, consistent with a long-term increase in observed air temperatures and modelled submarine melt rates as presented in Chapter 6. This mass loss has culminated in a retreat of $>$ 4 km and an acceleration of 2.5-3 km yr^{-1} since 2014, with maximum retreat positions in both 2017 and 2019 extending further inland than its maximum retreat during 2005. More importantly, the near-terminus region is currently 20-100 m thinner than it was in 2005, such that the front 5 km of the glacier is now within 25-50 m of flotation, indicating that the glacier is currently in a much more unstable configuration than during its previous maximum retreat in 2005. Moreover, reverse bed slopes extend for several kilometres inland beneath the northern and southern regions of the near-terminus, with the potential to exacerbate any future retreat. This suggestion of instability is supported by the results at Fenris and Midgard Glaciers which have been subject to a similar climate forcing and have also undergone persistent mass loss (Mouginot et al., 2019). The near-terminus regions of these glaciers thinned to flotation (in early-2018 at Fenris Glacier and in the late-2000s at Midgard Glacier), after which they underwent rapid retreat and

acceleration. Whilst the timing and magnitude of retreat differs, likely related to their respective ice thicknesses and basal topography (i.e., Catania et al., 2018), the fundamental mechanism driving the rapid retreat (thinning to flotation as a result of a persistent negative mass balance) is the same. These results therefore suggest that Helheim Glacier is poised for a dramatic and sustained retreat should atmospheric and oceanic temperatures continue to warm, in contrast to the re-advance following its' previous (2002-2005) retreat.

7.2 Implications of Results

The results of this thesis build upon previous research focused on understanding how the Greenland Ice Sheet dynamically responds to oceanic and atmospheric forcing. These results are now put in context with the key issues surrounding the future dynamics and stability of the Greenland Ice Sheet.

7.2.1 Dynamic impact of enhanced surface melting

Enhanced surface melting is projected to continue under ongoing climate warming (Hofer et al., 2020; Vaughan et al., 2013), yet whilst early work indicated that ice flow would scale positively with meltwater production within the southwest land-terminating sector of the Greenland Ice Sheet (Parizek and Alley, 2004; Zwally et al., 2002), more recent research and the results of this thesis indicate that this region of the ice sheet is instead resilient to the dynamic impacts of increases in surface meltwater production across multi-annual time scales (Stevens et al., 2016; Tedstone et al., 2015; Williams et al., 2020). There has, however, been recent debate as to the influence of hydro-dynamic coupling on ice motion, with radar-imagery-derived velocities suggesting that there has been no significant trend in ice velocity across much of the southwest ice-sheet margin between 2000/01 and 2016/17 (Joughin et al., 2018). By extending the study area of Tedstone et al., 2015 ∼120 km further south, increasing the area across which the time series is extracted from ∼400 km^2 to ∼4000 km^2, and removing any influence of inter-mission bias through the calculation of an ice velocity anomaly, the

results of this thesis provide greater confidence that hydro-dynamic coupling is indeed the key control on 'short-term' variability in ice motion within this sector of the ice sheet. Whilst our findings reveal that ice motion re-accelerates under the sustained cooler temperatures from 2013 through 2019, there is no evidence or expectation to suggest that air temperatures will remain at this level under continued climate change (Vaughan et al., 2013). Moreover, there is also no indication that climate change will result in more frequent short-term fluctuations between warm and cool periods within individual summer melt seasons, which would be required to drive transient increases in ice flow as the subglacial drainage system is repeatedly overwhelmed by large meltwater inputs, as observed during the exceptional July 2012 melt-event (Tedstone et al., 2013). As such, it is expected that on decadal timescales, there will continue to be an inverse relationship between ice motion and surface melt forcing within the southwest land-terminating margin.

Modelling studies have re-produced some of the characteristics of the observed hydro-dynamic coupling across Greenland's land-terminating margins over short-term (days to weeks) and seasonal timescales (Dow et al., 2014; Hewitt, 2013; Hoffman et al., 2016; Koziol and Arnold, 2018; Schoof, 2010). However, the results of recent efforts at modelling the response of the land-terminating margin to increased meltwater production on a decadal timescale project a future positive feedback between surface melting and ice velocity (Bougamont et al., 2014; Gagliardini and Werder, 2018), despite a range of independent observations to the contrary (Stevens et al., 2016; Tedstone et al., 2013, 2015; van de Wal et al., 2008, 2015; Williams et al., 2020). This may result from the use of a subglacial hydrological model in which the evolution of an efficient subglacial drainage system occurs over a period of months (Werder et al., 2013), whereas dye and SF6 tracer experiments indicate that it occurs over a period of days (Chandler et al., 2013; Cowton et al., 2013). In the case of an efficient drainage system evolving over a period of months, a distributed drainage system would persist for a much longer period of the summer melt season than in reality, resulting in an extended

period characterised by a positive melt/velocity feedback. To re-produce the observed impact of hydro-dynamic coupling more accurately, subglacial hydrological models should be validated against observational data, as has been done within recent modelling studies focusing on the impact of submarine melting on driving tidewater glacier retreat (Slater et al., 2019b).

The land-terminating sector offers a study site that is isolated from ice-ocean interactions, thereby allowing for the investigation into the dynamic response of these sectors of the ice-sheet to atmospheric forcing. Applying or indeed extrapolating the results of Chapter 4 to tidewater glacier margins, however, remains difficult due to both the extreme difficulty in conducting field studies on fast-flowing, heavily crevassed outlet glaciers (Catania et al., 2020; Nienow et al., 2017), and the wide variety of processes controlling tidewater glacier dynamics. As such, it is not clear to what extent subglacial channels can form beneath tidewater glaciers (Nienow et al., 2017), and if they can form, to what extent they influence glacier flow. Tidewater glaciers flow much faster (typically 1000 m yr^{-1} or more) than the southwest land-terminating margin ($\sim$100 m yr^{-1}), and theoretically fast-flowing ice should increase the rate of subglacial channel closure and only allow slow channel growth (Röthlisberger, 1972), such that channel formation may be limited beneath tidewater glaciers as has been seen at fast flowing surging glaciers (Kamb, 1987), especially where the bed deepens inland such that the ice thickness increases. This suggestion of inhibited subglacial channel formation is supported by a range of studies which infer the presence of a distributed subglacial drainage system beneath tidewater glaciers (Fried et al., 2015; Jackson et al., 2017; Slater et al., 2017). However and conversely, runoff-driven buoyant plumes are often observed in front of tidewater glacier termini (i.e., Bunce et al., 2021; Jackson et al., 2017; Slater et al., 2017), indicating the output of basal water from discrete sources, thus indicative of efficient subglacial channels. Indeed, a recent study of seasonal ice velocities across 45 Greenlandic outlet glaciers for the period 2015-2017 suggests that the underlying hydro-dynamic processes may be the same for both land- and marine-terminating margins, at least on a

seasonal timescale (Vijay et al., 2019). Similarly, recent work combining ice velocity measurements with plume modelling at Narsap Sermia, Kangiata Nunaata Sermia, and Akullersuup Sermia in southwest Greenland shows that during the years 2014-2019, these three tidewater glaciers all underwent a seasonal speed-up, usually coinciding with the onset of surface melting, and a subsequent slowdown to below pre-acceleration levels, with a gradual increase in ice velocity over the following winter (Davison et al., 2020b).

Whilst some evidence therefore now points towards tidewater glacier dynamics being controlled to some extent by changes in surface melting and the associated impacts upon the subglacial drainage system, the question remains concerning the likely influence of hydro-dynamic coupling on long-term tidewater glacier dynamics. If seasonal behaviour at some tidewater glaciers is indeed qualitatively consistent with the self-regulation of ice flow observed within the land-terminating sectors (Stevens et al., 2016; Tedstone et al., 2013, 2015; van de Wal et al., 2008, 2015; Williams et al., 2020), it may be expected that there would be a limited sensitivity of multi-annual ice motion to multi-annual changes in surface melt production. However, and as introduced in Chapter 2, enhanced surface melt may also drive increased submarine melting (Bunce et al., 2021; Motyka et al., 2003; Slater et al., 2015), enhanced fjord circulation and thus the delivery of more warm water to the glacier front at depth (Carroll et al., 2015; Cowton et al., 2016; Sciascia et al., 2013; Straneo et al., 2011), as well as enhanced crevassing near the terminus (Benn et al., 2007a; Cook et al., 2014; Nick et al., 2010; Van Der Veen, 1998), and these impacts may overprint any dynamical change driven by changes to the subglacial hydrological system. Indeed, whilst observations at Narsap Sermia suggest a seasonal hydro-dynamic control on ice flow (Davison et al., 2020b), this glacier underwent a dramatic retreat and acceleration, of $\sim$3.3 km and $>$1.5 km yr^{-1} respectively, between 2010 and 2014 which has been linked primarily to a large increase in submarine melting due to increased sea surface temperatures and subglacial discharge (Motyka et al., 2017). Consequently, whilst the evolution of the subglacial drainage system likely plays a role in the response of

tidewater glaciers to climate warming, it remains unclear the extent to which this controls their dynamics, especially over multi-annual timescales, when compared to processes associated with ice-ocean interactions.

7.2.2 Mass loss from Greenland's marine-terminating glaciers

The future contribution to sea level rise as a result of dynamic change at Greenland's tidewater outlet glaciers will be driven by thinning, retreat, and acceleration at the glacier termini, as well as the extent to which these dynamic changes are able to propagate upglacier into the ice sheet interior. With regards to the former, the results presented in Chapter 6 show that whilst local morphology and bed topography can result in differences in the timing, rate, and magnitude of the response of individual glaciers to climate warming (Catania et al., 2018), a long-term warming of the ocean and atmosphere represents the primary driver of mass loss, consistent with recent work investigating the centennial dynamic response of Jakobshavn Isbrae, Kangerlussuaq, and Helheim Glacier to changing climate forcings (Khan et al., 2020). Additional factors, such as the presence or absence of a rigid ice mélange (Bevan et al., 2019; Joughin et al., 2020) or the enhancement of the circulation within the fjord (Straneo and Cenedese, 2015; Straneo et al., 2011) also exert a control on tidewater glacier dynamics; however, these processes, and their impacts, are also inherently linked to oceanic and atmospheric warming.

This importance of long-term oceanic and atmospheric warming in driving tidewater glacier mass loss has implications for modelling the dynamic response of tidewater glaciers to climate warming. There are currently two main approaches for simulating the impact of ocean and atmospheric warming within ice sheet models; high-resolution models that aim to capture the calving process (Benn et al., 2017b; Bondzio et al., 2016; Todd et al., 2018, 2019) and more simple parameterisations of tidewater glacier retreat that are applicable at an ice-sheet-scale (Slater et al., 2019b, 2020). Whilst models following the former are increasingly able to capture the complexities of the calving process (Benn et al., 2017b), their spatial resolution (<100 m) is an order of magnitude finer than most current gen-

eration ice sheet models (Goelzer et al., 2018, 2020) and difficulties remain due to the range of calving styles, as well as the lack of a calving law that has been validated extensively at tidewater glaciers (Benn et al., 2017a). These issues with process complexity and the small spatial scales across which these processes operate have hindered efforts to represent calving within Greenland-scale ice sheet models (Slater et al., 2019b).

As a result of these difficulties, recent efforts to model the dynamic response of Greenland's tidewater glaciers to oceanic and atmospheric warming have focused primarily on practicality, whilst also aiming to maintain process fidelity (Catania et al., 2020; Slater et al., 2019b). This is the approach taken using the ice sheet models included within the Ice Sheet Model Intercomparison Project for CMIP6 (ISMIP6) (Edwards et al., 2021; Goelzer et al., 2018, 2020), whereby tidewater glacier terminus position is parameterised as a simple linear function of submarine melting, which is in turn estimated as a function of subglacial discharge and ocean temperature (Slater et al., 2019b). The reasoning behind this approach is that whilst individual glacier response to climate warming is heterogenous as a result of numerous factors including differences in ice geometry and local morphology, as observed in Chapter 6 and elsewhere (i.e., Bunce et al., 2018; Catania et al., 2018), more homogenous broad patterns of behaviour have been observed over larger spatial and temporal scales (Cowton et al., 2018; Porter et al., 2018b; Slater et al., 2019b). For example, combined variability in oceanic and atmospheric temperatures explained 54 % of the variability in terminus position across 10 tidewater glaciers in east Greenland between 1993 and 2012 (Cowton et al., 2018), and a recent study of 74 Greenlandic tidewater outlets observed a significant correlation ($R^2 = 0.81 \pm 0.15$, $p = 0.009$) between glacier dynamic thinning and local ocean heat content for regions outside of west Greenland (Porter et al., 2018b). The results presented in Chapter 6 further support this modelling approach, as although the tidewater glaciers studied respond to long-term ocean and atmospheric warming at different times, the long-term warming of the ocean and atmosphere is the key control on dynamic change

through its impact on long-term glacier mass balance. Fundamentally, it is less important to accurately model the precise timing and rate of retreat of an individual glacier as opposed to accurately modelling the overall magnitude of retreat of a broad population of glaciers, which this thesis argues will be primarily driven by oceanic and atmospheric warming.

In addition to the dynamic changes near the termini of Greenland's tidewater outlet glaciers, the importance of the inland propagation of these dynamic changes has been emphasised by modelling work, which estimates that more than 75 % of Greenland's projected sea level rise contribution will result from this long-term diffusive response (Price et al., 2011). Indeed, recent work hypothesises that smaller glaciers with a low mass flux, where dynamic perturbations can propagate great distances inland, are as important to Greenland's future sea level contribution as the more well-studied high-mass-flux glaciers, where the propagation of perturbations occurs over a far more limited extent (Felikson et al., 2020). The results of Chapter 5 lend observational support to this hypothesis by showing evidence of accelerated ice flow ∼90 km inland of Rinks Isbrae, Upernavik Isstrom, and Kong Oscar Glacier in northwest Greenland, consistent with estimated thinning limits of >400, >300, and 500 km respectively (Felikson et al., 2020). However, whilst Felikson et al., 2020 estimate thinning limits of 57.9 and 35.3 km for Jakobshavn Isbrae and Kangerlussuaq respectively, the observations in Chapter 5 show evidence of ice flow acceleration ∼117 and ∼135 km inland from these glaciers' termini. As a result, these glaciers are likely of particular importance as they are characterised by both an extremely high mass flux (i.e., Mankoff et al., 2020; Mouginot et al., 2019), as well as the ability for dynamic change to propagate considerable distances inland and thus draw greater volumes of thicker ice from the interior towards the ice-sheet margin.

The inland propagation of change initiated at the terminus and the limitations imposed by bed topography are included within the current state-of-the-art models used within ISMIP6 (Goelzer et al., 2020), and so in theory, these models

do incorporate the effects shown here in Chapter 5 and other studies (i.e., Felikson et al., 2017, 2020; Price et al., 2011). However, the majority (14/21) of these models have minimum spatial resolutions >= 1 km, and 8/21 have minimum spatial resolutions of at least 5 km (Goelzer et al., 2020, their Table A1). As a result, models of this resolution are unlikely to resolve the finer details of bed topography or ice geometry, and so they may not account for narrow deep troughs or small bedrock bumps and pinning points such that the effect of bed topography on facilitating or limiting the propagation of dynamic change inland may not be well captured. Whilst recent modelling studies have increased spatial resolution, reaching as fine as 100 m along the coast (Aschwanden et al., 2019; Morlighem et al., 2019), these models are largely limited in extent to localised regions of the ice sheet. High-resolution modelling has recently been expanded to an ice sheet scale with a spatial resolution of 200 m along the coast, incorporating 215 individual tidewater glaciers (Choi et al., 2021), and the resultant model is able to reproduce the contrasting dynamic response between glaciers as a result of differences in bed topography and the presence or absence of subglacial troughs. Nevertheless, for 67 of the 215 glaciers, largely located within the northeast and southeast sectors of the ice sheet, the bed topography data is poorly constrained such that the ice fronts are fixed in time (Choi et al., 2021). As such, at these glaciers, the model does not allow ice dynamics to feedback on terminus retreat, which represents a significant weakness as it is well understood that the ice sheet responds dynamically to calving front retreat through thinning and ice flow acceleration. This dynamic response in turn would be expected to drive further rapid retreat resulting in a stronger dynamic perturbation that is propagated inland, such that more mass is transported to the margin where it is subsequently removed (Felikson et al., 2017, 2020; Goelzer et al., 2020; Price et al., 2011). This lack of ice dynamical feedback on terminus retreat is also not accounted for within the simple linear parameterisation of tidewater glacier retreat within the ISMIP6 models (Goelzer et al., 2020; Slater et al., 2019b), thus representing a major limitation across many state of the art ice sheet models.

In summary, the current state of the art ice sheet models included within ISMIP6 parameterise tidewater glacier retreat in such a way that glacier response to oceanic and atmospheric forcing is accounted for and validated against existing observations. In addition, they also consider both the propagation of dynamic perturbations initiated at the terminus and the impacts of bed topography and ice geometry in facilitating or limiting the inland extent to which such propagation may reach. However, it is clear that significant limitations remain concerning the accurate modelling of the dynamic response of tidewater glaciers, and their inland drainage basins, to ongoing climate forcing.

7.3 Future Research

A number of challenges remain with regards to fully understanding the response of the Greenland Ice Sheet to continued climate warming. Within land-terminating regions of the ice sheet, these challenges include obtaining a better understanding of the response of higher elevation regions to surface melt forcing, the representation of subglacial hydrology within ice sheet models, and the influence of the growing number of proglacial lakes on ice dynamics. Similarly, there are a range of challenges to overcome in order to obtain a comprehensive understanding of how marine-terminating margins of the ice sheet will respond to future climate warming. These include identifying the extent to which hydrology-dynamic coupling exerts a control on ice flow within tidewater glacier system, obtaining more extensive and higher qualities measurements of submarine melting, bed topography, and fjord bathymetry, and representing key processes within the ice sheet models used to project the future response of the Greenland Ice Sheet to future climate change.

A primary limitation of the results presented in Chapter 4 is the inland extent to which dynamic change was assessed (∼50 km from the margin extending to ∼1300 m a.s.l.). Extending satellite-derived velocity estimates beyond the heavily-crevassed ablation area is difficult, as feature-tracking methods struggle

to track ice motion within inland regions in which there are few discernible surface features, especially when using pre-Landsat-8 imagery. Whilst the long-term dynamic response of inland regions of the ice sheet was quantified in Chapter 5, the sites inland of the southwest land-terminating sector were filtered out due to the poor data quality associated with the satellite-derived ice velocity estimates at these sites, and so current observations remain limited to sparse GPS measurements (Doyle et al., 2014; Tedstone et al., 2013; van de Wal et al., 2015). Understanding how the land-terminating accumulation zone will respond to future climate warming is further complicated as these GPS sites show contrasting responses to the same apparent melt forcing. At site 7 of their GPS transect (2.8, 1700 m a.s.l), Tedstone et al., 2013 observe a reduction in ice velocity in the extreme melt year of 2012/13 compared to 2011/12 and a 6 % reduction in net annual motion in 2012 compared to 2009, whereas at site S10 of the k-transect (2.8, 1840 m a.s.l), Doyle et al., 2014 observe a 2.2 % acceleration between 2009 and 2012. A possible explanation is that the increase in ice thickness at site S10 compared to site 7 is sufficient to prevent the development of an efficient subglacial drainage system (i.e., Chandler et al., 2013; Hooke et al., 1990; Schoof, 2010) such that melt and velocity scale positively at this site. It is clear that a greater spatial and temporal density of ice velocity measurements are required within the accumulation zone to better understand how this region of the ice sheet responds to an enhanced surface melt forcing over multi-annual timescales.

Within the ablation area, whilst the results of this thesis and other studies indicate that the land-terminating ice sheet should be resilient to the dynamic impacts of increased meltwater production, a potential mechanism by which this sector of the ice sheet could dynamically lose mass in the future is through the formation of proglacial lakes. The presence of proglacial lakes has been well-studied in alpine glacial environments, whereby glaciers terminating in lakes have been observed to flow faster and experienced enhanced terminus retreat (Baurley et al., 2020; Dell et al., 2019; King et al., 2018; Sugiyama et al., 2011; Tsutaki et al., 2019). As an example, at Breiðamerkurjökul in southeast Iceland, an increase in peak velocity

from 1.00 ± 0.36 m d^{-1} to 3.50 ± 0.25 m d^{-1} between 1991 and 2015, alongside a terminus retreat of ∼3.5 km, is observed for the lake-terminating eastern flow branch (Baurley et al., 2020). In contrast, the land-terminating flow branches saw no discernible velocity change during the same time period, and significantly less terminus retreat (Baurley et al., 2020). The presence of proglacial lakes has been observed in western Greenland, with 55 such lakes mapped using Landsat 7 ETM+ imagery along the west coast (Lewis and Smith, 2009), and UAV imagery revealing the presence of 23 ice-marginal lakes at Isunguata Sermia within the southwest land-terminating sector (Jones et al., 2018). Recent work has shown that proglacial lake frequency is increasing within Greenland (How et al., 2021), with an increase in proglacial lake frequency along Greenland's western margin by 75 %, from 387 lakes in 1985 (Carrivick and Quincey, 2014) to 678 lakes in 2017 (How et al., 2021). The increase in proglacial lake abundance has been attributed to both increasing surface melt (Carrivick and Quincey, 2014) and the retreat of the ice margin (How et al., 2021). Consequently, as both increases in surface melting and ice marginal retreat are projected to continue under future warming, it is likely that the abundance of proglacial lakes at the margins of the Greenland Ice Sheet will continue to increase. The continued growth of proglacial lakes may offer a currently unconsidered mechanism by which Greenland's future mass loss could be enhanced, despite the current negative feedback between surface melting and ice motion. This remains unclear, and thus represents a compelling topic for future research.

At the heart of improving future projections of Greenland's dynamic contribution to sea level rise is the ability to accurately model the response of tidewater glacier dynamics to oceanic and atmospheric warming (Catania et al., 2020). This in turn requires an improved understanding of ice dynamical processes, and thus increased and improved observations of these processes and the critical factors that control them. Spaceborne observations of Greenland have been acquired at an accelerating pace, and datasets of ice velocity and surface elevation are now generated automatically at an ice-sheet-scale (Gardner et al., 2018, 2019; Howat

et al., 2014; Joughin et al., 2010; Rosenau et al., 2015). However, observations remain far more limited in other aspects of ice dynamic change. For example, mapping terminus positions remains a time-consuming manual process, although improvements have been made through the use of cloud computing (Lea, 2018) and machine learning (Cheng et al., 2021; Mohajerani et al., 2019). In addition, whilst ocean properties exert a first order control on tidewater glacier dynamics, we still lack systematic long-term monitoring of such ocean properties around Greenland, particularly within Greenland's glacial fjords (Straneo et al., 2019). Mooring data has been collected from expensive, logistically difficult field campaigns (i.e., Carroll et al., 2018; Gladish et al., 2015; Mortensen et al., 2014; Straneo et al., 2010, 2011); however, these are spatially limited to select fjords and temporally limited to the past decade, with observations often not maintained in the long-term (Straneo et al., 2019).

Further, although submarine melting represents a crucial process by which the warming of both the ocean and atmosphere drives mass loss from Greenland's tidewater glaciers, our best estimates of submarine melt rates are subject to considerable uncertainty. Submarine melt rates have traditionally been derived from either model estimates (i.e., Jenkins, 2011; Slater et al., 2015; Xu et al., 2013), which may lack complexity and are constrained by limited direct observations, or from fjord hydrographic data (i.e., Inall et al., 2014; Rignot et al., 2010), which provide only a snapshot in time and do not account for variability in fjord circulation and ocean properties (Jackson and Straneo, 2016). More recently, direct measurements have been made from remotely operated platforms which can collect data from close to the glacier front (Jackson et al., 2017; Mankoff et al., 2016). However, these measurements remain limited spatially to a few glaciers and temporally to the summer season due to the lack of ice mélange. In addition, methods of estimating submarine melt rates from satellite data have been developed (Enderlin and Howat, 2013; Moyer et al., 2019; Moyer et al., 2017), which are less expensive and have much greater spatial coverage than field campaigns. Again however, these methods are limited to those glaciers characterised by the

presence of a floating ice tongue, and these appear to be limited in extent around Greenland (Reeh, 2017). Consequently, more detailed in-situ observations and/or improved methodologies with respect to modelling and remotely sensed data acquisition are required to provide better constraints on the rates of submarine melting at Greenland's tidewater glaciers.

The nature of the bed topography underlying the Greenland Ice Sheet is of fundamental importance concerning the ice sheets future response to climate warming. Tidewater glaciers situated on reverse sloping beds are considered to be more susceptible to rapid retreat from a given external forcing (Bunce et al., 2018; Carr et al., 2013; Catania et al., 2018, 2020; Meier and Post, 1987). In a recent study of 15 tidewater glaciers in west Greenland, the timing and extent of multi-annual tidewater glacier retreat are strongly correlated with the presence and size of overdeepenings (Catania et al., 2018). This influence of bed topography is also observed in our results reported in Chapter 6 whereby differences in bed topography likely explains the differing response times of neighbouring glaciers to a common climate forcing. The pattern of inland velocity change presented in Chapter 5 also reinforces the importance of obtaining high quality measurements of the bed topography beneath the Greenland Ice Sheet, as not only is Greenland's bed topography a primary control on ice flow (Morlighem et al., 2017), but it is also thought to facilitate or limit the ability for any dynamic change at the terminus to propagate inland (Felikson et al., 2017, 2020; Williams et al., 2021). Indeed, previous improvements in resolving Greenland's bed topography led to the detection of deep subglacial valleys extending below sea level for considerable distances inland and further than previously thought (Morlighem et al., 2014, 2017). It is these subglacial valleys that are hypothesised to facilitate the propagation of dynamic change inland, through both the enhanced driving stresses due to the thicker and warmer ice (Wang et al., 2012) and the absence of steep prograde bedrock slopes which are thought to limit the extent of inland thinning by enhancing the advection of a kinematic wave downstream relative to its' diffusion upstream (Felikson et al., 2017, 2020). However, large uncertainties and

limitations remain both in terms of our current estimates of Greenland's bed topography and therefore how it is represented in ice sheet models.

Our current best estimate of Greenland's bed topography is that of BedMachineV3 (Morlighem et al., 2017), which is calculated by combining a range of ice thickness, ice velocity, and reconstructed SMB data through mass conservation to infer the topography of the underlying bed. The accuracy of the bed topography estimates decreases as you move away from the radar derived ice-thickness survey lines (Morlighem et al., 2017), and so our current best estimates of Greenland's bed topography are limited by the spatial extent to which ice thickness measurements of sufficient quality have been taken. Moreover, difficulties also arise during the collection of radar derived ice thickness data , whereby the presence of crevasses, water on the ice sheet surface or stored within the ice, and deep subglacial valleys limit the ability for radar energy to propagate to the bed (Catania et al., 2020; Morlighem et al., 2017). Similar difficulties exist concerning the collection of fjord bathymetry, which is of fundamental importance to our understanding of how oceanic heat is transported to glacier termini, due to the fact that many glacier fjords are choked with icebergs and ice mélange year-round, limiting the access of ships required for data collection.

As a result, our current best estimates of subglacial bed topography are subject to considerable uncertainties, and there remain numerous glaciers at which values are poorly constrained (Morlighem et al., 2017), as observed for example at Midgard Glacier in Chapter 6. It is clear that future work is required to provide an improved spatial coverage and quality of ice thickness observations with which to constrain the bed topography under the Greenland Ice Sheet. This may be achieved through the use of drones (Catania et al., 2020) or future satellite missions (Freeman et al., 2017) which would offer radar ice thickness measurements over a much greater spatial scale than is currently available. In addition, high-resolution data from ice-penetrating radar could be collected for key sites, as has been done at Pine Island Glacier in Antarctica (Bingham et al., 2017),

although such field campaigns are logistically difficult and financially expensive (Catania et al., 2020).

As discussed in Section 7.2, simulating the impact of oceanic and atmospheric warming on ice dynamics within Greenland-scale ice sheet models remains challenging, and many uncertainties remain in our current best projections of future Greenland mass loss (Choi et al., 2021; Edwards et al., 2021; Goelzer et al., 2020; Slater et al., 2019b, 2020). A high grid resolution, and thus sufficient computing power, is required to resolve individual tidewater glaciers (Goelzer et al., 2020), and many ice sheet models are sufficiently coarse such that they are unable to do so, which is a major limitation if ice dynamics have a fundamental control on mass loss (Choi et al., 2021). High-resolution modelling has been achieved at individual glaciers (i.e., Nick et al., 2013) and on a regional scale (Aschwanden et al., 2019; Morlighem et al., 2019), but has only very recently been achieved at an ice sheet scale (Choi et al., 2021). However, as computing power improves, resolving individual tidewater glaciers within Greenland-scale ice sheet models should become increasingly feasible. Alternatively, given that just a handful of large glaciers (Enderlin et al., 2014; Mankoff et al., 2020) and smaller glaciers at which perturbations originating at the terminus are able to propagate great distances inland (Felikson et al., 2020) are of particular significance to mass loss from the Greenland Ice Sheet, a possible solution may be to include a variable mesh size in order to capture ice dynamic processes at key tidewater outlets, whilst retaining a coarser mesh, and simpler retreat parameterisations (Slater et al., 2019b), elsewhere. In addition, a poor understanding of key processes such as calving and submarine melting represents a major limitation of current generation ice sheet models (Goelzer et al., 2020). Parameterisation of calving processes is limited by a lack of a calving law that has been extensively validated at tidewater glaciers (Benn et al., 2017a), and the implementation of a submarine melt-driven control on modelled glacier retreat is limited by uncertainties in rates of submarine melting, in addition to issues resulting from our limited understanding of the calving process (Slater et al., 2020). It is clear that future

work is needed both in terms of improving the models themselves, but also in terms of improving our understanding of key ice dynamic processes such that we can better understand and accurately represent them within ice sheet models.

7.4 Concluding Remarks

The research presented in this thesis has advanced our understanding of ice dynamic processes, and their response to external climate forcing, on multi-annual to multi-decadal scales at both land- and marine-terminating margins of the Greenland Ice Sheet, as well as within the interior accumulation zone. It has shown that the multi-decadal ice dynamics of the southwest land-terminating sector of the ice sheet are driven by changes in the subglacial hydrological system in response to variability in the long-term surface melt forcing, during periods of both atmospheric warming and cooling (Chapter 4). Within the accumulation zone, this thesis presents the first direct observations of multi-decadal ice velocity change on an ice-sheet-wide scale. A complex pattern of inland dynamic change is observed, showing both evidence of propagation of dynamic change from some tidewater glacier termini to significant (>100 km) distances inland, accelerating the drawdown of mass towards the margin, and a lack of flow acceleration inland of others. This lack of inland acceleration is hypothesised to result from the presence of steep bedrock topographic steps at the heads of subglacial troughs (Chapter 5). Finally, a range of remotely sensed data sources are brought together to illustrate that Helheim Glacier, the second largest glacier on the Greenland Ice Sheet by solid ice discharge (Mankoff et al., 2020), is currently poised for a dramatic retreat as a result of persistent mass loss since 2003 (Chapter 6). Moreover, these data also show that differences in fjord morphology and glacier geometry influence the timing of the response of neighbouring glaciers to a common climate forcing, although the fundamental process driving rapid glacier retreat (an extended period of anomalously high oceanic and atmospheric temperatures driving a long-term negative mass balance and associated near-terminus thinning) is observed to be common to all three glaciers studied.

This thesis thus presents several critical advances in our understanding of the processes controlling ice dynamical change across the Greenland Ice Sheet. Such advancements are crucial in order to better constrain the models aiming to project the likely dynamic response of the Greenland Ice Sheet to future climate warming.

Bibliography

Ahlstrøm, A. P., S. B. Andersen, M. L. Andersen, H. Machguth, F. M. Nick, I. Joughin, et al. (July 2013). "Seasonal velocities of eight major marine-terminating outlet glaciers of the Greenland ice sheet from continuous in situ GPS instruments". In: *Earth System Science Data* 5.2, pp. 277–287. DOI: 10.5194/essd-5-277-2013.

Ahn, Y. and I. M. Howat (Aug. 2011). "Efficient automated glacier surface velocity measurement from repeat images using multi-image/multichip and null exclusion feature tracking". In: *IEEE Transactions on Geoscience and Remote Sensing* 49.8, pp. 2838–2846. DOI: 10.1109/TGRS.2011.2114891.

Åkesson, H., K. H. Nisancioglu, and F. M. Nick (June 2018). "Impact of fjord geometry on grounding line stability". In: *Frontiers in Earth Science* 6, p. 71. DOI: 10.3389/feart.2018.00071.

Alley, R. B., D. D. Blankenship, C. R. Bentley, and S. T. Rooney (1986). "Deformation of till beneath ice stream B, West Antarctica". In: *Nature* 322.6074, pp. 57–59. DOI: 10.1038/322057a0.

Alley, R. B. (1993). "In search of ice-stream sticky spots". In: *Journal of Glaciology* 39.133, pp. 447–454. DOI: 10.3189/s0022143000016336.

Amundson, J. M., M. Fahnestock, M. Truffer, J. Brown, M. P. Lüthi, and R. J. Motyka (Mar. 2010). "Ice mélange dynamics and implications for terminus stability, Jakobshavn Isbrse, Greenland". In: *Journal of Geophysical Research: Earth Surface* 115.1. DOI: 10.1029/2009JF001405.

Amundson, J. M. (Feb. 2016). "A mass-flux perspective of the tidewater glacier cycle". In: *Journal of Glaciology* 62.231, pp. 82–93. DOI: 10.1017/jog.2016.14.

An, L., E. Rignot, S. Elieff, M. Morlighem, R. Millan, J. Mouginot, et al. (Apr. 2017). "Bed elevation of Jakobshavn Isbrae, West Greenland, from high-resolution airborne gravity and other data". In: *Geophysical Research Letters* 44.8, pp. 3728–3736. DOI: 10.1002/2017GL073245.

Andersen, M., L. Stenseng, H. Skourup, W. Colgan, S. Khan, S. Kristensen, et al. (Jan. 2015). "Basin-scale partitioning of Greenland ice sheet mass balance components (2007–2011)". In: *Earth and Planetary Science Letters* 409, pp. 89–95. DOI: 10.1016/J.EPSL.2014.10.015.

Andresen, C. S., F. Straneo, M. H. Ribergaard, A. A. Bjørk, T. J. Andersen, A. Kuijpers, et al. (Jan. 2012). *Rapid response of Helheim Glacier in Greenland to climate variability over the past century*. DOI: 10.1038/ngeo1349.

Andrews, L. C., G. A. Catania, M. J. Hoffman, J. D. Gulley, M. P. Lüthi, C. Ryser, et al. (Oct. 2014). "Direct observations of evolving subglacial drainage beneath the Greenland Ice Sheet". In: *Nature* 514.7520, pp. 80–83. DOI: 10.1038/nature13796.

Aschwanden, A., M. A. Fahnestock, M. Truffer, D. J. Brinkerhoff, R. Hock, C. Khroulev, et al. (June 2019). "Contribution of the Greenland Ice Sheet to sea level over the next millennium". In: *Science Advances* 5.6, eaav9396. DOI: 10.1126/sciadv.aav9396.

Bamber, J. L., R. M. Westaway, B. Marzeion, and B. Wouters (June 2018). *The land ice contribution to sea level during the satellite era*. DOI: 10.1088/1748-9326/aac2f0.

Banwell, A., I. Hewitt, I. Willis, and N. Arnold (Dec. 2016). "Moulin density controls drainage development beneath the Greenland ice sheet". In: *Journal of Geophysical Research: Earth Surface* 121.12, pp. 2248–2269. DOI: 10.1002/2015JF003801.

Bartholomaus, T. C., C. F. Larsen, S. O'Neel, and M. E. West (Dec. 2012). "Calving seismicity from iceberg-sea surface interactions". In: *Journal of Geophysical Research: Earth Surface* 117.F4, n/a–n/a. DOI: 10.1029/2012JF002513.

Bartholomaus, T. C., R. S. Anderson, and S. P. Anderson (Jan. 2008). "Response of glacier basal motion to transient water storage". In: *Nature Geoscience* 1.1, pp. 33–37. DOI: 10.1038/ngeo.2007.52.

Bartholomew, I., P. Nienow, A. Sole, D. Mair, T. Cowton, M. King, et al. (July 2011a). "Seasonal variations in Greenland Ice Sheet motion: Inland extent and behaviour at higher elevations". In: *Earth and Planetary Science Letters* 307.3-4, pp. 271–278. DOI: 10.1016/j.epsl.2011.04.014.

Bartholomew, I., P. Nienow, D. Mair, A. Hubbard, M. A. King, and A. Sole (June 2010). "Seasonal evolution of subglacial drainage and acceleration in a Greenland outlet glacier". In: *Nature Geoscience* 3.6, pp. 408–411. DOI: 10.1038/ngeo863.

Bartholomew, I., P. Nienow, A. Sole, D. Mair, T. Cowton, S. Palmer, et al. (Apr. 2011b). "Supraglacial forcing of subglacial drainage in the ablation zone of the Greenland ice sheet". In: *Geophysical Research Letters* 38.8, n/a–n/a. DOI: 10.1029/2011GL047063.

Bartholomew, I., P. Nienow, A. Sole, D. Mair, T. Cowton, and M. A. King (Sept. 2012). "Short-term variability in Greenland Ice Sheet motion forced by time-varying meltwater drainage: Implications for the relationship between subglacial drainage system behavior and ice velocity". In: *Journal of Geophysical Research: Earth Surface* 117.F3, n/a–n/a. DOI: 10.1029/2011JF002220.

Bassis, J. N. and S. Jacobs (Oct. 2013). "Diverse calving patterns linked to glacier geometry". In: *Nature Geoscience* 6.10, pp. 833–836. DOI: 10.1038/ngeo1887.

Baurley, N. R., B. A. Robson, and J. K. Hart (Sept. 2020). "Long-term impact of the proglacial lake Jökulsárlón on the flow velocity and stability of Breiðamerkurjökull glacier, Iceland". In: *Earth Surface Processes and Landforms* 45.11, pp. 2647–2663. DOI: 10.1002/esp.4920.

Benn, D. and D. J. A. Evans (2010). *Glaciers and Glaciation, 2nd edition*. Routledge. DOI: 10.4324/9780203785010.

Benn, D. I., N. R. Hulton, and R. H. Mottram (2007a). "'Calving laws', 'sliding laws' and the stability of tidewater glaciers". In: *Annals of Glaciology*. Vol. 46. Cambridge University Press, pp. 123–130. DOI: 10.3189/172756407782871161.

Benn, D. I., C. R. Warren, and R. H. Mottram (June 2007b). "Calving processes and the dynamics of calving glaciers". In: *Earth-Science Reviews* 82.3-4, pp. 143–179. DOI: 10.1016/j.earscirev.2007.02.002.

Benn, D. I., T. Cowton, J. Todd, and A. Luckman (Dec. 2017a). *Glacier Calving in Greenland*. DOI: 10.1007/s40641-017-0070-1.

Benn, D. I., J. Aström, T. Zwinger, J. Todd, F. M. Nick, S. Cook, et al. (Aug. 2017b). "Melt-under-cutting and buoyancy-driven calving from tidewater glaciers: New insights from discrete element and continuum model simulations". In: *Journal of Glaciology* 63.240, pp. 691–702. DOI: 10.1017/jog.2017.41.

Bersch, M., I. Yashayaev, and K. P. Koltermann (June 2007). "Recent changes of the thermohaline circulation in the subpolar North Atlantic". In: *Ocean Dynamics* 57.3, pp. 223–235. DOI: 10.1007/s10236-007-0104-7.

Bevan, S. L., A. J. Luckman, and T. Murray (2012). "Glacier dynamics over the last quarter of a century at Helheim, Kangerdlugssuaq and 14 other major Greenland outlet glaciers". In: *Cryosphere* 6.5, pp. 923–937. DOI: 10.5194/tc-6-923-2012.

Bevan, S. L., A. J. Luckman, D. I. Benn, T. Cowton, and J. Todd (2019). "Impact of warming shelf waters on ice mélange and terminus retreat at a large SE Greenland glacier". In: *The Cryosphere* 13, pp. 2303–2315. DOI: 10.5194/tc-13-2303-2019.

Bevan, S. L., A. Luckman, S. A. Khan, and T. Murray (Apr. 2015). "Seasonal dynamic thinning at Helheim Glacier". In: *Earth and Planetary Science Letters* 415, pp. 47–53. DOI: 10.1016/j.epsl.2015.01.031.

Bevis, M. (2019). "Accelerating changes in ice mass within Greenland, and the ice sheet's sensitivity to atmospheric forcing". In: *Proc. Natl Acad. Sci. USA* 116, pp. 1934–1939.

Bingham, R. G., P. W. Nienow, and M. J. Sharp (2003). "Intra-annual and intra-seasonal flow dynamics of a High Arctic polythermal valley glacier". In: *Annals of Glaciology* 37, pp. 181–188. DOI: 10.3189/172756403781815762.

Bingham, R. G., P. W. Nienow, M. J. Sharp, and S. Boon (2005). "Subglacial drainage processes at a High Arctic polythermal valley glacier". In: *Journal of Glaciology* 51.172, pp. 15–24. DOI: 10.3189/172756505781829520.

Bingham, R. G., P. W. Nienow, M. J. Sharp, and L. Copland (Oct. 2006). "Hydrology and dynamics of a polythermal (mostly cold) High Arctic glacier". In: *Earth Surface Processes and Landforms* 31.12, pp. 1463–1479. DOI: 10.1002/esp.1374.

Bingham, R. G., D. G. Vaughan, E. C. King, D. Davies, S. L. Cornford, A. M. Smith, et al. (Dec. 2017). "Diverse landscapes beneath Pine Island Glacier influence ice flow". In: *Nature Communications* 8.1, pp. 1–9. DOI: 10.1038/s41467-017-01597-y.

Bishop, M. P., A. B. G. Bush, R. Furfaro, A. R. Gillespie, D. K. Hall, U. K. Haritashya, et al. (2014). "Theoretical Foundations of Remote Sensing for Glacier Assessment and Mapping". In: *Global Land Ice Measurements from Space*. Springer Berlin Heidelberg, pp. 23–52. DOI: 10.1007/978-3-540-79818-7_2.

Bjørk, A. A., N. K. Larsen, J. Olsen, A. E. Goldsack, K. K. Kjeldsen, M. Morlighem, et al. (Aug. 2018). "Holocene history of the Helheim Glacier, southeast Greenland". In: *Quaternary Science Reviews* 193, pp. 145–158. DOI: 10.1016/j.quascirev.2018.06.018.

Bjørk, A. A., K. H. Kjær, N. J. Korsgaard, S. A. Khan, K. K. Kjeldsen, C. S. Andresen, et al. (June 2012). "An aerial view of 80 years of climate-related glacier fluctuations in southeast Greenland". In: *Nature Geoscience* 5.6, pp. 427–432. DOI: 10.1038/ngeo1481.

Blankenship, D. D., C. R. Bentley, S. T. Rooney, and R. B. Alley (1986). "Seismic measurements reveal a saturated porous layer beneath an active Antarctic ice stream". In: *Nature* 322.6074, pp. 54–57. DOI: 10.1038/322054a0.

Bondzio, J. H., H. Seroussi, M. Morlighem, T. Kleiner, M. Rückamp, A. Humbert, et al. (Mar. 2016). "Modelling calving front dynamics using a level-set method: Application to Jakobshavn Isbræ, West Greenland". In: *Cryosphere* 10.2, pp. 497–510. DOI: 10.5194/tc-10-497-2016.

Boon, S., M. Sharp, and P. Nienow (Apr. 2003). "Impact of an extreme melt event on the runoff and hydrology of a high Arctic glacier". In: *Hydrological Processes* 17.6, pp. 1051–1072. DOI: 10.1002/hyp.1194.

Bougamont, M., P. Christoffersen, A. L. Hubbard, A. A. Fitzpatrick, S. H. Doyle, and S. P. Carter (Dec. 2014). "Sensitive response of the Greenland Ice Sheet to surface melt drainage over a soft bed". In: *Nature Communications* 5.1, p. 5052. DOI: 10.1038/ncomms6052.

Boulton, G. S. and R. C. A. Hindmarsh (Aug. 1987). "Sediment deformation beneath glaciers: Rheology and geological consequences". In: *Journal of Geophysical Research* 92.B9, p. 9059. DOI: 10.1029/JB092iB09p09059.

Boulton, G. (1996). "Theory of glacial erosion, transport and deposition as a consequence of subglacial sediment deformation". In: *Journal of Glaciology* 42.140, pp. 43–62. DOI: 10.3189/s0022143000030525.

Box, J. E., L. Yang, D. H. Bromwich, and L. S. Bai (July 2009). "Greenland ice sheet surface air temperature variability: 1840-2007". In: *Journal of Climate* 22.14, pp. 4029–4049. DOI: 10.1175/2009JCLI2816.1.

Box, J. E. and D. T. Decker (Dec. 2011). "Greenland marine-terminating glacier area changes: 2000-2010". In: *Annals of Glaciology* 52.59, pp. 91–98. DOI: 10.3189/172756411799096312.

Box, J. E. and W. Colgan (Sept. 2013). "Greenland ice sheet mass balance reconstruction. Part III: Marine ice loss and total mass balance (1840-2010)". In: *Journal of Climate* 26.18, pp. 6990–7002. DOI: 10.1175/JCLI-D-12-00546.1.

Brangers, I., H. Lievens, C. Miège, M. Demuzere, L. Brucker, and G. J. M. De Lannoy (Feb. 2020). "Sentinel-1 Detects Firn Aquifers in the Greenland Ice Sheet". In: *Geophysical Research Letters* 47.3. DOI: 10.1029/2019GL085192.

Brough, S., J. R. Carr, N. Ross, and J. M. Lea (May 2019). "Exceptional Retreat of Kangerlussuaq Glacier, East Greenland, Between 2016 and 2018". In: *Frontiers in Earth Science* 7, p. 123. DOI: 10.3389/feart.2019.00123.

Brown, N. E., B. Hallet, and D. B. Booth (Aug. 1987). "Rapid soft bed sliding of the Puget Glacial Lobe". In: *Journal of Geophysical Research* 92.B9, p. 8985. DOI: 10.1029/JB092iB09p08985.

Brunt, K. M., R. L. Hawley, E. R. Lutz, M. Studinger, J. G. Sonntag, M. A. Hofton, et al. (Mar. 2017). "Assessment of NASA airborne laser altimetry data using ground-based GPS data near Summit Station, Greenland". In: *Cryosphere* 11.2, pp. 681–692. DOI: 10.5194/tc-11-681-2017.

Bunce, C., J. R. Carr, P. W. Nienow, N. Ross, and R. Killick (2018). "Ice front change of marine-terminating outlet glaciers in northwest and southeast Greenland during the 21st century". In: *Journal of Glaciology* 64.246, pp. 523–535. DOI: 10.1017/jog.2018.44.

Bunce, C., P. Nienow, A. Sole, T. Cowton, and B. Davison (2021). "Influence of glacier runoff and near-terminus subglacial hydrology on frontal ablation at a large Greenlandic tidewater glacier". In: DOI: 10.1017/jog.2020.109.

Burgess, E. W., C. F. Larsen, and R. R. Forster (Dec. 2013). "Summer melt regulates winter glacier flow speeds throughout Alaska". In: *Geophysical Research Letters* 40.23, pp. 6160–6164. DOI: 10.1002/2013GL058228.

Cappelen, J., B. Vinther, C. Kern-Hansen, E. V. Laursen, and P. V. Jørgensen (2017). *Greenland – DMI Historical Climate Data Collection 1784-2016*. Tech. rep.

Cappelen, J., E. V. Laursen, C. Kern-Hansen, L. Boas, P. Wang, B. Jørgensen, et al. (2020). *Weather observations from Greenland 1958-2019. Danish Meteorological Institute Tech. Rep. 20-08*. Tech. rep. DMI.

Carr, J. R., A. Vieli, and C. Stokes (Sept. 2013). "Influence of sea ice decline, atmospheric warming, and glacier width on marine-terminating outlet glacier behavior

in northwest Greenland at seasonal to interannual timescales". In: *Journal of Geophysical Research: Earth Surface* 118.3, pp. 1210–1226. DOI: 10.1002/jgrf.20088.

Carrivick, J. L. and D. J. Quincey (May 2014). "Progressive increase in number and volume of ice-marginal lakes on the western margin of the Greenland Ice Sheet". In: *Global and Planetary Change* 116, pp. 156–163. DOI: 10.1016/j.gloplacha.2014.02.009.

Carroll, D., D. A. Sutherland, B. Hudson, T. Moon, G. A. Catania, E. L. Shroyer, et al. (Sept. 2016). "The impact of glacier geometry on meltwater plume structure and submarine melt in Greenland fjords". In: *Geophysical Research Letters* 43.18, pp. 9739–9748. DOI: 10.1002/2016GL070170.

Carroll, D., D. A. Sutherland, B. Curry, J. D. Nash, E. L. Shroyer, G. A. Catania, et al. (Sept. 2018). "Subannual and Seasonal Variability of Atlantic-Origin Waters in Two Adjacent West Greenland Fjords". In: *Journal of Geophysical Research: Oceans* 123.9, pp. 6670–6687. DOI: 10.1029/2018JC014278.

Carroll, D., D. A. Sutherland, E. L. Shroyer, J. D. Nash, G. A. Catania, and L. A. Stearns (Aug. 2015). "Modeling turbulent subglacial meltwater plumes: Implications for fjord-scale buoyancy-driven circulation". In: *Journal of Physical Oceanography* 45.8, pp. 2169–2185. DOI: 10.1175/JPO-D-15-0033.1.

Cassotto, R., M. Fahnestock, J. M. Amundson, M. Truffer, and I. Joughin (Feb. 2015). "Seasonal and interannual variations in ice melange and its impact on terminus stability, Jakobshavn Isbræ, Greenland". In: *Journal of Glaciology* 61.225, pp. 76–88. DOI: 10.3189/2015JoG13J235.

Catania, G. A. and T. A. Neumann (Jan. 2010). "Persistent englacial drainage features in the Greenland Ice Sheet". In: *Geophysical Research Letters* 37.2, n/a–n/a. DOI: 10.1029/2009GL041108.

Catania, G. A., L. A. Stearns, D. A. Sutherland, M. J. Fried, T. C. Bartholomaus, M. Morlighem, et al. (Aug. 2018). "Geometric Controls on Tidewater Glacier Retreat in Central Western Greenland". In: *Journal of Geophysical Research: Earth Surface* 123.8, pp. 2024–2038. DOI: 10.1029/2017JF004499.

Catania, G. A., L. A. Stearns, T. A. Moon, E. M. Enderlin, and R. H. Jackson (Feb. 2020). "Future Evolution of Greenland's Marine-Terminating Outlet Glaciers". In: *Journal of Geophysical Research: Earth Surface* 125.2. DOI: 10.1029/2018JF004873@10.1002/(ISSN)1944-9208.GRANDCHAL1.

Chandler, B. M. and D. J. Evans (Jan. 2021). "Glacial Processes and Sediments". In: *Encyclopedia of Geology*. Elsevier, pp. 830–856. DOI: 10.1016/b978-0-12-409548-9.11902-5.

Chandler, D. M., J. L. Wadham, G. P. Lis, T. Cowton, A. Sole, I. Bartholomew, et al. (Mar. 2013). "Evolution of the subglacial drainage system beneath the Greenland Ice Sheet revealed by tracers". In: *Nature Geoscience* 6.3, pp. 195–198. DOI: 10.1038/ngeo1737.

Chauché, N., A. Hubbard, J. C. Gascard, J. E. Box, R. Bates, M. Koppes, et al. (Aug. 2014). "Ice-ocean interaction and calving front morphology at two west Greenland tidewater outlet glaciers". In: *Cryosphere* 8.4, pp. 1457–1468. DOI: 10.5194/tc-8-1457-2014.

Chen, J., X. Zhu, J. E. Vogelmann, F. Gao, and S. Jin (Apr. 2011). "A simple and effective method for filling gaps in Landsat ETM+ SLC-off images". In: *Remote Sensing of Environment* 115.4, pp. 1053–1064. DOI: 10.1016/j.rse.2010.12.010.

Cheng, D., W. Hayes, E. Larour, Y. Mohajerani, M. Wood, I. Velicogna, et al. (Apr. 2021). "Calving Front Machine (CALFIN): glacial termini dataset and automated

deep learning extraction method for Greenland, 1972–2019". In: *The Cryosphere* 15.3, pp. 1663–1675. DOI: 10.5194/tc-15-1663-2021.

Choi, Y., M. Morlighem, E. Rignot, and M. Wood (Dec. 2021). "Ice dynamics will remain a primary driver of Greenland ice sheet mass loss over the next century". In: *Communications Earth & Environment* 2.1, p. 26. DOI: 10.1038/s43247-021-00092-z.

Christoffersen, P., R. I. Mugford, K. J. Heywood, I. Joughin, J. A. Dowdeswell, J. P. M. Syvitski, et al. (2011). "Warming of waters in an East Greenland fjord prior to glacier retreat: mechanisms and connection to large-scale atmospheric conditions". In: *The Cryosphere* 5, pp. 701–714. DOI: 10.5194/tc-5-701-2011.

Christoffersen, P., M. O'Leary, J. H. Van Angelen, and M. Van Den Broeke (Nov. 2012). "Partitioning effects from ocean and atmosphere on the calving stability of kangerdlugssuaq glacier, east greenland". In: *Annals of Glaciology* 53.60, pp. 249–256. DOI: 10.3189/2012AoG60A087.

Chu, V. W. (Feb. 2014). "Greenland ice sheet hydrology". In: *Progress in Physical Geography* 38.1, pp. 19–54. DOI: 10.1177/0309133313507075.

Chu, W., D. M. Schroeder, H. Seroussi, T. T. Creyts, S. J. Palmer, and R. E. Bell (Dec. 2016). "Extensive winter subglacial water storage beneath the Greenland Ice Sheet". In: *Geophysical Research Letters* 43.24, pp. 484–12. DOI: 10.1002/2016GL071538.

Clarke, G. K. (May 2005). "SUBGLACIAL PROCESSES". In: *Annual Review of Earth and Planetary Sciences* 33.1, pp. 247–276. DOI: 10.1146/annurev.earth.33.092203.122621.

Colgan, W., H. Rajaram, R. S. Anderson, K. Steffen, H. J. Zwally, T. Phillips, et al. (Sept. 2012). "The annual glaciohydrology cycle in the ablation zone of the Greenland ice sheet: Part 2. Observed and modeled ice flow". In: *Journal of Glaciology* 58.207, pp. 51–64. DOI: 10.3189/2012JoG11J081.

Cook, S., I. C. Rutt, T. Murray, A. Luckman, T. Zwinger, N. Selmes, et al. (2014). "The Cryosphere Modelling environmental influences on calving at Helheim Glacier in eastern Greenland". In: *The Cryosphere* 8, pp. 827–841. DOI: 10.5194/tc-8-827-2014.

Cooper, M. and L. Smith (Oct. 2019). "Satellite Remote Sensing of the Greenland Ice Sheet Ablation Zone: A Review". In: *Remote Sensing* 11.20, p. 2405. DOI: 10.3390/rs11202405.

Copland, L., M. J. Sharp, and P. W. Nienow (2003). "Links between short-term velocity variations and the subglacial hydrology of a predominantly cold polythermal glacier". In: *Journal of Glaciology* 49.166, pp. 337–348. DOI: 10.3189/172756503781830656.

Cowton, T. R., A. J. Sole, P. W. Nienow, D. A. Slater, and P. Christoffersen (July 2018). "Linear response of east Greenland's tidewater glaciers to ocean/atmosphere warming". In: *Proceedings of the National Academy of Sciences of the United States of America* 115.31, pp. 7907–7912. DOI: 10.1073/pnas.1801769115.

Cowton, T., P. Nienow, A. Sole, J. Wadham, G. Lis, I. Bartholomew, et al. (Mar. 2013). "Evolution of drainage system morphology at a land-terminating Greenlandic outlet glacier". In: *Journal of Geophysical Research: Earth Surface* 118.1, pp. 29–41. DOI: 10.1029/2012JF002540.

Cowton, T., D. Slater, A. Sole, D. Goldberg, and P. Nienow (Feb. 2015). "Modeling the impact of glacial runoff on fjord circulation and submarine melt rate using a new subgrid-scale parameterization for glacial plumes". In: *Journal of Geophysical Research: Oceans* 120.2, pp. 796–812. DOI: 10.1002/2014JC010324.

Cowton, T., A. Sole, P. Nienow, D. Slater, D. Wilton, and E. Hanna (Dec. 2016). "Controls on the transport of oceanic heat to Kangerdlugssuaq Glacier, East Greenland". In: *Journal of Glaciology* 62.236, pp. 1167–1180. DOI: 10.1017/jog.2016.117.

Csatho, B. M., A. F. Schenka, C. J. Van Der Veen, G. Babonis, K. Duncan, S. Rezvanbehbahani, et al. (Dec. 2014). "Laser altimetry reveals complex pattern of Greenland Ice Sheet dynamics". In: *Proceedings of the National Academy of Sciences of the United States of America* 111.52, pp. 18478–18483. DOI: 10.1073/pnas.1411680112.

Cuffey, K. and W. Paterson (2010). *The Physics of Glaciers*. 4th. Oxford: Butterworth-Heinemann.

Cullather, R. I., S. M. J. Nowicki, R. I. Cullather, and S. M. J. Nowicki (Mar. 2018). "Greenland Ice Sheet Surface Melt and Its Relation to Daily Atmospheric Conditions". In: *Journal of Climate* 31.5, pp. 1897–1919. DOI: 10.1175/JCLI-D-17-0447.1.

Das, S. B., I. Joughin, M. D. Behn, I. M. Howat, M. A. King, D. Lizarralde, et al. (May 2008). "Fracture propagation to the base of the Greenland Ice Sheet during supraglacial lake drainage." In: *Science (New York, N.Y.)* 320.5877, pp. 778–81. DOI: 10.1126/science.1153360.

Davison, B. J., T. R. Cowton, F. R. Cottier, and A. J. Sole (Dec. 2020a). "Iceberg melting substantially modifies oceanic heat flux towards a major Greenlandic tidewater glacier". In: *Nature Communications* 11.1, pp. 1–13. DOI: 10.1038/s41467-020-19805-7.

Davison, B. J., A. J. Sole, T. R. Cowton, J. M. Lea, D. A. Slater, D. Fahrner, et al. (Sept. 2020b). "Subglacial Drainage Evolution Modulates Seasonal Ice Flow Variability of Three Tidewater Glaciers in Southwest Greenland". In: *Journal of Geophysical Research: Earth Surface* 125.9, e2019JF005492. DOI: 10.1029/2019JF005492.

Davison, B. J., A. J. Sole, S. J. Livingstone, T. R. Cowton, and P. W. Nienow (Feb. 2019). "The Influence of Hydrology on the Dynamics of Land-Terminating Sectors of the Greenland Ice Sheet". In: *Frontiers in Earth Science* 7, p. 10. DOI: 10.3389/feart.2019.00010.

De Fleurian, B., M. A. Werder, S. Beyer, D. J. Brinkerhoff, I. Delaney, C. F. Dow, et al. (2018). "SHMIP The subglacial hydrology model intercomparison Project". In: *Journal of Glaciology* 64.248, pp. 897–916. DOI: 10.1017/jog.2018.78.

De Ridder, K. and H. Gallée (Nov. 1998). "Land surface-induced regional climate change in southern Israel". In: *Journal of Applied Meteorology* 37.11, pp. 1470–1485. DOI: 10.1175/1520-0450(1998)037<1470:LSIRCC>2.0.CO;2.

Debella-Gilo, M. and A. Kääb (Jan. 2011). "Sub-pixel precision image matching for measuring surface displacements on mass movements using normalized cross-correlation". In: *Remote Sensing of Environment* 115.1, pp. 130–142. DOI: 10.1016/j.rse.2010.08.012.

Debella-Gilo, M., A. Kääb, M. Debella-Gilo, and A. Kääb (Jan. 2012). "Measurement of Surface Displacement and Deformation of Mass Movements Using Least Squares Matching of Repeat High Resolution Satellite and Aerial Images". In: *Remote Sensing* 4.1, pp. 43–67. DOI: 10.3390/rs4010043.

de Fleurian, B., M. Morlighem, H. Seroussi, E. Rignot, M. R. van den Broeke, P. Kuipers Munneke, et al. (Oct. 2016). "A modeling study of the effect of runoff variability on the effective pressure beneath Russell Glacier, West Greenland". In: *Journal of Geophysical Research: Earth Surface* 121.10, pp. 1834–1848. DOI: 10.1002/2016JF003842.

Dehecq, A., N. Gourmelen, and E. Trouve (June 2015). "Deriving large-scale glacier velocities from a complete satellite archive: Application to the Pamir–Karakoram–Himalaya". In: *Remote Sensing of Environment* 162, pp. 55–66. DOI: 10.1016/j.rse.2015.01.031.

Dehecq, A., N. Gourmelen, A. S. Gardner, F. Brun, D. Goldberg, P. W. Nienow, et al. (Jan. 2019). "Twenty-first century glacier slowdown driven by mass loss in High Mountain Asia". In: *Nature Geoscience* 12.1, pp. 22–27. DOI: 10.1038/s41561-018-0271-9.

Delhasse, A., X. Fettweis, C. Kittel, C. Amory, and C. Agosta (Oct. 2018). "Brief communication: Impact of the recent atmospheric circulation change in summer on the future surface mass balance of the Greenland Ice Sheet". In: *Cryosphere* 12.11, pp. 3409–3418. DOI: 10.5194/tc-12-3409-2018.

Delhasse, A., C. Kittel, C. Amory, S. Hofer, D. Van As, R. S. Fausto, et al. (Mar. 2020). "Brief communication: Evaluation of the near-surface climate in ERA5 over the Greenland Ice Sheet". In: *Cryosphere* 14.3, pp. 957–965. DOI: 10.5194/tc-14-957-2020.

Dell, R., R. Carr, E. Phillips, and A. J. Russell (Apr. 2019). "Response of glacier flow and structure to proglacial lake development and climate at Fjallsjökull, south-east Iceland". In: *Journal of Glaciology* 65.250, pp. 321–336. DOI: 10.1017/jog.2019.18.

Dow, C., B. Kulessa, I. Rutt, S. Doyle, and A. Hubbard (July 2014). "Upper bounds on subglacial channel development for interior regions of the Greenland ice sheet". In: *Journal of Glaciology* 60.224, pp. 1044–1052. DOI: 10.3189/2014JoG14J093.

Doyle, S. H., A. L. Hubbard, C. F. Dow, G. A. Jones, A. Fitzpatrick, A. Gusmeroli, et al. (Jan. 2013). "Ice tectonic deformation during the rapid in situ drainage of a supraglacial lake on the Greenland Ice Sheet". In: *The Cryosphere* 7.1, pp. 129–140. DOI: 10.5194/tc-7-129-2013.

Doyle, S. H., A. Hubbard, A. A. W. Fitzpatrick, D. van As, A. B. Mikkelsen, R. Pettersson, et al. (Feb. 2014). "Persistent flow acceleration within the interior of the Greenland ice sheet". In: *Geophysical Research Letters* 41.3, pp. 899–905. DOI: 10.1002/2013GL058933.

Doyle, S. H., A. Hubbard, R. S. Van De Wal, J. E. Box, D. Van As, K. Scharrer, et al. (Aug. 2015). "Amplified melt and flow of the Greenland ice sheet driven by late-summer cyclonic rainfall". In: *Nature Geoscience* 8.8, pp. 647–653. DOI: 10.1038/ngeo2482.

Drusch, M., U. Del Bello, S. Carlier, O. Colin, V. Fernandez, F. Gascon, et al. (May 2012). "Sentinel-2: ESA's Optical High-Resolution Mission for GMES Operational Services". In: *Remote Sensing of Environment* 120, pp. 25–36. DOI: 10.1016/j.rse.2011.11.026.

Echelmeyer, K., T. S. Clarke, and W. Harrison (1991). "Surficial glaciology of Jakobshavns Isbræ, West Greenland: Part I. Surface morphology". In: *Journal of Glaciology* 37.127, pp. 368–382. DOI: 10.3189/s0022143000005803.

Echelmeyer, K. and W. D. Harrison (1990). "Jakobshavns Isbræ, West Greenland: Seasonal Variations in Velocity - or Lack Thereof". In: *Journal of Glaciology* 36.122, pp. 82–88. DOI: 10.3189/s0022143000005591.

Edwards, T. L., S. Nowicki, B. Marzeion, R. Hock, H. Goelzer, H. Seroussi, et al. (May 2021). "Projected land ice contributions to twenty-first-century sea level rise". In: *Nature* 593.7857, pp. 74–82. DOI: 10.1038/s41586-021-03302-y.

Enderlin, E. M., I. M. Howat, and A. Vieli (2013). "High sensitivity of tidewater outlet glacier dynamics to shape". In: *The Cryosphere* 7, pp. 1007–1015. DOI: 10.5194/tc-7-1007-2013.

Enderlin, E. M. and I. M. Howat (Mar. 2013). "Submarine melt rate estimates for floating termini of Greenland outlet glaciers (2000-2010)". In: *Journal of Glaciology* 59.213, pp. 67–75. DOI: 10.3189/2013JoG12J049.

Enderlin, E. M., I. M. Howat, S. Jeong, M.-J. Noh, J. H. van Angelen, and M. R. van den Broeke (Feb. 2014). "An improved mass budget for the Greenland ice sheet". In: *Geophysical Research Letters* 41.3, pp. 866–872. DOI: 10.1002/2013GL059010.

Enderlin, E. M., S. O'Neel, T. C. Bartholomaus, and I. Joughin (July 2018). "Evolving Environmental and Geometric Controls on Columbia Glacier's Continued Retreat". In: *Journal of Geophysical Research: Earth Surface* 123.7, pp. 1528–1545. DOI: 10.1029/2017JF004541.

F Straneo, P. H. (2013). "North Atlantic warming and the retreat of Greenland's outlet glaciers". In: *Nature* 504, pp. 36–43.

Fahnestock, M., T. Scambos, T. Moon, A. Gardner, T. Haran, and M. Klinger (Nov. 2016). "Rapid large-area mapping of ice flow using Landsat 8". In: *Remote Sensing of Environment* 185, pp. 84–94. DOI: 10.1016/j.rse.2015.11.023.

Fahrner, D., J. M. Lea, S. Brough, D. W. F. Mair, and J. Abermann (Mar. 2021). "Linear response of the Greenland ice sheet's tidewater glacier terminus positions to climate". In: *Journal of Glaciology*, pp. 1–11. DOI: 10.1017/jog.2021.13.

Falkner, K. K., H. Melling, A. M. Münchow, J. E. Box, T. Wohlleben, H. L. Johnson, et al. (Apr. 2011). "Context for the Recent Massive Petermann Glacier Calving Event". In: *Eos, Transactions American Geophysical Union* 92.14, pp. 117–118. DOI: 10.1029/2011EO140001.

Fecher, T., R. Pail, T. Gruber, W. D. Schuh, J. Kusche, J. M. Brockmann, et al. (May 2017). *GOCO05c: A New Combined Gravity Field Model Based on Full Normal Equations and Regionally Varying Weighting*. DOI: 10.1007/s10712-016-9406-y.

Felikson, D., T. C. Bartholomaus, G. A. Catania, N. J. Korsgaard, K. H. Kjær, M. Morlighem, et al. (May 2017). "Inland thinning on the Greenland ice sheet controlled by outlet glacier geometry". In: *Nature Geoscience* 10.5, pp. 366–369. DOI: 10.1038/ngeo2934.

Felikson, D., G. Catania, T. C. Bartholomaus, M. Morlighem, and B. P. Y. Noël (Dec. 2020). "Steep glacier bed knickpoints mitigate inland thinning in Greenland". In: *Geophysical Research Letters*. DOI: 10.1029/2020gl090112.

Fettweis, X., M. Tedesco, M. Van Den Broeke, and J. Ettema (2011). "Melting trends over the Greenland ice sheet (1958-2009) from spaceborne microwave data and regional climate models". In: *The Cryosphere* 5, pp. 359–375. DOI: 10.5194/tc-5-359-2011.

Fettweis, X. (2007). "Reconstruction of the 1979-2006 Greenland ice sheet surface mass balance using the regional climate model MAR". In: *Cryosphere* 1.1, pp. 21–40. DOI: 10.5194/tc-1-21-2007.

Fettweis, X., B. Franco, M. Tedesco, J. H. van Angelen, J. T. M. Lenaerts, M. R. van den Broeke, et al. (Mar. 2013). "Estimating the Greenland ice sheet surface mass balance contribution to future sea level rise using the regional atmospheric climate model MAR". In: *The Cryosphere* 7.2, pp. 469–489. DOI: 10.5194/tc-7-469-2013.

Fettweis, X., J. E. Box, C. Agosta, C. Amory, C. Kittel, C. Lang, et al. (Apr. 2017). "Reconstructions of the 1900–2015 Greenland ice sheet surface mass balance using

the regional climate MAR model". In: *The Cryosphere* 11.2, pp. 1015–1033. DOI: 10.5194/tc-11-1015-2017.

Fischer, M. P. and R. D. Powell (1998). "A simple model for the influence of push-morainal banks on the calving and stability of glacial tidewater termini". In: *Journal of Glaciology* 44.146, pp. 31–41. DOI: 10.3189/s002214300000232x.

Fitch, A. J., A. J. Fitch, A. Kadyrov, W. J. Christmas, and J. Kittler (2002). "Orientation correlation". In: *BRITISH MACHINE VISION CONFERENCE* 1, pp. 133–142. URL: http://citeseerx.ist.psu.edu/viewdoc/summary?doi=10.1.1.64.5662.

Fitzpatrick, A. A., A. Hubbard, I. Joughin, D. J. Quincey, D. V. As, A. P. Mikkelsen, et al. (July 2013). "Ice flow dynamics and surface meltwater flux at a land-terminating sector of the Greenland ice sheet". In: *Journal of Glaciology* 59.216, pp. 687–696. DOI: 10.3189/2013JoG12J143.

Flowers, G. E. (Apr. 2015). *Modelling water flow under glaciers and ice sheets*. DOI: 10.1098/rspa.2014.0907.

Foresta, L., N. Gourmelen, F. Pálsson, P. Nienow, H. Björnsson, and A. Shepherd (Dec. 2016). "Surface elevation change and mass balance of Icelandic ice caps derived from swath mode CryoSat-2 altimetry". In: *Geophysical Research Letters* 43.23, pp. 138–12. DOI: 10.1002/2016GL071485.

Foresta, L., N. Gourmelen, F. Weissgerber, P. Nienow, J. J. Williams, A. Shepherd, et al. (June 2018). "Heterogeneous and rapid ice loss over the Patagonian Ice Fields revealed by CryoSat-2 swath radar altimetry". In: *Remote Sensing of Environment* 211, pp. 441–455. DOI: 10.1016/j.rse.2018.03.041.

Forster, R. R., J. E. Box, M. R. Van Den Broeke, C. Miège, E. W. Burgess, J. H. Van Angelen, et al. (Feb. 2014). "Extensive liquid meltwater storage in firn within the Greenland ice sheet". In: *Nature Geoscience* 7.2, pp. 95–98. DOI: 10.1038/ngeo2043.

Fountain, A. G. and J. S. Walder (Aug. 1998). "Water flow through temperate glaciers". In: *Reviews of Geophysics* 36.3, pp. 299–328. DOI: 10.1029/97RG03579.

Fowler, A. C. (Aug. 1987). "A theory of glacier surges". In: *Journal of Geophysical Research* 92.B9, p. 9111. DOI: 10.1029/JB092iB09p09111.

Frank, T., H. Åkesson, B. de Fleurian, M. Morlighem, and K. Nisancioglu (2021). "Geometric Controls of Tidewater Glacier Dynamics". In: *The Cryosphere Discussions*, pp. 1–32. DOI: 10.5194/tc-2021-81.

Fraser, N. J. and M. E. Inall (Apr. 2018). "Influence of Barrier Wind Forcing on Heat Delivery Toward the Greenland Ice Sheet". In: *Journal of Geophysical Research: Oceans* 123.4, pp. 2513–2538. DOI: 10.1002/2017JC013464.

Freeman, A., X. Pi, and E. Heggy (Oct. 2017). "Radar Sounding Through the Earth's Ionosphere at 45 MHz". In: *IEEE Transactions on Geoscience and Remote Sensing* 55.10, pp. 5833–5842. DOI: 10.1109/TGRS.2017.2715838.

Fried, M. J., G. A. Catania, T. C. Bartholomaus, D. Duncan, M. Davis, L. A. Stearns, et al. (Nov. 2015). "Distributed subglacial discharge drives significant submarine melt at a Greenland tidewater glacier". In: *Geophysical Research Letters* 42.21, pp. 9328–9336. DOI: 10.1002/2015GL065806.

Fried, M. J., G. A. Catania, L. A. Stearns, D. A. Sutherland, T. C. Bartholomaus, E. Shroyer, et al. (July 2018). "Reconciling Drivers of Seasonal Terminus Advance and Retreat at 13 Central West Greenland Tidewater Glaciers". In: *Journal of Geophysical Research: Earth Surface* 123.7, pp. 1590–1607. DOI: 10.1029/2018JF004628.

Fürst, J. J., H. Goelzer, and P. Huybrechts (May 2015). "Ice-dynamic projections of the Greenland ice sheet in response to atmospheric and oceanic warming". In: *Cryosphere* 9.3, pp. 1039–1062. DOI: 10.5194/tc-9-1039-2015.

Gagliardini, O. and M. A. Werder (Oct. 2018). "Influence of increasing surface melt over decadal timescales on land-terminating Greenland-type outlet glaciers". In: *Journal of Glaciology* 64.247, pp. 700–710. DOI: 10.1017/jog.2018.59.

Gallee, H. and G. Schayes (Apr. 1994). "Development of a three-dimensional meso-γ primitive equation model: katabatic winds simulation in the area of Terra Nova Bay, Antarctica". In: *Monthly Weather Review* 122.4, pp. 671–685. DOI: 10.1175/1520-0493(1994)122<0671:DOATDM>2.0.CO;2.

Gardner, A. S., G. Moholdt, T. Scambos, M. Fahnstock, S. Ligtenberg, M. Van Den Broeke, et al. (Feb. 2018). "Increased West Antarctic and unchanged East Antarctic ice discharge over the last 7 years". In: *Cryosphere* 12.2, pp. 521–547. DOI: 10.5194/tc-12-521-2018.

Gardner, A. S., M. Fahnestock, and T. A. Scambos (2019). *[06/06/2019]: ITS_LIVE Regional Glacier and Ice Sheet Surface Velocities. Data archived at National Snow and Ice Data Center;* Boulder, Colorado USA. DOI: 10.5067/6II6VW8LLWJ7.

Gladish, C. V., D. M. Holland, A. Rosing-Asvid, J. W. Behrens, and J. Boje (Jan. 2015). "Oceanic boundary conditions for Jakobshavn Glacier. Part I: Variability and renewal of Ilulissat Icefjord waters, 2001-14". In: *Journal of Physical Oceanography* 45.1, pp. 3–32. DOI: 10.1175/JPO-D-14-0044.1.

Glen, J. (1955). "The creep of polycrystalline ice". In: *Proceedings of the Royal Society of London. Series A, Mathematical and Physical Sciences* 228.1175, pp. 519–538. URL: https://royalsocietypublishing.org/.

Goelzer, H., S. Nowicki, T. Edwards, M. Beckley, A. Abe-Ouchi, A. Aschwanden, et al. (Apr. 2018). "Design and results of the ice sheet model initialisation initMIP-Greenland: An ISMIP6 intercomparison". In: *Cryosphere* 12.4, pp. 1433–1460. DOI: 10.5194/tc-12-1433-2018.

Goelzer, H., S. Nowicki, A. Payne, E. Larour, H. Seroussi, W. H. Lipscomb, et al. (2020). "The future sea-level contribution of the Greenland ice sheet: a multi-model ensemble study of ISMIP6". In: *The Cryosphere* 14, pp. 3071–3096. DOI: 10.5194/tc-14-3071-2020.

Good, S. A., M. J. Martin, and N. A. Rayner (Dec. 2013). "EN4: Quality controlled ocean temperature and salinity profiles and monthly objective analyses with uncertainty estimates". In: *Journal of Geophysical Research: Oceans* 118.12, pp. 6704–6716. DOI: 10.1002/2013JC009067.

Gordon, S., M. J. Sharp, B. Hubbard, C. C. Smart, B. Ketterling, and I. Willis (1998). "Seasonal reorganization of subglacial drainage inferred from measurements in boreholes". In: *Hydrological Processes* 12.1, pp. 105–133.

Gourmelen, N., M. J. Escorihuela, A. Shepherd, L. Foresta, A. Muir, A. Garcia-Mondéjar, et al. (Sept. 2018). "CryoSat-2 swath interferometric altimetry for mapping ice elevation and elevation change". In: *Advances in Space Research* 62.6, pp. 1226–1242. DOI: 10.1016/j.asr.2017.11.014.

Gray, L., D. Burgess, L. Copland, M. N. Demuth, T. Dunse, K. Langley, et al. (Sept. 2015). "CryoSat-2 delivers monthly and inter-annual surface elevation change for Arctic ice caps". In: *Cryosphere* 9.5, pp. 1895–1913. DOI: 10.5194/tc-9-1895-2015.

Gray, L., D. Burgess, L. Copland, K. Langley, P. Gogineni, J. Paden, et al. (June 2019). "Measuring Height Change Around the Periphery of the Greenland Ice Sheet With Radar Altimetry". In: *Frontiers in Earth Science* 7, p. 146. DOI: 10.3389/feart.2019.00146.

Gregory, J. M., S. E. George, and R. S. Smith (Dec. 2020). "Large and irreversible future decline of the Greenland ice sheet". In: *Cryosphere* 14.12, pp. 4299–4322. DOI: 10.5194/tc-14-4299-2020.

Gudmundsson, G. H., J. Krug, G. Durand, L. Favier, and O. Gagliardini (2012). "The stability of grounding lines on retrograde slopes". In: *Cryosphere* 6.6, pp. 1497–1505. DOI: 10.5194/tc-6-1497-2012.

Hall, D. K., J. C. Comiso, N. E. DiGirolamo, C. A. Shuman, J. E. Box, and L. S. Koenig (May 2013). "Variability in the surface temperature and melt extent of the Greenland ice sheet from MODIS". In: *Geophysical Research Letters* 40.10, pp. 2114–2120. DOI: 10.1002/grl.50240.

Hallet, B. (Oct. 1990). "Spatial self-organization in geomorphology: from periodic bedforms and patterned ground to scale-invariant topography". In: *Earth Science Reviews* 29.1-4, pp. 57–75. DOI: 10.1016/0012-8252(0)90028-T.

Hanna, E., P. Huybrechts, K. Steffen, J. Cappelen, R. Huff, C. Shuman, et al. (Jan. 2008). "Increased runoff from melt from the Greenland Ice Sheet: A response to global warming". In: *Journal of Climate* 21.2, pp. 331–341. DOI: 10.1175/2007JCLI1964.1.

Hanna, E., S. H. Mernild, J. Cappelen, and K. Steffen (Oct. 2012). "Recent warming in Greenland in a long-term instrumental (1881-2012) climatic context: I. Evaluation of surface air temperature records". In: *Environmental Research Letters* 7.4, p. 15. DOI: 10.1088/1748-9326/7/4/045404.

Hanna, E., J. M. Jones, J. Cappelen, S. H. Mernild, L. Wood, K. Steffen, et al. (Mar. 2013). "The influence of North Atlantic atmospheric and oceanic forcing effects on 1900-2010 Greenland summer climate and ice melt/runoff". In: *International Journal of Climatology* 33.4, pp. 862–880. DOI: 10.1002/joc.3475.

Hanna, E., X. Fettweis, S. H. Mernild, J. Cappelen, M. H. Ribergaard, C. A. Shuman, et al. (Mar. 2014). "Atmospheric and oceanic climate forcing of the exceptional Greenland ice sheet surface melt in summer 2012". In: *International Journal of Climatology* 34.4, pp. 1022–1037. DOI: 10.1002/joc.3743.

Hanna, E., T. E. Cropper, R. J. Hall, and J. Cappelen (Dec. 2016). "Greenland Blocking Index 1851-2015: a regional climate change signal". In: *International Journal of Climatology* 36.15, pp. 4847–4861. DOI: 10.1002/joc.4673.

Hanna, E., J. Cappelen, |. X. Fettweis, S. H. Mernild, |. Thomas, L. Mote, et al. (2020). "Greenland surface air temperature changes from 1981 to 2019 and implications for ice-sheet melt and mass-balance change". In: *Int J Climatol*. DOI: 10.1002/joc.6771.

Haran, T., J. Bohlander, T. A. Scambos, T. Painter, and M. Fahnestock (2015). *MEaSUREs MODIS Mosaic of Greenland 2005 (MOG2005) Image Map. Data archived at the National Snow and Ice Data Center*. Boulder, Colorado USA.

Harper, J., N. Humphrey, W. T. Pfeffer, J. Brown, and X. Fettweis (Nov. 2012). "Greenland ice-sheet contribution to sea-level rise buffered by meltwater storage in firn". In: *Nature* 491.7423, pp. 240–243. DOI: 10.1038/nature11566.

Heid, T. and A. Kääb (Mar. 2012). "Evaluation of existing image matching methods for deriving glacier surface displacements globally from optical satellite imagery". In: *Remote Sensing of Environment* 118, pp. 339–355. DOI: 10.1016/j.rse.2011.11.024.

Helm, V., A. Humbert, and H. Miller (Aug. 2014). "Elevation and elevation change of Greenland and Antarctica derived from CryoSat-2". In: *The Cryosphere* 8.4, pp. 1539–1559. DOI: 10.5194/tc-8-1539-2014.

Hewitt, I. (June 2013). "Seasonal changes in ice sheet motion due to melt water lubrication". In: *Earth and Planetary Science Letters* 371-372, pp. 16–25. DOI: 10.1016/J.EPSL.2013.04.022.

Hill, E. A., J. R. Carr, and C. R. Stokes (Jan. 2017). *A review of recent changes in major marine-terminating outlet glaciers in northern Greenland*. DOI: 10.3389/feart.2016.00111.

Hill, E. A., J. Rachel Carr, C. R. Stokes, and G. Hilmar Gudmundsson (Oct. 2018). "Dynamic changes in outlet glaciers in northern Greenland from 1948 to 2015". In: *Cryosphere* 12.10, pp. 3243–3263. DOI: 10.5194/tc-12-3243-2018.

Hock, R. and R. L. Hooke (Apr. 1993). "Evolution of the internal drainage system in the lower part of the ablation area of Storglaciaren, Sweden". In: *Geological Society of America Bulletin* 105.4, pp. 537–546. DOI: 10.1130/0016-7606(1993)105<0537:EOTIDS>2.3.CO;2.

Hofer, S., A. J. Tedstone, X. Fettweis, and J. L. Bamber (June 2017). "Decreasing cloud cover drives the recent mass loss on the Greenland Ice Sheet". In: *Science Advances* 3.6, e1700584. DOI: 10.1126/sciadv.1700584.

Hofer, S., A. J. Tedstone, X. Fettweis, and J. L. Bamber (July 2019). "Cloud microphysics and circulation anomalies control differences in future Greenland melt". In: *Nature Climate Change* 9.7, pp. 523–528. DOI: 10.1038/s41558-019-0507-8.

Hofer, S., C. Lang, C. Amory, C. Kittel, A. Delhasse, A. Tedstone, et al. (Dec. 2020). "Greater Greenland Ice Sheet contribution to global sea level rise in CMIP6". In: *Nature Communications* 11.1, pp. 1–11. DOI: 10.1038/s41467-020-20011-8.

Hoffman, M. J., G. A. Catania, T. A. Neumann, L. C. Andrews, and J. A. Rumrill (Dec. 2011). "Links between acceleration, melting, and supraglacial lake drainage of the western Greenland Ice Sheet". In: *Journal of Geophysical Research* 116.F4, F04035. DOI: 10.1029/2010JF001934.

Hoffman, M. J., L. C. Andrews, S. F. Price, G. A. Catania, T. A. Neumann, M. P. Lüthi, et al. (Dec. 2016). "Greenland subglacial drainage evolution regulated by weakly connected regions of the bed". In: *Nature Communications* 7.1, p. 13903. DOI: 10.1038/ncomms13903.

Hoffman, M. J., M. Perego, L. C. Andrews, S. F. Price, T. A. Neumann, J. V. Johnson, et al. (Jan. 2018). "Widespread Moulin Formation During Supraglacial Lake Drainages in Greenland". In: *Geophysical Research Letters* 45.2, pp. 778–788. DOI: 10.1002/2017GL075659.

Holland, D. M., R. H. Thomas, B. De Young, M. H. Ribergaard, and B. Lyberth (Oct. 2008). "Acceleration of Jakobshavn Isbr triggered by warm subsurface ocean waters". In: *Nature Geoscience* 1.10, pp. 659–664. DOI: 10.1038/ngeo316.

Holliday, N. P., S. L. Hughes, S. Bacon, A. Beszczynska-Möller, B. Hansen, A. Lavín, et al. (Feb. 2008). "Reversal of the 1960s to 1990s freshening trend in the northeast North Atlantic and Nordic Seas". In: *Geophysical Research Letters* 35.3, p. L03614. DOI: 10.1029/2007GL032675.

Hooke, R. L., P. Calla, P. Holmlund, M. Nilsson, and A. Stroeven (1989). "A 3 year record of seasonal variations in surface velocity, Storglaciaren, Sweden". In: *Journal of Glaciology* 35.120, pp. 235–247. DOI: 10.3189/s0022143000004561.

Hooke, R. L., T. Laumann, and J. Kohler (1990). "Subglacial water pressures and the shape of subglacial conduits". In: *Journal of Glaciology* 36.122, pp. 67–71. DOI: 10.1017/S0022143000005566.

Hooke, R. L. (2005). *Principles of Glacier Dynamics, 2nd edition*. Cambridge University Press. DOI: https://doi.org/10.1017/CBO9780511614231.

Houghton, J. T., Y. Ding, D. J. Griggs, M. Noguer, P. J. Van Der Linden, X. Dai, et al. (2001). *Climate Change 2001: The Scientific Basis Contribution of Working Group I to the Third Assessment Report of the Intergovernmental Panel on Climate Change Published for the Intergovernmental Panel on Climate Change*. Tech. rep. URL: http://www.cambridge.org.

How, P., D. I. Benn, N. R. Hulton, B. Hubbard, A. Luckman, H. Sevestre, et al. (Nov. 2017). "Rapidly changing subglacial hydrological pathways at a tidewater glacier revealed through simultaneous observations of water pressure, supraglacial lakes, meltwater plumes and surface velocities". In: *The Cryosphere* 11.6, pp. 2691–2710. DOI: 10.5194/tc-11-2691-2017.

How, P., A. Messerli, E. Mätzler, M. Santoro, A. Wiesmann, R. Caduff, et al. (Dec. 2021). "Greenland-wide inventory of ice marginal lakes using a multi-method approach". In: *Scientific Reports* 11.1, p. 4481. DOI: 10.1038/s41598-021-83509-1.

Howat, I. M., I. Joughin, S. Tulaczyk, and S. Gogineni (2005). "Rapid retreat and acceleration of Helheim Glacier, east Greenland". In: *Geophys. Res. Lett* 32, p. 22502. DOI: 10.1029/2005GL024737.

Howat, I. M., S. De La Peña, P. Peña, J. H. Van Angelen, J. T. M. Lenaerts, and M. R. Van Den Broeke (2013). ""Expansion of meltwater lakes on the Greenland Ice Sheet"". In: *The Cryosphere* 7, pp. 201–204. DOI: 10.5194/tc-7-201-2013.

Howat, I. M., A. Negrete, and B. E. Smith (Aug. 2014). "The Greenland Ice Mapping Project (GIMP) land classification and surface elevation data sets". In: *The Cryosphere* 8.4, pp. 1509–1518. DOI: 10.5194/tc-8-1509-2014.

Howat, I. M., I. Joughin, and T. A. Scambos (Mar. 2007). "Rapid changes in ice discharge from Greenland outlet glaciers". In: *Science* 315.5818, pp. 1559–1561. DOI: 10.1126/science.1138478.

Howat, I. M., B. E. Smith, I. Joughin, and T. A. Scambos (Sept. 2008a). "Rates of southeast Greenland ice volume loss from combined ICESat and ASTER observations". In: *Geophysical Research Letters* 35.17, p. L17505. DOI: 10.1029/2008GL034496.

Howat, I. M., I. Joughin, M. Fahnestock, B. E. Smith, and T. A. Scambos (2008b). "Synchronous retreat and acceleration of southeast Greenland outlet glaciers 2000-06: Ice dynamics and coupling to climate". In: *Journal of Glaciology* 54.187, pp. 646–660. DOI: 10.3189/002214308786570908.

Howat, I. M., J. E. Box, Y. Ahn, A. Herrington, and E. M. McFadden (Oct. 2010). "Seasonal variability in the dynamics of marine-terminating outlet glaciers in Greenland". In: *Journal of Glaciology* 56.198, pp. 601–613. DOI: 10.3189/002214310793146232.

Howat, I. M., Y. Ahn, I. Joughin, M. R. van den Broeke, J. T. M. Lenaerts, and B. Smith (June 2011). "Mass balance of Greenland's three largest outlet glaciers, 2000-2010". In: *Geophysical Research Letters* 38.12, n/a–n/a. DOI: 10.1029/2011GL047565.

Howat, I. M. (2017). *[04/03/2021] MEaSUREs Greenland Ice Mapping Project (GIMP) 2000 Image Mosaic Version 1. [tile 3_1 band 8, tile 4_1 band 8]. Data archived at the National Snow and Ice Data Center*. Boulder, Colorado USA. DOI: https://doi.org/10.5067/4RNTRRE4JCYD.

Howat, I. M. (2020). *[11/11/2020]: MEaSUREs Greenland Ice Velocity: Selected Glacier Site Velocity Maps from Optical Images, Version 3 [E66_50N, E66_60N]. Data archived at National Snow and Ice Data Center;* Boulder, Colorado USA. DOI: https://doi.org/10.5067/RRFY5IW94X5W.

Hubbard, B. P., M. J. Sharp, I. C. Willis, M. K. Nielsen, and C. C. Smart (Jan. 1995). "Borehole water-level variations and the structure of the subglacial hydrological

system of Haut Glacier d'Arolla, Valais, Switzerland". In: *Journal of Glaciology* 41.139, pp. 572–583. DOI: 10.3189/S0022143000034894.

Hubbard, B. P., A. Hubbard, H. M. Mader, J. L. Tison, K. Grust, and P. W. Nienow (2003). "Spatial variability in the water content and rheology of temperate glaciers: Glacier de Tsanfleuron, Switzerland". In: *Annals of Glaciology* 37, pp. 1–6. DOI: 10.3189/172756403781815474.

Hubbard, B. and P. Nienow (Jan. 1997). "Alpine subglacial hydrology". In: *Quaternary Science Reviews* 16.9, pp. 939–955. DOI: 10.1016/S0277-3791(97)00031-0.

Huybrechts, P., A. Letreguilly, and N. Reeh (Mar. 1991). "The Greenland ice sheet and greenhouse warming". In: *Global and Planetary Change* 3.4, pp. 399–412. DOI: 10.1016/0921-8181(91)90119-H.

Huybrechts, P. and J. De Wolde (1999). *The Dynamic Response of the Greenland and Antarctic Ice Sheets to Multiple-Century Climatic Warming*. Tech. rep.

Hvidberg, C. S., A. Grinsted, D. Dahl-Jensen, S. Abbas Khan, A. Kusk, J. K. Andersen, et al. (2020). "Surface velocity of the Northeast Greenland Ice Stream (NEGIS): assessment of interior velocities derived from satellite data by GPS". In: *The Cryosphere* 14, pp. 3487–3502. DOI: 10.5194/tc-14-3487-2020.

Iken, A., H. Röthlisberger, A. Flotron, and W. Haeberli (1983). "The Uplift of Unteraargletscher at the Beginning of the Melt Season—A Consequence of Water Storage at the Bed?" In: *Journal of Glaciology* 29.101, pp. 28–47. DOI: 10.3189/s0022143000005128.

Iken, A. (1981). "The Effect of the Subglacial Water Pressure on the Sliding Velocity of a Glacier in an Idealized Numerical Model". In: *Journal of Glaciology* 27.97, pp. 407–421. DOI: 10.3189/s0022143000011448.

Iken, A. and R. A. Bindschadler (Jan. 1986). "Combined measurements of Subglacial Water Pressure and Surface Velocity of Findelengletscher, Switzerland: Conclusions about Drainage System and Sliding Mechanism". In: *Journal of Glaciology* 32.110, pp. 101–119. DOI: 10.3189/S0022143000006936.

Iken, A. and M. Truffer (1997). "The relationship between subglacial water pressure and velocity of Findelengletscher, Switzerland, during its advance and retreat". In: *Journal of Glaciology* 43.144, pp. 328–338. DOI: 10.3189/s0022143000003282.

Inall, M. E., T. Murray, F. R. Cottier, K. Scharrer, T. J. Boyd, K. J. Heywood, et al. (Feb. 2014). "Oceanic heat delivery via Kangerdlugssuaq Fjord to the south-east Greenland ice sheet". In: *Journal of Geophysical Research: Oceans* 119.2, pp. 631–645. DOI: 10.1002/2013JC009295.

IPCC (2013). *Climate change 2013 the physical science basis: Working Group I contribution to the fifth assessment report of the intergovernmental panel on climate change*. Vol. 9781107057, pp. 1–1535. ISBN: 9781107415324. DOI: 10.1017/CBO9781107415324.

Iverson, N. R., B. Hanson, R. L. B. Hooke, and P. Jansson (Jan. 1995). "Flow mechanism of glaciers on soft beds". In: *Science* 267.5194, pp. 80–81. DOI: 10.1126/science.267.5194.80.

Iverson, N. R., R. W. Baker, R. L. Hooke, B. Hanson, and P. Jansson (1999). "Coupling between a glacier and a soft bed: I. A relation between effective pressure and local shear stress determined from till elasticity". In: *Journal of Glaciology* 45.149, pp. 31–40. DOI: 10.3189/s0022143000003014.

Iverson, N. R. (1999). "Coupling between a glacier and a soft bed: II Model results". In: *Journal of Glaciology* 45.149, pp. 41–53. DOI: 10.3189/s0022143000003026.

Iverson, N. R. (2011). *Shear resistance and continuity of subglacial till: Hydrology rules*. DOI: 10.3189/002214311796406220.

Jackson, R. H., E. L. Shroyer, J. D. Nash, D. A. Sutherland, D. Carroll, M. J. Fried, et al. (July 2017). "Near-glacier surveying of a subglacial discharge plume: Implications for plume parameterizations". In: *Geophysical Research Letters* 44.13, pp. 6886–6894. DOI: 10.1002/2017GL073602.

Jackson, R. H., F. Straneo, and D. A. Sutherland (June 2014). "Externally forced fluctuations in ocean temperature at Greenland glaciers in non-summer months". In: *Nature Geoscience* 7.7, pp. 503–508. DOI: 10.1038/ngeo2186.

Jackson, R. H. and F. Straneo (Sept. 2016). "Heat, salt, and freshwater budgets for a glacial fjord in Greenland". In: *Journal of Physical Oceanography* 46.9, pp. 2735–2768. DOI: 10.1175/JPO-D-15-0134.1.

Jackson, R. H., S. J. Lentz, and F. Straneo (Nov. 2018). "The dynamics of shelf forcing in Greenlandic fjords". In: *Journal of Physical Oceanography* 48.11, pp. 2799–2827. DOI: 10.1175/JPO-D-18-0057.1.

Jakob, L., N. Gourmelen, M. Ewart, and S. Plummer (Apr. 2021). "Spatially and temporally resolved ice loss in High Mountain Asia and the Gulf of Alaska observed by CryoSat-2 swath altimetry between 2010 and 2019". In: *The Cryosphere* 15.4, pp. 1845–1862. DOI: 10.5194/tc-15-1845-2021.

James, T. D., T. Murray, N. Selmes, K. Scharrer, and M. O'Leary (July 2014). "Buoyant flexure and basal crevassing in dynamic mass loss at Helheim Glacier". In: *Nature Geoscience* 7.8, pp. 593–596. DOI: 10.1038/ngeo2204.

Jamieson, S. S., A. Vieli, S. J. Livingstone, C. Ó. Cofaigh, C. Stokes, C. D. Hillenbrand, et al. (Nov. 2012). "Ice-stream stability on a reverse bed slope". In: *Nature Geoscience* 5.11, pp. 799–802. DOI: 10.1038/ngeo1600.

Jenkins, A., K. W. Nicholls, and H. F. Corr (Oct. 2010). "Observation and parameterization of ablation at the base of Ronne Ice Ahelf, Antarctica". In: *Journal of Physical Oceanography* 40.10, pp. 2298–2312. DOI: 10.1175/2010JPO4317.1.

Jenkins, A. (Dec. 2011). "Convection-driven melting near the grounding lines of ice shelves and tidewater glaciers". In: *Journal of Physical Oceanography* 41.12, pp. 2279–2294. DOI: 10.1175/JPO-D-11-03.1.

Jeong, S. and I. M. Howat (Dec. 2015). "Performance of Landsat 8 Operational Land Imager for mapping ice sheet velocity". In: *Remote Sensing of Environment* 170, pp. 90–101. DOI: 10.1016/j.rse.2015.08.023.

Jeong, S., I. M. Howat, and Y. Ahn (Apr. 2017). "Improved Multiple Matching Method for Observing Glacier Motion With Repeat Image Feature Tracking". In: *IEEE Transactions on Geoscience and Remote Sensing* 55.4, pp. 2431–2441. DOI: 10.1109/TGRS.2016.2643699.

Jiskoot, H. (2011). "Dynamics of glaciers". In: *Encyclopedia of Earth Sciences Series*. Vol. Part 3. Springer Netherlands, pp. 245–256. DOI: 10.1007/978-90-481-2642-2_127.

Jiskoot, H., D. Juhlin, H. S. Pierre, and M. Citterio (Nov. 2012). "Tidewater glacier fluctuations in central east greenland coastal and fjord regions (1980s-2005)". In: *Annals of Glaciology* 53.60, pp. 35–44. DOI: 10.3189/2012AoG60A030.

Johansson, A., P. Jansson, and I. Brown (Jan. 2013). "Spatial and temporal variations in lakes on the Greenland Ice Sheet". In: *Journal of Hydrology* 476, pp. 314–320. DOI: 10.1016/j.jhydrol.2012.10.045.

Johnson, H. L., A. Münchow, K. K. Falkner, and H. Melling (Jan. 2011). "Ocean circulation and properties in Petermann Fjord, Greenland". In: *Journal of Geophysical Research* 116.C1, p. C01003. DOI: 10.1029/2010JC006519.

Jones, C., J. Ryan, T. Holt, and A. Hubbard (2018). "Structural glaciology of Isunguata Sermia". In: *Journal of Maps* 14.2, pp. 517–527. DOI: 10.1080/17445647.2018.1507952.

Joughin, I., B. E. Smith, D. E. Shean, and D. Floricioiu (Feb. 2014). "Brief communication: Further summer speedup of jakobshavn isbræ". In: *Cryosphere* 8.1, pp. 209–214. DOI: 10.5194/tc-8-209-2014.

Joughin, I., S. Tulaczyk, M. Fahnestock, and R. Kwok (Oct. 1996). "A mini-surge on the Ryder Glacier, Greenland, observed by satellite radar interferometry". In: *Science* 274.5285, pp. 228–230. DOI: 10.1126/science.274.5285.228.

Joughin, I., W. Abdalati, and M. Fahnestock (Dec. 2004). "Large fluctuations in speed on Greenland's Jakobshavn Isbræ glacier". In: *Nature* 432.7017, pp. 608–610. DOI: 10.1038/nature03130.

Joughin, I., I. Howat, R. B. Alley, G. Ekstrom, M. Fahnestock, T. Moon, et al. (Jan. 2008a). "Ice-front variation and tidewater behavior on Helheim and Kangerdlugssuaq Glaciers, Greenland". In: *Journal of Geophysical Research* 113.F1, F01004. DOI: 10.1029/2007JF000837.

Joughin, I., S. B. Das, M. A. King, B. E. Smith, I. M. Howat, and T. Moon (May 2008b). "Seasonal speedup along the western flank of the Greenland Ice Sheet." In: *Science (New York, N.Y.)* 320.5877, pp. 781–3. DOI: 10.1126/science.1153288.

Joughin, I., B. E. Smith, I. M. Howat, T. Scambos, and T. Moon (Sept. 2010). "Greenland flow variability from ice-sheet-wide velocity mapping". In: *Journal of Glaciology* 56.197, pp. 415–430. DOI: 10.3189/002214310792447734.

Joughin, I., R. B. Alley, and D. M. Holland (Nov. 2012). *Ice-sheet response to oceanic forcing*. DOI: 10.1126/science.1226481.

Joughin, I., B. E. Smith, and I. Howat (July 2018). "Greenland Ice Mapping Project: ice flow velocity variation at sub-monthly to decadal timescales". In: *The Cryosphere* 12.7, pp. 2211–2227. DOI: 10.5194/tc-12-2211-2018.

Joughin, I., D. E. Shean, B. E. Smith, and D. Floricioiu (Jan. 2020). "A decade of variability on Jakobshavn Isbræ: Ocean temperatures pace speed through influence on mélange rigidity". In: *Cryosphere* 14.1, pp. 211–227. DOI: 10.5194/tc-14-211-2020.

Kääb, A., S. Winsvold, B. Altena, C. Nuth, T. Nagler, and J. Wuite (July 2016). "Glacier Remote Sensing Using Sentinel-2. Part I: Radiometric and Geometric Performance, and Application to Ice Velocity". In: *Remote Sensing* 8.7, p. 598. DOI: 10.3390/rs8070598.

Kamb, B., C. F. Raymond, W. D. Harrison, H. Engelhardt, K. A. Echelmeyer, N. Humphrey, et al. (Feb. 1985). "Glacier surge mechanism: 1982-1983 surge of variegated glacier, Alaska". In: *Science* 227.4686, pp. 469–479. DOI: 10.1126/science.227.4686.469.

Kamb, B. and K. A. Echelmeyer (1986). "STRESS-GRADIENT COUPLING IN GLACIER FLOW: 1. LONGITUDINAL AVERAGING OF THE INFLUENCE OF ICE THICKNESS AND SURFACE SLOPE". In: *Journal of Glaciology* 32.111, pp. 267–284.

Kamb, B. (Aug. 1987). "Glacier surge mechanism based on linked cavity configuration of the basal water conduit system". In: *Journal of Geophysical Research* 92.B9, p. 9083. DOI: 10.1029/JB092iB09p09083.

Karlsson, N. B., A. M. Solgaard, K. D. Mankoff, F. Gillet-Chaulet, J. A. MacGregor, J. E. Box, et al. (Dec. 2021). "A first constraint on basal melt-water production of the Greenland ice sheet". In: *Nature Communications* 12.1, pp. 1–10. DOI: 10.1038/s41467-021-23739-z.

Kehrl, L. M., I. Joughin, D. E. Shean, D. Floricioiu, and L. Krieger (Sept. 2017). "Seasonal and interannual variabilities in terminus position, glacier velocity, and surface elevation at Helheim and Kangerlussuaq Glaciers from 2008 to 2016". In: *Journal of Geophysical Research: Earth Surface* 122.9, pp. 1635–1652. DOI: 10.1002/2016JF004133.

Khan, S. A., K. K. Kjeldsen, K. H. Kjaer, S. Bevan, A. Luckman, A. Aschwanden, et al. (2014). "Glacier dynamics at Helheim and Kangerdlugssuaq glaciers, southeast Greenland, since the Little Ice Age". In: *The Cryosphere* 8, pp. 1497–1507. DOI: 10.5194/tc-8-1497-2014.

Khan, S. A., A. Aschwanden, A. A. BjØrk, J. Wahr, K. K. Kjeldsen, and K. H. Kjaær (Apr. 2015). "Greenland ice sheet mass balance: A review". In: *Reports on Progress in Physics* 78.4, p. 046801. DOI: 10.1088/0034-4885/78/4/046801.

Khan, S. A., A. A. Bjørk, J. L. Bamber, M. Morlighem, M. Bevis, K. H. Kjær, et al. (Dec. 2020). "Centennial response of Greenland's three largest outlet glaciers". In: *Nature Communications* 11.1. DOI: 10.1038/s41467-020-19580-5.

Khan, S. A., K. H. Kjaer, N. J. Korsgaard, J. Wahr, I. R. Joughin, L. H. Timm, et al. (Mar. 2013). "Recurring dynamically induced thinning during 1985 to 2010 on Upernavik Isstrøm, West Greenland". In: *Journal of Geophysical Research: Earth Surface* 118.1, pp. 111–121. DOI: 10.1029/2012JF002481.

Khazendar, A., I. G. Fenty, D. Carroll, A. Gardner, C. M. Lee, I. Fukumori, et al. (Mar. 2019). "Interruption of two decades of Jakobshavn Isbrae acceleration and thinning as regional ocean cools". In: *Nature Geoscience*, p. 1. DOI: 10.1038/s41561-019-0329-3.

King, M. (2018). "Seasonal to decadal variability in ice discharge from the Greenland Ice Sheet". In: *Cryosphere* 12, pp. 3813–3825.

King, M. D., I. M. Howat, S. G. Candela, M. J. Noh, S. Jeong, B. P. Y. Noël, et al. (Dec. 2020). "Dynamic ice loss from the Greenland Ice Sheet driven by sustained glacier retreat". In: *Communications Earth & Environment* 1.1, p. 1. DOI: 10.1038/s43247-020-0001-2.

King, O., A. Dehecq, D. Quincey, and J. Carrivick (Aug. 2018). "Contrasting geometric and dynamic evolution of lake and land-terminating glaciers in the central Himalaya". In: *Global and Planetary Change* 167, pp. 46–60. DOI: 10.1016/j.gloplacha.2018.05.006.

Kjeldsen, K. K., N. J. Korsgaard, A. A. Bjørk, S. A. Khan, J. E. Box, S. Funder, et al. (Dec. 2015). "Spatial and temporal distribution of mass loss from the Greenland Ice Sheet since AD 1900". In: *Nature* 528.7582, pp. 396–400. DOI: 10.1038/nature16183.

Koenig, L. S., C. Miège, R. R. Forster, and L. Brucker (Jan. 2014). "Initial in situ measurements of perennial meltwater storage in the Greenland firn aquifer". In: *Geophysical Research Letters* 41.1, pp. 81–85. DOI: 10.1002/2013GL058083.

Konrad, H., L. Gilbert, S. L. Cornford, A. Payne, A. Hogg, A. Muir, et al. (Jan. 2017). "Uneven onset and pace of ice-dynamical imbalance in the Amundsen Sea Embayment, West Antarctica". In: *Geophysical Research Letters* 44.2, pp. 910–918. DOI: 10.1002/2016GL070733.

Korsgaard, N. J., C. Nuth, S. A. Khan, K. K. Kjeldsen, A. A. Bjørk, A. Schomacker, et al. (May 2016). *Digital elevation model and orthophotographs of Greenland based on aerial photographs from 1978-1987*. DOI: 10.1038/sdata.2016.32.

Koziol, C., N. Arnold, A. Pope, and W. Colgan (June 2017). "Quantifying supraglacial meltwater pathways in the Paakitsoq region, West Greenland". In: *Journal of Glaciology* 63.239, pp. 464–476. DOI: 10.1017/jog.2017.5.

Koziol, C. P. and N. Arnold (Mar. 2018). "Modelling seasonal meltwater forcing of the velocity of land-terminating margins of the Greenland Ice Sheet". In: *The Cryosphere* 12.3, pp. 971–991. DOI: 10.5194/tc-12-971-2018.

Krabill, W. (Dec. 2004). "Greenland Ice Sheet: Increased coastal thinning". In: *Geophysical Research Letters* 31.24, p. L24402. DOI: 10.1029/2004GL021533.

Krabill, W. B., W. Abdalati, E. B. Frederick, S. S. Manizade, C. F. Martin, J. G. Sonntag, et al. (Oct. 2002). "Aircraft laser altimetry measurement of elevation changes of the greenland ice sheet: Technique and accuracy assessment". In: *Journal of Geodynamics* 34.3-4, pp. 357–376. DOI: 10.1016/S0264-3707(02)00040-6.

Kulessa, B., A. L. Hubbard, A. D. Booth, M. Bougamont, C. F. Dow, S. H. Doyle, et al. (Aug. 2017). "Seismic evidence for complex sedimentary control of Greenland Ice Sheet flow". In: *Science Advances* 3.8, e1603071. DOI: 10.1126/sciadv.1603071.

Larsen, S. H., S. A. Khan, A. P. Ahlstrøm, C. S. Hvidberg, M. J. Willis, and S. B. Andersen (Feb. 2016). "Increased mass loss and asynchronous behavior of marine-terminating outlet glaciers at Upernavik Isstrøm, NW Greenland". In: *Journal of Geophysical Research: Earth Surface* 121.2, pp. 241–256. DOI: 10.1002/2015JF003507.

Lea, J. M., D. W. Mair, and B. R. Rea (2014). "Instruments and Methods :Evaluation of existing and new methods of tracking glacier terminus change". In: *Journal of Glaciology* 60.220, pp. 323–332. DOI: 10.3189/2014JoG13J061.

Lea, J. M. (July 2018). "The Google Earth Engine Digitisation Tool (GEEDiT) and the Margin change Quantification Tool (MaQiT) – simple tools for the rapid mapping and quantification of changing Earth surface margins". In: *Earth Surface Dynamics* 6.3, pp. 551–561. DOI: 10.5194/esurf-6-551-2018.

Leeson, A. A., E. Eastoe, and X. Fettweis (Mar. 2018). "Extreme temperature events on Greenland in observations and the MAR regional climate model". In: *The Cryosphere* 12.3, pp. 1091–1102. DOI: 10.5194/tc-12-1091-2018.

Lemos, A., A. Shepherd, M. McMillan, A. E. Hogg, E. Hatton, and I. Joughin (June 2018). *Ice velocity of Jakobshavn Isbræ, Petermann Glacier, Nioghalvfjerdsfjorden, and Zachariæ Isstrøm, 2015-2017, from Sentinel 1-a/b SAR imagery*. DOI: 10.5194/tc-12-2087-2018.

Lewis, G., E. Osterberg, R. Hawley, B. Whitmore, H. Peter Marshall, and J. Box (2017). "Regional Greenland accumulation variability from Operation IceBridge airborne accumulation radar". In: *The Cryosphere* 11, pp. 773–788. DOI: 10.5194/tc-11-773-2017.

Lewis, S. M. and L. C. Smith (July 2009). "Hydrologic drainage of the Greenland Ice Sheet". In: *Hydrological Processes* 23.14, pp. 2004–2011. DOI: 10.1002/hyp.7343.

Lindbäck, K., R. Pettersson, S. H. Doyle, C. Helanow, P. Jansson, S. S. Kristensen, et al. (Sept. 2014). "High-resolution ice thickness and bed topography of a land-terminating section of the Greenland Ice Sheet". In: *Earth System Science Data* 6.2, pp. 331–338. DOI: 10.5194/essd-6-331-2014.

Lliboutry, L. (1968). "General Theory of Subglacial Cavitation and Sliding of Temperate Glaciers". In: *Journal of Glaciology* 7.49, pp. 21–58. DOI: 10.3189/s0022143000020396.

Lliboutry, L. (1979). "Local Friction Laws for Glaciers: A Critical Review and New Openings". In: *Journal of Glaciology* 23.89, pp. 67–95. DOI: 10.3189/s0022143000029750.

Lliboutry, L. (Aug. 1987). "Realistic, yet simple bottom boundary conditions for glaciers and ice sheets". In: *Journal of Geophysical Research* 92.B9, p. 9101. DOI: 10.1029/JB092iB09p09101.

Luckman, A. (Apr. 2005). "Seasonal variation in velocity before retreat of Jakobshavn Isbræ, Greenland". In: *Geophysical Research Letters* 32.8, p. L08501. DOI: 10.1029/2005GL022519.

Luckman, A., T. Murray, R. de Lange, and E. Hanna (Feb. 2006). "Rapid and synchronous ice-dynamic changes in East Greenland". In: *Geophysical Research Letters* 33.3, p. L03503. DOI: 10.1029/2005GL025428.

Luckman, A., D. I. Benn, F. Cottier, S. Bevan, F. Nilsen, and M. Inall (Oct. 2015). "Calving rates at tidewater glaciers vary strongly with ocean temperature". In: *Nature Communications* 6.1, pp. 1–7. DOI: 10.1038/ncomms9566.

Lyapustin, A., M. Tedesco, Y. Wang, T. Aoki, M. Hori, and A. Kokhanovsky (Sept. 2009). "Retrieval of snow grain size over Greenland from MODIS". In: *Remote Sensing of Environment* 113.9, pp. 1976–1987. DOI: 10.1016/j.rse.2009.05.008.

Machguth, H., M. MacFerrin, D. van As, J. E. Box, C. Charalampidis, W. Colgan, et al. (Apr. 2016). "Greenland meltwater storage in firn limited by near-surface ice formation". In: *Nature Climate Change* 6.4, pp. 390–393. DOI: 10.1038/nclimate2899.

Mair, D., P. Nienow, I. Willis, and M. Sharp (2001). "Spatial patterns of glacier motion during a high-velocity event: Haut Glacier d'Arolla, Switzerland". In: *Journal of Glaciology* 47.156, pp. 9–20. DOI: 10.3189/172756501781832412.

Mair, D. (Aug. 2002). "Influence of subglacial drainage system evolution on glacier surface motion: Haut Glacier d'Arolla, Switzerland". In: *Journal of Geophysical Research* 107.B8, p. 2175. DOI: 10.1029/2001JB000514.

Mair, D., I. Willis, U. H. Fischer, B. Hubbard, P. Nienow, and A. Hubbard (2003). "Hydrological controls on patterns of surface, internal and basal motion during three "spring events": Haut Glacier d' Arolla, Switzerland". In: *Journal of Glaciology* 49.167, pp. 555–567. URL: https://www.cambridge.org/core..

Malczyk, G., N. Gourmelen, D. Goldberg, J. Wuite, and T. Nagler (Dec. 2020). "Repeat Subglacial Lake Drainage and Filling Beneath Thwaites Glacier". In: *Geophysical Research Letters* 47.23, e2020GL089658. DOI: 10.1029/2020GL089658.

Mankoff, K. D., A. Solgaard, W. Colgan, A. P. Ahlstrøm, S. Abbas Khan, and R. S. Fausto (2020). "Greenland Ice Sheet solid ice discharge from 1986 through March 2020". In: *Earth Syst. Sci. Data* 12, pp. 1367–1383. DOI: 10.5194/essd-12-1367-2020.

Mankoff, K. D., F. Straneo, C. Cenedese, S. B. Das, C. G. Richards, and H. Singh (Dec. 2016). "Structure and dynamics of a subglacial discharge plume in a Greenlandic fjord". In: *Journal of Geophysical Research: Oceans* 121.12, pp. 8670–8688. DOI: 10.1002/2016JC011764.

Mantelli, E., C. Camporeale, and L. Ridolfi (Sept. 2015). "Supraglacial channel inception: Modeling and processes". In: *Water Resources Research* 51.9, pp. 7044–7063. DOI: 10.1002/2015WR017075.

Mather, P. M. (2004). *Computer Processing of Remotely-Sensed Images*. John Wiley & Sons, Ltd.

Mcfadden, E. M., I. M. Howat, I. Joughin, B. E. Smith, and Y. Ahn (2011). "Changes in the dynamics of marine terminating outlet glaciers in west Greenland Arctic-DEM View project Evolution of sub-Ice Shelf Meltwater Channels in Antarctica and Greenland and Implications for Ice Shelf Stability View project Changes in the dynamics of marine terminating outlet glaciers in west Greenland (2000-2009)". In:

Article in Journal of Geophysical Research Atmospheres 116, p. 2022. DOI: 10.1029/2010JF001757.

McGrath, D., W. Colgan, N. Bayou, A. Muto, and K. Steffen (May 2013). "Recent warming at Summit, Greenland: Global context and implications". In: *Geophysical Research Letters* 40.10, pp. 2091–2096. DOI: 10.1002/grl.50456.

McMillan, M., A. Shepherd, A. Sundal, K. Briggs, A. Muir, A. Ridout, et al. (2014a). "Increased ice losses from Antarctica detected by CryoSat-2". In: *Geophysical Research Letters* 41.11, pp. 3899–3905. DOI: 10.1002/2014GL060111.

McMillan, M., A. Shepherd, N. Gourmelen, A. Dehecq, A. Leeson, A. Ridout, et al. (Dec. 2014b). "Rapid dynamic activation of a marine-based Arctic ice cap". In: *Geophysical Research Letters* 41.24, pp. 8902–8909. DOI: 10.1002/2014GL062255.

McMillan, M., A. Leeson, A. Shepherd, K. Briggs, T. W. K. Armitage, A. Hogg, et al. (July 2016). "A high-resolution record of Greenland mass balance". In: *Geophysical Research Letters* 43.13, pp. 7002–7010. DOI: 10.1002/2016GL069666.

McNabb, R. W. and R. Hock (Feb. 2014). "Alaska tidewater glacier terminus positions, 1948-2012". In: *Journal of Geophysical Research: Earth Surface* 119.2, pp. 153–167. DOI: 10.1002/2013JF002915.

Meier, M. F. and A. Post (Aug. 1987). "Fast tidewater glaciers". In: *Journal of Geophysical Research* 92.B9, p. 9051. DOI: 10.1029/JB092iB09p09051.

Meierbachtol, T., J. Harper, and N. Humphrey (Aug. 2013a). "Basal drainage system response to increasing surface melt on the Greenland ice sheet." In: *Science (New York, N.Y.)* 341.6147, pp. 777–9. DOI: 10.1126/science.1235905.

Meierbachtol, T., J. Harper, and N. Humphrey (Aug. 2013b). "Basal Drainage System Response to Increasing Surface Melt on the Greenland Ice Sheet". In: *Science* 341.6147, pp. 777–779. DOI: 10.1126/science.1235905.

Mercenier, R., M. P. Lüthi, and A. Vieli (Apr. 2020). "How Oceanic Melt Controls Tidewater Glacier Evolution". In: *Geophysical Research Letters* 47.8. DOI: 10.1029/2019GL086769.

Meredith, M., M. Sommerkorn, S. Cassotta, A. Derksen, A. Ekaykin, A. Hollowed, et al. (2019). "Polar Regions". In: *IPCC Special Report on the Ocean and Cryosphere in a Changing Climate*. Ed. by H.-O. Pörtner, D. Roberts, V. Masson-Delmotte, P. Zhai, M. Tignor, E. Poloczanska, et al.

Mernild, S. H., T. L. Mote, and G. E. Liston (Sept. 2011). "Greenland ice sheet surface melt extent and trends: 1960–2010". In: *Journal of Glaciology* 57.204, pp. 621–628. DOI: 10.3189/002214311797409712.

Mernild, S. H., N. T. Knudsen, M. J. Hoffman, J. C. Yde, E. Hanna, W. H. Lipscomb, et al. (Aug. 2013). "Volume and velocity changes at Mittivakkat Gletscher, southeast Greenland". In: *Journal of Glaciology* 59.216, pp. 660–670. DOI: 10.3189/2013JoG13J017.

Messerli, A. and A. Grinsted (Feb. 2015). "Image georectification and feature tracking toolbox: ImGRAFT". In: *Geoscientific Instrumentation, Methods and Data Systems* 4.1, pp. 23–34. DOI: 10.5194/gi-4-23-2015.

Miège, C., R. R. Forster, L. Brucker, L. S. Koenig, D. K. Solomon, J. D. Paden, et al. (Dec. 2016). "Spatial extent and temporal variability of Greenland firn aquifers detected by ground and airborne radars". In: *Journal of Geophysical Research: Earth Surface* 121.12, pp. 2381–2398. DOI: 10.1002/2016JF003869.

Miles, K. E., I. C. Willis, C. L. Benedek, A. G. Williamson, and M. Tedesco (July 2017). "Toward Monitoring Surface and Subsurface Lakes on the Greenland Ice Sheet Using

Sentinel-1 SAR and Landsat-8 OLI Imagery". In: *Frontiers in Earth Science* 5, p. 58. DOI: 10.3389/feart.2017.00058.

Miles, V. V., M. W. Miles, and O. M. Johannessen (Feb. 2016). "Satellite archives reveal abrupt changes in behavior of Helheim Glacier, southeast Greenland". In: *Journal of Glaciology* 62.231, pp. 137–146. DOI: 10.1017/jog.2016.24.

Millan, R., E. Rignot, J. Mouginot, M. Wood, A. A. Bjørk, and M. Morlighem (Mar. 2018). "Vulnerability of Southeast Greenland Glaciers to Warm Atlantic Water From Operation IceBridge and Ocean Melting Greenland Data". In: *Geophysical Research Letters* 45.6, pp. 2688–2696. DOI: 10.1002/2017GL076561.

Miller, O., D. K. Solomon, C. Miège, L. Koenig, R. Forster, N. Schmerr, et al. (Jan. 2018). "Direct Evidence of Meltwater Flow Within a Firn Aquifer in Southeast Greenland". In: *Geophysical Research Letters* 45.1, pp. 207–215. DOI: 10.1002/2017GL075707.

Mohajerani, Y., M. Wood, I. Velicogna, and E. Rignot (Jan. 2019). "Detection of Glacier Calving Margins with Convolutional Neural Networks: A Case Study". In: *Remote Sensing* 11.1, p. 74. DOI: 10.3390/rs11010074.

Moon, T., I. Joughin, B. Smith, and I. Howat (May 2012). "21st-century evolution of Greenland outlet glacier velocities". In: *Science* 336.6081, pp. 576–578. DOI: 10.1126/science.1219985.

Moon, T. and I. Joughin (June 2008). "Changes in ice front position on Greenland's outlet glaciers from 1992 to 2007". In: *Journal of Geophysical Research* 113.F2, F02022. DOI: 10.1029/2007JF000927.

Moon, T., I. Joughin, B. Smith, M. R. Van Den Broeke, W. J. Van De Berg, B. Noël, et al. (Oct. 2014). "Distinct patterns of seasonal Greenland glacier velocity". In: *Geophysical Research Letters* 41.20, pp. 7209–7216. DOI: 10.1002/2014GL061836.

Moon, T., I. Joughin, and B. Smith (May 2015). "Seasonal to multiyear variability of glacier surface velocity, terminus position, and sea ice/ice mélange in northwest Greenland". In: *Journal of Geophysical Research: Earth Surface* 120.5, pp. 818–833. DOI: 10.1002/2015JF003494.

Moon, T. A., A. S. Gardner, B. Csatho, I. Parmuzin, and M. A. Fahnestock (Nov. 2020). "Rapid Reconfiguration of the Greenland Ice Sheet Coastal Margin". In: *Journal of Geophysical Research: Earth Surface* 125.11, e2020JF005585. DOI: 10.1029/2020JF005585.

Morlighem, M., E. Rignot, J. Mouginot, X. Wu, H. Seroussi, E. Larour, et al. (Dec. 2013). "High-resolution bed topography mapping of Russell Glacier, Greenland, inferred from Operation IceBridge data". In: *Journal of Glaciology* 59.218, pp. 1015–1023. DOI: 10.3189/2013JoG12J235.

Morlighem, M., E. Rignot, J. Mouginot, H. Seroussi, and E. Larour (June 2014). "Deeply incised submarine glacial valleys beneath the Greenland ice sheet". In: *Nature Geoscience* 7.6, pp. 418–422. DOI: 10.1038/ngeo2167.

Morlighem, M., C. N. Williams, E. Rignot, L. An, J. E. Arndt, J. L. Bamber, et al. (Nov. 2017). "BedMachine v3: Complete Bed Topography and Ocean Bathymetry Mapping of Greenland From Multibeam Echo Sounding Combined With Mass Conservation". In: *Geophysical Research Letters* 44.21, pp. 051–11. DOI: 10.1002/2017GL074954.

Morlighem, M., M. Wood, H. Seroussi, Y. Choi, and E. Rignot (Mar. 2019). "Modeling the response of northwest Greenland to enhanced ocean thermal forcing and subglacial discharge". In: *The Cryosphere* 13.2, pp. 723–734. DOI: 10.5194/tc-13-723-2019.

Mortensen, J., J. Bendtsen, K. Lennert, and S. Rysgaard (Dec. 2014). "Seasonal variability of the circulation system in a west Greenland tidewater outlet glacier fjord, Godthåbsfjord (64°N)". In: *Journal of Geophysical Research: Earth Surface* 119.12, pp. 2591–2603. DOI: 10.1002/2014JF003267.

Motyka, R. J., W. P. Dryer, J. Amundson, M. Truffer, and M. Fahnestock (Oct. 2013). "Rapid submarine melting driven by subglacial discharge, LeConte Glacier, Alaska". In: *Geophysical Research Letters* 40.19, pp. 5153–5158. DOI: 10.1002/grl.51011.

Motyka, R. J., L. Hunter, K. A. Echelmeyer, and C. Connor (2003). "Submarine melting at the terminus of a temperate tidewater glacier, LeConte Glacier, Alaska, U.S.A". In: *Annals of Glaciology* 36, pp. 57–65. DOI: 10.3189/172756403781816374.

Motyka, R. J., M. Truffer, M. Fahnestock, J. Mortensen, S. Rysgaard, and I. Howat (Mar. 2011). "Submarine melting of the 1985 Jakobshavn Isbrae floating tongue and the triggering of the current retreat". In: *Journal of Geophysical Research: Earth Surface* 116.F1, n/a–n/a. DOI: 10.1029/2009JF001632.

Motyka, R. J., R. Cassotto, M. Truffer, K. K. Kjeldsen, D. Van As, N. J. Korsgaard, et al. (Apr. 2017). "Asynchronous behavior of outlet glaciers feeding Godthåbsfjord (Nuup Kangerlua) and the triggering of Narsap Sermia's retreat in SW Greenland". In: *Journal of Glaciology* 63.238, pp. 288–308. DOI: 10.1017/jog.2016.138.

Mouginot, J., E. Rignot, B. Scheuchl, I. Fenty, A. Khazendar, M. Morlighem, et al. (Dec. 2015). "Fast retreat of Zachariæ Isstrøm, northeast Greenland." In: *Science (New York, N.Y.)* 350.6266, pp. 1357–61. DOI: 10.1126/science.aac7111.

Mouginot, J., E. Rignot, A. A. Bjørk, M. v. d. Broeke, R. Millan, M. Morlighem, et al. (May 2019). "Forty-six years of Greenland Ice Sheet mass balance from 1972 to 2018". In: *Proceedings of the National Academy of Sciences* 116.19, pp. 9239–9244. DOI: 10.1073/PNAS.1904242116.

Mouginot, J., E. Rignot, B. Scheuchl, and R. Millan (Apr. 2017). "Comprehensive Annual Ice Sheet Velocity Mapping Using Landsat-8, Sentinel-1, and RADARSAT-2 Data". In: *Remote Sensing* 9.4, p. 364. DOI: 10.3390/rs9040364.

Moyer, A. N., D. A. Sutherland, P. W. Nienow, and A. J. Sole (Aug. 2019). "Seasonal Variations in Iceberg Freshwater Flux in Sermilik Fjord, Southeast Greenland From Sentinel-2 Imagery". In: *Geophysical Research Letters* 46.15, pp. 8903–8912. DOI: 10.1029/2019GL082309.

Moyer, A. N., P. W. Nienow, N. Gourmelen, A. J. Sole, and D. A. Slater (Dec. 2017). "Estimating Spring Terminus Submarine Melt Rates at a Greenlandic Tidewater Glacier Using Satellite Imagery". In: *Frontiers in Earth Science* 5, p. 107. DOI: 10.3389/feart.2017.00107.

Murray, T., K. Scharrer, T. D. James, S. R. Dye, E. Hanna, A. D. Booth, et al. (Aug. 2010). "Ocean regulation hypothesis for glacier dynamics in southeast Greenland and implications for ice sheet mass changes". In: *Journal of Geophysical Research* 115.F3, F03026. DOI: 10.1029/2009JF001522.

Murray, T., K. Scharrer, N. Selmes, A. D. Booth, T. D. James, S. L. Bevan, et al. (Aug. 2015). "Extensive retreat of Greenland tidewater glaciers, 2000–2010". In: *Arctic, Antarctic, and Alpine Research* 47.3, pp. 427–447. DOI: 10.1657/AAAR0014-049.

Myers, P. G., N. Kulan, and M. H. Ribergaard (Sept. 2007). "Irminger Water variability in the West Greenland Current". In: *Geophysical Research Letters* 34.17, p. L17601. DOI: 10.1029/2007GL030419.

Nagy, T., L. M. Andreassen, R. A. Duller, and P. J. Gonzalez (May 2019). "SenDiT: The Sentinel-2 Displacement Toolbox with Application to Glacier Surface Velocities". In: *Remote Sensing* 11.10, p. 1151. DOI: 10.3390/rs11101151.

Nghiem, S. V., D. K. Hall, T. L. Mote, M. Tedesco, M. R. Albert, K. Keegan, et al. (Oct. 2012). "The extreme melt across the Greenland ice sheet in 2012". In: *Geophysical Research Letters* 39.20. DOI: 10.1029/2012GL053611.

Nick, F. M., C. J. van der Veen, and J. Oerlemans (July 2007). "Controls on advance of tidewater glaciers: Results from numerical modeling applied to Columbia Glacier". In: *Journal of Geophysical Research* 112.F3, F03S24. DOI: 10.1029/2006JF000551.

Nick, F. M., C. J. Van Der Veen, A. Vieli, and D. I. Benn (Dec. 2010). "A physically based calving model applied to marine outlet glaciers and implications for the glacier dynamics". In: *Journal of Glaciology* 56.199, pp. 781–794. DOI: 10.3189/002214310794457344.

Nick, F. M., A. Vieli, I. M. Howat, and I. Joughin (Feb. 2009). "Large-scale changes in Greenland outlet glacier dynamics triggered at the terminus". In: *Nature Geoscience* 2.2, pp. 110–114. DOI: 10.1038/ngeo394.

Nick, F. M., A. Vieli, M. L. Andersen, I. Joughin, A. Payne, T. L. Edwards, et al. (May 2013). "Future sea-level rise from Greenland's main outlet glaciers in a warming climate". In: *Nature* 497.7448, pp. 235–238. DOI: 10.1038/nature12068.

Nick, F. (2012). "The response of Petermann Glacier, Greenland, to large calving events, and its future stability in the context of atmospheric and oceanic warming". In: *J. Glaciol.* 58, pp. 229–239.

Nienow, P. W., A. L. Hubbard, B. P. Hubbard, D. M. Chandler, D. W. F. Mair, M. J. Sharp, et al. (Dec. 2005). "Hydrological controls on diurnal ice flow variability in valley glaciers". In: *Journal of Geophysical Research: Earth Surface* 110.F4, n/a–n/a. DOI: 10.1029/2003JF000112.

Nienow, P. W., A. J. Sole, D. A. Slater, and T. R. Cowton (Dec. 2017). "Recent Advances in Our Understanding of the Role of Meltwater in the Greenland Ice Sheet System". In: *Current Climate Change Reports* 3.4, pp. 330–344. DOI: 10.1007/s40641-017-0083-9.

Nienow, P., M. Sharp, and I. Willis (Sept. 1998). "Seasonal changes in the morphology of the subglacial drainage system, Haut Glacier d'Arolla, Switzerland". In: *Earth Surface Processes and Landforms* 23.9, pp. 825–843. DOI: 10.1002/(SICI)1096-9837(199809)23:9<825::AID-ESP893>3.0.CO;2-2.

Nilsson, J., P. Vallelonga, S. B. Simonsen, L. S. Sørensen, R. Forsberg, D. Dahl-Jensen, et al. (May 2015). "Greenland 2012 melt event effects on CryoSat-2 radar altimetry". In: *Geophysical Research Letters* 42.10, pp. 3919–3926. DOI: 10.1002/2015GL063296.

Nilsson, J., A. Gardner, L. Sandberg Sørensen, and R. Forsberg (2016). "Improved retrieval of land ice topography from CryoSat-2 data and its impact for volume-change estimation of the Greenland Ice Sheet". In: *The Cryosphere* 10, pp. 2953–2969. DOI: 10.5194/tc-10-2953-2016.

Noël, B., W. J. Van De Berg, E. Van Meijgaard, P. Kuipers Munneke, R. S. W. Van De Wal, and M. R. Van Den Broeke (2015). "Evaluation of the updated regional climate model RACMO2.3: summer snowfall impact on the Greenland Ice Sheet". In: *The Cryosphere* 9, pp. 1831–1844. DOI: 10.5194/tc-9-1831-2015.

Noël, B., W. J. Van De Berg, S. Lhermitte, B. Wouters, H. Machguth, I. Howat, et al. (Mar. 2017). "A tipping point in refreezing accelerates mass loss of Greenland's glaciers and ice caps". In: *Nature Communications* 8.1, pp. 1–8. DOI: 10.1038/ncomms14730.

Noël, B., W. J. Van De Berg, J. M. Van Wessem, E. Van Meijgaard, D. Van As, J. T. Lenaerts, et al. (Mar. 2018). "Modelling the climate and surface mass balance of po-

lar ice sheets using RACMO2 - Part 1: Greenland (1958-2016)". In: *The Cryosphere* 12.3, pp. 811–831. DOI: 10.5194/tc-12-811-2018.

Noh, M. J. and I. M. Howat (July 2017). "The Surface Extraction from TIN based Search-space Minimization (SETSM) algorithm". In: *ISPRS Journal of Photogrammetry and Remote Sensing* 129, pp. 55–76. DOI: 10.1016/j.isprsjprs.2017.04.019.

Nye, J. F. (1953). *The Flow Law of Ice from Measurements in Glacier Tunnels, Laboratory Experiments and the Jungfraufirn Borehole Experiment*. DOI: 10.2307/99248.

Nye, J. F. (July 1960). "The response of glaciers and ice-sheets to seasonal and climatic changes". In: *Proceedings of the Royal Society of London. Series A. Mathematical and Physical Sciences* 256.1287, pp. 559–584. DOI: 10.1098/rspa.1960.0127.

Nye, J. F. (May 1963). "On the Theory of the Advance and Retreat of Glaciers". In: *Geophysical Journal International* 7.4, pp. 431–456. DOI: 10.1111/j.1365-246X.1963.tb07087.x.

O'Leary, M. and P. Christoffersen (2013). "Calving on tidewater glaciers amplified by submarine frontal melting". In: *Cryosphere* 7.1, pp. 119–128. DOI: 10.5194/tc-7-119-2013.

Oerlemans, J. (Mar. 1991). "The mass balance of the Greenland ice sheet: sensitivity to climate change as revealed by energy-balance modelling". In: *The Holocene* 1.1, pp. 40–48. DOI: 10.1177/095968369100100106.

OMG (2020). *[07/10/2020]: Glacier elevation data from the GLISTIN-A campaigns. Ver. 1. Data archived at PO.DAAC*. CA, USA. DOI: https://dx.doi.org/10.5067/OMGEV-GLNA1.

Oppenheimer, M., B. C. Glavovic, J. Hinkel, R. van de Wal, A. K. Magnan, A. Abd-Elgawad, et al. (2019). "Sea Level Rise and Implications for Low-Lying Islands, Coasts and Communities". In: *IPCC Special Report on the Ocean and Cryosphere in a Changing Climate*. Ed. by H.-O. Pörtner, D. Roberts, V. Masson-Delmotte, P. Zhai, M. Tignor, E. Poloczanska, et al.

Overland, J., E. Hanna, and I. Hanssen-Bauer (2019). "Surface air temperature". In: *Arctic Report Card*. Ed. by J. Richter-Menge, M. Druckenmiller, and M. Jeffries. URL: http://eprints.lincoln.ac.uk/id/eprint/34615/.

Palmer, S., A. Shepherd, P. Nienow, and I. Joughin (Feb. 2011). "Seasonal speedup of the Greenland Ice Sheet linked to routing of surface water". In: *Earth and Planetary Science Letters* 302.3-4, pp. 423–428. DOI: 10.1016/j.epsl.2010.12.037.

Parizek, B. R. and R. B. Alley (May 2004). "Implications of increased Greenland surface melt under global-warming scenarios: ice-sheet simulations". In: *Quaternary Science Reviews* 23.9-10, pp. 1013–1027. DOI: 10.1016/j.quascirev.2003.12.024.

Pattyn, F., C. Ritz, E. Hanna, X. Asay-Davis, R. DeConto, G. Durand, et al. (Dec. 2018). *The Greenland and Antarctic ice sheets under 1.5 °C global warming*. DOI: 10.1038/s41558-018-0305-8.

Payne, A. J., A. Vieli, A. P. Shepherd, D. J. Wingham, and E. Rignot (Dec. 2004). "Recent dramatic thinning of largest West Antarctic ice stream triggered by oceans". In: *Geophysical Research Letters* 31.23, pp. 1–4. DOI: 10.1029/2004GL021284.

Petrunin, A. G., I. Rogozhina, A. P. Vaughan, I. T. Kukkonen, M. K. Kaban, I. Koulakov, et al. (Sept. 2013). "Heat flux variations beneath central Greenland's ice due to anomalously thin lithosphere". In: *Nature Geoscience* 6.9, pp. 746–750. DOI: 10.1038/ngeo1898.

Pfeffer, W. T. (Aug. 2007). "A simple mechanism for irreversible tidewater glacier retreat". In: *Journal of Geophysical Research* 112.F3, F03S25. DOI: 10.1029/2006JF000590.

Pfeffer, W. T., M. F. Meier, and T. H. Illangasekare (Dec. 1991). "Retention of Greenland runoff by refreezing: Implications for projected future sea level change". In: *Journal of Geophysical Research* 96.C12, p. 22117. DOI: 10.1029/91JC02502.

Phillips, T., H. Rajaram, and K. Steffen (Oct. 2010). "Cryo-hydrologic warming: A potential mechanism for rapid thermal response of ice sheets". In: *Geophysical Research Letters* 37.20, n/a–n/a. DOI: 10.1029/2010GL044397.

Phillips, T., H. Rajaram, W. Colgan, K. Steffen, and W. Abdalati (Sept. 2013). "Evaluation of cryo-hydrologic warming as an explanation for increased ice velocities in the wet snow zone, Sermeq Avannarleq, West Greenland". In: *Journal of Geophysical Research: Earth Surface* 118.3, pp. 1241–1256. DOI: 10.1002/jgrf.20079.

Piotrowski, J. A., D. M. Mickelson, S. Tulaczyk, D. Krzyszkowski, and F. W. Junge (Dec. 2001). "Were deforming subglacial beds beneath past ice sheets really widespread?" In: *Quaternary International* 86.1, pp. 139–150. DOI: 10.1016/S1040-6182(01)00056-8.

Piotrowski, J. A., N. K. Larsen, and F. W. Junge (May 2004). "Reflections on soft subglacial beds as a mosaic of deforming and stable spots". In: *Quaternary Science Reviews* 23.9-10, pp. 993–1000. DOI: 10.1016/j.quascirev.2004.01.006.

Poinar, K., I. Joughin, S. B. Das, M. D. Behn, J. T. M. Lenaerts, and M. R. van den Broeke (Mar. 2015). "Limits to future expansion of surface-melt-enhanced ice flow into the interior of western Greenland". In: *Geophysical Research Letters* 42.6, pp. 1800–1807. DOI: 10.1002/2015GL063192.

Poinar, K., I. Joughin, J. T. Lenaerts, and M. R. Van Den Broeke (Feb. 2017). "Englacial latent-heat transfer has limited influence on seaward ice flux in western Greenland". In: *Journal of Glaciology* 63.237, pp. 1–16. DOI: 10.1017/jog.2016.103.

Poinar, K., C. F. Dow, and L. C. Andrews (May 2019). "Long-Term Support of an Active Subglacial Hydrologic System in Southeast Greenland by Firn Aquifers". In: *Geophysical Research Letters* 46.9, pp. 4772–4781. DOI: 10.1029/2019GL082786.

Polyakov, I. V., A. Beszczynska, E. C. Carmack, I. A. Dmitrenko, E. Fahrbach, I. E. Frolov, et al. (Sept. 2005). "One more step toward a warmer Arctic". In: *Geophysical Research Letters* 32.17, pp. 1–4. DOI: 10.1029/2005GL023740.

Pope, A., W. Rees, A. Fox, A. Fleming, A. Pope, W. G. Rees, et al. (July 2014). "Open Access Data in Polar and Cryospheric Remote Sensing". In: *Remote Sensing* 6.7, pp. 6183–6220. DOI: 10.3390/rs6076183.

Porter, C. C., P. Morin, I. Howat, M.-J. Noh, B. Bates, K. Peterman, et al. (2018a). *ArcticDEM. Data archived at Harvard Dataverse*. DOI: https://doi.org/10.7910/DVN/OHHUKH.

Porter, D. F., K. J. Tinto, A. L. Boghosian, B. M. Csatho, R. E. Bell, and J. R. Cochran (July 2018b). "Identifying Spatial Variability in Greenland's Outlet Glacier Response to Ocean Heat". In: *Frontiers in Earth Science* 6, p. 90. DOI: 10.3389/feart.2018.00090.

Post, A. (1975). *Preliminary hydrography and historic terminal changes of Columbia Glacier, Alaska*. Tech. rep. DOI: 10.3133/ha559.

Post, A. and R. J. Motyka (Jan. 1995). "TAKU AND LE CONTE GLACIERS, ALASKA: CALVING-SPEED CONTROL OF LATE-HOLOCENE ASYNCHRONOUS ADVANCES AND RETREATS". In: *Physical Geography* 16.1, pp. 59–82. DOI: 10.1080/02723646.1995.10642543.

Post, A., S. O'Neel, R. J. Motyka, and G. Streveler (Sept. 2011). "A complex relationship between calving glaciers and climate". In: *Eos, Transactions American Geophysical Union* 92.37, pp. 305–306. DOI: 10.1029/2011EO370001.

Price, S., A. Payne, G. Catania, and T. Neumann (Sept. 2008). "Seasonal acceleration of inland ice via longitudinal coupling to marginal ice". In: *Journal of Glaciology* 54.185, pp. 213–219. DOI: 10.3189/002214308784886117.

Price, S. F., A. J. Payne, I. M. Howat, and B. E. Smith (May 2011). "Committed sea-level rise for the next century from Greenland ice sheet dynamics during the past decade". In: *Proceedings of the National Academy of Sciences of the United States of America* 108.22, pp. 8978–8983. DOI: 10.1073/pnas.1017313108.

Pritchard, H. D., S. B. Luthcke, and A. H. Fleming (2011). *Understanding ice-sheet mass balance: Progress in satellite altimetry and gravimetry*. DOI: 10.3189/002214311796406194.

Pritchard, H. D., R. J. Arthern, D. G. Vaughan, and L. A. Edwards (Oct. 2009). "Extensive dynamic thinning on the margins of the Greenland and Antarctic ice sheets". In: *Nature* 461.7266, pp. 971–975. DOI: 10.1038/nature08471.

Raymond, C. (1996). "Shear margins in glaciers and ice sheets". In: *Journal of Glaciology* 42.140, pp. 90–102. DOI: 10.3189/s0022143000030550.

Reeh, N., H. H. Thomsen, A. K. Higgins, and A. Weidick (2001). "Sea ice and the stability of north and northeast Greenland floating glaciers". In: *Annals of Glaciology* 33, pp. 474–480. DOI: 10.3189/172756401781818554.

Reeh, N. (1968). "On The Calving of Ice From Floating Glaciers and Ice Shelves". In: *Journal of Glaciology* 7.50, pp. 215–232. DOI: 10.3189/s0022143000031014.

Reeh, N. (2017). "Greenland Ice Shelves and Ice Tongues". In: Springer, pp. 75–106. DOI: 10.1007/978-94-024-1101-0_4.

Riel, B., B. Minchew, and I. Joughin (Jan. 2021). "Observing traveling waves in glaciers with remote sensing: New flexible time series methods and application to Sermeq Kujalleq (Jakobshavn Isbræ), Greenland". In: *Cryosphere* 15.1, pp. 407–429. DOI: 10.5194/tc-15-407-2021.

Rignot, E. and P. Kanagaratnam (2006a). "Changes in the velocity structure of the Greenland Ice Sheet". In: *Science* 311, pp. 986–990.

Rignot, E., I. Velicogna, M. R. van den Broeke, A. Monaghan, and J. T. M. Lenaerts (Mar. 2011). "Acceleration of the contribution of the Greenland and Antarctic ice sheets to sea level rise". In: *Geophysical Research Letters* 38.5, n/a–n/a. DOI: 10.1029/2011GL046583.

Rignot, E., I. Fenty, D. Menemenlis, and Y. Xu (Nov. 2012). "Spreading of warm ocean waters around Greenland as a possible cause for glacier acceleration". In: *Annals of Glaciology* 53.60, pp. 257–266. DOI: 10.3189/2012AoG60A136.

Rignot, E., Y. Xu, D. Menemenlis, J. Mouginot, B. Scheuchl, X. Li, et al. (June 2016). "Modeling of ocean-induced ice melt rates of five west Greenland glaciers over the past two decades". In: *Geophysical Research Letters* 43.12, pp. 6374–6382. DOI: 10.1002/2016GL068784.

Rignot, E. and S. S. Jacobs (June 2002). "Rapid bottom melting widespread near antarctic ice sheet grounding lines". In: *Science* 296.5575, pp. 2020–2023. DOI: 10.1126/science.1070942.

Rignot, E. and P. Kanagaratnam (Feb. 2006b). "Changes in the velocity structure of the Greenland Ice Sheet". In: *Science* 311.5763, pp. 986–990. DOI: 10.1126/science.1121381.

Rignot, E., J. E. Box, E. W. Burgess, and E. Hanna (2008). "Mass balance of the Greenland ice sheet from 1958 to 2007". In: *Geophysical Research Letters* 35.20, p. L20502. DOI: 10.1029/2008GL035417..

Rignot, E., M. Koppes, and I. Velicogna (Mar. 2010). "Rapid submarine melting of the calving faces of West Greenland glaciers". In: *Nature Geoscience* 3.3, pp. 187–191. DOI: 10.1038/ngeo765.

Rippin, D. M., I. C. Willis, N. S. Arnold, A. J. Hodson, and M. Brinkhaus (2005). "Spatial and temporal variations in surface velocity and basal drag across the tongue of the polythermal glacier midre Lovénbreen, Svalbard". In: *Journal of Glaciology* 51.175, pp. 588–600. DOI: 10.3189/172756505781829089.

Rosenau, R., M. Scheinert, and R. Dietrich (Nov. 2015). "A processing system to monitor Greenland outlet glacier velocity variations at decadal and seasonal time scales utilizing the Landsat imagery". In: *Remote Sensing of Environment* 169, pp. 1–19. DOI: 10.1016/j.rse.2015.07.012.

Röthlisberger, H. (Jan. 1972). "Water Pressure in Intra- and Subglacial Channels". In: *Journal of Glaciology* 11.62, pp. 177–203. DOI: 10.3189/S0022143000022188.

Roy, D. P., M. A. Wulder, T. R. Loveland, W. C.E., R. G. Allen, M. C. Anderson, et al. (Apr. 2014). "Landsat-8: Science and product vision for terrestrial global change research". In: *Remote Sensing of Environment* 145, pp. 154–172. DOI: 10.1016/j.rse.2014.02.001.

Ryan, J. C., L. C. Smith, D. Van As, S. W. Cooley, M. G. Cooper, L. H. Pitcher, et al. (Mar. 2019). "Greenland Ice Sheet surface melt amplified by snowline migration and bare ice exposure". In: *Science Advances* 5.3, eaav3738. DOI: 10.1126/sciadv.aav3738.

Sandberg Sørensen, L., S. B. Simonsen, R. Forsberg, K. Khvorostovsky, R. Meister, and M. E. Engdahl (Aug. 2018). "25 years of elevation changes of the Greenland Ice Sheet from ERS, Envisat, and CryoSat-2 radar altimetry". In: *Earth and Planetary Science Letters* 495, pp. 234–241. DOI: 10.1016/J.EPSL.2018.05.015.

Sasgen, I., B. Wouters, A. S. Gardner, M. D. King, M. Tedesco, F. W. Landerer, et al. (Dec. 2020). "Return to rapid ice loss in Greenland and record loss in 2019 detected by the GRACE-FO satellites". In: *Communications Earth & Environment* 1.1, pp. 1–8. DOI: 10.1038/s43247-020-0010-1.

Scambos, T. A., C. Hulbe, M. Fahnestock, and J. Bohlander (2000). "The link between climate warming and break-up of ice shelves in the Antarctic Peninsula". In: *Journal of Glaciology* 46.154, pp. 516–530. DOI: 10.3189/172756500781833043.

Scambos, T. A., M. J. Dutkiewicz, J. C. Wilson, and R. A. Bindschadler (Dec. 1992). "Application of image cross-correlation to the measurement of glacier velocity using satellite image data". In: *Remote Sensing of Environment* 42.3, pp. 177–186. DOI: 10.1016/0034-4257(92)90101-O.

Schild, K. M. and G. S. Hamilton (Aug. 2013). "Seasonal variations of outlet glacier terminus position in Greenland". In: *Journal of Glaciology* 59.216, pp. 759–770. DOI: 10.3189/2013JoG12J238.

Schoof, C. (Mar. 2005). "The effect of cavitation on glacier sliding". In: *Proceedings of the Royal Society A: Mathematical, Physical and Engineering Sciences* 461.2055, pp. 609–627. DOI: 10.1098/rspa.2004.1350.

Schoof, C. (Dec. 2010). "Ice-sheet acceleration driven by melt supply variability". In: *Nature* 468.7325, pp. 803–806. DOI: 10.1038/nature09618.

Sciascia, R., F. Straneo, C. Cenedese, and P. Heimbach (May 2013). "Seasonal variability of submarine melt rate and circulation in an East Greenland fjord". In: *Journal of Geophysical Research: Oceans* 118.5, pp. 2492–2506. DOI: 10.1002/jgrc.20142.

Seaberg, S. Z., J. Z. Seaberg, R. L. Hooke, and D. W. Wiberg (1988). "Character of the Englacial and Subglacial Drainage System in the Lower Part of the Ablation

Area of Storglaciären, Sweden, as Revealed by Dye-Trace Studies". In: *Journal of Glaciology* 34.117, pp. 217–227. DOI: 10.3189/s0022143000032263.

Seale, A., P. Christoffersen, R. I. Mugford, and M. O'Leary (Sept. 2011). "Ocean forcing of the Greenland Ice Sheet: Calving fronts and patterns of retreat identified by automatic satellite monitoring of eastern outlet glaciers". In: *Journal of Geophysical Research: Earth Surface* 116.3. DOI: 10.1029/2010JF001847.

Selmes, N., T. Murray, and T. D. James (Feb. 2013). "Characterizing supraglacial lake drainage and freezing on the Greenland Ice Sheet". In: *The Cryosphere Discussions* 7.1, pp. 475–505. DOI: 10.5194/tcd-7-475-2013.

Serreze, M. C. and R. G. Barry (May 2011). "Processes and impacts of Arctic amplification: A research synthesis". In: *Global and Planetary Change* 77.1-2, pp. 85–96. DOI: 10.1016/j.gloplacha.2011.03.004.

Sharp, M., J. C. Gemmell, and J.-L. Tison (Mar. 1989). "Structure and stability of the former subglacial drainage system of the glacier De Tsanfleuron, Switzerland". In: *Earth Surface Processes and Landforms* 14.2, pp. 119–134. DOI: 10.1002/esp.3290140204.

Shepherd, A., A. Hubbard, P. Nienow, M. King, M. McMillan, and I. Joughin (Jan. 2009). "Greenland ice sheet motion coupled with daily melting in late summer". In: *Geophysical Research Letters* 36.1, p. L01501. DOI: 10.1029/2008GL035758.

Shepherd, A., E. R. Ivins, G. A, V. R. Barletta, M. J. Bentley, S. Bettadpur, et al. (Nov. 2012). "A Reconciled Estimate of Ice-Sheet Mass Balance". In: *Science* 338.6111, pp. 1183–1189. DOI: 10.1126/SCIENCE.1228102.

Shepherd, A., E. Ivins, E. Rignot, B. Smith, M. van den Broeke, I. Velicogna, et al. (Mar. 2019). "Mass balance of the Greenland Ice Sheet from 1992 to 2018". In: *Nature* 579.7798, pp. 233–239. DOI: 10.1038/s41586-019-1855-2.

Shreve, R. L. (1972). "Movement of Water in Glaciers". In: *Journal of Glaciology* 11.62, pp. 205–214. DOI: 10.3189/s002214300002219x.

Shuman, C. A., D. K. Hall, N. E. Digirolamo, T. K. Mefford, and M. J. Schnaubelt (Sept. 2014). "Comparison of near-surface air temperatures and MODIS ice-surface temperatures at summit, Greenland (2008-13)". In: *Journal of Applied Meteorology and Climatology* 53.9, pp. 2171–2180. DOI: 10.1175/JAMC-D-14-0023.1.

Simonsen, S. B. and L. S. Sørensen (Mar. 2017). "Implications of changing scattering properties on Greenland ice sheet volume change from Cryosat-2 altimetry". In: *Remote Sensing of Environment* 190, pp. 207–216. DOI: 10.1016/j.rse.2016.12.012.

Slater, D. A., P. W. Nienow, T. R. Cowton, D. N. Goldberg, and A. J. Sole (Apr. 2015). "Effect of near-terminus subglacial hydrology on tidewater glacier submarine melt rates". In: *Geophysical Research Letters* 42.8, pp. 2861–2868. DOI: 10.1002/2014GL062494.

Slater, D. A., P. W. Nienow, D. N. Goldberg, T. R. Cowton, and A. J. Sole (Mar. 2017). "A model for tidewater glacier undercutting by submarine melting". In: *Geophysical Research Letters* 44.5, pp. 2360–2368. DOI: 10.1002/2016GL072374.

Slater, D. A., F. Straneo, S. B. Das, C. G. Richards, T. J. W. Wagner, and P. W. Nienow (Nov. 2018). "Localized Plumes Drive Front-Wide Ocean Melting of A Greenlandic Tidewater Glacier". In: *Geophysical Research Letters* 45.22, pp. 350–12. DOI: 10.1029/2018GL080763.

Slater, D., F. Straneo, D. Felikson, C. Little, H. Goelzer, X. Fettweis, et al. (May 2019a). "Past and future response of Greenland's tidewater glaciers to submarine melting". In: *The Cryosphere Discussions*, pp. 1–32. DOI: 10.5194/tc-2019-98.

Slater, D. A., F. Straneo, D. Felikson, C. M. Little, H. Goelzer, X. Fettweis, et al. (Sept. 2019b). "Estimating Greenland tidewater glacier retreat driven by submarine melting". In: *Cryosphere* 13.9, pp. 2489–2509. DOI: 10.5194/tc-13-2489-2019.

Slater, D. A., D. Felikson, F. Straneo, H. Goelzer, C. M. Little, M. Morlighem, et al. (Mar. 2020). *Twenty-first century ocean forcing of the Greenland ice sheet for modelling of sea level contribution*. DOI: 10.5194/tc-14-985-2020.

Smith, B., H. A. Fricker, A. S. Gardner, B. Medley, J. Nilsson, F. S. Paolo, et al. (Apr. 2020). "Pervasive ice sheet mass loss reflects competing ocean and atmosphere processes". In: *Science*, eaaz5845. DOI: 10.1126/science.aaz5845.

Smith, L. C., V. W. Chu, K. Yang, C. J. Gleason, L. H. Pitcher, A. K. Rennermalm, et al. (Jan. 2015). "Efficient meltwater drainage through supraglacial streams and rivers on the southwest Greenland ice sheet". In: *Proceedings of the National Academy of Sciences of the United States of America* 112.4, pp. 1001–1006. DOI: 10.1073/pnas.1413024112.

Smith, L. C., K. Yang, L. H. Pitcher, B. T. Overstreet, V. W. Chu, Å. K. Rennermalm, et al. (Dec. 2017). "Direct measurements of meltwater runoff on the Greenland ice sheet surface". In: *Proceedings of the National Academy of Sciences of the United States of America* 114.50, E10622–E10631. DOI: 10.1073/pnas.1707743114.

Sohn, H.-G., K. C. Jezek, and C. J. van der Veen (July 1998). "Jakobshavn Glacier, west Greenland: 30 years of spaceborne observations". In: *Geophysical Research Letters* 25.14, pp. 2699–2702. DOI: 10.1029/98GL01973.

Sole, A., T. Payne, J. Bamber, P. Nienow, and W. Krabill (Dec. 2008). "Testing hypotheses of the cause of peripheral thinning of the Greenland Ice Sheet: is land-terminating ice thinning at anomalously high rates?" In: *The Cryosphere* 2.2, pp. 205–218. DOI: 10.5194/tc-2-205-2008.

Sole, A. J., D. W. F. Mair, P. W. Nienow, I. D. Bartholomew, M. A. King, M. J. Burke, et al. (Aug. 2011). "Seasonal speedup of a Greenland marine-terminating outlet glacier forced by surface melt–induced changes in subglacial hydrology". In: *Journal of Geophysical Research* 116.F3, F03014. DOI: 10.1029/2010JF001948.

Sole, A., P. Nienow, I. Bartholomew, D. Mair, T. Cowton, A. Tedstone, et al. (Aug. 2013). "Winter motion mediates dynamic response of the Greenland Ice Sheet to warmer summers". In: *Geophysical Research Letters* 40.15, pp. 3940–3944. DOI: 10.1002/grl.50764.

Stearns, L. A. and G. S. Hamilton (Mar. 2007). "Rapid volume loss from two East Greenland outlet glaciers quantified using repeat stereo satellite imagery". In: *Geophysical Research Letters* 34.5. DOI: 10.1029/2006GL028982.

Stein, M. (2006). "North Atlantic Subpolar Gyre Warming – Impacts on Greenland Offshore Waters". In: *J. Northw. Atl. Fish. Sci* 36, pp. 43–54. DOI: 10.2960/J.v36.m568.

Stenborg, T. (Apr. 1969). "Studies of the Internal Drainage of Glaciers". In: *Geografiska Annaler: Series A, Physical Geography* 51.1-2, pp. 13–41. DOI: 10.1080/04353676.1969.11879788.

Stevens, L. A., M. D. Behn, S. B. Das, I. Joughin, B. P. Y. Noël, M. R. van den Broeke, et al. (Nov. 2016). "Greenland Ice Sheet flow response to runoff variability". In: *Geophysical Research Letters* 43.21, pp. 295–11. DOI: 10.1002/2016GL070414.

Stone, D. B. and G. K. Clarke (Apr. 1996). "In situ measurements of basal water quality and pressure as an indicator of the character of subglacial drainage system". In: *Hydrological Processes* 10.4, pp. 615–628. DOI: 10.1002/(sici)1099-1085(199604)10:4<615::aid-hyp395>3.0.co;2-m.

Straneo, F. and C. Cenedese (Jan. 2015). "The Dynamics of Greenland's Glacial Fjords and Their Role in Climate". In: *Annual Review of Marine Science* 7.1, pp. 89–112. DOI: 10.1146/annurev-marine-010213-135133.

Straneo, F., G. S. Hamilton, D. A. Sutherland, L. A. Stearns, F. Davidson, M. O. Hammill, et al. (Mar. 2010). "Rapid circulation of warm subtropical waters in a major glacial fjord in East Greenland". In: *Nature Geoscience* 3.3, pp. 182–186. DOI: 10.1038/ngeo764.

Straneo, F., R. G. Curry, D. A. Sutherland, G. S. Hamilton, C. Cenedese, K. Våge, et al. (May 2011). "Impact of fjord dynamics and glacial runoff on the circulation near Helheim Glacier". In: *Nature Geoscience* 4.5, pp. 322–327. DOI: 10.1038/ngeo1109.

Straneo, F., D. A. Sutherland, D. Holland, C. Gladish, G. S. Hamilton, H. L. Johnson, et al. (Nov. 2012). "Characteristics of ocean waters reaching greenland's glaciers". In: *Annals of Glaciology* 53.60, pp. 202–210. DOI: 10.3189/2012AoG60A059.

Straneo, F. and P. Heimbach (Dec. 2013). *North Atlantic warming and the retreat of Greenland's outlet glaciers*. DOI: 10.1038/nature12854.

Straneo, F., D. A. Sutherland, L. Stearns, G. Catania, P. Heimbach, T. Moon, et al. (Mar. 2019). *The case for a sustained Greenland Ice sheet-Ocean Observing System (GrIOOS)*. DOI: 10.3389/fmars.2019.00138.

Sugiyama, S., P. Skvarca, N. Naito, H. Enomoto, S. Tsutaki, K. Tone, et al. (Sept. 2011). "Ice speed of a calving glacier modulated by small fluctuations in basal water pressure". In: *Nature Geoscience* 4.9, pp. 597–600. DOI: 10.1038/ngeo1218.

Sundal, A. V., A. Shepherd, P. Nienow, E. Hanna, S. Palmer, and P. Huybrechts (Jan. 2011). "Melt-induced speed-up of Greenland ice sheet offset by efficient subglacial drainage". In: *Nature* 469.7331, pp. 521–524. DOI: 10.1038/nature09740.

Sutherland, D. A., R. H. Jackson, C. Kienholz, J. M. Amundson, W. P. Dryer, D. Duncan, et al. (July 2019). "Direct observations of submarine melt and subsurface geometry at a tidewater glacier". In: *Science* 365.6451, pp. 369–374. DOI: 10.1126/science.aax3528.

Sutherland, D. A. and R. S. Pickart (2008). "The East Greenland Coastal Current: Structure, variability, and forcing". In: DOI: 10.1016/j.pocean.2007.09.006.

Tedesco, M. and X. Fettweis (Dec. 2012). "21st century projections of surface mass balance changes for major drainage systems of the Greenland ice sheet". In: *Environmental Research Letters* 7.4, p. 045405. DOI: 10.1088/1748-9326/7/4/045405.

Tedesco, M., J. Box, J. Cappelen, R. S. Fausto, X. Fettweis, K. Hansen, et al. (2017). *Greenland Ice Sheet [in Arctic Report Card 2017]*. Tech. rep. URL: ftp://ftp.oar.noaa.gov/arctic/documents/ArcticReportCard_full_report2017.pdf.

Tedesco, M. and X. Fettweis (Apr. 2020). "Unprecedented atmospheric conditions (1948-2019) drive the 2019 exceptional melting season over the Greenland ice sheet". In: *Cryosphere* 14.4, pp. 1209–1223. DOI: 10.5194/tc-14-1209-2020.

Tedstone, A. J., P. W. Nienow, A. J. Sole, D. W. F. Mair, T. R. Cowton, I. D. Bartholomew, et al. (Dec. 2013). "Greenland ice sheet motion insensitive to exceptional meltwater forcing." In: *Proceedings of the National Academy of Sciences of the United States of America* 110.49, pp. 19719–24. DOI: 10.1073/pnas.1315843110.

Tedstone, A. J. and N. S. Arnold (Aug. 2012). "Automated remote sensing of sediment plumes for identification of runoff from the Greenland ice sheet". In: *Journal of Glaciology* 58.210, pp. 699–712. DOI: 10.3189/2012JoG11J204.

Tedstone, A. J., P. W. Nienow, N. Gourmelen, A. Dehecq, D. Goldberg, and E. Hanna (Oct. 2015). "Decadal slowdown of a land-terminating sector of the Greenland

Ice Sheet despite warming". In: *Nature* 526.7575, pp. 692–695. DOI: 10.1038/nature15722.

Tedstone, A. J. (2015). "Hydrological controls on Greenland Ice Sheet motion". PhD thesis. University of Edinburgh.

Thomas, R. and M. Studinger (2010). *[07/10/2020]: Pre-IceBridge ATM L2 Icessn Elevation, Slope, and Roughness, Version 1. Data archived at National Snow and Ice Data Center*. Boulder, Colorado USA. DOI: https://doi.org/10.5067/6C6WA3R918HJ.

Thomas, R., T. Akins, B. Csatho, M. Fahnestock, P. Gogineni, C. Kim, et al. (July 2000). "Mass balance of the Greenland Ice Sheet at high elevations". In: *Science* 289.5478, pp. 426–428. DOI: 10.1126/science.289.5478.426.

Thomas, R. H., B. M. Csathó, S. Gogineni, K. C. Jezek, and K. Kuivinen (Jan. 1998). "Thickening of the western part of the Greenland ice sheet". In: *Journal of Glaciology* 44.148, pp. 653–658. DOI: 10.3189/S002214300000215X.

Thomas, R. H. (Dec. 2001). "Program for Arctic Regional Climate Assessment (PARCA): Goals, key findings, and future directions". In: *Journal of Geophysical Research: Atmospheres* 106.D24, pp. 33691–33705. DOI: 10.1029/2001JD900042.

Thomas, R. H., W. Abdalati, E. Frederick, W. B. Krabill, S. Manizade, and K. Steffen (2003). "Investigation of surface melting and dynamic thinning on Jakobshavn Isbræ, Greenland". In: *Journal of Glaciology* 49.165, pp. 231–239. DOI: 10.3189/172756503781830764.

Thomas, R. H. (Sept. 2004). "Force-perturbation analysis of recent thinning and acceleration of Jakobshavn Isbræ, Greenland". In: *Journal of Glaciology* 50.168, pp. 57–66. DOI: 10.3189/172756504781830321.

Thomason, J. F. and N. R. Iverson (2008). "A laboratory study of particle ploughing and pore-pressure feedback: A velocity-weakening mechanism for soft glacier beds". In: *Journal of Glaciology* 54.184, pp. 169–181. DOI: 10.3189/002214308784409008.

Todd, J., P. Christoffersen, T. Zwinger, P. Råback, N. Chauché, D. Benn, et al. (Mar. 2018). "A Full-Stokes 3-D Calving Model Applied to a Large Greenlandic Glacier". In: *Journal of Geophysical Research: Earth Surface* 123.3, pp. 410–432. DOI: 10.1002/2017JF004349.

Todd, J., P. Christoffersen, T. Zwinger, P. Räback, and D. I. Benn (June 2019). "Sensitivity of a calving glacier to ice-ocean interactions under climate change: New insights from a 3-d full-stokes model". In: *Cryosphere* 13.6, pp. 1681–1694. DOI: 10.5194/tc-13-1681-2019.

Truffer, M., W. Harrison, and R. March (Sept. 2005). "Record negative glacier balances and low velocities during the 2004 heatwave in Alaska, USA: implications for the interpretation of observations by Zwally and others in Greenland". In: *Journal of Glaciology* 51.175, pp. 663–664. DOI: 10.3189/172756505781829016.

Truffer, M. and R. J. Motyka (Mar. 2016). *Where glaciers meet water: Subaqueous melt and its relevance to glaciers in various settings*. DOI: 10.1002/2015RG000494.

Trusel, L. (2018). "Nonlinear rise in Greenland runoff in response to post-industrial Arctic warming". In: *Nature* 564, pp. 104–108.

Tsutaki, S., K. Fujita, T. Nuimura, A. Sakai, S. Sugiyama, J. Komori, et al. (Oct. 2019). "Contrasting thinning patterns between lake- And land-terminating glaciers in the Bhutanese Himalaya". In: *The Cryosphere* 13.10, pp. 2733–2750. DOI: 10.5194/tc-13-2733-2019.

Van De Wal, R. S., W. Boot, C. J. Smeets, H. Snellen, M. R. Van Den Broeke, and J. Oerlemans (Aug. 2012). "Twenty-one years of mass balance observations along the

6515 K-transect, West Greenland". In: *Earth System Science Data* 4.1, pp. 31–35. DOI:
6516 10.5194/essd-4-31-2012.
6517 van den Broeke, M., J. Bamber, J. Ettema, E. Rignot, E. Schrama, W. J. van de Berg,
6518 et al. (Nov. 2009). "Partitioning Recent Greenland Mass Loss". In: *Science* 326.5955,
6519 pp. 984–986. DOI: 10.1126/science.1178176.
6520 van den Broeke, M. R., E. M. Enderlin, I. M. Howat, P. Kuipers Munneke, B. P. Y.
6521 Noël, W. J. van de Berg, et al. (Sept. 2016). "On the recent contribution of the
6522 Greenland ice sheet to sea level change". In: *The Cryosphere* 10.5, pp. 1933–1946.
6523 DOI: 10.5194/tc-10-1933-2016.
6524 Van Der Veen, C. J. (Feb. 1998). "Fracture mechanics approach to penetration of surface
6525 crevasses on glaciers". In: *Cold Regions Science and Technology* 27.1, pp. 31–47. DOI:
6526 10.1016/S0165-232X(97)00022-0.
6527 Van Der Veen, (1996). "Tidewater calving". In: *Journal of Glaciology* 42.141, pp. 375–
6528 385. DOI: 10.3189/s0022143000004226.
6529 van der Veen, C. J. (Dec. 2001). "Greenland ice sheet response to external forcing".
6530 In: *Journal of Geophysical Research: Atmospheres* 106.D24, pp. 34047–34058. DOI:
6531 10.1029/2001JD900032.
6532 van der Veen, C. J. (Mar. 2002). "Calving glaciers". In: *Progress in Physical Geography:*
6533 *Earth and Environment* 26.1, pp. 96–122. DOI: 10.1191/0309133302pp327ra.
6534 van der Veen, C. J. (Jan. 2007). "Fracture propagation as means of rapidly transferring
6535 surface meltwater to the base of glaciers". In: *Geophysical Research Letters* 34.1,
6536 p. L01501. DOI: 10.1029/2006GL028385.
6537 van de Wal, R. S. W., W. Boot, M. R. van den Broeke, C. J. P. P. Smeets, C. H. Reijmer,
6538 J. J. A. Donker, et al. (July 2008). "Large and Rapid Melt-Induced Velocity Changes
6539 in the Ablation Zone of the Greenland Ice Sheet". In: *Science* 321.5885, pp. 111–113.
6540 DOI: 10.1126/science.1158540.
6541 van de Wal, R. S. W., C. J. P. P. Smeets, W. Boot, M. Stoffelen, R. van Kampen, S. H.
6542 Doyle, et al. (Apr. 2015). "Self-regulation of ice flow varies across the ablation area
6543 in south-west Greenland". In: *The Cryosphere* 9.2, pp. 603–611. DOI: 10.5194/tc-
6544 9-603-2015.
6545 van de Wal, R. and J. Oerlemans (Jan. 1994). "An energy balance model for the
6546 Greenland ice sheet". In: *Global and Planetary Change* 9.1-2, pp. 115–131. DOI:
6547 10.1016/0921-8181(94)90011-6.
6548 Van Tricht, K., S. Lhermitte, J. T. Lenaerts, I. V. Gorodetskaya, T. S. L'Ecuyer, B.
6549 Noël, et al. (Jan. 2016). "Clouds enhance Greenland ice sheet meltwater runoff". In:
6550 *Nature Communications* 7.1, pp. 1–9. DOI: 10.1038/ncomms10266.
6551 Vaughan, D. G., J. C. Comiso, I. Allison, J. Carrasco, G. Kaser, R. Kwok, et al. (2013).
6552 *Observations: Cryosphere. In: Climate Change 2013: The Physical Sci-ence Basis.*
6553 *Contribution of Working Group I to the Fifth Assessment Report of the Intergovern-*
6554 *mental Panel on Climate Change Coordinating Lead Authors: Lead Authors.* Tech.
6555 rep.
6556 Velicogna, I., T. C. Sutterley, and M. R. van den Broeke (Nov. 2014). "Regional ac-
6557 celeration in ice mass loss from Greenland and Antarctica using GRACE time-
6558 variable gravity data". In: *Geophysical Research Letters* 41.22, pp. 8130–8137. DOI:
6559 10.1002/2014GL061052.
6560 Velicogna, I. and J. Wahr (Sept. 2006). "Acceleration of Greenland ice mass loss in
6561 spring 2004". In: *Nature* 443.7109, pp. 329–331. DOI: 10.1038/nature05168.

Vieli, A., J. Jania, H. Blatter, and M. Funk (2004). "Short-term velocity variations on Hansbreen, a tidewater glacier in Spitsbergen". In: *Journal of Glaciology* 50.170, pp. 389–398. DOI: 10.3189/172756504781829963.

Vijay, S., S. A. Khan, A. Kusk, A. M. Solgaard, T. Moon, and A. A. Bjørk (Feb. 2019). "Resolving Seasonal Ice Velocity of 45 Greenlandic Glaciers With Very High Temporal Details". In: *Geophysical Research Letters* 46.3, pp. 1485–1495. DOI: 10.1029/2018GL081503.

Vizcaino, M., U. Mikolajewicz, F. Ziemen, C. B. Rodehacke, R. Greve, and M. R. Broeke (May 2015). "Coupled simulations of Greenland Ice Sheet and climate change up to A.D. 2300". In: *Geophysical Research Letters* 42.10, pp. 3927–3935. DOI: 10.1002/2014GL061142.

Wagner, T. J., F. Straneo, C. G. Richards, D. A. Slater, L. A. Stevens, S. B. Das, et al. (Mar. 2019). "Large spatial variations in the flux balance along the front of a Greenland tidewater glacier". In: *Cryosphere* 13.3, pp. 911–925. DOI: 10.5194/tc-13-911-2019.

Walder, J. and B. Hallet (1979). "Geometry of Former Subglacial Water Channels and Cavities". In: *Journal of Glaciology* 23.89, pp. 335–346. DOI: 10.3189/s0022143000029944.

Walder, J. S. (1982). "Stability of Sheet Flow of Water Beneath Temperate Glaciers and Implications for Glacier Surging". In: *Journal of Glaciology* 28.99, pp. 273–293. DOI: 10.3189/s0022143000011631.

Walder, J. S. (1986). "Hydraulics of Subglacial Cavities". In: *Journal of Glaciology* 32.112, pp. 439–445. DOI: 10.3189/s0022143000012156.

Walder, J. S. and A. Fowler (1994). "Channelized subglacial drainage over a deformable bed". In: *Journal of Glaciology* 40.134, pp. 3–15. DOI: 10.3189/s0022143000003750.

Walsh, K. M., I. M. Howat, Y. Ahn, and E. M. Enderlin (2012). "Changes in the marine-terminating glaciers of central east Greenland, 2000-2010". In: *The Cryosphere* 6, pp. 211–220. DOI: 10.5194/tc-6-211-2012.

Wang, W., J. Li, and H. J. Zwally (Sept. 2012). "Dynamic inland propagation of thinning due to ice loss at the margins of the Greenland ice sheet". In: *Journal of Glaciology* 58.210, pp. 734–740. DOI: 10.3189/2012JoG11J187.

Warren, C., D. Benn, V. Winchester, and S. Harrison (2001). "Buoyancy-driven lacustrine calving, Glaciar Nef, Chilean Patagonia". In: *Journal of Glaciology* 47.156, pp. 135–146. DOI: 10.3189/172756501781832403.

Warren, C. R. and N. F. Glasser (1992). "Contrasting Response of South Greenland Glaciers to Recent Climatic Change". In: *Arctic and Alpine Research* 24.2. DOI: 10.1080/00040851.1992.12002937.

Weertman, J. (1957). "On the Sliding of Glaciers". In: *Journal of Glaciology* 3.21, pp. 33–38. DOI: 10.3189/s0022143000024709.

Weertman, J. (1964). "The Theory of Glacier Sliding". In: *Journal of Glaciology* 5.39, pp. 287–303. DOI: 10.3189/s0022143000029038.

Weertman, J. (Feb. 1972). "General theory of water flow at the base of a glacier or ice sheet". In: *Reviews of Geophysics* 10.1, p. 287. DOI: 10.1029/RG010i001p00287.

Weertman, J. (1974). "Stability of the Junction of an Ice Sheet and an Ice Shelf". In: *Journal of Glaciology* 13.67, pp. 3–11. DOI: 10.3189/s0022143000023327.

Werder, M. A., I. J. Hewitt, C. G. Schoof, and G. E. Flowers (Dec. 2013). "Modeling channelized and distributed subglacial drainage in two dimensions". In: *Journal of Geophysical Research: Earth Surface* 118.4, pp. 2140–2158. DOI: 10.1002/jgrf.20146.

Williams, J. J., N. Gourmelen, and P. Nienow (Dec. 2020). "Dynamic response of the Greenland ice sheet to recent cooling". In: *Scientific Reports* 10.1, pp. 1–11. DOI: 10.1038/s41598-020-58355-2.

Williams, J. J., N. Gourmelen, and P. Nienow (Mar. 2021). "Complex multi-decadal ice dynamical change inland of marine-terminating glaciers on the Greenland Ice Sheet". In: *Journal of Glaciology*, pp. 1–14. DOI: 10.1017/jog.2021.31.

Williamson, A. G., A. F. Banwell, I. C. Willis, and N. S. Arnold (Sept. 2018). "Dual-satellite (Sentinel-2 and Landsat 8) remote sensing of supraglacial lakes in Greenland". In: *Cryosphere* 12.9, pp. 3045–3065. DOI: 10.5194/tc-12-3045-2018.

Willis, M. J., W. Zheng, W. J. Durkin, M. E. Pritchard, J. M. Ramage, J. A. Dowdeswell, et al. (Nov. 2018). "Massive destabilization of an Arctic ice cap". In: *Earth and Planetary Science Letters* 502, pp. 146–155. DOI: 10.1016/j.epsl.2018.08.049.

Wood, M., E. Rignot, I. Fenty, D. Menemenlis, R. Millan, M. Morlighem, et al. (Aug. 2018). "Ocean-Induced Melt Triggers Glacier Retreat in Northwest Greenland". In: *Geophysical Research Letters* 45.16, pp. 8334–8342. DOI: 10.1029/2018GL078024.

Woodcock, C. E., R. Allen, M. Anderson, A. Belward, R. Bindschadler, W. Cohen, et al. (May 2008). *Free access to landsat imagery*. DOI: 10.1126/science.320.5879.1011a.

Wright, P. J., J. T. Harper, N. F. Humphrey, and T. W. Meierbachtol (June 2016). "Measured basal water pressure variability of the western Greenland Ice Sheet: Implications for hydraulic potential". In: *Journal of Geophysical Research: Earth Surface* 121.6, pp. 1134–1147. DOI: 10.1002/2016JF003819.

Wulder, M. A., J. C. White, C. E. Woodcock, A. S. Belward, W. B. Cohen, E. A. Fosnight, et al. (Nov. 2016). "The global Landsat archive: Status, consolidation, and direction". In: *Remote Sensing of Environment* 185, pp. 271–283. DOI: 10.1016/J.RSE.2015.11.032.

Wulder, M. A., T. R. Loveland, D. P. Roy, C. J. Crawford, J. G. Masek, C. E. Woodcock, et al. (May 2019). "Current status of Landsat program, science, and applications". In: *Remote Sensing of Environment* 225, pp. 127–147. DOI: 10.1016/j.rse.2019.02.015.

Xu, Y., E. Rignot, I. Fenty, D. Menemenlis, and M. M. Flexas (Sept. 2013). "Subaqueous melting of Store Glacier, west Greenland from three-dimensional, high-resolution numerical modeling and ocean observations". In: *Geophysical Research Letters* 40.17, pp. 4648–4653. DOI: 10.1002/grl.50825.

Zheng, W., M. E. Pritchard, M. J. Willis, and L. A. Stearns (Dec. 2019). "The Possible Transition From Glacial Surge to Ice Stream on Vavilov Ice Cap". In: *Geophysical Research Letters* 46.23, pp. 13892–13902. DOI: 10.1029/2019GL084948.

Zhu, Z., M. A. Wulder, D. P. Roy, C. E. Woodcock, M. C. Hansen, V. C. Radeloff, et al. (Apr. 2019). "Benefits of the free and open Landsat data policy". In: *Remote Sensing of Environment* 224, pp. 382–385. DOI: 10.1016/j.rse.2019.02.016.

Zwally, H. J., W. Abdalati, T. Herring, K. Larson, J. Saba, and K. Steffen (July 2002). "Surface melt-induced acceleration of Greenland ice-sheet flow". In: *Science* 297.5579, pp. 218–222. DOI: 10.1126/science.1072708.

Zwally, H. J., J. Li, A. C. Brenner, M. Beckley, H. G. Cornejo, J. DiMarzio, et al. (Sept. 2011). "Greenland ice sheet mass balance: distribution of increased mass loss with climate warming; 2003–07 versus 1992–2002". In: *Journal of Glaciology* 57.201, pp. 88–102. DOI: 10.3189/002214311795306682.

Williams et al., 2020, *Scientific Reports*

SCIENTIFIC REPORTS

nature research

OPEN

Dynamic response of the Greenland ice sheet to recent cooling

Joshua J. Williams*, Noel Gourmelen & Peter Nienow

The subglacial hydrological system critically controls ice motion at the margins of the Greenland Ice Sheet. However, over multi-annual timescales, the net impact of hydro-dynamic coupling on ice motion remains poorly understood. Here, we present annual ice velocities from 1992–2019 across a ~10,600 km^2 land-terminating area of southwest Greenland. From the early-2000s through to ~2012, we observe a slowdown in ice motion in response to increased surface melt, consistent with previous research. From 2013 to 2019 however, we observe an acceleration in ice motion coincident with atmospheric cooling and a ~15% reduction in mean surface melt production relative to 2003–2012. We find that ice velocity speed-up is greater in marginal areas, and is strongly correlated with ice thickness. We hypothesise that under thinner ice, increases in basal water pressure offset a larger proportion of the ice overburden pressure, leading to reduced effective pressure and thus greater acceleration when compared to thicker ice further inland. Our findings indicate that hydro-dynamic coupling provides the major control on changes in ice motion across the ablation zone of land terminating margins of the Greenland Ice Sheet over multi-annual timescales.

The Greenland Ice Sheet (GrIS) has lost mass at an accelerating rate over the past two decades, with persistent mass loss observed since 1998[1–5]. Approximately 52% of this mass loss can be attributed to surface melt[6], which increased in the late 2000s and early 2010s to levels unprecedented since at least 1900[7]. Increases in surface melt have been driven by increasing air temperatures over Greenland since the mid-1980s[7,8] and variability in cloud cover, both of which are forced by larger scale circulation patterns[9–13]. Increased cloud-cover warms the ice sheet interior through the trapping of longwave radiation[14,15], whereas a reduction in summer cloud cover since 1995 has driven enhanced melt in the ablation zone through increasing the shortwave flux[10,16]. Moreover, the seasonal migration of the snowline causes the exposure of dark bare-ice, decreasing the albedo of the ice surface and reducing meltwater re-freezing, further driving surface melt and runoff[17]. Alongside changes in surface mass balance, roughly 48% of mass loss is due to increases in ice discharge through Greenland's marine terminating outlet glaciers[6]. However, the dynamic response of the ice sheet to variability in surface mass balance and ocean conditions remains a large source of uncertainty in projecting future sea level rise[18].

Land-terminating margins are isolated from processes acting at the ice/ocean boundary, and thus provide ideal study sites for investigating how the ice-sheet responds to atmospheric, and thus surface melt forcing[19,20]. This is particularly prescient as the largely land-terminating margin in South West Greenland exhibits a strong and sustained negative mass balance[21,22], and is projected to make a greater contribution to sea level rise with continued atmospheric warming and associated increases in surface runoff[23].

Each summer, surface meltwaters drain from the ice-sheet surface to the bed via moulins and crevasses[24–27] where their impact on friction at the ice-bed interface is fundamentally important in controlling ice velocity[28,29]. Whilst initial research postulated that as these seasonal meltwaters drain to the base of the ice sheet, they would pressurise the basal hydrological system, reduce friction at the bed and so enhance glacier sliding[30], other studies have argued that variability in meltwater input, rather than the volume itself, is more critical for driving ice acceleration[31,32].

Both short-term and sustained increases in surface meltwater delivery to the glacier bed drive an increase in basal water pressure above the ice overburden pressure, reducing friction at the bed and so forcing a transient acceleration[32–34]. These inputs force a morphological switch from an inefficient, distributed subglacial drainage system to an efficient, channelised system when and where subglacial discharge is sufficiently turbulent to open subglacial channels[26,32,35,36]. This introduces a negative feedback whereby as the drainage system capacity increases in response to enhanced meltwater input, basal water pressures decrease as subglacial channels allow the efficient evacuation of subglacial water[26,37], forcing a deceleration of the ice later in the melt season[27,32,38].

School of Geosciences, University of Edinburgh, Edinburgh, EH8 9XP, UK. *email: j.j.williams-4@sms.ed.ac.uk

More recently, research has focused on whether this hydro-dynamical coupling of ice flow at land-terminating margins results in a long-term trend in ice-motion in response to long-term increases in surface melt[39,40]. Multi-annual ice velocity slowdowns in southwest Greenland since the early-mid 2000s have been reported by numerous studies based on both GPS data[41–43] and large-scale satellite-derived observations[40,44]. Ice velocities from GPS stations along a transect in Southwest Greenland, extending ~150 km inland from the margin between surface elevations of 340 m and 1850 m above sea level (a.s.l), show a 10% average slowdown from 1991–2007[41,42], coincident with increasing surface melt, and GPS data at North Lake show a slowdown of $-0.9 \pm 1.1\,m\,yr^{-2}$ from 2006–2014[43]. Over a much larger 8000 km^2 region of Southwest Greenland, Tedstone *et al.*[40] showed that ice velocity had decreased by 12% in 2007–14 compared to 1985–94, despite a 50% increase in surface meltwater production, with ice velocity decreasing by 1.5 m yr^2 between 2002 and 2014. This long-term slowdown is attributed to the expansion of subglacial channels, both up-glacier and in their dimensions, as a result of the long-term increase in surface melt, enhancing the drainage of waters from the more extensive distributed component of the subglacial drainage system, thus reducing regional basal water pressures and so ice velocities[38,40]. The distributed component of the subglacial drainage system encompasses varying degrees of connectivity, and it is hypothesised that the reduction of basal water pressures in the weakly-connected areas of the drainage system specifically[27,39] are critical to the observed slow-down as their recharge is slow (on the order of years[39]), resulting in widespread and extended depressurisation and so increased basal traction.

Since the record surface melt in 2012[3], a period of relative stability in mass balance[45] has been observed across Greenland, with 2017 having the lowest maximum surface melt extent since 1996[46]. This stability is coincident with positive Arctic and North Atlantic Oscillations, promoting cyclonic conditions thereby reducing incoming solar radiation and enhancing precipitation[46]. Given that the proposed hydro-dynamic mechanism for a long-term velocity slowdown requires a continual increase in surface melt[39,40], it would be expected that ice motion would respond to a sustained change in surface run-off and begin to stabilise or accelerate as surface melt decreases and the distributed subglacial hydrological system re-pressurises. Under reduced surface melt forcing, we would expect the up-glacier extent of efficient subglacial channels to decrease, allowing regions of the distributed drainage system that were, in previous years, drained by efficient channels to re-pressurise through the gradual recharge of meltwater via basal melting. Numerous GPS data show that this process occurs on a seasonal timescale, whereby following the deceleration of ice motion to a minimum in the late melt season, measured ice velocities show a gradual increase over the following winter[41,47,48]; this process has not however been observed to-date on a multi-annual timescale. This study therefore extends the West Greenland ice velocity time series, both spatially and temporally, in order to investigate how ice motion has responded to recent reductions in surface melt forcing, with the ultimate aim of improving our understanding of the mechanisms driving ice sheet motion.

Here we present observations of ice velocity from 1992–2019 across a predominantly land-terminating area of ~10,600 km^2 in SW Greenland, extending ~300 km along the margin and ~50 km inland to an elevation of 1300 m. Our study region is considerably larger than that of Tedstone *et al.*[41], extending a further ~120 km to the south. We apply feature tracking to 2665 pairs of Landsat scenes, separated by 352–384 days, over 14 path/row combinations. Subsequently, we derive robust ice velocity and uncertainty estimates[49,50] for periods of 1, 2 and 4 years to construct a time series from 1992 to 2019, and assess the spatial distribution of velocity change between 1992–2003 and 2003–2012, and 2010–2012 and 2017–2019. Finally, we assess the implications of our results for future land-terminating ice-sheet motion in a warming climate in light of the dynamic response of the study region to the recent variability in meltwater forcing.

Results

Spatial pattern of velocity change. Ice velocity displays a clear slowdown across the study site (Fig. 1A) between the periods 1992–2003 and 2003–2012, with 93.1% (9895 km^2) of the region exhibiting reduced velocity in the latter period, and a mean regional slowdown of ~15.3% (Fig. 2A). The slowdown is greatest at lower ice thicknesses and decreases in magnitude inland as surface elevation and ice thickness increase (Fig. 2C), although deceleration characterises all ice thicknesses assessed and extends further inland than in previous work[40]. We would expect this to be the case as at higher elevations further inland, lower surface melt rates, thicker ice and shallower surface slopes slow channel growth, allowing subglacial water pressures to remain higher in smaller subglacial channels[26,49,50].

Subsequently, we observe a mean region-wide acceleration of ~7.9% between the periods 2010–2012 and 2017–2019 (Fig. 1B), with 89.6% (8218 km^2) of this second change map exhibiting increased velocity during the latter period (Fig. 2B). This acceleration in ice motion is proportionally largest at lower ice thicknesses and decreases as ice thickness increases but is observed across all ice thicknesses studied (Fig. 2D).

Ice velocity and surface melt/runoff time series. To investigate changes in ice motion (Fig. 3A), we follow recent work by assessing anomalies in annual velocity (see SI) whereby only pixels common to all the velocity fields presented in the time series are used in the computation of the median velocity anomalies[50]. Most of the common points fall between 600 m and 1000 m elevation (a.s.l.) due to the hypsometry of our study region (Fig. 4), although we observe >50% coverage in each 100 m elevation band between 100 m and 900 m. In total, we compute velocity anomalies across 71703 common measurements (4130 km^2), an order of magnitude greater than previous work[40] (their Fig. 2C).

Over the time period from 1992 to 2019, the ice velocity anomaly time series reveals a mean slowdown of $-0.72 \pm 0.08\,m\,yr^{-2}$ ($R^2 = 0.70$, $p < 0.01$). The quality of the fit is further improved via break point analysis (see SI) which recognises three statistically distinct periods based on the pattern of velocity changes ($R^2 = 0.85$ (Fig. 3A)). Between 1992 and 2003, we observe a period exhibiting no significant trend ($-0.03 \pm 0.23\,m\,yr^{-2}$, $p = 0.48$). A substantial slowdown of $-1.64 \pm 0.37\,m\,yr^{-2}$ ($p < 0.05$), starting around 2003 (but which could range from

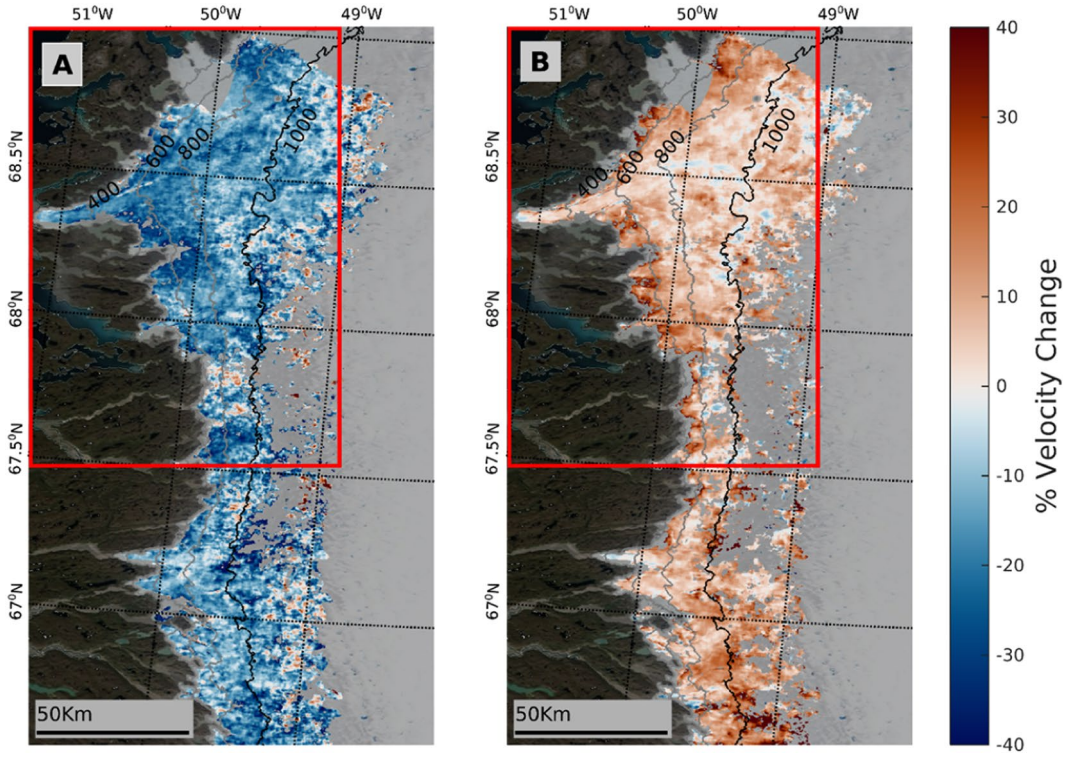

Figure 1. Spatial change in ice velocity (%) between the **(A)** 2003–2012 and 1992–2003 and **(B)** 2017–2019 and 2010–2012 reference periods. Data above 1300 m a.s.l. are filtered out in order to remove spurious points that characterise higher elevations. The red rectangle denotes the region studied in Tedstone et al.[40]. Ice surface elevation contours (grey lines) are from Howat et al.[88], with the 1000 m contour bold to make clear the area across which the velocity time series was calculated (Fig. 3). The two tidewater glaciers to the north of the study region are masked out as they are undergoing different dynamic processes to the rest of the region. The base image is a MODIS (Terra) corrected reflectance image from EOSDIS NASA Worldview (https://worldview.earthdata.nasa.gov/).

2002–2004 due to a gap in our data), occurs until 2012, after which the most recent period of ice motion exhibits a significant increasing trend ($0.58 \pm 0.37\,m\,yr^{-2}$, $p < 0.05$).

We use the regional climate model MAR v3.10[7,9] to calculate the mean surface melt production anomaly during the three distinct periods identified in our ice velocity anomaly time series; 1992–2003, 2003–2012, and 2012–2019 (Fig. 3B). Mean surface melt production anomalies across our study region rose by ~30% from $-0.18\,m\,yr^{-1}$ to $0.45\,m\,yr^{-1}$ (w.e.) (~$2.15\,m\,yr^{-1}$ to ~$2.77\,m\,yr^{-1}$ (w.e.)) between 1992–2003 and 2003–2012. Following this period of sustained higher surface melt production, a ~15% decrease to $0.06\,m\,yr^{-1}$ (~$2.39\,m\,yr^{-1}$) is observed for 2012–2019, when compared to the 2003–2012 mean. The period of ice velocity decrease therefore coincides with a period of enhanced ice surface melt, while rates of constant and accelerating ice velocity occur during periods of lower surface melt.

Previous work has argued that there is a significant relationship between antecedent surface melt production and ice velocity[40]. More recent work however suggests that this may be a statistical construct[43], whereby as more antecedent melt years are included in the average value, R^2 tends further towards 1 (Supplementary Fig. 12) as the data becomes increasingly smoothed and the individual points become less independent. With only one period of sustained slowdown, we are unable to test whether ice velocity slowdown is in response to a gradual increase in surface melt or to the passing of some surface melt threshold. Moreover, the response times of ice velocity to increases and decreases in surface melt forcing appear to differ – surface melt displays a long-term increasing trend from the early-mid 1990s before ice velocities begin to decrease in ~2003, whereas ice velocities stabilise and begin accelerating almost instantly in response to the large reduction in surface melt forcing from 2013 onwards. To investigate the impact of year-to-year variability in surface melt production on year-to-year velocity, we calculate a linear regression through detrended velocity and melt production anomaly time series (Fig. S13), which gives an R^2 of 0.08 ($p = 0.11$), indicating that there is no significant relationship between annual ice velocity and annual runoff, consistent with earlier work[41,43,48].

Discussion

Changes in ice thickness and surface gradient can contribute to changes in ice motion through their associated impacts on driving stress. Thinning at the margins of the Greenland Ice Sheet has been observed since the early 1990s[2], and from 1992–1998, the South West Greenland land-terminating sector thinned by ~0.02–0.4 $m\,yr^{-1}$ [51,52]. A period of stability characterised the late 1990s and early to mid-2000s[52], followed by rapid thinning (~

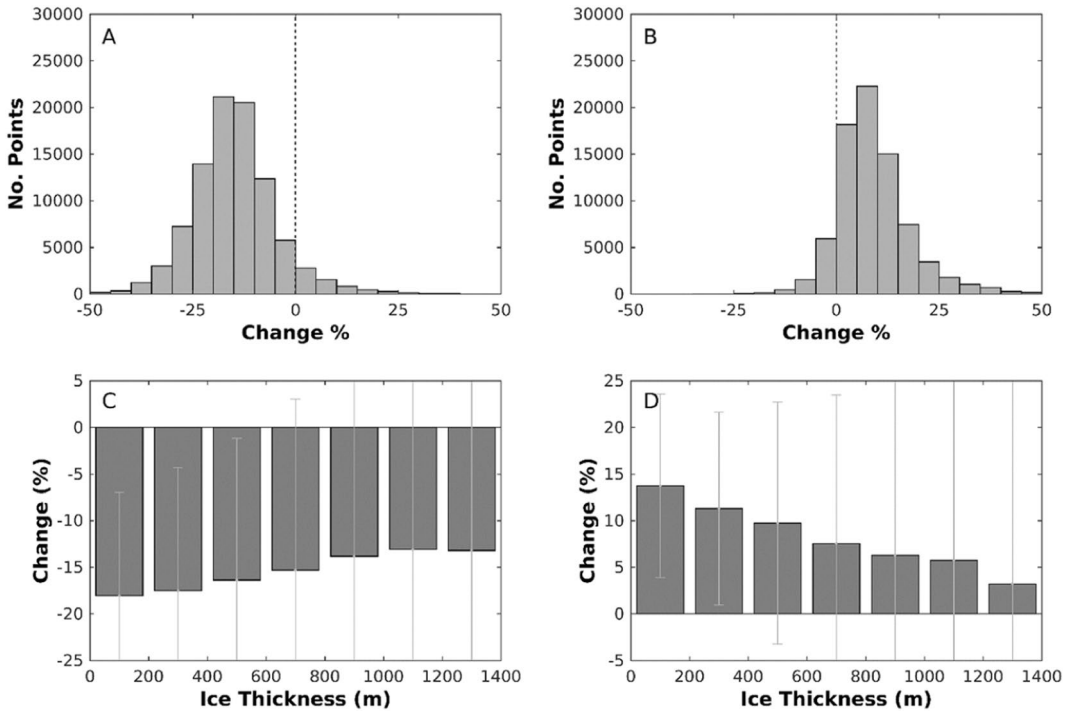

Figure 2. Histogram of ice velocity change across the study region and percentage change across ice thicknesses for the two changemaps displayed in Fig. 1. Plots A and C relate to Fig. 1A (2003/2012–1992/2003), and plots B and D relate to Fig. 1B (2017/2019–2010/2012). **(A)** Percentage change in ice velocities across the region displayed in Fig. 1A in 5% bins. **(B)** Percentage change in ice velocities across the region displayed in Fig. 1B in 5% bins. **(C)** Median percentage change in each 200 m ice thickness band between 0 m and 1400 m for the changemap displayed in Fig. 1A. (**D**) Median percentage change in each 200 m ice thickness band between 0 m and 1400 m for the changemap displayed in Fig. 1B. The error bars display the interquartile range. Ice surface elevation data is from Howat *et al.*[88], and ice thickness data are from Morlighem *et al.*[89].

1–1.5 m yr^{-1}). Whilst some datasets assume a constant thinning of a similar magnitude through to 2014[53], recent work points to a maximum thinning rate in 2012, after which thinning has continued at a more moderate rate[54], albeit with differences in thinning trends between drainage basins[52,55]. Prior modelling work in our study region[40] indicates that changes in driving stress due to thinning could only explain 17–33% of the slowdown signal beyond 10 km from the ice-margin, and none of the signal beyond 50 km. This modelling work applied 20 m of thinning over 30 years, equating to a thinning rate of −0.66 m yr^{-1}. Outside of the period 2007–2011, there is no evidence for thinning rates greater than this during our study period[51–53,56], and we thus do not believe that thinning rates could be responsible for more slowdown than already reported in Tedstone *et al.*[40]. Moreover, continued thinning from 2012 would be expected to continue to reduce ice motion, which contrasts with the acceleration in ice velocity observed during this period. As such, these findings imply that most of the ice velocity signal is controlled by processes operating at the ice-bed interface.

The subglacial hydrological system exerts a critical control on ice motion at land-terminating margins of the Greenland Ice Sheet[38,57]. Our results provide support for a previously postulated mechanism[40], whereby under a sustained multi-annual increase in surface meltwater production, the subglacial drainage system is characterised by both a gradual increase in the extent of channelisation, as well as the time during which these channels remain open and are thus able to evacuate water from the surrounding distributed drainage system[58]. These conditions promote the drainage of waters from weakly-connected[39] regions of the distributed drainage system, thereby reducing basal water pressure and associated basal lubrication and hence ice velocity over longer (decadal) timescales as effective pressures increase. Whilst it is hypothesised that increasing runoff to the bed will increase sediment pore water pressure, resulting in reduced sediment shear strength, increased sediment deformation and thus enhanced ice flow[59], such behaviour contrasts with the observations reported here and elsewhere[40–42,44]. Consequently, our results suggest either that extensive layers of subglacial till are not ubiquitous across our study region or if they are present, the tills have not deformed pervasively in response to the sustained period of enhanced meltwater input.

Surface melt production in our study region peaks in 2012, decreasing thereafter (although surface mass balance remains negative), consistent with trends observed across the ice-sheet[46]. Concurrent with decreasing meltwater runoff, we observe an acceleration in ice velocity. During the period of sustained high melt, the drainage of basal waters from a larger area of the distributed drainage system causes a gradual depressurisation of the background water pressure with an associated increase in effective pressure. Reduced surface meltwater production would result in seasonally less extensive and smaller subglacial channels and consequently these channels will undergo faster creep closure[32]. This results in a reduced time-period over which the main subglacial channels

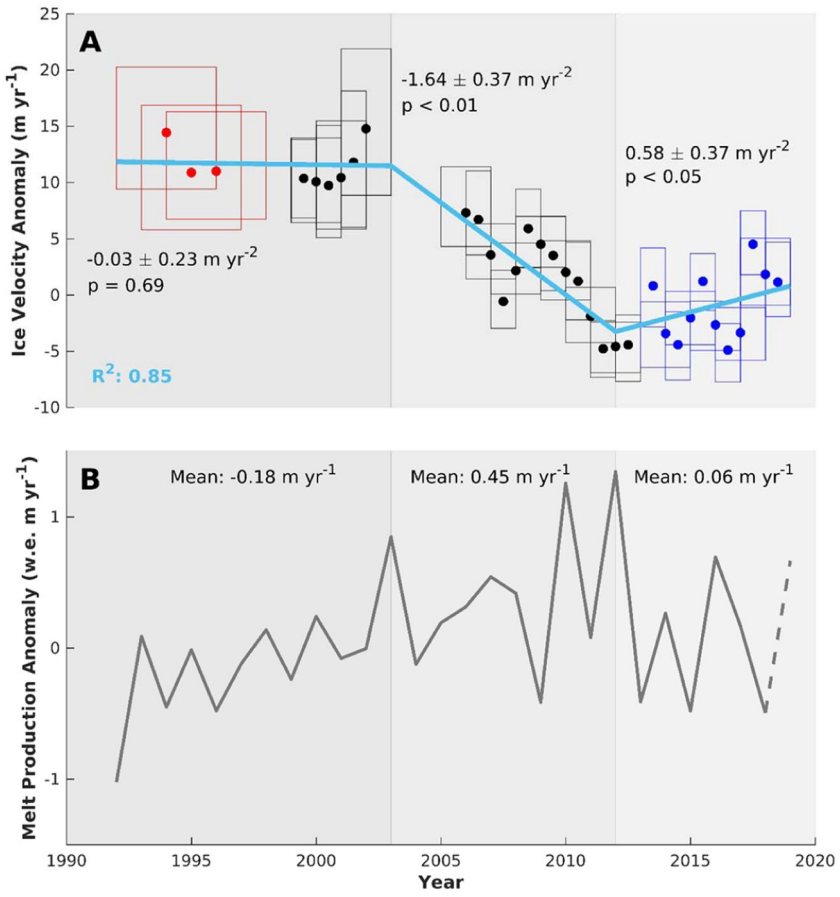

Figure 3. (**A**) Median ice velocity anomalies (m yr^{-1}) during each period calculated by sampling the common pixels between all velocity fields in the times series. Red boxes indicate Landsat 5 data, black boxes indicate Landsat 7 data, and blue boxes indicate Landsat 8 data. The width of each box corresponds to the total time period of the pairs in Landsat scenes fused for each period. The height of each box corresponds to the interquartile range and the light blue line displays the trends in ice velocity computed by a segmented linear regression (see Methods and SI). **(B)** Annual modelled surface melt production anomaly (grey)[7] in water equivalent (w.e.) m yr^{-1} (see Methods and SI). A dotted line is used to display the data for 2019 as this was incomplete at the time of processing. The background shades are used to differentiate the three distinct periods of dynamic behaviour.

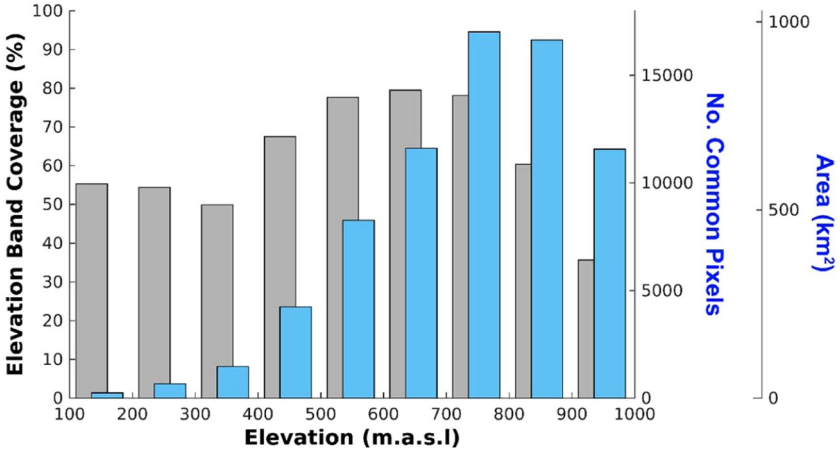

Figure 4. Percentage coverage of each 100 m elevation band by common sampling pixels (grey, left axis) and the altitudinal distribution in the common sampling pixels used in the computation of median ice velocities (blue, right axes).

can evacuate water from the surrounding weakly connected, hydraulically distributed regions. As water pressure is no longer being systematically reduced, the background water pressure can increase through a gradual re-pressurisation of the subglacial hydrological system, as meltwater can recharge from basal melting without being evacuated by efficient subglacial channels.

Effective pressure (N) is calculated as $N = Pi - Pw$, where Pi refers to the ice overburden pressure and Pw to the basal water pressure[32,60]. Repressurising the subglacial hydrological system causes basal water pressure (Pw) to increase, thus reducing effective pressure and causing ice to accelerate. As effective pressure is a function of ice thickness, for the same increase in basal water pressure we would anticipate acceleration to be greater where ice is thinner. Although we expect channel closure to occur earlier and faster under thicker ice (due to higher ice overburden pressure)[26,49,50], modelling studies suggest that once channel pressure falls to 90% of overburden pressure, there is less than 2 days difference in closure time for channels with a cross-sectional area of 10 m^2 compared to <1 m^2 [50]. Moreover, it has been suggested that maximum channel closure rates are similar at both marginal and interior sites[49]. Consequently, we argue that any variation in repressurisation due to channel closure rates will only have a small impact upon effective pressures when compared to variability in ice thickness (which ranges from 0–1400 m across our study area). As a result, we hypothesise that the observed acceleration is greater for marginal regions of thinner ice due to the impact of basal meltwater recharge on water pressure in these areas offsetting a larger proportion of the ice overburden pressure (Fig. 2D).

The inland limit and spatial extent of efficient channel formation is subject to considerable debate[38,61]. Borehole and tracer studies and ice velocity records have been used to infer channels extending 40–80 km inland[19,25,26,34,62–64], with high flow velocities of traced waters and the rapid transmission of pulses of meltwater from the ice sheet surface to the margin indicating efficient drainage[38,65]. These observations are supported by modelling studies, whereby efficient channels have been modelled up to 50 km inland, under 900 m thick ice[66,67]. The spatial extent of channelisation is influenced by the distribution of surface-to-bed connections, with high moulin density conducive to widespread and rapid channel development[68]. Further inland, ice thickness increases, surface slopes become shallower and runoff production decreases, leading to enhanced creep closure due to higher effective pressures and reductions in hydropotential gradients and wall-melting[32,61,69,70]. Under these conditions, modelling studies suggest that at a certain elevation and ice-thickness, efficient subglacial channels will not develop[49,50] in which case melt and ice-velocity are expected to scale positively[71]. Velocity measurements 140 km from the margin[71], within the accumulation area of the Leverett catchment, indicate a 2.2% increase in annual velocity between 2009 and 2012. In our study, we are unable to determine whether a positive change in ice velocity has occurred at elevations above 1300 m (a.s.l.) due to increasing noise in our dataset further inland. However, GPS observations reveal reduced velocities to at least 80 km inland (at ~1500 m a.s.l) in the years of record surface melt in 2010[48] and 2012[37] when compared to 2009.

Whilst multi-annual ice velocity slowdowns in southwest Greenland since the early-mid 2000s are observed here and in a number of other studies[40–44], differences between studies exist regarding the magnitude of slowdown, and the proposed mechanism(s) driving this dynamic change. For example, whilst GPS data show a slowdown of -0.9 ± 1.1 m yr^{-2} at North Lake from 2006–2014[43], satellite radar data from 2000/01 to 2016/17 reveal no significant trend (-0.2 m yr^{-2}, $p = 0.62$)[44]. At a regional scale, this radar data suggests a weaker slowdown trend than that reported either here, or by Tedstone *et al.*[40] (-1.5 m yr^{-2} from 2002–2014, -12% between 1985–1994 and 2007–2014), across the same study area, with little in the way of significant changes between 2001/01 and 2016/17 across much of the southwest margin[44]. Methodological differences between the studies may affect the conclusions drawn as this study and that of Tedstone *et al.*[40] applied feature tracking to image pairs either side of an annual baseline (352–400 days in Tedstone *et al.*[40], 352–384 days here), whereas Joughin *et al.*[44] composed mosaics of winter velocities, comprised of data sampled between September and May. Regardless, this raises the possibility that the previously observed slowdown[40] may be related to some local process, rather than regional-scale surface melt forcing[44], for example water piracy as a result of dynamic thinning on Jakobshavn Isbrae has been suggested as a driver of slowdown in the north of the West Greenland land-terminating sector[44]. However, by extending the study area ~120 km to the south, and by increasing the number of common pixels used in our time series by an order of magnitude compared to that of Tedstone *et al.*[40], we extend confidence in the observed slowdown of ice motion from the early-mid 2000s. Moreover, by calculating an ice velocity anomaly[72], we remove the influence of any biases between sensors from the observed trends, further increasing confidence that this sector of the ice sheet underwent significant deceleration during this period.

A variety of models exist to simulate the subglacial drainage system and its impact on ice dynamics in response to increasing meltwater fluxes in a warming climate[73]. However, whilst current models can reproduce observed dynamics of Greenland's land-terminating margins over days/weeks[32,50], on a seasonal timescale[39,67,74], and across several years[66,75], there is a need to consider the longer, decadal and multi-decadal response of ice motion to surface meltwater forcing in order to better reproduce observed dynamics and project future change. On a decadal scale, recent modelling predicts increased ice-motion and thus ice flux into the ablation zone under enhanced summer melt within 44 km of the ice-margin[76] (their Figure 5C). These predictions contrast with the results presented both here and from other GPS and satellite-derived observations[37,40–44]. Further work is therefore required to investigate what aspects of the model set-up or framework cause the modelled ice-motion to accelerate on a multi-annual timescale in response to increasing surface runoff, in contrast to numerous observations reported in this and other studies. Whilst we do observe reduced slowdown as ice thickness increases, our results and those of others show that ice motion within the ablation area has slowed as a result of increased surface runoff, and we do not observe any appreciable or spatially extensive increases in ice velocity as a result of an extended period of high surface melt. We therefore argue that in order to better represent ice dynamical processes and project future changes in coupled hydro-dynamic models, the models must better utilise the available data from field and satellite observations both in model set-up and for assessing model performance, and there is a need for changes in the numeric representation of processes, including ice-hydrology coupling.

Our findings demonstrate that ice at surface elevations below 1300 m (a.s.l.) in the South West land-terminating region of the GrIS underwent deceleration during the mid to late-2000s and early-2010s with subsequent acceleration following sustained reductions in surface melt production, with this acceleration proportionally greater in areas of thinner ice. We hypothesise that this recent acceleration is driven by increases in basal water pressure offsetting a larger proportion of ice overburden pressure, and thus causing a greater reduction in effective pressure under thinner ice. This behaviour has not been observed previously on a multi-annual timescale. Whilst we have demonstrated that changes affecting the subglacial hydrological system are the most likely driver of ice velocity change in our study region, we are unable to conclusively state whether antecedent melt production is the predominant factor controlling ice motion, or whether some threshold in the amount of melt is required in order to drive a change in velocity. However, it is clear from our results that the period of ice deceleration occurred during a period of sustained high melt production, and ice motion accelerated subsequently as melt production decreased to consistently lower values from 2013 onwards. Moreover, we observed no indication of an ongoing slowdown once surface melt production exhibited a sustained decrease. Thus, the behaviour observed supports a process-based understanding of the links between hydrology and ice dynamics in this land-terminating sector of the Greenland ice sheet. The results displayed in this study show that the observed trends in ice velocity are not statistical artefacts or the result of biases between sensors[72]. Further, we see no evidence of speed-up at the elevations studied under a warming climate, irrespective of the bed conditions. Future work is required to improve observations of change at higher elevations, and at other land-terminating sectors of the ice sheet, in order to assess the extent to which these processes operate on an ice sheet scale.

Furthermore, while the results presented here relate specifically to land-terminating margins, it has been argued that the dynamics of tidewater glaciers are a product of both oceanic and atmospheric forcing[77,78], with the latter potentially driving a positive feedback as a result of its influence upon fjord water circulation and thus submarine melt[77,79,80]. This positive feedback contrasts with our findings at land-terminating margins, indicating that at an ice-sheet scale, the relationship between hydrology and ice dynamics is complex and spatially variable. Since the extent to which surface melt processes impact on tidewater glacier dynamics remains uncertain, analysis of existing large-scale, multi-decadal datasets[5] at marine-terminating margins should be undertaken with respect to surface melt change, in order to better project the future response of the Greenland ice sheet to changing atmospheric and oceanic conditions.

Methods

Remote sensing of ice velocity. We apply optical feature tracking[40,81] to all Landsat pairs for the 14 path/row combinations that intersect our study region (66.41 to 69.52N, −51.78 to −45.45 W, Figures S1–S3). A pair length of 368 ± 16 days is used to minimise the impact of any seasonal variability in interannual ice velocity (Fig. S4). We use oriented correlation, matching the feature of gradient orientation for each pixel[82], and use a combination of spectral bands at wavelengths ~0.52–0.69 μm (bands 2 + 3 for Landsat 5 and 7, 3 + 4 for Landsat 8). We enhance the images by applying a principal component analysis to these bands, and subsequently, a high-pass gaussian filter is used to enhance surface features such as crevasses and reduce the impact of temporally stable features relating to the basal topography[40,81]. We use a reference window of 80 pixels and set the search window based upon prior velocity estimates[83]. Following Tedstone *et al.*[40], we apply a median coregistration to the output velocity fields in order to remove errors associated with georeferencing.

The coregistered velocity fields are then fused via a spatio-temporal median over annual or multi-year periods. Low-quality velocity estimates are removed through filtering by a threshold signal-to-noise ratio value (snr threshold = 6), identified by calculating the value beyond which the median absolute deviation of velocities over stable ground becomes asymptotic[81]. The final velocity field for each time period is composed of the median value of all velocity fields within the time period at each pixel. To calculate uncertainty at each pixel, we compute a 1σ confidence interval for each component of the velocity field in the form:

$$\sigma = \frac{k}{2} \cdot \frac{MAD}{N^{\alpha}}$$

Where MAD is the median absolute deviation over stable ground, N is the number of velocity fields used in the computation of the median velocity, σ is the 1σ confidence interval, and k and α are parameters determined for each time period from the stable ground velocity which is known to equal zero. This relationship is extrapolated on-ice using the appropriate values of MAD and N at each pixel. Following Tedstone *et al.*[40], we discard pixels with $\sigma > 60$ myr^{-1} from the subsequent analyses. In addition, we mask out the tidewater glaciers to the very north of the study region, limit our analysis to pixels below 1000 m above sea-level, and retain only the velocity fields with an area coverage above 9250 km^2. The median velocity is subsequently calculated across the 71703 pixels common to all the remaining merged velocity fields (Fig. S5) in order to avoid spatial bias influencing the change signal.

Anomaly-based time series. Recent work indicates that velocity magnitude has a biased mean, with this bias increasing with the standard deviation of the velocity components (and so with noise), causing an artificial negative velocity trend[72]. To mitigate this effect, we follow the velocity anomaly approach of Dehecq *et al.*[72]. First, we calculate a mean of all velocity pairs covering the period 1992–2019 described as V_0. The velocity anomaly is defined as the value of the difference vector $V_t - V_0$ projected on the mean velocity vector:

$$dv = \frac{(V_t - V_0) \cdot V_0}{\|V_0\|} = \frac{(V_{x,t} - V_{x,0})V_{x,0} + (V_{y,t} - V_{y,0})V_{y,0}}{\|V_0\|}$$

The result of this approach is to centre the noise distribution symmetrically around zero (Fig. S6) such that there is no bias in the mean value, removing any artificial slowdown trends due to variability in noise magnitude between sensors[72]. The resultant velocity anomaly fields are displayed in Fig. S7.

To assess the long-term trends in our time series, we first compute a simple linear regression through the data, and then test whether the data can be divided into three statistically different segments (Figures S8–S10) using the non-parametric Mann-Whitney Wilcoxon Test. We select the pair of breakpoints with the lowest RMSE, and that are statistically significant with 99% certainty, which gives breaks at 2003 and 2012.

Spatial trends in ice velocity. We construct change maps displaying the percentage ice velocity change between the following periods; 1992–2003 and 2003–2012, 2010–2012 and 2017–2019. For each pair, median ice velocity for each period was calculated through fusing all constituent velocity fields via a spatio-temporal median, and uncertainty of the percentage change was calculated through a linear combination of the uncertainties of each period:

$$\sqrt{{c_1}^2 + {c_2}^2}$$

where c_1 is the first period (i.e. 1992–2003) and c_2 is the second period (i.e. 2003–2012). We remove pixels with uncertainty greater than 60 m yr^{-1}. We also filter by Velocity Vector Coherence (VVC)[81], which follows the form:

$$VVC(i,\, j) = \frac{\left\| \sum_{t \in T} \underset{V}{\rightarrow} (i,\, j,\, t) \right\|}{\left\| \sum_{t \in T} \underset{V}{\rightarrow} (i,\, j,\, t) \right\|}$$

where T is the set of N velocity estimates V(i,j,t) merged to obtain the median velocity $\overline{V}$(i,j) at pixel(i,j). We filter out all pixels with VVC < 0.45. In addition, we erode the edge of our ice mask by 3 pixels in order to limit the influence of noise at the ice margin.

Surface mass balance. We obtain surface mass balance (SMB) data from the MAR v3.10 regional climate model[7], forced by NCEP-NCARv1 from 1992 to 2019. We limit our analyses of SMB below an ice surface elevation upper limit of 1600 m (a.s.l.). Little lake drainage occurs above this elevation[84–86] and it has been argued that this is an approximate maximum elevation where crevasses, and thus moulins, are likely to form[87]. Whilst surface meltwater can runoff from elevations above this, surficial drainage is less likely to occur in high elevation regions due to the shallower surface slope[86]. Consequently, below this threshold elevation, we can be confident that surface meltwater drains to the ice-bed interface, and so influences ice motion. Regardless, melt at all elevations has increased from the 1958–1987 average in the period 1988–2013[87], with the difference between the means of the period being positive at $p < 0.05$ from 400–2600 m (a.s.l.).

Data availability

The Landsat imagery used in this study was provided by the United States Geological Survey and the European Space Agency third party missions program and are freely available.

Received: 5 July 2019; Accepted: 13 January 2020;
Published online: 03 February 2020

References

1. Rignot, E., Velicogna, I., van den Broeke, M.R., Monaghan, A., & Lenaerts, J.T.M. Acceleration of the contribution of the Greenland and Antarctic ice sheets to sea level rise. *Geophysical Research Letters* **38**(5), https://doi.org/10.1029/2011GL046583 (2011).
2. Shepherd, A. *et al.* A Reconciled Estimate of Ice-Sheet Mass Balance. *Science* **338**(6111), 1183–1189 (2012).
3. Hanna, E. *et al.* The influence of North Atlantic atmospheric and oceanic forcing effects on 1900-2010 Greenland summer climate and ice melt/runoff. *International Journal of Climatology* **33**(4), 862–880 (2013).
4. van den Broeke, M. R. *et al.* On the recent contribution of the Greenland ice sheet to sea level change. *The Cryosphere* **10**(5), 1933–1946 (2016).
5. Mouginot, J. *et al.* Forty-six years of Greenland Ice Sheet mass balance from 1972 to 2018. *Proceedings of the National Academy of Sciences* **116**(19), 9239–9244 (2019).
6. Shepherd, A. *et al.* Mass balance of the Greenland Ice Sheet from 1992 to 2018. *Nature* (2019).
7. Fettweis, X. *et al.* Reconstructions of the 1900–2015 Greenland ice sheet surface mass balance using the regional climate MAR model. *The Cryosphere* **11**(2), 1015–1033 (2017).
8. Cappelen, J., Vinther, B. M., Kern-Hansen, C., Laursen, E. V. & Jorgensen, P. V. Greenland – DMI Historical Climate Data Collection 1784-2016, *Danish Meteorol. Inst. Rep.*, 17–04 (2017).
9. Fettweis, X. *et al.* Estimating the Greenland ice sheet surface mass balance contribution to future sea level rise using the regional atmospheric climate model MAR. *The Cryosphere* **7**(2), 469–489 (2013).
10. Hofer, S., Tedstone, A. J., Fettweis, X. & Bamber, J. L. Cloud microphysics and circulation anomalies control differences in future Greenland melt. *Nature Climate Change* **9**(7), 523–530 (2019).
11. Serreze, M. C. & Barry, R. G. Processes and impacts of Arctic amplification: A research synthesis. *Global Planetary Change* **77**(1–2), 85–96 (2011).
12. Nghiem, S.V. et al. The extreme melt across the Greenland ice sheet in 2012. *Geophysical Research Letters* **39**(20), https://doi.org/10.1029/2012GL053611 (2012).
13. Hanna, E., Cropper, T. E., Hall, R. J. & Cappelen, J. Greenland Blocking Index 1851-2015: a regional climate change signal. *International Journal of Climatology* **36**(15), 4847–4861 (2016).
14. Van Tricht, K. *et al.* Clouds enhance Greenland ice sheet meltwater runoff. *Nature Communications* **7**, 10226 (2016).
15. Cullather, R. I. & Nowicki, S. M. J. Greenland Ice Sheet surface melt and its relation to daily atmospheric conditions. *Journal of Climate* **31**, 1897–1919 (2018).

16. Hofer, S., Tedstone, A. J., Fettweis, X. & Bamber, J. L. Decreasing cloud cover drives the recent mass loss on the Greenland Ice Sheet. *Science Advances* **3**(6), e1700584 (2017).
17. Ryan, J. C. *et al*. Greenland Ice Sheet surface melt amplified by snowline migration and bare ice exposure. *Science Advances* **5**(3), eaav3738 (2019).
18. IPCC. *Climate change 2013: the physical science basis. Contribution of Working Group I to the Fifth Assessment Report of the Intergovernmental Panel on Climate Change*. In: Stocker, T. F., *et al* editors. Cambridge, UK and New York, NY, USA: Cambridge University Press. p.1535. (2013).
19. Fitzpatrick, A. A. W. *et al*. Ice flow dynamics and surface meltwater flux at a land-terminating sector of the Greenland ice sheet. *Journal of Glaciology* **59**(216), 687–696 (2013).
20. Lindbäck, K. *et al*. High-resolution ice thickness and bed topography of a land-terminating section of the Greenland Ice Sheet. *Earth System Science. Data* **6**(2), 331–338 (2014).
21. van den Broeke, M. *et al*. Partitioning Recent Greenland Mass Loss. *Science* **326**(5955), 984–986 (2009).
22. Andersen, M. L. *et al*. Basin-scale partitioning of Greenland ice sheet mass balance components (2007–2011). *Earth and Planetary Science Letters* **409**, 89–95 (2015).
23. Tedesco, M. & Fettweis, X. 21st century projections of surface mass balance changes for major drainage systems of the Greenland ice sheet. *Environmental Research Letters* **7**(4), https://doi.org/10.1088/1748-9326/7/4/045405 (2012).
24. van der Veen, C. J. Fracture propagation as means of rapidly transferring surface meltwater to the base of glaciers. *Geophysical Research Letters* **34**(1), L01501 (2007).
25. Das, S. B. *et al*. Fracture propagation to the base of the Greenland Ice Sheet during supraglacial lake drainage. *Science* **320**(5877), 778–81 (2008).
26. Chandler, D. M. *et al*. Evolution of the subglacial drainage system beneath the Greenland Ice Sheet revealed by tracers. *Nature Geoscience* **6**(3), 195–198 (2013).
27. Andrews, L. C. *et al*. Direct observations of evolving subglacial drainage beneath the Greenland Ice Sheet. *Nature* **514**(7520), 80–83 (2014).
28. Iken, A. & Bindschadler, R. A. Combined measurements of Subglacial Water Pressure and Surface Velocity of Findelengletscher, Switzerland: Conclusions about Drainage System and Sliding Mechanism. *Journal of Glaciology* **32**(110), 101–119 (1986).
29. Fountain, A. G. & Walder, J. S. Water flow through temperate glaciers. *Reviews of Geophysics* **36**(3), 299–328 (1998).
30. Zwally, H. J. *et al*. Surface melt-induced acceleration of Greenland ice-sheet flow. *Science* **297**(5579), 218–22 (2002).
31. Bartholomaus, T. C., Anderson, R. S. & Anderson, S. P. Response of glacier basal motion to transient water storage. *Nature Geoscience* **1**(1), 33–37 (2008).
32. Schoof, C. Ice-sheet acceleration driven by melt supply variability. *Nature* **468**(7325), 803–806 (2010).
33. Bartholomew, I. *et al*. Seasonal evolution of subglacial drainage and acceleration in a Greenland outlet glacier. *Nature Geoscience* **3**(6), 408–411 (2010).
34. Bartholomew, I. et al. Supraglacial forcing of subglacial drainage in the ablation zone of the Greenland ice sheet. *Geophysical Research Letters* **38**(8), https://doi.org/10.1029/2011GL047063 (2011).
35. Kamb, B. Glacier surge mechanism based on linked cavity configuration of the basal water conduit system. *Journal of Geophysical Research: Solid Earth* **92**(B9), 9083 (1987).
36. Bingham, R. G., Nienow, P. W., Sharp, M. J. & Boon, S. Subglacial drainage processes at a High Arctic polythermal valley glacier. *Journal of Glaciology* **51**(172), 15–24 (2005).
37. Tedstone, A. J. *et al*. Greenland ice sheet motion insensitive to exceptional meltwater forcing. *Proceedings of the National Academy of Sciences* **110**(49), 19719–24 (2013).
38. Nienow, P. W., Sole, A. J., Slater, D. A. & Cowton, T. R. Recent Advances in Our Understanding of the Role of Meltwater in the Greenland Ice Sheet System. *Current Climate Change Reports* **3**(4), 330–344 (2017).
39. Hoffman, M. J. *et al*. Greenland subglacial drainage evolution regulated by weakly connected regions of the bed. *Nature Communications* **7**(1), 13903 (2016).
40. Tedstone, A. J. *et al*. Decadal slowdown of a land-terminating sector of the Greenland Ice Sheet despite warming. *Nature* **526**(7575), 692–695 (2015).
41. van de Wal, R. S. W. *et al*. Self-regulation of ice flow varies across the ablation area in south-west Greenland. *The Cryosphere* **9**(2), 603–611 (2015).
42. van de Wal, R. S. W. *et al*. Large and Rapid Melt-Induced Velocity Changes in the Ablation Zone of the Greenland Ice Sheet. *Science* **321**(5885), 111–113 (2008).
43. Stevens, L. A. *et al*. Greenland Ice Sheet flow response to runoff variability. *Geophysical Research Letters* **43**(21), 11,295–11,303 (2016).
44. Joughin, I., Smith, B. E. & Howat, I. Greenland Ice Mapping Project: ice flow velocity variation at sub-monthly to decadal timescales. *The Cryosphere* **12**(7), 2211–2227 (2018).
45. Bevis, M. *et al*. Accelerating changes in ice mass within Greenland, and the ice sheet's sensitivity to atmospheric forcing. *Proceedings of the National Academy of Sciences* **116**(6), 1934–1939 (2019).
46. Tedesco, M. *et al*. Greenland Ice Sheet [in Arctic Report Card 2017], http://www.arctic.noaa.gov/Report-Card (2017).
47. Joughin, I. *et al*. Seasonal speedup along the Western flank of the Greenland Ice Sheet. *Science* **320**(5877), 781–783 (2008).
48. Sole, A. *et al*. Winter motion mediates dynamic response of the Greenland Ice Sheet to warmer summers. *Geophysical Research Letters* **40**(15), 3940–3944 (2013).
49. Meierbachtol, T., Harper, J. & Humphrey, N. Basal Drainage System Response to Increasing Surface Melt on the Greenland Ice Sheet. *Science* **341**(6147), 777–779 (2013).
50. Dow, C. F., Kulessa, B., Rutt, I. C., Doyle, S. H. & Hubbard, A. Upper bounds on subglacial channel development for interior regions of the Greenland ice sheet. *Journal of Glaciology* **60**(224), 1044–1052 (2014).
51. Sole, A., Payne, T., Bamber, J., Nienow, P. & Krabill, W. Testing hypotheses of the cause of peripheral thinning of the Greenland Ice Sheet: is land-terminating ice thinning at anomalously high rates? *The Cryosphere* **2**(2), 205–218 (2008).
52. Sandberg Sørensen, L. *et al*. 25 years of elevation changes of the Greenland Ice Sheet from ERS, Envisat, and CryoSat-2 radar altimetry. *Earth and Planetary Science Letters* **495**, 234–241 (2018).
53. Helm, V., Humbert, A. & Miller, H. Elevation and elevation change of Greenland and Antarctica derived from CryoSat-2. *The Cryosphere* **8**(4), 1539–1559 (2014).
54. McMillan, M. *et al*. A high-resolution record of Greenland mass balance. *Geophysical Research Letters* **43**(13), 7002–7010 (2016).
55. Nilsson, J., Gardner, A., Sandberg Sørenson, L. & Forsberg, R. Improved retrieval of land ice topography from CryoSat-2 data and its impact for volume-change estimation of the Greenland Ice Sheet. *The Cryosphere* **10**, 2953–2969 (2016).
56. Pritchard, H. D., Arthern, R. J., Vaughan, D. G. & Edwards, L. A. Extensive dynamic thinning on the margins of the Greenland and Antarctic ice sheets. *Nature* **461**(7266), 971–975 (2009).
57. Chu, V. W. Greenland ice sheet hydrology. *Progress in Physical Geography* **38**(1), 19–54 (2014).
58. Hubbard, B. P., Sharp, M. J., Willis, I. C., Nielsen, M. K. & Smart, C. C. Borehole water-level variations and the structure of the subglacial hydrological system of Haut Glacier d'Arolla, Valais, Switzerland. *Journal of Glaciology* **41**(139), 572–583 (1995).
59. Kulessa, B. *et al*. Seismic evidence for complex sedimentary control of Greenland Ice Sheet flow. *Science Advances* **3**(8), e1603071 (2017).

60. Meier, M. F. & Post, A. Fast tidewater glaciers. *Journal of Geophysical Research* **92**(B9), 9051–9058 (1987).
61. Davison, B. J., Sole, A. J., Livingstone, S. J., Cowton, T. R. & Nienow, P. W. The influence of hydrology on the dynamics of land-terminating sectors of the Greenland Ice Sheet. *Frontiers in Earth Science* **7**(10), https://doi.org/10.3389/feart.2019.00010 (2019).
62. Bartholomew, I. D. *et al*. Seasonal variations in Greenland Ice Sheet motion: inland extent and behaviour at high elevations. *Earth and Planetary Science Letters* **307**(3–4), 271–278 (2011).
63. Bartholomew, I. D. *et al*. Short-term variability in Greenland Ice Sheet motion forced by time-varying meltwater drainage: Implications for the relationship between subglacial drainage system behaviour and ice velocity. *Journal of Geophysical Research* **117**(F03002), https://doi.org/10.1029/2011JF002220 (2012).
64. Doyle, S. H. *et al*. Ice tectonic deformation during the rapid *in situ* drainage of a supraglacial lake on the Greenland Ice Sheet. *The Cryosphere* **7**(1), 129–140 (2013).
65. Smith, L. C. *et al*. Direct measurements of meltwater runoff on the Greenland ice sheet surface. *Proceedings of the National Academy of Sciences* **114**(50), 10622–10631 (2017).
66. De Fleurian, B. *et al*. A modelling study of the effect of runoff variability on the effective pressure beneath Russell Glacier, West Greenland. *Journal of Geophysical Research: Earth Surface* **121**, 1834–1848 (2016).
67. Koziol, C. P. & Arnold, N. Modelling seasonal meltwater forcing of the velocity of land-terminating margins of the Greenland Ice Sheet. *The Cryosphere* **12**(3), 971–991 (2018).
68. Banwell, A., Hewitt, I., Willis, I. & Arnold, N. Moulin density controls drainage development beneath the Greenland Ice Sheet. *Journal of Geophysical Research: Earth Surface* **121**, 2248–2269 (2016).
69. Nye, J. F. The flow law of ice from measurements in glacier tunnels, laboratory experiments and the Jungfraufirn borehole experiment. *Proceedings of the Royal Society of London: Series A* **219**(1139), 477–489 (1953).
70. Hooke, R. L., Laumann, T. & Kohler, J. Subglacial water pressures and the shape of subglacial conduits. *Journal of Glaciology* **36**(122), 67–71 (1990).
71. Doyle, S. H. *et al*. Persistent flow acceleration within the interior of the Greenland ice sheet. *Geophysical Research Letters* **41**(3), 899–905 (2014).
72. Dehecq, A. *et al*. Twenty-first century glacier slowdown driven by mass loss in High Mountain Asia. *Nature Geoscience* **12**(1), 22–27 (2019).
73. De Fleurian, B., Werder, M. A., Beyer, S. & Brinkerhoff, D. J. SHMIP The subglacial hydrology model intercomparison Project. *Journal of Glaciology* **64**(248), 897–916 (2018).
74. Hewitt, I. J. Seasonal changes in ice sheet motion due to melt water lubrication. *Earth and Planetary Science Letters* **371–372**, 16–25 (2013).
75. Poinar, K., Dow, C. F. & Andrews, L. C. Long-term support of an active subglacial hydrologic system in Southeast Greenland by firn aquifers. *Geophysical Research Letters* **46**, 4772–4781 (2019).
76. Gagliardini, O. & Werder, M. A. Influence of increasing surface melt over decadal timescales on land-terminating Greenland-type outlet glaciers. *Journal of Glaciology* **64**(247), 700–710 (2018).
77. Cowton, T. R., Sole, A. J., Nienow, P. W., Slater, D. A. & Christoffersen, P. Linear response of east Greenland's tidewater glaciers to ocean/atmosphere warming. *Proceedings of the National Academy of Sciences* **115**(31), 7907–7912 (2018).
78. Slater, D. *et al*. Past and future response of Greenland's tidewater glaciers to submarine melting. *The Cryosphere Discussions*, https://doi.org/10.5194/tc-2019-98 (2019).
79. Slater, D., Nienow, P., Goldberg, D., Cowton, T. & Sole, A. A model for tidewater glacier undercutting by submarine melting. *Geophysical Research Letters* **44**(5), 2360–2368 (2017).
80. Slater, D. *et al*. Localized plumes drive front-wide ocean melting of a Greenlandic tidewater glacier. *Geophysical Research Letters* **45**(22), 12350–12358 (2018).
81. Dehecq, A., Gourmelen, N. & Trouve, E. Deriving large-scale glacier velocities from a complete satellite archive: Application to the Pamir–Karakoram–Himalaya. *Remote Sensing of Environment* **162**, 55–66 (2015).
82. Fitch, A. J., Fitch, A. J., Kadyrov, A., Christmas, W. J. & Kittler, J. Orientation correlation. *Br Mach Vis Conf* **1**, 133–142 (2002).
83. Joughin, I., Smith, B. E., Howat, I. M., Scambos, T. & Moon, T. Greenland flow variability from ice-sheet-wide velocity mapping. *Journal of Glaciology* **56**(197), 415–430 (2010).
84. Howat, I. M., de la Peña, S., van Angelen, J. H., Lenaerts, J. T. M. & van den Broeke, M. R. Brief Communication: Expansion of meltwater lakes on the Greenland Ice Sheet. *The Cryosphere* **7**(1), 201–204 (2013).
85. Johansson, A. M., Jansson, P. & Brown, I. A. Spatial and temporal variations in lakes on the Greenland Ice Sheet. *Journal of Hydrology* **476**, 314–320 (2013).
86. Selmes, N., Murray, T. & James, T. D. Characterizing supraglacial lake drainage and freezing on the Greenland Ice Sheet. *The Cryosphere Discussions* **7**(1), 475–505 (2013).
87. Poinar, K. *et al*. Limits to future expansion of surface-melt-enhanced ice flow into the interior of western Greenland. *Geophysical Research Letters* **42**(6), 1800–1807 (2015).
88. Howat, I. M., Negrete, A. & Smith, B. E. The Greenland Ice Mapping Project (GIMP) land classification and surface elevation data sets. *The Cryosphere* **8**(4), 1509–1518 (2014).
89. Morlighem, M. *et al*. BedMachine v3: Complete Bed Topography and Ocean Bathymetry Mapping of Greenland From Multibeam Echo Sounding Combined With Mass Conservation. *Geophysical Research Letters* **44**(21), 11,051–11,061 (2017).

Acknowledgements

J.J.W. and P.N. were funded by a UK Natural Environment Research Council (NERC) doctoral training partnership grant (NE/L002558/1). N.G was funded by ESA grants Dragon10302 and Dragon32437. The Landsat imagery was provided by the United States Geological Survey and the European Space Agency third party missions program. We would also like to thank Dr. Xavier Fettweis for providing the MAR v3.10 SMB data.

Author contributions

J.J.W., N.G. and P.N. contributed to the design of the study and writing of the paper. J.J.W. performed the data processing and analyses.

Competing interests

The authors declare no competing interests.

Additional information

Supplementary information is available for this paper at https://doi.org/10.1038/s41598-020-58355-2.

Correspondence and requests for materials should be addressed to J.J.W.

Reprints and permissions information is available at www.nature.com/reprints.

Williams et al., 2021, *Journal of Glaciology*

Journal of Glaciology

Article

Cite this article: Williams JJ, Gourmelen N, Nienow P (2021). Complex multi-decadal ice dynamical change inland of marine-terminating glaciers on the Greenland Ice Sheet. *Journal of Glaciology* 1–14. https://doi.org/10.1017/jog.2021.31

Received: 9 December 2020
Revised: 19 February 2021
Accepted: 22 February 2021

Keywords:
Arctic glaciology; atmosphere-ice-ocean interactions; glacier flow; ice dynamics

Author for correspondence:
Joshua J. Williams,
Email: j.j.williams-4@sms.ed.ac.uk

cambridge.org/jog

Complex multi-decadal ice dynamical change inland of marine-terminating glaciers on the Greenland Ice Sheet

Joshua J. Williams, Noel Gourmelen and Peter Nienow

School of Geosciences, University of Edinburgh, Edinburgh, EH8 9XP, UK

Abstract

Greenland's future contribution to sea-level rise is strongly dependent on the extent to which dynamic perturbations, originating at the margin, can drive increased ice flow within the ice-sheet interior. However, reported observations of ice dynamical change at distances >∼50 km from the margin have a very low spatial and temporal resolution. Consequently, the likely response of the ice-sheet's interior to future oceanic and atmospheric warming is poorly constrained. Through combining GPS and satellite-image-derived ice velocity measurements, we measure multi-decadal (1993–1997 to 2014–2018) velocity change at 45 inland sites, encompassing all regions of the ice sheet. We observe an almost ubiquitous acceleration inland of tidewater glaciers in west Greenland, consistent with acceleration and retreat at glacier termini, suggesting that terminus perturbations have propagated considerable distances (>100 km) inland. In contrast, outside of Kangerlussuaq, we observe no acceleration inland of tidewater glaciers in east Greenland despite terminus retreat and near-terminus acceleration, and suggest propagation may be limited by the influence of basal topography and ice geometry. This pattern of inland dynamical change indicates that Greenland's future contribution to sea-level will be spatially complex and will depend on the capacity for dynamic changes at individual outlet glacier termini to propagate inland.

1. Introduction

The Greenland Ice Sheet (GrIS) has lost mass to the ocean at an increasing rate over recent decades (Rignot and others, 2008, 2011; Shepherd and others, 2012, 2020; Enderlin and others, 2014; King and others, 2018; Mouginot and others, 2019), and now has the largest contribution to global sea-level rise of any individual ice body (Vaughan and others, 2013; Bamber and others, 2018). Estimates indicate that ∼48–66% of this mass loss can be attributed to glacier dynamics, with this dynamic loss driven by the acceleration and retreat of marine-terminating glaciers and increasing by 14% between 1985–1999 and 2007–2018 (King and others, 2020), and the remaining ∼34–52% due to surface mass balance (SMB) (Mouginot and others, 2019; Shepherd and others, 2020). Following a step-increase in ice discharge in the early-2000s, the GrIS is suggested to have entered a state of persistent mass loss (King and others, 2020), and recent model intercomparison work projects a future sea-level rise contribution of 32 ± 17 to 90 ± 50 mm by 2100 (Goelzer and others, 2020). Almost all of our current observations of long-term change are concentrated at the margins of the ice sheet, which have been characterised by thinning (Pritchard and others, 2009; McMillan and others, 2016; Sørensen and others, 2018) and both substantial velocity accelerations (Rignot and Kanagaratnam, 2006; Joughin and others, 2010, 2018; Moon and others, 2012) and near-ubiquitous retreat of marine-terminating outlet glaciers (Murray and others, 2015; Bunce and others, 2018), especially in the northwest and southeast.

In contrast, our understanding of changes in the dynamics of inland regions of the ice sheet is far more limited, and yet any such changes would be important for several reasons. At land-terminating margins, while the impacts of variable hydrological forcing on ice flow have been well-studied near the ice margin (van de Wal and others, 2008, 2015; Bartholomew and others, 2010; Sole and others, 2013; Tedstone and others, 2015), it remains unclear whether meltwater can access the bed, and efficient subglacial channels form, further into the ice-sheet interior where the ice is thicker and rates of surface melting are lower (Nienow and others, 2017). This is particularly important given that as the ELA rises in response to projected increases in surface melt (Hanna and others, 2008), the area of the ice-sheet surface undergoing melt will increase exponentially due to the hypsometry of the ice-sheet surface (Bartholomew and others, 2011; Machguth and others, 2016). Furthermore, some studies have postulated that ice motion will scale positively with surface melting at high elevations (Doyle and others, 2014; Gagliardini and Werder, 2018), and others that the presence of liquid water within the englacial hydrological system may increase ice deformation rates over time scales of years to decades (Phillips and others, 2010, 2013). More generally, considering conservation of mass, the thickness of ice in the interior is considerably greater than that at the margin, and so any increase in ice motion has the potential to result in a much larger increase in mass flux when compared to marginal regions (Doyle and others, 2014), particularly for marine-terminating margins which are characterised by faster flow velocities and can

6673

discharge any increase in mass flux directly into the ocean. As a consequence, future sea-level change projections are strongly dependent on how quickly mass can be transported from the ice-sheet interior to the margin (Price and others, 2008, 2011; Felikson and others, 2017, 2020), as well as the time required for the ice sheet to reach a new steady-state following a perturbation. For example, modelling work indicates that ~75% of the projected sea-level rise from Greenland, which would result from the response of the ice sheet to forcing over the past few decades, is yet to come (Price and others, 2011). Furthermore, additional estimates suggest thinning may continue for hundreds (Wang and others, 2012) to thousands (Price and others, 2008) of years until a new steady-state is reached.

Several mechanisms have been proposed to drive a change in the ice dynamics within regions inland of Greenland's tidewater glacier termini. Changes to the surface slope and thickness of the ice, as a result of ice dynamical and/or SMB change, impact upon the driving stress, in turn affecting the rates of ice flow through internal deformation of the ice (Cuffey and Paterson, 2010). Such a change in driving stress, and thus internal deformation, can be driven through the up-glacier propagation of changes at the terminus of tidewater glaciers (i.e. Howat and others, 2008; Price and others, 2008, 2011; Nick and others, 2009; Felikson and others, 2017, 2020); for example, the loss of back-stress as a result of the loss of a floating ice tongue, or an increase in strain rate as the terminus retreats into deeper water (Price and others, 2011). This perturbs the force-balance, and the resultant acceleration leads to thinning of nearby upstream ice, steepening the local glacier surface thereby increasing the driving stress, resulting in further acceleration causing thinning and acceleration to propagate upstream (Nick and others, 2009). The propagation of this thinning can be modelled as a diffusive kinematic wave (Nye, 1960, 1963; Nick and others, 2009; Price and others, 2011; Felikson and others, 2017, 2020). This process can initiate a dramatic change in inland velocities, as observed during large 'surging' events at some Arctic ice caps (i.e. McMillan and others, 2014; Willis and others, 2018; Zheng and others, 2019).

Recent work (Felikson and others, 2017, 2020) suggests there may be geometrical constraints on the ability for thinning (and thus velocity) perturbations to propagate inland. These studies calculate the Péclet number (Pe), which describes the ratio of the rate at which a kinematic wave diffuses upstream or advects downstream. A threshold value of $Pe = 3$ is argued to represent the location at which 89% of dynamic change has occurred (Felikson and others, 2020), thus offering a possible empirical threshold by which to measure the ability of changes at the margin to propagate inland. Through applying this to 141 tidewater glaciers across the GrIS, Felikson and others (2020) suggest two end-member geometries describe those glaciers with the greatest potential for dynamic mass loss; those with a relatively low mass flux but with basal topography permitting thinning to diffuse far inland (i.e. northwest Greenland), and those with high mass flux but with thinning limits close to the margin (i.e. southeast Greenland).

In spite of the wealth of studies, there is little observational data to constrain these theoretical and model results, especially at higher elevations further inland. Direct observations of velocity change inland of fast-flowing marine-terminating outlet glaciers are limited to sparse GPS measurements of seasonal flow variations at a few individual glaciers (Sole and others, 2011; Ahlstrøm and others, 2013), and a single long-term (multi-decadal) study observing changes in ice motion extending ~80–100 km from the grounding line at Zachariae Isstrøm in northeast Greenland (Mouginot and others, 2015). Recent measurements of mass change from ICESat and ICESat-2 show thinning extending inland to elevations of 2000–2500 m (a.s.l.) in western and southern Greenland, particularly inland of Jakobshavn Isbrae and tidewater glaciers in the northwest, and to 1500 m (a.s.l.) in northeast Greenland (Smith and others, 2020), although thinning is the result of both dynamic change and changes in SMB. To disentangle the relative contribution of dynamic and SMB, thereby isolating the dynamic signal of mass loss, surface elevation change (SEC) can be corrected with SMB fields derived from regional climate models (Pritchard and others, 2009; Zwally and others, 2011; McMillan and others, 2016; Felikson and others, 2017). The majority of pronounced dynamic thinning is found in a relatively narrow set of regions; Jakobshavn Isbrae, Upernavik Isstrøm and Steenstrup Glacier on the west coast, Kangerlussuaq in the southeast, and Zachariae Isstrøm in the northeast (McMillan and others, 2016). While dynamic thinning has been observed to penetrate inland of fast-flowing outlet glaciers (Pritchard and others, 2009; Zwally and others, 2011; McMillan and others, 2016), the amplitude of thinning from a small perturbation in ice velocity is expected to be well below the combined uncertainty of altimetry and SMB models and so the inland limit of dynamic thinning comes with large uncertainty. Consequently, there is a need for additional robust measurements of dynamics, and thus potentially dynamic change, within the accumulation zone of the GrIS in order to quantify how the interior of the GrIS has responded to climate warming and associated ice marginal dynamic perturbations.

During the period 1993–1997, a line of 161 stakes located ~30 km apart was installed in a 'girdle' around the entire GrIS at ~2000 m elevation as part of the NASA-led Program for Arctic Regional Climate Assessment (PARCA) project, in order to estimate the mass balance of the ice-sheet interior (Thomas and others, 1998, 2000, 2001). At each stake, annual ice velocity was calculated using GPS observations recorded over a 1-year return period sometime between 1993 and 1997. This period was characterised by stable mass balance (Sørensen and others, 2018) and preceded both the recent rapid acceleration in ice motion observed at many of Greenland's marine-terminating outlet glaciers (Thomas and others, 2003; Joughin and others, 2004; Luckman and others, 2006; Holland and others, 2008; Murray and others, 2010; Bevan and others, 2012; Hill and others, 2018), and the slowdown in the southwest land-terminating sector (Tedstone and others, 2015; van de Wal and others, 2015; Stevens and others, 2016; Williams and others, 2020), which both began in the late-1990s to early-2000s. While inland velocity measurements have previously been limited to GPS data, the launch of Landsat-8 in 2013, among other advances in satellite imaging, has led to the extension of large-scale feature tracking into the ice-sheet interior (Fahnestock and others, 2016; Gardner and others, 2018, 2019). Since 2013, some marine-terminating glaciers have continued to accelerate while others have stabilised or slowed down (Joughin and others, 2018, 2020; Lemos and others, 2018; Khazendar and others, 2019; Mankoff and others, 2020). Few, however, have remained stable since the 1990s or returned to speeds comparable to those prior to the initial acceleration (Bevan and others, 2012; Joughin and others, 2018).

Here, we compare recent satellite-image-derived velocities in the ice-sheet interior to those collected at the PARCA GPS stakes along the 2000 m elevation contour in the mid-1990s to quantify how the interior of the GrIS has responded to the period of dramatic change observed at marine-terminating margins of the GrIS during the 2000s and 2010s. We measure multi-decadal ice velocity change at 45 sites inland of tidewater margins, encompassing all regions of the ice sheet. Subsequently, we assess the observed pattern of change with respect to the patterns of velocity change at the margins, ice geometrical constraints and modelled SMB from MAR v3.10 (Fettweis and others, 2017).

6674

2. Data and methods

2.1 PARCA ice velocities around the 2000 m traverse

The PARCA dataset consists of GPS receivers at 161 stakes, located ~30 km apart and spanning the entire 2000 m elevation contour of the GrIS, except for the southwest where the stakes were placed at higher elevations to avoid nunataks, mountains and crevasses (Thomas and others, 1998, 2000). At each GPS station, an annual ice velocity (m a^{-1}) was recorded within the period 1993–1997, as well as surface elevation (m a.s.l.) and ice thickness (m), the latter of which was measured by ice-penetrating radar. The precision of annual velocity measurements from these GPS sites is <0.5 m a^{-1}, and better than 0.2 m a^{-1} in most cases (Thomas and others, 1998). We apply a conservative uncertainty of ±0.5 m a^{-1} at all sites.

It should be noted that while the GPS sites are located at approximately the same surface elevation, there are considerable differences in the distance from their respective glacier termini (Fig. S6), with a notable increase in distance inland in the north and northeast.

2.2 NASA MEaSUREs ITS-LIVE ice velocities

Recent advances in satellite imaging have enabled the routine mapping of ice velocities (Dehecq and others, 2015; Fahnestock and others, 2016), with enhanced coverage in the interiors of the ice sheets (Gardner and others, 2018). Here, we use the NASA MEaSUREs ITS-LIVE annual velocity mosaics (v0) of the GrIS, generated from Landsat imagery through the auto-RIFT feature tracking processing chain (Gardner and others, 2018), covering the period 1985–2018 and gridded to 240 m (Gardner and others, 2019). Full documentation of this dataset is available from https://its-live.jpl.nasa.gov/#documentation. We use this dataset as the ice velocity measurements extend to the 2000 m elevation contour and both effective pair length (dt) and centre date are provided at each pixel such that we can assess the impact of any seasonality introduced in our analyses. Moreover, a recent assessment of satellite-image-derived ice velocities within the Greenland interior shows that when compared to GPS velocities from 2015 to 2019, located ~150 km from the ice divide in the Northeast Greenland Ice Stream (NEGIS; 75°38N, 35°60W), ITS-LIVE velocities from 2013 to 2018 are characterised by the lowest bias (0.31 m) of all velocity products assessed (Hvidberg and others, 2020). For the calculation of multi-decadal ice velocity change, we use the data spanning 2014–2018, produced from Landsat-8 imagery. While Landsat-8 imagery was used to compute the 2013 velocity field, it was used in conjunction with Landsat-7 imagery, and so the uncertainties are much higher than for 2014–2018 given the lower radiometric resolution of Landsat-7 compared to Landsat-8. Given the slow ice speeds within the interior, any such uncertainty can make up a considerable part of the observed change, hence we do not include data earlier than 2014 in our analyses.

2.3 ITS-LIVE velocity extraction at PARCA GPS sites

Prior to velocity extraction, we exclude pixels with a velocity below 10 m a^{-1}, reasoning that the associated uncertainties constitute an unacceptably high percentage at very low velocities. Following this thresholding, we extract ice velocity (m a^{-1}), ice velocity uncertainty (m a^{-1}), effective pair length (days) and effective centre date from a 3 × 3-pixel (720 × 720 m) window around each of the 161 PARCA GPS sites, taking the median value of each from the extracted window. We repeat this for each year in the period 2014–2018, and then calculate the median velocity and uncertainty across the 2014–2018 period (calculated from whichever years we have data at a given GPS site) to account for any year-to-year variability in ice velocity.

Seasonal variability in ice velocities has been observed near the margins of tidewater glaciers in Greenland (Lemos and others, 2018), as well as up to at least ~70 km inland at Kangiata Nunaata Sermia in southwest Greenland (Sole and others, 2011) and at an elevation of 1850 m (a.s.l.), 140 km inland in the southwest land-terminating sector (Doyle and others, 2014). We calculate the potential impact of such seasonality on the satellite-image-derived velocity data at the PARCA GPS sites, as described in Supplementary Text 1, and observe no coherent pattern showing any clear evidence of seasonality in the velocity data at these elevations.

2.4 Calculating velocity change

For each GPS site, we use the 2014–2018 median ITS-LIVE velocity to calculate a decadal velocity change through the following:

$$\text{Velocity change (m a}^{-1}) = \text{ITS\_LIVE velocity}_{2014-2018} - \text{GPS velocity}$$

$$\text{Velocity change (\%)} = \frac{\text{ITS\_LIVE velocity}_{2014-2018} - \text{GPS velocity}}{\text{GPS velocity}} \times 100$$

It should be noted that for inland regions where the ice is flowing much more slowly than at the margins, any uncertainties in the ice velocity measurements may equal a considerable proportion of any measured velocity change. Following this, we first remove any sites where the measured velocity change (m a^{-1}) is less than or equal to the 2014–2018 median velocity uncertainty (m a^{-1}) extracted from the ITS-LIVE data added to the 0.5 m uncertainty of the GPS measurements (Thomas and others, 1998). To assess temporal variability, at each GPS site, we calculate the std dev. of the annual velocity for the period 2014–2018. We remove any GPS sites where our measured velocity change (2014–2018 median) is less than or equal to the std dev. at that site. The locations of these sites are shown in Figure S7. Following this filtering, we measure decadal velocity change at 45 GPS sites.

At these 45 sites, ITS-LIVE velocity uncertainties range from 0.1 to 11.5 m a^{-1}, with a mean uncertainty of 1.8 m a^{-1}, for the years 2014–2018 (Fig. S8). At the majority of the GPS sites included in our analyses, both median ice velocity uncertainty (m a^{-1}) and the ice velocity std dev. (m a^{-1}) across the 2014–2018 ITS-LIVE data are very low, often <1–2 m a^{-1} (Fig. S8). In addition, almost all of the GPS sites have ITS-LIVE data in all 5 years (2014–2018, Fig. S8D), such that the median velocity and velocity uncertainty are representative of the entire period, thereby limiting any temporal bias.

We observe absolute magnitudes of change ranging from −9.4 ± 3.3 to +28.1 ± 8.3 m a^{-1} (Fig. 1a), and also report these as percentage changes (Fig. 1b). Where there are multiple GPS sites inland of a glacier, we report the range of velocity change values observed across these sites, and we also report the combined ITS-LIVE and GPS uncertainties.

2.5 Velocity time series creation

To compare acceleration in the interior with changes in ice motion at the margins, we create time series of ice velocity at the ice-sheet margin using the full ITS-LIVE dataset from 1985 to 2018 (Gardner and others, 2018, 2019). For each glacier studied, we define an area of interest (AOI) near the terminus. Within this AOI, we then remove pixels that are flowing slower than a specified minimum velocity, as well as pixels with an uncertainty greater

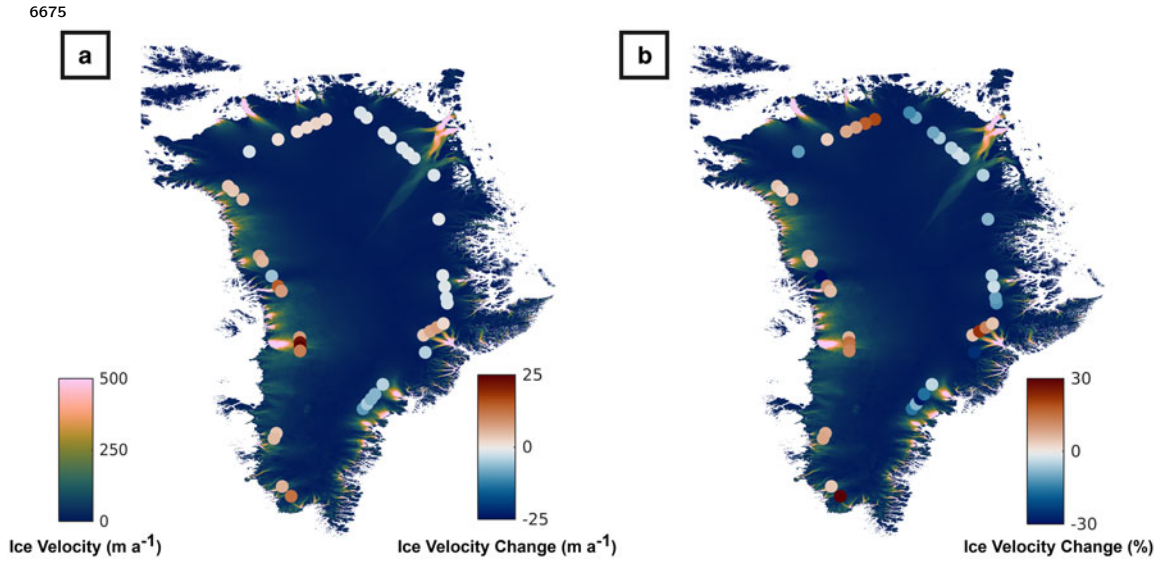

Fig. 1. Ice velocity change (a: m a^{-1}, b: %) at 45 GPS sites inland of tidewater margins between the periods 1993–1997 and 2014–2018. The base image is the 2016 velocity field from the NASA MEaSUREs ITS-LIVE v0 product (Gardner and others, 2018, 2019).

than a specified threshold value, for each year of ITS-LIVE data. These velocity and uncertainty thresholds differ between sites, with full input parameters given in Table S1. We then calculate the pixels common to all years of ITS-LIVE data within the AOI, such that there is no spatial bias influencing the time series. These pixels are shown for each site in Figures S9–S25.

At fast-flowing outlet glaciers, the pair lengths used to compute velocity are often smaller than those further inland where greater temporal separation is necessary to measure displacement given the slower flow speeds. Seasonal velocity variability has been observed at several of Greenland's tidewater glaciers from both GPS measurements (Sole and others, 2011) and satellite remote sensing (Lemos and others, 2018), and may impact upon the extracted velocities and thus time series. As such, we calculate the percentage of summer (JJA) coverage at each common pixel for each year using the centre-date and effective pair length, as described in Supplementary Text 1. We then calculate the median summer coverage across all common pixels for each year of data, and colour-code the scatter points in Figures 2–4 by these values.

2.6 Surface mass balance

Changes in ice motion can be driven by changes in SMB, for example, through meltwater input to the bed (Tedstone and others, 2015), cryo-hydrologic warming (Phillips and others, 2010, 2013) or simply the impact on local driving stress through ice thinning and surface slope change (Tedstone and others, 2015). We obtain SMB data from the MAR v3.10 regional climate model (Fettweis and others, 2017), forced by NCEP-NCARv1 from 1992 to 2019. Modelled melt production and SMB are extracted from a 3-by-3-pixel window around each GPS station, for the years 1990–1999 and 2014–2018. Mean values are calculated for each of these time periods, which are then differenced to calculate the change in modelled melt production and SMB between the GPS and satellite velocity measurement periods.

3. Results

3.1 Multi-decadal velocity change around the 2000 m traverse

We observe a near-ubiquitous acceleration inland of marine-terminating glaciers on the west coast (Fig. 1). Across four GPS sites ~117 km inland of the terminus of Jakobshavn Isbrae, the largest and fastest flowing outlet glacier of the GrIS (Joughin and others, 2004, 2020; Holland and others, 2008; Khazendar and others, 2019), we observe an acceleration ranging from 7.6 ± 4.2 to 28.1 ± 7.8 m a^{-1}.

Similarly, we observe accelerations up-glacier from Narsap Sermia (3.6 ± 0.8 to 4.6 ± 1.6 m a^{-1}) in the southwest, and inland of Rink Isbrae (7.8 ± 2.7 to 14.6 ± 7.5 m a^{-1}), Upernavik Isstrøm (4.9 ± 1.9 to 6.3 ± 2.2 m a^{-1}) and Kong Oscar Gletsjer (3.3 ± 1.0 to 3.7 ± 2.4 m a^{-1}) in central to northwest Greenland. The only glacier where we observe inland deceleration on the west coast is Umiammakku Isbrae (−5.5 ± 2.8 m a^{-1}).

North Greenland is characterised by very small changes in inland flow (−1.8 ± 0.7 to +2.1 ± 0.8 m a^{-1}), with minor accelerations of 1.1 ± 0.4 m a^{-1} and 1.0 ± 0.3 to 2.1 ± 0.3 m a^{-1} inland of Petermann Gletsjer and Ryder Gletsjer, respectively. In contrast, the NEGIS (which drains into 79 North Glacier and Zachariae Isstrøm) has seen a slowdown of −1.3 ± 0.7 to −1.8 ± 0.6 m a^{-1}. To the north of the NEGIS, Academy Gletsjer also shows inland deceleration (−1.3 ± 0.2 to −1.8 ± 0.2 m a^{-1}).

In contrast to west Greenland, interior acceleration has been largely absent from the east coast. In central-east Greenland, the inland region draining into Daugaard-Jensen Gletsjer has decelerated by −1.3 ± 0.4 to −1.5 ± 0.3 m a^{-1}. Further south, Kangerlussuaq has a more complex pattern, with a 1.7 ± 0.8 to 7.5 ± 2.2 m a^{-1} interior acceleration inland of two of its flow branches, and a −4.0 ± 1.9 m a^{-1} deceleration inland of the most southerly branch. In the southeast, we observe decelerations inland of Helheim Gletsjer (−4.1 ± 1.2 to −6.8 ± 1.3 m a^{-1}) and Ikertivaq (−4.9 ± 2.0 to −9.4 ± 2.8 m a^{-1}).

We next assess multi-decadal (1985–2018) time series of near-terminus ITS-LIVE ice velocity (Gardner and others, 2018, 2019) downstream of our inland velocity change measurements to investigate whether the observed inland velocity change may be driven by the up-glacier propagation of acceleration at the terminus.

3.2 Near-terminus velocity change

Numerous studies have measured multi-annual ice velocity change near the terminus of Greenland's tidewater glaciers (e.g. Rignot and Kanagaratnam, 2006; Howat and others, 2007, 2008; Joughin and others, 2008, 2010, 2018; Murray and others, 2010; Bevan and others, 2012; Moon and others, 2012; Mouginot and others, 2015). Through assessing ITS-LIVE ice velocity change (Gardner

6676

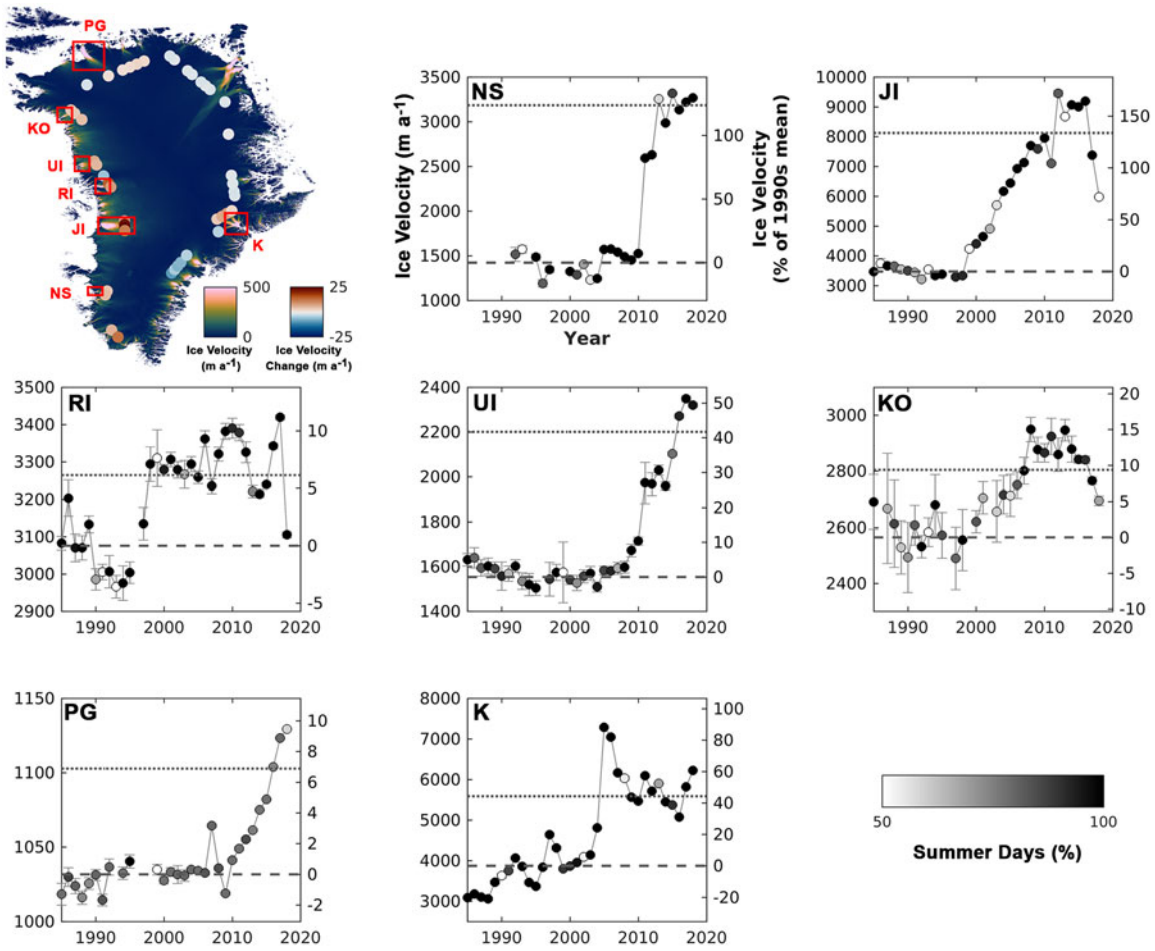

Fig. 2. Time series of ITS-LIVE ice velocity (m a^{-1}) from 1985 to 2018 measured near the terminus (see Supplementary Figs S9–S15 for exact locations) for glaciers inland of which multi-decadal acceleration is observed; (NS) Narsap Sermia, (JI) Jakobshavn Isbrae, (RI) Rink Isbrae, (UI) Upernavik Isstrøm (Central), (KO) Kong Oscar Gletsjer, (PG) Petermann Gletsjer, (K) Kangerlussuaq. Scatter points are colour-coded in greyscale by the percentage of summer (JJA) days over which ice velocities were measured in that particular year (see Methods/Supplementary Information). At each site, only points common to every annual velocity field included in the time series were used for velocity extraction (see Supplementary Figs S9–S15). The dashed line displays the average velocity between 1990 and 1999, and the dotted line displays the average velocity between 2014 and 2018. Input parameters are given in Table S1.

and others, 2018, 2019) from 1985 to 2018 at tidewater glacier margins (Fig. 2) alongside these studies, we observe that those sites where ice velocities were greater between 2014 and 2018 than during the 1990s have also undergone large and/or rapid perturbations downstream. Conversely, five of the six sites without inland acceleration also exhibit acceleration downstream (Fig. 3).

Where multiple GPS sites are present upstream of an individual glacier terminus, inland change is largely consistent across these GPS sites (Fig. 1). At Kangerlussuaq however, the response is more complex. While the glacier terminus underwent a substantial acceleration between 2000 and 2006 (Rignot and Kanagaratnam, 2006; Howat and others, 2007, 2008; Bevan and others, 2012; Moon and others, 2012; Khan and others, 2014), flow diverges into four distinct branches inland (Fig. 4), with acceleration inland of the central flow branches (2 and 3) and deceleration inland of the most southerly branch (1) between 1993–1997 and 2014–2018. For the flow branches (2 and 3) where we observe inland acceleration (of 3.2 ± 1.0 to 6.5 ± 1.4 m a^{-1} and 1.7 ± 0.8 to 7.5 ± 2.2 m a^{-1} respectively, Fig. 1), we observe downstream speed-ups of ~ 100 m a^{-1} (~25%) and 75 m a^{-1} (~20%) between ~2000 and ~2008. A similar ~100 m a^{-1} acceleration is observed at the most easterly branch (4), although the GPS sites inland of this flow branch are filtered out of our analysis. For the most southerly flow branch (1), inland of which we observe a deceleration (-4.0 ± 1.9 m a^{-1}, Fig. 1), we observe minimal downstream change, indicating that differences in downstream flow dynamics may explain the different inland responses of upstream tributaries at Kangerlussuaq.

3.3 Influence of ice geometry

While glaciers that show interior acceleration are characterised by downstream acceleration, several glaciers that have also experienced downstream speed-up exhibit no inland acceleration. Consequently, dynamical change at the margin alone is not necessarily indicative of interior acceleration. To assess whether downstream ice geometry can explain the inland heterogeneity in velocity change between 1993–1997 and 2014–2018, we compare the observed velocity change to basal topography and the extent of subglacial troughs (Fig. 5, Table 1). It is clear that for six out of the eight glaciers where we observe inland acceleration, the overdeepened subglacial trough extends further or at least a comparable distance inland to the PARCA GPS stations (Table 1). This is most evident at Jakobshavn Isbrae, where we observe inland acceleration at four GPS sites, all of which lie within an extensive region underlain by deep basal topography (Fig. 5). Conversely, for four of the seven glaciers where we observe inland deceleration, the GPS stations are largely located far beyond the maximum extent of any subglacial trough, indicating that subglacial topography (and thus ice geometry) may play an important role limiting the propagation distance of perturbations at the terminus for certain glaciers. This pattern, however, is not

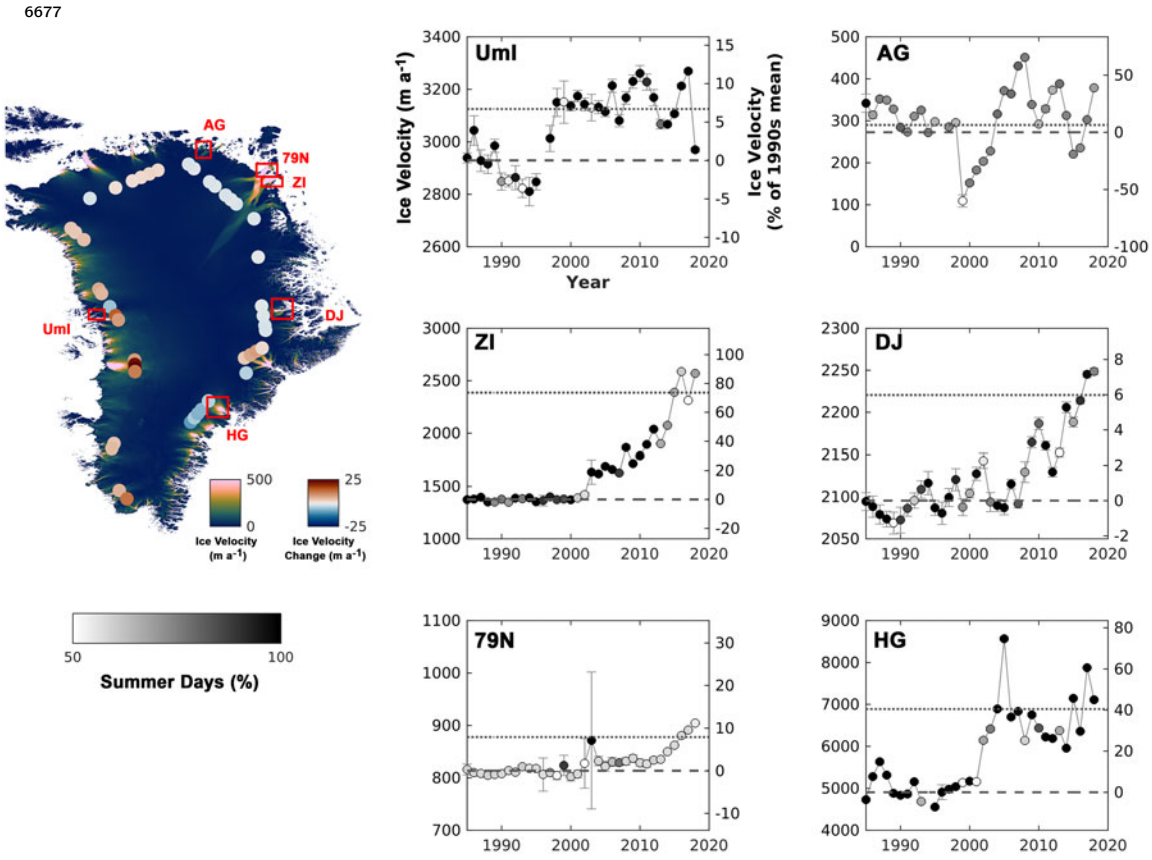

Fig. 3. Time series of ITS-LIVE ice velocity (m a^{-1}) from 1985 to 2018 measured near the terminus (see Supplementary Figs S17–S22 for exact locations) for glaciers inland of which no multi-decadal acceleration is observed; (Uml) Umiammakku Isbrae, (AG) Academy Gletsjer, (79N) 79 North Glacier, (ZI) Zachariae Isstrøm, (DJ) Daugaard-Jensen Gletsjer, (HG) Helheim Gletsjer. Scatter points are colour-coded in greyscale by the percentage of summer days over which ice velocities were measured for that particular year (see Methods/Supplementary Information). At each site, only the points common to every velocity field included in the time series were used for velocity extraction (see Supplementary Figs S16–S21). The dashed line displays the average velocity between 1990 and 1999, and the dotted line displays the average velocity between 2014 and 2018. Input parameters are given in Table S1.

ubiquitous; for example, we do not observe inland acceleration at 79 North Glacier or Zachariae Isstrøm despite extensive subglacial troughs while conversely, we observe acceleration inland of Kangerlussuaq despite the GPS sites being located ~50 km further inland than the head of the respective subglacial trough.

3.4 Influence of surface mass balance

Within the accumulation zone in southwest Greenland, increases in surface melt have been hypothesised to drive acceleration through hydro-dynamic coupling (Doyle and others, 2014) and/or cryo-hydrologic warming (Phillips and others, 2010, 2013). Data from MAR v3.10 (Fettweis and others, 2017) suggest ice-sheet-wide increases in modelled surface melt production within the interior (Figs 6a, b) between the periods 1990–1999 and 2014–2018. The largest increases (42–270 mm a^{-1}) are observed in the west and southeast, whereas increases in the north and northeast are very small (0–45 mm a^{-1}). All of the PARCA GPS sites are characterised by positive SMBs during both the 1990–1999 and 2014–2018 periods (Figs 6c, d), which range from ~90–200 mm a^{-1} in the north to more positive values of ~200–1900 and ~300–650 mm a^{-1} along the east and west coasts, respectively.

4. Discussion

4.1. Mechanisms driving inland change

Our results reveal a complex pattern of inland velocity change over the ~20-year period between 1993–1997 and 2014–2018, for which there exist several possible driving mechanisms.

While we do observe increases in modelled surface melt production at all of the GPS sites, and decreases in modelled SMB at most (Fig. 6), we see no evidence that any of the sites have undergone a transition from the accumulation to the ablation zone during the study period. Although cryo-hydrologic warming may also occur in the wet snow zone of the lower accumulation zone (Phillips and others, 2013), all 45 sites remain well within the accumulation zone as evidenced by positive modelled SMBs during 2014–2018 (all >~10 cm w.e., with a mean of 43 cm w.e., Fig. 6d). This is consistent with in situ stake observations which show no evidence of negative SMB above ~1700 m (a.s.l.) across 17 sites in Greenland (Machguth and others, 2016), and a persistent positive SMB at site S10 (1850 m a.s.l.) of the K-transect in southwest Greenland (van de Wal and others, 2012), despite increases in surface melt at this site (Doyle and others, 2014). Furthermore, analysis of surface strain rates indicates that moulins and crevasses are unlikely to form above 1600 m (a.s.l.), and so meltwater access to the englacial drainage system is likely limited at these elevations (Poinar and others, 2015) and will instead flow along surface streams into moulins further downstream.

Ice flow may also be affected by the presence of firn aquifers, which are thought to be extensive in southeast Greenland (Miège and others, 2016; Brangers and others, 2020) and which may store significant quantities of meltwater for several decades (Harper and others, 2012; Forster and others, 2014; Miller and others, 2018). Water stored in firn may increase ice motion through latent heat transfer (Phillips and others, 2010, 2013; Poinar and others, 2017) and/or through drainage to the bed (Miège and others, 2016; Poinar and others, 2017, 2019). In the case of the

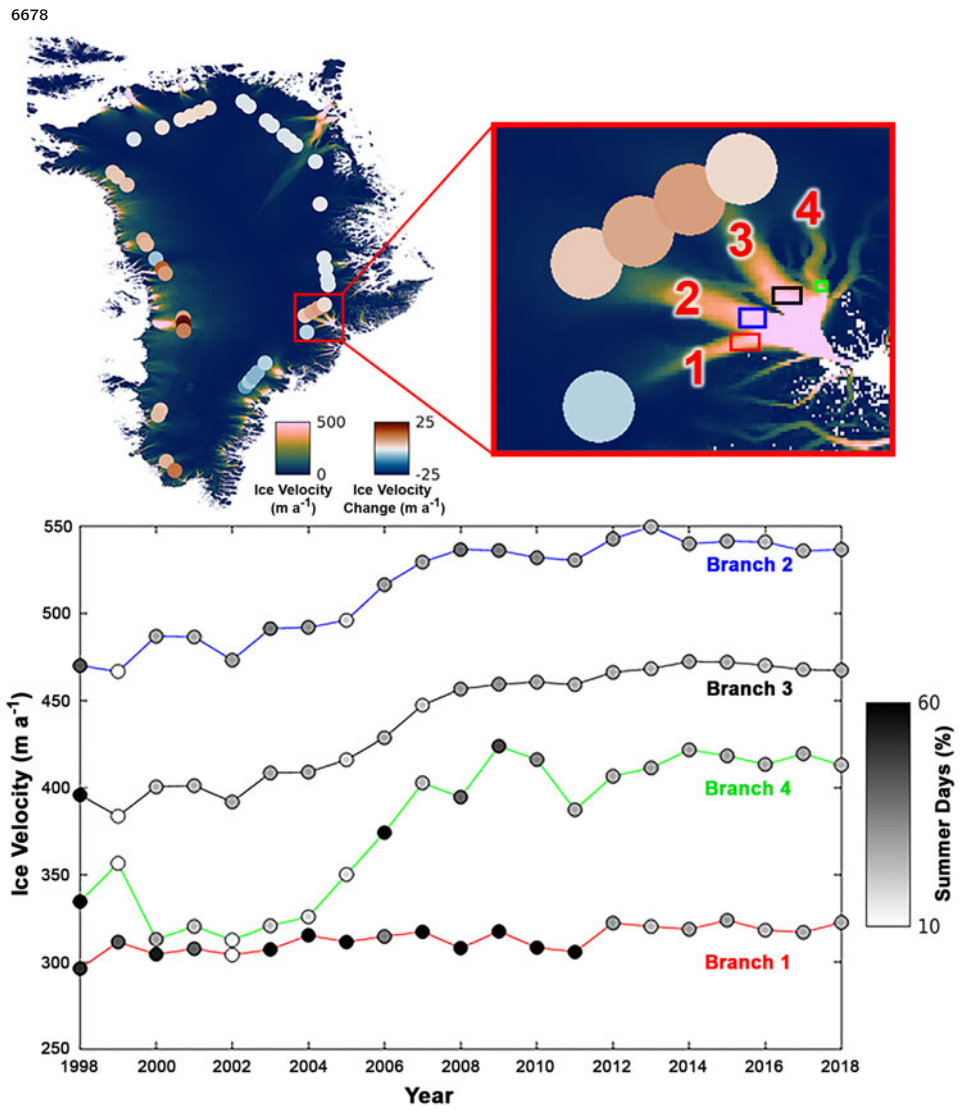

Fig. 4. Time series of ITS-LIVE ice velocity (m a^{-1}) from 1998 to 2018 measured at the four flow branches of Kangerlussuaq, with velocity extraction from pixels within the rectangle on each branch. Scatter points are colour-coded by the percentage of summer days over which ice velocities were measured for that particular year (see Methods/Supplementary Information). At each site, only the points common to every velocity field included in the time series were used for velocity extraction (see SI Figs S22–S25). Input parameters are given in Table S1.

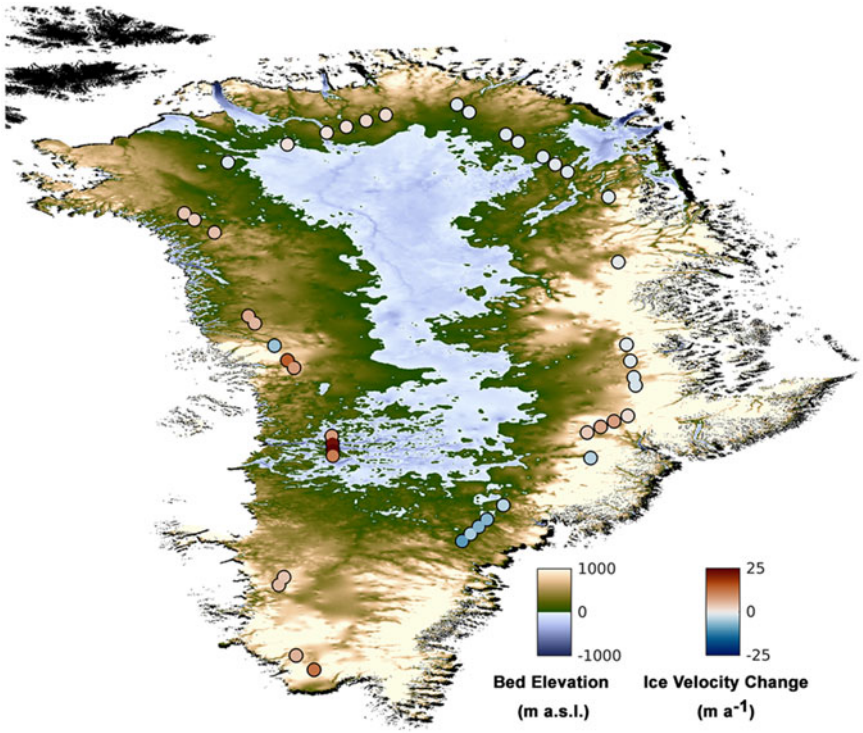

Fig. 5. Ice velocity change (m a^{-1}) at 45 GPS sites inland of tidewater margins between the periods 1993–1997 and 2014–2018, compared to basal topography from BedMachineV3 (Morlighem and others, 2017).

6679

Table 1. Comparison of PARCA GPS distance inland and measured velocity change (m a^{-1}) between 1993–1997 and 2014–2018 with the extent of subglacial troughs (Morlighem and others, 2014, Table S1) at 15 tidewater glaciers on the Greenland Ice Sheet

Glacier name Location	Distance of PARCA GPS site from terminus (km)		Subglacial trough length (km)[a] (Morlighem and others, 2014)	Trough length – average distance inland (km)	Inland velocity change (m a^{-1})	
	Min	Max			Min	Max
Central and southwest						
Narsap Sermia	92	92	77	−15	3.6	4.6
Jakobshavn Isbrae	117	118	170	52.5	7.6	28.1
Northwest						
Rink Isbrae	90	94	88	−4	7.8	14.6
Umiammakku Isbrae	115	115	39	−76	−5.5	−5.5
Upernavik Isstrøm (C)	97	97	90	−7	4.9	6.3
Kong Oscar Gletsjer	85	86	101	15.5	3.3	3.7
North						
Petermann Gletsjer	200	200	400	200	1.1	1.1
Ryder Gletsjer	180	216	191	−7	1	2.1
Academy Gletsjer	153	165	102	−57	−1.8	−1.3
Northeast						
79 North Glacier	210	219	404	189.5	−1.6	−1.5
Zachariae Isstrøm	190	240	377	162	−1.8	−1.3
Central and southeast						
Daugaard-Jensen Gletsjer	108	137	70[b]	−52.5	−1.5	−1.3
Kangerlussuaq	131	141	87	−49	−4	7.5
Helheim Gletsjer	118	120	68	−51	−6.8	−4.1
Ikertivaq	96	130	0	−113	−9.4	−4.9

As neighbouring GPS sites may have differing distances from the margin, we compare the average distance of these sites inland of a particular glacier to the subglacial trough length at that glacier.
[a]Subglacial trough lengths were calculated by Morlighem and others (2014, Table S1) using the longest flowline that connects the ice front to the interior of the ice sheet, and do not necessarily follow the glacier centreline.
[b]Daugaard-Jensen Gletsjer is stated to have a trough length of 70 km in the main manuscript, with a maximum trough length of 124 km given in Supplementary Information.

latter, the presence of a firn aquifer may buffer the supply of meltwater to the bed, and thus possibly mask any long-term trend between ice velocity and meltwater production. However, drainage from firn aquifers is thought to most likely occur where there exists a downstream crevasse field through which it can drain to the bed (Miège and others, 2016), and so may have a limited impact upon ice flow at the inland locations assessed in this study.

Changes in surface slope and/or ice thickness through both ice dynamical and SMB-related processes cause changes in driving stress and can thus contribute to changes in ice motion through changes to the internal deformation rate. To assess whether the velocity changes observed may be explained by changes in local driving stress, we estimate the expected change in velocity as a result of changes in ice thickness and surface slope at PARCA GPS site 36, inland of Jakobshavn Isbrae, where we observe the largest velocity increase. Applying this calculation elsewhere is difficult as the observed velocity changes are small (Fig. 1), the uncertainties associated with the SEC are proportionally large, and the potential errors associated with the following 20-year approximate SEC reconstruction, and thus the 1990s slope estimate, are too great, thus reducing confidence in our ability to make any meaningful comparison.

We extract ice thickness and surface slope, the latter calculated using surface elevation and under the assumption that ice flows in the direction of the steepest slope, at this location from BedMachineV3 (Morlighem and others, 2017), and consider this as a representative for the period 2014–2018. We then use the CCI SEC v2.0 product (Simonsen and Sørensen, 2017; Sørensen and others, 2018) to calculate the cumulative SEC at each pixel within the 3 × 3-pixel window surrounding site 36, across the periods 1993–1997, 1998–2002, 2003–2007, 2007–2011 and 2012–2016. By adding this SEC to the ice thickness from BedMachineV3, we get a rough estimate of the initial ice thickness in 1993. Similarly, by adding the cumulative SEC to the BedMachineV3 surface elevation within the same 3 × 3-pixel window, we calculate an approximate initial surface slope for 1993. We subsequently calculate the change in ice thickness and surface slope.

The first-order relative change in surface velocity (δu_s) as a result of changes in ice thickness and surface slope can be characterised by the following (Tedstone and others, 2015):

$$\delta u_s = u_s\left(3\frac{\delta S}{S} + 4\frac{\delta H}{H}\right)$$

where u_s represents the initial ice surface velocity (194.5 m a^{-1}), S and H represent the initial surface slope (0.018 m m^{-1}) and ice thickness (1740.2 m), respectively, and δS and δH represent the change in surface slope (0.001 m m^{-1}) and ice thickness (−7.2 m), respectively. The resultant approximation for a change in deformational velocity is 35.02 m a^{-1}, which is within the uncertainty range of the observed velocity change (28.1 ± 7.8 m a^{-1}) and thus compares well.

We also assess the role that SMB-driven thickness changes play in driving velocity change (Mernild and others, 2013). There has been extensive SMB-driven thinning around Greenland (van den Broeke and others, 2009; Mouginot and others, 2019), for example, at site 36, modelled melt production increases by 150 mm a^{-1} between the 1990–1999 and 2014–2018 means (Fig. 6a). However, we observe no obvious spatial correlation between changes in ice velocity (Fig. 1) and modelled surface melt production. While we do observe large increases in surface melting (>100 mm a^{-1}) at some GPS sites where we observe acceleration (i.e. inland of Jakobshavn Isbrae, Upernavik Isstrøm and Kong Oscar Gletsjer in the central to northwest), the GPS sites on the east coast show an almost pervasive deceleration despite increases in modelled melt production. This is most notable at the south-eastern GPS sites, where increases in modelled melt production are of a similar or greater magnitude (47–270 mm a^{-1}) to those in the central and northwest (42–162 mm a^{-1}).

To assess the impact of this SMB forcing alone, we follow Tedstone and others (2015) by taking a 100 km transect, extending 50 km on either side of site 36, and calculating the slope change from the linear change in ice thickness over this distance.

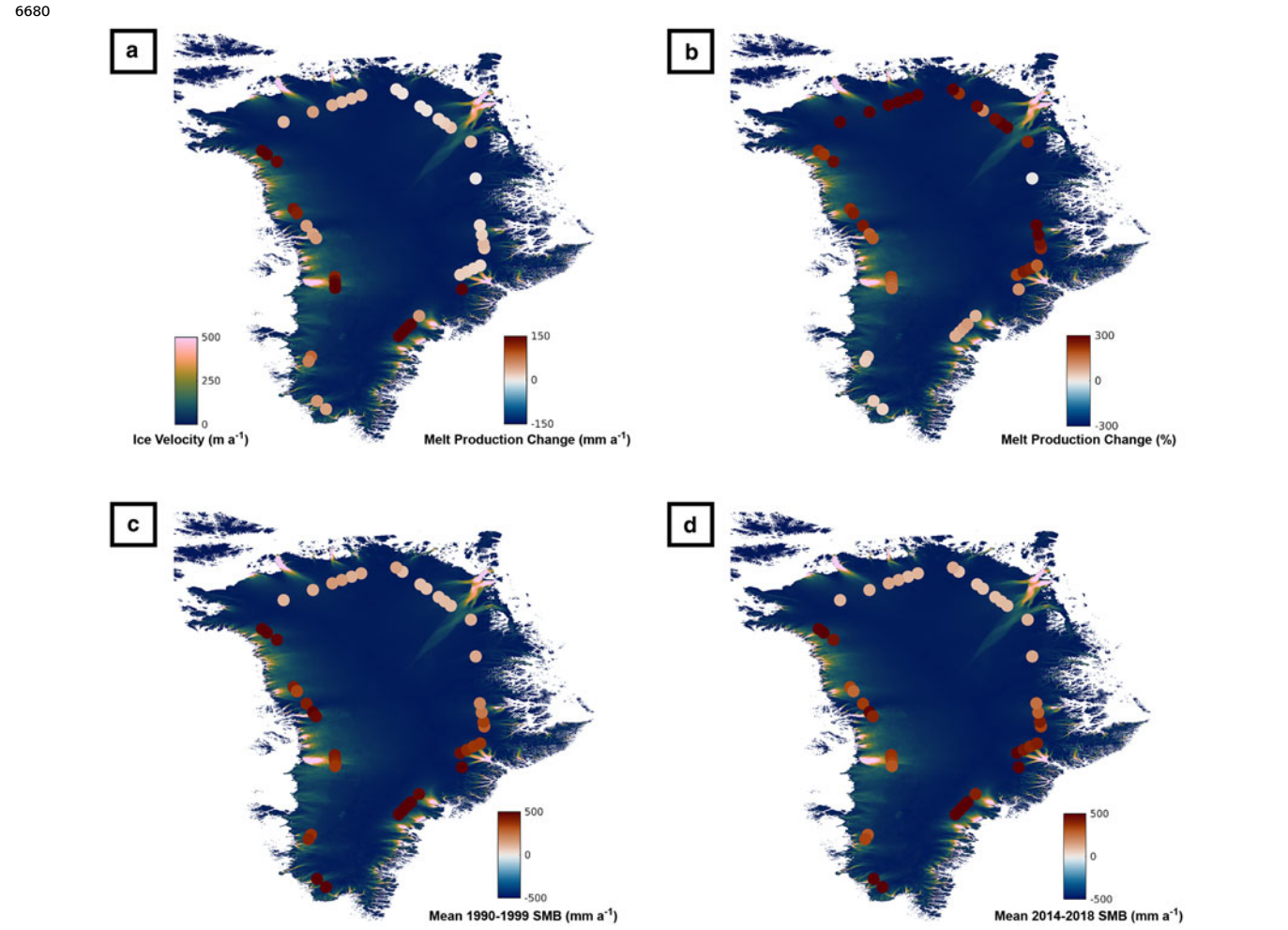

Fig. 6. (a) Modelled surface melt production change (mm a^{-1}), (b) modelled surface melt production change (%), (c) mean modelled 1990–1999 SMB (mm a^{-1}) and (d) mean modelled 2014–2018 SMB (mm a^{-1}) at 45 GPS sites inland of tidewater margins. Modelled melt production change is calculated between the 1990–1999 and 2014–2018 means. The base image is the 2016 velocity field from the NASA MEaSUREs ITS-LIVE v0 product (Gardner and others, 2018, 2019). Modelled surface melt production and SMB data are from MAR v3.10 (Fettweis and others, 2017).

Modelled melt production increased by 184.5 and 41.3 mm a^{-1} between the 1990–1999 and 2014–2018 means at the downstream and upstream ends of the transect, respectively, a difference of 143.2 mm a^{-1}, and the concurrent change in accumulation rate is negligible. Assuming a linear increase in melt production over 20 years, this gives a total thinning of 1.5 m and a steepening of 0.000015 m m^{-1}.

Applying the above equation, we estimate the associated change in deformational velocity as −0.18 m a^{-1}, indicating that at site 36, SMB changes alone are unable to explain the observed velocity acceleration, and counteract some of the observed velocity increase. The modelling therefore suggests that in this inland region of the ice sheet, changes in surface slope are insufficient to overcome the reduction in driving stress caused by thinning. At all other sites where we observe acceleration, modelled melt production increase is either similar (northwest Greenland) or less than that observed inland of Jakobshavn Isbrae (Fig. 6a). As such, assuming a relatively consistent ice-sheet hypsometry, this suggests that a change in SMB may often act to oppose acceleration and is unlikely to drive an inland velocity change of more than several tens of cm a^{-1}.

Changes to SMB have also been hypothesised to influence ice motion through cryo-hydrologic warming in regions transitioning from the accumulation to the ablation region (Phillips and others, 2010, 2013). Despite increases in modelled melt production, we observe that all of the PARCA GPS sites have strongly positive modelled SMB in both the 1990–1999 and 2014–2018 periods (Figs 6c, d), and so we observe no evidence of a transition between accumulation and ablation zones at any site, with all 45 GPS sites remaining well within the accumulation zone.

As a result, we argue that our observations of inland acceleration are most likely driven by the upstream propagation of changes initiated at the terminus (Howat and others, 2005, 2007; Joughin and others, 2008; Price and others, 2008, 2011; Nick and others, 2009; Felikson and others, 2017). This mechanism is discussed in more detail in the subsequent sections.

4.2. Observed velocity changes and regional differences

We observe almost ubiquitous acceleration across the GPS sites inland of tidewater glaciers in west Greenland with a slowdown at Umiammakku Isbrae being the only exception. The largest acceleration is observed ~117 km inland from the terminus of Jakobshavn Isbrae (7.6 ± 4.2 to 28.1 ± 7.8 m a^{-1}), which is unsurprising given the high magnitude of acceleration and thinning observed near the terminus between the late-1990s and early-2010s (Joughin and others, 2004, 2008, 2014, 2018; Luckman and Murray, 2005; Holland and others, 2008; Moon and others, 2012), primarily as a result of reduced back-stress through the loss of its floating ice tongue (Joughin and others, 2004; Thomas, 2004; Holland and others, 2008; Motyka and others, 2011). Moreover, modelling of dynamic thinning suggests that faster ice flow facilitates a larger magnitude propagation inland, with modelled thinning rates at 2000 m elevation of nearly

6681
$-0.4\ m\ a^{-1}$ within a drainage system with a mean flow velocity of $\sim 120\ m\ a^{-1}$ as opposed to an ice-sheet-wide average of $\sim -0.1\ m\ a^{-1}$ with a mean velocity of $\sim 60\ m\ a^{-1}$ (Wang and others, 2012), and Jakobshavn Isbrae is the fastest flowing outlet glacier on the GrIS (i.e. Joughin and others, 2014, 2018).

We also observe inland acceleration at other tidewater glaciers in west Greenland that have undergone terminus retreat and associated near-terminus acceleration, such that their 2014–2018 ice velocities were greater than during the 1990s (Fig. 2). For example, the northern and central branches of Upernavik Isstrøm underwent rapid calving, retreat and acceleration beginning during the mid-late 2000s (Khan and others, 2013; Larsen and others, 2016), and Narsap Sermia accelerated and retreated by ~3.3 km between 2010 and 2014, primarily as a result of increased submarine melting (Motyka and others, 2017). Similarly, Kong Oscar Gletsjer and Rink Isbrae retreated by several kilometres during the mid-2000s (Bevan and others, 2012) and the mid-late 1990s (Catania and others, 2018) respectively, in conjunction with acceleration (Fig. 2). Inland of these west coast glaciers, we observe acceleration ranging from 3.3 ± 1.0 to $3.7 \pm 2.4\ m\ a^{-1}$ inland of Kong Oscar Gletsjer up to $14.6 \pm 7.5\ m\ a^{-1}$ inland of Rink Isbrae. However, we observe a clear contrast between the dynamics of west and east Greenland. While outlet glaciers on the west coast almost all demonstrate inland acceleration, there is little evidence of propagation of downstream change inland of tidewater glacier termini on the east coast. We observe no evidence of inland acceleration at Helheim Gletsjer, Zachariae Isstrøm and 79 North Glacier, all of which have undergone significant frontal retreat and acceleration at some point between our measurement periods of 1993–1997 and 2014–2018 (Howat and others, 2005, 2007, 2008; Rignot and Kanagaratnam, 2006; Murray and others, 2010; Bevan and others, 2012; Mouginot and others, 2015; our Fig. 3).

The duration of a specific terminus perturbation does not appear to control the likelihood of that perturbation propagating inland. We observe inland acceleration at sites with long-term perturbations (Jakobshavn Isbrae, Upernavik Isstrøm, Kong Oscar Gletsjer) as well as at sites with relatively short-term accelerations (i.e. Kangerlussuaq, Narsap Sermia), although all sites where we observe acceleration were flowing faster in their terminus regions during 2014–2018 than during 1990–1999. Moreover, we observe no inland acceleration at Zachariae Isstrøm despite continual acceleration since the early-2000s, or at Helheim Gletsjer which underwent a rapid speed-up of short duration from ~2002 to 2005 (Fig. 3). It may be that perturbations at the terminus have yet to propagate to the PARCA GPS sites inland of some tidewater glaciers, particularly in the north and northeast (Fig. S6) where the GPS sites are ~165–240 km inland from the terminus as opposed to ~85–141 km on the east and west coasts. Thinning has been observed to propagate along ice streams in West Antarctica at the rates of 6–15 $km\ a^{-1}$ (Konrad and others, 2017) while acceleration near the terminus of Kangerlussuaq propagated 10 km up-glacier between 2005 and 2006 (Howat and others, 2007). While recent work observes propagation rates in the lowest 20 km of Jakobshavn Isbrae an order of magnitude faster than the local mean flow speed (Riel and others, 2020), the rates of propagation have not been observed further inland, or elsewhere in Greenland, and we are unable to determine propagation rates given the gap in our time series. Surface velocities derived from Landsat missions prior to Landsat-8 are characterised by both a reduced spatial coverage in inland regions, due to insufficient radiometric resolution to measure subtle features on the ice-sheet surface (Fahnestock and others, 2016), and increased uncertainties, which are particularly problematic given the slow surface velocities as one moves inland. Regardless, it is plausible that perturbations have not yet had the time to propagate sufficiently far inland to be observed at the PARCA GPS sites in northeast Greenland, especially given that the rate of propagation will slow as it moves further inland (van der Veen, 2001). This is supported by separate velocity measurements, which show no evidence of acceleration beyond ~80–100 and ~50 km inland of Zachariae Isstrøm and 79 North Glacier, respectively (Mouginot and others, 2015; their Fig. 2). Further south at Daugaard-Jensen and Helheim Gletsjers however, the PARCA GPS sites are a comparable distance inland to those on the west coast, as well as those at Kangerlussuaq, which have undergone acceleration in response to terminus perturbations, indicating that there may be an alternative control on the speed and/or limit of propagation (i.e. Felikson and others, 2017, 2020).

4.3. Influence of basal topography and ice geometry

Basal topography is a crucial factor controlling ice flow. Beneath the GrIS, widespread ice-filled valleys have been observed to extend significantly deeper below sea level and farther inland than previously thought (Morlighem and others, 2014), thereby channelling ice flow over distances from tens to hundreds of kilometres. Since deep troughs and the associated thicker ice lead to both higher driving stresses and warmer ice, they will encourage faster ice flow and potentially greater propagation distances (Wang and others, 2012). We observe almost ubiquitous interior acceleration in the central and northwest regions, across areas that are characterised by low surface slopes and bed topography that remains below sea level for tens to hundreds of kilometres inland (Morlighem and others, 2017).

For example, Jakobshavn Isbrae flows through a subglacial valley extending ~170 km inland (Morlighem and others, 2014), whereas the PARCA GPS sites are located ~117 km from the terminus (Table 1). Under these conditions, not only do we observe the large acceleration at the terminus, but this acceleration is likely to be channelled to, and beyond, the site at which we measure inland velocity change in this study. Similar patterns are observed at other west coast glaciers, where PARCA GPS sites are closer to the margin than the extent of the associated subglacial valleys, or, if further inland than the head of the valley, are at least within the theoretical stress-coupling length (4–10× the ice-thickness (Kamb and Echelmeyer, 1986)) of the maximum subglacial valley extent. In contrast, the one glacier on the west coast where we do not observe inland acceleration is Umiammakku Isbrae, despite near-terminus flow velocities $\sim 200\ m\ a^{-1}$ greater in the 2000s and 2010s compared to the early- to mid-1990s (Fig. 3). Here, an overdeepened subglacial valley extends just ~39 km from the terminus (Morlighem and others, 2014), whereas the PARCA GPS site is located ~115 km inland.

In the north, we observe no inland acceleration at Academy Gletsjer, where the head of the submarine valley is ~57 km closer to the terminus than the PARCA GPS sites. Similarly, outside of two flow branches of Kangerlussuaq, we observe no evidence of interior propagation on the east coast, where despite the existence of deep subglacial valleys (Morlighem and others, 2017), basal topography rises quickly to plateaus above sea level (Morlighem and others, 2014), suggesting that these rapid rises in basal topography may limit the inland propagation of any thinning perturbation. This is the case at Helheim Gletsjer and Daugaard-Jensen Gletsjer, which are both grounded below sea-level for ~70 km, whereupon rises in basal topography over a short-distance have been theorised to prevent rapid glacier retreat or ice-sheet drawdown (Morlighem and others, 2014). Given that the PARCA GPS sites inland of Helheim Gletsjer and Daugaard-Jensen Gletsjer are ~118–120 and 108–137 km from the terminus, respectively, it is plausible that any perturbation at the terminus is limited

6682

by the rapid rise in basal topography at the end of the subglacial trough, such that no inland response is observed in our study.

This hypothesis, and our observations, is largely consistent with recent work that argues that steep rises (termed 'knickpoints') in bedrock topography act to limit the extent of inland thinning, such that the gentle basal topography of the northwest facilitates the propagation of thinning far into the ice-sheet interior, and the mountainous basal topography of the central east and southeast limits propagation to near the margin (Felikson and others, 2020). We observe inland acceleration at Rink Isbrae, Upernavik Isstrøm and Kong Oscar Gletsjer in the northwest, consistent with proposed thinning limits of >400, >300 and ~500 km, respectively (Felikson and others, 2020). Likewise, our observation of no inland speed-up at Umiammakku Isbrae is consistent with a thinning limit of 43.8 km, considerably downstream of the PARCA GPS site. Our results are also in agreement on the east coast, where Daugaard-Jensen Gletsjer and Helheim Gletsjer are characterised by thinning limits of 53.5 and 26.7 km (Felikson and others, 2020), again located >50 km downstream of the PARCA GPS sites and in line with the lack of inland acceleration observed in this study. While both 79 North and Zachariae Isstrøm show no inland acceleration despite extensive subglacial valleys extending beyond the PARCA GPS sites, as noted previously, it is plausible that since these sites are several hundred kilometres from the margin, the propagation speed is such that any downstream perturbation has not yet reached them. Alternatively, knickpoints in bed topography may limit any dynamic propagation to ~100–120 km inland of the termini of these glaciers, considerably downstream from the PARCA GPS sites in this region (Felikson and others, 2020).

Our observations of inland acceleration at Jakobshavn Isbrae, Narsap Sermia and Kangerlussuaq, however, are in contrast to the thinning limits suggested by Felikson and others (2020) at these glaciers (57.9, 37.3 and 35.3 km, respectively). Since Felikson and others (2020) argue that the Pe = 3 threshold accounts for 89% (with an interquartile range of 76–100%) of the total dynamic loss, our observations of acceleration inland of these glaciers may represent the remaining ~11% of dynamic change that has propagated beyond the empirical thinning limit. Alternatively, at Jakosbhavn Isbrae, there may be some uncertainty associated with the choice of flowline within the Pe analysis, with earlier work indicating a thinning limit of 240 km (Felikson and others, 2017) compared to the more recent 57.9 km estimate (Felikson and others, 2020).

While we observe acceleration inland of the suggested thinning limits at Jakobshavn Isbrae and Narsap Sermia, these accelerations remain consistent with the extent of underlying subglacial troughs (Table 1). In contrast, at Kangerlussuaq, our observed acceleration is both ~100 km inland of the thinning limit proposed by Felikson and others (2020), and ~49 km inland of the maximum subglacial trough extent. Consequently, while basal topography and ice geometry appear to offer a compelling explanation for much of the observed inland velocity change, it is clear that the processes controlling tidewater glacier dynamics are complex. As such, multiple controls will likely impact the ability of a terminus perturbation to propagate inland, thus affecting how different inland regions of the GrIS have responded and will continue to respond to climate warming.

4.4. Comparison with other studies

Recent measurements of mass change between 2003 and 2019 from ICESat and ICESat-2 show a clear pattern of coastal thinning around the entire periphery of the GrIS, which decreases inland and changes to thickening at 2000–2500 m (a.s.l.) in southern and western Greenland, and at 1500 m (a.s.l.) in the northeast (Smith and others, 2020). Thinning extends furthest inland at Jakobshavn Isbrae and in the northwest, consistent with our observations of multi-decadal accelerations in these inland regions. Similarly, mass change is far more limited in extent in the central east and northeast regions where we do not observe inland acceleration, although in the southeast, thinning appears to extend to approximately the locations of the GPS sites at which we observe no acceleration. As the dynamic component of mass change is not isolated in these ICESat and ICESat-2 data, the south-eastern thinning may be influenced by a decrease in SMB, which has contributed to 36 ± 12% of mass loss in this region between 1972 and 2018 (Mouginot and others, 2019).

Measurements of SEC can be used to isolate the dynamic component of a thinning signal through the differencing of measured elevation change and modelled SMB (i.e. Pritchard and others, 2009; McMillan and others, 2016). This methodology has revealed extensive dynamic thinning, penetrating deep into the ice-sheet interior. At Jakobshavn Isbrae, thinning has been observed ~120 km inland (Pritchard and others, 2009), extending upwards of 2000 m surface elevation as early as 2001 (Thomas and others, 2003). Similar pervasive thinning has been observed inland of other fast-flowing tidewater glaciers, notably Helheim Gletsjer, Kangerlussuaq, Upernavik Isstrøm and Zachariae Isstrøm (Pritchard and others, 2009; McMillan and others, 2016). On a regional scale, the northwest and southeast margins are characterised by the strongest dynamic thinning (Pritchard and others, 2009; Zwally and others, 2011; Csatho and others, 2014) although the furthest propagation of thinning inland is observed in the west and northwest, with thinning in the southeast less extensive (Zwally and others, 2011; Csatho and others, 2014). Moreover, in the southeast, the inland extent of dynamic thinning has been observed to rapidly decrease between the period 2003–2005 and 2009 (Csatho and others, 2014), and outside of Kangerlussuaq, significant signals of dynamic thinning are not clear (McMillan and others, 2016).

These observations are reinforced by modelling work, which indicates that dynamic thinning may penetrate deep into the ice sheet in as little as 10 years of an initial perturbation, with modelled thinning rates of up to 40 cm a^{-1} extending to 2000 m elevation in central west and northwest Greenland (Wang and others, 2012). For the fast-flowing outlet glaciers of Jakobshavn Isbrae, Helheim Gletsjer and Kangerlussuaq, modelling of dynamic thinning along the centre-profile between 2003 and 2005 suggests thinning during this period would reach ~80–100 km inland of the terminus at Jakobshavn Isbrae and ~30–40 km inland at both Helheim Gletsjer and Kangerlussuaq (Price and others, 2011).

Our work largely supports these studies. We observe a strong interior acceleration inland of Jakobshavn Isbrae, a region characterised by extremely strong dynamic thinning (Pritchard and others, 2009; Zwally and others, 2011; Csatho and others, 2014; McMillan and others, 2016), with speed-ups of smaller magnitude inland of other west coast tidewater glaciers. We observe interior acceleration upstream of two of the main flow branches of Kangerlussuaq on the east coast, and do not measure any long-term interior acceleration inland of Helheim Gletsjer or Zachariae Isstrøm, despite indications of some penetration of dynamic thinning inland at these glaciers (Pritchard and others, 2009; McMillan and others, 2016). Our observations in northeast Greenland are supported by other satellite-image-derived velocities, which indicate little if any interior acceleration inland of Zachariae Isstrøm and 79 North Glacier beyond ~80–100 and ~50 km from the terminus, respectively (Mouginot and others, 2015).

5. Conclusions

In this study, we present the first multi-decadal analysis of ice-sheet-wide changes in ice velocity within the accumulation

6683

zone of the GrIS. Along the west coast, we observe evidence of inland acceleration, most likely in response to perturbations originating at tidewater glacier termini. In contrast, away from Kangerlussuaq, we observe no inland acceleration on the east coast, despite acceleration and thinning at the terminus of many of these marine-terminating glaciers. The complexity within the observed pattern of inland change likely reflects a range of controls, including the speed at which a perturbation can propagate inland, and the influence of ice geometry and basal topography in facilitating or limiting the extent to which a perturbation can propagate up-glacier.

These findings are of great importance with regards to Greenland's future contribution to global sea-level rise, as they indicate that ice acceleration at many tidewater glaciers has the potential to propagate considerable distances into the ice-sheet interior, accelerating the draw-down of greater volumes of thicker ice towards the margins, thus accelerating mass loss. Moreover, our results indicate that this mass loss as a result of the draw-down of ice from the interior should be further exacerbated by future acceleration and thinning perturbations at tidewater margins. However, our results also support recent work that indicates that local ice geometry and bed topography are crucial in facilitating or limiting the ability for a perturbation at the terminus to propagate inland (Morlighem and others, 2014, 2017; Felikson and others, 2017, 2020), and suggest that as a result of steep down-glacier bed topography, inland regions in east Greenland may be more resilient to the impacts of future outlet glacier acceleration than those in the west. This is consistent with recent work that suggests that the presence of steep subglacial knickpoints limits the extent to which thinning can diffuse inland, particularly in the southeast, whereas the gentle bed topography of the northwest facilitates the propagation of thinning hundreds of kilometres inland (Felikson and others, 2020). Consequently, we expect that Greenland's future contribution to global sea-level rise will be spatially complex and will depend on the ability for dynamic changes at the termini of individual outlet glaciers to propagate inland.

Supplementary material. The supplementary material for this article can be found at https://doi.org/10.1017/jog.2021.31

Acknowledgements. J.J.W. was funded by a UK Natural Environment Research Council (NERC) doctoral training partnership grant (NE/L002558/1). We thank Xavier Fettweis for providing the MAR v3.10 SMB data, and Denis Felikson for helpful discussions with regards to the propagation of terminus perturbations inland. We also thank the two reviewers whose suggestions and comments helped improve the manuscript.

Author contributions.
J.J.W., N.G. and P.N. contributed to the design of the study and the writing of the paper. J.J.W. performed data processing and analyses.

References

Ahlstrøm AP and 13 others (2013) Seasonal velocities of eight major marine-terminating outlet glaciers of the Greenland ice sheet from continuous in situ GPS instruments. *Earth System Science Data* **5**(2), 277–287.

Bamber JL, Westaway RM, Marzeion B and Wouters B (2018) The land ice contribution to sea level during the satellite era. *Environmental Research Letters* **13**(6), 099502.

Bartholomew I and 5 others (2010) Seasonal evolution of subglacial drainage and acceleration in a Greenland outlet glacier. *Nature Geoscience* **3**(6), 408–411.

Bartholomew ID and 6 others (2011) Seasonal variations in Greenland Ice Sheet motion: inland extent and behaviour at high elevations. *Earth and Planetary Science Letters* **307**(3–4), 271–278.

Bevan SL, Luckman AJ and Murray T (2012) Glacier dynamics over the last quarter of a century at Helheim, Kangerdlugssuaq and 14 other major Greenland outlet glaciers. *The Cryosphere* **6**, 923–937.

Brangers I and 5 others (2020) Sentinel-1 detects firn aquifers in the Greenland Ice Sheet. *Geophysical Research Letters* **47**(3), https://doi.org/10.1029/2019GL085192.

Bunce C, Carr R, Nienow PW, Ross N and Killick R (2018) Ice front change of marine-terminating outlet glaciers in northwest and southeast Greenland during the 21st century. *Journal of Glaciology* **64**(246), 523–535.

Catania G and 7 others (2018) Geometric controls on tidewater glacier retreat in central western Greenland. *Journal of Geophysical Research: Earth Surface* **123**(1), 2024–2038.

Csatho BM and 9 others (2014) Laser altimetry reveals complex pattern of Greenland ice sheet dynamics. *Proceedings of the National Academy of Sciences* **111**, 18478–18483.

Cuffey KM and Paterson WSB (2010) *The Physics of Glaciers*, 4th Edn. Oxford: Butterworth-Heinemann.

Dehecq A, Gourmelen N and Trouvé E (2015) Deriving large-scale glacier velocities from a complete satellite archive: application to the Pamir-Karakoram-Himalaya. *Remote Sensing of Environment* **162**, 55–66.

Doyle SH and 6 others (2014) Persistent flow acceleration within the interior of the Greenland ice sheet. *Geophysical Research Letters* **41**(3), 899–905.

Enderlin EM and 5 others (2014) An improved mass budget for the Greenland ice sheet. *Geophysical Research Letters* **41**(3), 866–872.

Fahnestock M and 5 others (2016) Rapid large-area mapping of ice flow using Landsat 8. *Remote Sensing of Environment* **185**, 84–94.

Felikson D and 11 others (2017) Inland thinning on the Greenland ice sheet controlled by outlet glacier geometry. *Nature Geoscience* **10**(5), 366–369.

Felikson D, Catania G, Bartholomaus TC, Morlighem M and Noël B (2020) Steep glacier bed knickpoints mitigate inland thinning in Greenland. *Geophysical Research Letters*. doi: 10.1029/2020GL090112.

Fettweis X and 8 others (2017) Reconstructions of the 1900–2015 Greenland ice sheet surface mass balance using the regional climate MAR model. *The Cryosphere* **11**(2), 1015–1033.

Forster RR and 12 others (2014) Extensive liquid meltwater storage in firn within the Greenland ice sheet. *Nature Geoscience* **7**, 95–98.

Gagliardini O and Werder MA (2018) Influence of increasing surface melt over decadal timescales on land-terminating Greenland-type outlet glaciers. *Journal of Glaciology* **64**(247), 700–710.

Gardner AS and 6 others (2018) Increased West Antarctic and unchanged East Antarctic ice discharge over the last 7 years. *The Cryosphere* **12**(2), 521–547.

Gardner AS, Fahnestock MA and Scambos TA (2019) ITS_LIVE regional glacier and ice sheet surface velocities, data archived at National Snow and Ice Data Center (data accessed 06/06/2019). doi: 10.5067/6II6VW8LLWJ7.

Goelzer H and 41 others (2020) The future sea-level contribution of the Greenland ice sheet: a multi-model ensemble study of ISMIP6. *The Cryosphere* **14**(9), 3071–3096.

Hanna E and 8 others (2008) Increased runoff from melt from the Greenland Ice Sheet: a response to global warming. *Journal of Climate* **21**(2), 331–341.

Harper J, Humphrey N, Pfeffer WT, Brown J and Fettweis X (2012) Greenland ice-sheet contribution to sea-level rise buffered by meltwater storage in firn. *Nature* **491**, 240–243.

Hill EA, Carr R, Stokes CR and Gudmundsson H (2018) Dynamic changes in outlet glaciers in northern Greenland from 1948 to 2015. *The Cryosphere* **12**, 3243–3263.

Holland DM, Thomas RH, de Young B, Ribergaard MH and Lyberth B (2008) Acceleration of Jakobshavn Isbrae triggered by warm subsurface ocean waters. *Nature Geoscience* **1**, 659–664.

Howat IM, Joughin I, Fahnestock M, Smith BE and Scambos TA (2008) Synchronous retreat and acceleration of southeast Greenland outlet glaciers 2000–06 ice dynamics and coupling to climate. *Journal of Glaciology* **54**, 646–660.

Howat IM, Joughin I and Scambos TA (2007) Rapid changes in ice discharge from Greenland outlet glaciers. *Science (New York, N.Y.)* **315**(5818), 1559–1561.

Howat IM, Joughin I, Tulaczyk S and Gogineni S (2005) Rapid retreat and acceleration of Helheim Glacier, east Greenland. *Geophysical Research Letters* **32**, L22502. doi: 10.1029/2005GL024737.

Hvidberg CS and 10 others (2020) Surface velocity of the Northeast Greenland Ice Stream (NEGIS): assessment of interior velocities derived from satellite data by GPS. *The Cryosphere* **14**, 3487–3502.

Joughin I and 8 others (2008) Ice-front variation and tidewater behaviour on Helheim and Kangerdlugssuaq Glaciers, Greenland. *Journal of Geophysical Research* **113**, F01004. doi: 10.1029/2007JF000837.

6684
Joughin I, Abdalati W and Fahnestock M (2004) Large fluctuations in speed on Greenland's Jakobshavn Isbrae glacier. *Nature* **432**, 608–610.
Joughin I, Shean DE, Smith BE and Floricoiu D (2020) A decade of variability on Jakobshavn Isbrae: ocean temperatures pace speed through influence on melange rigidity. *The Cryosphere* **14**(1), 211–227.
Joughin I, Smith BE and Howat I (2018) Greenland Ice Mapping Project: ice flow velocity variation at sub-monthly to decadal timescales. *The Cryosphere* **12**(7), 2211–2227.
Joughin I, Smith BE, Howat IM, Scambos T and Moon T (2010) Greenland flow variability from ice-sheet-wide velocity mapping. *Journal of Glaciology* **56**(197), 415–430.
Joughin I, Smith BE, Shean DE and Floricoiu D (2014) Brief communication: further summer speedup of Jakobshavn Isbrae. *The Cryosphere* **8**, 209–214.
Kamb B and Echelmeyer KA (1986) Stress-gradient coupling in glacier flow: I. Longitudinal averaging of the influence of ice thickness and surface slope. *Journal of Glaciology* **32**, 267–284.
Khan SA and 13 others (2013) Recurring dynamically induced thinning during 1985 to 2010 on Upernavik Isstrøm, west Greenland. *Journal of Geophysical Research: Earth Surface* **118**, 11–121. doi: 10.1029/2012JF002481.
Khan SA and 12 others (2014) Sustained mass loss of the northeast Greenland ice sheet triggered by regional warming. *Nature Climate Change* **4**, 292–299.
Khazendar A and 13 others (2019) Interruption of two decades of Jakobshavn Isbrae acceleration and thinning as regional ocean cools. *Nature Geoscience* **12**, 277–283.
King MD and 6 others (2018) Seasonal to decadal variability in ice discharge from the Greenland Ice Sheet. *The Cryosphere* **12**, 3813–3825.
King MD and 8 others (2020) Dynamic ice loss from the Greenland Ice Sheet driven by sustained glacier retreat. *Communications Earth & Environment* **1**, https://doi.org/10.1038/s43247-020-0001-2.
Konrad H and 6 others (2017) Uneven onset and pace of ice-dynamical imbalance in the Amundsen Sea Embayment, West Antarctica. *Geophysical Research Letters* **44**(2), 910–918.
Larsen SH and 5 others (2016) Increased mass loss and asynchronous behaviour of marine-terminating outlet glaciers at Upernavik Isstrøm, NW Greenland. *Journal of Geophysical Research: Earth Surface* **121**, 241–256. doi: 10.1002/2015JF003507.
Lemos A and 5 others (2018) Ice velocity of Jakobshavn Isbræ, Petermann Glacier, Nioghalvfjerdsfjorden, and Zachariæ Isstrøm, 2015–2017, from Sentinel 1-a/b SAR imagery. *The Cryosphere* **12**(6), 2087–2097.
Luckman A and Murray T (2005) Seasonal variation in velocity before retreat of Jakobshavn Isbrae, Greenland. *Geophysical Research Letters* **32**(8), L08501. doi: 10.1029/2005GL022519.
Luckman A, Murray T, de Lange R and Hanna E (2006) Rapid and synchronous ice-dynamic changes in east Greenland. *Geophysical Research Letters* **33**(3), L03503. doi: 10.1029/2005GL025428.
Machguth H and 9 others (2016) Greenland meltwater storage in firn limited by near-surface ice formation. *Nature Climate Change* **6**(4), 390–393.
Mankoff KD and 5 others (2020) Greenland Ice Sheet solid ice discharge from 1986 through March 2020. *Earth System Science Data* **12**, 1367–1383.
McMillan M and 14 others (2014) Rapid dynamic activation of a marine-based Arctic ice cap. *Geophysical Research Letters* **41**(24), 8902–8909.
McMillan M and 14 others (2016) A high-resolution record of Greenland mass balance. *Geophysical Research Letters* **43**(13), 7002–7010.
Mernild SH and 7 others (2013) Volume and velocity changes at Mittivakkat Gletscher, southeast Greenland. *Journal of Glaciology* **59**(216), 660–670.
Miège C and 12 others (2016) Spatial extent and temporal variability of Greenland firn aquifers detected by ground and airborne radars. *Journal of Geophysical Research: Earth Surface* **121**(12), 2381–2398.
Miller O and 7 others (2018) Direct evidence of meltwater flow within a firn aquifer in southeast Greenland. *Geophysical Research Letters* **45**(1), 207–215.
Moon T, Joughin I, Smith B and Howat I (2012) 21st-century evolution of Greenland outlet glacier velocities. *Science (New York, N.Y.)* **336**, 576–578.
Morlighem M and 31 others (2017) BedMachine v3: complete bed topography and ocean bathymetry mapping of Greenland from multibeam echo sounding combined with mass conservation. *Geophysical Research Letters* **44**(21), 11051–11061.
Morlighem M, Rignot E, Mouginot J, Seroussi H and Larour E (2014) Deeply incised submarine glacial valleys beneath the Greenland ice sheet. *Nature Geoscience* **7**(6), 418–422.
Motyka RJ and 5 others (2011) Submarine melting of the 1985 Jakobshavn Isbrae floating tongue and the triggering of the current retreat. *Journal of Geophysical Research: Earth Surface* **116**, F01007. doi: 10.1029/2009JF001632.
Motyka RJ and 11 others (2017) Asynchronous behavior of outlet glaciers feeding Godthåbsfjord (Nuup Kangerlua) and the triggering of Narsap Sermia's retreat in SW Greenland. *Journal of Glaciology* **63**(238), 288–308.
Mouginot J and 7 others (2015) Fast retreat of Zachariæ Isstrøm, northeast Greenland. *Science (New York, N.Y.)* **350**(6266), 1357–1361.
Mouginot J and 8 others (2019) Forty-six years of Greenland Ice Sheet mass balance from 1972 to 201. *Proceedings of the National Academy of Sciences* **116**(19), 9239–9244.
Murray T and 10 others (2010) Ocean regulation hypothesis for glacier dynamics in southeast Greenland and implications for ice sheet mass changes. *Journal of Geophysical Research: Earth Surface* **115**, F03026. doi: 10.1029/2009JF001522.
Murray T and 14 others (2015) Extensive retreat of Greenland tidewater glaciers, 2000–2010. *Arctic, Antarctic, and Alpine Research* **47**(3), 427–447.
Nick FM, Vieli A, Howat IM and Joughin I (2009) Large-scale changes in Greenland outlet glacier dynamics triggered at the terminus. *Nature Geoscience* **2**(2), 110–114.
Nienow PW, Sole AJ, Slater DA and Cowton TR (2017) Recent advances in our understanding of the role of meltwater in the Greenland Ice Sheet system. *Current Climate Change Reports* **3**, 330–344.
Nye JF (1960) The response of glaciers and ice-sheets to seasonal and climatic changes. *Proceedings of the Royal Society A* **256**, 559–584.
Nye JF (1963) On the theory of the advance and retreat of glaciers. *Geophysical Journal of the Royal Astronomical Society* **7**(4), 431–456.
Phillips T, Rajaram H, Colgan W, Steffen K and Abdalati W (2013) Evaluation of cryo-hydrologic warming as an explanation for increased ice velocities in the wet snow zone, Sermeq Avannarleq, West Greenland. *Journal of Geophysical Research: Earth Surface* **118**(3), 1241–1256.
Phillips T, Rajaram H and Steffen K (2010) Cryo-hydrologic warming: a potential mechanism for rapid thermal response of ice sheets. *Geophysical Research Letters* **37**(20), L20503. doi: 10.1029/2010GL044397.
Poinar K and 5 others (2015) Limits to future expansion of surface-melt-enhanced ice flow into the interior of western Greenland. *Geophysical Research Letters* **42**(6), 1800–1807.
Poinar K and 5 others (2017) Drainage of Southeast Greenland firn aquifer water through crevasses to the bed. *Frontiers in Earth Science* **5**(5), https://doi.org/10.3389/feart.2017.00005.
Poinar K, Dow CF and Andrews LC (2019) Long-term support of an active subglacial hydrologic system in Southeast Greenland by firn aquifers. *Geophysical Research Letters* **46**(9), 4772–4781.
Price SF, Payne AJ, Catania GA and Neumann TA (2008) Seasonal acceleration of inland ice via longitudinal coupling to marginal ice. *Journal of Glaciology* **54**(185), 213–219.
Price SF, Payne AJ, Howat IM and Smith BE (2011) Committed sea-level rise for the next century from Greenland ice sheet dynamics during the past decade. *Proceedings of the National Academy of Sciences* **108**, 8978–8983.
Pritchard HD, Arthern RJ, Vaughan DG and Edwards LA (2009) Extensive dynamic thinning on the margins of the Greenland and Antarctic ice sheets. *Nature* **461**(7266), 971–975.
Riel B, Minchew B and Joughin I (2020) Observing traveling waves in glaciers with remote sensing: new flexible time series methods and application to Sermeq Kujalleq (Jakobshavn Isbræ), Greenland. *The Cryosphere Discussions*, https://doi.org/10.5194/tc-2020-193.
Rignot E, Box JE, Burgess E and Hanna E (2008) Mass balance of the Greenland ice sheet from 1958 to 2007. *Geophysical Research Letters* **35**, L20502.
Rignot E and Kanagaratnam P (2006) Changes in the velocity structure of the Greenland Ice Sheet. *Science (New York, N.Y.)* **311**(5763), 986–990.
Rignot E, Velicogna I, van den Broeke MR, Monaghan A and Lenaerts J (2011) Acceleration of the contribution of the Greenland and Antarctic ice sheets to sea level rise. *Geophysical Research Letters* **38**(5), L05503.
Shepherd A and 45 others (2012) A reconciled estimate of ice-sheet mass balance. *Science (New York, N.Y.)* **338**(6111), 1183–1189.
Shepherd A and 88 others (2020) Mass balance of the Greenland Ice Sheet from 1992 to 2018. *Nature* **579**, 233–239.
Simonsen SB and Sørensen LS (2017) Implications of changing scattering properties on Greenland ice sheet volume change from Cryosat-2 altimetry. *Remote Sensing of Environment* **190**, 207–216.
Smith B and 14 others (2020) Pervasive ice sheet mass loss reflects competing ocean and atmospheric processes. *Science (New York, N.Y.)* **368**(6496), 1239–1242.

6685
Sole AJ and 6 others (2011) Seasonal speedup of a Greenland marine-terminating outlet glacier forced by surface melt-induced changes in subglacial hydrology. *Journal of Geophysical Research* **116**, F03014, http://dx.doi.org/10.1029/2010JF001948.

Sole A and 6 others (2013) Winter motion mediates dynamic response of the Greenland Ice Sheet to warmer summers. *Geophysical Research Letters* **40** (15), 3940–3944.

Sørensen LS and 5 others (2018) 25 years of elevation changes of the Greenland Ice Sheet from ERS, Envisat, and CryoSat-2 radar altimetry. *Earth and Planetary Science Letters* **495**, 234–241.

Stevens LA and 6 others (2016) Greenland Ice Sheet flow response to runoff variability. *Geophysical Research Letters* **43**(21), 11295–11303.

Tedstone AJ and 5 others (2015) Decadal slowdown of a land-terminating sector of the Greenland Ice Sheet despite warming. *Nature* **526**(7575), 692–695.

Thomas R and 6 others (2000) Mass balance of the Greenland Ice Sheet at high elevations. *Science (New York, N.Y.)* **289**(5478), 426–428.

Thomas RH and PARCA Investigators (2001) Program for Arctic Regional Climate Assessment (PARCA): goals, key findings, and future directions. *Journal of Geophysical Research* **106**(D24), 33691–33705.

Thomas RH and 5 others (2003) Investigation of surface melting and dynamic thinning on Jakobshavn Isbrae, Greenland. *Journal of Glaciology* **49**(165), 231–239.

Thomas RH (2004) Force-perturbation analysis of recent thinning and acceleration of Jakobshavn Isbrae, Greenland. *Journal of Glaciology* **50**(168), 57–66.

Thomas RH, Csatho BM, Gogineni S, Jezek KC and Kuivinen K (1998) Thickening of the western part of the Greenland Ice Sheet. *Journal of Glaciology* **44**(148), 653–658.

van den Broeke M and 8 others (2009) Partitioning recent Greenland mass loss. *Science (New York, N.Y.)* **326**, 984–986.

van der Veen CJ (2001) Greenland ice sheet response to external forcing. *Journal of Geophysical Research: Atmospheres* **106**(D24), 34047–34058.

van de Wal RSW and 6 others (2008) Large and rapid melt-induced velocity changes in the ablation zone of the Greenland Ice Sheet. *Science (New York, N.Y.)* **321**(5885), 111–113.

van de Wal RSW and 5 others (2012) Twenty-one years of mass balance observations along the K-transect, west Greenland. *Earth System Science Data* **4**, 31–35.

van de Wal RSW and 10 others (2015) Self-regulation of ice flow varies across the ablation area in south-west Greenland. *The Cryosphere* **9**(2), 603–611.

Vaughan DG and 13 others (2013) Observations: cryosphere. In Stocker TF **and 9 others** (eds), *Climate Change 2013: The Physical Science Basis. Contribution of Working Group I to the Fifth Assessment Report of the Intergovernmental Panel on Climate Change*. Cambridge and New York: Cambridge University Press, pp. 317–382.

Wang W, Li J and Zwally HJ (2012) Dynamic inland propagation of thinning due to ice loss at the margins of the Greenland ice sheet. *Journal of Glaciology* **58**(210), 734–740.

Williams JJ, Gourmelen N and Nienow P (2020) Dynamic response of the Greenland ice sheet to recent cooling. *Scientific Reports* **10**, 1647, https://doi.org/10.1038/s41598-020-58355-2.

Willis MJ and 11 others (2018) Massive destabilization of an Arctic ice cap. *Earth and Planetary Science Letters* **502**, 146–155.

Zheng W, Pritchard ME, Willis MJ and Stearns LA (2019) The possible transition from glacial surge to ice stream on Vavilov ice cap. *Geophysical Research Letters* **46**(23), 13892–13902.

Zwally H and 11 others (2011) Greenland ice sheet mass balance: distribution of increased mass loss with climate warming. *Journal of Glaciology* **57**, 88–102.